MEDICINAL PLANTS IN GASTROINTESTINAL CANCERS AND TUMOR MICROENVIRONMENTS

EDITED BY: Qingmin Sun, Youhua Xu, Cristiana Perrotta and Chao Sun
PUBLISHED IN: Frontiers in Pharmacology and Frontiers in Oncology

frontiers Research Topics

frontiers

ISSN 1664-8714
ISBN978-2-88976-938-4
DOI 10.3389/978-2-88976-938-4

About Frontiers

Frontiers is more than just an open-access publisher of scholarly articles: it is a pioneering approach to the world of academia, radically improving the way scholarly research is managed. The grand vision of Frontiers is a world where all people have an equal opportunity to seek, share and generate knowledge. Frontiers provides immediate and permanent online open access to all its publications, but this alone is not enough to realize our grand goals.

Frontiers Journal Series

The Frontiers Journal Series is a multi-tier and interdisciplinary set of open-access, online journals, promising a paradigm shift from the current review, selection and dissemination processes in academic publishing. All Frontiers journals are driven by researchers for researchers; therefore, they constitute a service to the scholarly community. At the same time, the Frontiers Journal Series operates on a revolutionary invention, the tiered publishing system, initially addressing specific communities of scholars, and gradually climbing up to broader public understanding, thus serving the interests of the lay society, too.

Dedication to Quality

Each Frontiers article is a landmark of the highest quality, thanks to genuinely collaborative interactions between authors and review editors, who include some of the world's best academicians. Research must be certified by peers before entering a stream of knowledge that may eventually reach the public - and shape society; therefore, Frontiers only applies the most rigorous and unbiased reviews.
Frontiers revolutionizes research publishing by freely delivering the most outstanding research, evaluated with no bias from both the academic and social point of view. By applying the most advanced information technologies, Frontiers is catapulting scholarly publishing into a new generation.

What are Frontiers Research Topics?

Frontiers Research Topics are very popular trademarks of the Frontiers Journals Series: they are collections of at least ten articles, all centered on a particular subject. With their unique mix of varied contributions from Original Research to Review Articles, Frontiers Research Topics unify the most influential researchers, the latest key findings and historical advances in a hot research area! Find out more on how to host your own Frontiers Research Topic or contribute to one as an author by contacting the Frontiers Editorial Office: frontiersin.org/about/contact

MEDICINAL PLANTS IN GASTROINTESTINAL CANCERS AND TUMOR MICROENVIRONMENTS

Topic Editors:
Qingmin Sun, Affiliated Hospital of Nanjing University of Chinese Medicine, China
Youhua Xu, Macau University of Science and Technology Taipa, SAR China
Cristiana Perrotta, University of Milan, Italy
Chao Sun, Tianjin Medical University General Hospital, China

Citation: Sun, Q., Xu, Y., Perrotta, C., Sun, C., eds. (2022). Medicinal Plants in Gastrointestinal Cancers and Tumor Microenvironments.
Lausanne: Frontiers Media SA. doi: 10.3389/978-2-88976-938-4

Table of Contents

frontiers in Pharmacology

REVIEW
published: 18 May 2021
doi: 10.3389/fphar.2021.681477

Does Oral Apigenin Have Real Potential for a Therapeutic Effect in the Context of Human Gastrointestinal and Other Cancers?

Eva F. DeRango-Adem[1] *and Jonathan Blay*[1,2]*

[1]School of Pharmacy, University of Waterloo, Waterloo, ON, Canada, [2]Department of Pathology, Dalhousie University, Halifax, NS, Canada

Apigenin (4′, 5, 7-trihydroxyflavone) is a plant flavone that has been found to have various actions against cancer cells. We evaluated available evidence to determine whether it is feasible for apigenin to have such effects in human patients.

Apigenin taken orally is systemically absorbed and recirculated by enterohepatic and local intestinal pathways. Its bioavailability is in the region of 30%. Once absorbed from the oral route it reaches maximal circulating concentration (C_{max}) after a time (T_{max}) of 0.5–2.5h, with an elimination half-life ($T^1/_2$) averaging 2.52 ± 0.56h.

Using a circulating concentration for efficacy of 1–5μmol/L as the target, we evaluated data from both human and rodent pharmacokinetic studies to determine if a therapeutic concentration would be feasible. We find that oral intake of dietary materials would require heroic ingestion amounts and is not feasible. However, use of supplements of semi-purified apigenin in capsule form could reach target blood levels using amounts that are within the range currently acceptable for other supplements and medications. Modified formulations or parenteral injection are suitable but may not be necessary.

Further work with direct studies of pharmacokinetics and clinical outcomes are necessary to fully evaluate whether apigenin will contribute to a useful clinical strategy, but given emerging evidence that it may interact beneficially with chemotherapeutic drugs, this is worthy of emphasis. In addition, more effective access to intestinal tissues from the oral route raises the possibility that apigenin may be of particular relevance to gastrointestinal disorders including colorectal cancer.

Keywords: apigenin, pharmacokinetics, pharmacodynamics, colorectal carcinoma, cancer, natural health products (NHPs), dietary contituents, therapeutics

OPEN ACCESS

Edited by:
Cristiana Perrotta, University of Milan, Italy

Reviewed by:
Eswar Shankar, Case Western Reserve University, United States
Ajay Sharma, University of Texas Health Science Center at Houston, United States

***Correspondence:**
Jonathan Blay
jonathan.blay@uwaterloo.ca

Specialty section:
This article was submitted to Pharmacology of Anti-Cancer Drugs, a section of the journal Frontiers in Pharmacology

Received: *18 March 2021*
Accepted: *30 April 2021*
Published: *18 May 2021*

Citation:
DeRango-Adem EF and Blay J (2021) Does Oral Apigenin Have Real Potential for a Therapeutic Effect in the Context of Human Gastrointestinal and Other Cancers? Front. Pharmacol. 12:681477. doi: 10.3389/fphar.2021.681477

INTRODUCTION

Natural products have long been appreciated for their potential as molecular sources for novel chemotherapeutic and chemopreventive agents(Cassady et al., 1990). Among the diverse possibilities, flavonoids have shown particular promise as either natural molecules in the diet, or lead compounds for drug development (Kale et al., 2008; Androutsopoulos et al., 2010; Batra and Sharma, 2013). Among the flavonoids, one that has captured the attention of researchers such as

ourselves has been apigenin, a flavone that is substituted by hydroxy groups at positions 4′, 5 and 7(National Center for Biotechnology Information, 2021). This plant-derived molecule has been of clinical interest since the 1950s, following observations that it is able to modulate histamine release and is bronchodilatory(Hava and Janku, 1958; Spicak and Subrt, 1958). However more recently, we and others have drawn attention to the possibility that apigenin may have useful properties against cancer(Lefort and Blay, 2013; Shankar et al., 2017; Yan et al., 2017). In particular, we have noted that apigenin's action at the cellular level is distinct from that of closely related flavones such as kaempferol and genistein(Lefort and Blay, 2011; Lefort et al., 2020).

Our research has focused particularly on gastrointestinal cancers(Lefort and Blay, 2013). However, apigenin has potentially advantageous effects on cellular processes in many solid cancers, including those of the breast, prostate, lung and lymphoma, and leukemias (Lefort and Blay, 2013), supporting contentions that it may have a general benefit in managing different neoplasias (Shankar et al., 2017; Yan et al., 2017).

Among the challenges in taking advantage of such molecules in their natural context or an extracted form is their capacity to reach biologically active concentrations at the target site and their selectivity of action. Together these two considerations define the potential efficacy as a therapeutic or adjunct, and side effect profile. Although many effects can be demonstrated *ex vivo* or in preclinical models, the question of whether natural product molecules are clinically relevant *via* the ingestion route, or whether clinically important activity can only be attained with additional drug-delivery technologies or chemical modification, is often not clear.

For the oral route, there is the question of whether clinically relevant concentrations of natural product molecules can be achieved by simple dietary manipulation, or whether artificial supplements are necessary to reach the required dosing level. When addressing cancer, we face two different situations in that accessing most cancers depends on the phases of absorption and systemic distribution after oral ingestion of the molecule of interest. However for gastrointestinal cancers, which are our primary interest, dietary apigenin has relatively direct access to neoplastic tissue that is positioned close to the intestinal lumen, particularly in early stage disease.

In this article, we review the currently available data on pharmacokinetics and pharmacodynamics of apigenin, and place these data in the context of the apigenin's potential for meaningful intervention in gastrointestinal and other oncopathologies. We will consider apigenin's physical and physiological properties, chemical properties (e.g., solubility), the comparative evidence for *in vitro* and *in vivo* therapeutic effects, and pharmacokinetic properties (absorption, distribution, metabolism, elimination).

METHODS

Article Sourcing and Data Extraction

A database of 1,447 literature sources within the laboratory relating to flavonoid action in the gastrointestinal tract was used as the initial resource and to define best search parameters to capture all relevant articles relating to the pharmacokinetic and pharmacodynamic profile of apigenin.

To capture all articles relevant to the pharmacokinetics of apigenin, a broad search strategy using those two terms was used on PubMed, considering only articles written in English or available as an English translation. This yielded (as of September 2020) an additional 314 articles which were manually curated together with those already available to provide the basis for this review. Selection was for relevance to the questions posed, informed by the perspectives of the authors. We considered i) wide information from a variety of analytical and preclinical models, ii) comparisons between oral and other administration routes, and iii) all information relevant to absorption, distribution, metabolism and excretion (ADME; the four parts of pharmacokinetics or how the body handles a bioactive molecule).

To capture cellular mechanistic and pharmacodynamic data with particular attention to gastrointestinal cancers, the following search strategies were used in the same framework:

1. apigenin AND (vill* OR mucosa OR "lamina propria" OR mesentary OR capillar* OR lympat*)
2. apigenin AND ("plasma membrane" OR endosom* OR nucle* OR transporter*)
3. apigenin AND (conversion OR deglycos* OR hydroxy* OR hydroph*)
4. apigenin AND (HT-29 OR HT29 OR HCT-116 OR HCT116 OR HRT-18 OR HRT18 OR Caco-2 OR Caco2 OR T84 OR SW480 OR SW620 OR Colo-320 OR Colo320)
5. apigenin AND (cancer OR carcino*) AND (gastrointes* OR colo*)

Ths enabled interpretation of pharmacokinetic data with particular emphasis on intestinal cellular action and gastrointestinal oncopathologies, as is the focus of this review.

String Interactome Mapping

STRING is a web-based database of known and predicted protein-protein interactions that allows protein-protein interaction mapping based on both direct (physical) and indirect (functional) associations (Szklarczyk et al., 2019). Potential protein interactions involving apigenin and the cellular regulators identified in the pharmacodynamic review of this project were subjected to STRING analysis using *Homo sapiens* as the model organism. Proteins analyzed included APC, p34 (CDK2), p21 (CDKN1A), CDK1, cyclin B1, PARP, Bcl-XL, Mcl1, Stat3, Bax, Cytochrome C, Caspase-3, Caspase-8, Caspase-9, CHOP (DDIT3), DR5 (TNFRSF10B), Nag1 (GDF15), p53, p21, Erk (p38, MAPK1), Beta-Catenin 1 (CTNNB1), Snail, NFKB1, AKT1, C-myc, cyclin D1, PKM2, PTBP1, DPP4, ADA, and CK2 (CSNK2A1). These proteins are represented as nodes on the STRING map, with connections ranked as specified in the figure legend.

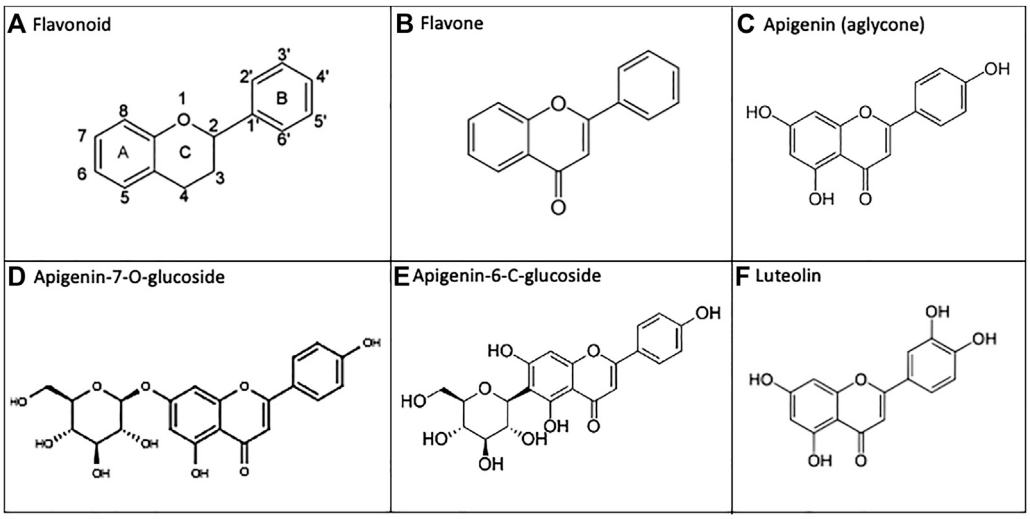

FIGURE 1 | Apigenin and related chemical structures. **(A)** General flavonoid structure as 15-carbon molecules containing two phenyl groups and a heterocyclic carbon ring. **(B)** The flavone sub-class of flavonoids have a C2-C3 double bond, unsubstituted C3 carbon, and a C4 ketone oxidization. **(C)** Apigenin is a 4′, 5, 7-trihydroxyflavone. **(D, E)** In nature, apigenin is commonly found as a 7-O-glucoside, 6-C-glucoside or 8-C-glucoside, which is enzymatically metabolized to free apigenin prior to intestinal absorption. **F)** Apigenin undergoes phase I metabolism *via* CYP1A2, and to a lesser extent CYP3A4, generating the 3′-hydroxylated product luteolin.

CURRENT KNOWLEDGE AND ANALYSIS

Structure of Apigenin and its Relationship With Other Plant Flavones

Flavonoids are polyphenolic natural products derived from plants and present in high amounts within leaves, flowers, and fruits(Hostetler et al., 2017). These diverse chemical compounds serve as native signaling mediators, allow UV protection, or enable pesticidal control within multiple plant phyla(Hostetler et al., 2017; Nunes et al., 2018). When plants are consumed by animals, including humans, some of these molecules also exhibit anti-inflammatory and antioxidant properties which are believed to translate to health benefits. However, the low bioavailability of flavonoids constitutes a barrier to their efficacy via the oral route (Thilakarathna and Rupasinghe, 2013). Flavones are a sub-class of flavonoids, having a C2-C3 double bond, unsubstituted C3 carbon, and ketone oxidization at C4 (Panche et al., 2016) (**Figure 1**).

We have noted particular health potential for apigenin–a plant flavone found in high concentrations within parsley, chamomile, celery, spinach, artichokes and oregano(Shankar et al., 2017). Apigenin is a 4′, 5, 7-trihydroxyflavone (National Center for Biotechnology Information, 2021), and it is the free hydroxyl groups present on the A/B rings of apigenin that are responsible for the antioxidant effects of this flavone(Singh et al., 2014). In natural sources, apigenin is commonly found as an 7-O-glucoside, 6-C-glucoside, or 8-C-glucoside (14, 18) (**Figure 1**). After ingestion of the plant material, these glucosides are enzymatically metabolized *in vivo* into free apigenin (*i.e.,* the aglycone form) and subsequently absorbed(Hostetler et al., 2013; Hostetler et al., 2017). Luteolin is another plant flavonoid, and it is also an apigenin metabolite–produced as a result of phase I cytochrome P450 (CYP) enzyme hydroxylation *in vivo* (Hostetler et al., 2017) (**Figure 1**).

Physico-Chemical Properties of Apigenin and Their Effect on Uptake

Flavonoids as a sub-class are poorly bioavailable from the diet due to their low water solubility, chemical instability, and rapid metabolism in the body (Leonarduzzi et al., 2009). Apigenin itself is however lipophilic and a weak acid, and therefore will be most permeable to cell membranes in the unionized form within acidic environments, allowing it to be better absorbed in lower pH environments along the gastrointestinal tract, including the stomach (Leonarduzzi et al., 2009). In the pH range of the intestinal tract, hydrophobic apigenin is still able to permeate lipid membranes–enabling absorption along the full length of the intestines, but does so most effectively in the duodenum (Tang et al., 2017).

Apigenin is a Class II molecule under the Biopharmaceutics Classification System (BCS) (Tsume et al., 2014), exhibiting low water solubility and high permeability (Leonarduzzi et al., 2009). Water solubility increases with ionization in more basic environments. The maximal aqueous solubility of apigenin occurs at a pH of 7.5, up to a concentration of 0.183mg/ml (National Center for Biotechnology Information, 2021).

Overall Uptake of Apigenin From the Diet

Observational studies looking at consumption of apigenin within whole foods in the human diet indicate daily intake between 0.45 and 1.17mg–varying between age and demographic(Meyer et al.,

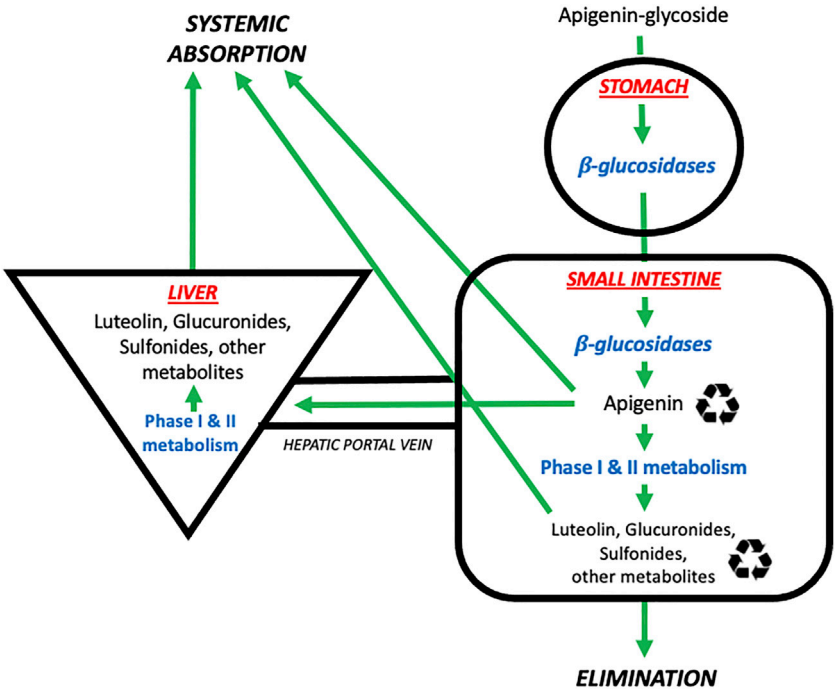

FIGURE 2 | The absorption, distribution, metabolism, and elimination of apigenin. Apigenin is present in the diet in glycosylated forms found in nature (e.g., 7-O-glucoside, 6-C-glucoside or 8-C-glucoside). These glycosides are then metabolized by *β*-glucosidases in the stomach and small intestines to generate free apigenin (i.e., the aglycone form). Free apigenin can be directly absorbed systemically, or undergo downstream phase I and II metabolism in the small intestines and liver to generate hydroxylated metabolites such as luteolin, or glucuronidated and sulfonated metabolites. These metabolites enter four possible pathways: i) direct systemic absorption, ii) elimination (mostly via the urine, to a lesser extent the feces), iii) local enteric recycling, or iv) enterohepatic recycling via the bile. ♻Denotes that molecules are subject to recycling through enteric and/or enterohepatic routes. Image adapted from (Thilakarathna and Rupasinghe, 2013).

2006; Somerset and Johannot, 2008). Meyer and colleagues studied the bioavailability of apiin (apigenin-7-O-apiosylglucoside) following a single bolus of parsley–a food source with an exceedingly high concentration of apigenin (Meyer et al., 2006). Blood and urine samples from 11 German adults (ages 23–41) were taken following a meal consisting of 2g parsley/kg body weight–which was equivalent to ~17mg of apigenin (Meyer et al., 2006). Plasma concentrations of apigenin ranged from 28–337nmol/L at 6–10h after consumption, and fell below detection at 28h (Meyer et al., 2006). A total of 0.039mg (±0.03) of apigenin was recovered over 24h from urine samples (Meyer et al., 2006). These low plasma and urine concentrations are expected based on some of the pharmacokinetic parameters that will be discussed below - such as rapid metabolism, excretion of unabsorbed apigenin in non-urinary pathways, or hydrolysis by colonic microflora (Meyer et al., 2006).

Absorption of Apigenin in the Gastrointestinal Tract

A schematic summary of the physiological processes leading to the absorption, distribution, metabolism, and elimination of apigenin is shown in **Figure 2**. As mentioned above, apigenin is ingested in a glycosylated form. These apigenin glucosides must be metabolized to the aglycone form by enzymes in the stomach and/or small intestines–such as epithelial *β*-glucosidases–or within endogenous colon microflora, prior to systemic absorption (Srinivas, 2015). *Eubacterium ramulus* and *Bacteroides distasonis* have been identified as major bacterial species essential to the biotransformation of 7-glycosides into aglyconated apigenin (Hanske et al., 2009). *Ex vivo* hydrolytic deglycosylation studies of apigenin and luteolin into their respective aglycone forms using rat models suggest variability in deglycosylation rate according to location within the gastrointestinal tract (Lu et al., 2010).

Oral administration of extracts of *Chrysanthemum morifolium,* which contain high levels of apigenin in its 7-O-β-D-glucosidic form, has been studied in rats (Lu et al., 2010). There is substantial and fairly rapid early deglycosylation after ingestion in the stomach and upper intestine, with absorption beginning in the duodenum; the stomach seems to be a site for early hydrolysis and retention of the compound (Lu et al., 2010). These authors concluded that the upper intestine, particularly the jejunum, play the major role in flavonoid absorption (Lu et al., 2010). However, other studies have shown that for apigenin, amounts absorbed were the highest in the colon (40%) and the lowest in the terminal ileum (21%) (Chen et al., 2003). *In vivo* intestinal absorption was mediated by both passive and active carrier-mediated transport in the duodenum and jejunum, as well as concentration-dependent membrane permeability (Zhang et al., 2012). Absorption in the ileum and colon was largely *via* passive transport, in a concentration-independent manner (Zhang et al., 2012).

TABLE 1 | Pharmacokinetic parameters of apigenin in the literature. Four kinetic studies on oral and IV administered apigenin in rat models have been published. Doses ranged from 13.5 to 60 mg/kg. Significant variability was observed between peak plasma concentrations and the respective T_{max}. Relative oral bioavailability (F) of apigenin is low, at ~30%. Note: parameters were calculated to equivalent units.

Study data source	Model	Admin	Molecule	Dose (mg/kg)	C_{max} (ng/ml)	T_{max} (h)	AUC(0-t) (ng*h/ml)	$T^1/_2$
Teng et al. (2012)	Rats	Oral	Apigenin	13.5	42 ± 2	0.50±0.01	659 ± 25	2.11 ± 0.03
			Glucuronide metabolite		43 ± 4	1.23 ± 0.13	351 ± 13	4.69 ± 0.05
			Sulfonate metabolite		13 ± 2	1.07±0.09	20 ± 2	10.97 ± 0.13
Ding et al. (2014)	Rats	Oral	Apigenin	60	1330 ± 240	2.5±0.33	11763 ± 1520	4.198 ± 0.29
Wan et al. (2007)	Rats	IV	Apigenin	20	10934 ± 1730	IV admin (N/A)	3312 ± 473	1.75 ± 1.18
			Luteolin metabolite		78.16 ± 26.23	0.08	28.73 ± 11.33	0.97 ± 1.25
Chen et al. (2011)	Rats	IV	Apigenin-7-O-glucoside	18	0.68 ± 0.04	IV admin (N/A)	1.34 ± 0.11	2.03 ± 1.32

Some flavonoids, including apigenin, are able to modulate intestinal smooth muscle peristalsis–potentially facilitating their absorption(Gharzouli and Holzer, 2004). *In vitro* studies in guinea pigs show that apigenin interferes with muscle excitation and/or excitation-contraction, to decrease distension sensitivity and peristaltic performance in a concentration-dependent manner, thereby advantaging the absorption process (Gharzouli and Holzer, 2004). Biliary excretion and recycling enables a significantly increased half-life of the compound and prolonged exposure of the intestinal mucosa (Chen et al., 2003; Min et al., 2017). In addition to enterohepatic recycling, apigenin can also undergo local enteric recycling, in a concentration and metabolite-dependent manner (Hu et al., 2003). These enterohepatic/enteric recycling processes will tend to favor the persistence of apigenin in the gastrointestinal tract but reduce net systemic absorption.

Variability in Apigenin Absorption, and Bioavailability

Intra-individual variability of small molecule absorption in the intestinal tract is in part related to the presence and activity of efflux pumps within the intestinal epithelium, such as the ABC transporters. ABC transporters limit flavonoid bioavailability by mediating efflux from intestinal cells into the lumen for excretion (Ravisankar et al., 2019). In Caco-2 cell monolayer models, potential dietary concentrations of apigenin (0.01–1.0μmol/L) significantly inhibited the expression of the ABC transporters ABCB–MDR1 (P-glycoprotein), ABCC–MRP2, ABCC-MRP3, and ABCG–BCRP (Ravisankar et al., 2019). This effect was synergistic with co-treatment of quercetin–another plant flavonoid (Ravisankar et al., 2019). This inhibition is believed to be mediated by directly blocking the ATP-binding site, or allosteric mechanisms (Ravisankar et al., 2019). Apigenin and quercetin enhance their own and each other's bioavailability by downregulating the activity of ABC transporters (Ravisankar et al., 2019). Of interest to the tissue distribution patterns of apigenin, to be discussed below, *in vitro* studies of this small molecule indicate it is also able to bind and inhibit the MRP efflux protein on human erythrocytes (Łania-Pietrzak et al., 2005).

Apigenin-specific pharmacokinetic parameters from four comprehensive studies using intact animal models are presented in **Table 1**. Relative bioavailability (F) of oral apigenin can be calculated by dividing the area under the curve (AUC) of an orally administered subset, over that of an intravenously administered subset. Using published values for the oral AUC (Teng et al., 2012) and IV AUC (Wan et al., 2007) and correcting for different doses, this represents ~30% bioavailability (976.29ng*h/ml/3313.10ng*h/ml). Oral bioavailabilities of small molecules in humans below 50% are considered to be low (Kim et al., 2014). After oral dosing the maximal circulating concentration (C_{max}) was reached after a time (T_{max}) of 0.5–2.5h, with considerable variation in the C_{max} reported in different studies. The highest C_{max} reported was 1330 ± 0.24ng/ml with an oral dose of 60mg/kg (Ding et al., 2014). Following IV administration of apigenin (20mg/kg) in rats, a mean residence time (MRT) of 0.65 ± 0.5h was calculated (Wan et al., 2007). Values for the circulating half-life ($T^1/_2$) for apigenin in these studies ranged from 1.8–4.2h with an average value of 2.52 ± 0.56h (Wan et al., 2007; Chen et al., 2011; Teng et al., 2012; Ding et al., 2014). With systematic dosing this would translate to reaching steady state within ~12h.

Tissue Distribution of Apigenin After Systemic Uptake

In terms of plasma protein binding affinities, fluorescent spectroscopic quenching and molecular modeling analyses suggest apigenin binds to human serum transferrin glycoprotein at the Fe^{3+}-binding site (Zhang et al., 2013). Specifically, this interaction is mediated by electrostatic and hydrogen bonding between the C5 and C7 hydroxyl groups of apigenin's B-ring, and Lys-291 and Tyr-188 of transferrin (Zhang et al., 2013). There is additional hydrogen-bonding between the carbonyl of apigenin's C-ring, and transferrin's Arg-124 (Zhang et al., 2013).

Structural, physiological, and clinical data suggest that apigenin distributes to tissues well–as would be expected due to its high molecular lipophilicity and plasma binding capacity. Apigenin has a large Volume of Distribution (Vd) *in vivo*. Following IV administration of 20mg/kg of apigenin in rats,

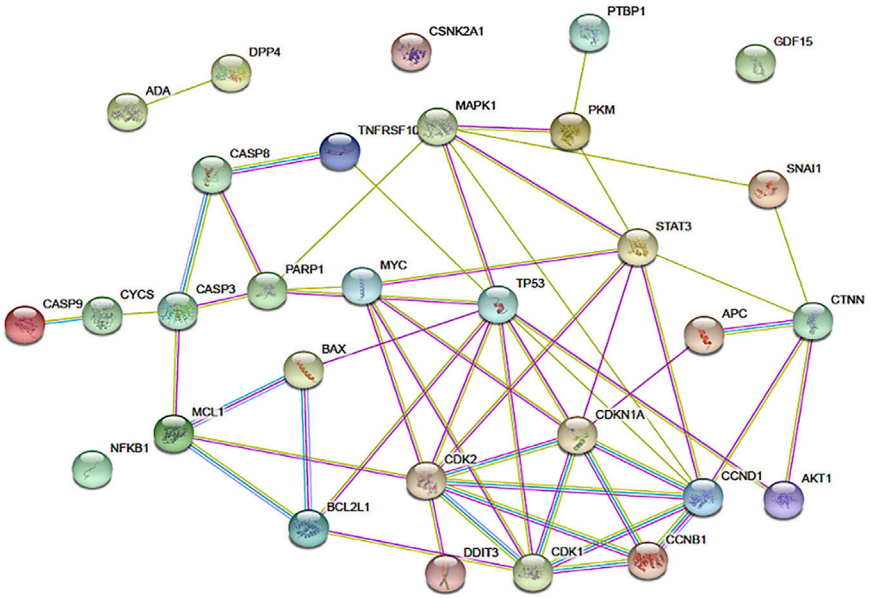

FIGURE 3 | The network of connections between regulatory pathways and molecules that are known to be impacted by apigenin. The functional protein association tool STRING was used to map the inter-connectedness of impacted proteins, identified through physical protein interactions in *Homo sapiens*, as shown. Connections between nodes are color coded depending on the interaction type: blue, curated databases; fuchsia, experimentally determined; green, textmining; light purple, protein homology. Connections within this network for DPP4, ADA, CSNK2A1, and CDF15 are not shown, but published data on non-physical interactions (e.g., gene co-expression) indicate that such links exist.

the Vd of apigenin was 15.75 ± 11.73L/kg–much larger than the Total Body Water (TBW) of rodents, at 0.67L/kg (Wan et al., 2007). Another study using 5.4mg/kg IV apigenin in rats showed a comparatively lower Vd at 2.07 ± 0.14L/kg, and a Vd of its metabolite luteolin at 0.868 ± 0.1L/kg–however both values are still above the TBW of rodents, indicating distribution and accumulation into tissue (Chen et al., 2012; Ninfali et al., 2013).

Lipinski's "Rule of Five" points to whether the physical properties of chemical compounds increase their propensity of being orally active drug candidates. According to the criteria, an orally active drug cannot have a logP >5 (i.e., the drug cannot be too lipophilic). The logP of apigenin is 2.84, making it a lipophilic agent that is permeable to drugs membrane and has the ability to bypass the blood-brain barrier, but still remains orally active (Yang et al., 2014).

Specific tissues that apigenin distributes to include gastrointestinal and hepatic tissues (Lu et al., 2010). Following oral administration of *Chrysanthemum* plant extracts in rats, apigenin and luteolin were observed to distribute to tissues throughout the gastrointestinal tract–from the stomach to terminal colon - following systemic absorption and circulation (Lu et al., 2010). Both luteolin and apigenin concentrations were 3–10X higher in the jejunum, as compared to other segments of the intestines (68.2nmol/g and 84nmol/g for the two flavonoids, respectively), (Lu et al., 2010). Extracts of oral *Eclipta prostrata* in rats indicate that apigenin and luteolin accumulate most in the liver, 10 min following oral administration (Du et al., 2018). The formation rates of glucuronated and sulfonated apigenin in the liver occurs at a faster rate than apigenin excretion, by 2.5–6X and 4–6X for the respective metabolites–directly contributing to the flavonoids' ability to accumulate in tissue(Tang et al., 2017).

The Cellular Pharmacodynamics of Apigenin With Neoplasias as the Target

As a small molecule (MW 270g/mol), it is not surprising that apigenin interacts with multiple cellular components. However, there is accumulating evidence that these varied interactions allow apigenin to modulate cellular regulatory pathways in ways that alter the behavior of both normal and neoplastic cells, particularly those of epithelial origin. This may depend on the state of lineage differentiation; we have shown that the ability of apigenin to upregulate the cell-surface regulator CD26/DPP4 on colon epithelial cells depends on the degree of differentiation in a series of carcinoma cell lines (Lefort et al., 2020).

The network of cellular regulatory proteins known to be impacted by apigenin is shown in **Figure 3**. This includes a number of pathways relating to the cell cycle, growth, proliferation, autophagy, and apoptosis–many of which are intrinsically linked. Indeed, apigenin has a plethora of actions on intracellular pathways that underlie its potential for a net anti-cancer effect (**Figure 4**). Some of the affected proteins are at the cell surface, such as the dipeptidyl peptidase DPP4 (also referred to as CD26) and its bound ligand ecto-adenosine deaminase (ADA), which we have examined extensively for their roles in tumor expansion and metastasis (Tan et al., 2006; Lefort and Blay, 2011; Cutler et al., 2015). The peptidase activity of DPP4 modulates the bioactivity of the chemokine CXCL12, which

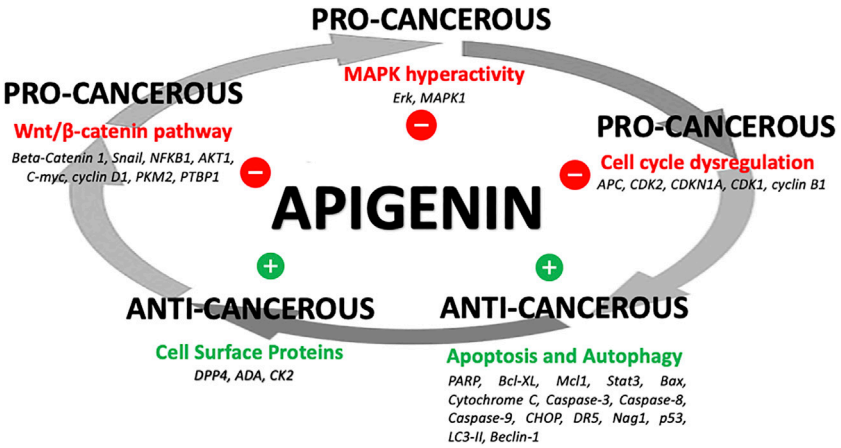

FIGURE 4 | Apigenin influences on cancer processes. A summary of how apigenin is a key regulator in a number of linked cellular pathways, inhibiting pro-cancerous activity or promoting anti-cancerous activity, yielding a potential overall anti-cancer effect.

acts upon the cell-surface receptor CXCR4 to control both the propensity of colorectal and other carcinoma cells to accumulate in their secondary tissue sites and form metastasis (Richard et al., 2006; Richard and Blay, 2008). This may be one route by which apigenin or related ligands could have an effect in constraining metastasis (Lefort and Blay, 2011; Lefort and Blay, 2013). However, the ability of apigenin to regulate the function of cell-surface proteins is not directly exerted at the external face of the plasma membrane. For example, the ability of apigenin to upregulate DPP4 depends on inhibition of an intracellular kinase, casein kinase 2 (CK2) (Lefort et al., 2020).

Indeed, apigenin primarily acts on intracellular protein targets such as CK2. Firstly, apigenin impacts proximal signaling through MAPK protein kinases. Hyperactivity of the MAPK pathway is linked to cancer proliferation and progression (Dhillon et al., 2007). HCT116 colon cancer cells treated with apigenin show increased MAPK phosphorylation (Dross et al., 2003). Apigenin induced 15 and 4.3-fold increases in expression of phosphorylated ERK and p38, respectively (Dross et al., 2003). This led to significantly increased transcriptional activation of downstream effectors in the MAPK pathway in a dose-dependent manner–including a 7.4-fold increase in the phosphorylation of Elk (a phosphorylation target of ERK) and a 3.2-fold increase in the phosphorylation of activating transcription factor-2 (ATF-2, a phosphorylation target of p38) (Dross et al., 2003). These data suggest apigenin's cellular regulatory activity is in part mediated by modulating phosphorylation events of the MAPK pathway (Dross et al., 2003).

Apigenin can also modulate different aspects of the Wnt/β-catenin signaling pathway. This pathway regulates cellular behaviors including migration and the formation of tissue structures, and plays a key role in both the formation and progression of cancers, including colorectal carcinoma (Yuan et al., 2020; Bugter et al., 2021; Caspi et al., 2021). The transcription factor Snail promotes Wnt target gene expression, and downstream interactions with beta-catenin–ultimately promoting growth and proliferation (Stemmer et al., 2008). Treatment of HCT116 cells with 10–20μmol/L of apigenin led to decreased expression of Snail (also a regulator of the epithelial-to-mesenchymal transition of cancer cells) and NF-κB (a transcriptional regulator of Snail) at the RNA and protein level in a dose-dependent manner (Tong et al., 2019). In SW480 cells, apigenin inhibited β-catenin signaling activation in a dose-dependent manner - blocking β-catenin nuclear entry, expression of the Wnt proto-oncogene and downstream effector genes (e.g., C-myc, cyclin d1) (Xu et al., 2016). In HCT116 cells, apigenin affected cancer cell metabolism in a multi-modal manner *via* the Wnt/β-catenin pathway. Apigenin can directly bind and allosterically inhibit tumor-specific pyruvate kinase M2 (PKM2)–blocking glycolysis (Shan et al., 2017). However it can also inhibit expression of PKM2 at the RNA and protein level by blocking the β-catenin/c-Myc/PTBP1 pathway (Shan et al., 2017).

Apigenin interferes with cellular proliferation by effects on intracellular protein targets. An effect of apigenin on the cell cycle was observed in three different human colon cancer cell lines: SW480, HT-29 and Caco-2 (Wang et al., 2000). Cells treated with apigenin were found to be stalled at G2/M phase in the cell cycle–a phenomenon that was both time and dose-dependent (Wang et al., 2000). As the number of cells stalled at G2/M increased with time and apigenin concentration, the percentage of cells in G1 phase decreased (Wang et al., 2000; Ai et al., 2017; Wang and Zhao, 2017). This translated to 64% of SW480 cells, 42% of HT-29 cells and 26% of Caco-2 cells in G2/M arrest. Greater levels of cell cycle arrest correlated with lower IC50 concentrations of apigenin (*i.e.,* SW480 cells had the smallest IC50) (Wang et al., 2000). Apigenin treatment resulted in a significant reduction of the kinase activity of p34 (a key cyclin-dependent kinase during G2/M), p34 protein expression, and cyclin B1 protein expression (Wang et al., 2000). Apigenin may also mediate G2/M stalling by upregulation of the CDK1 inhibitor p21, and subsequently downregulating CDK1 (Takagaki et al., 2005; Oishi et al., 2013). Alternatively, *in vitro* proteomic binding assays in HT-29 cells suggest apigenin directly binds ribosomal protein S9

(RPS9), and that knockdown of RPS9 induces G2/M arrest by downregulating and destabilizing CDK1 (Oishi et al., 2013).

Finally, through its intracellular actions apigenin has effects on cellular survival by altering apoptosis and autophagy pathways. Apigenin-mediated apoptosis involves diverse regulators of cell death. Apigenin suppresses cell proliferation and induces apoptosis in a caspase- and concentration-dependent manner in colorectal HT29, COLO320, DLD-1, and HCT116 cells (Maeda et al., 2018). Notable effects include the following: i) marked increases in the cleavage of PARP, ii) downregulation of anti-apoptotic Bcl2 proteins (Bcl-xL and Mcl-l) *via* apigenin-directed inhibition of STAT3 (a Bcl2-activating kinase), iii) increased expression of pro-apoptosis regulators of both the intrinsic (Bax proteins, Cytochrome C, caspases -3,-8, -9) and extrinsic (CHOP, DR5, caspase-8) pathways, iv) increased expression of pro-apoptotic proteins NAG1 and p53, and v) increased expression of the cell cycle inhibitor p21 (Horinaka et al., 2006; Zhang et al., 2009; Zhong et al., 2010; Ai et al., 2017; Wang and Zhao, 2017; Maeda et al., 2018).

In p53-mutant HT29 human colon adenocarcinoma cells, 90μmol/L of apigenin over 72h led to apoptosis in 24.92% of cells - as well as 2.6-fold and 3.7-fold increases in caspase-3 and caspase-8 mRNA expression, respectively, (Zhang et al., 2009). The effects of apigenin on autophagy pathways in colorectal cancer cells is less clear. However, the presence of autophagosomes and the autophagy marker LC3-II were observed upon apigenin treatment in HCT116 human colon cancer cells (Zhang et al., 2009). Apigenin's effects on apoptosis and autophagy may be mediated by destabilizing a common pathway involving PI3K/Akt/mTOR–which is known to promote tumor cell survival (Chen et al., 2019).

Metabolism and Recycling of Apigenin and its Metabolites

In addition to its poor solubility, apigenin is also poorly bioavailable in part due to extensive first-pass metabolism and phase II conjugation by hepatic UDP-glucuronosyltransferase (UGT; specifically UGT1A1 and potentially UGT2B1) and sulfotransferase (SULT) enzymes (Wang et al., 2009). Following intestinal metabolism, the aglycone form of apigenin is more rapidly absorbed when further metabolized into phase II metabolites *via* glucuronidation and sulfation–also an essential step for the enterohepatic recycling of this flavone (Liu et al., 2003; Srinivas, 2015). In rat microsomal models, apigenin undergoes phase II metabolism to produce three different monoglucuronidated species, and a monosulfonated species (Gradolatto et al., 2004). Metabolism is 5.5-fold faster in the jejunum as compared to the colon, and both intestinal and liver microsomes are saturated at an apigenin concentration of 100μmol/L (Chen et al., 2003) *In vitro* assays on human liver microsomes suggest apigenin glucuronidation occurs at a much faster rate than sulfonation, and this may translate to different *in vivo* rates of phase II metabolism (Cai et al., 2007).

Further, metabolism to glucuronide and sulfonide species occurs to a greater extent in intestinal tissue, as compared to hepatic tissue (Cai et al., 2007). Apigenin also undergoes phase I metabolism *via* CYP1A2, and to a lesser extent CYP3A4 and CYP2B–generating the 3′-hydroxylated product luteolin (Breinholt et al., 2002). *In vitro* models show induction of CYP1A and CYP2B led to a 39% increase in luteolin formation, and luteolin formation was strongly inhibited by blocking the metabolic activity of CYP2E1, CYP3A, CYP2B, and CYP2C9 (Gradolatto et al., 2004). Luteolin phase II conjugates in rats include four monoglucoronidated species, and two monosulfoconjugates (Gradolatto et al., 2004).

Table 2 outlines the major CYPs affecting apigenin metabolism, as well as common compounds and/or medications known to be inducers or inhibitors of these phase I hepatic enzymes (Kleinschmidt and Delaney, 2015). Patients taking these medications would encounter elevated (with CYP inhibitors) or reduced (with CYP inducers) plasma levels of apigenin if taken concomitantly.

Apigenin phase II conjugates are excreted throughout the gastrointestinal tract, but largely in the jejunum (Chen et al., 2003). In rat models, approximately 33% of total apigenin is excreted into the gut, while 7% is excreted into the bile (Chen et al., 2003). Assays of steady-state concentration in bile suggest significantly higher concentrations than those used initially for perfusion–indicating that apigenin has the ability to concentrate in bile (Chen et al., 2003). Similar to many plant flavonoids, apigenin is able to undergo enterohepatic recycling (Chen et al., 2003). During enterohepatic recycling, the glucuronide and sulfonate metabolites are excreted into the intestines *via* the bile or enterocytes. The metabolites can then re-convert into aglycones *via* glucuronidases or sulfatases in the colon (Min et al., 2017). In Caco-2 cell monolayer models, low concentrations of apigenin resulted in sulfonated metabolites being excreted apically to a concentrated level through high-affinity, low-capacity transport(Hu et al., 2003). Higher concentrations of apigenin resulted in more glucoronidated metabolites being excreted basolaterally (Hu et al., 2003).

Clearance and Elimination of Apigenin and its Metabolites

Apigenin's high Vd and enterohepatic/enteric recycling processes indicate the elimination patterns of this lipophilic molecule will be delayed. Indeed, the elimination patterns in rat models using a single dose of 10mg of radiolabeled apigenin supports this (Gradolatto et al., 2005). Following oral administration, ~50% of apigenin was recovered in urine and ~12% in feces (Gradolatto et al., 2005). Unchanged, glucuronidated, and to a lesser extent sulfonated species, were recovered in all excrements (Gradolatto et al., 2005). Although most products were excreted within the first 24 h, about 25% of the original apigenin dose was retained 10 days after treatment (Gradolatto et al., 2005). Plasma clearance was estimated at 2ml/h (Gradolatto et al., 2005). For humans, monoglucoronidated and monosulfonated species of apigenin have been recovered from urine and identified by HPLC (Nielsen and Dragsted, 1998).

There are differences in rates of clearance between apigenin and its primary metabolite luteolin. Following 5.4mg/kg IV administration of apigenin in rats, the clearance of luteolin

TABLE 2 | Apigenin as a substrate for phase I CYP enzymes. Based on studies looking at the induction or inhibition of luteolin production (a primary metabolite of free apigenin), data suggests that apigenin metabolism is induced by CYP1A and CYP2B enzymes, and inhibited by CYP2E1, CYP3A, CYP2B, CYP2C9 (Breinholt et al., 2002; Gradolatto et al., 2004). If these effects are corroborated *in vivo*, drug interactions involving medications that induce or inhibit these CYP enzymes would lead to increased apigenin metabolism (and lower plasma levels), or decreased metabolism (and increased plasma levels), respectively.

Apigenin metabolizer	Common inducers	Common inhibitors
CYP1A2	*Nafcillin, Rifampin, Primaquine, Carbamazepine, Secobarbital, Pentobarbital, Phenobarbital, Phenytoin, Nelfinavir, Ritonavir*, Lansoprazole, Omeprazole, Antipyrine, Coffee, Cruciferous vegetables, Insulin, Sulfinpyrazone, St. John's Wort, Teriflunomide*	Ciprofloxacin*, enoxacin*, Norfloxacin, Macrolides, Duloxetine, Fluvoxamine*, Acyclovir, efavirenz, Peginterferon-α-2a, *Amiodarone, Mexiletine, Propafenone, Ticlopidine, Verapamil, Rofecoxib, Tolfenamic acid, Allopurinol, Cimetidine, Disulfiram, Famotidine, Grapefruit juice, Methoxsalen, Oral contraceptives, Zafirlukast**
CYP2B6	*Artemisinin antimalarials, Rifampin, Carbamazepine*, Phenobarbital, Phenytoin, Antiretrovirals, Efavirenz, Nelfinavir, Nevirapine, Ritonavir, Cyclophosphamide, Metamizole, St. John's Wort, Statins, Vitamin D*	*17-α-ethynylestradiol, Clopidogrel, Clotrimazole, Mifepristone (RU-486), Phencyclidine, Sertraline, Tenofovir, ThioTEPA, Ticlopidine, Voriconazole*
CYP2C9	*Rifampin, Rifapentine, Amobarbital, Carbamazepine, Pentobarbital, Phenobarbital, Phenytoin, Secobarbital, Nelfinavir, Nevirapine, Ritonavir*, Dexamethasone, Prednisone, Aminoglutethimide, Antipyrine, Aprepitant, Avasimibe, Bosentan, Smoking, Cyclophosphamide, Enzalutamide, Glutethimide, Nifedipine, St. John's Wort, Statins*	*Clarithromycin, Erythromycin, Troleandomycin, Isoniazid*, Metronidazole*, Rifampin, Sulfamethoxazole, Trimethoprim, Fluoxetine, Fluvoxamine, Paroxetine, Sertraline, Felbamate, Valproic acid, Fluconazole*, Itraconazole, Ketoconazole, Miconazole, Sulfaphenazole, Voriconazole, Efavirenz, Ritonavir*, Fluvastatin, Lovastatin, Amiodarone, Cimetidine, Disulfiram, Grapefruit juice*
CYP2C19	*Analgesics, Antipyrine, Salicylates, Antibiotics, Artemisinin antimalarials, Rifampin*, Rifapentin*, Carbamazepine, Phenobarbital, Phenytoin, Efavirenz, Nelfinavir, Ritonavir*, Dexamethasone, Prednisone, Enzalutamide, St. John's Wort*	*Clarithromycin, Erythromycin, Troleandomycin, Chloramphenicol, Isoniazid, Citalopram, Fluoxetine*, Fluvoxamine*, Moclobemide*, Paroxetine, Sertraline, Antiepileptics, Felbamate, Oxcarbazepine, Topiramate, Valproic acid, Fluconazole*, Ketoconazole, Voriconazole, Esomeprazole, Lansoprazole, Omeprazole*, Pantoprazole, Rabeprazole, Cimetidine, Clopidogrel, Grapefruit juice, Indomethacin, Oral contraceptives, Ritonavir*, Ticlopidine**
CYP2E1	*Acetone, ATRA, Ethanol, Isoniazid, Smoking, St. John's wort, Styrene, Toluene*	*Clomethiazole, Diethyldithiocarbamate, Disulfiram, 4-Methylpyrazole, Orphenadrine*
CYP3A4	*Nafcillin, Rifabutin, Rifampin*, Rifapentine, Troleandomycin, Amobarbital, Carbamazepine*, Felbamate, Oxcarbazepine, Pentobarbital, Phenobarbital, Phetharbital, Phenytoin*, Rufinamide, Topiramate, Valproic acid, Amprenavir, Efavirenz, Etravirine, Nelfinavir, Nevirapine, Ritonavir*, Tipranavir, Bexarotene, Enzalutamide*, Imatinib, Mitotane*, Vinblastine, Dexamethasone, Methylprednisolone, Prednisolone, Prednisone, Alitretinoin, Antipyrine, Aprepitant, Armodafinil, Artemisinin antimalarials, Avasimibe, Bosentan, Ethanol, Gingko biloba, Metamizole, Miconazole, Modafinil, Organochlorine compounds, Phenylbutazone, Pioglitazone, St. John's Wort*, Statins, Sulfinpyrazone, Troglitazone*	*Clarithromycin*, Erythromycin, Telithromycin*, Troleandomycin*, Azithromycin, Chloramphenicol, Ciprofloxacin, Isoniazid, Norfloxacin, Fluoxetine, Fluvoxamine, Nefazodone*, Norfluoxetine, Paroxetine, Sertraline, Amiodarone, Dronedarone, Quinine, Clotrimazole, Fluconazole Itraconazole*, Ketoconazole*, Miconazole, Posaconazole*, Voriconazole*, Cimetidine, Ranitidine, Amprenavir, Atazanavir*, Cobicistat*, Danoprevir*, Elvitegravir*, Fosamprenavir, Indinavir*, Lopinavir*, Nelfinavir*, Paritaprevir*, Ritonavir*, Saquinavir*, Tipranavir*, Amlodipine, Diltiazem*, Nicardipine, Nifedipine, Verapamil, Ergotamines, Ticagrelor, crizotinib, Idelalisib*, Imatinib, Irinotecan, Boceprevir*, Telaprevir*, Cyclosporine, Tacrolimus, Aprepitant, Chlorzoxazone, Cilostazol, cocaine, Conivaptan*, Ethinylestradiol, Felbamate, Fosaprepitant, Grapefruit Juice*, Istradefylline, Ivacaftor, Lomitapide, Mifepristone (RU-486), Nicotine, Olanzapine, Propofol, Ranolazine, Tofisopam, Zileuton*

**indicates the medication is a potent inhibitor/inducer.*

was 0.450 ± 0.03L/h/kg (Chen et al., 2012; Ninfali et al., 2013). Apigenin clearance was 0.065 ± 0.005L/h/kg (Chen et al., 2012; Ninfali et al., 2013). Studies using primary rat hepatocytes suggest this faster rate of elimination for luteolin is likely due to rapid metabolism by phase I metabolism, in addition to phase II metabolism by UGTs, SULTs, and COMT–whereas apigenin is mostly metabolized *via* UGT and SULTs (Chen et al., 2012; Ninfali et al., 2013).

The Capacity for Drug Interactions Between Apigenin and Medications

As mentioned, apigenin in its aglycone form can undergo phase I metabolism by CYP enzymes. The flavonoid chemical structure (i.e., C2-C3 double bonds and A-ring hydroxylation) makes these small molecules as a class potent inhibitors of CYP1A1, CYP1A2 and CYP1B1 in yeast, rat and human models (Androutsopoulos et al., 2010; Kimura et al., 2010). Apigenin is also a potent inhibitor of CYP1A2 and CYP2C9 (Kale et al., 2008; Si et al., 2009). Concomitant use of apigenin and certain drugs (**Table 2**) could result in either a Class C-D drug-drug interactions, or complete contraindications as defined in the healthcare professional resource Lexicomp (Lexicomp Inc, 2021).

Potentially more worrisome are drug interactions involving medications that are substrates of CYP enzymes affected by apigenin–resulting in toxicity or supratherapeutic effects of the prescribed medications at high apigenin levels. In the context of cancer, the principal chemotherapies and/or supportive care drugs metabolized by the key CYP enzymes that are inhibited by apigenin are listed in **Table 3** (Kleinschmidt and Delaney, 2015). It is important to note that where there are prodrugs that are metabolized by apigenin-inhibitable CYPs, there is a risk of subtherapeutic effects of the active drug. Similarly, drugs metabolized for elimination by CYPs inhibited by apigenin

TABLE 3 | CYP enzymes inhibited by apigenin, and their respective substrates of relevance to cancer treatment. Studies have indicated that apigenin is an inhibitor of CYP1A2, CYP2C9, and CYP3A4 (Kleinschmidt and Delaney, 2015). This implicates apigenin in potential drug interactions with a number of chemotherapies and medications used in the supportive care of cancer. If this flavone were to be taken in conjunction with any one of the interacting substrates, this would lead to decreased metabolism and potentially supratherapeutic or toxic plasma levels.

Enzyme inhibited by apigenin	Substrates
CYP1A2	- Nausea and vomiting *Alosetron*, Ondansetron, Ramosetron*, Olanzapine* - Cancer-induced VTE *Warfarin* - Hormones *Estradiol*
CYP2C9	- Chemotherapy and other cancer treatments *Cyclophosphamide, Tamoxifen* - Chemo-induced nausea and vomiting *Tetrahydrocannabinol* - Cancer-induced VTE *Warfarin**
CYP3A4	- Chemotherapy and other cancer treatments *Cyclophosphamide, Dasatinib, Docetaxel, Erlotinib, Etoposide, Gefitinib, Ibrutinibb, Ifosfamide, Imatinib, Irinotecan, Teniposide, Vincristine*, Tamoxifen, Flutamide* - Chemo-induced nausea and vomiting *Granisetron, Ondansetron, Haloperidol, Dexamethasone, Alprazolam, clonazepam, Diazepam, Midazolam*, Triazolam*, Tetrahydrocannabinol* - Cancer-induced VTE *Warfarin* - Chemo-induced Diarrhea *Loperamide* - Chemo-induced Immune-mediated reactions *Chlorpheniramine, Desloratadine, Ebastine*, Loratadine, Terfenadine*, Cortisol, Hydrocortisone, Methylprednisolone, Prednisone* - Hormones *Estradiol, Progesterone, Testosterone*

**Indicates the compound has a narrow therapeutic range and/or highly metabolized by the CYP enzyme*

TABLE 4 | Concentrations of apigenin necessary to produce cellular responses in human cancer cells. A representative series of examples were taken from the literature cited in this review. The main experimental readouts are indicated, although studies included more detail. All targets are human cells, and in all cases involve a single dose of apigenin except for one example in which colony formation was evaluated over seven days and apigenin was added on a daily basis (Shan et al., 2017).

Study data source	Model	Readout of interest	Typical exposure time	Lowest effective concentration	EC50 or IC50
Wang et al. (2000)	Colorectal cancer cells	Cell cycle G2/M arrest	24–48h	30μmol/L	40–70μmol/L[a]
Horinaka et al. (2006)	Multiple cancer cell lines	Cell-surface DR5 (TRAILR2)	24h	20μmol/L[b]	–
Lefort and Blay (2011)	Colorectal cancer cells	Cell-surface CD26/DPP4	48h	1μmol/L	3–30μmol/L[a]
Oishi et al. (2013)	Prostate cancer cells	Mitochondrial ANT2	24h	20μmol/L[b]	–
Xu et al. (2016)	Colorectal cancer cells	Viability, proliferation, migration	48h	5μmol/L	18–24μmol/L[a]
Shan et al. (2017)	Colorectal cancer cells	Colony formation, survival	24h, 7d	10μmol/L	28–90μmol/L[a]
Wang and Zhao (2017)	Colorectal cancer cells	Cell growth, apoptosis	24–72h	40μmol/L	78–98μmol/L[a]
Maeda et al. (2018)	Colorectal cancer cells	Proliferation, apoptosis	48h	5μmol/L	~15μmol/L[b]
Tong et al. (2019)	Colorectal cancer cells	Viability, EMT, migration	24h	10μmol/L	34–47μmol/L[a]
Lefort et al. (2020)	Colorectal cancer cells	Cell-surface CD26/DPP4	48h	3μmol/L	~10μmol/L[b]

[a]*Depending on parameter measured.*
[b]*Estimated from data provided.*

will exhibit enhanced therapeutic effects but also a higher risk of toxicity.

We are currently unaware of the existence of clear guidelines for potential apigenin interactions with other medications (or indeed sound evidence-based justifications for its clinical efficacy in disease situations). However, the Therapeutic Research Center Natural Medicines database for healthcare professionals has detailed professional monographs for various natural products, including parsley, German chamomile and chrysanthemum–key plant sources with some of the highest contents of apigenin found in nature (Natural Medicines TRC, 2021a; Natural Medicines TRC, 2021b; Natural Medicines TRC, 2021c).

The Required Local Concentration of Apigenin to Exert Cellular Actions

The concentrations of apigenin required to produce a cellular effect vary substantially between different studies and the cellular response being measured, but the lowest effective concentration is within a significant proportion of the studies is in the range 1–5μmol/L (**Table 4**). It is notable that in this limited sample of studies, the lower threshold concentrations are seen with a 48h exposure time, whereas higher concentrations are required for treatments with a shorter (24h) exposure to the single apigenin doses used. This would be consistent with a model in which apigenin's effects on cells involve multiple successive pathways that interact to give the final change in overall cell phenotype.

We will use 1–5μmol/L as the minimal local extracellular apigenin concentration that has to be attained at a particular location *in vivo* in order to provoke a cellular response in the cell population of interest, and the necessary plasma concentration. This is likely to be a generous estimate as most experimental studies (and all listed in **Table 4**) use only a single treatment, which would result in a progressively declining apigenin concentration. However, appropriate *in vivo* dosing is repetitive and offsets any degradation or metabolism of the agent. In our work on down-regulation of DPPIV on human colorectal cancer cells by adenosine, it was necessary to use a single dose concentration of 300μmol/L to produce a robust effect. However, allowing for degradation half-life and using lower doses (and a reduced overall amount) successively over the 48h response period reduced the exposure level, with no change in effect, to 12.5μmol/L or lower, a 24-fold alteration in requirement (Tan et al., 2004). There has been no comparable study of the effect of dosing frequency for apigenin, but based on a biological half-life of ~2.5h, a spaced dosing regimen would be optimal for a response that takes ~48h to develop and involves the sequential participation of successive cellular pathways. As well, there is no active mixing in cell culture models, leading to an unstirred fluid layer next to the cell surface which reduces the concentration of ligand that is available to interact with cells (Shibayama et al., 2015; Kono et al., 2016). This again necessitates higher concentrations in the bulk fluid medium than are truly necessary for a response. This of course is not the case in perfused tissue. For both of these reasons, we believe the 1–5μmol/L target to be a very conservative estimate for the extracellular apigenin concentration required for activity *in vivo*. The cell lines used in these preclinical studies (**Table 4**) are immortalized cell lines from tumor sources, so this rationale is applicable to affecting cancer cells.

The Utility of Apigenin Taken Orally in its Natural Herbal Form

Humans consume on average between 0.45–1.17mg of apigenin daily (Meyer et al., 2006; Somerset and Johannot, 2008). In the bioavailability study of Meyer and colleagues, adult volunteers consumed a meal containing 2g parsley/kg body weight–corresponding to 149 ± 35g of parsley (mean body weight 75kg) and providing an average of 18 ± 4mg (66 ± 15μmol) of apigenin (Meyer et al., 2006). Such dosing led to mean plasma concentrations that exceeded 100nmol/L between 6–9h after parsley consumption and reached a maximum of 337nmol/L (Meyer et al., 2006) These established plasma levels (0.1–0.3μmol/L) begin to approach the target range of 1–5μmol/L. However, this corresponds to almost two cups of this low density herb, representing in the region of 15 to 40-fold the normal daily intake. Attaining an apigenin level with sufficient capacity to influence cell function at systemic locations would require of the order of 100-fold the regular daily dietary intake of even apigenin-rich foods. As a therapeutic or assistive option, this would be unreasonable - especially in cancer populations, where malnutrition secondary to nausea, vomiting, and poor appetite is common. Thus, the use of pure apigenin extracts, dry-powder capsules, and/or IV treatments are essential to take advantage of the beneficial effects of this flavone.

The Utility of Apigenin Taken Orally as a Semi-purified Preparation

Comprehensive *in vivo* studies looking at the pharmacokinetic properties of purified apigenin given by the oral route have not yet been conducted in humans. In rats, doses of apigenin assessed were 13.5 and 60mg/kg (see **Table 1** above). While it is difficult to compare the gastrointestinal physiology of rats to humans, in a 70kg adult person, this is equivalent to apigenin doses of 0.9 and 4.2 g, respectively. Compared with the dosing with dietary parsley mentioned above, this would be approximately a 50–240-fold reduction in bulk intake yet should take plasma concentrations into the bioactive range in humans (by simple extrapolation, to at least 5μmol/L). Measurements in rats at the higher oral dose gave a maximal plasma concentration of 1330ng/ml(Ding et al., 2014). With a molecular mass for apigenin of 270g/mol, this equates to 4.9μmol/L. Although an approximation based upon limited data, both the rat model and extrapolation from human data therefore suggest that doses used and approved in experimentation reach systemic levels into the range to achieve biological effects. Indeed, it should be noted that substantially higher doses of apigenin of up to 300mg/kg have been used in mouse models, with no overt toxicity or effect on body weight up to 68 days of exposure (Ai et al., 2017; Tong et al., 2019).

Taking the higher 4.2g dose and with the density of apigenin being ~1.5g/ml (National Center for Biotechnology Information, 2021), this would correlate to a product volume of 2.8ml. The largest commonly used capsules hold 1.37ml of material(Medisca, 2021). Therefore, 2.8ml of apigenin powder (which represents the dose we predict should yield a 5μmol/L plasma concentration of apigenin) would require two large capsules of purified flavone to provide this oral dosage in humans. This is feasible.

Therefore in principle it should be possible, using oral dosing of apigenin capsules, to reach circulatory concentrations that are able to influence the biology of systemic targets. Circulatory apigenin should be available to act through the extracellular milieu for a substantial time. As indicated above there is a persistence of 6–9h after oral ingestion from human parsley consumption (Meyer et al., 2006) and a $T^1/_2$ of 2.1–4.2h in rodents (Teng et al., 2012; Ding et al., 2014). With reasonable

dosing several times per day, effective levels could be maintained for long enough a period to exert effects on the cell behaviors described in this review.

The oral dosage form necessary in a therapeutic context therefore needs to be of a reasonably purified form of apigenin itself, since the doses of apigenin that are therapeutically relevant cannot be achieved by oral consumption of whole plant products such as parsley. Parsley leaf itself is available in capsule form as a health supplement, with the typical recommended ingestion amount being 2 capsules for a total dose of 900mg. Using an apigenin content for dried parsley of 45mg/g (Sung et al., 2016), this would equate to a daily dose of approximately 40mg apigenin, less than 1% of what is needed for a meaningful clinical outcome on cancer cell behavior, although it may have other beneficial effects on health. Crude plant products are therefore not adequate in this context.

Purified forms of apigenin itself (CAS# 520–36–5) are however readily available for research purposes and could be upscaled for human ingestion following appropriate protocols. Purity levels of 95–98% are available from multiple suppliers globally, both sourced from natural products (citrus, chamomile) and synthetic. Naturally sourced apigenin is purified via chromatographic methods and produced in powder or recrystallized forms. Incorporation into capsules at a typical 97% purity level would not compromise feasibility and other than the capsule casing comprised of cellulose or gelatin, no other excipients (binding agents, lubricants, fillers, colors) would be required.

Parenteral Delivery of Apigenin

While IV administration of apigenin would be disfavoured in humans as not being overtly justified, it would be predicted to enable biologically active concentrations. Indeed, IV delivery of apigenin (20mg/kg) in rats yielded a C_{max} of 11.0 ± 1.7μg/ml (Wan et al., 2007), which represents a plasma concentration in excess of 40μmol/L, sufficient to produce a response in all of the cell systems studied (**Table 4**).

Options to Enhance the Bioavailability of Apigenin Taken Orally

If taken in a [semi]-purified form for health beneficial purposes, additional measures can be used to ensure circulatory apigenin levels reach the higher concentrations apparently necessary (in single-dose *ex vivo* studies) for certain cellular responses (**Table 4**). Apigenin can be generated in different dosage forms beyond simple encapsulation. Improved bioavailability of oral dosage forms have been evaluated by using apigenin-loaded water-in-oil-in-water emulsions (Kim et al., 2016). These emulsions were tested using *in vitro* simulations of digestion, confirming that the carriers enable the delivery of bioactive compounds in a water phase, while minimizing degradation and potentially improving *in vivo* bioavailability (Kim et al., 2016). In another effort to improve solubility in oral dosage forms, apigenin and its potassium salt form were compared using Caco-2 cell monolayers (Sánchez-Marzo et al., 2019). While solubility was vastly improved in the salt form, both apigenin and its salt exhibited similar intestinal apparent permeabilities (Sánchez-Marzo et al., 2019).

Emerging technologies to enhance apigenin oral delivery include nanoparticles, also using surfactants for enhanced drug solubility. Such nanoparticle delivery systems increase bioavailability in a number of ways: i) protection from chemical degradation in the gastrointestinal tract, ii) improved absorption via the lymphatic system, iii) protection from first-pass metabolism, iv) sustained release, and v) site-of-action targeting (e.g., solid tumor) (Leonarduzzi et al., 2009; Wang et al., 2013). Three examples of these nanoparticle technologies include mixed micelle systems (Zhang et al., 2017), pharmacosomes (Telange et al., 2017), and self-microemulsifying drug delivery systems (Zhao et al., 2013). The improved pharmacokinetic parameters of these nanocarrier systems would translate to improved delivery of apigenin as a pharmacologic agent. There is also the potential to increase efficacy of apigenin actions. Indeed, liposomal formulations of apigenin have been shown to enhance antineoplastic efficacy against colorectal cancer both *in vitro* and *in vivo* (Banerjee et al., 2017).

Furthermore, there are methods under development that would more effectively deliver apigenin to the intended site of action following oral administration. For example, TPGS (d-alpha-tocopheryl polyethylene glycol 1,000 succinate) is a water-soluble co-polymer derived from vitamin E. This forms amphiphilic nanoparticles comprised of a hydrophilic PEG head and hydrophobic tocopherol tail, that have unique advantages as drug carriers (Gorain et al., 2018). In the context of cytotoxic chemotherapeutics, paclitaxel-loaded TPGS nanocarriers enable enhanced drug solubilization, inhibition of P-gp-mediated drug resistance (paclitaxel being a substrate of P-gp), improved cancer cell permeability, promotion of cell cycle arrest and apoptosis (Gorain et al., 2018). Mixed micelles including TPGS for the co-delivery of synergistic chemotherapeutics show promise in diverse oncopathologies. For example, polylactide-co-glycolide/D-alpha-tocopherol polyethylene glycol 1000 succinate (PLGA/TPGS) nanocarriers are able to co-deliver docetaxel and salinomycin to strategic benefit (Gao et al., 2019). These carriers were successful in delivering and maintaining 1:1M ratios of these synergistically cytotoxic agents both *in vitro* and *in vivo* to breast cancer cells and their stem cells (Gao et al., 2019). Similar positive results have been shown using TPGS mixed micelles targeted toward liver cancer (docetaxel and piperine), as well as ovarian cancer (paclitaxel and fenretinide) (Ding et al., 2020; Wang et al., 2020). Such a TPGS-based dual delivery system may prove advantageous in combining apigenin with primary chemotherapeutics.

Bioactive Self-Nanoemulsifying Drug Delivery Systems (Bio-SNEDDSs) have been used with apigenin and are effective in improving solubility and bioavailability of the flavonoid, both *in vitro* and *in vivo* (Kazi et al., 2020). Nanoemulsion of apigenin results in decreased drug particle size that can be absorbed to a greater extent and potentially bypass degradation in the gastrointestinal tract (Kazi et al., 2020). Studies in rat models have indicated that Bio-SNEDDS result in the formation of nanosized and homogenous apigenin-loaded particles that lead

to significantly improved C_{max} concentrations and AUCs (by 105 and 91%, respectively) compared to administration of pure apigenin powder (Kazi et al., 2020). As well, the bioactive and nutritive lipid excipients in the delivery system may in fact have additional therapeutic effects (Kazi et al., 2020). Such a delivery approach may further increase the feasibility of using oral apigenin clinically.

While our focus here is on oral delivery of apigenin and its formulations, nanoparticles would also be advantageous if an intravenous route were being considered and would likely circumvent problems such as apigenin's rapid crystallization into plasma post-delivery (Karim et al., 2017). Injectable nanoparticle drug delivery systems include lipid nanocapsules, polymeric nanoscapsules, and liposomes (Karim et al., 2017). These confer a number of benefits, including: i) good encapsulation of apigenin and loading capacity, ii) stability during storage, iii) reduced cytotoxicity, and iv) extended release of apigenin due to a less pronounced carrier burst effect (Karim et al., 2017).

DISCUSSION

Challenges and Opportunities in the Therapeutic Use of Apigenin

Careful examination of the available data indicates that it is unlikely that dietary ingestion of apigenin-containing plant materials–even those with very high levels such as parsley–will lead to biologically meaningful effects on cells through the vascular route without heroic levels of intake. This does not completely exclude the possibility that local high concentrations of apigenin acting directly from the gastrointestinal lumen could affect intestinal tissues in the gut wall, including primary tumors. The potential for locally efficaceous concentrations could be examined by local tissue measurements of apigenin uptake, perhaps using the microdialysis approach that we introduced for measuring metabolites in solid tumors (Blay et al., 1997).

Use of apigenin supplements, with purified apigenin in capsules, can achieve biologically relevant plasma concentrations that would be capable of influencing cellular behaviors. From the therapeutic perspective the flavonoid structure, although well handled by the body as a natural product, has challenges in terms of delivery and subsequent metabolism of the bioactive molecule. The molecular characteristics of apigenin and related flavones lead to poor solubility, moderate permeability, and chemical instability (Zhao et al., 2019). These properties can be attributed to a number of structural characteristics of flavones, including i) a planar structure due to double bonds between positions 2 and 3 of the flavones, resulting in tight molecular arrangements and poor penetration, ii) frequent glucoronidation and sulfation of flavone hydroxyl groups in the gastrointestinal tract, leading to luminal efflux and inadequate net oral absorption, and iii) sensitivity of hydroxyl, ketone and unsaturated double bonds to pH and enzyme attack (Zhao et al., 2019). This constitutes a hurdle to an effective therapeutic strategy.

However, the chemical simplicity of apigenin and the presence of modifiable groups also facilitates strategies to modify and improve apigenin's delivery and access to the target location. The interference due to basic physicochemical characteristics can be bypassed with the development of prodrugs, glycosylation, the use of absorption enhancers such as cyclopentadecalactone, and the nanotechnologies discussed above (Gorain et al., 2018; Gao et al., 2019; Zhao et al., 2019; Ding et al., 2020; Kazi et al., 2020; Wang et al., 2020). Indeed, there is an opportunity to capitalize on the unique features of this small molecule. The flavone structure is a ready scaffold for further modification using medicinal chemistry (Singh et al., 2014). In our own work, we have shown that changes in hydroxylation or glycosylation have dramatic effects on the ability of apigenin to upregulate CD26, and thus potentially affect hallmarks of cancer (Lefort and Blay, 2011; Lefort et al., 2020). Therefore, using apigenin as a lead compound in drug development may be a valuable option for optimizing a small molecule to fully capture the beneficial effects that have been identified.

Caveats in the Therapeutic Use of Apigenin in Oncology Based Upon Current Knowledge.

Whether the administration of apigenin will indeed achieve clinically beneficial outcomes requires focused studies that combine direct measurements of plasma apigenin levels with clinical outcomes during chemotherapy. Although studies of oral and parenteral administration of apigenin in rat models have produced some valuable pharmacokinetic data (Wan et al., 2007; Chen et al., 2011; Teng et al., 2012; Ding et al., 2014) there has been very little direct pharmacokinetic assessment in humans and it has been restricted to dosing with the dietary natural product such as parsley (Meyer et al., 2006). Full assessment of apigenin and metabolites, and particular intra-patient variability given the variation in apigenin absorption and bioavailability noted above, need to be factored in alongside assessment of safety and toxicity in phase I clinical trials.

There is substantial evidence for beneficial anti-cancer effects of apigenin, particular in the context of gastrointestinal cancers (Lefort and Blay, 2013). However, much of the preclinical *in vitro* data utilizes highly selected lines of cancer cells that have been adapted to culture and that in monolayer may not well represent the behavior of cells within 3-dimensional tissue frameworks (Lowthers et al., 2003; Howes et al., 2014). These cell populations may have different genotypes and behaviors compared with primary tumor isolates. As well, few *in vivo* studies use cancers implanted orthotopically, which better recapitulate the disease evolution compared to subcutaneous tumors (Lensch et al., 2002; Flatmark et al., 2004).

In addition, most pharmacodynamic studies characterizing the mode(s) of action of apigenin involve treatment using the flavonoid as a monotherapy (Wang et al., 2000; Horinaka et al., 2006; Lefort and Blay, 2011; Oishi et al., 2013; Xu et al., 2016; Shan et al., 2017; Wang and Zhao, 2017; Maeda et al., 2018; Tong et al., 2019; Lefort et al., 2020), whereas clinical oncology uses combination regimens and the addition of a component such

as apigenin would be as a further agent in addition to the combination used against the category and stage of neoplasic being addressed. However, we have found that apigenin has a valuable and potentially synergistic advantage when given together with chemotherapeutics in certain cancer readouts (Lefort and Blay, 2011), meaning that its addition to existing combinations is inherently worthy of study. As we have illustrated in this review and elsewhere (Lefort and Blay, 2011; Lefort and Blay, 2013; Lefort et al., 2020), there is a great diversity of cellular responses that has been shown for apigenin in preclinical cancer models. It is therefore important that in early studies of efficacy in humans, all relevant cellular markers of progression are evaluated. As patients may have comorbidities for which they are receiving other medications, it will also be important to take account of possible drug reactions as we have indicated in **Table 3**.

Possible Beneficial Effects of Apigenin Concurrent With Chemotherapy

Although not justifiable in itself as a therapeutic strategy, the status of apigenin as an inhibitor of CYP1A2, CYP2C9 and CYP3A4 means that it may enhance rather than inhibit the action of certain cancer medications by altering their pharmacokinetics in a beneficial way. Apigenin can also improve the pharmacokinetic parameters of the chemotherapeutic agents docetaxel and paclitaxel–two microtubular depolymerization inhibitors with poor bioavailability (Kumar et al., 2015). Co-administration of 10mg/kg of apigenin to adult male rats *via* oral gavage with 40mg/kg docetaxel significantly increased docetaxel C_{max} (137%) and AUC (162%)–without affecting $T^1/_2$ (Teng et al., 2012). Co-administration of apigenin with paclitaxel led to the AUC, C_{max}, MRT, and $T^1/_2$ of paclitaxel increasing with apigenin in a concentration-dependent manner, likely due to both CYP3A4 and P-gp efflux pump inhibition in the intestines (Kumar et al., 2015). These data suggest apigenin may enhance the bioavailability of taxanes–potentially requiring a lower dose of these chemotherapies for adequate clinical effect.

P-gp overexpression is a key player in multi-drug chemotherapy failure of human cancer cells. P-gp is an ABC efflux pump found in epithelial cells of the liver, kidney and intestines, and chemoresistance is secondary to its enhanced efflux activity - translating to poor drug accumulation and suboptimal cytotoxic action (Lohner et al., 2007). In a study of 14 different flavonoids, apigenin was the only small molecule that did not induce P-gp expression in human intestinal Caco-2 cells at the protein level (Lohner et al., 2007). Molecular docking and quantitative structure-activity relationship modeling confirm apigenin as an agent with high P-gp inhibitor binding and potency (Mohana et al., 2016).

Apigenin may have multiple productive interactions with chemotherapeutic agents through its effects on cellular signaling pathways, and this might be of particular importance in cancer cells that have developed further resistance mechanisms (Lefort and Blay, 2011). Apigenin has a synergistic effect with the chemotherapeutic agent 5-FU in inducing apoptosis in p53-mutant human colon adenocarcinoma cells (Zhang et al., 2009). It induces the autophagy mediators LC3-II and Beclin-1 in colorectal carcinoma cells resistant to cisplatin (Chen et al., 2019). Apigenin also enhances the effect of doxorubicin in chemotherapy-resistant hepatocarcinoma cells, likely by down-regulating the PI3K/Akt pathway (Ga et al., 2013). Finally, apigenin is thought to down-regulate the PI3K/Akt pathway and in reduce expression of nuclear factor erythroid 2-related factor (a key player in chemoresistance) at the RNA and protein level (Ga et al., 2013). Combining apigenin with chemotherapeutic drugs may be a worthwhile clinical strategy for the support of cytotoxic action as a chemosensitizer.

AUTHOR CONTRIBUTIONS

JB defined the parameters of this review, ED-A carried out the literature searches and composed the majority of the text and tables/figures, JB contributed a portion of the text and tables, and final editing and revisions for publication were done jointly by ED-A and JB. Both authors approved the final version of this manuscript.

ACKNOWLEDGMENTS

We thank B. Diaconu for assisting with early collection of references. JB is a Senior Scientist of the BHCRI.

REFERENCES

Ai, X.-Y., Qin, Y., Liu, H.-J., Cui, Z.-H., Li, M., Yang, J.-H., et al. (2017). Apigenin Inhibits Colonic Inflammation and Tumorigenesis by Suppressing STAT3-NF-Kb Signaling. *Oncotarget* 8 (59), 100216–100226. doi:10.18632/oncotarget.22145

Androutsopoulos, V. P., Papakyriakou, A., Vourloumis, D., Tsatsakis, A. M., and Spandidos, D. A. (2010). Dietary Flavonoids in Cancer Therapy and Prevention: Substrates and Inhibitors of Cytochrome P450 CYP1 Enzymes. *Pharmacol. Ther.* 126 (1), 9–20. doi:10.1016/j.pharmthera.2010.01.009

Banerjee, K., Banerjee, S., and Mandal, M. (2017). Enhanced Chemotherapeutic Efficacy of Apigenin Liposomes in Colorectal Cancer Based on Flavone-Membrane Interactions. *J. Colloid Interf. Sci.* 491, 98–110. doi:10.1016/j.jcis.2016.12.025

Batra, P., and Sharma, A. K. (2013). Anti-cancer Potential of Flavonoids: Recent Trends and Future Perspectives. *3 Biotech.* 3 (6), 439–459. doi:10.1007/s13205-013-0117-5

Blay, J., White, T. D., and Hoskin, D. W. (1997). The Extracellular Fluid of Solid Carcinomas Contains Immunosuppressive Concentrations of Adenosine. *Cancer Res.* 57 (13), 2602–2605.

Breinholt, V. M., Offord, E. A., Brouwer, C., Nielsen, S. E., Brøsen, K., and Friedberg, T. (2002). *In vitro* investigation of Cytochrome P450-Mediated Metabolism of Dietary Flavonoids. *Food Chem. Toxicol.* 40 (5), 609–616. doi:10.1016/S0278-6915(01)00125-9

Bugter, J. M., Fenderico, N., and Maurice, M. M. (2021). Mutations and Mechanisms of WNT Pathway Tumour Suppressors in Cancer. *Nat. Rev. Cancer* 21 (1), 5–21. doi:10.1038/s41568-020-00307-z

Cai, H., Boocock, D. J., Steward, W. P., and Gescher, A. J. (2007). Tissue Distribution in Mice and Metabolism in Murine and Human Liver of

Apigenin and Tricin, Flavones with Putative Cancer Chemopreventive Properties. *Cancer Chemother. Pharmacol.* 60 (2), 257–266. doi:10.1007/s00280-006-0368-5

Caspi, M., Wittenstein, A., Kazelnik, M., Shor-Nareznoy, Y., and Rosin-Arbesfeld, R. (2021). Therapeutic Targeting of the Oncogenic Wnt Signaling Pathway for Treating Colorectal Cancer and Other Colonic Disorders. *Adv. Drug Deliv. Rev.* 169, 118–136. doi:10.1016/j.addr.2020.12.010

Cassady, J. M., Baird, W. M., and Chang, C.-J. (1990). Natural Products as a Source of Potential Cancer Chemotherapeutic and Chemopreventive Agents. *J. Nat. Prod.* 53 (1), 23–41. doi:10.1021/np50067a003

Chen, J., Lin, H., and Hu, M. (2003). Metabolism of Flavonoids via Enteric Recycling: Role of Intestinal Disposition. *J. Pharmacol. Exp. Ther.* 304 (3), 1228–1235. doi:10.1124/jpet.102.046409

Chen, X., Xu, H., Yu, X., Wang, X., Zhu, X., and Xu, X. (2019). Apigenin Inhibits In Vitro and In Vivo Tumorigenesis in Cisplatin-Resistant Colon Cancer Cells by Inducing Autophagy, Programmed Cell Death and Targeting M-TOR/PI3K/Akt Signalling Pathway. *J. BUON* 24 (2), 488–493.

Chen, Z., Tu, M., Sun, S., Kong, S., Wang, Y., Ye, J., et al. (2012). The Exposure of Luteolin Is Much Lower Than that of Apigenin in Oral Administration of Flos Chrysanthemi Extract to Rats. *Drug Metab. Pharmacokinet.* 27 (1), 162–168. doi:10.2133/dmpk.DMPK-11-RG-081

Chen, Z., Ying, X., Meng, S., Zhu, X., Jiang, H., Cao, Q., et al. (2011). High-performance Liquid Chromatographic Determination and Pharmacokinetic Study of Apigenin-7-O-β-D-Glucoside in Rat Plasma after Intravenous Administration. *Arch. Pharm. Res.* 34 (5), 741–746. doi:10.1007/s12272-011-0507-3

Cutler, M. J., Lowthers, E. L., Richard, C. L., Hajducek, D. M., Spagnuolo, P. A., and Blay, J. (2015). Chemotherapeutic Agents Attenuate CXCL12-Mediated Migration of Colon Cancer Cells by Selecting for CXCR4-Negative Cells and Increasing Peptidase CD26. *BMC Cancer* 15, 882. doi:10.1186/s12885-015-1702-2

Dhillon, A. S., Hagan, S., Rath, O., and Kolch, W. (2007). MAP Kinase Signalling Pathways in Cancer. *Oncogene* 26 (22), 3279–3290. doi:10.1038/sj.onc.1210421

Ding, S., Zhang, Z.-h., Song, J., Cheng, X.-d., Jiang, J., and Jia, X.-b. (2014). Enhanced Bioavailability of Apigenin via Preparation of a Carbon Nanopowder Solid Dispersion. *Int. J. Nanomedicine* 9, 2327–2333. doi:10.2147/IJN.S60938

Ding, Y., Ding, Y., Wang, Y., Wang, C., Gao, M., Xu, Y., et al. (2020). Soluplus/TPGS Mixed Micelles for Co-delivery of Docetaxel and Piperine for Combination Cancer Therapy. *Pharm. Develop. Tech.* 25 (1), 107–115. doi:10.1080/10837450.2019.1679834

Dross, R. V., Xue, Y., Knudson, A., and Pelling, J. C. (2003). The Chemopreventive Bioflavonoid Apigenin Modulates Signal Transduction Pathways in Keratinocyte and Colon Carcinoma Cell Lines. *Int. Res. Conf. Food Nutr. Cancer*, 3800–3804.

Du, G., Fu, L., Jia, J., Pang, X., Yu, H., Zhang, Y., et al. (2018). Validated UPLC-MS/MS Method for Quantification of Seven Compounds in Rat Plasma and Tissues: Application to Pharmacokinetic and Tissue Distribution Studies in Rats after Oral Administration of Extract ofEclipta prostrataL. *Biomed. Chromatogr.* 32 (6), e4191–12. doi:10.1002/bmc.4191

Flatmark, K., Mælandsmo, G. M., Martinsen, M., Rasmussen, H., and Fodstad, Ø. (2004). Twelve Colorectal Cancer Cell Lines Exhibit Highly Variable Growth and Metastatic Capacities in an Orthotopic Model in Nude Mice. *Eur. J. Cancer* 40 (10), 1593–1598. doi:10.1016/j.ejca.2004.02.023

Gao, A.-M., Ke, Z.-P., Wang, J.-N., Yang, J.-Y., Chen, S.-Y., and Chen, H. (2013). Apigenin Sensitizes Doxorubicin-Resistant Hepatocellular Carcinoma BEL-7402/ADM Cells to Doxorubicin via Inhibiting PI3K/Akt/Nrf2 Pathway. *Carcinogenesis* 34 (8), 1806–1814. doi:10.1093/carcin/bgt108

Gao, J., Liu, J., Xie, F., Lu, Y., Yin, C., and Shen, X. (2019). Co-Delivery of Docetaxel and Salinomycin to Target Both Breast *Cancer* Cells and Stem Cells by PLGA/TPGS Nanoparticles. *Int. J. Nanomedicine* 14, 9199–9216. doi:10.2147/IJN.S230376

Gharzouli, K., and Holzer, P. (2004). Inhibition of guinea Pig Intestinal Peristalsis by the Flavonoids Quercetin, Naringenin, Apigenin and Genistein. *Pharmacology* 70 (1), 5–14. doi:10.1159/000074237

Gorain, B., Choudhury, H., Pandey, M., and Kesharwani, P. (2018). Paclitaxel Loaded Vitamin E-TPGS Nanoparticles for Cancer Therapy. *Mater. Sci. Eng. C* 91, 868–880. doi:10.1016/j.msec.2018.05.054

Gradolatto, A., Basly, J.-P., Berges, R., Teyssier, C., Chagnon, M.-C., Siess, M.-H., et al. (2005). Pharmacokinetics and Metabolism of Apigenin in Female and Male Rats after a Single Oral Administration. *Drug Metab. Dispos* 33 (1), 49–54. doi:10.1124/dmd.104.000893.nicity

Gradolatto, A., Canivenc-Lavier, M.-C., Basly, J.-P., Siess, M.-H., and Teyssier, C. (2004). Metabolism of Apigenin by Rat Liver Phase I and Phase II Enzymes and by Isolated Perfused Rat Liver. *Drug Metab. Dispos* 32 (1), 58–65. doi:10.1124/dmd.32.1.58

Hanske, L., Loh, G., Sczesny, S., Blaut, M., and Braune, A. (2009). The Bioavailability of Apigenin-7-Glucoside Is Influenced by Human Intestinal Microbiota in Rats. *J. Nutr.* 139 (6), 1095–1102. doi:10.3945/jn.108.102814

Hava, M., and Janku, I. (1958). [The Bronchodilating Activity of Apigenin]. *Arch. Int. Pharmacodyn Ther.* 117 (1-2), 23–29.

Horinaka, M., Yoshida, T., Shiraishi, T., Nakata, S., Wakada, M., and Sakai, T. (2006). The Dietary Flavonoid Apigenin Sensitizes Malignant Tumor Cells to Tumor Necrosis Factor-Related Apoptosis-Inducing Ligand. *Mol. Cancer Ther.* 5 (4), 945–951. doi:10.1158/1535-7163.MCT-05-0431

Hostetler, G. L., Ralston, R. A., and Schwartz, S. J. (2017). Flavones: Food Sources, Bioavailability, Metabolism, and Bioactivity. *Adv. Nutr.* 8, 423–435. doi:10.3945/an.116.012948

Hostetler, G. L., Riedl, K. M., and Schwartz, S. J. (2013). Effects of Food Formulation and Thermal Processing on Flavones in Celery and Chamomile. *Food Chem.* 141 (2), 1406–1411. doi:10.1016/j.foodchem.2013.04.051

Howes, A. L., Richardson, R. D., Finlay, D., and Vuori, K. (2014). 3-Dimensional Culture Systems for Anti-cancer Compound Profiling and High-Throughput Screening Reveal Increases in EGFR Inhibitor-Mediated Cytotoxicity Compared to Monolayer Culture Systems. *PLoS One* 9 (9), e108283. doi:10.1371/journal.pone.0108283

Hu, M., Chen, J., and Lin, H. (2003). Metabolism of Flavonoids via Enteric Recycling: Mechanistic Studies of Disposition of Apigenin in the Caco-2 Cell Culture Model. *J. Pharmacol. Exp. Ther.* 307 (1), 314–321. doi:10.1124/jpet.103.053496

Kale, A. G. S., and Kotwal, S. (2008). *Cancer* Phytotherapeutics: Role for Flavonoids at the Cellular Level. *Phytotherapy Res.* 22 (4), 544–549. doi:10.1002/ptr10.1002/ptr.2283

Karim, R., Palazzo, C., Laloy, J., Delvigne, A.-S., Vanslambrouck, S., Jerome, C., et al. (2017). Development and Evaluation of Injectable Nanosized Drug Delivery Systems for Apigenin. *Int. J. Pharmaceutics* 532 (2), 757–768. doi:10.1016/j.ijpharm.2017.04.064

Kazi, M., Alhajri, A., Alshehri, S. M., Elzayat, E. M., Al Meanazel, O. T., Shakeel, F., et al. (2020). Enhancing Oral Bioavailability of Apigenin Using a Bioactive Self-Nanoemulsifying Drug Delivery System (Bio-SNEDDS): *In Vitro*, *In Vivo* and Stability Evaluations. *Pharmaceutics* 12 (8), 749. doi:10.3390/pharmaceutics12080749

Kim, B.-K., Cho, A.-R., and Park, D.-J. (2016). Enhancing Oral Bioavailability Using Preparations of Apigenin-Loaded W/O/W Emulsions: *In vitro* and In Vivo Evaluations. *Food Chem.* 206, 85–91. doi:10.1016/j.foodchem.2016.03.052

Kim, M. T., Sedykh, A., Chakravarti, S. K., Saiakhov, R. D., and Zhu, H. (2014). Critical Evaluation of Human Oral Bioavailability for Pharmaceutical Drugs by Using Various Cheminformatics Approaches. *Pharm. Res.* 31 (4), 1002–1014. doi:10.1007/s11095-013-1222-1

Kimura, Y., Ito, H., Ohnishi, R., and Hatano, T. (2010). Inhibitory Effects of Polyphenols on Human Cytochrome P450 3A4 and 2C9 Activity. *Food Chem. Toxicol.* 48 (1), 429–435. doi:10.1016/j.fct.2009.10.041

Kleinschmidt, K. C., and Delaney, K. A. (2015). 13 : Biochemical and Metabolic Principles. *Goldfrank's Toxicologic Emergencies* 11e83, 170–188.

Kono, Y., Iwasaki, A., Matsuoka, K., and Fujita, T. (2016). Effect of Mechanical Agitation on Cationic Liposome Transport across an Unstirred Water Layer in Caco-2 Cells. *Biol. Pharm. Bull.* 39 (8), 1293–1299. doi:10.1248/bpb.b16-00050

Kumar, K. K., Priyanka, L., Gnananath, K., Babu, P. R., and Sujatha, S. (2015). Pharmacokinetic Drug Interactions between Apigenin, Rutin and Paclitaxel Mediated by P-Glycoprotein in Rats. *Eur. J. Drug Metab. Pharmacokinet.* 40 (3), 267–276. doi:10.1007/s13318-014-0203-z

Lefort, É. C., and Blay, J. (2013). Apigenin and its Impact on Gastrointestinal Cancers. *Mol. Nutr. Food Res.* 57 (1), 126–144. doi:10.1002/mnfr.201200424

Lefort, É. C., and Blay, J. (2011). The Dietary Flavonoid Apigenin Enhances the Activities of the Anti-metastatic Protein CD26 on Human Colon Carcinoma Cells. *Clin. Exp. Metastasis* 28 (4), 337–349. doi:10.1007/s10585-010-9364-6

Lefort, É. C., Diaconu, B., Bentley, V. L., and Blay, J. (2020). Apigenin Upregulation of CD26/DPPIV on Colon Epithelial Cells Requires Inhibition of Casein Kinase 2. *Food Sci. Nutr.* 8, 5321–5329. doi:10.1002/fsn3.1823

Lensch, R., Götz, C., Andres, C., Bex, A., Lehmann, J., Zwergel, T., et al. (2002). Comprehensive Genotypic Analysis of Human Prostate Cancer Cell Lines and Sublines Derived from Metastases after Orthotopic Implantation in Nude Mice. *Int. J. Oncol.* 21 (4), 695–706. doi:10.3892/ijo.21.4.695

Leonarduzzi, G., Testa, G., Sottero, B., Gamba, P., and Poli, G. (2010). Design and Development of Nanovehicle-Based Delivery Systems for Preventive or Therapeutic Supplementation with Flavonoids. *Cmc* 17 (1), 74–95. doi:10.2174/092986710789957760

Lexicomp Inc (2021). "Apigenin," in *Specific Lexicomp Online Database Interactions Database* (Hudson (OH): Wolters Kluwer Health).

Liu, Y., Liu, Y., Dai, Y., Xun, L., and Hu, M. (2003). Enteric Disposition and Recycling of Flavonoids and Ginkgo Flavonoids. *J. Altern. Complement. Med.* 9 (5), 631–640. doi:10.1089/107555303322524481

Lohner, K., Schnäbele, K., Daniel, H., Oesterle, D., Rechkemmer, G., Göttlicher, M., et al. (2007). Flavonoids Alter P-Gp Expression in Intestinal Epithelial Cells In Vitro and In Vivo. *Mol. Nutr. Food Res.* 51 (3), 293–300. doi:10.1002/mnfr.200600225

Lowthers, E. L., Richard, C. L., and Blay, J. (2003). Differential Sensitivity to Short-Chain Ceramide Analogues of Human Intestinal Carcinoma Cells Grown in Tumor Spheroids versus Monolayer Culture. *In Vitro Cel Dev Biol Anim* 39 (8-9), 340–342. doi:10.1290/1543-706X(2003)039<0340:DSTSCA>2.0.CO;2

Lu, X.-Y., Sun, D.-L., Chen, Z.-J., Chen, T., Li, L.-P., Xu, Z.-H., et al. (2010). Relative Contribution of Small and Large Intestine to Deglycosylation and Absorption of Flavonoids fromChrysanthemun morifoliumExtract. *J. Agric. Food Chem.* 58 (19), 10661–10667. doi:10.1021/jf102992r

Maeda, Y., Takahashi, H., Nakai, N., Yanagita, T., Ando, N., Okubo, T., et al. (2018). Apigenin Induces Apoptosis by Suppressing Bcl-Xl and Mcl-1 Simultaneously via Signal Transducer and Activator of Transcription 3 Signaling in Colon Cancer. *Int. J. Oncol.* 52 (5), 1661–1673. doi:10.3892/ijo.2018.4308

Medisca (2021). "International Capsule Size Chart," in *Reference Charts* (Plattsburgh (NY): Medisca).

Meyer, H., Bolarinwa, A., Wolfram, G., and Linseisen, J. (2006). Bioavailability of Apigenin from Apiin-Rich Parsley in Humans. *Ann. Nutr. Metab.* 50 (3), 167–172. doi:10.1159/000090736

Min, Z., Rongjin, S., Sumit, B., Yong, M., Shufan, G., Taijun, Y., et al. (2017). Disposition of Flavonoids via Recycling: Direct Biliary Excretion of Enterically or Extrahepatically Derived Flavonoid Glucuronides. *Physiol. Behav.* 176 (3), 139–148. doi:10.1016/j.physbeh.2017.03.040

Mohana, S., Ganesan, M., Agilan, B., Karthikeyan, R., Srithar, G., Beaulah Mary, R., et al. (2016). Screening Dietary Flavonoids for the Reversal of P-Glycoprotein-Mediated Multidrug Resistance in Cancer. *Mol. Biosyst.* 12 (8), 2458–2470. doi:10.1039/c6mb00187d

National Center for Biotechnology Information (2021). "PubChem Compound Summary for CID 5280443, Apigenin," in *PubChem* (Bethesda (MD): National Library of Medicine (US)).

Natural Medicines TRC (2021a). "Chrysanthemum," in *Food, Herbs & Supplements* (Stockton (CA): TRC Healthcare).

Natural Medicines TRC (2021b). "German Chamomile," in *Food, Herbs & Supplements* (Stockton (CA): TRC Healthcare).

Natural Medicines TRC (2021c). "Parsley," in *Food, Herbs & Supplements* (Stockton (CA): TRC Healthcare).

Nielsen, S. E., and Dragsted, L. O. (1998). Column-switching High-Performance Liquid Chromatographic Assay for Determination of Apigenin and Acacetin in Human Urine with Ultraviolet Absorbance Detection. *J. Chromatogr. B: Biomed. Sci. Appl.* 713 (2), 379–386. doi:10.1016/s0378-4347(98)00187-x

Ninfali, P., Dominici, S., Angelino, D., Gennari, L., Buondelmonte, C., and Giorgi, L. (2013). An Enzyme-Linked Immunosorbent Assay for the Measurement of Plasma Flavonoids in Mice Fed Apigenin-C -glycoside. *J. Sci. Food Agric.* 93 (12), 3087–3093. doi:10.1002/jsfa.6143

Nunes, A. R., Vieira, Í. G. P., Queiroz, D. B., Leal, A. L. A. B., Maia Morais, S., Muniz, D. F., et al. (2018). Use of Flavonoids and Cinnamates, the Main Photoprotectors with Natural Origin. *Adv. Pharmacol. Sci.* 2018, 1–9. doi:10.1155/2018/5341487

Oishi, M., Iizumi, Y., Taniguchi, T., Goi, W., Miki, T., and Sakai, T. (2013). Apigenin Sensitizes Prostate *Cancer* Cells to Apo2L/TRAIL by Targeting Adenine Nucleotide Translocase-2. *PLoS ONE* 8 (2), e55922. doi:10.1371/journal.pone.0055922

Panche, A. N., Diwan, A. D., and Chandra, S. R. (2016). Flavonoids: An Overview. *J. Nutr. Sci.* 5, 5. doi:10.1017/jns.2016.41

Ravisankar, S., Agah, S., Kim, H., Talcott, S., Wu, C., and Awika, J. (2019). Combined Cereal and Pulse Flavonoids Show Enhanced Bioavailability by Downregulating Phase II Metabolism and ABC Membrane Transporter Function in Caco-2 Model. *Food Chem.* 279, 88–97. doi:10.1016/j.foodchem.2018.12.006

Richard, C. L., and Blay, J. (2008). CXCR4 in *Cancer* and its Regulation by PPARγ. *PPAR Res.* 2008, 1–19. doi:10.1155/2008/769413

Richard, C. L., Tan, E. Y., and Blay, J. (2006). Adenosine Upregulates CXCR4 and Enhances the Proliferative and Migratory Responses of Human Carcinoma Cells to CXCL12/SDF-1α. *Int. J. Cancer* 119 (9), 2044–2053. doi:10.1002/ijc.22084

Sánchez-Marzo, N., Pérez-Sánchez, A., Ruiz-Torres, V., Martínez-Tébar, A., Castillo, J., Herranz-López, M., et al. (2019). Antioxidant and Photoprotective Activity of Apigenin and its Potassium Salt Derivative in Human Keratinocytes and Absorption in Caco-2 Cell Monolayers. *Int. J. Mol. Sci.* 20 (9), 2148–2213. doi:10.3390/ijms20092148

Shan, S., Shi, J., Yang, P., Jia, B., Wu, H., Zhang, X., et al. (2017). Apigenin Restrains Colon *Cancer* Cell Proliferation via Targeted Blocking of Pyruvate Kinase M2-dependent Glycolysis. *J. Agric. Food Chem.* 65 (37), 8136–8144. doi:10.1021/acs.jafc.7b02757

Shankar, E., Goel, A., Gupta, K., and Gupta, S. (2017). Plant Flavone Apigenin: An Emerging Anticancer Agent. *Curr. Pharmacol. Rep.* 3 (6), 423–446. doi:10.1007/s40495-017-0113-2

Shibayama, T., Morales, M., Zhang, X., Martínez-Guerrero, L. J., Berteloot, A., Secomb, T. W., et al. (2015). Unstirred Water Layers and the Kinetics of Organic Cation Transport. *Pharm. Res.* 32 (9), 2937–2949. doi:10.1007/s11095-015-1675-5

Si, D., Wang, Y., Zhou, Y.-H., Guo, Y., Wang, J., Zhou, H., et al. (2009). Mechanism of CYP2C9 Inhibition by Flavones and Flavonols. *Drug Metab. Dispos* 37 (3), 629–634. doi:10.1124/dmd.108.023416

Singh, M., Kaur, M., and Silakari, O. (2014). Flavones: An Important Scaffold for Medicinal Chemistry. *Eur. J. Med. Chem.* 84, 206–239. doi:10.1016/j.ejmech.2014.07.013

Somerset, S. M., and Johannot, L. (2008). Dietary Flavonoid Sources in Australian Adults. *Nutr. Cancer* 60 (4), 442–449. doi:10.1080/01635580802143836

Spicak, V., and Subrt, F. (1958). [Effect of Apigenin on Histamine Liberation]. *Cesk Fysiol* 7 (3), 263–264.

Srinivas, N. R. (2015). Recent Trends in Preclinical Drug-Drug Interaction Studies of Flavonoids - Review of Case Studies, Issues and Perspectives. *Phytother. Res.* 29 (11), 1679–1691. doi:10.1002/ptr.5447

Stemmer, V., de Craene, B., Berx, G., and Behrens, J. (2008). Snail Promotes Wnt Target Gene Expression and Interacts with β-catenin. *Oncogene* 27 (37), 5075–5080. doi:10.1038/onc.2008.140

Sung, B., Chung, H. Y., and Kim, N. D. (2016). Role of Apigenin in *Cancer* Prevention via the Induction of Apoptosis and Autophagy. *J. Cancer Prev.* 21 (4), 216–226. doi:10.15430/JCP.2016.21.4.216

Szklarczyk, D., Gable, A. L., Lyon, D., Junge, A., Wyder, S., Huerta-Cepas, J., et al. (2019). STRING V11: Protein-Protein Association Networks with Increased Coverage, Supporting Functional Discovery in Genome-wide Experimental Datasets. *Nucleic Acids Res.* 47 (D1), D607–D613. doi:10.1093/nar/gky1131

Takagaki, N., Sowa, Y., Oki, T., Nakanishi, R., Yogosawa, S., and Sakai, T. (2005). Apigenin Induces Cell Cycle Arrest and p21/WAF1 Expression in a P53-independent Pathway. *Int. J. Oncol.* 26 (1), 185–189. doi:10.3892/ijo.26.1.185

Tan, E. Y., Mujoomdar, M., and Blay, J. (2004). Adenosine Down-Regulates the Surface Expression of Dipeptidyl Peptidase IV on HT-29 Human Colorectal Carcinoma Cells. *Am. J. Pathol.* 165 (1), 319–330. doi:10.1016/S0002-9440(10)63299-3

Tan, E. Y., Richard, C. L., Zhang, H., Hoskin, D. W., and Blay, J. (2006). Adenosine Downregulates DPPIV on HT-29 Colon Cancer Cells by Stimulating Protein Tyrosine Phosphatase(s) and Reducing ERK1/2 Activity via a Novel Pathway.

Am. J. Physiology-Cell Physiol. 291 (3), C433–C444. doi:10.1152/ajpcell.00238.2005

Tang, D., Chen, K., Huang, L., and Li, J. (2017). Pharmacokinetic Properties and Drug Interactions of Apigenin, a Natural Flavone. *Expert Opin. Drug Metab. Toxicol.* 13 (3), 323–330. doi:10.1080/17425255.2017.1251903

Telange, D. R., Patil, A. T., Pethe, A. M., Fegade, H., Anand, S., and Dave, V. S. (2017). Formulation and Characterization of an Apigenin-Phospholipid Phytosome (APLC) for Improved Solubility, In Vivo Bioavailability, and Antioxidant Potential. *Eur. J. Pharm. Sci.* 108, 36–49. doi:10.1016/j.ejps.2016.12.009

Teng, Z., Yuan, C., Zhang, F., Huan, M., Cao, W., Li, K., et al. (2012). Intestinal Absorption and First-Pass Metabolism of Polyphenol Compounds in Rat and Their Transport Dynamics in Caco-2 Cells. *PLoS ONE* 7 (1), e29647–9. doi:10.1371/journal.pone.0029647

Thilakarathna, S. H., and Rupasinghe, H. P. (2013). Flavonoid bioavailability and attempts for bioavailability enhancement. *Nutrients* 5 (9), 3367–3387. doi:10.3390/nu5093367

Tong, J., Shen, Y., Zhang, Z., Hu, Y., Zhang, X., and Han, L. (2019). Apigenin Inhibits Epithelial-Mesenchymal Transition of Human Colon Cancer Cells through NF-κB/Snail Signaling Pathway. *Biosci. Rep.* 39 (5), 1–11. doi:10.1042/BSR20190452

Tsume, Y., Mudie, D. M., Langguth, P., Amidon, G. E., and Amidon, G. L. (2014). The Biopharmaceutics Classification System: Subclasses for In Vivo Predictive Dissolution (IPD) Methodology and IVIVC. *Eur. J. Pharm. Sci.* 57, 152–163. doi:10.1016/j.ejps.2014.01.009

Wan, L., Guo, C., Yu, Q., Li, Y., Wang, X., Wang, X., et al. (2007). Quantitative Determination of Apigenin and its Metabolism in Rat Plasma after Intravenous Bolus Administration by HPLC Coupled with Tandem Mass Spectrometry. *J. Chromatogr. B* 855 (2), 286–289. doi:10.1016/j.jchromb.2007.05.007

Wang, B., and Zhao, X.-H. (2017). Apigenin Induces Both Intrinsic and Extrinsic Pathways of Apoptosis in Human Colon Carcinoma HCT-116 Cells. *Oncol. Rep.* 37 (2), 1132–1140. doi:10.3892/or.2016.5303

Wang, S. W. J., Kulkarni, K. H., Tang, L., Wang, J. R., Yin, T., Daidoji, T., et al. (2009). Disposition of Flavonoids via Enteric Recycling: UDP-Glucuronosyltransferase (UGT) 1As Deficiency in Gunn Rats Is Compensated by Increases in UGT2Bs Activities. *J. Pharmacol. Exp. Ther.* 329 (3), 1023–1031. doi:10.1124/jpet.108.147371

Wang, S., Zhang, J., Chen, M., and Wang, Y. (2013). Delivering Flavonoids into Solid Tumors Using Nanotechnologies. *Expert Opin. Drug Deliv.* 10 (10), 1411–1428. doi:10.1517/17425247.2013.807795

Wang, W., Heideman, L., Chung, C. S., Pelling, J. C., Koehler, K. J., and Birt, D. F. (2000). Cell-cycle Arrest at G2/M and Growth Inhibition by Apigenin in Human Colon Carcinoma Cell Lines. *Mol. Carcinog.* 28 (2), 102–110. doi:10.1002/1098-2744(200006)28:2<102::AID-MC6>3.0.CO;2-2

Wang, Y., Ding, Y., Xu, Y., Wang, C., Ding, Y., Gao, M., et al. (2020). Mixed Micelles of TPGS and Soluplus for Co-delivery of Paclitaxel and Fenretinide: In Vitro and In Vivo Anticancer Study. *Pharm. Develop. Tech.* 25 (7), 865–873. doi:10.1080/10837450.2020.1753770

Xu, M., Wang, S., Song, Y., Yao, J., Huang, K., and Zhu, X. (2016). Apigenin Suppresses Colorectal Cancer Cell Proliferation, Migration and Invasion via Inhibition of the Wnt/β-Catenin Signaling Pathway. *Oncol. Lett.* 11 (5), 3075–3080. doi:10.3892/ol.2016.4331

Yan, X., Qi, M., Li, P., Zhan, Y., and Shao, H. (2017). Apigenin in Cancer Therapy: Anti-cancer Effects and Mechanisms of Action. *Cell Biosci* 7 (1), 1–16. doi:10.1186/s13578-017-0179-x

Yang, Y., Bai, L., Li, X., Xiong, J., Xu, P., Guo, C., et al. (2014). Transport of Active Flavonoids, Based on Cytotoxicity and Lipophilicity: An Evaluation Using the Blood-Brain Barrier Cell and Caco-2 Cell Models. *Toxicol. Vitro* 28 (3), 388–396. doi:10.1016/j.tiv.2013.12.002

Yuan, S., Tao, F., Zhang, X., Zhang, Y., Sun, X., and Wu, D. (2020). Role of Wnt/β-Catenin Signaling in the Chemoresistance Modulation of Colorectal *Cancer*. *Biomed. Res. Int.* 2020, 1–9. doi:10.1155/2020/9390878

Zhang, J., Liu, D., Huang, Y., Gao, Y., and Qian, S. (2012). Biopharmaceutics Classification and Intestinal Absorption Study of Apigenin. *Int. J. Pharmaceutics* 436 (1-2), 311–317. doi:10.1016/j.ijpharm.2012.07.002

Zhang, X.-f., Han, R.-m., Sun, X.-r., Li, G.-y., Yang, Q.-f., Li, Q., et al. (2013). The Effect of the Skeleton Structure of Flavanone and Flavonoid on Interaction with Transferrin. *Bioorg. Med. Chem. Lett.* 23 (24), 6677–6681. doi:10.1016/j.bmcl.2013.10.042

Zhang, Y.-J., Dai, Q., Sun, D.-F., Xiong, H., Tian, X.-Q., Gao, F.-H., et al. (2009). mTOR Signaling Pathway Is a Target for the Treatment of Colorectal *Cancer*. *Ann. Surg. Oncol.* 16 (9), 2617–2628. doi:10.1245/s10434-009-0555-9

Zhang, Z., Cui, C., Wei, F., and Lv, H. (2017). Improved Solubility and Oral Bioavailability of Apigenin via Soluplus/Pluronic F127 Binary Mixed Micelles System. *Drug Develop. Ind. Pharm.* 43 (8), 1276–1282. doi:10.1080/03639045.2017.1313857

Zhao, J., Yang, J., and Xie, Y. (2019). Improvement Strategies for the Oral Bioavailability of Poorly Water-Soluble Flavonoids: An Overview. *Int. J. Pharmaceutics* 570, 118642. doi:10.1016/j.ijpharm.2019.118642

Zhao, L., Zhang, L., Meng, L., Wang, J., and Zhai, G. (2013). Design and Evaluation of a Self-Microemulsifying Drug Delivery System for Apigenin. *Drug Develop. Ind. Pharm.* 39 (5), 662–669. doi:10.3109/03639045.2012.687378

Zhong, Y., Krisanapun, C., Lee, S.-H., Nualsanit, T., Sams, C., Peungvicha, P., et al. (2010). Molecular Targets of Apigenin in Colorectal Cancer Cells: Involvement of P21, NAG-1 and P53. *Eur. J. Cancer* 46 (18), 3365–3374. doi:10.1016/j.ejca.2010.07.007

Łania-Pietrzak, B., Michalak, K., Hendrich, A. B., Mosiadz, D., Grynkiewicz, G., Motohashi, N., et al. (2005). Modulation of MRP1 Protein Transport by Plant, and Synthetically Modified Flavonoids. *Life Sci.* 77 (15), 1879–1891. doi:10.1016/j.lfs.2005.04.005

Conflict of Interest: The authors declare that the research was conducted in the absence of any commercial or financial relationships that could be construed as a potential conflict of interest.

frontiers in Pharmacology

ORIGINAL RESEARCH
published: 02 July 2021
doi: 10.3389/fphar.2021.699842

Evidence That Tumor Microenvironment Initiates Epithelial-To-Mesenchymal Transition and Calebin A can Suppress it in Colorectal Cancer Cells

*Constanze Buhrmann[1,2], Aranka Brockmueller[1], Choudhary Harsha[3], Ajaikumar B. Kunnumakkara[3], Peter Kubatka[4], Bharat B. Aggarwal[5] and Mehdi Shakibaei[1]**

[1]Musculoskeletal Research Group and Tumor Biology, Chair of Vegetative Anatomy, Faculty of Medicine, Institute of Anatomy, Ludwig-Maximilian-University Munich, Munich, Germany, [2]Faculty of Medicine, Institute of Anatomy and Cell Biology, University of Augsburg, Augsburg, Germany, [3]Cancer Biology Laboratory and DBT-AIST International Center for Translational and Environmental Research (DAICENTER), Department of Biosciences and Bioengineering, Indian Institute of Technology Guwahati, Guwahati, India, [4]Department of Medical Biology, Jessenius Faculty of Medicine, Comenius University in Bratislava, Martin, Slovakia, [5]Inflammation Research Center, San Diego, CA, United States

OPEN ACCESS

Edited by:
Cristiana Perrotta,
University of Milan, Italy

Reviewed by:
Héctor R. Contreras,
University of Chile, Chile
Dingcheng Gao,
Cornell University, United States

***Correspondence:**
Mehdi Shakibaei
mehdi.shakibaei@med.uni-muenchen.de

Specialty section:
This article was submitted to Pharmacology of Anti-Cancer Drugs, a section of the journal Frontiers in Pharmacology

Received: 14 May 2021
Accepted: 23 June 2021
Published: 02 July 2021

Citation:
Buhrmann C, Brockmueller A, Harsha C, Kunnumakkara AB, Kubatka P, Aggarwal BB and Shakibaei M (2021) Evidence That Tumor Microenvironment Initiates Epithelial-To-Mesenchymal Transition and Calebin A can Suppress it in Colorectal Cancer Cells. Front. Pharmacol. 12:699842. doi: 10.3389/fphar.2021.699842

Background: Tumor microenvironment (TME) has a pivotal impact on tumor progression, and epithelial-mesenchymal transition (EMT) is an extremely crucial initial event in the metastatic process in colorectal cancer (CRC) that is not yet fully understood. Calebin A (an ingredient in *Curcuma longa*) has been shown to repress CRC tumor growth. However, whether Calebin A is able to abrogate TME-induced EMT in CRC was investigated based on the underlying pathways.

Methods: CRC cell lines (HCT116, RKO) were exposed with Calebin A and/or a FAK inhibitor, cytochalasin D (CD) to investigate the action of Calebin A in TME-induced EMT-related tumor progression.

Results: TME induced viability, proliferation, and increased invasiveness in 3D-alginate CRC cultures. In addition, TME stimulated stabilization of the master EMT-related transcription factor (Slug), which was accompanied by changes in the expression patterns of EMT-associated biomarkers. Moreover, TME resulted in stimulation of NF-κB, TGF-β1, and FAK signaling pathways. However, these effects were dramatically reduced by Calebin A, comparable to FAK inhibitor or CD. Finally, TME induced a functional association between NF-κB and Slug, suggesting that a synergistic interaction between the two transcription factors is required for initiation of EMT and tumor cell invasion, whereas Calebin A strongly inhibited this binding and subsequent CRC cell migration.

Conclusion: We propose for the first time that Calebin A modulates TME-induced EMT in CRC cells, at least partially through the NF-κB/Slug axis, TGF-β1, and FAK signaling. Thus, Calebin A appears to be a potential agent for the prevention and management of CRC.

Keywords: tumor microenvironment, colorecal cancer, Calebin A, EMT, focal adhesion kinase, NF- kappa B, slug, TGF - β1

INTRODUCTION

Colorectal cancer (CRC) is ranked third in incidence and second in associated mortality worldwide (Bray et al., 2018; Bray et al., 2020; Siegel et al., 2020). CRC rising incidences have been linked to the aging population, poor lifestyle, and diet in particular, among other factors (Dekker et al., 2019). Although, it has been observed that the incidence of CRC has been decreasing in recent years (Mauri et al., 2019), additionally it has been reported that the quality of life is often compromised by chronic side effects in CRC patients after therapies (Buccafusca et al., 2019). This indicates the importance of developing an alternative effective treatment option with few side effects in order to control the overall CRC mortality statistics.

The major etiological factor of CRC is chronic infection in the gastrointestinal tract that causes an active pro-inflammatory tumor microenvironment (TME) supported by defensive cells such as T-lymphocytes, macrophages, natural killer cells and other cells that may play a key role in tumor development (Elinav et al., 2013). The TME contributes significantly to the proliferation, survival, and migration of the underlying cellular neoplastic system. In addition, tumor cells possess some of the signaling proteins of the inherent immune system, such as chemokines, cytokines and their receptors that contribute to migration and metastasis (Coussens and Werb, 2002). Further, the inflammatory TME attracts immune cells and other protective cells which secrete pro-inflammatory mediators. These factors, in turn, can lead to greater alteration of intracellular signaling pathways, initiation and accumulation of mutations in tumor cells that induce active and rapid proliferation and protect the cancer cells from apoptosis. As a result, CRC cells lose the epithelial phenotype and simultaneously acquire the mesenchymal phenotype, thus undergoing an epithelial-mesenchymal transition (EMT) that gives them the ability to metastasize (Virchow, 1881; Coussens and Werb, 2002; de Visser et al., 2006; Medzhitov, 2008; Buhrmann et al., 2020a). Therefore, targeting the TME might provide new therapeutic approaches for controlling tumor development.

EMT and its associated progression and occurrence of metastasis is a major contributor to mortality in CRC patients, and the underlying mechanisms are still under exploration. EMT has been shown to play a determinant function in cancer development as it leads to disruption of cell-cell adherences, extracellular matrix (ECM) re-modelling and increased motility of the tumor cells (Martin, 2014). In addition, EMT inhibits E-cadherin expression, causing impaired adhesion and cell polarity during the development of epithelial tumors (carcinomas) and becomes evident at the stage of invasion (mesenchymal phenomenon), when tumor cells detach from the primary tumor and acquire the ability to cross the surrounding area (Behrens et al., 1992; Stetler-Stevenson et al., 1993; Christofori and Semb, 1999; Tepass et al., 2000; Thiery, 2002; Prieto-García et al., 2017) and this promotes formation of cancer stem cells (Mani et al., 2008; Polyak and Weinberg, 2009). Interestingly, it has been previously reported that down-regulation of E-cadherin expression in tumor cells may involve both genetic and epigenetic modifications (Christofori and Semb, 1999). Among the epigenetic and genetic modifications, excessive methylation of the E-cadherin promoter and transcriptional suppression are observed as major activities in most carcinomas (Yoshiura et al., 1995; Tamura et al., 2000; Cheng et al., 2001; Hajra et al., 2002). In addition, transcriptional repressors of the Snail zinc finger transcription factor family, such as Snail and Slug, play an essential role in the activation and induction of EMT, as this alters the expression patterns of EMT biomarkers in favor of the mesenchymal phenotype (LaBonne and Bronner-Fraser, 2000; del Barrio and Nieto, 2002; Nieto, 2002). Indeed, the inflammatory TME has been further shown to induce cancer initiation, and metastasis through stimulating the EMT process (Buhrmann et al., 2016). Stromal cells in the TME are recognized to have a pivotal function in the stimulation of EMT in tumor cells (Guo and Deng, 2018) and TME-mediated EMT induction in tumor cells is stimulated by activating various cell signaling pathways including TNF-β, NF-κB and Wnt signaling connected with cancer progression (Jing et al., 2011). Moreover, pro-inflammatory TNF-α or TNF-β, have been previously reported to act as potential endogenous tumor-promoting factors and an important mechanism of cytokines in this action is to induce EMT in different types of tumor cells (Soria et al., 2011; Buhrmann et al., 2020a). In addition, focal adhesion kinase (FAK), cytoskeletal proteins and their receptors have previously demonstrated to have a major function in the context of EMT-mediated tumor cell survival and invasion, as well as progression. These upstream signaling molecules are potential therapeutic targets to control tumor metastasis as well as tumor proliferation (Seguin et al., 2015).

NF-κB is a very important and pro-inflammatory transcription factor that is induced by diverse inflammatory signals, oxidative stress, and various carcinogens in diverse cells. Moreover, NF-κB is known to initially reside in an inactive state in the cytoplasm in various cells and consists of a heterotrimer with p50 and p65 subunits and an inhibitory IκBα subunit (Bhat-Nakshatri et al., 2010). It has been shown that most of the processes involved in pro-inflammatory and carcinogenic pathways are linked to NF-κB signaling. After activation and phosphorylation, NF-κB translocates to the nucleus to control the protein expression of pro-inflammatory genes. Interestingly, it is found that phosphorylation of NF-κB leads to various stages of inflammation, survival, proliferation, migration, angiogenesis, tumor development, and also tumor cell metastasis and drug resistance (Aggarwal, 2004).

The transforming growth factor-β1 (TGF-β1) is identified to be a potent enabler of EMT in the initial phase of tumor progression and tumor metastasis (Buhrmann et al., 2016). In addition, TGF-β1 specifically promotes receptor complex activity, leading to the initiation of Smad2 phosphorylation in the nucleus, in which they functionally associate to transcription factors such as Snail and Slug, suppressing the expression of epithelial biomarkers and stimulating the expression of mesenchymal biomarkers at mRNA level (Zhang et al., 2018).

Further, activation of EMT signaling pathways has been described to be regulated at the epigenetic and post-translational level (Prieto-García et al., 2017) and identification of novel agents targeting EMT may provide possible new

therapeutic approaches in cancer treatment (Kalluri and Weinberg, 2009). Calebin A [4-(3-methoxy-4-hydroxyphenyl)-2-oxo-3-enebutanyl 3-(3-methoxy-4-hydroxyphenyl) propenoate] is drived from curcumin-free turmeric (*Curcuma longa L., Zingiberaceae*), first described by Park and Kim (Park and Kim, 2002) and since then, other isomers of Calebin A have been discovered (Zeng et al., 2007). Calebin A has been reported to possess potent anti-inflammatory and anti-tumor potential, such as inhibiting cell viability, proliferation, and migration, and promoting apoptosis in various resistant and solid tumor cells by blocking several cellular signaling pathways (Aggarwal et al., 2013; Buhrmann et al., 2019; Nair et al., 2019; Buhrmann et al., 2020a).

However, so far, to our knowledge, there are not any clear studies published on the possible inhibition of EMT process and metastasis in CRC-TME by Calebin A. Therefore, the present study targeted to test the sub-regulatory promotions of Calebin A on CRC cells in a pro-inflammatory multicellular TME model. In this work, we report for the first time that Calebin A suppresses TME-induced invasion and malignancy of CRC cells by modulating EMT signaling pathways, thus highlighting Calebin A.

MATERIALS AND METHODS

Antibodies and Chemicals

Monoclonal antibodies to phospho-specific-FAK, PARP, p65-NF-κB, phospho-specific p65-NF-κB, and activated-Caspase-3 were from R&D Systems (Heidelberg, Germany). Antibodies to β-Actin, cytochalasin D (CD), MTT reagent [3-(4,5-dimethylthiazol-2-yl)-2,5-diphenyltetrazolium bromide], DAPI (4,6-diamidino-2-phenylindole), dithiothreitol (DTT) and alginate were from Sigma-Aldrich (Taufkirchen, Germany). Anti-E-cadherin, anti-vimentin, anti-TGF-β1, anti-p-Smad2 and anti-Slug were from Santa Cruz Biotechnology (Santa Cruz, CA, United States). Secondary antibodies for immunofluorescence were procured from Dianova (Hamburg, Germany). Alkaline phosphatase-linked antibodies for Western blotting were obtained from EMD Millipore (Schwalbach, Germany). Calebin A (CA), was a generous gift from Sabinsa Corporation (East Windsor, NJ, United States). Calebin A was diluted and 10,000 μM stock solution was prepared in DMSO, and this was further diluted in cell culture medium. Final concentration of DMSO did not exceed 0.1% during the experiments. Focal adhesion kinase inhibitor (FAK-I) (PF-562271) was purchased from Sellekchem (Munich, Germany). Stock sample of 10 mM FAK-I was prepared in DMSO and diluted again in serum-starved medium to make working samples.

Cell Lines and Cell Culture Conditions

Two distinct colorectal cancer cell lines (HCT116 and RKO), and a stromal fibroblast cell line (MRC-5) were purchased from the European Collection of Cell Cultures (Salisbury, United Kingdom) and a human T-lymphocyte cell line (Jurkat) was obtained from the Leibniz Institute (DSMZ-German Collection of Microorganisms and Cell Cultures). Jurkat was cultured in suspension and HCT116, RKO, and MRC-5 were cultured as monolayers in normal cell growth medium containing 10% FCS under standard conditions (37°C, 5% CO_2) (Shakibaei et al., 2015).

Study Design

TME cultures were set up by co-culturing stromal cells (MRC-5), T-lymphocyte cell line (Jurkat) and CRC cells (HCT116, RKO) to investigate the potential of Calebin A on the suppression of epithelial-to-mesenchymal transition in CRC cells as described previously (Buhrmann et al., 2020a). To establish the multicellular TME, CRC cells (HCT116, RKO) in 3-dimensional (3D) alginate cultures (1×10^6/ml alginate) were transferred to petri dishes containing monolayer fibroblasts ($3{,}000/cm^2$) and in suspension T-lymphocytes (20.000/ml medium). These cells were cultured in serum-starved medium (3% FCS) for 10 days. The CRC cells cultured in alginate beads alone were termed as "basal control". All experiments were performed with serum starved medium containing only 3% FCS.

Alginate Culture

As described in detail in our previous studies (Shakibaei and De Souza, 1997; Shakibaei et al., 2015), CRC cells ($1x10^6$/ml) were suspended in alginate and dropwise (size: 0.5 cm) added into a sterile $CaCl_2$ solution (100 mM) where the drops polymerized into beads after 10 min. After continued washing with NaCl (15 mM), alginate beads were incubated for 1 h in serum starved medium. For the experiments, cells were left untreated or treated with CD in a dose dependent manner (0.1, 1, 2, and 4 μg/ml) for 30 min and then encapsulated in alginate beads, and TME cultures were established as described above. Further, primarily untreated TME cultures were treated with Calebin A (1, 2, 5, and 10 μM) or with FAK-I (0.01, 0.1, 1, and 10 μM). As basal control, CRC were encapsulated in alginate beads without fibroblasts or Jurkat and either left untreated or treated with 5 μM Calebin A. Medium was changed three times a week and cultures were investigated after 10 days.

Viability Assay

Impact of Calebin A on the proliferation of CRC cells in TME cultures was examined by the MTT reagent, as described before (Buhrmann et al., 2020a). Shortly, CRC cells treated as described above were detached from alginate using a sterile sodium citrate solution (55 mM), were re-suspended in altered medium (no phenol red, no vitamin C, 3% FCS) and 10 μl MTT solvent (5 mg/ml) was spread per well in a 96-well plate in triplicate. Incubation was stopped after 2 h by adding 10% Triton x-100/acidic isopropanol and metabolically active cells were estimated using a multiscanner plate ELISA reader (Bio-Rad Laboratories Inc. Munich, Germany).

Invasion Test

The cell invasion assay was examined using alginate beads (Shakibaei et al., 2015; Buhrmann et al., 2020a). Shortly, 1 $x10^6$/ml cells were embedded in alginate and treated as described above. After incubation for 10 days, the noninvasive

cells and alginate matrix were removed from the petri dishes while the invasive cells that migrated across the alginate beads adhered and made colonies in opposite to fibroblasts cells on the bottom of the petri dish. These invasive cells were stained with toluidine blue for 1 h and accurate washed two times with PBS and photographed under the light microscope (Zeiss, Germany). The amount of migrating and positively stained attached colonies was quantified and analyzed by counting all colonies.

Immunofluorescence

Immunofluorescence labeling of Slug was performed in a modified TME as described (Buhrmann et al., 2020a). Shortly, HCT116, and RKO cells were seeded on glass plates (5,000/plate) and after adherence, they were either left untreated or treated with CD (1, 2 μg/ml) for 30 min and then placed on a steel-net bridge in petri dishes containing monolayer of fibroblasts ($10.000/cm^2$) and T-lymphocytes in suspension (20.000/ml) to establish TME. Additionally, cultures were either left untreated or treated with Calebin A (1, 5 μM) for 24 h. For basal control, CRC cells were cultured only on glass plates without creating the TME and either left untreated or were treated with Calebin A (5 μM).

Western Blot Analysis

Samples from the TME were processed in the same manner as earlier detailed (Shakibaei et al., 2015; Buhrmann et al., 2017). Shortly, alginate samples were suspended in sterile sodium citrate solution for 20 min, lyzed on ice (50 mM Tris/HCl, pH 7.2/ 150 mM NaCl/(v/v) Triton X-100/1 mM sodium orthovanadate/ 50 mM sodium pyrophosphate/100 mM sodium fluoride/4 μg/ml pepstatin A/1 mM PMSF), total protein content was measured, and fractionated by SDS-PAGE under reducing conditions. After blotting on a nitrocellulose membrane (Transblot apparatus, Bio-Rad, Munich, Germany), membranes were incubated overnight with primary antibody (1:10,000) at 4°C and incubated for 1.5 h with secondary antibody (1:10,000). Positive binding was determined using nitroblue tetrazolium and 5-bromo-4-chloro-3-indoyl phosphate (VWR, Germany), quantification of bands was performed using the "Quantity One" program (Bio-Rad, Munich, Germany).

DNA-Binding Assay

To address the role of Calebin A in modulating NF-κB attachment on DNA, we performed a DNA-binding assay with dithiothreitol (DTT) as earlier detailed (Buhrmann et al., 2020a). TME cultures were established and then nuclei and cytoplasm were separated from each other, from CRC cells that remained untreated and/or treated with Calebin A (1, 2, and 5 μM) plus DTT (5 mM) alone or in both for 1 h, as has been thoroughly outlined in previous work (Buhrmann et al., 2020a; Buhrmann et al., 2020b; Buhrmann et al., 2020c). The nuclei were then prepared, separated by SDS-PAGE and blotted as indicated earlier. PARP was used to normalize the samples to the controls.

Immunoprecipitation Assay

The immunoprecipitation assay was performed as outlined (Shakibaei et al., 2012) to explore the endogenous interaction of NF-κB and Slug on CRC grown in TME cultures. Whole cell extracts of HCT116 and RKO from TME cultures were incubated with 25 μl of either normal rabbit IgG-serum or normal mouse IgG-serum and *Staphylococcus aureus* cells as pre-clearing. Further, samples were incubated with primary antibodies (anti-p-NF-κB-p65 or anti-Slug) diluted in washing buffer [0.1% Tween 20, 150 mM NaCl, 50 mM Tris-HCl (pH 7.2), 1 mM $CaCl_2$, 1 mM $MgCl_2$ and 1 mM PMSF] for 1.5 h (4°C), with *S. aureus* cells for 1 h and washed three times with washing buffer and once with 50 mM Tris-HCl (pH 7.2). Finally, samples were boiled in SDS-PAGE sample buffer and immunoblotting (anti-p-NF-κB-p65 or anti-Slug) was performed as described above. Additionally, samples were incubated with non-immune rabbit anti-mouse IgG alone as control immunoprecipitations.

Statistics

Each individual assay was tested separately three times using three separate sets of replicates. A Wilcoxon-Mann-Whitney test was used for statistical analysis. Results were presented as mean ± SD or SEM and compared by one-way, two-way or three-way ANOVA using SPSS Statistics if the normality test was satisfied (Kolmogorov-Smirnov test). A p-value of <0.05 was regarded as evidence of statistically important results.

RESULTS

The objective of this presentation was to investigate the sub-regulatory actions of Calebin A (a component of *C. longa*) (**Figure 1A**) on CRC cells in a pro-inflammatory multicellular TME model to represent an *in vivo* approach TME. In this work, we show for the first time that Calebin A suppresses TME-induced CRC cell invasion and malignancy by modulating EMT signaling during the early onset of CRC.

Calebin A Blocks TME-Induced Viability and Proliferation of CRC Cells, Comparable to FAK Inhibitor or Cytochalasin D

Given that the organization and rearrangement of the cytoskeleton is essential for the cancer cell invasion, migration, and proliferation (Tai et al., 2015), we first investigated whether Calebin A modifies colorectal cancer cell proliferation and viability in TME, similar to FAK inhibitor or cytochalasin D. Serum-starved HCT116 or RKO cells were kept untreated or treated with different concentrations of Calebin A or FAK inhibitor or CD. Cell viability and proliferation were determined using MTT assay as outlined in Materials and Methods. TME significantly increased cell viability and proliferation of HCT116 and RKO cells compared with basal control (**Figures 1B,C**). In contrast, Calebin A, similar to FAK inhibitor, or CD reduced markedly TME-promoted cell viability and proliferation of cells in 3D-alginate tumor cultures in both basal control and TME in a dose-dependent way. Collectively, the anti-proliferative action of Calebin A resembles FAK inhibitor or cytochalasin D and these proteins may play a role in its efficacy.

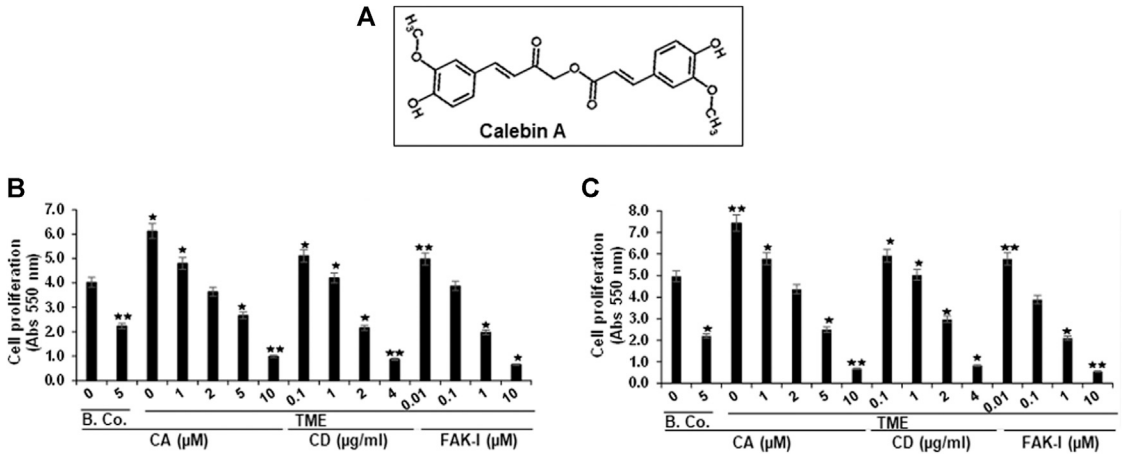

FIGURE 1 | Calebin A or FAK inhibitor or cytochalasin D action on colorectal cancer cell survival. **(A)** Chemical bodies of Calebin A. **(B)** HCT116 and **(C)** RKO cells in alginate beads by themselves (basal control = B. Co.) or in TME were firstly not treated, and secondly, were exposed to a series of doses of Calebin A (CA) (1, 2, 5, 10 μM) or cytochalasin D (CD) (0.1, 1, 2, and 4 μg/ml) or FAK inhibitor (FAK-I) (0.01, 0.1, 1, and 10 μM) for 10 days and cell survival was monitored by MTT. All tests were checked on three different occasions each. $*p < 0.05$, $**p < 0.01$ relative to basal control.

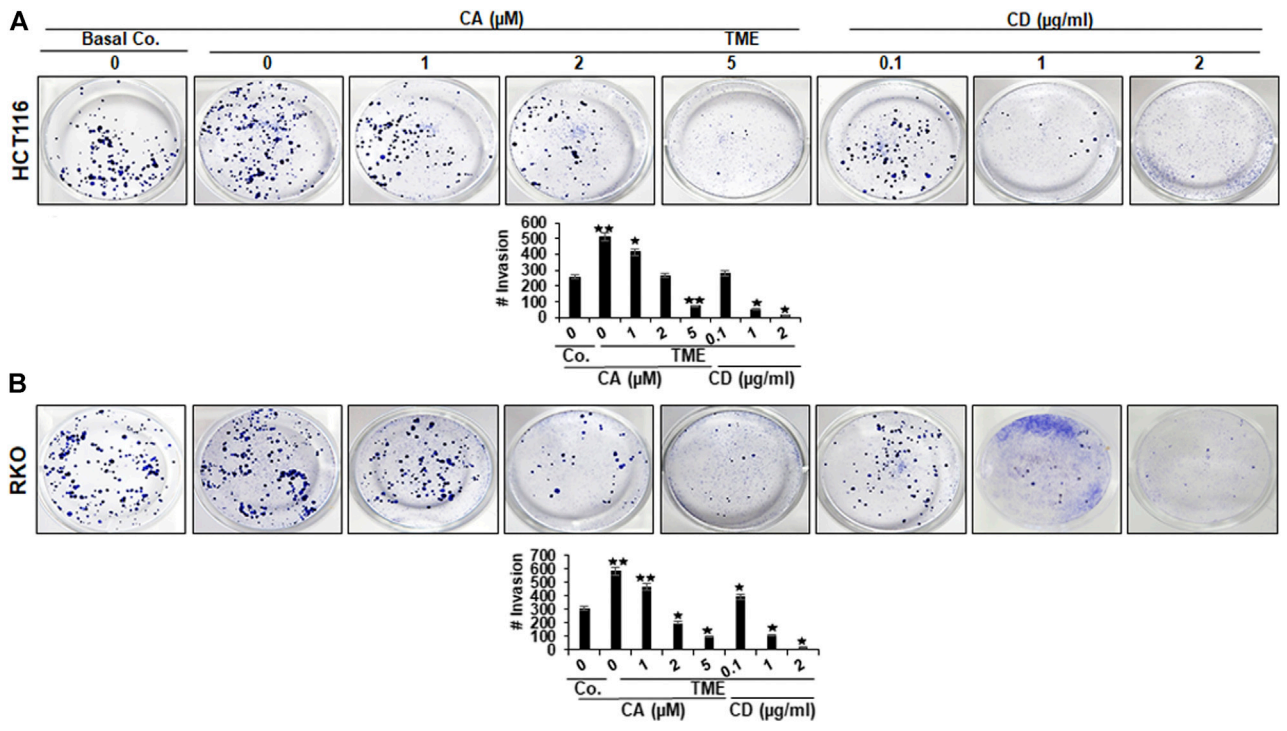

FIGURE 2 | Calebin A or cytochalasin D actions on colorectal cancer cells migration in TME. **(A)** HCT116 and **(B)** RKO cells in alginate beads by themselves (Basal Co.) or in TME were treated with increasing concentration of Calebin A (CA) (1, 2, and 5 μM), of cytochalasin D (CD) (0.1, 1, and 2 μg/ml) or culture medium as control for 10 days in alginate and migrated spheroids were identified by toluidine blue-based labeling as outlined in the Materials and Methods. Results of all tests were scored at a minimum of three counts. $*p < 0.05$, $**p < 0.01$ relatively to basal control.

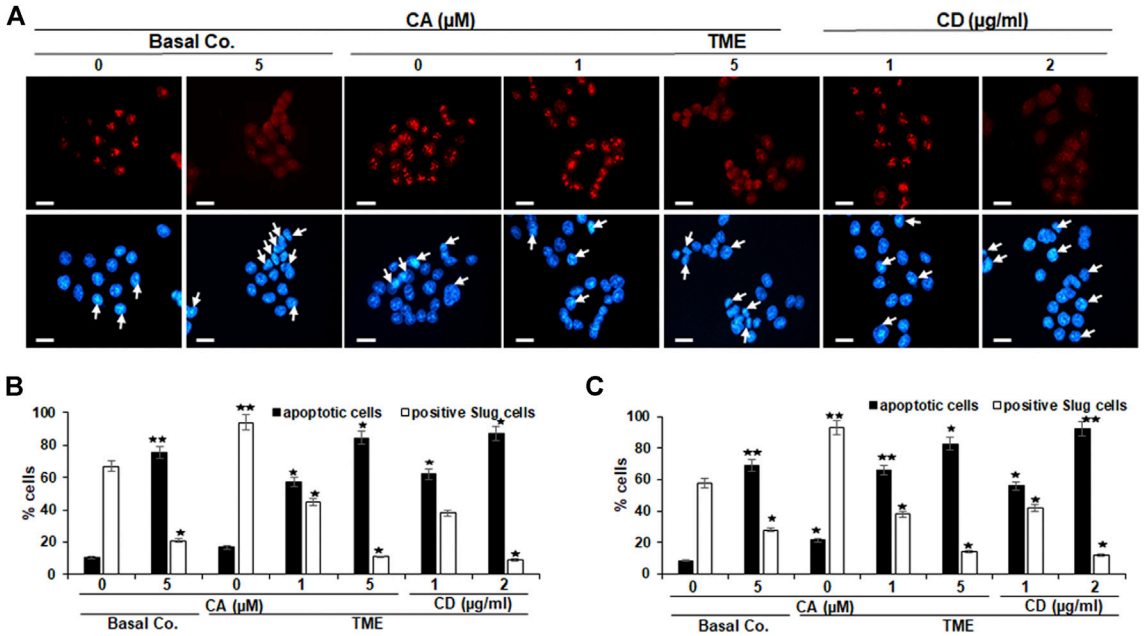

FIGURE 3 | Calebin A or cytochalasin D action on EMT-related transcription factor (Slug) expression in colorectal cancer cells. HCT116 **(A–B)** and RKO **(C)** cells by themselves (basal co.) subjected to Calebin A (CA) (5 μM), or in TME were kept alone untreated, subjected to graded doses of Calebin A (CA) (1, 5 μM) or cytochalasin D (CD) (1, 2 μg/ml) for 4 h in monolayer cultures and underwent immunofluorescence staining with anti-Slug and nuclear counterstaining with DAPI as stated in the Materials and Methods of this study. Magnification 400x; bars = 30 nm. All assays were performed three times each, and the number of apoptotic nuclei (arrows) has been determined by scoring 400–500 cells taken at 25 separate microscopic areas **(B–C)**. $^{*}p < 0.05$, $^{**}p < 0.01$ compared to basal control.

Calebin A Blocks TME-Induced 3D-Alginate CRC Cell Migration and Invasion, Comparable to Cytochalasin D

To assess the action of Calebin A or CD on the motility and invasion ability of CRC cells through the TME, HCT116, and RKO cells were grown in a 3D-alginate-matrix TME that more closely represents *in vivo* conditions and handled as outlined in detail in Materials and Methods. As shown in **Figures 2A,B**, the untreated TME significantly promoted tumor cell migration in CRC cell through the 3D-alginate-based matrix compared with the basal untreated TME control. In contrast, treatment of CRC cells with Calebin A (1, 2, and 5 μM), similar to CD (0,1, 1, and 2 μg/ml), blocked CRC cell migration and invasion across the alginate matrix in TME cultures in a dose-dependent way. Taken together, this is consistent with the results of the MTT assay, which showed that Calebin A, similar to CD inhibited CRC cell viability and proliferation, and these data highlight the importance of the involvement of cytoskeletal signaling proteins in the anti-metastasis properties supported by Calebin A in TME.

Calebin A Down-Regulated EMT-Related Transcription Factor (Slug) in CRC Cells Comparable to Cytochalasin D, as Shown by Immunofluorescence Microscopy

Slug is a component of the Snail generation of zinc-finger transcription factors (Blanco et al., 2002), and it has been proposed that Slug is participating in the modulation of cell motility during tumor cell invasion and migration (Cobaleda et al., 2007). To explore the impact of Calebin A on Slug expression in CRC cells, HCT116 and RKO cultures were left untreated or treated with different concentrations of Calebin A or CD and immunolabeled with anti-Slug as described above and evaluated by immunofluorescence microscopy and nuclear labeling with DAPI. In the control TME cultures, HCT116 and RKO cells showed significantly stronger labeling for Slug in the nucleus compared with the basal control (**Figures 3A–C**). Calebin A treatment, similarly to CD, significantly downregulated the expression of Slug in CRC cells and its nuclear localization in TME cultures, indicating the important pro-inflammatory effects of TME on CRC cells that support tumor promotion. Taken together, these results highlight that Slug is one of the major target proteins of Calebin A for its anti-metastatic or anti-EMT mechanisms in CRC cell TME (**Figures 3A–C**). Apoptosis was in fact verified by analyzing the apoptosis indicating morphological alterations in the nucleus with DAPI nuclear labeling (**Figures 3A–C**). Nuclear staining showed that untreated control HCT116 (**Figures 3A,B**) and RKO (**Figure 3C**) cell cultures had generally normal nuclear dimensions with only a few apoptotic nuclei in the cultured cells. In contrary, a significant increase in apoptotic cells was observed in cells treated with Calebin A or CD in HCT116 or RKO cells with nuclear morphological alterations (pyknosis, fragmented nuclei, chromatin condensation) in a dose-dependent fashion (**Figures 3A–C**). Taken together, these

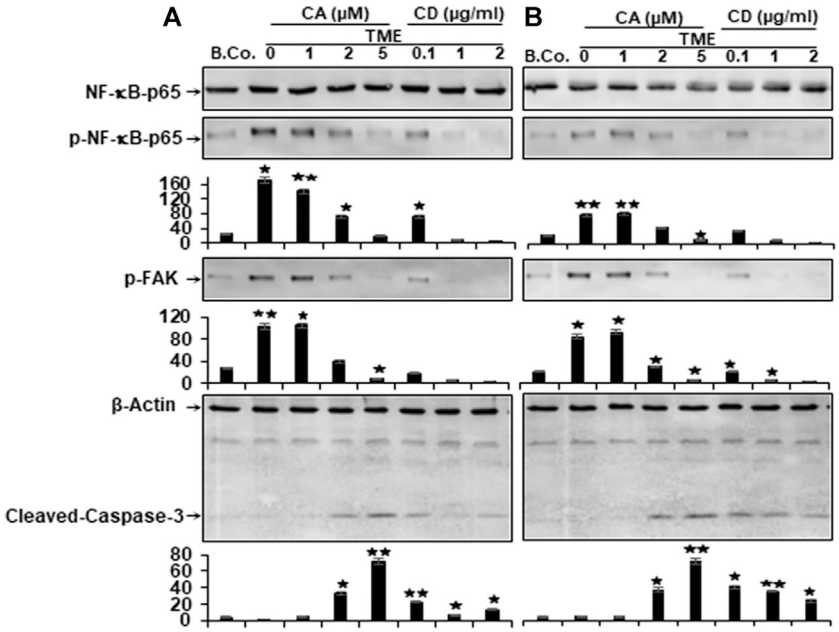

FIGURE 4 | Calebin A or cytochalasin D actions on NF-κB, FAK, and caspase-3 expression in colorectal cancer cells. **(A)** HCT116 and **(B)** RKO cells in alginate beads (B. Co.) or in TME were kept by themselves or treated with variable amounts of Calebin A (CA) (1, 2, and 5 μM) or cytochalasin D (CD) (0.1, 1, and 2 μg/ml) for 10 days as outlined in Materials and Methods. Immunoblotting on total samples was performed through Western blotting using antibodies to p65-NF-κB, phospho-p65-NF-κB, p-FAK, and Caspase-3. Indicated are the results of at least three separate assays, with β-Actin serving as control. The densitometric analysis has been carried out for the indicated proteins. $^{*}p < 0.05$, $^{**}p < 0.01$ relatively to basal control.

outcomes are in agreement with MTT findings and indicate Calebin A has the ability to act to suppress the pro-tumor actions of TME in CRC cells through repression of EMT as well as induction of apoptosis.

Calebin A Suppressed TME-Induced p-NF-κB-p65, FAK, and Activated TME-Inhibited Caspase-3, Comparable to Cytochalasin D, in CRC Cells

In the past, TMEs have been shown to promote NF-κB activation and phosphorylation, which has been linked to tumor cell migration and metastasis (Ghosh et al., 1998; Lind et al., 2001; Cho et al., 2007; Sutnar et al., 2007). Therefore, we investigated the expression and phosphorylation of NF-κB in relation to malignancy and metastasis of CRC cells. Starved HCT116 and RKO cells were grown in alginate matrix beads and co-cultured in TME conditions, followed by treatment with incremental concentrations of Calebin A (1, 2, and 5 μM), CD (0.1, 1, and 2 μg/ml) or in culture medium as a control for 10 days as detailed in the Materials and Methods. Samples were immunolabeled using antibodies to p65, phospho-specific p65-NF-κB, p-FAK, and Caspase-3.

The levels of p65-NF-κB and p-FAK phosphorylation of HCT116 and RKO-alginate cultures were found to be notably increased in TME compared with basal control cultures. Interestingly, in a manner consistent with the disruption of the cytoskeleton by CD, treatment of TME with Calebin A markedly down-regulated the phosphorylation of p-NF-κB-p65 and p-FAK in a concentration-dependent way in both cells (**Figure 4**). Calebin A based treatment of TME, similar to CD disruption of the cytoskeleton, significantly upregulated cleaved Caspase-3 protein expression in CRC cells in a dose-dependent way (**Figure 4**). Contrary, treatment with CD resulted in less cleaved Caspase-3 protein compared with Calebin A, and cleavage of Caspase-3 was greater in RKO than in HCT116 CRC cells (**Figure 4**). These results suggest that Calebin A suppresses TME-mediated migration and invasion in CRC cells *via* inhibition of NF-κB, p-FAK and stimulation of caspase-3.

Calebin A Modulated TME-Induced TGF-β1 Signaling, Comparable to Cytochalasin D in CRC Cells

The cytokine transforming growth factor-β1 (TGF-β1) is a crucial factor in tumor progression and a strong enhancer of EMT during tumor invasion and metastasis (Massagué, 2000; Siegel and Massagué, 2003; Derynck and Akhurst, 2007), therefore, next, to determine whether TGF-β1 is implicated in augmenting tumor cell proliferation, migration, and the factors that stimulate cancer, we studied TGF-β1 protein expression in HCT116 and RKO cells. Starved cells grown in the TME cultures were either kept untreated or treated as mentioned in the "Materials and Methods" paragraph. Both CRC cells exhibited low expression of TGF-β1 and p-Smad-2 proteins in basal control (**Figure 5**). Whereas, immunoblotting showed substantially increased levels of TGF-β1 and p-Smad-2

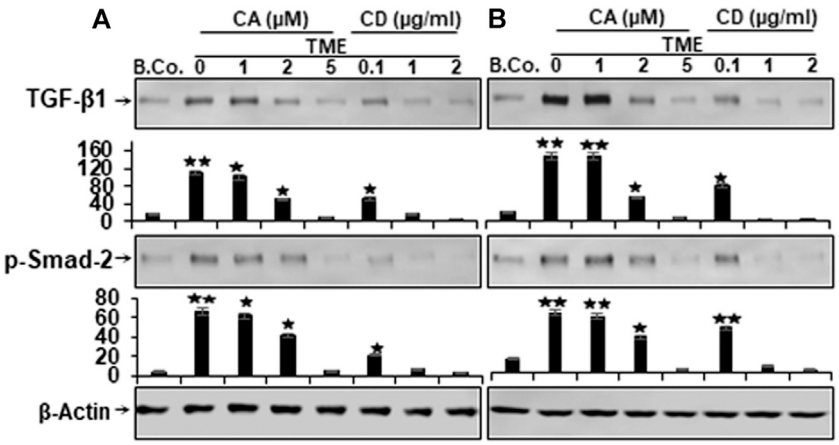

FIGURE 5 | Calebin A or cytochalasin D actions on TGF-β1 and p-Smad-2 expression in colorectal cancer cells. **(A)** HCT116 and **(B)** RKO cells in alginate beads (B. Co.) or in TME were maintained untreated or treated as outlined to the previous. Immunoblotting of total samples was performed by Western blotting using antibodies to TGF-β1 and p-Smad-2. Indicated are the results of at least three separate assays, with β-Actin serving as loading control. Densitometric analysis was performed for the indicated proteins. $^{*}p < 0.05$, $^{**}p < 0.01$ relatively to basal control.

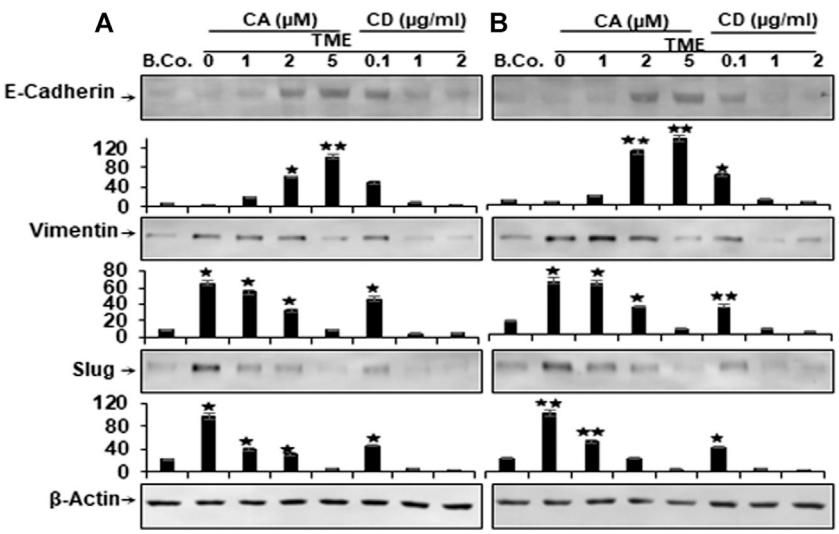

FIGURE 6 | Calebin A or cytochalasin D actions on EMT-specific biomarkers in colorectal cancer cells. HCT116 **(A)** and RKO cells **(B)** in alginate beads (B. Co.) or in TME were maintained alone or treated as outlined to the previous. Immunoblotting of total samples was performed by Western blotting using antibodies to E-Cadherin, vimentin and Slug. Indicated are the results of at least three separate assays, with β-Actin serving as loading control. Densitometric analysis was performed for the indicated proteins. $^{*}p < 0.05$, $^{**}p < 0.01$ relatively to basal control.

expression in both HCT116 and RKO cells obtained by TME (**Figure 5**). Importantly, in a manner resembling CD-treated cultures, Calebin A was found to considerably down-regulate the expression of the biomarkers mentioned above in a concentration-dependent way (**Figure 5**). Taken together, these outcomes are consonant with those of several other studies documenting that TGF-β1 and cytokines are the major contributors to progression, invasion, and metastasis within the TME (Derynck and Akhurst, 2007; Li et al., 2014; Jang et al., 2015). Collectively, Calebin A acts against the TMEs and has a potent suppressive effect on the mentioned processes.

Calebin A Modulated TME-Induced Altering the Expression of EMT-Specific Biomarkers, Comparable to Cytochalasin D in CRC Cells

To learn more about the multifunctional role of the Calebin A, in TME-induced tumor malignancy and metastasis in CRC cells, in relation to motility and EMT, we examined the level of EMT-related pathway protein expression, including E-cadherin, vimentin, and Slug. EMT has been reported to have a major function in carcinogenesis by leading to

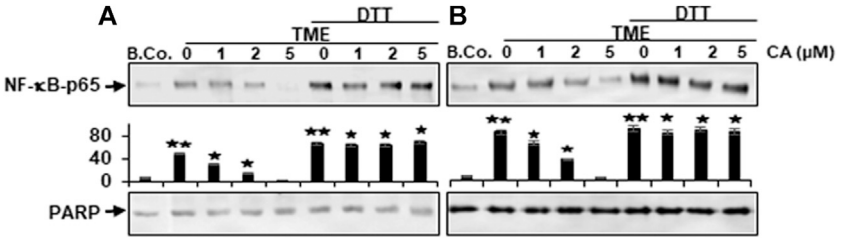

FIGURE 7 | Calebin A acts on TME-induced p-NF-κB-p65 engagement with DNA in colorectal cancer cells. **(A)** HCT116 and **(B)** RKO cells in alginate beads were cultured alone (B. Co.) or in TME were cultured alone or subjected to Calebin A (CA) as outlined in the Materials and Methods. Dissected nuclei of basal control or TME cells that has been allowed to incubate for 30 min with the stated concentrations of Calebin A in the presence or absence of 5 mM DTT were processed, then examined for p-NF-κB-p65 linkage to DNA using Western blotting. PARP acted as control. Densitometric assessment was done for the indicated proteins. $^{*}p < 0.05$, $^{**}p < 0.01$ relatively to basal control.

weakening of cell-cell adhesion, alteration of ECM, and increased motility of cancer cells (Martin, 2014). We investigated the expression of EMT biomarkers for tumorigenicity and the possible effects of Calebin A on these biomarkers. Alginate basal control HCT116 and RKO cells revealed a basal level expression of the aforementioned EMT markers (**Figure 6**). In contrast, Western blot results showed markedly down-regulated expression of E-cadherin and markedly up-regulated expression of vimentin and Slug in both cells from TME cultures (**Figure 6**). However, similar to CD, treatment with Calebin A resulted in up-regulation of E-cadherin expression and, in contrast, significant down-regulation of vimentin and Slug expression in a concentration-dependent way, indicating the prominent targeting impact of Calebin A on the EMT signaling pathway (**Figure 6**). The densitometric analysis of the immunoblots supported the presented findings (**Figure 6**). Taken together, such data clearly demonstrate the critical function of Calebin A in regulating TME-stimulated EMT pathway, as well as Calebin A mediates anti-metastasis effects in part by down-regulating the EMT pathway of CRC cells in the TME.

DTT Blocks Calebin A-Suppressive Effects of NF-κB Binding to DNA in CRC Cells

We further wanted to know whether Calebin A has the ability to trigger the repression of NF-κB phosphorylation by directly interfering with its binding to DNA. To address this question, we treated isolated nuclei obtained from HCT116 (A) and RKO (B) cells as indicated in Materials and Methods. To this end, Calebin A markedly attenuated the association of NF-κB binding to DNA in a dose-dependent way, as demonstrated in **Figures 7A,B**. Since the position 38 cysteine region in p65 protein is required for DNA binding, an assay to remove the cysteine regions was performed with DTT either with or without Calebin A. Indeed, our study revealed that the blocking effect of Calebin A toward the attachment of p65-NF-κB on DNA has been abolished when DTT was applied to the nuclei of RKO cells, similar to HCT116 cells, indicating a specific effect of Calebin A in regulating the interaction of NF-κB with DNA and this is not cell specific (**Figures 7A,B**). Taken together, these data suggest that Calebin A directly modulates the binding of p65-NF-κB to DNA.

Calebin A Inhibits TME-Induced p-NF-κB-p65 Association With the Master EMT-Related Transcription Factor (Slug), Comparable to Cytochalasin D in CRC Cells

Cell motility, cytoskeletal remodeling, cell adhesion, FAK signaling pathways, and NF-κB have already been shown to be linked to the regulation of cancer cell growth, viability, and invasiveness (Cary and Guan, 1999; Schlaepfer et al., 1999; Cheng et al., 2001; Aggarwal, 2004; Zhang et al., 2009). The functional link between the proteins that have a metastasis-promoting effect in the TME and their contribution to cancer metastasis is known. We next performed co-immunoprecipitation experiment to provide evidence for a potentially interaction of NF-κB and Slug in CRC cells in TME. Cells were treated as described in Materials and Methods, and cell lysates immunoprecipitated using antibodies directed to p-NF-κB or to Slug, that was subsequently immunoblotted using Slug or p-NF-κB antibodies. As shown in **Figure 8**, surprisingly, in both CRC cells, we found markedly strong co-immunoprecipitation of NF-κB protein with Slug protein in TME (**Figure 8**). Marginal co-immunoprecipitation of NF-κB protein with the Slug protein was observed in untreated basal control cultures (**Figure 8**). However, similar to CD, treatment with Calebin A significantly inhibited this co-immunoprecipitation of NF-κB protein with Slug protein. Densitometric analysis of immunoblots supported the results presented at the top (**Figure 8**). Overall, our data strongly indicate that, on the one hand TME promotes the formation of the NF-κB/Slug complex during tumorigenesis, resulting in malignancy and metastasis in CRC cells, and, on the other hand Calebin A prevents TME-induced EMT, partly due to blockage of the NF-κB/Slug route.

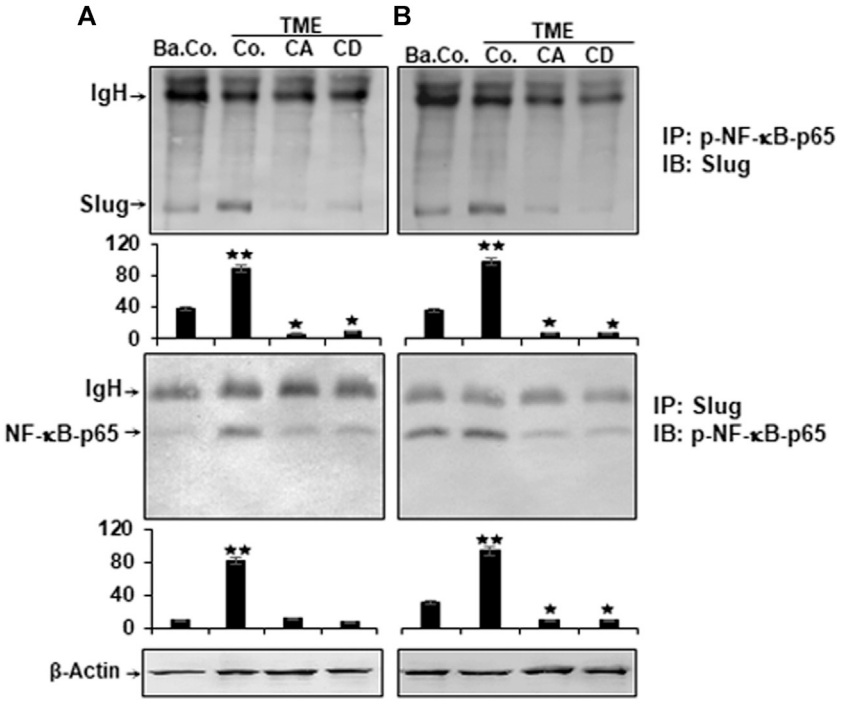

FIGURE 8 | Calebin A or cytochalasin D impact on TME-induced p-NF-κB-p65 association with master EMT-related transcription factor (Slug) in colorectal cancer cells. HCT116 **(A)** and RKO **(B)** cells in alginate matrix alone (B. Co.) or in TME were kept without treatment (Co.) or treated with Calebin A (CA) or Cytochalasin D (CD) as outlined in the Materials and Methods. The lysate samples were immunoprecipitated (IP) using anti-p-NF-κB-p65 or with anti-Slug. Finally, each immunoprecipitates was fractionated by SDS-PAGE and subjected to immunoblotting (IB) with anti-Slug or anti-p-NF-κB-p65. Densitometric assays on protein levels as displayed with immunoblotting were carried out in triplicate. The initial samples were subjected to antibody against β-Actin as control. Values were comparable with the reference control. $p < 0.05$ (*), $p < 0.01$ (**). IgH = immunoglobulin heavy chain.

DISCUSSION

The present work has allowed us to establish a CRC cell 3D-alginate pro-inflammatory multicellular TME culture mimicking the heterogeneous TME *in vivo* to evaluate the anti-tumor actions observed with Calebin A, mainly the anti-EMT effect. We provided the following insights and investigated the role of TME in promoting CRC tumor progression (tumor migration and EMT) and the modulatory actions of Calebin A in this process. 1) The TME induced viability, proliferation, and alterations in the expression of biomarkers related to EMT (elevated vimentin, depressed E-cadherin), leading to higher motility and invasiveness in CRC cells. 2) However, these effects were dramatically decreased by Calebin A, similar to FAK inhibitor or CD. 3) In addition, TME induced stabilization of master EMT-related transcription factor (Slug), activation of NF-κB, increased TGF-β1- and p-Smad-2-expression, and FAK signaling pathways. 4) Calebin A treatment, similar to CD, significantly reduced TME-induced NF-κB, FAK and Slug signaling and cell migration in both CRC cell lines as well. 5) Calebin A selectively down-regulated the binding of p65-NF-κB on DNA in the two CRC cells, thereby modulating NF-κB-dependent TME-induced EMT signaling. 6) Finally, TME induced a functional connection between NF-κB and Slug, which could enhance Slug-dependent up-regulation of EMT, whereas Calebin A, similar to CD strongly blocked this association of the two transcription factors, thereby blocking EMT.

It has been repeatedly shown in the recent past that three-dimensional tumor cultures have excellent culture conditions compared to two-dimensional tumor cultures, as these cultures have a set of suitable *in vivo* conditions for tumor cell survival (Luca et al., 2013; Shakibaei et al., 2015; Stankevicius et al., 2017). The alginate-based substrate provides the appropriate 3D microenvironment for tumor cells to proliferate, form typical tumor spheroids and, very importantly, provides conditions for tumor cells to migrate through the alginate substrate and eventually metastasize. Interestingly, the alginate bead culture is solubilized readily and the living CRC tumor cells can be tested as to their multiple properties in the early steps of proliferation and metastasis further supporting the TME in a manner comparable to *in vivo* (Shakibaei et al., 2015; Buhrmann et al., 2016).

Increasing evidences indicate that there is a direct strong link between inflammation, inflammatory mediators and tumorigenesis. However, the mechanisms by which TME and inflammation enable tumor progression remain poorly understood. It is now recognized that inflammation-induced migration, EMT and metastasis of tumor cells in the TME is a major target of many clinical challenges in tumor treatment

(Cordon-Cardo and Prives, 1999; Coussens and Werb, 2002; López-Novoa and Nieto, 2009). In this report, we have shown in invasion assays that the TME induced invasion of cells and this was significantly down-regulated through Calebin A, similar to CD or FAK-inhibitor. This similar mode of action of Calebin A and CD is due to an important target in the cell, namely cytoskeletal proteins, which are critical and essential for cancer cell proliferation, migration and invasion and thus EMT (Tai et al., 2015). This target of Calebin A was further confirmed by the fact that Calebin A also simultaneously inhibits the enzyme responsible for polymerization of cytoskeletal proteins, FAK. In addition, focal contacts are membrane-bound complex structures that create connection among the cytoskeleton and the ECM. FAK plays an essential role as an integrator of biochemical signals and mechanical stimuli and also dominates in active and motile cells. Furthermore, FAK found to have an integral function in controlling DNA synthesis and cytoskeletal organization, thereby regulating cell division, proliferation, and migration (Zhao et al., 1998; Oktay et al., 1999). However, it has been shown that high expression of FAK and FAK signal transduction pathways in various tumor cells and tumor stem cells results in anti-apoptotic effects and tumor cell survival. Indeed, FAK plays a fundamental role in modulating tumor aggressiveness and metastasis, and high FAK expression is always associated with a negative prognosis of tumors (Hungerford et al., 1996; Almeida et al., 2000; Sonoda et al., 2000; Kong et al., 2015; Tai et al., 2015).

We also demonstrated that the transcription factor NF-κB is one of the important stimulated inflammatory down-stream signaling pathways for TME. Similar to the CD pathway, Calebin A has a specific modulatory effect against TME-promoted activation of NF-κB pathway as well as NF-κB-regulated proteins in CRC cells. This finding and our previous studies are consistent with previous research demonstrating that NF-κB becomes activated in tumor cells in responding to diverse groups of pro-inflammatory substances, including cytokines and TME, and inhibits apoptosis (Baeuerle and Baichwal, 1997; Buhrmann et al., 2019; Buhrmann et al., 2020a). After its translocation into the nucleus, it associates with the targeted sequence in DNA, leading in turn to gene transcription. It has already been reported that NF-κB is a promising target for the development of anti-tumor drugs (Van Antwerp et al., 1996; Wang et al., 1996). Indeed, TME-induced NF-κB, is known to be among the major mediators of cancer progression, and thus proliferation and EMT. Thus, NF-κB is associated with tumor metastasis (Pikarsky et al., 2004; Wu and Zhou, 2010). Therefore, compounds like Calebin A, which can block the phosphorylation of NF-κB, have the ability to block tumor promotion and metastasis.

Our data further showed that cytokine transforming growth factor-β1 (TGF-β1) and simultaneously, p-Smad-2 expression was significantly up-regulated in TME in both CRC cells. Indeed, it has been previously reported that TME-induced TGF-β1 expression in CRC cells in a Smad2-dependent process (Jang et al., 2015), and it is known to play a major role in TGF-β1-induced tumor progression, migration, and EMT (Li et al., 2014). TGF-β1 induces the signaling pathway for EMT *via* a heteromeric complex of two transmembrane serine/threonine kinase receptors type I and type-II. This leads to phosphorylation of Smad2 and 3 and 4, whereupon these trimers are transported to the nucleus, where they associate with transcription factors such as Snail and Slug to repress the expression of epithelial markers and induce the expression of mesenchymal markers at the mRNA level (Zhang et al., 2018). Moreover, TGF-β1 has been shown to promote tumor cell progression and metastasis mainly through EMT and EMT-linked proteins during tumor invasion and metastasis (Buhrmann et al., 2016; Kaowinn et al., 2017).

Interestingly, the concomitant expression of epithelial cell marker (E-cadherin) was markedly decreased and the expression of mesenchymal biomarkers (vimentin and Slug) was markedly increased in the TME. Indeed, down-regulated E-cadherin expression is known to be a specific feature of the EMT process in tumorigenesis (Bendris et al., 2012). Our results clearly show that Calebin A reversed TME-induced changes in the expression of TGF-β1, p-Smad-2, and EMT biomarkers, similar to CD, in a concentration-dependent manner, suggesting that TME-stimulated EMT can be attenuated in CRC cells. Furthermore, available evidence has recently clearly demonstrated that both genetic and epigenetic influences and factors play important roles in silencing E-cadherin expression in various tumor types (Christofori and Semb, 1999; Cheng et al., 2001). Indeed, it has been further reported that there are some inhibitors of E-cadherin such as the Snail family of zinc finger transcription factors. These transcription factors, as well as Slug, have now been shown to be important modulators of EMT and many other important processes *via* the influence on E-cadherin in various tumors (Batlle et al., 2000; Cano et al., 2000; Grooteclaes and Frisch, 2000; Comijn et al., 2001; Perez-Moreno et al., 2001; Blanco et al., 2002). It was further reported and clearly demonstrated that Slug, a major EMT-related transcription factor, has a specific repressive effect on the mouse E-cadherin promoter. Besides, overexpression of Slug in MDCK cells and breast cancer cell lines have been reported to significantly repress endogenous E-cadherin expression, thereby significantly inhibiting cell EMT (invasion and migration) (Hajra et al., 2002; Bolós et al., 2003).

Moreover, our data show that the TME clearly induces the expression of EMT-related transcription factors such as Slug and NF-κB, indicating targeted EMT activation, and they are known to be highly expressed especially in tumor stem cells and invaded tumor cells (Bhat-Nakshatri et al., 2010; Jang et al., 2015), and Calebin A suppressed the TME-induced expression of Slug and NF-κB. Indeed, a large body of literature indicates that TME-induced cytokines and pro-inflammatory signaling may promote tumor cell metastasis and EMT signaling (Virchow, 1881; Coussens and Werb, 2002; de Visser et al., 2006; Medzhitov, 2008; Balkwill, 2009; Buhrmann et al., 2020a).

We demonstrated further that TME strongly augmented CRC cell migration and invasion by triggering the EMT signaling pathway *via* NF-κB-mediated Slug axis stabilization and activation, which plays a critical role in CRC cell metastasis. These results suggest that a synergistic functional interaction of Slug and NF-κB is required for initiation of EMT and migration of tumor cells. However, when the 3D-alginate CRC tumor cells

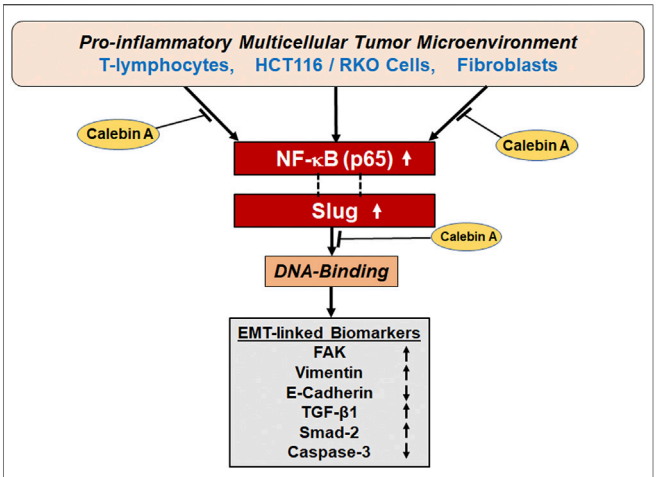

FIGURE 9 | A graphic presentation of the antitumorigenic actions of Calebin A *via* modulation of EMT and Slug/NF-κB axis of colorectal cancer cells in pro-inflammatory multicellular TME.

were treated with Calebin A, similar to CD, NF-κB/Slug-axis-activation was markedly inhibited, EMT-related protein expression was significantly reversed, and TME-stimulated active migration and invasion were dramatically reduced.

CONCLUSION

In conclusion, our results report the first evidence that Calebin A can attenuate the TME-promoted EMT, invasion in CRC cells in 3D-alginate beads, similar to CD or FAK-inhibitor *via* regulation of FAK, EMT biomarkers, and TGF-β1/Smad-2 expression. The inhibitory effect of Calebin A on TME-induced EMT is also associated with suppression of the NF-κB/Slug axis pathway. Thus, as a multitargeted component, Calebin A is a promising therapeutic phytopharmaceutical for the treatment of CRC (**Figure 9**).

DATA AVAILABILITY STATEMENT

The raw data supporting the conclusions of this article will be made available by the authors, without undue reservation, to any qualified researcher.

AUTHOR CONTRIBUTIONS

Conceptualization, CB, AB, AK, and MS; methodology, formal analysis and investigation, CB, AB, BA, PK, and MS; writing—original draft preparation, CB, AB, and MS; writing—review and editing, CH, PK, CB, AB, BA, and MS, supervision, MS; project administration, MS. All authors have read and agreed to the published version of the manuscript.

ACKNOWLEDGMENTS

We thank Sabine Miech, Anna-Lena Mueller and Andreas Eimannsberger for excellent technical assistance. We also thank Sabinsa Corporation (East Windsor, NJ, United States) for providing Calebin A as a generous gift.

SUPPLEMENTARY MATERIAL

The Supplementary Material for this article can be found online at: https://www.frontiersin.org/articles/10.3389/fphar.2021.699842/full#supplementary-material

REFERENCES

Aggarwal, B. B. (2004). Nuclear Factor-Kb. *Cancer Cell* 6, 203–208. doi:10.1016/j.ccr.2004.09.003

Aggarwal, B. B., Yuan, W., Li, S., and Gupta, S. C. (2013). Curcumin-free Turmeric Exhibits Anti-inflammatory and Anticancer Activities: Identification of Novel Components of Turmeric. *Mol. Nutr. Food Res.* 57, 1529–1542. doi:10.1002/mnfr.201200838

Almeida, E. A. C., Ilić, D., Han, Q., Hauck, C. R., Jin, F., Kawakatsu, H., et al. (2000). Matrix Survival Signaling. *J. Cel Biol* 149, 741–754. doi:10.1083/jcb.149.3.741

Baeuerle, P. A., and Baichwal, V. R. (1997). NF-κB as a Frequent Target for Immunosuppressive and Anti-inflammatory Molecules**This Article Was Accepted for Publication on 27 September 1996. *Adv. Immunol.* 65, 111–137. doi:10.1016/s0065-2776(08)60742-7

Balkwill, F. (2009). Tumour Necrosis Factor and Cancer. *Nat. Rev. Cancer* 9, 361–371. doi:10.1038/nrc2628

Batlle, E., Sancho, E., Francí, C., Domínguez, D., Monfar, M., Baulida, J., et al. (2000). The Transcription Factor Snail Is a Repressor of E-Cadherin Gene Expression in Epithelial Tumour Cells. *Nat. Cel Biol* 2, 84–89. doi:10.1038/35000034

Behrens, J., Frixen, U., Schipper, J., Weidner, M., and Birchmeier, W. (1992). Cell Adhesion in Invasion and Metastasis. *Semin. Cell Biol.* 3, 169–178. doi:10.1016/s1043-4682(10)80013-3

Bendris, N., Arsic, N., Lemmers, B., and Blanchard, J. M. (2012). Cyclin A2, Rho GTPases and EMT. *Small GTPases* 3, 225–228. doi:10.4161/sgtp.20791

Bhat-Nakshatri, P., Appaiah, H., Ballas, C., Pick-Franke, P., Goulet, R., Jr., Badve, S., et al. (2010). SLUG/SNAI2 and Tumor Necrosis Factor Generate Breast Cells with CD44+/CD24- Phenotype. *BMC Cancer* 10, 411. doi:10.1186/1471-2407-10-411

Blanco, M. J., Moreno-Bueno, G., Sarrio, D., Locascio, A., Cano, A., Palacios, J., et al. (2002). Correlation of Snail Expression with Histological Grade and Lymph Node Status in Breast Carcinomas. *Oncogene* 21, 3241–3246. doi:10.1038/sj.onc.1205416

Bolós, V., Peinado, H., Pérez-Moreno, M. A., Fraga, M. F., Esteller, M., and Cano, A. (2003). The Transcription Factor Slug Represses E-Cadherin Expression and Induces Epithelial to Mesenchymal Transitions: a Comparison with Snail and E47 Repressors. *J. Cel Sci* 116, 499–511.

Bray, F., Ferlay, J., Soerjomataram, I., Siegel, R. L., Torre, L. A., and Jemal, A. (2018). Global Cancer Statistics 2018: GLOBOCAN Estimates of Incidence and Mortality Worldwide for 36 Cancers in 185 Countries. *CA: A Cancer J. Clin.* 68, 394–424. doi:10.3322/caac.21492

Bray, F., Ferlay, J., Soerjomataram, I., Siegel, R. L., Torre, L. A., and Jemal, A. (2020). Erratum: Global Cancer Statistics 2018: GLOBOCAN Estimates of Incidence and Mortality Worldwide for 36 Cancers in 185 Countries. *CA Cancer J. Clin.* 70, 313. doi:10.3322/caac.21609

Buccafusca, G., Proserpio, I., Tralongo, A. C., Rametta Giuliano, S., and Tralongo, P. (2019). Early Colorectal Cancer: Diagnosis, Treatment and Survivorship Care. *Crit. Rev. Oncology/Hematology* 136, 20–30. doi:10.1016/j.critrevonc.2019.01.023

Buhrmann, C., Kunnumakkara, A. B., Popper, B., Majeed, M., Aggarwal, B. B., and Shakibaei, M. (2020a). Calebin A Potentiates the Effect of 5-FU and TNF-β (Lymphotoxin α) against Human Colorectal Cancer Cells: Potential Role of NF-Kb. *Int. J. Mol. Sci.* 21. doi:10.3390/ijms21072393

Buhrmann, C., Popper, B., Kunnumakkara, A. B., Aggarwal, B. B., and Shakibaei, M. (2019). Evidence that Calebin A, a Component of Curcuma Longa Suppresses NF-B Mediated Proliferation, Invasion and Metastasis of Human Colorectal Cancer Induced by TNF-β (Lymphotoxin). *Nutrients* 11, 2904. doi:10.3390/nu11122904

Buhrmann, C., Shayan, P., Banik, K., Kunnumakkara, A. B., Kubatka, P., Koklesova, L., et al. (2020b). Targeting NF-Kb Signaling by Calebin A, a Compound of Turmeric, in Multicellular Tumor Microenvironment: Potential Role of Apoptosis Induction in CRC Cells. *Biomedicines* 8, 236. doi:10.3390/biomedicines8080236

Buhrmann, C., Shayan, P., Brockmueller, A., and Shakibaei, M. (2020c). Resveratrol Suppresses Cross-Talk between Colorectal Cancer Cells and Stromal Cells in Multicellular Tumor Microenvironment: A Bridge between *In Vitro* and *In Vivo* Tumor Microenvironment Study. *Molecules* 25, 4292. doi:10.3390/molecules25184292

Buhrmann, C., Shayan, P., Goel, A., and Shakibaei, M. (2017). Resveratrol Regulates Colorectal Cancer Cell Invasion by Modulation of Focal Adhesion Molecules. *Nutrients* 9, 1073. doi:10.3390/nu9101073

Buhrmann, C., Shayan, P., Popper, B., Goel, A., and Shakibaei, M. (2016). Sirt1 Is Required for Resveratrol-Mediated Chemopreventive Effects in Colorectal Cancer Cells. *Nutrients* 8, 145. doi:10.3390/nu8030145

Cano, A., Pérez-Moreno, M. A., Rodrigo, I., Locascio, A., Blanco, M. J., Del Barrio, M. G., et al. (2000). The Transcription Factor Snail Controls Epithelial-Mesenchymal Transitions by Repressing E-Cadherin Expression. *Nat. Cell Biol.* 2, 76–83. doi:10.1038/35000025

Cary, L. A., and Guan, J. L. (1999). Focal Adhesion Kinase in Integrin-Mediated Signaling. *Front. Biosci.* 4, D102–D113. doi:10.2741/cary

Cheng, C.-W., Wu, P.-E., Yu, J.-C., Huang, C.-S., Yue, C.-T., Wu, C.-W., et al. (2001). Mechanisms of Inactivation of E-Cadherin in Breast Carcinoma: Modification of the Two-Hit Hypothesis of Tumor Suppressor Gene. *Oncogene* 20, 3814–3823. doi:10.1038/sj.onc.1204505

Cho, Y. B., Lee, W. Y., Song, S. Y., Shin, H. J., Yun, S. H., and Chun, H.-K. (2007). Matrix Metalloproteinase-9 Activity Is Associated with Poor Prognosis in T3-T4 Node-Negative Colorectal Cancer. *Hum. Pathol.* 38, 1603–1610. doi:10.1016/j.humpath.2007.03.018

Christofori, G., and Semb, H. (1999). The Role of the Cell-Adhesion Molecule E-Cadherin as a Tumour-Suppressor Gene. *Trends Biochem. Sci.* 24, 73–76. doi:10.1016/s0968-0004(98)01343-7

Cobaleda, C., Pérez-Caro, M., Vicente-Dueñas, C., and Sánchez-García, I. (2007). Function of the Zinc-Finger Transcription FactorSNAI2in Cancer and Development. *Annu. Rev. Genet.* 41, 41–61. doi:10.1146/annurev.genet.41.110306.130146

Comijn, J., Berx, G., Vermassen, P., Verschueren, K., Van Grunsven, L., Bruyneel, E., et al. (2001). The Two-Handed E Box Binding Zinc finger Protein SIP1 Downregulates E-Cadherin and Induces Invasion. *Mol. Cel.* 7, 1267–1278. doi:10.1016/s1097-2765(01)00260-x

Cordon-Cardo, C., and Prives, C. (1999). At the Crossroads of Inflammation and Tumorigenesis. *J. Exp. Med.* 190, 1367–1370. doi:10.1084/jem.190.10.1367

Coussens, L. M., and Werb, Z. (2002). Inflammation and Cancer. *Nature* 420, 860–867. doi:10.1038/nature01322

De Visser, K. E., Eichten, A., and Coussens, L. M. (2006). Paradoxical Roles of the Immune System during Cancer Development. *Nat. Rev. Cancer* 6, 24–37. doi:10.1038/nrc1782

Dekker, E., Tanis, P. J., Vleugels, J. L. A., Kasi, P. M., and Wallace, M. B. (2019). Colorectal Cancer. *The Lancet* 394, 1467–1480. doi:10.1016/s0140-6736(19)32319-0

Del Barrio, M. G., and Nieto, M. A. (2002). Overexpression of Snail Family Members Highlights Their Ability to Promote Chick Neural Crest Formation. *Development* 129, 1583–1593. doi:10.1242/dev.129.7.1583

Derynck, R., and Akhurst, R. J. (2007). Differentiation Plasticity Regulated by TGF-β Family Proteins in Development and Disease. *Nat. Cel Biol* 9, 1000–1004. doi:10.1038/ncb434

Elinav, E., Nowarski, R., Thaiss, C. A., Hu, B., Jin, C., and Flavell, R. A. (2013). Inflammation-induced Cancer: Crosstalk between Tumours, Immune Cells and Microorganisms. *Nat. Rev. Cancer* 13, 759–771. doi:10.1038/nrc3611

Ghosh, S., May, M. J., and Kopp, E. B. (1998). NF-Kb and REL PROTEINS: Evolutionarily Conserved Mediators of Immune Responses. *Annu. Rev. Immunol.* 16, 225–260. doi:10.1146/annurev.immunol.16.1.225

Grooteclaes, M. L., and Frisch, S. M. (2000). Evidence for a Function of CtBP in Epithelial Gene Regulation and Anoikis. *Oncogene* 19, 3823–3828. doi:10.1038/sj.onc.1203721

Guo, S., and Deng, C.-X. (2018). Effect of Stromal Cells in Tumor Microenvironment on Metastasis Initiation. *Int. J. Biol. Sci.* 14, 2083–2093. doi:10.7150/ijbs.25720

Hajra, K. M., Chen, D. Y., and Fearon, E. R. (2002). The SLUG Zinc-finger Protein Represses E-Cadherin in Breast Cancer. *Cancer Res.* 62, 1613–1618.

Hungerford, J. E., Compton, M. T., Matter, M. L., Hoffstrom, B. G., and Otey, C. A. (1996). Inhibition of pp125FAK in Cultured Fibroblasts Results in Apoptosis. *J. Cell Biol.* 135, 1383–1390. doi:10.1083/jcb.135.5.1383

Jang, M. H., Kim, H. J., Kim, E. J., Chung, Y. R., and Park, S. Y. (2015). Expression of Epithelial-Mesenchymal Transition-Related Markers in Triple-Negative Breast Cancer: ZEB1 as a Potential Biomarker for Poor Clinical Outcome. *Hum. Pathol.* 46, 1267–1274. doi:10.1016/j.humpath.2015.05.010

Jing, Y., Han, Z., Zhang, S., Liu, Y., and Wei, L. (2011). Epithelial-Mesenchymal Transition in Tumor Microenvironment. *Cell Biosci.* 1, 29. doi:10.1186/2045-3701-1-29

Kalluri, R., and Weinberg, R. A. (2009). The Basics of Epithelial-Mesenchymal Transition. *J. Clin. Invest.* 119, 1420–1428. doi:10.1172/jci39104

Kaowinn, S., Kim, J., Lee, J., Shin, D. H., Kang, C.-D., Kim, D.-K., et al. (2017). Cancer Upregulated Gene 2 Induces Epithelial-Mesenchymal Transition of Human Lung Cancer Cells *via* TGF-β Signaling. *Oncotarget* 8, 5092–5110. doi:10.18632/oncotarget.13867

Kong, D., Chen, F., and Sima, N. (2015). Inhibition of Focal Adhesion Kinase Induces Apoptosis in Bladder Cancer Cells *via* Src and the Phosphatidylinositol 3-kinase/Akt Pathway. *Exp. Ther. Med.* 10, 1725–1731. doi:10.3892/etm.2015.2745

Labonne, C., and Bronner-Fraser, M. (2000). Snail-related Transcriptional Repressors Are Required in Xenopus for Both the Induction of the Neural Crest and its Subsequent Migration. *Develop. Biol.* 221, 195–205. doi:10.1006/dbio.2000.9609

Li, N., Xu, H., Fan, K., Liu, X., Qi, J., Zhao, C., et al. (2014). Altered β1,6-GlcNAc Branched N -glycans Impair TGF-β-mediated Epithelial-to-Mesenchymal Transition through Smad Signalling Pathway in Human Lung Cancer. *J. Cell. Mol. Med.* 18, 1975–1991. doi:10.1111/jcmm.12331

Lind, D. S., Hochwald, S. N., Malaty, J., Rekkas, S., Hebig, P., Mishra, G., et al. (2001). Nuclear Factor-Kb Is Upregulated in Colorectal Cancer. *Surgery* 130, 363–369. doi:10.1067/msy.2001.116672

López-Novoa, J. M., and Nieto, M. A. (2009). Inflammation and EMT: an alliance towards Organ Fibrosis and Cancer Progression. *EMBO Mol. Med.* 1, 303–314. doi:10.1002/emmm.200900043

Luca, A. C., Mersch, S., Deenen, R., Schmidt, S., Messner, I., Schäfer, K. L., et al. (2013). Impact of the 3D Microenvironment on Phenotype, Gene Expression, and EGFR Inhibition of Colorectal Cancer Cell Lines. *PLoS One* 8, e59689. doi:10.1371/journal.pone.0059689

Mani, S. A., Guo, W., Liao, M.-J., Eaton, E. N., Ayyanan, A., Zhou, A. Y., et al. (2008). The Epithelial-Mesenchymal Transition Generates Cells with Properties of Stem Cells. *Cell* 133, 704–715. doi:10.1016/j.cell.2008.03.027

Martin, T. A. (2014). The Role of Tight Junctions in Cancer Metastasis. *Semin. Cell Develop. Biol.* 36, 224–231. doi:10.1016/j.semcdb.2014.09.008

Massagué, J. (2000). How Cells Read TGF-β Signals. *Nat. Rev. Mol. Cell Biol.* 1, 169–178. doi:10.1038/35043051

Mauri, G., Sartore-Bianchi, A., Russo, A. G., Marsoni, S., Bardelli, A., and Siena, S. (2019). Early-onset Colorectal Cancer in Young Individuals. *Mol. Oncol.* 13, 109–131. doi:10.1002/1878-0261.12417

Medzhitov, R. (2008). Origin and Physiological Roles of Inflammation. *Nature* 454, 428–435. doi:10.1038/nature07201

Nair, A., Amalraj, A., Jacob, J., Kunnumakkara, A. B., and Gopi, S. (2019). Non-Curcuminoids from Turmeric and Their Potential in Cancer Therapy and Anticancer Drug Delivery Formulations. *Biomolecules* 9, 13. doi:10.3390/biom9010013

Nieto, M. A. (2002). The Snail Superfamily of Zinc-finger Transcription Factors. *Nat. Rev. Mol. Cel Biol.* 3, 155–166. doi:10.1038/nrm757

Oktay, M., Wary, K. K., Dans, M., Birge, R. B., and Giancotti, F. G. (1999). Integrin-mediated Activation of Focal Adhesion Kinase Is Required for Signaling to Jun

NH2-terminal Kinase and Progression through the G1 Phase of the Cell Cycle. *J. Cell Biol.* 145, 1461–1470. doi:10.1083/jcb.145.7.1461

Park, S.-Y., and Kim, D. S. H. L. (2002). Discovery of Natural Products fromCurcumalongathat Protect Cells from Beta-Amyloid Insult: A Drug Discovery Effort against Alzheimer's Disease. *J. Nat. Prod.* 65, 1227–1231. doi:10.1021/np010039x

Pérez-Moreno, M. A., Locascio, A., Rodrigo, I., Dhondt, G., Portillo, F., Nieto, M. A., et al. (2001). A New Role for E12/E47 in the Repression ofE-Cadherin Expression and Epithelial-Mesenchymal Transitions. *J. Biol. Chem.* 276, 27424–27431. doi:10.1074/jbc.m100827200

Pikarsky, E., Porat, R. M., Stein, I., Abramovitch, R., Amit, S., Kasem, S., et al. (2004). NF-κB Functions as a Tumour Promoter in Inflammation-Associated Cancer. *Nature* 431, 461–466. doi:10.1038/nature02924

Polyak, K., and Weinberg, R. A. (2009). Transitions between Epithelial and Mesenchymal States: Acquisition of Malignant and Stem Cell Traits. *Nat. Rev. Cancer* 9, 265–273. doi:10.1038/nrc2620

Prieto-García, E., Díaz-García, C. V., García-Ruiz, I., and Agulló-Ortuño, M. T. (2017). Epithelial-to-mesenchymal Transition in Tumor Progression. *Med. Oncol.* 34, 122. doi:10.1007/s12032-017-0980-8

Schlaepfer, D. D., Hauck, C. R., and Sieg, D. J. (1999). Signaling through Focal Adhesion Kinase. *Prog. Biophys. Mol. Biol.* 71, 435–478. doi:10.1016/s0079-6107(98)00052-2

Seguin, L., Desgrosellier, J. S., Weis, S. M., and Cheresh, D. A. (2015). Integrins and Cancer: Regulators of Cancer Stemness, Metastasis, and Drug Resistance. *Trends Cell Biol.* 25, 234–240. doi:10.1016/j.tcb.2014.12.006

Shakibaei, M., and De Souza, P. (1997). Differentiation of Mesenchymal Limb Bud Cells to Chondrocytes in Alginate Beads. *Cell Biol. Int.* 21, 75–86. doi:10.1006/cbir.1996.0119

Shakibaei, M., Kraehe, P., Popper, B., Shayan, P., Goel, A., and Buhrmann, C. (2015). Curcumin Potentiates Antitumor Activity of 5-fluorouracil in a 3D Alginate Tumor Microenvironment of Colorectal Cancer. *BMC Cancer* 15, 250. doi:10.1186/s12885-015-1291-0

Shakibaei, M., Shayan, P., Busch, F., Aldinger, C., Buhrmann, C., Lueders, C., et al. (2012). Resveratrol Mediated Modulation of Sirt-1/Runx2 Promotes Osteogenic Differentiation of Mesenchymal Stem Cells: Potential Role of Runx2 Deacetylation. *PLoS One* 7, e35712. doi:10.1371/journal.pone.0035712

Siegel, P. M., and Massagué, J. (2003). Cytostatic and Apoptotic Actions of TGF-β in Homeostasis and Cancer. *Nat. Rev. Cancer* 3, 807–820. doi:10.1038/nrc1208

Siegel, R. L., Miller, K. D., Goding Sauer, A., Fedewa, S. A., Butterly, L. F., Anderson, J. C., et al. (2020). Colorectal Cancer Statistics, 2020. *CA A. Cancer J. Clin.* 70, 145–164. doi:10.3322/caac.21601

Sonoda, Y., Matsumoto, Y., Funakoshi, M., Yamamoto, D., Hanks, S. K., and Kasahara, T. (2000). Anti-apoptotic Role of Focal Adhesion Kinase (FAK). *J. Biol. Chem.* 275, 16309–16315. doi:10.1074/jbc.275.21.16309

Soria, G., Ofri-Shahak, M., Haas, I., Yaal-Hahoshen, N., Leider-Trejo, L., Leibovich-Rivkin, T., et al. (2011). Inflammatory Mediators in Breast Cancer: Coordinated Expression of TNFα & IL-1β with CCL2 & CCL5 and Effects on Epithelial-To-Mesenchymal Transition. *BMC Cancer* 11, 130. doi:10.1186/1471-2407-11-130

Stankevicius, V., Kunigenas, L., Stankunas, E., Kuodyte, K., Strainiene, E., Cicenas, J., et al. (2017). The Expression of Cancer Stem Cell Markers in Human Colorectal Carcinoma Cells in a Microenvironment Dependent Manner. *Biochem. Biophys. Res. Commun.* 484, 726–733. doi:10.1016/j.bbrc.2017.01.111

Stetler-Stevenson, W. G., Liotta, L. A., and Kleiner, D. E., Jr. (1993). Extracellular Matrix 6: Role of Matrix Metalloproteinases in Tumor Invasion and Metastasis. *Faseb J* 7, 1434–1441. doi:10.1096/fasebj.7.15.8262328

Sutnar, A., Pesta, M., Liska, V., Treska, V., Skalicky, T., Kormunda, S., et al. (2007). Clinical Relevance of the Expression of mRNA of MMP-7, MMP-9, TIMP-1, TIMP-2 and CEA Tissue Samples from Colorectal Liver Metastases. *Tumor Biol.* 28, 247–252. doi:10.1159/000110897

Tai, Y. L., Chen, L. C., and Shen, T. L. (2015). Emerging Roles of Focal Adhesion Kinase in Cancer. *Biomed. Res. Int.* 2015, 690690. doi:10.1155/2015/690690

Tamura, G., Yin, J., Wang, S., Fleisher, A. S., Zou, T., Abraham, J. M., et al. (2000). E-cadherin Gene Promoter Hypermethylation in Primary Human Gastric Carcinomas. *J. Natl. Cancer Inst.* 92, 569–573. doi:10.1093/jnci/92.7.569

Tepass, U., Truong, K., Godt, D., Ikura, M., and Peifer, M. (2000). Cadherins in Embryonic and Neural Morphogenesis. *Nat. Rev. Mol. Cell Biol.* 1, 91–100. doi:10.1038/35040042

Thiery, J. P. (2002). Epithelial-mesenchymal Transitions in Tumour Progression. *Nat. Rev. Cancer* 2, 442–454. doi:10.1038/nrc822

Van Antwerp, D. J., Martin, S. J., Kafri, T., Green, D. R., and Verma, I. M. (1996). Suppression of TNF-Alpha -Induced Apoptosis by NF-Kappa B. *Science* 274, 787–789. doi:10.1126/science.274.5288.787

Virchow, R. (1881). An Address on the Value of Pathological Experiments. *Bmj* 2, 198–203. doi:10.1136/bmj.2.1075.198

Wang, C.-Y., Mayo, M. W., and Baldwin, A. S., Jr. (1996). TNF- and Cancer Therapy-Induced Apoptosis: Potentiation by Inhibition of NF-Kappa B. *Science* 274, 784–787. doi:10.1126/science.274.5288.784

Wu, Y., and Zhou, B. P. (2010). TNF-α/NF-κB/Snail Pathway in Cancer Cell Migration and Invasion. *Br. J. Cancer* 102, 639–644. doi:10.1038/sj.bjc.6605530

Yoshiura, K., Kanai, Y., Ochiai, A., Shimoyama, Y., Sugimura, T., and Hirohashi, S. (1995). Silencing of the E-Cadherin Invasion-Suppressor Gene by CpG Methylation in Human Carcinomas. *Proc. Natl. Acad. Sci.* 92, 7416–7419. doi:10.1073/pnas.92.16.7416

Zeng, Y., Qiu, F., Takahashi, K., Liang, J., Qu, G., and Yao, X. (2007). New Sesquiterpenes and Calebin Derivatives from Curcuma Longa. *Chem. Pharm. Bull.* 55, 940–943. doi:10.1248/cpb.55.940

Zhang, Q., Helfand, B. T., Jang, T. L., Zhu, L. J., Chen, L., Yang, X. J., et al. (2009). Nuclear Factor-Kb-Mediated Transforming Growth Factor-β-Induced Expression of Vimentin Is an Independent Predictor of Biochemical Recurrence after Radical Prostatectomy. *Clin. Cancer Res.* 15, 3557–3567. doi:10.1158/1078-0432.ccr-08-1656

Zhang, X., Zhang, P., Shao, M., Zang, X., Zhang, J., Mao, F., et al. (2018). SALL4 Activates TGF-β/SMAD Signaling Pathway to Induce EMT and Promote Gastric Cancer Metastasis. *Cmar* 10, 4459–4470. doi:10.2147/cmar.s177373

Zhao, J.-H., Reiske, H., and Guan, J.-L. (1998). Regulation of the Cell Cycle by Focal Adhesion Kinase. *J. Cell Biol.* 143, 1997–2008. doi:10.1083/jcb.143.7.1997

Conflict of Interest: The authors declare that the research was conducted in the absence of any commercial or financial relationships that could be construed as a potential conflict of interest.

frontiers in Oncology

SYSTEMATIC REVIEW
published: 04 August 2021
doi: 10.3389/fonc.2021.632168

Efficacy and Safety of *Astragalus*-Containing Traditional Chinese Medicine Combined With Platinum-Based Chemotherapy in Advanced Gastric Cancer: A Systematic Review and Meta-Analysis

Mengqi Cheng[1†], Jiaqi Hu[2†], Yuwei Zhao[2†], Juling Jiang[1], Runzhi Qi[1], Shuntai Chen[1,2], Yaoyuan Li[1], Honggang Zheng[1], Rui Liu[1], Qiujun Guo[1], Xing Zhang[1], Yinggang Qin[1] and Baojin Hua[1*]*

[1] Department of Oncology, Guang'anmen Hospital, China Academy of Chinese Medical Sciences, Beijing, China,
[2] Graduate School, Beijing University of Chinese Medicine, Beijing, China

Background: *Astragalus*-containing traditional Chinese medicine (TCM) is widely used as adjunctive treatment to platinum-based chemotherapy (PBC) in patients with advanced gastric cancer (AGC) in China. However, evidence regarding its efficacy remains limited. This study aimed to evaluate the efficacy and safety of *Astragalus*-containing TCM combined with PBC in AGC treatment.

Methods: We searched for literature (up to July 19, 2020) in eight electronic databases. The included studies were reviewed by two researchers. The main outcomes were the objective response rate (ORR), disease control rate (DCR), survival rate, quality of life (QOL), adverse drug reactions (ADRs), and peripheral blood lymphocyte levels. The effect estimate of interest was the risk ratio (RR) or mean difference (MD) with 95% confidence intervals (CIs). Trial sequential analysis (TSA) was used to detect the robustness of the primary outcome and to calculate the required information size (RIS). Certainty of the evidence was assessed using the GRADE profiler.

Results: Results based on available literature showed that, compared with patients treated with PBC alone, those treated with *Astragalus*-containing TCM had a better ORR (RR: 1.24, 95% CI: 1.15–1.34, P < 0.00001), DCR (RR: 1.10, 95% CI: 1.06–1.14, P < 0.00001), 1-year survival rate (RR: 1.41, 95% CI: 1.09–1.82, P = 0.009), 2-year survival rate (RR: 3.13, 95% CI: 1.80–5.46, P < 0.0001), and QOL (RR: 2.03, 95% CI: 1.70–2.43, P < 0.00001 and MD: 12.39, 95% CI: 5.48–19.30, P = 0.0004); higher proportions of $CD3^+$ T cells and $CD3^+$ $CD4^+$ T cells; higher ratio of $CD4^+/CD8^+$ T cells; nature killer cells; and lower incidence of ADRs. Subgroup analysis showed that both oral and injection administration of *Astragalus*-containing TCM increased tumor response. Whether treatment duration was ≥8 weeks or <8 weeks, *Astragalus*-containing TCM could

Edited by:
Youhua Xu,
Macau University of Science and Technology, SAR China

Reviewed by:
Qingmin Sun,
Affiliated Hospital of Nanjing University of Chinese Medicine, China
Tingting Zhao,
Macau University of Science and Technology, SAR China

***Correspondence:**
Baojin Hua
huabaojinxs@126.com
Yinggang Qin
theoldq@126.com

[†]These authors have contributed equally to this work and share first authorship

Specialty section:
This article was submitted to Pharmacology of Anti-Cancer Drugs, a section of the journal Frontiers in Oncology

Received: *22 November 2020*
Accepted: *12 July 2021*
Published: *04 August 2021*

Citation:
Cheng M, Hu J, Zhao Y, Jiang J, Qi R, Chen S, Li Y, Zheng H, Liu R, Guo Q, Zhang X, Qin Y and Hua B (2021) Efficacy and Safety of Astragalus-Containing Traditional Chinese Medicine Combined With Platinum-Based Chemotherapy in Advanced Gastric Cancer: A Systematic Review and Meta-Analysis. Front. Oncol. 11:632168. doi: 10.3389/fonc.2021.632168

increase tumor response in AGC patients. Furthermore, *Astragalus*-containing TCM combined with oxaliplatin-based chemotherapy could increase the ORR and DCR; when with cisplatin, it could only increase the ORR.

Conclusion: Current low to moderate evidence revealed that *Astragalus*-containing TCM combined with PBC had better efficacy and less side effects in the treatment of AGC; however, more high-quality randomized studies are warranted.

Systematic Review Registration: PROSPERO, identifier CRD42020203486.

Keywords: *Astragalus*, platinum, advanced gastric cancer, traditional Chinese medicine, meta-analysis

INTRODUCTION

As a global health problem, gastric cancer remains the third most common cause of cancer-related death worldwide accounting for 8.2% of cancer-related deaths in 2018, equating to 1 in every 12 deaths (1). Unfortunately, a considerable number of patients with gastric cancer are diagnosed at advanced stage, meaning that the opportunity for surgical treatment has been lost (2). Platinum-based chemotherapy (PBC) is widely used in the treatment of advanced gastric cancer (AGC), and platinum (cisplatin or oxaliplatin) plus fluoropyrimidine regimen is suggested as the first-line chemotherapy regimen according to the National Comprehensive Cancer Network (NCCN) guidelines (version 2.2020) (3, 4). However, in clinical practice, the adverse events of and chemotherapy resistance to PBC have exposed the limitations of PBC, prompting researchers and clinicians to pay more attention to the study of alternative and complementary therapies.

In China, Chinese herb medicine used in Traditional Chinese Medicine (TCM) is frequently combined with chemotherapy in the treatment of AGC; specifically, it has been shown to improve the efficacy of chemotherapy and reduce its side effects (5–7). *Astragalus* (also called *Huangqi* in Chinese) is sourced from the leguminous plant *Astragalus membranaceus (Fisch.)*, which has been recognized as one of the primary tonic herbs in TCM over 2,000 years and is widely used in the treatment of malignant tumors in China.

Many researchers have examined the effectiveness and safety of *Astragalus*-containing TCM combined with PBC in the treatment of colorectal cancer and non-small-cell lung cancer (8–11). However, the effects of *Astragalus*-containing Chinese medicines plus PBC in AGC treatment have not been systematically assessed.

In recent decades, a large number of trials on the use of *Astragalus*-containing Chinese herbal therapies combined with PBC for AGC treatment have been published. This study aimed to provide a systematic analysis of the results obtained in these studies in order to understand the safety and efficacy of *Astragalus*-containing TCM in combination with PBC during AGC treatment. To do so, we performed a meta-analysis of the available studies on *Astragalus*-containing TCM combined with PBC in order to further clinically investigate the effects on safety and efficacy.

Abbreviations: TCM, traditional Chinese medicine; AGC, advanced gastric cancer; PBC, platinum-based chemotherapy; RCTs, randomized controlled trials; RR, risk ratio; MD, mean difference; CI, confidence interval; TSA, trial sequential analysis; GRADE, grading of recommendations assessment, development, and evaluation; RIS, required information size; ORR, objective response rate; DCR, disease control rate; QOL, quality of life; ADRs, adverse drug reactions.

METHODS

This study was conducted following the Preferred Reporting Items for Systematic Reviews and Meta-Analyses (PRISMA) guidelines. The protocol has been registered on PROSPERO, under the number CRD42020203486.

Search Strategy

PubMed, EMBASE, Cochrane Central Register of Controlled Trials (CENTRAL), clinicaltrials.gov, Chinese Biomedical Literature database (CBM), China Academic Journals (CNKI), Chinese Science and Technology Journals (CQVIP), and Wanfang Database were searched systematically for all articles published from inception to July 19, 2020. The following search terms were used: ([gastr* OR stomach* OR digest* OR epigastr*] AND [carcin* OR cancer* OR neoplas* OR tumour* OR tumor* OR growth* OR adenocarcin* OR malig*]) AND (*Astragalus* OR radix astragali OR huang qi OR huangqi). All retrievals were implemented using MeSH and free words (the detailed search strategy is available in **Supplementary 1**). The languages were restricted to Chinese and English.

Inclusion and Exclusion Criteria

Inclusion criteria: (1) All studies were randomized controlled trials (RCTs) or quasi-RCTs. (2) Patients who had TNM stage III-IV AGC and were diagnosed using the histopathological and cytological diagnostic criteria. (3) The experimental group of patients was given *Astragalus*-based herbal therapy combined with PBC. Any form of *Astragalus* (Huang qi) preparation, including water decoction, extracts, granules, or injection, among other forms, regardless of administration route, were included. The control group of patients was given PBC alone. (4) Outcomes were identified as the tumor response, survival

rate, QOL, ADRs, and peripheral blood lymphocytes levels, and at least one of these outcomes was reported; and (5) for repeated publication studies, we selected the data with the most comprehensive report and the longest follow-up.

Exclusion Criteria: (1) Patients who underwent radiotherapy, chemotherapy, or other antitumor therapy within 1 month before treatment; (2) patients with severe infection, other malignant tumors, and severe medical diseases; (3) the prescription of *Astragalus*-based herbal therapy was not fixed; (4) studies for which the data could not be extracted; and (5) the baseline data of patients in two groups were not comparable.

Study Selection and Data Extraction

Studies were selected independently by two reviewers according to the above inclusion and exclusion criteria. Two reviewers independently extracted the data. Disagreements were discussed with and resolved by the third reviewer. The following data were extracted: first author (year of publication), sample sizes, gender, age, study arm, drug delivery, treatment duration, follow-up time, outcomes, and criteria. Data presented graphically were extracted using WebPlotDigitizer (https://automeris.io/WebPlotDigitizer).

Risk of Bias Assessment

Two reviewers independently assessed the quality of the selected studies according to the Cochrane Collaboration's tool for RCTs. Items were sorted into three categories: low risk of bias, unclear bias, and high risk of bias. The following characteristics were evaluated: Random sequence generation (selection bias), allocation concealment (selection bias), blinding of participants and personnel (performance bias), incomplete outcome data (attrition bias), selective reporting (reporting bias), and other biases. Results from these evaluations were graphed and assessed using Review Manager 5.3.

Outcome Definition

Tumor response and the survival rate were the main outcomes. Tumor response, containing the objective response rate (ORR) and disease control rate (DCR), was based on the World Health Organization (WHO) criteria (12) or Response Evaluation Criteria in Solid Tumors (RECIST) (13). Complete response (CR), partial response (PR), stable disease (SD), and progressive disease (PD) were used as indicators. The CR plus PR rates were as equal to the ORR; the CR plus PR, and SD rates were equal to the DCR.

Quality of life (QOL), adverse drug reactions (ADRs), and peripheral blood lymphocytes levels were the second outcomes. QOL was considered improved when the Karnofsky Performance Status (KPS) score was 10 points higher after treatment than before treatment. ADRs were accessed by measuring hematotoxicity (neutropenia, anemia, and thrombocytopenia), gastrointestinal toxicity (nausea and vomiting, diarrhea), hepatic and renal dysfunction, neurotoxicity, alopecia, and stomatitis, based on WHO criteria (12) or NCI Common Terminology Criteria for Adverse Events (CTCAE) (14). The peripheral blood lymphocyte levels were evaluated by measuring the T-lymphocyte subsets such as the percentage of $CD3^+$, $CD3^+CD4^+$, and $CD3^+CD8^+$ T cells, as well as the $CD4^+/CD8^+$ T cells ratio and the percentage of natural killer (NK) cells.

Data Analysis

The Review Manager 5.3 and Stata V16.0 software were used in this study. The risk ratio (RR) and 95% confidence interval (CI) were used to assess dichotomous variables, while mean difference (MD) with a 95% CI was used to assess continuous variables. Statistical heterogeneity was measured by the I^2 statistic and the Chi-squared test. The summary RR, MD, and 95% CI were estimated by a random-effect model. P values were used to calculate outcomes, and $P < 0.05$ was considered statistically significant. The funnel plots and Egger's tests were applied to examine potential publication bias when studies ≥10. In accordance with the drug delivery of *Astragalus*-containing TCM, PBC regimen, and treatment duration, subgroup analyses were performed to reveal the clinical heterogeneity and its influence on tumor response.

Trial sequential analysis software (TSA, version 0.9.5.10 beta) was used to determine the robustness of main outcomes and to calculate the required information size (RIS) in the meta-analysis (15). If the cumulative Z-curve stretched across the monitoring boundaries, a sufficient level of evidence for the intervention effect may have been reached and no further studies were needed. Type I and II errors were needed to perform the TSA. In this review, the RIS was estimated using $\alpha = 0.05$ (two sided) with power equal to 80%.

Evidence Quality Assessment

Two reviewers independently assessed the quality of the evidence for each outcome using the GRADE approach (16). Disagreements were discussed with and resolved by the third reviewer. The quality of evidence was classified as being high, moderate, low, and very low. The quality was downgraded according to the following five domains: (1) risk of bias (if most trials showed an unclear risk, with or without high risk, but the results had good robustness, the evidence was rated down by only one level; if the results showed poor robustness, the evidence was downgraded by two levels); (2) inconsistency (statistical heterogeneity was present and the results of the sensitivity analysis had poor robustness); (3) indirectness (the participants, intervention, outcomes, or comparison of the study did not meet the objectives of this study); (4) imprecision (the sample size for each outcome was fewer than 300 cases); and (5) reporting bias (publication bias). Except for the risk of bias, evidence was downgraded by one level.

RESULTS

Search Results

A total of 2,873 records were identified through database searching. All records were screened by two reviewers with a three-step process. Firstly, we screened the titles and removed duplicates, after which 1,829 records remained. Secondly, we

included 227 full texts by reading the title or abstract. Thirdly, we evaluated the full texts and excluded 192 trials by following the inclusion and exclusion criteria. In the end, 35 eligible studies involving 2,670 stage III/IV AGC patients were included in our study (**Figure 1**).

Characteristics of the Included Studies

The characteristic information of the included studies is shown in **Table 1**. All 35 studies were single-centered and conducted in China. There were 1,572 male and 1,098 female patients, and sample sizes ranged from 30 to 240. Eighteen studies used the oral TCM administration, and 17 studies used commercial TCM injections. All clinical trials were designed to use *Astragalus*-containing TCM as the principal drug together with PBC. Follow-up lasted from 4 weeks to 3 years. Twenty trials reported the tumor responses according to the WHO guidelines, and 12 reported them according to RECIST guidelines. Eighteen trials reported the ADRs using WHO criteria, three using NCI CTCAE criteria, and eight using unknown criteria.

Risk of Bias

All 35 studies referred to randomization; however, only eight studies (23, 25, 29, 30, 43, 47, 50, 52) used a random number table to generate a random sequence, one study used a lottery approach (24), and two studies (35, 49) used admission order, which was inappropriate. One study used an envelope method (44) to perform the allocation concealment, while the other studies did not report the method. Only one study mentioned single blinding (25), and none of the studies adequately reported the blinding of the investigators, patients, and outcome assessors. Selective reporting existed in one study (40) that failed to completely report the DCR. One study (20) had a high risk of other bias because it was funded by the industry. The risk of bias for the individual trials is summarized in **Figure 2**.

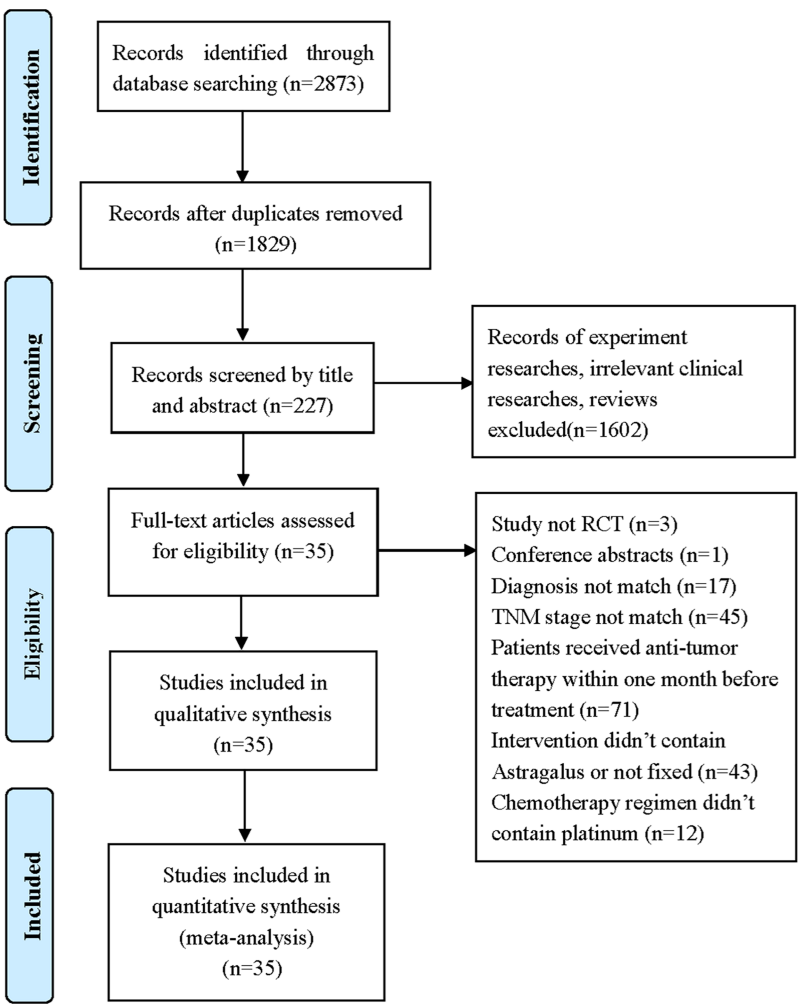

FIGURE 1 | Flow diagram of selection process (17).

TABLE 1 | Characteristics of the included studies.

Study	Advanced gastric cancer (AGC)			Interventions			Fellow up	Criteria	Outcome
	E/C	M/F	TNM stage	*Astragalus*-containing TCM	Drug delivery	Platinum-based regimen			
Yang, J. 2005 (18)	16/16	22/10	IV	*Astragalus*-based formulae: Astragalus, Codonopsis, Atractylodis macrocephala, Poria cocos, Pinellia ternate, Citrus reticulata, Fructus aurantii, Coix seed, Dioscoreae opposita, Hedyotis diffusa, Nightshade, Curcuma zedoary, Rice sprout, Malt, Radix scutellariae, Glycyrrhiza, 300 ml/d, 8w	Orally	5-Fu: 250 mg/m^2, d1–14; OXA: 130 mg/m^2, d1, d8, d15, 28d/C; 2 cycles	8w	WHO, WHO	O1,2,4,5
Gong, L.Y. 2006 (19)	26/30	31/25	IIIB: 17, IV: 9/IIIB: 19, IV: 11	Aidi: Astragalus, Ginseng, Cantharides, Eleutherococcus senticosus, 50 ml/d, 21d/C, 4 cycles	Injection	PTX: 135 mg/m^2, d1; 5-Fu: 500 mg/m^2, d1–5; CF: 100 mg/m^2, d1–5; DDP: 30 mg/m^2, d1–3, 3w/C, 4 cycles	>12m	RECIST, WHO	O1,2,3,5,6
Chen, P. 2007 (20)	64/64	90/38	IV	Cidan Capsule: Astragalus, Curcuma zedoary, Brucea javanica, Pleione bulbocodioides, Semen strychni, Nidus vespae, 5.4 g/d, 28d/C, 3 cycles	Orally	OXA: 100 mg, d1, d8; CF: 50 mg, d1–5; 5-Fu: 0.5–0.75 g, d1–5; 4w/C, 3 cycles	12w	WHO, WHO	O1,2,5
Li, A.M. 2007 (21)	64/64	86/42	III, IV	*Astragalus*-based formulae: Astragalus, Codonopsis, Atractylodis macrocephala, Poria cocos, Radix ophiopogonis, Spatholobus suberctu, Radix salviae miltiorrhizae, Ligustrum lucidum ait, Hedyotis diffusa, 400 ml/d, d1–21, 28d/C, 3 cycles	Orally	DDP: 20 mg/m^2, d1–5; LV: 200 mg/m^2, d1–5; 5-FU: 500 mg/m^2, d1–5; 4w/C, 3 cycles	12w	WHO, WHO	O1,2,5
Wang, L. 2007 (22)	15/15	23/7	IIIB, IV	*Astragalus*-based formulae: Astragalus, Atractylodis macrocephala, Radix pseudostellariae, Noria cocos, Dioscoreae opposita, Pinellia ternate, Citrus reticulata, Coix seed, Galli gigerii endothelium corneum, Hedyotis diffusa, Scutellariae barbatae, Rice sprout, Malt, Glycyrrhiza, 300 ml/d, 8w	Orally	PTX: 135 mg/m^2, d1, d8; OXA: 130 mg/m^2, d1, d8; 5-Fu: 500 mg/m^2, d1–5; 4w/C, 2 cycles	>8w	WHO, WHO	O1,2,4,5
He, Z.Q. 2008 (23)	65/58	68/55	IV	Delisheng: Astragalus, Red ginseng, Arenobufagin, Cantharides, 40 ml/d, 20 d/C, 4–6 cycles	Injection	OXA: 85 mg/m^2, d1; CF: 200 mg/m^2, d1–2; 5-Fu: 400 mg/m^2, d1–2; 5-Fu: 600 mg/m^2, d1–2; 2w/C, 4–6 cycles	Unknow	RECIST, WHO	O1,2,5,6
Liu, L.H. 2009 (24)	30/30	34/26	IIIB: 17, IV: 13/IIIB: 14, IV: 16	Aidi: Astragalus, Ginseng, Cantharides, Eleutherococcus senticosus, 50 ml/d, d1–10, 28d/C, 2 cycles	Injection	PTX: 175 mg/m^2, d1; DDP: 20 mg/m^2, d1–5; 5-Fu: 600 mg/m^2, d1–5; 28d/C, 2 cycles	8w	WHO, WHO	O1,2,4,5
Liu, X.Q. 2009 (25)	30/30	42/18	IV	Kangai: Astragalus, Ginseng, Matrine, 60 ml/d, 10d/C, 2 cycles	Injection	CF: 200 mg/m^2, d1–2; 5-Fu: 2.0 g/m^2,48 h; DOC: 50 mg/m^2, d1; DDP: 25 mg/m^2, d2–3; 14d/C; 2 cycles	4w	RECIST, NCI	O1,2,4,5
Zhu, Y. 2010 (26)	20/20	23/17	III, IV	*Astragalus*-based formulae: Astragalus, Codonopsis, Angelica sinensis, Paeonia lactiflora, Costusroot, Bupleurum, Coix seed, Notoginseng radix, Fructus aurantii, Rhizoma bletillae, Curcuma zedoary, Glycyrrhiza, Radix platycodi, Fritillary bulb, Crotonis fructus, 400 ml/d, 6w	Orally	OXA: 130 mg/m^2, d1; CF: 300 mg, d1–5; 5-Fu: 500 mg, d1–5; 3w/C, 2 cycles	6w–1y	RECIST, WHO	O1,2,3,4,5
Chen, Q.S. 2011 (27)	30/30	37/23	III: 17, IV: 13/III: 19, IV: 11	*Astragalus*-based formulae: Astragalus, Codonopsis, Atractylodis macrocephala, Noria cocos, Ninellia ternate, Ganoderma, Agrimonia pilosa, Prunellae spica, Hedyotis diffusa, Glycyrrhiza, 400 ml/d, 21d/C, 2 cycles	Orally	OXA: 85 mg/m^2, d1; CF: 200 mg/m^2, d1–2; 5-Fu: 400 mg/m^2, d1–2; 5-Fu: 600 mg/m^2, d1–2; 21d/C, 2 cycles	6w–1y	WHO,Un	O1,2,3,4,5,6
Du, C.J. 2011 (28)	120/120	122/118	IV	*Astragalus*-based formulae: Astragalus, Atractylodis macrocephala, Poria cocos, Pinellia ternate, Citrus reticulata, Rhizoma polygonati, Glycyrrhiza, Ligustrum lucidum ait, Sanguisorbae radix, Spatholobus suberctu, Donkey-hide glue, Radix actinidiae, 400 ml/d, 21d/C, 2 cycles	Orally	OXA: 100 mg/m^2, d1; CF: 200 mg/m^2, d1–5; 5-Fu: 500 mg/m^2, d1–5; 21d/C, 2 cycles	6w	RECIST	O1,2
Fan, C.M.	23/28	33/18	IIIA: 8, IIIB: 10, IV: 5/	Aidi: Astragalus, Ginseng, Cantharides, Eleutherococcus senticosus, 50 ml/d,10d/C, 4 cycles	Injection	OXA: 85 mg/m^2, d1; S-1: 80 mg/m^2, d1–14; 21d/C, 4 cycles	>12w	WHO, WHO	O1,2,3,4,5

(Continued)

TABLE 1 | Continued

Study	Advanced gastric cancer (AGC)			Interventions			Fellow up	Criteria	Outcome
	E/C	M/F	TNM stage	*Astragalus*-containing TCM	Drug delivery	Platinum-based regimen			
2011 (29)			IIIA: 10, IIIB: 13, IV:5						
Hu, F.S. 2011 (30)	51/48	69/30	IV	*Astragalus*-based formulae: Astragalus, Codonopsis, Radix pseudostellariae, Atractylodis macrocephala, Poria cocos, Fructus lycii, Ligustrum lucidum ait, Semen cuscutae, Spatholobus suberctu, Paeonia rubra, Curcuma zedoary, Polyphylla, Hedyotis diffusa, Radix actinidiae, 400 ml/d, 21d/C, 3 cycles	Orally	CAP: 1,000 mg/m^2, d1–14; OXA: 130 mg/m^2, d1; 21d/C, 3 cycles	9w	WHO, WHO	O1,2,4,5,6
Ren, Y.Z. 2012 (31)	33/32	30/35	IV	Shenqi Fuzheng: Astragalus, Codonopsis, 250 ml/d, 14d/C, 3 cycles	Injection	OXA: 85 mg/m^2, d1; CF: 300 mg/m^2, d1–2; 5-Fu: 400 mg/m^2, d1–2; 5-Fu: 600 mg/m^2, d1–2; 2w/C, 3 cycles	6w	WHO	O1,2
Wang, J.R. 2012 (32)	26/24	32/18	III: 15, IV: 11/III: 14, IV: 10	Shenqi Fuzheng: Astragalus, Codonopsis, 250 ml/d, 14d/C, 2 cycles	Injection	DOC: 75 mg/m^2, d1; DDP: 20 mg/m^2, d1–5; 5-Fu:750 mg/m^2, d1–5; 28d/C, 2 cycles	8w-24w	RECIST, WHO	O1,2,4,5
Li, H.Y. 2013 (33)	35/35	35/35	III: 14, IV: 21/III: 16, IV: 19	Shenqi Fuzheng: Astragalus, Codonopsis, 250 ml/d,14d/C, 4 cycles	Injection	OXA: 85 mg/m^2, d1; CF: 200 mg/m^2, d1–2; 5-Fu: 400 mg/m^2, d1–2; 5-Fu: 600 mg/m^2, d1–2; 2w/C, 4 cycles	8w	WHO,Un	O1,2,5
Tan, G. 2013 (34)	26/22	26/22	IV	*Astragalus*-based formulae: Astragalus, Codonopsis, Atractylodis macrocephala, Poria cocos, Dioscoreae opposita, Citrus reticulata, Amomum, Galli gigerii endothelium corneum, Aflatoxin, Salviae miltiorrhizae, Cowherb seed, Hedyotis diffusa, Ganoderma, Scutellariae barbatae, 400 ml/d, 28d/C, 2 cycles	Orally	OXA: 85 mg/m^2, d1; CF: 200 mg/m^2, d–5; 5-Fu: 400 mg/m^2, d1–2; 5-Fu: 600 mg/m^2, d1–2; 2w/C, 4 cycles	8w	WHO, WHO	O1,2,4
Yin, L.L. 2013 (35)	26/27	27/26	III: 16, IV: 10/III: 14, IV: 13	Shenqi Fuzheng: Astragalus, Codonopsis, 250 ml/d, 14d/C, 2 cycles	Injection	S-1: 120 mg/d, d1–21; DDP: 20 mg/m^2, d1–5; 4w/C, 2 cycles	8w	WHO, NCI	O1,2,5,6
Fei, Y.H. 2014 (36)	40/40	54/26	III: 21, IV: 19/III: 18, IV: 22	*Astragalus*-based formulae: Astragalus, Codonopsis, Ganoderma, Atractylodis macrocephala, Poria cocos, Radix ophiopogonis, Polyporus umbellatus, Pinellia ternate, Fructus aurantii, Coix seed, Hedyotis diffusa, Curcuma, Bambusae caulis in taenias, 400 ml/d, 3w	Orally	DOC: 40 mg/m^2, d1, d8; DDP: 15 mg/m^2, d1–5; 5-Fu, 600 mg/m^2, d1–5; 28d/C, 2 cycles	6w	WHO	O1,2,6
Wen, J. 2014 (37)	15/15	23/7	IIIB: 5, IIIC: 6, IV: 4/IIIB: 7, IIIC: 4, IV: 4	Shenqi Fuzheng: Astragalus, Codonopsis, 250 ml/d, 14d/C, 4 cycles	Injection	OXA: 85 mg/m^2, d1; CF: 200 mg/m^2, d1–2; 5-Fu: 400 mg/m^2, d1–2; 5-Fu: 600 mg/m^2, d1–2; 2w/C, 4 cycles	8w	RECIST, WHO	O1,2,4,5
Xiang, S.L. 2014 (38)	33/33	28/38	IIIB: 19, IV: 14/IIIB: 18, IV: 15	Aidi: Astragalus, Ginseng, Cantharides, Eleutherococcus senticosus, 50 ml/d, d1–10, 28d/C, 2 cycles	Injection	PTX: 175 mg/m^2, d1; DDP: 20 mg/m^2, d1–5; 5-Fu: 600 mg/m^2, d5–9; 28d/C, 2 cycles	8w	WHO, WHO	O1,2,4,5
Zhang, L. 2014 (39)	32/32	35/29	IIIA: 6, IIIB: 27, IV: 31	Aidi: Astragalus, Ginseng, Cantharides, Eleutherococcus senticosus, 50–80 ml/d, 21d/C, 2 cycles	Injection	OXA: 85 mg/m^2, d1; CF: 200 mg/m^2, d1–2; 5-Fu: 400 mg/m^2, d1–2; 5-Fu: 600 mg/m^2, d1–2; 2w/C, 2 cycles	6w	WHO, WHO	O1,2,5

(Continued)

TABLE 1 | Continued

Study	Advanced gastric cancer (AGC)			Interventions			Fellow up	Criteria	Outcome
	E/C	M/F	TNM stage	*Astragalus*-containing TCM	Drug delivery	Platinum-based regimen			
Zhang, M.J. 2014 (40)	48/48	54/42	IIIB: 27, IV: 21/IIIB: 30, IV: 18	Aidi: Astragalus, Ginseng, Cantharides, Eleutherococcus senticosus, 50 ml/d, 21d/C, 2 cycles	Injection	OXA: 130 mg/m^2, d1; 5-Fu: 400 mg/m^2, d1; 5-Fu: 2,600 mg/m^2, d1–5; CF: 200 mg/m^2, d1; 21d/C; 2 cycles	6w	RECIST, Un	O1,4,5
Zhang, Y.N. 2015 (41)	46/38	49/35	IV	*Astragalus*-based formulae: Astragalus, Codonopsis, Radix pseudostellariae, Atractylodis macrocephala, Poria cocos, Fructus lycii, Ligustrum lucidum ait, Semen cuscutae, Spatholobus suberctu, Paeonia rubra, Curcuma zedoary, Polyphylla, Hedyotis diffusa, Radix actinidiae, 400 ml/d, 21d/C, 3 cycles	Orally	CAP: 1,000 mg/m^2, d1–14; OXA: 130 mg/m^2, d1; 21d/C, 3 cycles	9w	WHO	O1,2,4,6
Duan, F. 2016 (42)	46/46	51/41	IIIB: 35, IV: 11/IIIB: 33, IV: 13	Aidi: Astragalus, Ginseng, Cantharides, Eleutherococcus senticosus, 50 ml/d, 21d/C, 2 cycles	Injection	PTX: 175 mg/m^2, d1; DDP: 25 mg/m^2, d1–5; 5-Fu: 600 mg/m^2, d5–9; 28d/C, 2 cycles	8w	WHO, WHO	O1,2,4,5
Hu, Q. 2016 (43)	21/21	18/24	III, IV	Weining Granule: Astragalus, Hedyotis diffusa, Curcuma zedoary, Fructus lycii, Poria cocos, 400 ml/d, 28d/C, 3 cycles	Orally	OXA: 130 mg/m^2, d1; S-1: BSA <1.25 m^2, 80mg/d, 1.25–1.50 m^2, 120 mg/d, >1.25 m^2,160 mg/d; 42d/C, 2 cycles	12w	WHO	O4,5,6
Huang, P. 2016 (44)	34/33	36/31	IIIB-IV	*Astragalus*-based formulae: Astragalus, Radix pseudostellariae, Coix seed, Paeonia lactiflora, Agrimonia pilosa, Pinellia ternate, Citrus reticulata, Radix ophiopogonis, Curcuma zedoary, Hedyotis diffusa, Rice sprout, Malt, 200 ml/d, 21d/C, 2 cycles	Orally	OXA: 130 mg/m^2, d1; S-1: 80 mg/m^2, d1–14; 21d/C, 2 cycles	6w	WHO, Un	O1,2,3,4,5,6
Ma, M. 2016 (45)	22/22	26/18	III, IV	*Astragalus*-based formulae: Astragalus, Ground beeltle, Radix cynanchi panicullati, 400 ml/d, 21d/C, 2 cycles	Orally	OXA: 130 mg/m^2, d1; S-1: 80 mg/m^2, d1–14; 21d/C, 2 cycles	6w	WHO, Un	O1,2,4,5
Shao, K.F. 2016 (46)	31/31	34/28	III: 17, IV: 14/III: 15, IV: 16	*Astragalus*-based formulae: Astragalus, Codonopsis, Atractylodis macrocephala, Poria cocos, Coix seed, Semen lablab album, Amomum, Angelica Sinensis, Rhizoma cimicifugae, Dioscoreae opposita, Lotus seed, Bupleurum, Citrus reticulata, Radix platycodi, Glycyrrhiza, 400 ml/d, 4w	Orally	OXA: 85 mg/m^2, d1; CF: 200 mg/m^2, d1–2; 5-Fu: 400 mg/m^2, d1–2; 5-Fu: 600 mg/m^2, d1–2; 2w/C, 2 cycles	4w	WHO	O5
Hu, Q. 2017 (47)	18/18	22/14	IIIA: 5, IIIB: 6, IV: 7/IIIA: 6, IIIB: 8, IV: 4	Kangai: Astragalus, Ginseng, Matrine, 50 ml/d, d1–14, 21d/C, 6 cycles	Injection	OXA: 130 mg/m^2, d1; S-1: 120 mg/m^2, d1–14; 21d/C, 6 cycles	>2y	RECIST, NCI	O1,2,3,5
Pan, B.Y. 2018 (48)	58/54	60/52	IV	Bo-Er-Ning Capsule: Astragalus, Ligustrum lucidum ait, Pleione bulbocodioides, Purslane, Rhizoma paridis, Nightshade, Perilla fruit, Galli gigerii endothelium corneum, Rhubarb, Ornel, Bombyx batryticatus, 1.8g/d, d1–14; 21d/C, 3 cycles	Orally	Tegafur: 80–120 mg/d, d1–14; DDP: 40 mg, d1–3; 21d/C, 3 cycles	3y	/	O3,4
Xu, W. 2019 (49)	66/66	79/53	III: 29, IV: 37/III: 30, IV: 36	*Astragalus*-based formulae: Astragalus, Codonopsis, Atractylodis macrocephala, Poria cocos, Pinellia ternate, Citrus reticulata, Coix seed, Dioscoreae opposita, Atractylodis macrocephala, Hedyotis diffusa, Glycyrrhiza, 400 ml/d, 8w	Orally	OXA: 85 mg/m^2, d1; CF: 200 mg/m^2, d1–2; 5-Fu: 400 mg/m^2, d1–2; 5-Fu: 600 mg/m^2, d1–2; 2w/C, 4 cycles	8w	RECIST, Un	O1,2,5,6
Yuan, D.D. 2019 (50)	60/60	76/44	III: 22, IV: 38/III: 24, IV: 36	Shenqi Fuzheng: Astragalus, Codonopsis, 250 ml/d,14d/C, 4 cycles	Injection	DOC: 75 mg/m^2, d1; DDP: 20 mg/m^2, d1-5; 5-Fu: 750 mg/m^2, d1–5; 28d/C, 4 cycles	16w	WHO,Un	O1,2,5
Zhu, Y.F.	30/30	48/12	IV	Aidi: Astragalus, Ginseng, Cantharides, Eleutherococcus senticosus, 40 ml/d, 21d/C, 4 cycles	Injection	S-1: BSA<1.25 m^2, 80 mg/d, >1.25 m^2, 120 mg/d, d1–14; OXA: 130	12w	RECIST, WHO	O1,2,4,5

(Continued)

TABLE 1 | Continued

Study	Advanced gastric cancer (AGC)			Interventions			Fellow up	Criteria	Outcome
	E/C	M/F	TNM stage	*Astragalus*-containing TCM	Drug delivery	Platinum-based regimen			
2019 (51)						mg/m^2, d1; DOC: 75 mg/m^2, d1; 21d/C, 4 cycles			
Hou, Y. 2020 (52)	45/45	49/41	IV	*Astragalus*-based formulae: Astragalus, Atractylodis macrocephala, Glycyrrhiza, Ginseng, Angelica sinensis, Rhizoma cimicifugae, Bupleurum, Citrus reticulata, 400 ml/d, 6w	Orally	CAP: 1,000 mg/m^2, d1–14; OXA: 130 mg/m^2, d1; 21d/C, 2 cycles	6w–2y	RECIST, Un	O1,2,3,5

E/C, experimental group (Astragalus-containing TCM with PBC)/control group (PBC alone); PBC, platinum-based chemotherapy; M/F, male/female; 5-Fu, 5-fluorouracil; OXA, oxaliplatin; PTX, paclitaxel; DDP, cisplatin; CF, Calcium folinate; DOC, docetaxel; BSA, body surface area; CAP, capecitabine; WHO, World Health Organization guidelines for solid tumor responses; RECIST, Response Evaluation Criteria in Solid Tumors; Un, unclear; O, outcomes; O1, objective response rate (ORR); O2, disease control rate (DCR); O3, survival rate; O4, quality of life (QOL); O5, adverse drug reactions (ADRs); O6, peripheral blood lymphocyte levels.

Tumor Response

Thirty-two trials with 2,454 patients reported the ORR following WHO or RECIST guidelines. The random-effects meta-analysis showed that *Astragalus*-based herbal therapy plus PBC enhanced the ORR, which showed a statistically significant difference (RR: 1.24, 95% CI: 1.15–1.34, P < 0.00001, I^2 = 0%, **Figure 3**).

Thirty-one trials with 2,358 cases reported the DCR. The meta-analysis using a random-effects model showed that *Astragalus*-based TCM plus PBC increased the DCR; the difference was statistically significant (RR: 1.10, 95% CI: 1.06–1.14, P < 0.00001, I^2 = 11%, **Figure 4**).

Survival Rate

Six trials (19, 26, 27, 29, 44, 52) reported the survival rate (**Figure 5**). Additionally, in two trials (47, 48), the survival rate was extracted from survival curves. Thus, eight trials containing 512 cases were included. The results demonstrated that there was no significant difference in the half-year survival rate between the two groups (RR: 1.14, 95% CI: 0.89–1.45, P = 0.31, I^2 = 90%). However, compared with the PBC-treated control group, the 1- and 2-year survival rates in the *Astragalus*-based TCM group were significantly improved (RR: 1.41, 95% CI: 1.09–1.82, P = 0.005, I^2 = 65%; RR: 3.13, 95% CI: 1.80–5.46, P = 0.84, I^2 = 0%).

Quality of Life (QOL)

In the included studies, two types of data were applied to report the QOL changes on KPS score. First, the number of patients who reported QOL improvement (KPS score 10 points higher after treatment). And second, the mean ± standard deviation (SD) of the KPS score before and after treatment. As shown in **Figure 6**, the number of patients with improved QOL based on the KPS score were reported in 14 studies (RR: 2.03, 95% CI: 1.70–2.43, P < 0.00001, I^2 = 0%); and the mean ± SD of KPS score were reported in other six studies (MD: 12.39, 95% CI: 5.48–19.30, P = 0.0004, I^2 = 95%) (**Figure 7**). Taken together, compared with PBC, the study results showed that *Astragalus*-containing TCM plus PBC significantly improved QOL.

Adverse Drug Reactions (ADRs)

Twenty-nine trials that included 2,053 patients reported ADRs principally according to the WHO criteria (12) (**Table 2** and **Figures S1–10**). The results of the random-effects meta-analysis demonstrated that, compared with PBC alone, *Astragalus*-containing TCM plus PBC significantly reduced the risk of neutropenia (RR: 0.65, 95% CI: 0.54–0.79, P < 0.00001), anemia (RR: 0.68, 95% CI: 0.52–0.89, P = 0.005), thrombocytopenia (RR: 0.65, 95% CI: 0.51–0.82, P = 0.0004), nausea and vomiting (RR: 0.73, 95% CI: 0.64–0.82, P < 0.00001), diarrhea (RR: 0.58, 95% CI: 0.45–0.75, P < 0.0001), hepatic dysfunction (RR: 0.55, 95% CI: 0.40–0.77, P = 0.0005), renal dysfunction (RR: 0.48, 95% CI: 0.26–0.88, P = 0.02), neurotoxicity (RR: 0.78, 95% CI: 0.65–0.92, P = 0.004), and alopecia (RR: 0.77, 95% CI: 0.61–0.97, P = 0.03), but not the stomatitis rate (RR: 0.73, 95% CI: 0.53–1.00, P = 0.05).

Peripheral Blood Lymphocyte Levels

Ten trials that included 796 patients reported the peripheral blood lymphocyte levels. The results of $CD3^+$ $CD8^+$ T cell levels

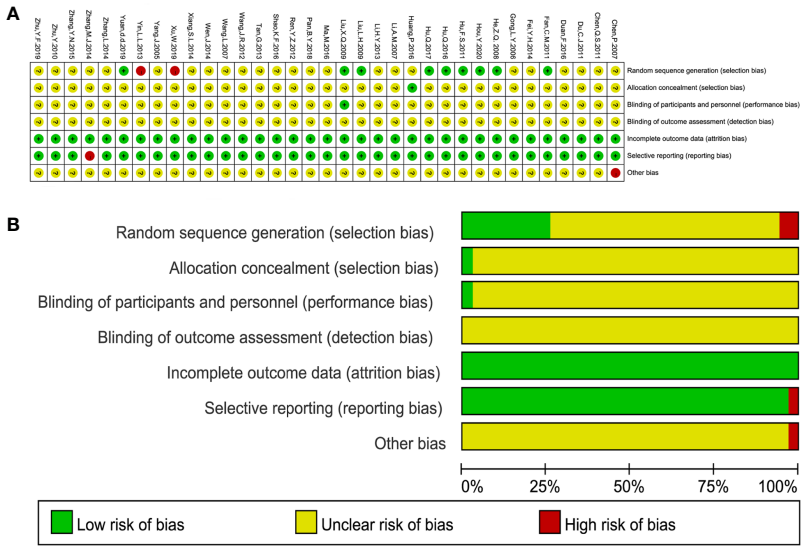

FIGURE 2 | Risk of bias summary and diagram. **(A)** Risk of bias summary. **(B)** Risk of bias diagram.

displayed poor clinical consistency. Therefore, we only evaluated the MD of the $CD3^+$ T cells, $CD3^+$ $CD4^+$ T cells, the $CD4^+/CD8^+$ T cells ratio, and NK cells using a random-effects model. Our results indicated that *Astragalus*-containing TCM plus PBC significantly enhanced the ratio of $CD3^+$ T cells (MD: 11.51, 95% CI: 5.94–17.08, P < 0.0001), $CD3^+$ $CD4^+$ T cells (MD: 6.44, 95% CI: 4.25–8.62, P < 0.00001), NK cells (MD: 4.58, 95% CI: 2.41–6.76, P < 0.0001) (**Figure 8**), and the $CD4^+/CD8^+$ T cells

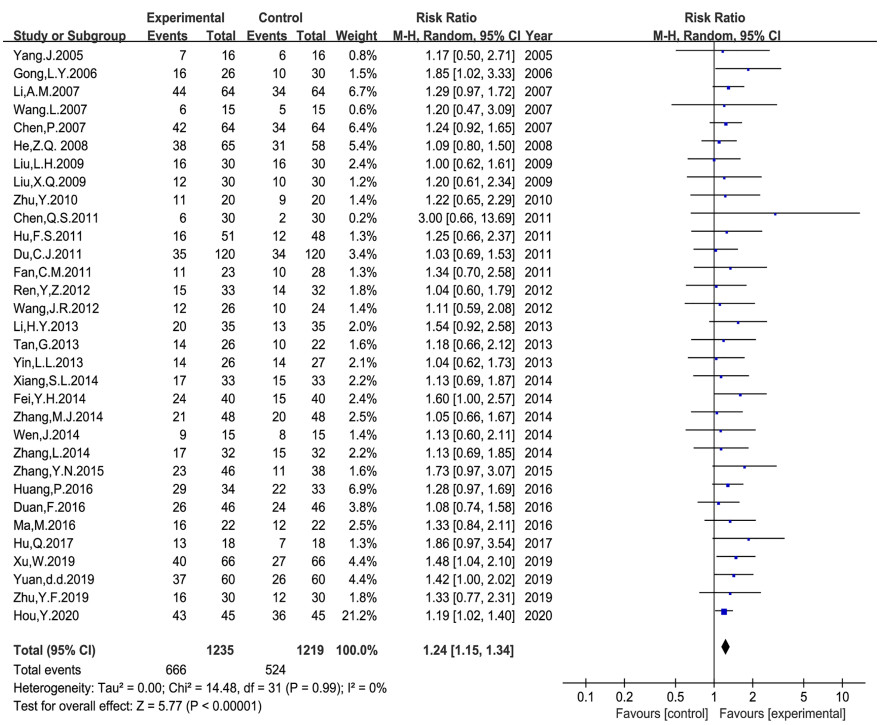

FIGURE 3 | Meta-analysis results of objective response rate (ORR) between the two groups.

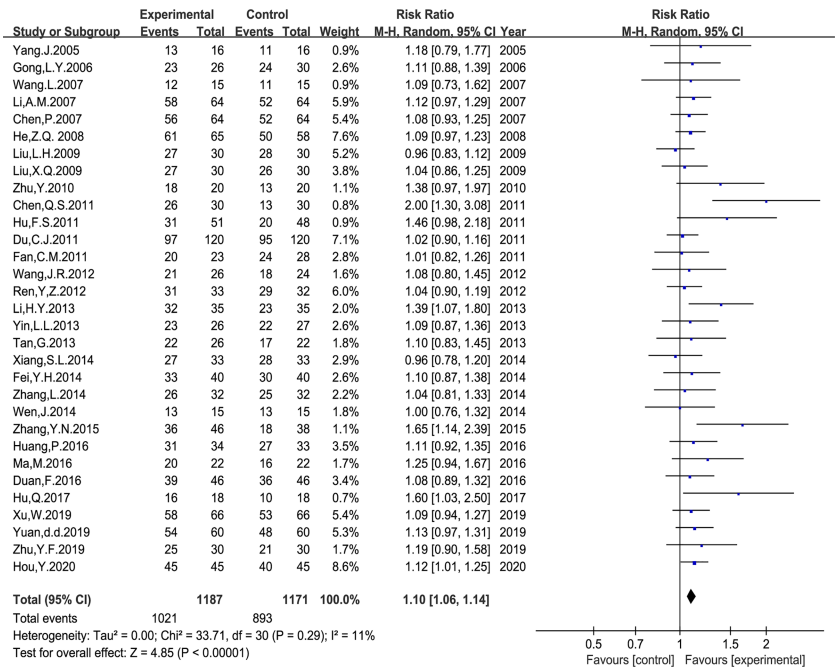

FIGURE 4 | Meta-analysis results of disease control rate (DCR) between the two groups.

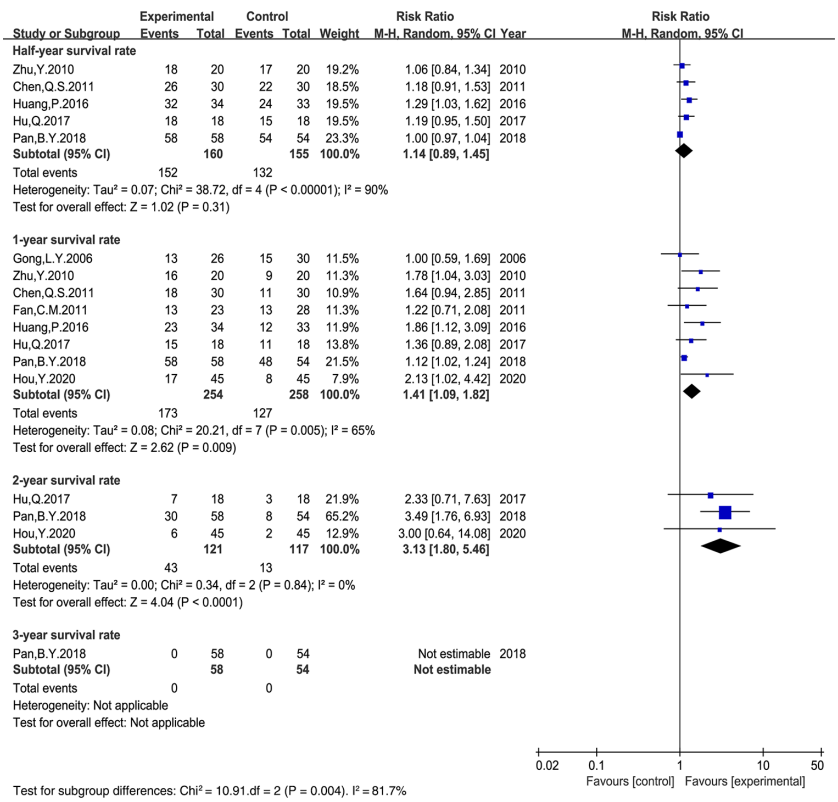

FIGURE 5 | Meta-analysis results of survival rate between the two groups.

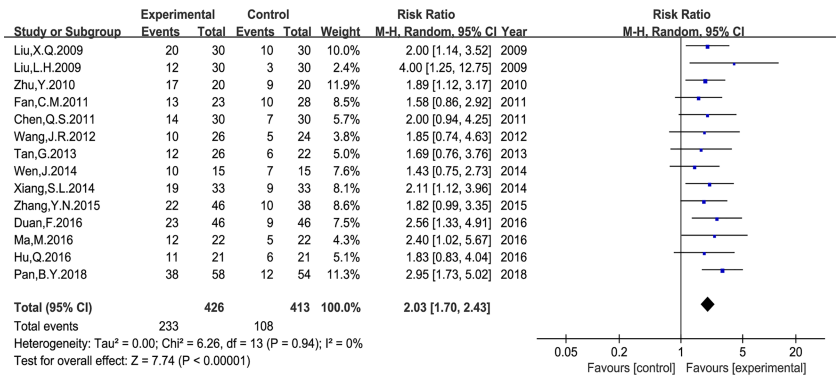

FIGURE 6 | Meta-analysis results of quality of life (QOL) according to the number of KPS improved patients.

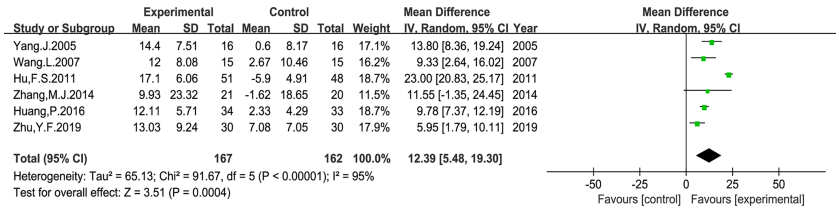

FIGURE 7 | Meta-analysis results of QOL according to mean ± SD.

TABLE 2 | Meta-analysis results of adverse drug reactions (ADRs).

Outcomes	Trials	Experimental group (Events/Total)	Control group (Events/Total)	SM	RR, 95%CI	I^2	P
Neutropenia	20	269/698	416/696	REM	0.65 [0.54, 0.79]	79%	<0.00001
Anemia	13	135/379	195/375	REM	0.68 [0.52, 0.89]	70%	0.005
Thrombocytopenia	20	155/602	237/595	REM	0.65 [0.51, 0.82]	62%	0.0004
Nausea and vomiting	19	263/647	377/646	REM	0.73 [0.64, 0.82]	32%	<0.00001
Diarrhea	10	62/307	111/301	REM	0.58 [0.45, 0.75]	0%	<0.0001
Hepatic dysfunction	14	45/442	86/446	REM	0.55 [0.40, 0.77]	0%	0.0005
Renal dysfunction	10	14/324	34/323	REM	0.48 [0.26, 0.88]	0%	0.02
Neurotoxicity	12	123/389	162/379	REM	0.78 [0.65, 0.92]	0%	0.004
Alopecia	4	50/145	61/138	REM	0.77 [0.61, 0.97]	0%	0.03
Stomatitis	6	45/174	62/174	REM	0.73 [0.53, 1.00]	0%	0.05

RR, risk ratio; CI, confidence interval; SM, statistical method; REM, random-effect model.

ratio (MD: 0.41, 95% CI: 0.27–0.55, P < 0.00001) (**Figure 9**) after treatment.

Subgroup Analysis of ORR and DCR

We performed subgroup analyses in accordance with the drug delivery of *Astragalus*-containing TCM, PBC regimen, and treatment duration to reveal the influence of the addition of *Astragalus*-containing TCM on the ORR and DCR (**Figures S11–16**). The drug delivery of *Astragalus*-containing TCM was either orally or by injection. Subgroup analysis showed that *Astragalus*-containing TCM could improve the ORR and DCR regardless of whether it was administered orally or by injection, respectively (**Table 3**). PBC regimens were cisplatin-based chemotherapy and oxaliplatin-based chemotherapy regimens. Subgroup analysis displayed that *Astragalus*-containing TCM plus oxaliplatin-based chemotherapy could enhance both the ORR and DCR; however, when combined with cisplatin-based chemotherapy, it could only enhance the ORR (**Table 3**). Finally, the treatment durations were ≥8 weeks and <8 weeks. As shown in **Table 3**, whether the treatment duration was ≥8 weeks or <8 weeks, the combination of *Astragalus*-containing TCM and PBC could improve the ORR and DCR.

Sensitivity Analysis

We performed sensitivity analysis by omitting each study in turn to check the robustness of the main outcome, including ORR, DCR, and

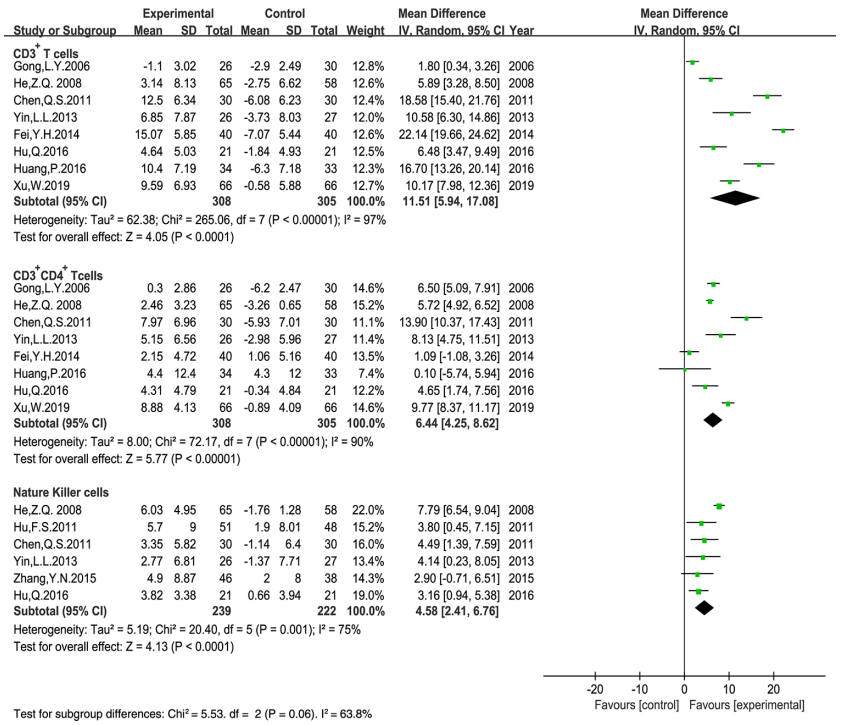

FIGURE 8 | Meta-analysis results of $CD3^+$ T cells, $CD3^+$ $CD4^+$ T cells, Nature Killer cells between the two groups.

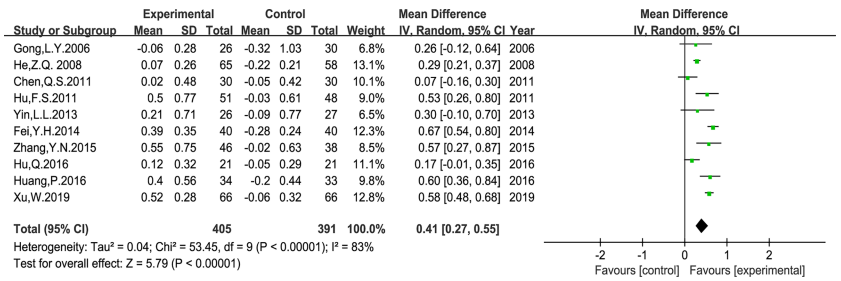

FIGURE 9 | Meta-analysis results of $CD4^+/CD8^+$ T cells ratio between the two groups.

survival rate. This analysis showed that the pooled RR values of the ORR, DCR, and 1-year survival rate were stable, except for the half-year survival rate (**Table 4**). Considering that the half-year survival rate was extracted from survival curves in the study of Pan, B.Y.2018 (48), we excluded this study, and the I^2 decreased from 90 to 0%.

As shown in **Figures S17, 18**, the TSA for the ORR and DCR showed that the Z-curve (blue dashed line) crossed the conventional boundary (brown dotted line), the trial sequential monitoring boundary for benefit (lower red solid line), and the RIS of the TSA (vertical red line; 660 for ORR, 574 for DCR), which suggested that the findings of the meta-analysis were robust for the ORR and DCR.

The TSA for the half-year survival rate (**Figure S19**) showed that the Z-curve did not cross either the conventional or trial sequential monitoring boundary, as well as the RIS (equal to 2920), which indicated that the evidence on the effect of half-year survival rate was insufficient. TSA for 1-year survival rate (**Figure S20**) showed that the Z-curve crossed the conventional and trial sequential monitoring boundary for benefit, but not the RIS (equal to 611). This indicates that the combination of *Astragalus*-containing TCM and PBC might enhance the 1-year survival rate for AGC patients. However, we did not have enough power to confirm the conclusion before RIS of 611 participants. The TSA for the 2-year survival rate (**Figure S21**) showed that the Z-curve crossed the conventional boundary and RIS (equal to 95), which indicated that the evidence on the effect of the 2-year survival rate was robust. Due to insufficient data, we failed to evaluate the effect on the 3-year survival rate.

TABLE 3 | Subgroup analysis of ORR and DCR.

Subgroups	Number of studies	RR (95% CI)	Z	P	Heterogeneity	
					I^2	P_h
1.Objective response rate (ORR)						
Drug delivery						
Orally	15	1.27 (1.15, 1.39)	4.93	<0.00001	0%	0.96
Injection	17	1.20 (1.07, 1.35)	3.08	0.002	0%	0.94
PBC regimens						
DDP-based chemotherapy regimen	10	1.25 (1.09, 1.44)	3.21	0.001	0%	0.79
OXA-based chemotherapy regimen	22	1.24 (1.13, 1.35)	4.81	<0.00001	0%	0.99
Treatment duration						
≥8 weeks	22	1.27 (1.15, 1.40)	4.74	<0.00001	0%	0.98
<8 weeks	10	1.21 (1.08, 1.35)	3.36	0.0008	0%	0.88
2.Disease control rate (DCR)						
Drug delivery						
Orally	15	1.14 (1.07, 1.22)	4.03	<0.0001	27%	0.16
Injection	16	1.07 (1.02, 1.12)	2.73	0.006	0%	0.65
PBC regimens						
DDP-based chemotherapy regimen	10	1.06 (1.00, 1.13)	2.06	0.04	0%	0.93
OXA-based chemotherapy regimen	21	1.13 (1.07, 1.20)	4.25	<0.0001	31%	0.09
Treatment duration						
≥8 weeks	22	1.10 (1.05, 1.16)	4.14	<0.0001	6%	0.38
<8 weeks	9	1.09 (1.02, 1.18)	2.45	0.01	28%	0.19

RR, risk ratio; CI, confidence interval; DDP, cisplatin; OXA, oxaliplatin.

TABLE 4 | Sensitivity analysis.

Indicators	Trials	SM	RR (95% CI)	I^2	Excluded trials	Trials	SM	RR (95% CI)	I^2
half-year survival rate	5	REM	1.14 [0.89, 1.45]	90%	Pan, B.Y. 2018 (48)	4	REM	1.18 [1.05, 1.33]	0%

SM, statistical method; REM, random-effects model; RR, risk ratio; CI, confidence interval.

Publication Bias

The funnel plots (**Figures S22–33**) were not strictly symmetrical in the meta-analysis of the ORR, DCR, QOL, neutropenia, anemia, thrombocytopenia, nausea and vomiting, diarrhea, hepatic dysfunction, renal dysfunction, neurotoxicity, and $CD4^+/CD8^+$ T cells ratio. However, as shown in Egger's test (**Table 5**), no significant publication bias existed among the meta-analysis of ORR (P = 0.3986), QOL (P = 0.7377), diarrhea (P = 0.3092), hepatic dysfunction (P = 0.5113), renal dysfunction (P = 0.9436), and $CD4^+/CD8^+$ T cells ratio (P=0.5250).

TABLE 5 | Egger's test.

Meta-analysis of publication bias	P value
ORR	0.3986
DCR	0.0021
QOL	0.7377
Neutropenia	0.0000
Anemia	0.0487
Thrombocytopenia	0.0000
Nausea and vomiting	0.0002
Diarrhea	0.3092
Hepatic dysfunction	0.5113
Renal dysfunction	0.9436
Neurotoxicity	0.0388
$CD4^+/CD8^+$ T cells ratio	0.5250

ORR, objective response rate; DCR, disease control rate; QOL, quality of life.

Quality of Evidence

In summary, the quality was moderate for the ORR, 1-year survival rate, QOL, hepatic dysfunction, renal dysfunction, stomatitis, and levels of peripheral blood lymphocytes; low for DCR, neutropenia, anemia, thrombocytopenia, nausea and vomiting, diarrhea, and neurotoxicity; and very low for other results (**Table 6**).

DISCUSSION

Gastric cancer has high incidence and morbidity levels around the world. In China, patients with AGC have poor clinical outcomes and a low 5-year survival rate of <20% (53). PBC is widely used and plays a crucial role in the treatment of AGC (54). However, the survival benefit in patients with AGC is still limited; therefore, it is necessary to develop effective combination therapies to increase the efficacy of PBC and reduce side effects in order to prolong the survival time and improve QOL in these patients.

As an important part of the comprehensive treatment of cancer, TCM, especially *Astragalus*-containing TCM, is used in combination with chemotherapy and broadly prescribed for AGC patients in China. To evaluate whether *Astragalus*-containing TCM with PBC improves the clinical efficacy and its safety, 35 RCTs involving 2,670 patients with AGC were included in this meta-analysis. To the best of our knowledge, it is

TABLE 6 | GRADE evidence profile.

TABLE 6a | GRADE evidence profile of clinical efficacy and safety.

Outcomes (Trials)	Quality assessment					No. of patients		Risk ratios (95% CI)	Quality
	Risk of bias	Inconsistency	Indirectness	Imprecision	Reporting bias	*Astragalus*-Containing TCM	PBC		
ORR (32)	Serious[a]	No	No	No	No	666/1,235 (53.9%)	524/1,219 (43%)	RR 1.24 (1.15 to 1.34)	⊕⊕⊕O Moderate
DCR (32)	Serious[a]	No	No	No	Serious	1,021/1,187 (86%)	893/1,171 (76.3%)	RR 1.10 (1.06 to 1.14)	⊕⊕OO Low
Half-year survival rate (5)	Very Serious[d]	Serious[g]	No	No	No	152/160 (95%)	132/155 (85.2%)	RR 1.14 (0.89 to 1.45)	⊕OOO Very Low
1-year survival rate (8)	Serious[c]	No[f]	No	No	No	173/254 (68.1%)	127/258 (49.2%)	RR 1.41 (1.09 to 1.82)	⊕⊕⊕O Moderate
2-year survival rate (3)	Very Serious[d]	No	No	Serious[e]	No	43/121 (35.5%)	13/117 (11.1%)	RR 3.13 (1.80 to 5.46)	⊕OOO Very Low
3-year survival rate (1)	Very Serious[d]	No	No	Serious[e]	No	0/58 (0%)	0/54 (0%)	Not pooled	⊕OOO Very Low
QOL, according to the number of KPS improved patients (14)	Serious[c]	No	No	No	No	233/426 (54.7%)	108/413 (26.2%)	RR 2.03 (1.70 to 2.43)	⊕⊕⊕O Moderate
Neutropenia (21)	Serious[a]	No[f]	No	No	Serious	269/698 (38.5%)	416/696 (59.8%)	RR 0.65 (0.54 to 0.79)	⊕⊕OO Low
Anemia (13)	Serious[a]	No[f]	No	No	Serious	135/379 (35.6%)	195/375 (52%)	RR 0.68 (0.52 to 0.89)	⊕⊕OO Low
Thrombocytopenia (21)	Serious[a]	No[f]	No	No	Serious	155/602 (25.7%)	237/595 (39.8%)	RR 0.65 (0.51 to 0.82)	⊕⊕OO Low
Nausea and vomiting (20)	Serious[a]	No[f]	No	No	Serious	263/647 (40.6%)	377/646 (58.4%)	RR 0.73 (0.64 to 0.82)	⊕⊕OO Low
Diarrhea (10)	Serious[c]	No	No	No	Serious	62/307 (20.2%)	111/301 (36.9%)	RR 0.58 (0.45 to 0.75)	⊕⊕OO Low
Hepatic dysfunction (14)	Serious[a]	No	No	No	No	45/442 (10.2%)	86/446 (19.3%)	RR 0.55 (0.40 to 0.77)	⊕⊕⊕O Moderate
Renal dysfunction (10)	Serious[a]	No	No	No	No	14/324 (4.3%)	34/323 (10.5%)	RR 0.48 (0.26 to 0.88)	⊕⊕⊕O Moderate
Neurotoxicity (12)	Serious[a]	No	No	No	Serious	123/389 (31.6%)	162/379 (42.7%)	RR 0.78 (0.65 to 0.92)	⊕⊕OO Low
Alopecia (4)	Very Serious[d]	No	No	Serious[e]	No	50/145 (34.5%)	61/138 (44.2%)	RR 0.77 (0.61 to 0.97)	⊕OOO Very Low
Stomatitis (6)	Serious[a]	No	No	No	No	45/174 (25.9%)	62/174 (35.6%)	RR 0.73 (0.53 to 1.00)	⊕⊕⊕O Moderate

ORR, objective response rate; DCR, disease control rate; QOL, quality of life; NK cells, natural killer cells; CI, confidence interval.

[a]*Most trials had unclear risk, and with high risk, but the result had good robustness. The evidence was rated down by only one level.*

[b]*Most trials had unclear risk and with high risk, and the result had poor robustness. The evidence was rated down by two levels.*

[c]*Most trials had unclear risk and the trials were no high risk, but the result had good robustness. The evidence was rated down by only one level.*

[d]*Most trials had unclear risk and the trials were no high risk, but the result had poor robustness. The evidence was rated down by two levels.*

[e]*The sample size for each outcome was fewer than 300 cases. Therefore, the evidence was rated down by one level.*

[f]*Heterogeneity presented in them, and the results had good robustness. Not rated down.*

[g]*Heterogeneity presented in them, and the result had poor robustness. The evidence was rated down by one level.*

TABLE 6 | GRADE evidence profile.

TABLE 6b | GRADE evidence profile of QOL (mean ± SD) and levels of peripheral blood lymphocytes.

Outcomes (Trials)	Quality assessment					No. of patients		Mean difference (95% CI)	Quality
	Risk of bias	Inconsistency	Indirectness	Imprecision	Reporting bias	*Astragalus*-Containing TCM	PBC		
QOL, according to mean ± SD (6)	Serious[a]	No[f]	No	No	No	167	162	MD 12.39 higher (5.48 to 19.3 higher)	⊕⊕⊕O Moderate
$CD3^+$ T cells (8)	Serious[a]	No[f]	No	No	No	308	305	MD 11.51 higher (5.94 to 17.08 higher)	⊕⊕⊕O Moderate
$CD3^+CD4^+$ T cells (8)	Serious[a]	No[f]	No	No	No	308	305	MD 6.44 higher (4.25 to 8.62 higher)	⊕⊕⊕O Moderate
$CD4^+/CD8^+$ T cells ratio (10)	Serious[a]	No[f]	No	No	No	405	391	MD 0.41 higher (0.27 to 0.55 higher)	⊕⊕⊕O Moderate
NK cells (6)	Serious[a]	No[f]	No	No	No	239	222	MD 4.58 higher (2.41 to 6.76 higher)	⊕⊕⊕O Moderate

ORR, objective response rate; DCR, disease control rate; QOL, quality of life; NK cells, natural killer cells; CI, confidence interval.

[a]Most trials had unclear risk, and with high risk, but the result had good robustness. The evidence was rated down by only one level.

[b]Most trials had unclear risk and with high risk, and the result had poor robustness. The evidence was rated down by two levels.

[c]Most trials had unclear risk and the trials were no high risk, but the result had good robustness. The evidence was rated down by only one level.

[d]Most trials had unclear risk and the trials were no high risk, but the result had poor robustness. The evidence was rated down by two levels.

[e]The sample size for each outcome was fewer than 300 cases. Therefore, the evidence was rated down by one level.

[f]Heterogeneity presented in them, and the results had good robustness. Not rated down.

[g]Heterogeneity presented in them, and the result had poor robustness. The evidence was rated down by one level.

the first systematic review and meta-analysis that has evaluated the efficacy and safety of *Astragalus*-containing TCM in combination with PBC for AGC treatment.

Our results indicated that *Astragalus*-containing TCM could enhance the ORR and DCR of PBC, meaning that the experimental group had a better short-term efficacy. Furthermore, we also performed subgroup analyses according to the drug delivery method of *Astragalus*-containing TCM, PBC regimen, and treatment duration. The results suggested that compared with PBC alone, both oral and injection-based administration of *Astragalus*-containing TCM resulted in better tumor response in AGC patients. In addition, both *Astragalus*-containing TCM combined with cisplatin-based chemotherapy and oxaliplatin-based chemotherapy resulted in a better ORR than chemotherapy alone. AGC patients that were given *Astragalus*-containing TCM plus oxaliplatin-based chemotherapy had better DCR; however, those who were given *Astragalus*-containing TCM plus cisplatin-based chemotherapy showed no difference in DCR. In addition, the subgroup analysis results also showed that *Astragalus*-containing TCM plus PBC resulted in better tumor response in AGC patients regardless of the duration of administration. Moreover, basic studies also showed that *Astragalus* and its main components could reduce or stabilize the gastric tumor by inducing antiproliferation, promoting apoptosis, and modulating the invasiveness of tumor cells, among other mechanisms (55–57). These results provided indirect basic and mechanistic evidences for the antitumor mechanisms of using *Astragalus*-containing TCM in AGC.

In terms of the survival rate, our study indicated that *Astragalus*-containing TCM plus PBC enhanced the 1- ($P = 0.009$) and 2-year survival rates ($P < 0.0001$) compared with PBC alone. However, due to the small number of included trials ($n = 8$), the data available for subgroup and sensitivity analyses were limited. In addition, none of the included studies completely reported the overall survival, progression-free survival, 5-year survival rate, which were important clinical survival outcomes. Therefore, conducting a meta-analysis on these outcome measures was not possible. More evidence is needed to support our findings.

PBC often leads to many adverse drug reactions in patients with AGC, which seriously impacts QOL. Therefore, reducing chemotherapy side effects while maintaining the curative effect has become a popular and urgent topic. More and more evidence has shown that *Astragalus* and its main components (such as *Astragalus* polysaccharide, flavonoid compounds, saponins compounds, alkaloids, etc.) have the potential to reduce side effects of chemotherapeutic agents (58–61). According to our results, *Astragalus*-containing TCM plus PBC reduced ADRs (bone marrow suppression, gastrointestinal reaction, hepatic and renal dysfunction, neurotoxicity, and alopecia) in patients with stage III/IV AGC ($P < 0.05$) and brought significantly improvement on their QOL based on KPS.

The human immune system plays a vital role in immune surveillance of malignant cells. Patients with AGC have low immune function, and PBC often aggravates the immunosuppressive state in patients, impairing the antitumor response (62), which increases the risk of tumor invasion and metastasis. Therefore, improving immunity is of great significance in

antitumor therapy. An increasing number of pharmacological studies have shown that *Astragalus* and its ingredients could improve chemotherapy-induced immunosuppression, which is associated with protective effects on immune organs by regulating leukocytes, lymphocytes, and macrophages, among other cells (63–65). In clinical settings, determination of peripheral blood lymphocytes is an effective method for evaluating the immune function of patients. This meta-analysis showed that *Astragalus*-containing TCM plus PBC significantly increased the percentages of $CD3^+$, $CD3^+CD4^+$, $CD4^+/CD8^+$, and NK cells in the peripheral blood.

This study has several limitations. Firstly, we only searched for literature from Chinese and English databases; thus, some related studies from Japanese, Korean, or other databases might have been missed. All of the RCTs included in our study were conducted in China, and only one study was published in an international journal (48); Funnel plots and egger's test results reflected that there was some potential publication bias. Secondly, only nine studies clearly described the use of randomization methods. In most included trials, allocation concealment and blinding were "unclear", which might result in potential implementation bias and selective bias. Thirdly, in all included trials, the follow-up duration was relatively short (≤3 years). We look forward to more longer-term follow-up studies to support our findings. Fourthly, there was substantial heterogeneity (I^2 > 50%) among studies for many outcomes, such as the half- and 1-year survival rate, peripheral blood lymphocyte levels, neutropenia, anemia, and thrombocytopenia, among others, which might have weakened the evidence strength of this meta-analysis. Therefore, more well-designed RCTs are needed to support our findings. Fifthly, in the treatment of AGC, *Astragalus* is rarely used as single-agent therapy; it usually is combined with other different herbal medicines. Additional researches are needed to further understand the specific immunological and cytotoxic mechanisms of *Astragalus* as an adjuvant to chemotherapy in the treatment of AGC. And lastly, based on the GRADE approach, the quality of outcomes was moderate to very low; most trials we included in our manuscript might not be reported strictly in accordance with the CONSORT reporting standards. All of these limitations might have resulted in insufficient evaluation of the outcome. However, we hope that our manuscript will make more and more doctors realize the potential benefits of *Astragalus*-containing TCM in AGC, and conduct more well-designed clinical trials adhering to CONSORT guidelines to verify the efficacy of *Astragalus*-containing TCM in the future.

CONCLUSION

Our study demonstrated the potencies of *Astragalus*-containing TCM with PBC to enhance the efficacy and safety for patients with AGC, and more efforts are needed to promote the application of *Astragalus*-containing TCM in the clinic. Furthermore, the long-term efficacy of *Astragalus*-containing TCM plus PBC in AGC treatment still needs to be verified in future well-designed clinical trials that adhere to CONSORT guidelines.

DATA AVAILABILITY STATEMENT

The original contributions presented in the study are included in the article/**Supplementary Material**. Further inquiries can be directed to the corresponding authors.

AUTHOR CONTRIBUTIONS

BH and YQ designed the research. MC, JH, and YZ performed literature search. YL and JJ performed article selection. RL and QG assessed methodological bias risk. XZ and YQ performed data extraction. JJ, RQ, SC, and HZ conducted a meta-analysis and assessed study quality. MC finished the manuscript draft. All authors contributed to the article and approved the submitted version.

FUNDING

This study was supported by the National Natural Science Foundation of China (Grant Nos. 81673961, 81774294), Beijing Municipal Science and Technology Commission (No. Z181100001618006), Beijing Natural Science Foundation (No. 7172186), Institution Subject of Guang'anmen Hospital, China Academy of Chinese Medical Sciences (Grant No. 2019S452).

SUPPLEMENTARY MATERIAL

The Supplementary Material for this article can be found online at: https://www.frontiersin.org/articles/10.3389/fonc.2021.632168/full#supplementary-material

REFERENCES

1. Bray F, Ferlay J, Soerjomataram I, Siegel RL, Torre LA, Jemal A. Global Cancer Statistics 2018: GLOBOCAN Estimates of Incidence and Mortality Worldwide for 36 Cancers in 185 Countries. *CA Cancer J Clin* (2018) 68:394–424. doi: 10.3322/caac.21492
2. Eusebi LH, Telese A, Marasco G, Bazzoli F, Zagari RM. Gastric Cancer Prevention Strategies: A Global Perspective. *J Gastroenterol Hepatol* (2020) 35:1495–502. doi: 10.1111/jgh.15037
3. Hwang IG, Ji JH, Kang JH, Lee HR, Lee HY, Chi KC, et al. A Multi-Center, Open-Label, Randomized Phase III Trial of First-Line Chemotherapy With Capecitabine Monotherapy Versus Capecitabine Plus Oxaliplatin in Elderly Patients With Advanced Gastric Cancer. *J Geriatr Oncol* (2017) 8:170–5. doi: 10.1016/j.jgo.2017.01.002
4. National Comprehensive Cancer Network. (NCCN). *Clinical Practice Guidelines in Oncology. Gastric Cancer, Version 2.2020*. Available at: https://www.nccn.org/professionals/physician_gls/pdf/gastric.pdf (Accessed May 21, 2020).

5. Li Y, Sui X, Su Z, Yu C, Shi X, Johnson NL, et al. Meta-Analysis of Paclitaxel-Based Chemotherapy Combined With Traditional Chinese Medicines for Gastric Cancer Treatment. *Front Pharmacol* (2020) 11:132. doi: 10.3389/fphar.2020.00132
6. Li J, Niu J, Yang M, Ye P, Zhai J, Yuan W, et al. Using Single-Patient (N-of-1) Trials to Determine Effectiveness of Traditional Chinese Medicine on Chemotherapy-Induced Leukopenia in Gastric Cancer: A Feasibility Study. *Ann Transl Med* (2019) 7:124. doi: 10.21037/atm.2019.02.03
7. Yao K, Ma Y, Ma W, Hu J, Wang C, Chen J, et al. Shenqifuzheng Injection Combined With Chemotherapy in the Treatment of Advanced Gastric Cancer: A Systematic Review and Meta-Analysis. *J Cancer Res Ther* (2014) 10:70–4. doi: 10.4103/0973-1482.139768
8. Lin S, An X, Guo Y, Gu J, Xie T, Wu Q, et al. Meta-Analysis of *Astragalus*-Containing Traditional Chinese Medicine Combined With Chemotherapy for Colorectal Cancer: Efficacy and Safety to Tumor Response. *Front Oncol* (2019) 9:749. doi: 10.3389/fonc.2019.00749
9. Cao A, He H, Wang Q, Li L, An Y, Zhou X. Evidence of *Astragalus* Injection Combined Platinum-Based Chemotherapy in Advanced Nonsmall Cell Lung Cancer Patients: A Systematic Review and Meta-Analysis. *Med (Baltimore)* (2019) 98:e14798. doi: 10.1097/MD.0000000000014798
10. Wang SF, Wang Q, Jiao LJ, Huang YL, Garfield D, Zhang J, et al. *Astragalus*-Containing Traditional Chinese Medicine, With and Without Prescription Based on Syndrome Differentiation, Combined With Chemotherapy for Advanced non-Small-Cell Lung Cancer: A Systemic Review and Meta-Analysis. *Curr Oncol* (2016) 23:e188–95. doi: 10.3747/co.23.2920
11. McCulloch M, See C, Shu XJ, Broffman M, Kramer A, Fan WY, et al. *Astragalus*-Based Chinese Herbs and Platinum-Based Chemotherapy for Advanced non-Small-Cell Lung Cancer: Meta-Analysis of Randomized Trials. *J Clin Oncol* (2006) 24:419–30. doi: 10.1200/JCO.2005.03.6392
12. Miller AB, Hoogstraten B, Staquet M, Winkler A. Reporting Results of Cancer Treatment. *Cancer* (1981) 47:207–14. doi: 10.1002/1097-0142(19810101)47:1<207::aid-cncr2820470134>3.0.co;2-6
13. Watanabe H, Yamamoto S, Kunitoh H, Sekine I, Yamamoto N, Ohe Y, et al. Tumor Response to Chemotherapy: The Validity and Reproducibility of RECIST Guidelines in NSCLC Patients. *Cancer Sci* (2003) 94:1015–20. doi: 10.1111/j.1349-7006.2003.tb01394.x
14. Trotti A, Colevas A, Setser A, Rusch V, Jaques D, Budach V, et al. CTCAE V3.0: Development of a Comprehensive Grading System for the Adverse Effects of Cancer Treatment. *Semin Radiat Oncol* (2003) 13:176–81. doi: 10.1016/s1053-4296(03)00031-6
15. Wetterslev J, Jakobsen JC, Gluud C. Trial Sequential Analysis in Systematic Reviews With Meta-Analysis. *BMC Med Res Methodol* (2017) 17:39. doi: 10.1186/s12874-017-0315-7
16. Guyatt GH, Oxman AD, Vist GE, Kunz R, Falck-Ytter Y, Alonso-Coello P, et al. GRADE: An Emerging Consensus on Rating Quality of Evidence and Strength of Recommendations. *BMJ* (2008) 336:924–6. doi: 10.1136/bmj.39489.470347.AD
17. Moher D, Liberati A, Tetzlaff J, Altman DG, The PRISMA Group. Preferred Reporting Items for Systematic Reviews and Meta-Analyses: The PRISMA Statement. *PLoS Med* (2009) 6(7):e1000097. doi: 10.1371/journal.pmed1000097
18. Yang J. *The Clinical Investigation About Advanced Gastric Cancer With Supplementing Spleen, Retrieving Gastric Function, Expelling Dampness, Removing Stasis and Relieving Poison Associated With Oxaliplatin/5-Fu Regimen*. Nanjing: Nanjing University of Chinese Medicine (2005).
19. Gong LY, Jiang CM, Zhao YZ. Ai-Di Injection Combined With Chemotherapy in the Treatment for 56 Cases With Advanced Gastric Cancer. *J Oncol* (2006) 12:424–25. doi: 10.3969/j.issn.1671-170X.2006.05.023
20. Chen P, Zheng WD, Gao HL, Song BJ. Clinical Analysis on the Treatment of Late Gastric Cancer by the Combination of Cidan Capsule With ELF Chemotherapy Plan. *World J Integr Trad Western Med* (2007) 2:167–69. doi: 10.3969/j.issn.1673-6613.2007.03.015
21. Li AM, Li FZ. Evaluation of Therapeutic Effect of FLP Regimen Combined With Xiaoai Jiandu Decoction in the Treatment of Advanced Gastric Cancer. *J Modern Med Health* (2007) 23:2260. doi: 10.3969/j.issn.1009-5519.2007.15.033
22. Wang L. *The Clinical Investigation About Advanced Gastric Cancer With Supplementing Spleen, Dissipating Phlegm, Removing Stasis, Relieving Poison Associated With Chemotherapy of Paclitaxel, Oxalipatin, 5-Fu*. Nanjing: Nanjing University of Chinese Medicine (2007).
23. He ZQ, Cheng DY, Gong H, Cheng J, Xu ZJ, Chen D, et al. The Clinical Efficacy of FOLFOX4 Chemotherapy Combined With Delisheng in Therapy of Advanced Gastric Cancer. *Modern Oncol* (2008) 16:408–11. doi: 10.3969/j.issn.1672-4992.2008.03.032
24. Liu LH, Zhang CX. Clinical Efficacy of Aidi Injection Combined With TPF in the Treatment of Advanced Gastric Carcinoma. *China Mod Doct* (2009) 47:16–7. doi: 10.3969/j.issn.1673-9701.2009.29.007
25. Liu XQ. *The Clinical Research of Kang'ai Injection Combined With Modified DCF Regimen for Patients With Advanced Gastric Cancer*. Fujian: Fujian University of Traditional Chinese Medicine (2009).
26. Zhu Y, Yuan WJ, Zhang XJ, Li X. Clinical Study of Modified Sanwu Bai San Prescription in the Treatment of Advanced Gastric Cancer. *J Emergency Tradit Chin Med* (2010) 19:578–80. doi: 10.3969/j.issn.1004-745X.2010.04.020
27. Chen QS. Clinical Observation on 30 Cases of Advanced Gastric Cancer Treated With Yiqi Jianpi Decoction Combined With FOLFOX Regimen. *Yunnan J Tradit Chin Med Mater Med* (2011) 32:45–7. doi: 10.3969/j.issn.1007-2349.2011.04.029
28. Du CJ, Wang TL, Guo YS. Clinical Observation of Jianpi Bushen Yiqi Yangxue Recipe in Improving the Quality of Life of Advanced Gastric Cancer. *J Hebei TCM Pharmacol* (2011) 26:24–5. doi: 10.3969/j.issn.1007-5615.2011.02.015
29. Fan CM, Ge CH, Lu F, Chen Y, Xu CY, Zhu JP, et al. Therapeutic Efficacy of Aidi Injection Combined With S-1 and Oxaliplatin in Treating Patients With Advanced Gastric Cancer. *Modern J Integr Tradit Chin Western Med* (2011) 20:4607–9. doi: 10.3969/j.issn.1008-8849.2011.36.004
30. Hu FS. *Summary of Professor Yu Rencun's Academic Thought and Clinical Experience and Clinical Observation of Yiqi Huoxue Jiedu Recipe Combined With Chemotherapy in the Treatment of Advanced Gastric Cancer*. Beijing: Beijing University of Chinese Medicine (2011).
31. Ren YZ, Wang F. Influence of Advanced Gastric Cancer Treated With Shenqi Fuzheng Injection Combined With Chemotherapy on Effect and Immune Function. *J Basic Clin Oncol* (2012) 25:394–96. doi: 10.3969/j.issn.1673-5412.2012.05.009
32. Wang JR, Wang JW, Wang J, Wang ZX, Wang KM. Clinical Observation of Shengifuzheng Injection in Combination With Chemotherapy in the Treatment of Patients With Advanced Gastric Carcinoma. *China Med Herald* (2012) 9:79–81. doi: 10.3969/j.issn.1673-7210.2012.33.030
33. Li HY, Ji WM, Tu J, Shen YL. Clinical Analysis of Shenqi Fuzheng Injection Combined With Chemotherapy in Patients With Advanced Gastric Cancer. *China Med Herald* (2013) 10:99–101. doi: 10.3969/j.issn.1673-7210.2013.15.035
34. Tan G. Clinical Observation of Jianpi Anticancer Decoction Combined With FOLFOX Regimen in the Treatment of Advanced Gastric Cancer. *Inner Mongol J Tradit Chin Med* (2013) 32:75–6. doi: 10.3969/j.issn.1006-0979.2013.19.071
35. Yin LL, Jiang CY. Observation on the Influence of Shenqi-Fuzheng Injection on T-Lymphocyte Subsets, NK Cell and the Leukocyte of the Patients With Advanced Gastric Cancer. *Int J Trad Chin Med* (2013) 35:22–4. doi: 10.3760/cma.j.issn.1673-4246.2013.01.007
36. Fei YH, Wang NY, Wang Q. Clinical Study on Fuzheng Huayu Formula Combined With Chemotherapy in the Treatment of Advanced Gastric Cancer. *Henan Tradit Chin Med* (2014) 34:2182–183. doi: 10.16367/j.issn.1003-5028.2014.11.036
37. Wen J. *Clinical Observation of Advanced Gastric Cancer Treated With Shenqi Fuzheng Injection Combined With Chemotherapy*. Yangzhou: Yangzhou University (2014).
38. Xiang SL, Zhao Y. Clinical Observation of Aidi Injection Combined With TPF Regimen in the Treatment of Advanced Gastric Cancer. *Med Inf* (2014) 27:108. doi: 10.3969/j.issn.1006-1959.2014.37.142
39. Zhang L. Study on Aidi Injection Combined With FOLFOX4 Chemotherapy for Advanced Gastric Cancer. *Cardiovasc Dis Elec J Integr Tradit Chin Western Med* (2014) 2:49–50.
40. Zhang MJ, Zuo CF. Observation on the Therapeutic Effect of Aidi Injection in Patients With Advanced Gastric Cancer. *Guide Chin Med* (2014) 12:190–91. doi: 10.15912/j.cnki.gocm.2014.04.177

41. Zhang YN, Zhang M, Li XF, Zhou HP. Clinical Observation on 46 Cases of Advanced Gastric Cancer Treated With Traditional Chinese Medicine for Supplementing Qi and Activating Blood Circulation. *Zhejiang J Tradit Chin Med* (2015) 50:656. doi: 10.13633/j.cnki.zjtcm.2015.09.023
42. Duan F. Observation on the Efficacy of Aidi Injection Combined With Chemotherapy in the Treatment of Advanced Gastric Cancer. *Chin J Clin Ration Drug Use* (2016) 9:55–6. doi: 10.15887/j.cnki.13-1389/r.2016.02.034
43. Hu Q. *Observe the Clinical Curative Effect for the Treatment of Advanced Gastric Cancer With Weining Particles Combination Chemotherapy*. Guangxi: Guangxi University of Traditional Medicine (2016).
44. Huang P, Tao MX, Xu C, Pan YY. Clinical Effects of Jianpi Huoxue Decoction Combined With Chemotherapy on Quality of Life and Immune Function in Patients With Advanced Gastric Cancer. *J Hubei Univ Chin Med* (2016) 18:37–9. doi: 10.3969/j.issn.1008-987x.2016.06.11
45. Ma M, Liu DS, Liang ES, Li XD, Cheng W, Huai XH. Clinical Observation of Fuzheng Xiaojia Recipe Combined With Chemotherapy in the Treatment of Advanced Gastric Cancer. *Chin J Gerontol* (2016) 36:5719–721. doi: 10.3969/j.issn.1005-9202.2016.22.105
46. Shao KF, Xiao P. Effects of Modified Shenling Baizhu San on Immune Function and Toxicity Reaction of Advanced Gastric Cancer Patients in Chemotherapy. *Guiding J Tradit Chin Med Pharm* (2016) 22:26–8+32. doi: 10.13862/j.cnki.cn43-1446/r.2016.08.008
47. Hu Q, Yang XY, Sun YS. Observation on the Therapeutic Effect of Kangai Injection Combined With Chemotherapy in Patients With Advanced Gastric Cancer. *Modem Pract Med* (2017) 29:886–89. doi: 10.3969/j.issn.1671-0800.2017.07.024
48. Pan B, Zang J, He J, Wang Z, Liu L. Add-On Therapy With Chinese Herb Medicine Bo-Er-Ning Capsule (BENC) Improves Outcomes of Gastric Cancer Patients: A Randomized Clinical Trial Followed With Bioinformatics-Assisted Mechanism Study. *Am J Cancer Res* (2018) 8:1090–105.
49. Xu W. Observation on the Efficacy and Safety of Jianpi Jiedu Recipe in Adjuvant Chemotherapy in the Treatment of Advanced Gastric Cancer. *Guangming J Chin Med* (2019) 34:767–69. doi: 10.3969/j.issn.1003-8914.2019.05.047
50. Yuan DD, Yue HG, Li LX. The Effects of Shenqifuzheng Injection on Serum miR-124 Level in Patients With Advanced Gastric Cancer. *J Med Theor & Prac* (2019) 32:1799–800+812. doi: 10.19381/j.issn.1001-7585.2019.12.002
51. Zhu YF, Zhang DW, Yu MH, Su Y, Wang CH, Xu XZ, et al. Efficacy of Aidi Injection Combined With Chemotherapy in Treatment of Advanced Gastric Cancer and Its Effects on Cancer-Related Fatigue, Quality of Life and Toxic and Side Effects. *J Hubei Univ Chin Med* (2019) 21:29–33. doi: 10.3969/j.issn.1008-987x.2019.04.07
52. Hou Y, Yan B. Effects of Buzhong Yiqi Decoction Combined With XELOX Regimen on Short-Term Efficacy and Long-Term Survival Rate in Advanced Gastric Cancer. *World Chin Med* (2020) 15:426–29. doi: 10.3969/j.issn.1673-7202.2020.03.027
53. Peng W, Zhang F, Wang Z, Li D, He Y, Ning Z, et al. Large Scale, Multicenter, Prospective Study of Apatinib in Advanced Gastric Cancer: A Real-World Study From China. *Cancer Manag Res* (2020) 12:6977–85. doi: 10.2147/CMAR.S249153
54. Cheng J, Cai M, Shuai X, Gao J, Wang G, Tao K. First-Line Systemic Therapy for Advanced Gastric Cancer: A Systematic Review and Network Meta-Analysis. *Ther Adv Med Oncol* (2019) 11:1–44. doi: 10.1177/1758835919877726
55. Yu J, Ji H, Dong X, Feng Y, Liu A. Apoptosis of Human Gastric Carcinoma MGC-803 Cells Induced by a Novel *Astragalus* Membranaceus Polysaccharide *via* Intrinsic Mitochondrial Pathways. *Int J Biol Macromol* (2019) 126:811–9. doi: 10.1016/j.ijbiomac.2018.12.268
56. Auyeung KK, Han QB, Ko JK. *Astragalus* Membranaceus: A Review of its Protection Against Inflammation and Gastrointestinal Cancers. *Am J Chin Med* (2016) 44:1–22. doi: 10.1142/S0192415X16500014
57. Auyeung KK, Woo PK, Law PC, Ko JK. *Astragalus* Saponins Modulate Cell Invasiveness and Angiogenesis in Human Gastric Adenocarcinoma Cells. *J Ethnopharmacol* (2012) 141:635–41. doi: 10.1016/j.jep.2011.08.010
58. Ma Q, Xu Y, Tang L, Yang X, Chen Z, Wei Y, et al. *Astragalus* Polysaccharide Attenuates Cisplatin-Induced Acute Kidney Injury by Suppressing Oxidative Damage and Mitochondrial Dysfunction. *BioMed Res Int* (2020) 2020:2851349. doi: 10.1155/2020/2851349
59. You X, Xu Y, Huang J, Zhi Y, Wu F, Ding F, et al. A Data Mining-Based Analysis of Medication Rules in Treating Bone Marrow Suppression by Kidney-Tonifying Method. *Evid Based Complement Alternat Med* (2019) 2019:1907848. doi: 10.1155/2019/1907848
60. Yan W, Xu Y, Yuan Y, Tian L, Wang Q, Xie Y, et al. Renoprotective Mechanisms of Astragaloside IV in Cisplatin-Induced Acute Kidney Injury. *Free Radic Res* (2017) 51:669–83. doi: 10.1080/10715762.2017.1361532
61. Liu W, Gao FF, Li Q, Lv JW, Wang Y, Hu PC, et al. Protective Effect of *Astragalus* Polysaccharides on Liver Injury Induced by Several Different Chemotherapeutics in Mice. *Asian Pac J Cancer Prev* (2014) 15:10413–20. doi: 10.7314/apjcp.2014.15.23.10413
62. Rébé C, Ghiringhelli F. Cytotoxic Effects of Chemotherapy on Cancer and Immune Cells: How can it be Modulated to Generate Novel Therapeutic Strategies? *Future Oncol* (2015) 19:2645–54. doi: 10.2217/fon.15.198
63. Li S, Sun Y, Huang J, Wang B, Gong Y, Fang Y, et al. Anti-Tumor Effects and Mechanisms of *Astragalus* Membranaceus (AM) and its Specific Immunopotentiation: Status and Prospect. *J Ethnopharmacol* (2020) 258:1–9. doi: 10.1016/j.jep.2020.112797
64. Yang B, Xiao B, Sun T. Antitumor and Immunomodulatory Activity of *Astragalus* Membranaceus Polysaccharides in H22 Tumor-Bearing Mice. *Int J Biol Macromol* (2013) 62:287–90. doi: 10.1016/j.ijbiomac.20-13.09.016
65. Li J, Bao Y, Lam W, Li W, Lu F, Zhu X, et al. Immunoregulatory and Anti-Tumor Effects of Polysaccharopeptide and *Astragalus* Polysaccharides on Tumor-Bearing Mice. *Immunopharmacol Immunotoxicol* (2008) 30:771–82. doi: 10.1080/08923970802279183

Conflict of Interest: The authors declare that the research was conducted in the absence of any commercial or financial relationships that could be construed as a potential conflict of interest.

Publisher's Note: All claims expressed in this article are solely those of the authors and do not necessarily represent those of their affiliated organizations, or those of the publisher, the editors and the reviewers. Any product that may be evaluated in this article, or claim that may be made by its manufacturer, is not guaranteed or endorsed by the publisher.

frontiers in Pharmacology

SYSTEMATIC REVIEW
published: 27 October 2021
doi: 10.3389/fphar.2021.714287

The Therapeutic Principle of Combined Strengthening Qi and Eliminating Pathogens in Treating Middle-Advanced Primary Liver Cancer: A Systematic Review and Meta-Analysis

*Yingqi She[1†], Qinfeng Huang[2†], Zhen Ye[1], Yu Hu[1], Mingquan Wu[3], Kaihua Qin[4], Ailing Wei[5], Xin Yang[1], Yuyao Liu[6], Cuihan Zhang[6] and Qiaobo Ye[1]**

[1]School of Basic Medical Sciences, Chengdu University of Traditional Chinese Medicine, Chengdu, China, [2]Department of Oncology, The First Affiliated Hospital, Guangxi University of Chinese Medicine, Nanning, China, [3]Department of Pharmacy, Sichuan Provincial Orthopedic Hospital, Chengdu, China, [4]Health Preservation and Rehabilitation College, Chengdu University of Traditional Chinese Medicine, Chengdu, China, [5]Department of Liver Disease, The First Affiliated Hospital, Guangxi University of Chinese Medicine, Nanning, China, [6]Pharmacy College, Chengdu University of Traditional Chinese Medicine, Chengdu, China

OPEN ACCESS

Edited by:
Qingmin Sun, Affiliated Hospital of Nanjing University of Chinese Medicine, China

Reviewed by:
Yun K. Tam, Sinoveda Canada Inc., Canada
Bunleu Sungthong, Mahasarakham University, Thailand

***Correspondence:**
Qiaobo Ye
yeqiaobo@cdutcm.edu.cn

[1]These authors contributed equally to this work

Specialty section:
This article was submitted to Ethnopharmacology, a section of the journal Frontiers in Pharmacology

Received: *25 May 2021*
Accepted: *27 September 2021*
Published: *27 October 2021*

Citation:
She Y, Huang Q, Ye Z, Hu Y, Wu M, Qin K, Wei A, Yang X, Liu Y, Zhang C and Ye Q (2021) The Therapeutic Principle of Combined Strengthening Qi and Eliminating Pathogens in Treating Middle-Advanced Primary Liver Cancer: A Systematic Review and Meta-Analysis. Front. Pharmacol. 12:714287. doi: 10.3389/fphar.2021.714287

Background: The combination of strengthening Qi and eliminating pathogens is an available therapeutic principle in traditional Chinese medicine (TCM) for primary liver cancer (PLC) at middle-advanced stage. However, there is a lack of reasonable evidence to support the proper application of this therapeutic principle. This meta-analysis aims to evaluate the efficacy and safety of Chinese medicinal formulas (CMFs), including two subgroup analyses of the principle of strengthening Qi and eliminating pathogens.

Method: Clinical trials were obtained through searching of EMBASE, Web of Science, PubMed, Cochrane Library, Chinese National Knowledge Infrastructure, Wanfang Database, Chinese Scientific Journal Database, Chinese Biomedical Literature Database, and two clinical trial registries. The randomized controlled trials with the combination of CMFs and transcatheter arterial chemoembolization (TACE) in the experiment group were acceptable, in contrast to the TACE alone in the control group. The statistics analysis was performed on Review Manager 5.4.

Results: A total of eligible 24 trials were accessed in this work. Overall, CMFs could improve the survival duration of 6 months, 1 year, and 2 years, Karnofsky Performance Status, tumor objective response rate (ORR), AFP, and symptom. In the subgroup analysis, trials complying with the principle of single strengthening Qi did not show any significant difference in increasing tumor ORR. Meanwhile, the principle of combined strengthening Qi and eliminating pathogens was uncertain in improving symptoms and 1-year and 2-year survival time. In addition, the outcome indexes of ALT and AST were heterogeneous. In last, the total occurrence of adverse events could not be reduced via using CMFs. Patients treated with CMFs exhibited liver injury, fever, and white blood cell decline, with mild events occurring more frequently and severe events occurring less.

Conclusion: CMFs are an effective treatment method to cure PLC at the middle-advanced stage. Adopting the principle of single strengthening Qi presents better efficacy in the long term by prolonging the survival duration. Following the principle of combined strengthening Qi and eliminating pathogens could be more beneficial to patients in short term by lessening the tumor size. CMFs have the advantage of reducing certain serious adverse events.

Keywords: Chinese medicinal formulas, transcatheter arterial chemoembolization, drastic medicinals, therapeutic principle, primary liver cancer, meta-analysis

INTRODUCTION

Primary liver cancer (PLC) is one of the common digestive system neoplasms, including most of the hepatocellular carcinoma (HCC), a small part of cholangiocarcinoma (CCC), and combined hepatocholangiocarcinoma (HCC-ICC). According to GLOBOCAN 2020 (Sung et al., 2021), 906,000 new PLC cases and 830,000 PLC death cases were reported. Based on cancer statistics published by the American Cancer Society in 2020 (Siegel et al., 2020), liver cancer (LC) was the fastest-growing one among tumor diseases, increasing at the rate of 2-3% per year during 2007–2016 in the United States. In all the regions and nations, China could not be ignored as it has the largest population of HCC patients (Zhu et al., 2016). Although both male and female morbidity and mortality dropped from 2000 to 2015 in China, the PLC still ranked fourth in new cases and second place in cancer mortality (Zhang et al., 2020).

Typically, due to the substantial compensation of hepatic function, PLC patients usually do not have clinical symptoms, such as liver pain and hepatomegaly, until the disease develops to the middle-late stage. Thus, a large number of patients miss the radical therapeutic time windows because of the delay in early diagnosis. With the innovation of medical technology, the lifespan of HCC patients has been extended (Tang et al., 2018); however, the burden of PLC should be paid more attention. From 2005 to 2015, absolute years of life lost in HCC increased 4.5% (Yang et al., 2019). Also, the countries with resource scarcity and those with a small number of doctors per 10,000 persons are more likely to face an early onset of LC (Are et al., 2017). For average families, the treatment of PLC can bring a huge economic burden. For countries, it also increases the financial burden on the public medical system and leads to the loss of social productivity.

Transcatheter Arterial Chemoembolization (TACE) has been regarded as the most common nonsurgical treatment for LC since Yamada was reported in Japan (Imai et al., 2014). And it has been the first-line treatment for PLC patients in the intermediate stage (BCLC stage B) (Galle et al., 2018). Although sorafenib is the current primary medicine for treating advanced hepatocellular carcinoma, BRIDGE's real-world clinical research noted that almost 50% of patients, ranging from stage 0 to D, were treated with TACE (Raoul et al., 2019). As early as 2011, it was reported in the Asian Consensus Workshop that TACE and surgical resection have been applied to the treatment for advanced hepatocellular carcinoma in Korea, China, and Japan (Han et al., 2011). Therefore, there is no doubt that TACE is a standard treatment for middle-late stage PLC.

TACE is a treatment in which embolic agents and chemotherapy drugs are mixed together and injected from the hepatic artery to the tumor site, serving to embolize the tumor-feeding arteries and induce ischemic necrosis in the tumor tissue. Depending on the embolic agent, there are conventional TACE (cTACE) treatments using iodine oil and drug-eluting bead TACE (DEB-TACE) that enables drugs to sustainedly release up to a month (Raoul et al., 2019). Adriamycin, mitomycin, and cisplatin are three chemotherapeutic agents frequently used in TACE (Galle et al., 2017). It is common for patients to suffer from postembolization syndrome after TACE treatment because of the toxic effects from chemotherapeutic agents and the stress response caused by the embolization of local tissues. Approximately 35–100% of patients experience abdominal pain, fever, and nausea, and some of them choose to discontinue TACE therapy in response to severe adverse reactions and liver failure (Raoul et al., 2011). Mason also pointed out that the postembolization syndrome was associated with an increased risk of death (Mason et al., 2015). Meanwhile, the tumor hypoxic microenvironment, resulting from artery occlusion, can induce the release of angiogenic factors and promote tumor neovascularization (Bruix et al., 2015). Consequently, it is urgent to find new antihepatoma drugs or new therapies. Currently, the clinical application of combining traditional or complementary medicine with TACE therapy is widespread, especially in China. Nevertheless, the efficacy and safety of traditional Chinese medicine (TCM) still need evidence-based reviews to provide more informative clinical proof.

TCM is gaining popularity, especially in tumor patients, since TCM focuses on the whole body of the patient and aims to make the patient adapt to chemotherapy by improving the patient's immunity and reducing side effects with the application of Chinese medicinal formulas (CMFs). Generally speaking, there are two common therapeutic principles for tumor patients, respectively, the principle of single strengthening Qi (PSSQ) and the principle of combined strengthening Qi and eliminating pathogens (PCSQEP). The former consists of Qi replenishing medicinals and the latter add drastic medicinals to Qi replenishing formulas to eliminate pathogens. Hitherto,

there has been no evidence from evidence-based medicine indicating which treatment regimen is more beneficial for PLC patients at the intermediate-advanced stage when TCM is used in conjunction with TACE. In this meta-analysis, drastic medicinals were defined, including toxic medicinals recorded in the China Pharmacopeia and characterized by a strong effect on dispersing stagnant Qi, purging fluid, dissipating mass, and breaking blood stasis. Overall, there is a need to assess the efficacy and safety of CMFs and figure out the applicable conditions for PSSQ and PCSQEP.

METHODS

This study was conducted by the Preferred Reporting Items for Systematic Reviews and Meta-Analyses (PRISMA) statement (Moher et al., 2009).

Search Strategies

The electronic search was from their inception until December 18, 2020, which was performed in the Chinese National Knowledge Infrastructure (CNKI), the Wanfang Database, the Chinese Scientific Journal Database (VIP), the Chinese Biomedical Literature Database (CBM), Excerpta Medica Database (EMBASE), Web of Science, PubMed, and Cochrane Library. The search formulation adopted a combination of free texts and medical subject heading (MeSH), which was developed to meet the requirements according to the search habits of each database. At the same time, there is no restriction of search formulation on language or country. The search formula for each database is shown in the Supplementary Material. References that meet the requirements would be taken into consideration as well. Two clinical trial registries (http://www.chictr.org.cn/and http://www.clinicaltrials.gov/) were also searched. We also contacted the trial registrants by email to try to obtain their raw data in case we missed some of the trials that were appropriate for this study.

Study Selection

Types of Participants

All participants enrolled in the study met the diagnostic criteria for intermediate-advanced PLC, which meant that trials involving participants with secondary hepatic carcinoma or participants at an early stage were excluded. The studies that did not mention the staging of LC were also excluded.

Types of Intervention

All patients had to receive TACE treatment or symptomatic and supportive treatment after TACE. On the basis of the TACE, the experimental group was treated with CMFs containing Qi replenishing medicinals in basic formulas by oral, lasting at least 1 week. Studies were also excluded if the experimental group used single Chinese medicinal, acupuncture, moxibustion, qigong, plaster, Chinese medicine injections, psychological interventions, and other Western medicine. Trials that did not report prescriptions were also excluded.

Types of Comparison

Except for TACE treatment, other treatment plans in control groups such as TACE combined with surgical resection, radiofrequency ablation, radiotherapy, and targeted therapy were excluded.

Outcomes

Referring to the Guidelines for Clinical Research of Malignant Tumors on New Traditional Chinese Medicines (GCRMTNTCM), the 6-month, 1-year, and 2-year survival rates and the efficient rate in Karnofsky Performance Status (KPS) were the primary outcome. The secondary outcomes were the tumor objective response rate (ORR), ALT, AST, AFP, symptoms improvement, and adverse events. Adverse events included nausea and vomit, inappetence, digestive symptoms, fever, liver injury, white blood cell (WBC) reduction, platelet reduction, hemoglobin reduction, bone marrow suppression, and neurotoxicity. Trials without relevant outcomes and sufficient data for statistical analysis were excluded.

Type of Studies

Only randomized controlled trials (RCTs) were accepted. Animal experiments, meta-analyses, systematic reviews, retrospective studies, case reports, and reviews were not eligible.

Others

To improve the quality of each included trial and to protect efficacy from other factors, we also set the inclusive condition for clinical trials according to the approach of RCTs design (**Supplementary Table S1**). Only the clinical trials that meet the following requirements can be included: 1) all patients who received primary treatment or had undergone a washout period before trials entry; 2) studies with comparable baseline; 3) studies with diagnostic, inclusion, and exclusion criteria; 4) studies with efficacy evaluation standard. Additionally, the studies would be excluded, if they were derived from conference papers or dissertations.

Data Collection and Extraction

First, She Y.Q. was responsible for searching according to the established search formulation, screening the eligible literature, and extracting the records. Second, Liu Y.Y. and Zhang C.H. independently screened the titles and abstracts of the trials and excluded those that were not compliant with the criteria. After merging the results of the two, She Y.Q. and Hu Y. proceeded to the full-text screening stage. When they encountered disagreement, it was handed over to the senior reviewers Wei A.L. for judgment. At the end of the screening process, all literature was reviewed or rechecked by the senior reviewers Qin K.H. Finally, from the included studies, information was extracted by two reviewers: Liu Y.Y. extracted the data, and She Y.Q. was in charge of reviewing it (see **Supplementary Figure S1**).

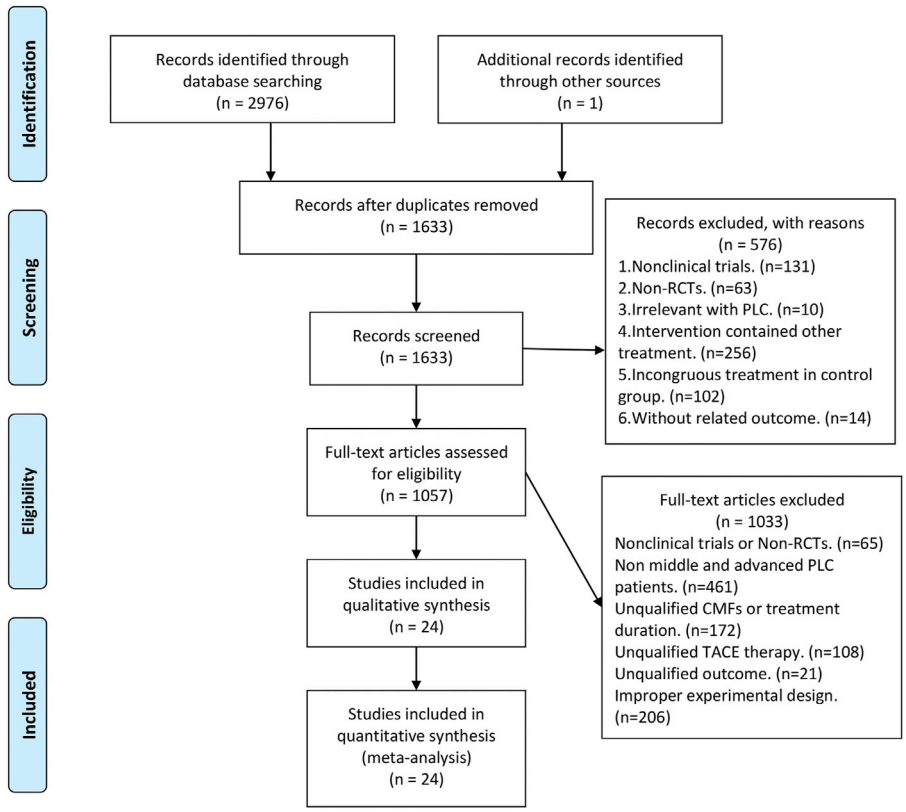

FIGURE 1 | PRISMA flow diagram.

Assessment of Risk of Bias

Regarding the Cochrane Handbook (Higgins et al., 2019), two reviewers independently analyzed the risk bias of the included trials. The following seven items were evaluated: 1) random sequence generation; 2) allocation concealment; 3) blinding of participants and personnel; 4) blinding of outcome assessment; 5) incomplete outcome data; 6) selective reporting; and 7) other biases. Each domain was graded on three levels based on methodological quality: high risk, low risk, and unclear risk.

Statistical Analysis

RevMan5.4 and Stata 16 were the software used for meta-analysis. According to the outcome category, continuous data were calculated as a weighted mean difference (WMD) with a 95% confidence interval (CI), while categorical data were calculated as the risk ratio (RR) with 95% CI. $p < 0.05$ was considered statistically significant. Heterogeneity was assessed by the chi-square test and I^2 statistic. When the $p > 0.1$ and $I^2 \leq 50\%$, these outcomes were regarded as homogeneity, using a fixed effect model. Conversely, when the $p \leq 0.1$ and $I^2 > 50\%$, these outcomes were deemed to have heterogeneity with a random effect model. A subgroup analysis was performed according to whether drastic medicinals were involved in the CMFs. Besides, if there were heterogeneity in the results, we would look for heterogeneity sources and perform a sensitivity analysis by converting the random effect model and fixed effect model to determine whether the results are stable. Publication bias was analyzed visually through funnel plots.

RESULTS

Study Identification

Figure 1 shows the flowchart of clinical trials screening in the meta-analysis, which was derived from the PRISMA statement (Moher et al., 2009). A total of 2,977 studies were obtained after searching in the database as well as hand retrieval, of which 1,344 were duplicates. 1,633 articles were entered into the records screening, and 576 articles were excluded. The remaining 1,057 articles were read in full text, where the more stringent inclusion criteria were implemented based on PICOS and experimental design (**Supplementary Table S2**), resulting in the exclusion of 1,033 articles. There were finally 24 eligible papers enrolled in this meta-analysis (Zhang et al., 2007; Huang et al., 2009; Chi et al., 2010; Li et al., 2011; Ding, 2012; Ji et al., 2012; Liu et al., 2013; Rong et al., 2013; Deng et al., 2014; Cheng, 2015; Feng and Chen, 2015; Tang et al., 2015; Wang, 2015; Ye et al., 2015; Wang et al., 2016; Li and Xu, 2017; Song et al., 2017; Zhang et al., 2017; Du et al., 2018; Jiang et al., 2020; Shen et al., 2020; Wang et al., 2020; Wang et al., 2020; Zhang, 2020).

TABLE 1 | Basic characteristics of the included studies.

First author and year	Staging criteria	Stage	Sample size (E/C)	Age (year)	Male/female	Child-Pugh	KPS	Drastic medicinals added	Treatment period	Washout period	Outcome measure
Zhang (2020)	BCLC	CD	20/20	E:59.6 ± 9.3 C:59.6 ± 9.3	E:15/5 C:15/5	—	>70	No	8 w	4 w	abei
Shen L. N. (2020)	GDTPLCC (2017)	IIb and III	30/30	E:60.03 ± 9.48 C:58.37 ± 11.05	E:24/6 C:25/5	AB	—	No	5 w	Primary treatment	fgj
Feng and Chen (2015)	—	II and III	42/42	—	—	—	>60	No	12 w	Primary treatment	de
Cheng M. F. (2015)	DTCCCC (1991)	II and III	42/42	—	—	—	—	No	2 w	4 w	abfgj
Deng L. (2014)	CDSCPLCC (2001)	II and III	42/38	E:66.78 ± 3.98 C:65.68 ± 4.69	E:26/12 C:25/17	AB	≥60	No	12 w	4 w	abefghij
Liu X. (2013)	CPG·CS	II and III	32/32	E:51.7 ± 10.3 C:52.2 ± 9.74	E:27/5 C:26/6	AB	≥60	No	8 w	4 w	deij
Ji J. (2012)	DTCCCC (1991)	II and III	28/28	E:44.3 ± 11.6 C:43.6 ± 12.8	E:18/10 C:16/12	AB	≥60	No	4 w	8 w	dej
Li Y.H. (2011)	CDSCPLCC (2001)	II and III	38/36	E:52.7 C:54.1 (median age)	E:29/7 C:31/7	AB	≥60	No	60 d	4 w	abcdehij
Chi H. C. (2010)	DTCCCC (1991)	Middle-advanced	60/60	—	E:36/24 C:38/22	—	—	No	4 m	4 w	bcdej
Wang A. M. (2020)	BCLC	BC	30/30	E:49.24 ± 13.74 C:48.64 ± 14.48	C:18/12 E:17/13	AB	—	No	4 w	4 w	fgj
Song Y. N. (2017)	GDTPLCC (2017)	Middle-advanced	40/40	E:54.48 ± 8.36 C:53.7 ± 8.27	E:18/22 C:30/10	—	60–80	No	3 rounds, 6–8 w per round	Primary treatment	abcefgh
Ye W. D. (2015)	BCLC	BC	34/34	E:55.15 C:55.24 (median age)	E:29/5 C:30/4	—	≥70	No	5 w	4 w	efj
Huang J. Y. (2009)	DTCCCC (1990)	II and III	30/30	E:54.5 C:56.1	E:21/9 C:20/10	—	≥50	Yes	60 d	4 w	dej
Wang (2015)	GDTPLC (2011)	II, III, and IV	46/46	E:41.2 ± 11.7 C:40.6 ± 12.4	E:25/21 C:27/19	—	>50	Yes	4 w	2 w	eh
Rong Z. (2013)	NDDTCCCC	Middle-advanced	30/30	E:52.73 ± 10.42 C:55.37 ± 10.68	E:18/12 C:16/14	AB	≥60	Yes	8 w	4 w	efgh
Wang Q. M. (2016)	CPG·CS	III and IV	30/30	E:46.67 ± 7.19 C:46.47 ± 7.38	E:24/6 C:22/8	AB	≥60	Yes	8 w	4 w	deij
Du H. P. (2018)	—	II and III	35/34	—	E:24/10 C:21/14	ABC	>60	Yes	3 m	Primary treatment	fgj
Wang X. D. (2020)	GDTPLCC (2017)	IIb and IIIa	25/25	E:56.52 ± 13.40 C:55.52 ± 12.58	E:20/5C:23/2	AB	≥60	Yes	6 w	4 w	defghij
Jiang R. R. (2020)	TNM	II and III	45/45	E:50.6 ± 8.1 C:49.7 ± 8.0	E:25/20 C:23/22	AB	>75	Yes	12 w	Primary treatment or 4 w	ehj
Tang Q. Y. (2015)	CDSCPLCC (2002)	Middle-advanced	53/53	E:53.67 ± 11.18 C:55.38 ± 10.72	E:46/7 C:48/5	AB	≥60	Yes	12 w	8 w	defg
Ding R. F. (2012)	—	III and IV	33/30	E:53.9 C:56.4	E:17/13 C:19/14	AB	—	Yes	2 rounds, 3–5 w per round	Primary treatment	e
Zhang Q. (2007)	DTCCCC (1991)	Middle-advanced	58/54	E:58.0 ± 7.0 C:56.5 ± 8.5	E:35/19 C:38/20	—	≥50	Yes	2 m	4 w	abcdej
Zhang Z. Y. (2017)	TNM	II, III, and IV	38/38	E:39.42 ± 5.37 C:39.61 ± 5.42	E:25/13 C:26/12	AB	>60	Yes	90 d	4 w	efgh
			40/38			AB	≥60	Yes	60 d		bcdj

(Continued on following page)

TABLE 1 | (*Continued*) Basic characteristics of the included studies.

First author and year	Staging criteria	Stage	Sample size (E/C)	Age (year)	Male/female	Child-Pugh	KPS	Drastic medicinals added	Treatment period	Washout period	Outcome measure
Li and Xu (2017)	GDTPLC (2011)	Middle-advanced		E:49.08 ± 11.27 C:46.18 ± 10.65	E:30/8 C:32/8					Primary treatment	

BCLC, Barcelona clinic liver cancer; GDTPLCC (2017), Guidelines for Diagnosis and Treatment of Primary Liver Cancer in China (2017 Edition); DTCCCC (1991), the Diagnosis and Treatment Criterion for Common Cancer in China (1991 Edition); CDSCPLCC (2001), Clinical Diagnosis and Staging Criteria of Primary Liver Cancer in China (2001 Edition); CPG·CS, Clinical Practice Guideline·Cancer Section; DTCCCC (1990), the Diagnosis and Treatment Criterion for Common Cancer in China (1991 Edition); GDTPLC (2011), Guidelines on the Diagnosis and Treatment of Primary Liver Cancer (2011 Edition); NDDTCCCC, New edition of the Diagnosis and Treatment Criterion for Common Cancer in China (1999 Edition); TNM, TNM Classification of Malignant Tumors; CDSCPLCC (2002), Clinical Diagnosis and Staging Criteria of Primary Liver Cancer in China (2002 Edition); E, experiment group; C, control group; d, day; w, week; m, month; a, 6-month survival; b, 1-year survival; c, 2-year survival; d, KPS; e, ORR; f, ALT; g, AST; h, AFP; i, TCM symptom improvement; j, adverse events.

Study Characteristics

To conduct the research, the researchers enrolled 1,786 patients. The 24 included trials were all completed in China, with sample sizes ranging from 40 to 120. Baseline information for each trial was shown in **Table 1**, and clinical data were comparable across all studies. Neoplasm staging systems were mentioned in 21 among 24 trials, two studies used the criteria developed by the Union for International Cancer (UICC), and three studies utilized the Barcelona staging. The remaining 16 trials adopted the standard established in China. Although no staging criteria were reported, three further trials included PLC patients at the intermediate-advanced stage. Except for nine studies in which Child-Pugh scores were not recorded and one trial that enrolled patients with Child-Pugh class C, the residual studies were all Child-Pugh class A or B patients. The KPS recorded in all 19 articles was greater than 50, indicating that at least the patients in these studies were able to live on their own and did not require heavy dependence on others. The details of the intervention are shown in **Table 2** and **Supplementary Table S3**. Regarding the choice of dosage form, two trials were administered in the form of capsules, one trial was administered in the form of oral solution, one trial was administered in the form of tablets, one trial was administered in the form of pills, and 19 trials were administered in the form of decoctions. As syndrome differentiation is one of the features of TCM, TCM physicians will modify the decoctions based on the severity of the disease and symptoms (e.g., abdominal distension, jaundice, and insomnia). As a result, 13 trials treated patients with the modified formulas, and six trials used the basic formulas. The proportion of included studies with and without drastic medicinals was 1:1. Furthermore, one trial did not account for the agents used for TACE. The duration of treatment ranged from 2 to 12 weeks. Patients either received TACE for the first time or experienced at least a 2-week washout period before enrolling in the trial.

Risk of Bias

Supplementary Figures S2, S3 showed the methodological quality of 24 trials. Eight trials applied a random number list. No studies described allocation concealment, blinding of participants and personnel, or blinding for outcomes, so their risks were unknown. All of the outcome data were complete, of which nine trials performed follow-up visits and one trial documented the reason for loss to follow-up and how these cases were handled. Two trials had poor adverse events reporting such that this outcome could not be incorporated into meta-analysis and were rated as high risk in the item of selective reporting. No clinical trial registration numbers were found for the remaining 22 studies, and the risk of selective reporting was unknown. Other risks of bias were also unclear.

Primary Outcome

Survival Time

A total of eight clinical trials reported the survival times of 6 months, 1 year, and 2 years of which the results were all shown by **Figure 2**, **Figure 3**, and **Figure 4**. Six trials reported 6-month survival rates [n = 473; RR = 1.18; 95%CI (1.06, 1.31); $p = 0.002$; $I^2 = 0\%$], with patients in the CMFs group having a higher survival rate than the TACE group. Subgroup analysis suggested that the trials complying with PSSQ improved the 6-month survival rate of patients in CMFs group [n = 361; RR = 1.20; 95%CI (1.06, 1.35); $p = 0.004$; $I^2 = 0\%$], while those trials complying with PCSQEP were not statistically significant [n = 112; RR = 1.12; 95%CI (0.92, 1.36); $p = 0.27$]. For the statistical analysis of 1-year survival, meta-analysis showed that the RR of 1-year survival was higher in the CMFs group than in the TACE group [n = 671; RR = 1.34; 95% CI (1.14, 1.57); $p = 0.09$; $I^2 = 43\%$]. In the subgroup analysis, the RR in the trials complying with PSSQ was higher in CMFs group [n = 481; RR = 1.43; 95%CI (1.22, 1.66); $p = 0.85$; $I^2 = 0\%$], while the trials complying with PCSQEP was not statistically significant [n = 190; RR = 1.18; 95%CI (0.80, 1.74); $p = 0.04$; $I^2 = 77\%$]. The sensitivity analysis showed that the study reported by Li L was the source of heterogeneity. CMFs also enhanced survival rate at 2 years [n = 464; RR = 1.63; 95%CI (1.27, 2.09); $p = 0.0001$; $I^2 = 0\%$]. In the subgroup analysis, trials complying with PSSQ [n = 274; RR = 1.62; 95%CI (1.13, 2.34); $p = 0.009$; $I^2 = 0\%$] and PCSQEP [n = 190; RR = 1.64; 95%CI

TABLE 2 | Details of interventions.

First author and year	Formula	Ingredients of drastic medicinals	Control intervention
Zhang (2020)	Modified Sanjinchaihushusan decoction$^{\triangle}$	—	TACE (5-FU and OXA)
Shen L. N. (2020)	Modified Gexiazhuyu decoction$^{\triangle}$	—	TACE (5-FU, OXA, CF, ADM, and MMC)
Feng and Chen (2015)	Gexiazhuyu decoction$^{\triangle}$	—	TACE (5-FU, DDP, and ADM)
Cheng M. F. (2015)	Modified Yiganxiaogu decoction$^{\triangle}$	—	TACE (5-FU, DDP, and EPI)
Deng L. (2014)	Modified Jianpiyigan decoction$^{\triangle}$	—	TACE (5-FU, OXA, and MMC)
Liu X. (2013)	Modified WD-2 decoction$^{\triangle}$	—	TACE (5-FU, OXA, MMC, HCPT, DDP, and EPI)
Ji J. (2012)	Xiaoyaosan decoction$^{\triangle}$	—	TACE (5-FU, MMC, and DDP)
Li Y. H. (2011)	Chinese medicinals decoction$^{\triangle}$	—	TACE (5-FU, THP, and DDP)
Chi H. C. (2010)	Modified Shuganjianpi decoction$^{\triangle}$	—	TACE (5-FU, DDP, and EPI)
Wang A. M. (2020)	Modified Bazhen decoction$^{\triangle}$	—	TACE (EPI)
Song Y. N. (2017)	Modified Wenyangjiedu decoction$^{\triangle}$	—	TACE (CBP, THP, and MMC)
Ye W. D. (2015)	Modified Fupitiaogan decoction$^{\triangle}$	—	TACE
Huang J. Y. (2009)	Shenyi capsule and Cidan capsule$^{\#}$	*é zhú* (the dried rhizoma of *Curcuma kwangsiensis* S.G.Lee and C.F.Liang), *shān cí gū* (the dried pseudobulb of *Cremastra appendiculata* (D.Don) Makino), *mǎ qián zǐ* (the mature seed of *Strychnos nux-vomica* L.), *fēng fáng* (the nest of *Polistes olivaceous* (DeGeer)), *yā dǎn zǐ* (the mature fruit of *Brucea javanica* (L.) Merr.), and *rén gōng niú huáng* (*Calculus Bovis Artifactus*)	TACE (5-FU, HCTP, DDP, and MMC)
Wang (2015)	Yangzhengxiaoji capsule$^{\#}$	*é zhú* (the dried rhizoma of *Curcuma kwangsiensis* S.G.Lee and C.F.Liang) and *tǔ biē chóng* (the dried insect body of *Eupolyphaga sinensis* Walker)	TACE (DDP, 5-FU, ADM, and MMC)
Rong Z. (2013)	Dujieqing oral liquid$^{\#}$	*wú gōng* (the dried insect body of *Scolopendra subspinipes mutilans* L. Koch), *bā jiǎo lián* (the dried rhizoma and root of *Podophyllum versipelle* Hance), and *tǔ biē chóng* (the dried insect body of *Eupolyphaga sinensis* Walker)	TACE (DDP, GEM, and PYM)
Wang Q. M. (2016)	Ganxi tablet$^{\#}$	*zǎo xiū* (the dried rhizome of *Paris polyphylla var. yunnanensis* (Franch.) Hand.-Mazz.)	TACE (arsenic trioxide)
Du H. P. (2018)	Biejiajian pill$^{\#}$	*tǔ biē chóng* (the dried insect body of *Eupolyphaga sinensis* Walker), *fēng fang* (the nest of *Polistes olivaceous* (DeGeer)), *qiāng lǎng* (the dried insect body of *Catharsius molossus* (Linnaeus)), *shǔ fù* (the dried insect body of *Armadillidium vurgare* (Latrelle)), and *xiāo shí* (Saltpetre)	TACE (5-FU, EPI, and HCPT)
Wang X. D. (2020)	Modified Fuzhengquxieyiai decoction$^{\#}$	*tǔ biē chóng* (the dried insect body of *Eupolyphaga sinensis* Walker) and *é zhú* (the dried rhizoma of *Curcuma kwangsiensis* S.G.Lee and C.F.Liang)	TACE (DDP and AZM)
Jiang R. R. (2020)	Fuhebiehua decoction$^{\#}$	*é zhú* (the dried rhizoma of *Curcuma kwangsiensis* S.G.Lee and C.F.Liang)	TACE (5-FU and OXA)
Tang Q. Y. (2015)	Modified Aitongxiao decoction$^{\#}$	*é zhú* (the dried rhizoma of *Curcuma kwangsiensis* S.G.Lee and C.F.Liang) and *sān léng* (the dried tuber of *Sparganium stoloniferum* (Buch.-Ham. ex Graebn.) Buch.-Ham. ex Juz.)	TACE (5-FU, THP, and MMC)
Ding R. F. (2012)	Modified Fuzheng decoction$^{\#}$	*é zhú* (the dried rhizoma of *Curcuma kwangsiensis* S.G.Lee and C.F.Liang)	TACE (OXA and GEM)
Zhang Q. (2007)	Gubenyiliu II decoction$^{\#}$	*é zhú* (the dried rhizoma of *Curcuma kwangsiensis* S.G.Lee and C.F.Liang)	TACE (DDP, 5-FU, VDS, and EPI)
Zhang Z. Y. (2017)	Qingganhuayu decoction$^{\#}$	*é zhú* (the dried rhizoma of *Curcuma kwangsiensis* S.G.Lee and C.F.Liang) and *sān léng* (the dried tuber of *Sparganium stoloniferum* (Buch.-Ham. ex Graebn.) Buch.-Ham. ex Juz.)	TACE (5-FU, EPI, MMC, and DDP)
Li and Xu (2017)	Baoyuan decoction and Xiaoyao decoction$^{\#}$	*é zhú* (the dried rhizoma of *Curcuma kwangsiensis* S.G.Lee and C.F.Liang)	TACE (5-FU, THP, and DDP)

Abbreviations: 5-FU, 5-fluorouracil; DDP, cisplatin; OXA, oxaliplatin; CBP, carboplatin; CF, calcium folinate; ADM, doxorubicin; EPI, epirubicin; THP, pirarubicin; MMC, mitomycin; AZM, azithromycin; GZM, gemcitabine; PYM, bleomycin A5; HCPT, hydroxycamptothecin; VDS, vindesine sulfate. $^{\triangle}$CMFs adopt the therapeutic principles of PSSQ. $^{\#}$CMFs adopt the therapeutic principles of PCSQEP.

(1.17, 2.29); $p = 0.004$; $I^2 = 0\%$] both reported that CMFs group performed better than TACE group.

The Efficient Rate of Karnofsky Performance Status

According to the KPS defined by World Health Organization (WHO) (Palmer, 1982), the quality of life of patients whose postoperative KPS increased or decreased by no more than 10 points is considered stabilized or improved, which is called the efficient rate of KPS. The results of 11 trials showed that the CMFs group had a more significant improvement and stabilization effect on patients' quality of life than the TACE group [n = 864; RR = 1.42; 95%CI (1.31, 1.55); $p < 0.00001$; $I^2 = 0\%$]. Concerning the subgroup analysis, five trials complying with PSSQ illustrated that the CMFs group enhanced the efficiency of

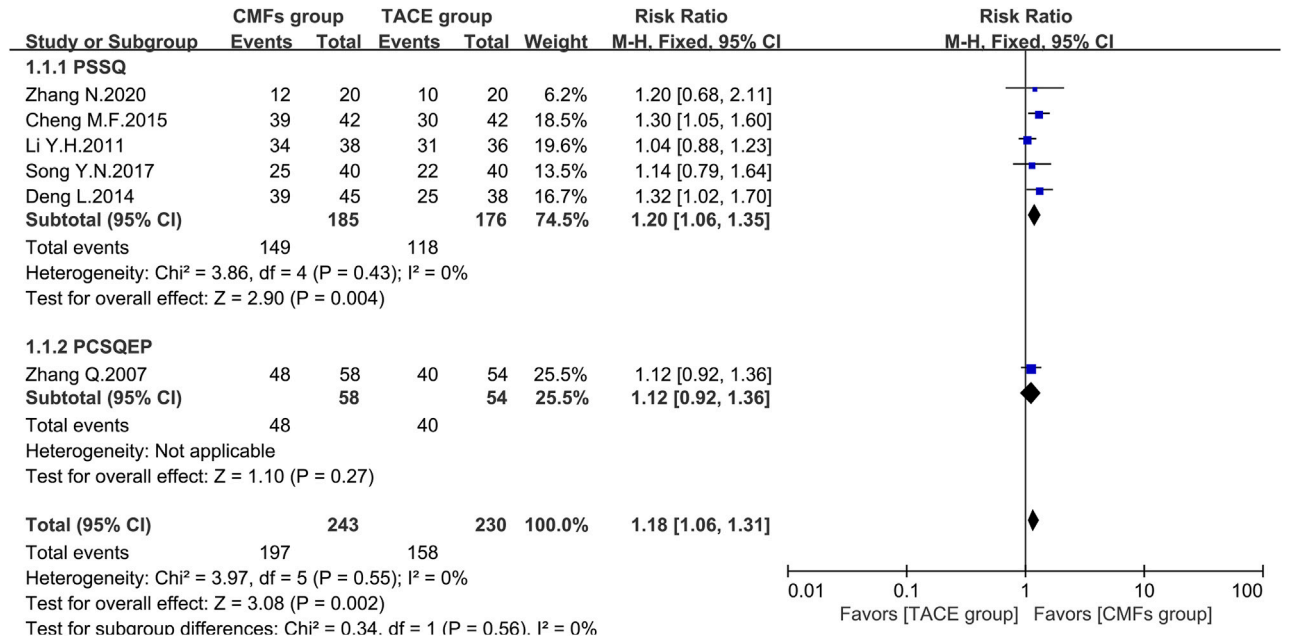

FIGURE 2 | Effect of CMFs group versus TACE group on 6-month survival, including a comparison between PSSQ and PCSQEP in the subgroup.

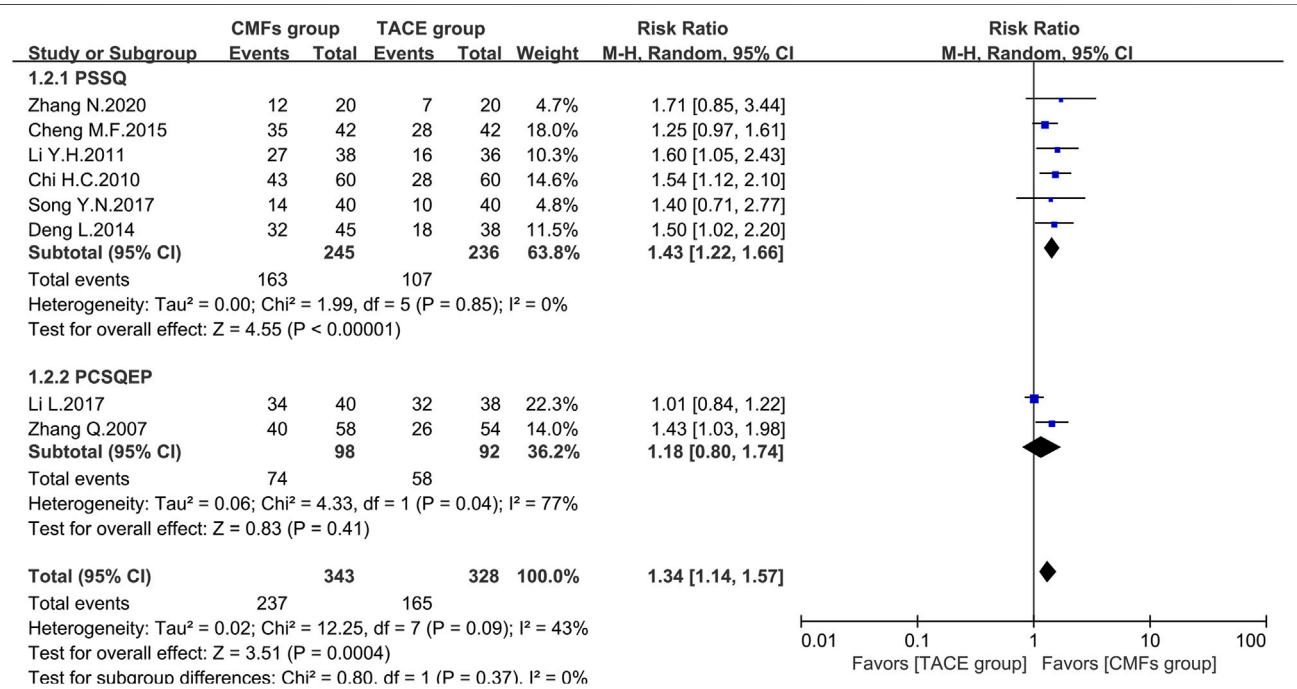

FIGURE 3 | Effect of CMFs group versus TACE group on 1-year survival, including a comparison between PSSQ and PCSQEP in the subgroup.

KPS compared to the TACE group [n = 398; RR = 1.43; 95%CI (1.26, 1.62); $p < 0.00001$; $I^2 = 0\%$], which was similar to the result of remaining four trials in PCSQEP group [n = 466; RR = 1.42; 95%CI (1.26, 1.60); $p < 0.00001$; $I^2 = 25\%$] (**Figure 5**).

Secondary Outcome

ORR

Nineteen clinical trials evaluated the efficacy of solid tumors with the benefit of two different evaluation criteria, the determination

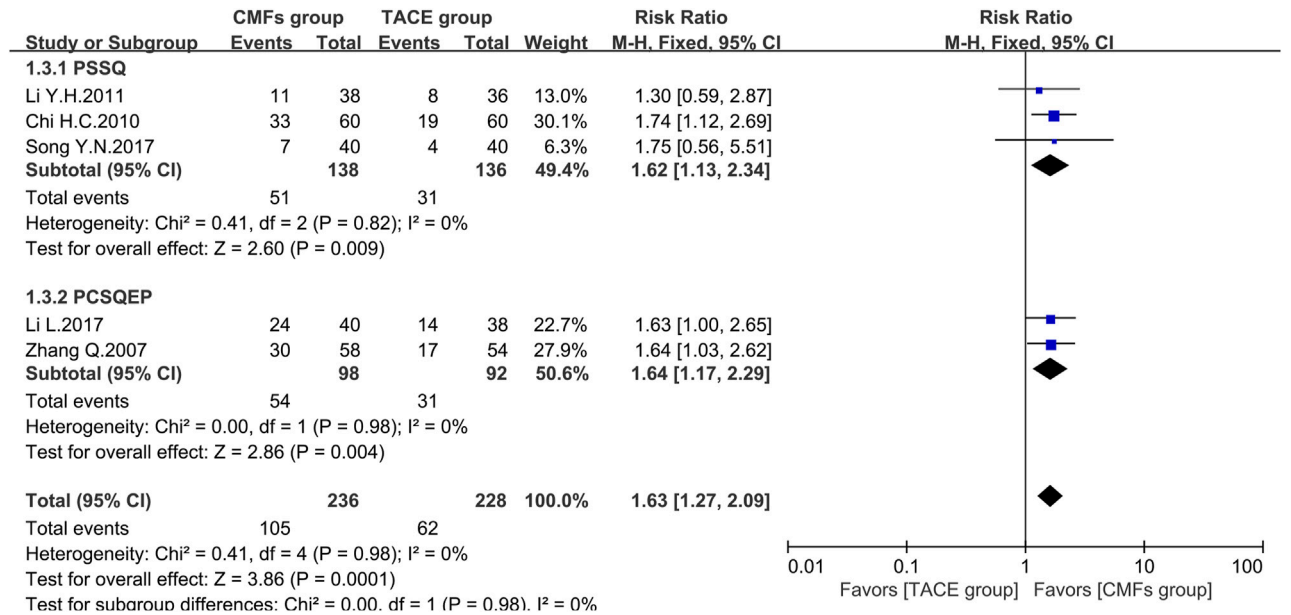

FIGURE 4 | Effect of CMFs group versus TACE group on 2-year survival, including a comparison between PSSQ and PCSQEP in the subgroup.

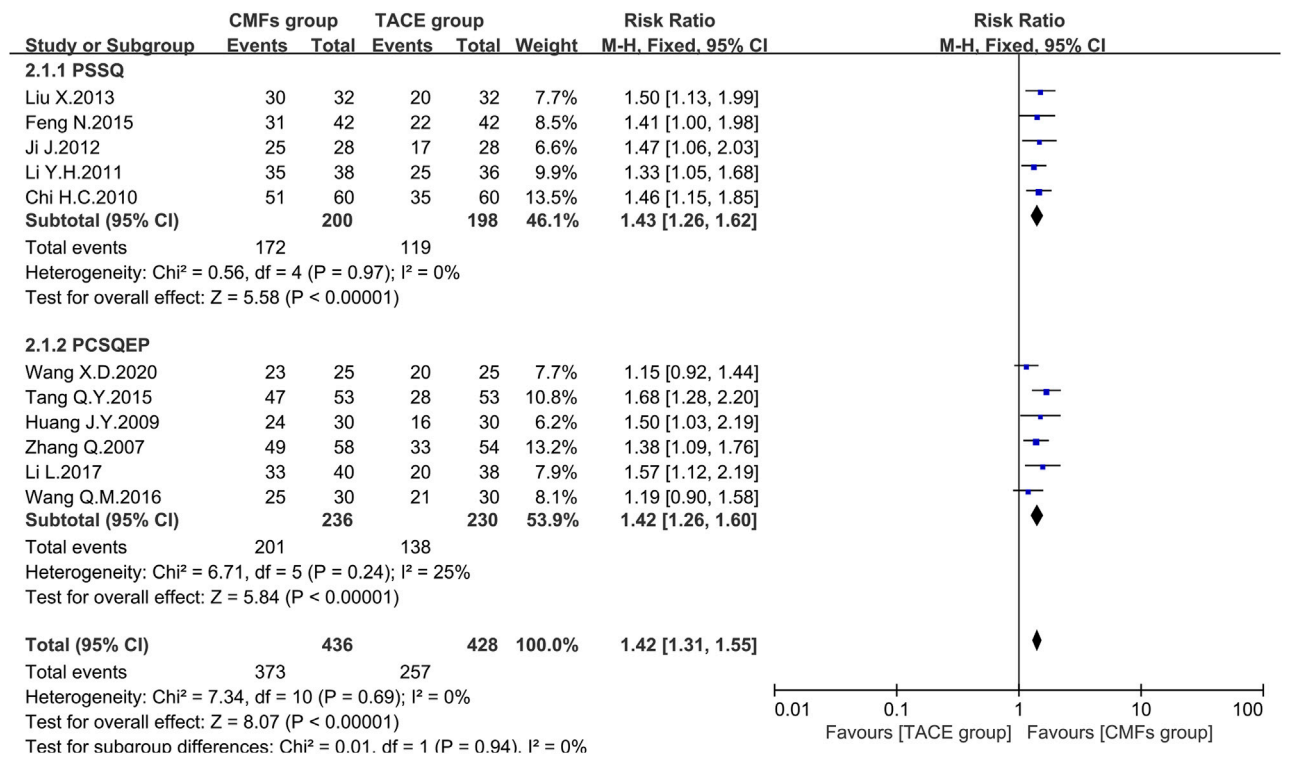

FIGURE 5 | Effect of CMFs group versus TACE group on the efficient rate of KPS, including a comparison between PSSQ and PCSQEP in the subgroup.

of overall response in solid tumors from WHO (Palmer, 1982), and response evaluation criteria in solid tumors (RECIST) (Therasse et al., 2000). ORR, the proportion of patients whose tumors shrank to a certain level and remained there for a certain period, was taken as an outcome indicator. A total of 12 clinical trials applied WHO criteria, and the results showed a more

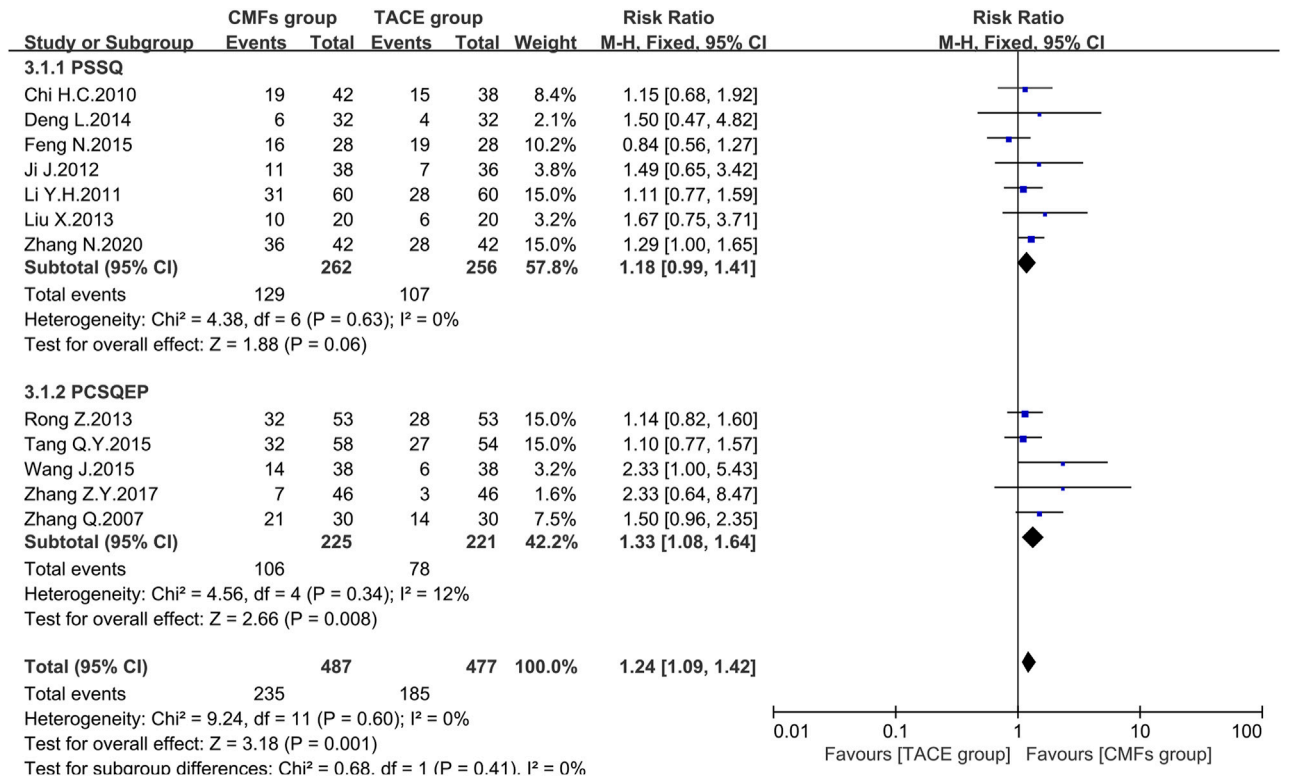

FIGURE 6 | Effect of CMFs group versus TACE group on ORR applied the WHO criteria, including a comparison between PSSQ and PCSQEP in the subgroup.

significant effect on reducing tumor size in the CMFs group than in the TACE group [n = 964; RR = 1.24; 95%CI (1.09, 1.42); p = 0.001; I^2 = 0%]. RECIST criteria were applied to the remaining seven clinical studies and the results were consistent with the former [n = 471; RR = 1.28; 95%CI (1.06, 1.56); p = 0.01; I^2 = 0%]. In the subgroup analysis, none of the trials complying with PSSQ were statistically significant using either the WHO criteria [n = 518; RR = 1.18; 95%CI (0.99, 1.41); p = 0.06; I^2 = 0%] or the RECIST criteria [n = 148; RR = 1.19; 95%CI (0.74, 1.90); p = 0.47; I^2 = 0%]. However, the trials complying with PCSQEP showed that CMFs were able to remarkably improve the ORR in WHO criteria [n = 446; RR = 1.33; 95%CI (1.08, 1.64); p = 0.008; I^2 = 12%] and RECIST criteria [n = 323; RR = 1.31; 95%CI (1.06, 1.62); p = 0.01; I^2 = 0%] (**Figure 6** and **Figure 7**).

ALT

A sum of 11 articles reported the effect of the combination of CMFs and TACE on ALT levels; see **Figure 8**. Overall, ALT levels were significantly reduced after treatment with CMFs [n = 793; MD = −12.15; 95%CI (−16.72, −7.58); p < 0.00001; I^2 = 94%]. The result of six trials complying with PSSQ reported beneficial results for the CMFs group [n = 432; MD = −18.01; 95%CI (−26.58, −9.45); p < 0.00001; I^2 = 93%], while the five trials complying with PCSQEP showed no statistical significance [n = 361; MD = −6.14; 95%CI (−12.58, 0.29); p < 0.00001; I^2 = 95%]. In addition, the effects of the PCSQEP group changed with the use of different effect models, which proved that the efficacy of trials complying with PCSQEP was unclear. As both subgroup and overall analyses exhibited a large heterogeneity, a random-effects model was used for the analyses. We speculated that the inconsistent timing of postoperative evaluation of ALT may be contributing to the heterogeneity. Therefore, four trials meeting the requirements that measured ALT after 4 weeks of TACE were analyzed, as shown in **Figure 9**. Similar to the results of those studies that did not limit the evaluation time, the CMFs [n = 294; MD = −11.90; 95%CI (−18.57, −5.23); p = 0.0005; I^2 = 84%] were able to reduce ALT levels. Trials complying with PSSQ [n = 188; MD = −14.61; 95%CI (−23.84, −5.37); p = 0.002; I^2 = 87%] achieved the same results. Interestingly, trials complying with PCSQEP group showed no statistical significance between CMFs group and TACE group [n = 106; MD = −4.61; 95%CI (−10.38, 1.16); p = 0.12]. Since studies are heterogeneous, a random-effects model was selected. Notably, the study of Wang A. M was a source of heterogeneity because excluding her study resulted in an I^2 = 0% for the PSSQ group and an I^2 = 29% overall.

AST

Ten articles reported the effects of the combination of CMFs and TACE on AST levels, and the results are shown in **Figure 10**. Owing to considerable heterogeneity, a random-effects model was conducted for meta-analysis. The CMFs group was able to reduce AST levels compared to TACE group [n = 725; MD = −10.55; 95%CI (−15.03, −6.07); p < 0.00001; I^2 = 89%]. Similarly, trials complying with PSSQ [n = 364; MD = −13.23; 95%CI (−24.45, −2.01); p <

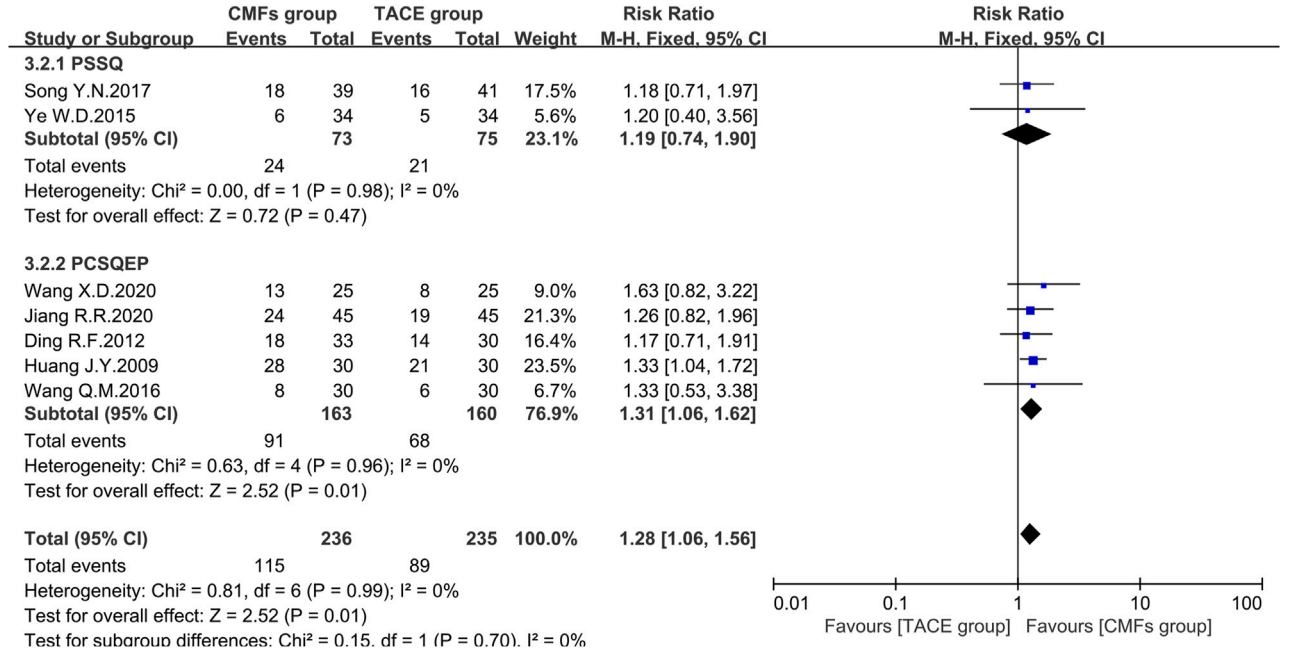

FIGURE 7 | Effect of CMFs group versus TACE group on ORR applied the RECIST criteria, including a comparison between PSSQ and PCSQEP in the subgroup.

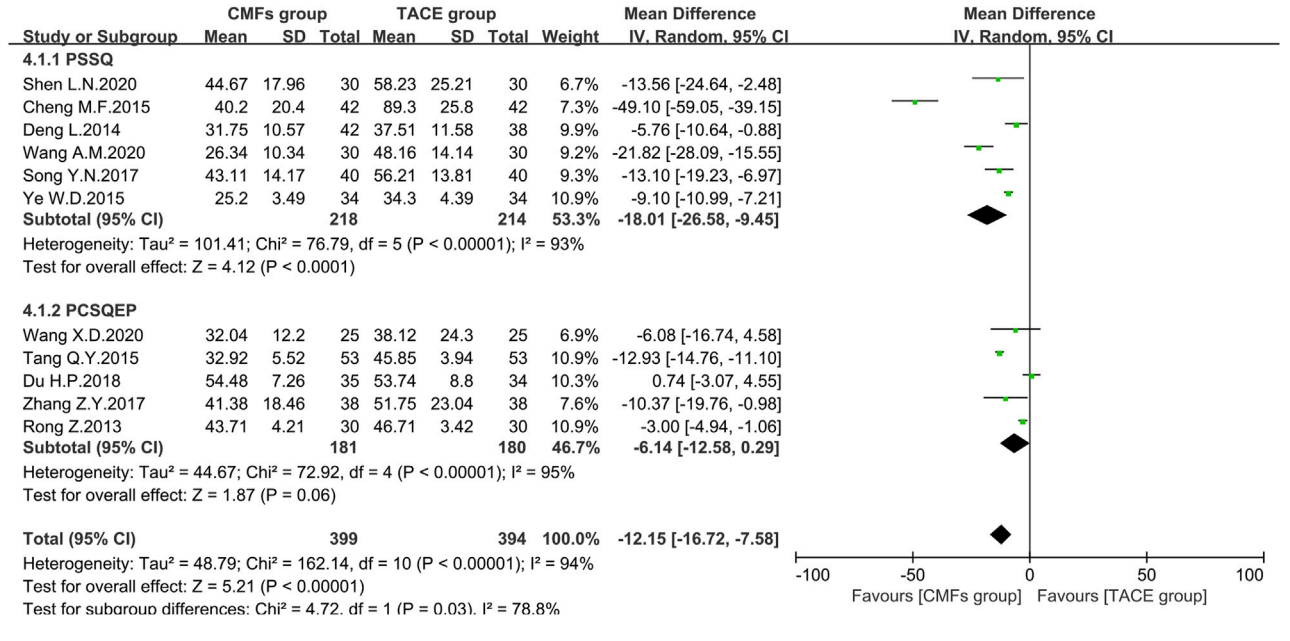

FIGURE 8 | Effect of CMFs group versus TACE group on ALT, including a comparison between PSSQ and PCSQEP in the subgroup.

0.00001; $I^2 = 92\%$] and PCSQEP [n = 361; MD = −7.13; 95%CI (−11.51, −2.75); $p < 0.0001$; $I^2 = 84\%$] both suggested that CMFs group achieved better reduction of AST levels. The reasons for the high heterogeneity of AST results are the same as ALT. There were three clinical studies in which AST was measured 4 weeks after TACE, and the results were shown in **Figure 11**. Since $I^2 = 80\%$ for the three articles, a random-effects model was still used. The overall efficacy was not statistically significant between CMFs group and TACE group [n = 226; MD = −3.49; 95%CI (−12.79, 5.80); $p = 0.46$; $I^2 = 80\%$], and trials complying with PSSQ demonstrated a diminution in AST in the CMFs group [n = 120; MD = −8.58; 95%CI (−14.87, −2.28); $p = 0.008$; $I^2 = 15\%$], while PCSQEP was also nonstatistically significant [n = 106; MD = 2.13;

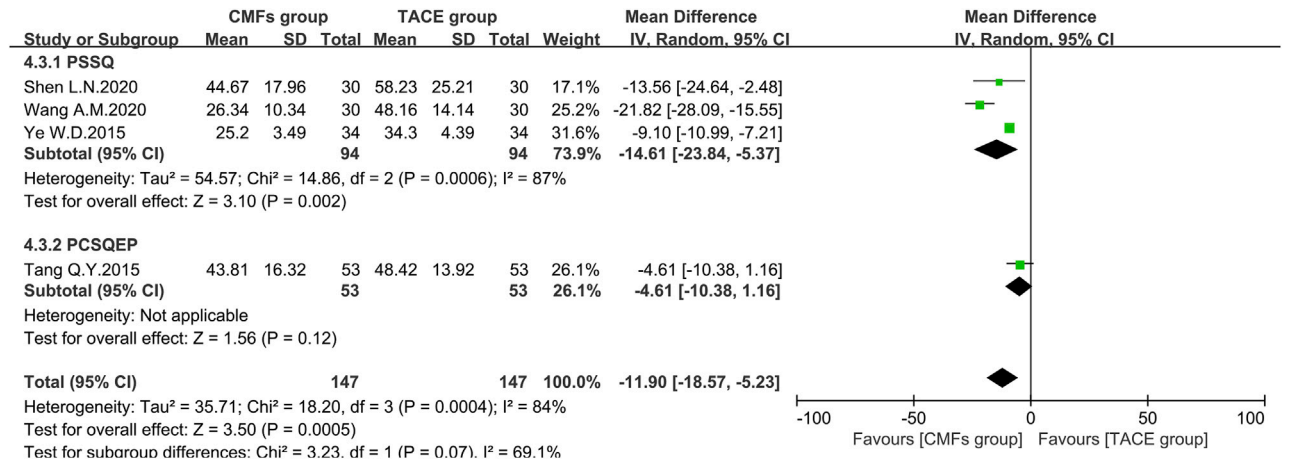

FIGURE 9 | Effect of CMFs group versus TACE group on ALT after treated with TACE for 4 weeks, including a comparison between PSSQ and PCSQEP in the subgroup.

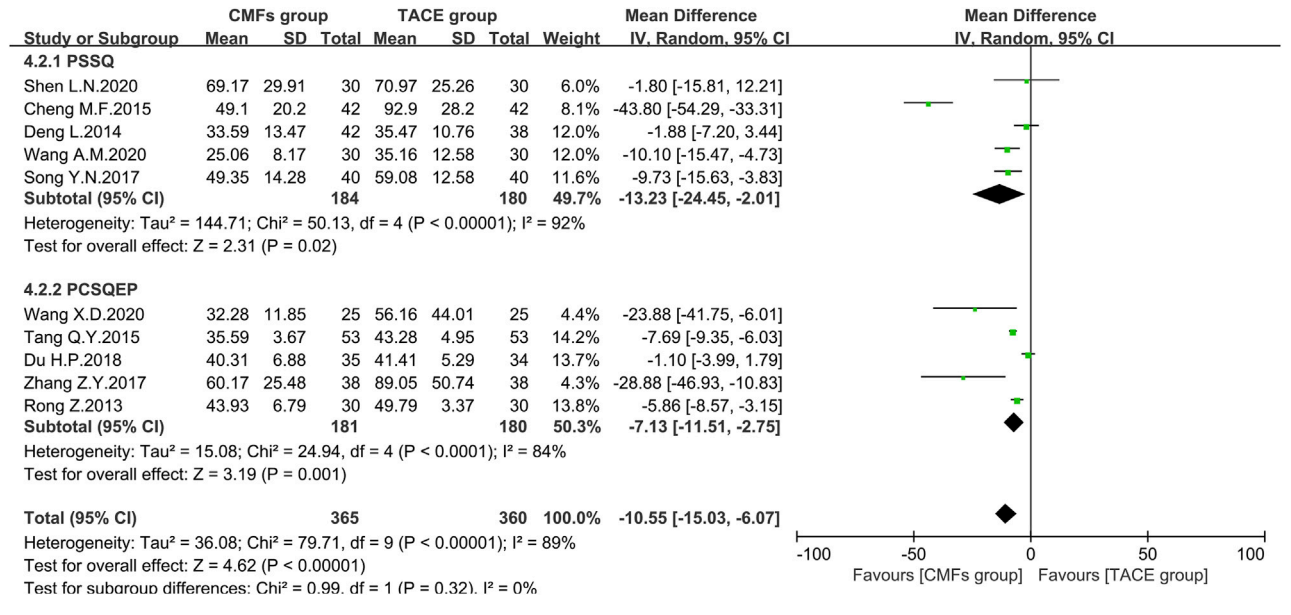

FIGURE 10 | Effect of CMFs group versus TACE group on AST, including a comparison between PSSQ and PCSQEP in the subgroup.

95%CI (−3.17, 7.43); $p = 0.43$]. Nevertheless, after applying a fixed-effects model, the overall AST outcome was statistically significant.

AFP

Eight clinical trials with AFP outcomes were reported, five of which were included in the meta-analysis. The remaining three could not be pooled because one clinical trial reported by Wang J (Wang, 2015) used units of iu/ml, one was dominated by Rong Z (Rong et al., 2013), which evaluated patients with AFP <400 ng/ml and >400 ng/ml separately, and one used categorical data (Li et al., 2011). The results of the remaining studies included in the meta-analysis were presented in **Figure 12**. The CMFs group was able to reduce AFP levels in comparison to the TACE group [n = 376; MD = -62.46; 95%CI (−90.94, −33.99); $p < 0.0001$; $I^2 = 40\%$], and similar results were obtained in the trials complying with PSSQ [n = 160; MD = −84.82; 95%CI (−134.92, −34.72); $p = 0.0009$; $I^2 = 0\%$] and PCSQEP [n = 216; MD = −56.81; 95%CI (−93.87, −19.74); $p = 0.003$; $I^2 = 55\%$]. A random-effects model was applied regarding the $I^2 > 50\%$ in the PCSQEP group. Wang X. D's study was a source of heterogeneity, and the outcome of trials complying with PCSQEP was invariant after this trial exclusion (Wang et al., 2020). In Wang J's study, the decrease in AFP was more pronounced in the CMFs group with the addition of drastic medicinals [n = 92; MD = −10.93; 95%CI (−16.10, −5.76); $p < 0.0001$] (Wang, 2015). In Rong Z's study, the decrease in AFP after the combination of CMFs and TACE was

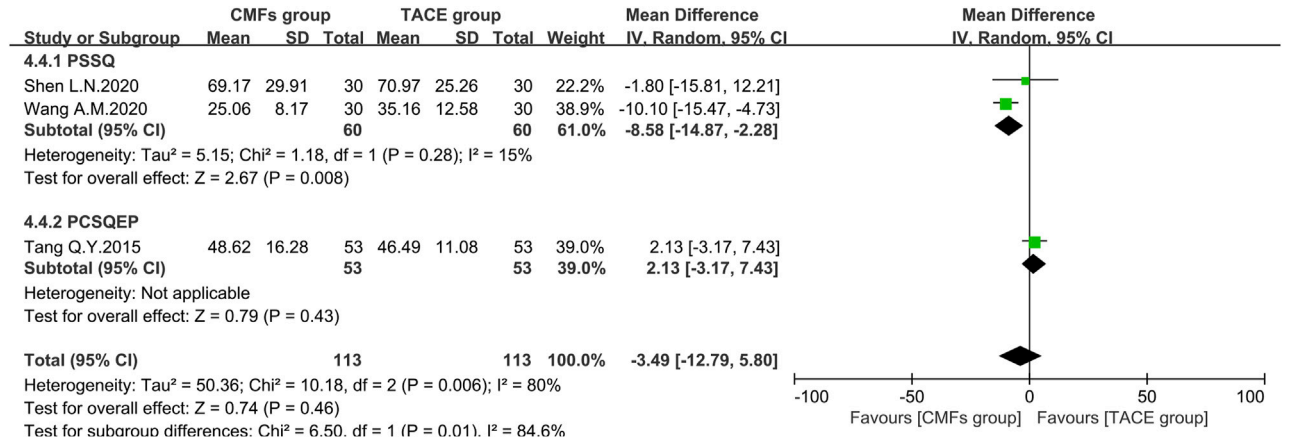

FIGURE 11 | Effect of CMFs group versus TACE group on AST after treated with TACE for 4 weeks, including a comparison between PSSQ and PCSQEP in the subgroup.

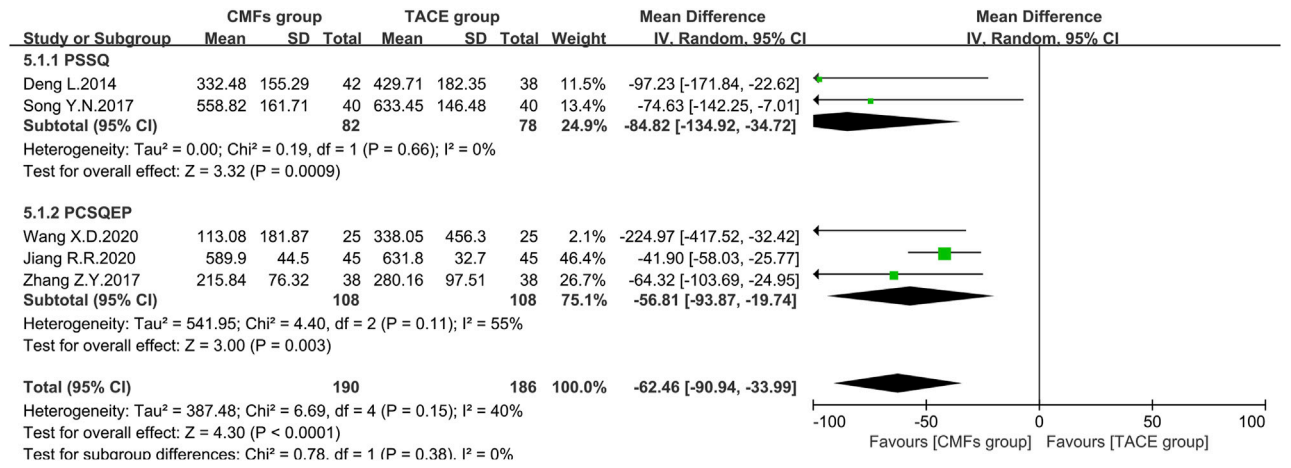

FIGURE 12 | Effect of CMFs group versus TACE group on AFP, including a comparison between PSSQ and PCSQEP in the subgroup.

not statistically significant in patients with AFP < 400 ng/ml before treatment, while it was significant in patients with AFP > 400 ng/ml [n = 22; MD = 14.12; 95%CI (−67.96, 96.20); $p = 0.74$]. In Li Y. H's study (Li et al., 2011), the improvement rate of AFP was 26.3% in the CMFs group and 22.2% in the TACE group (Rong et al., 2013).

The Improvement Rate of Symptoms

Referring to Guidelines of Clinical Research of New Drugs of Traditional Chinese Medicine, patients with hepatic cancer would have typical symptoms such as liver pain, abdominal distension, belching, and bitterness in the mouth. The authors of six trials scored according to the severity of the symptoms before treatment and then rated a significant improvement if the score after treatment dropped > 3/2. The meta-analysis results of symptom improvement rate were shown in **Figure 13**. In general, the improvement rate of symptoms in the CMFs group was higher than that in the TACE group [n = 368; RR = 1.67; 95%CI (1.18, 2.37); $p = 0.004$; $I^2 = 0\%$]. In the subgroup analysis, the trials complying with PSSQ revealed that CMFs could increase the number of people whose symptom score decreased by more than 3/2 compared with the TACE group [n = 258; RR = 1.62; 95%CI (1.10, 2.39); $p = 0.02$; $I^2 = 0\%$]. However, the result of trials complying with PCSQEP had no statistically significant [n = 110; RR = 1.88; 95%CI (0.87, 4.06); $p = 0.11$; $I^2 = 17\%$].

Adverse Events

A total of 13 studies reported adverse events after the combination of CMFs and TACE treatment. The trial of Wang X.D.2020 (Wang et al., 2020) reported that no adverse events occurred in the included patients, and the study of Liu X.2013 (Liu et al., 2013) and Ji J.2012 (Ji et al., 2012) did not provide enough adverse events data for meta-analysis. The remaining 10 studies adopted different evaluation standards; for example, some studies (Zhang

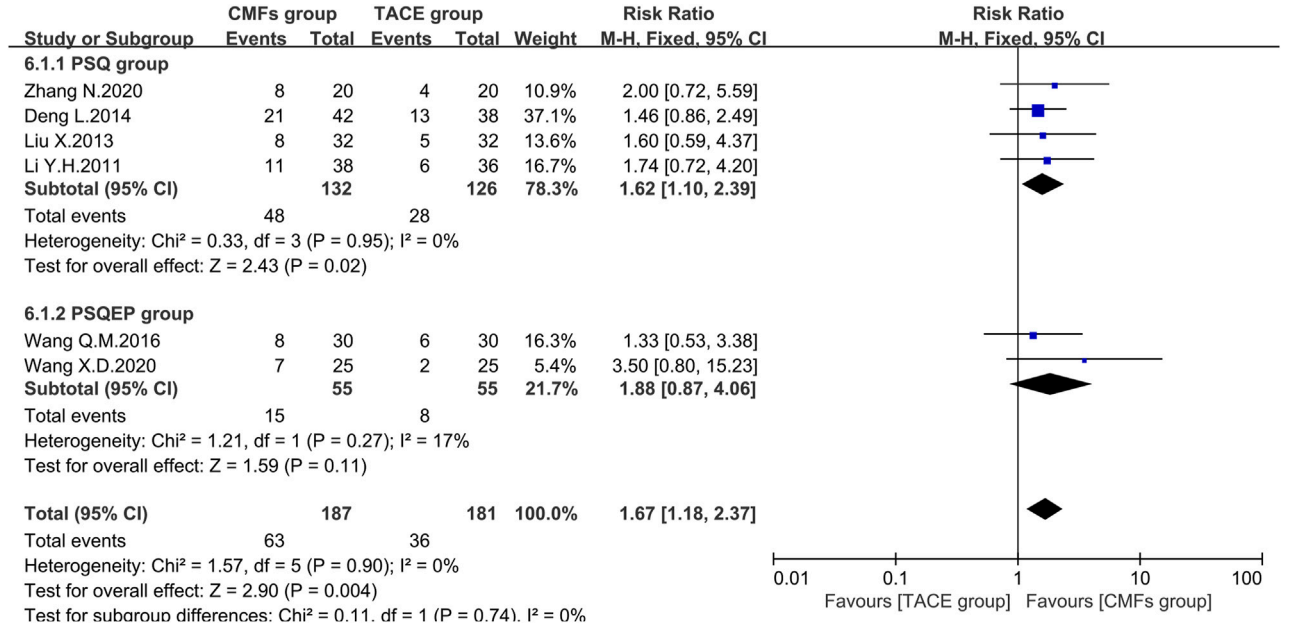

FIGURE 13 | Effect of CMFs group versus TACE group on the improvement of symptoms, including a comparison between PSSQ and PCSQEP in the subgroup.

et al., 2007; Chi et al., 2010; Ye et al., 2015; Wang et al., 2016) adopted the assessment of acute and subacute toxic effects from WHO (Palmer, 1982), and Ding R. F's research (Ding R.F., 2012) adopted the Common Terminology Criteria for Adverse Events version 3.0 (CTCAE) (Trotti et al., 2003). Therefore, we merged the data to be comparative and representative and presented it in **Supplementary Table S4**. As long as there was $I^2 > 50\%$ in the subgroup or the overall, the random-effects model was employed for analysis. Three trials reported the overall incidence of adverse events with nonstatistically significant results. In terms of fever, total hepatotoxicity incidence, neurotoxicity, total leukocyte decline rate, all grades of platelet decline, and hemoglobin decline, there were no statistically significant in both overall and subgroups. However, CMFs played a role in alleviating nausea and vomiting and bone marrow suppression whether the result of subgroup or overall supported this finding. In addition, patients with inappetence and gastrointestinal symptoms exhibited less incidence in the CMFs group. Although the CMFs group was not statistically significant in improving the toxicity of chemotherapy to platelets and hemoglobin, trials complying with the PCSQEP group or PSSQ showed the improvement in CMFs was superior to TACE. It was worth noting that some studies have graded the toxicity of adverse effects by severity, such as gastrointestinal symptoms, fever, hepatotoxicity, and leukocyte decline. CMFs group was not as good as the TACE group or was not statistically significant in relieving the above symptoms of mild degrees, but it could reduce serious adverse events. The results for the WBC decline and digestive symptoms I were unstable. After switching the effect model, the CMFs group would increase the incidence of digestive symptoms I and WBC levels compared with the TACE group.

Publication Bias

A funnel plot analysis of the KPS efficiency rate in the primary outcome was conducted because the number of trials for the survival outcome was too small and the power of the test was insufficient to assess symmetry (Higgins et al., 2019). For this reason, the method proposed by Harbord was used to explore the publication bias in survival rates, which was performed in Stata 16. The result shown in **Supplementary Figures S4, S5, and S7** indicated that there was no publication bias for the KPS efficiency rate and 6-month and 2-year survival. Publication bias was found in the 1-year survival rate (see **Supplementary Figure S6**).

DISCUSSION

TACE can only be used as a palliative treatment for patients. Although the survival time could be prolonged after accepting TACE treatment, the median survival time reported in the previous study was only 21 months (Yang et al., 2019). Moreover, the side effects always appear when receiving TACE treatment, such as vomiting, hair loss, and sensory disturbances. The endpoint of antitumor treatment is emphasized with providing the longest survival and less impaired quality of life (Bruix et al., 2015). Actually, CMFs could prolong survival time corresponding with improving the quality of life of cancer patients by the combination of multiple compounds. At present, the research on the antitumor mechanism of TCM mainly focuses on several ways: 1)

Inhibit tumor proliferation and migration. An effective anticancer component β-elemene extracted from *Curcumae Rhizoma* could inhibit HepG2 cell proliferation, induce cell cycle arrest, and mediate apoptosis by regulating topoisomerase, microtubular polymerization, and FasL (Zhai et al., 2019). 2) Improve immunity and general condition. Various herbal compounds have been shown to have positive effects on the immune system. For example, ginsenoside Rg3 could promote the differentiation of naive T cells to Th1 cells in LC mice by activating DCs (Wang et al., 2020). Cachexia is a common syndrome in patients with intermediate-advanced malignant tumors. Imperatorin inhibits STAT3 phosphorylation by directly binding to the SH2 domain of STAT3, which can reduce muscle wasting (Chen et al., 2020). 3) Reduce the side effects of chemotherapy drugs in the body, especially to protect normal cells and tissues in the body from damage caused by chemotherapy or radiotherapy. Cell death caused by damaging DNA is a therapeutic target of anticancer treatment and also a trigger for the occurrence of side effects in patients. It has been reported that rocaglamide could reduce DNA damage-induced toxicity in nonmalignant cells by inhibiting the p53 pathway (Becker et al., 2014). 4) Reduce resistance to chemotherapeutic agents in order to proceed to the next chemotherapeutic intervention as soon as possible. Astragaloside II was found to sensitize human hepatocellular carcinoma cells to 5-FU by inhibiting cellular autophagy involved in the MAPK-mTOR signaling pathway (Wang et al., 2017). Hence, as an adjuvant therapy, the antitumor treatment of CMFs is very promising.

In this study, the survival rate of PLC patients within 6 months, 1 year, and 2 years was enhanced, and so does the KPS. In addition, the scores of typical LC symptoms, including flank pain, belching, depression, and bitter mouth, were reduced through CMFs treatment. This evidence demonstrated that the combination of CMFs and TACE could improve the quality of life of patients. Assessment of solid tumor responses has proved to be a surrogate index for survival (Sieghart et al., 2015). Based on the relevant assessing standard followed by the RECIST or/and WHO, the tumor lesions were markedly reduced or even disappeared after using CMFs. AFP is also another classic tumor marker, which is mainly used for predicting advanced disease and poor prognosis (Bruix et al., 2015). A meta-analysis including five RCTs and three clinical trials of descriptive statistics indicated an apparent decrease of AFP after the treatment of CMFs. This result suggests that CMFs had a positive effect on tumor marker, which was consistent with the finding of Cheng Y. (Cheng et al., 2020). Generally speaking, CMFs could prolong the survival rate, ameliorate the quality of life, diminish solid tumors, and lower tumor markers in PLC patients at the intermediate-advanced stage. It is interesting that the utilization of traditional, complementary, and alternative medicine is as high as 80% in less developed countries according to WHO report (Hill et al., 2019). The finding in this meta-analysis could support that CMFs as an anticancer treatment had a good application prospect, which contributed to reducing the cost of treatment for cancer patients in low-income countries with obtaining the same medical benefits.

The drug caused ischemic necrosis of the tumor tissue along with transient or chronic liver injury after treating TACE (Miksad et al., 2019). Moreover, the level of AST/ALT ratio is also closely related to liver necrosis, and it may aggravate the hepatic neoplasm invasion (Zhang et al., 2019). Thus, liver function is necessary to evaluate. However, there existed a great heterogeneity in ALT and AST outcomes. Based on the knowledge for this disease, the heterogeneity resulted from five aspects, such as the liver function of patients before treatment, the type and dosage of drugs used in TACE, the course of TACE, the evaluation time after TACE treatment, and the liver toxicity of TCM.

Firstly, the total heterogeneity of ALT becomes $I^2 = 92\%$ ($n = 7$) when removing trials that involved patients with Child-Pugh C or did not record the Child-Pugh level of patients. The total heterogeneity of AST becomes $I^2 = 77\%$ ($n = 8$), with no heterogeneity being changed after liver function unified. Secondly, the types of chemotherapeutic drugs used in clinical trials were different. Simultaneously, some studies emphasized that the dosage of chemotherapeutic drugs would be adjusted according to the patient's tumor size, hepatorenal function, and general conditions (Deng et al., 2014; Zhang et al., 2017; Shen et al., 2020), which rendered the inconsistent use of chemotherapeutic drugs. Lack of standardized TACE treatment protocols is also a current problem (Sieghart et al., 2015). Besides, cTACE and DEB-TACE have different toxicity on the liver. Some studies have shown that the drug-related systemic and liver toxicity of the DEB-TACE group was pronouncedly turned down, comparing with the cTACE group (Sieghart et al., 2015). While other studies have illustrated, DEB-TACE increased the risk of liver-related damage (Raoul et al., 2019). More rigorous RCTs are required to prove the severity of the liver injury of DEB-TACE and cTACE. Thirdly, the duration and interval of TACE are also essential elements affecting liver function. And the successful efficiency of TACE can be reflected by the evaluation of tumor response (Sieghart et al., 2015). However, it is sporadic to achieve the goal of treatment in a single course of TACE treatment. Therefore, the Assessment for Retreatment with TACE (ART) score, tumor size, tumor number, AFP level, Child-Pugh class, Objective Response after TACE (SNACOR) model, AFP level, BCLC stage, Child-Pugh class, Response after TACE (ABCR score), and Hepatoma Arterial-embolization Prognostic (HAP) score are the reference tools used by doctors to assess whether a patient can undergo TACE again (Chon et al., 2019). So far, there is an absence of high-quality evidence to prove the optimal interval between two TACE treatments. Shortening the interval between two TACE treatments may result in hepatic dysfunction or liver failure (Intaraprasong et al., 2016). Meanwhile, there is a greater chance of liver failure after repeating TACE treatments (Raoul et al., 2011). Fourthly, transient liver injury generally takes 1 month to recover after

TACE (Barzakova et al., 2019; Miksad et al., 2019). Accordingly, those clinical trials that evaluated liver function after being treated with TACE for 4 weeks were selected to assess its effect on ALT and AST. When conducting sensitive analysis on selected trials, the RCT performed by Wang A.M (Wang et al., 2020) brought a significant heterogeneity on ALT and AST. Before removing this trial, the overall heterogeneity remained significant, and the impact of CMFs on AST was not statistically significant. Finally, drug-induced liver injury (DILI) caused by herbal medicine is the potential aspect leading to heterogeneity (Andrade et al., 2019). Herbs contain thousands of chemical compounds. Some compounds have been proved to be hepatotoxins including volatile compounds, phytotoxic proteins, glycosides, terpenoid lactones, terpenoids, alkaloids, anthraquinones, and phenolic acids (Quan et al., 2020). However, it is unclear that if the proper application of formulas containing these medicinals contributes to liver injury or not. Among the included trials, the longest treating period with CMFs is 3 months, during which the toxic chemical components may continually accumulate in the liver and eventually damage the liver cell.

Holism is a major feature of the TCM theoretical system. TCM holds the point that disease is by the imbalance of the body (So et al., 2019). TACE is considered a local treatment, which can cause ischemic necrosis of neoplasm and eliminate the pathogenic factors. The CMFs emphasize synergism and detoxification through the combination of chief medicinal, deputy medicinal, assistant medicinal, and envoy medicinal (Wei et al., 2018). CMFs are characterized by multicomponent and multitarget effects (Luan et al., 2020). In the treating practice, in order to treat simultaneously both the whole body and the local lesions, TCM physicians often adopt PCSQEP with drastic medicinals and Qi replenishing medicinals in their prescriptions.

LC was stubbornly intertwined with phlegm, blood stasis, and toxin, so drastic medicinals accurate in intervening cancer cells were frequently applied to eliminate pathogens. Pharmacological experiments demonstrated that drastic medicinals can fight against tumors (Yoon et al., 2018; Chang et al., 2020; Jia et al., 2021), promote blood circulation, and curb pain caused by oxaliplatin. However, the evidence of clinical studies was inadequate to explain that drastic medicinals had a strong tumor-suppressive effect and its rationality in clinic usage. It is worth noting that excessive usage of drastic medicinals would be emerging resulting by the physician differentiate the syndrome of the disease improperly, which would further damage the healthy Qi, disrupt the balance of homeostasis, and ultimately promote the development of the disease. In terms of the therapeutic effect of TACE, the necessity for applying the combination of drastic medicinals and TACE on PLC needs to be urgently evaluated.

Depending on the properties and dosage of the medicinals, the drastic medicinals are generally divided into three categories. The first is the medicinals with an obvious drug bias, such as the bitter-cold medicinal *bái huā shé shé cāo* (the whole plant of *Sclerotrion diffusum* (Willd.) R.J.Wang); the second is high-dose medication (generally more than 50 g); the third is toxic medicinals and overactive medicinals, which are mostly used in malignant diseases. It is worth clarifying that only the third category meets the entry requirements in this work. The clinical trials that applied drastic medicinals are believed to follow the PCSQEP.

The results displayed that trials complying with PSSQ or PCSQEP could improve the 2-year survival rate, stabilize or increase the KPS score, and decrease the AFP level. Interestingly, the CMFs group following PSSQ could improve the survival rate of 6 months and1 year and the curative effect of TCM symptoms, but the PCSQEP group had no statistical significance for these outcomes. There was no statistically significant ORR for the RECIST and WHO criteria in trials complying with PSSQ, while the trials complying with PCSQEP displayed a remarkable improvement. In particular, the survival rate reflected the long-term impact of treatment, and the solid tumor response reflected the direct effect of the drug on the tumor, which is a manifestation of the short-term impact. PSSQ and PCSQEP show different efficacy in long-term and short-term impact, which may be related to PLC patients' weak physical status. The reason why CMFs following PSSQ achieved better efficacy in the long term may stem from Qi replenishing medicinals with the effects of immunity-boosting and energy-supplementing (Wang et al., 2017). However, following PCSQEP, the cytotoxic effects of TACE and drastic medicinals synergistically fighting cancer were too intense to keep the normal life activities of the body for a long time. Perhaps by adjusting the compatibility of CMFs or using the two therapeutic regimens at intervals, it is possible to achieve the goal of improving both the short-term and the long-term curative effect of middle to advanced PLC. Notably, few studies adopted PCSQEP treatment regimens and followed up for 6 months or more, so the results in the subgroup analysis should be treated with caution.

Postembolism syndrome is reported as a typical adverse reaction of TACE treatment. Meanwhile, some Chinese medicinals applied in CMFs may cause adverse events. It is unclear whether the therapeutic effect of CMFs is greater than its damage due to the key role of liver metabolism. This study indicated that the entire adverse events of the combination of CMFs and TACE treatment were uncertain, but the reductions of nausea and vomiting, inappetence, digestive symptoms, and bone marrow suppression were clear. Interestingly, the combination of CMFs and TACE increased the risk of certain mild adverse events but reduced the incidence of serious adverse events. This suggests that physicians needed to be cautious when using Chinese medicinals in clinical practice, especially in East Asia, where herbal medicine is prevalent and chronic hepatitis B virus infection is the main reason for the high incidence of HCC patients (Ashtari et al., 2015). Studies have shown that, in a large number of DILI populations, 10% have preexisting liver disease. Besides this, slow acetylator genotype in East Asian ancestry would cause accumulation of toxic components in the body and aggravate the adverse events (Andrade et al., 2019). From another perspective, mild adverse events would gradually disappear with routine expectant treatment. On the contrary, the drop of serious adverse events reflected the therapeutic effect of CMFs that enhanced the patients' quality of life to a certain extent and prepared them for the next TACE operation. Drastic medicinals were known to be toxic, and in this meta-analysis, they did not have a statistically significant influence on the overall

occurrence of adverse events. Although we were particularly concerned about the incidence of various adverse events of drastic medicinals, due to the few included studies, the current results only showed that drastic medicinals had to alleviate effects on nausea and vomiting, digestive symptoms, and bone marrow suppression. More evidence is needed to support whether drastic medicinals will aggravate the burden of liver function in PLC patients and cause more serious adverse events.

The methodological quality of RCTs of TCM treatment is generally low and has been criticized for a long time (Li et al., 2014). In the full-text screening, several trials did not detail the randomization generation and no studies were blinded to the researchers and patients. Most of the interventions in the included studies were decoctions, but it was impractical to use a placebo of decoctions because it was challenging to design placebos to smell, look, and taste like a medicinal liquid in fact (Zhong et al., 2010). Therefore, the restrictive conditions of the experimental design were established to promote the credibility and authenticity of this study consulting the approach of RCTs (**Supplementary Table S1**).

Trials with diagnostic criteria, inclusion criteria, and exclusion criteria were regarded as stringency and reliability and the comparable baseline information was suitable for accurately evaluating the efficacy of the interventions. At the same time, the washout period of included studies could exclude the interference of antecedent treatments on TACE and TCM treatment. The remaining studies were from journals and were more authentic after review, which could also ensure the reliability of the conclusions in this study and the quality of the whole article.

CONCLUSION

This meta-analysis confirmed that the combination of CMFs and TACE treatment ameliorated the primary outcome, survival time, KPS, and secondary outcomes, ORR, AFP, and TCM symptoms in PLC patients at the intermediate-advanced stage. CMFs reduced some adverse events after TACE but may increase the occurrence of mild adverse events. Moreover, adopting PCSQEP was shown to be beneficial to patients in the short-term effect, while PSSQ made the patient benefit more in the long-term impact. Appropriate reduction drastic medicinals use or reasonable choice PCSQEP and PSSQ treating methods may prolong the lifespan of patients. As is well known, the meta-analysis aims to evaluate the efficacy and safety of PSSQ and PCSQEP in PLC. The research reveals that the anticancer effect with drastic medicinals not only comes from TCM theory and experimental research but also was supported by evidence-based medicine. Due to the limited quality and a small number of included studies, the results of this meta-analysis still needed to be kept with caution and required validation by more high-quality studies in the future.

DATA AVAILABILITY STATEMENT

The original contributions presented in the study are included in the article/**Supplementary Material**; further inquiries can be directed to the corresponding author.

AUTHOR CONTRIBUTIONS

Conception and design: YS, ZY, MW, and QY; data collection: YS; data extraction: YL, CZ, and YH; data verification: AW and KQ; email trial registrants: XY; data analysis: YS; manuscript drafting: YS, ZY, and YH; manuscript validation; MW, QH, and ZY.

FUNDING

This work was supported by the National Science Foundation of China, No. 81760851, and the Doctoral Research Start-Up Fund of Guangxi University of Chinese Medicine Introduced, No. 2019BS035.

SUPPLEMENTARY MATERIAL

The Supplementary Material for this article can be found online at: https://www.frontiersin.org/articles/10.3389/fphar.2021.714287/full#supplementary-material

REFERENCES

Andrade, R. J., Aithal, G. P., Björnsson, E. S., Kaplowitz, N., Kullak-Ublick, G. A., Larrey, D., et al. (2019). EASL Clinical Practice Guidelines: Drug-induced liver injury. *J. Hepatol.* 70 (6), 1222–1261. doi:10.1016/j.jhep.2019.02.014

Are, C., Meyer, B., Stack, A., Ahmad, H., Smith, L., Qian, B., et al. (2017). Global trends in the burden of liver cancer. *J. Surg. Oncol.* 115 (5), 591–602. doi:10.1002/jso.24518

Ashtari, S., Pourhoseingholi, M. A., Sharifian, A., and Zali, M. R. (2015). Hepatocellular carcinoma in Asia: Prevention strategy and planning. *World J. Hepatol.* 7 (12), 1708–1717. doi:10.4254/wjh.v7.i12.1708

Barzakova, E. S., Schulze-Hagen, M., Zimmermann, M., Lurje, G., Bednarsch, J., Pedersoli, F., et al. (2019). Monitoring Liver Function of Patients Undergoing Transarterial Chemoembolization (TACE) by a 13C Breath Test (LiMAx). *Cardiovasc. Intervent Radiol.* 42 (12), 1702–1708. doi:10.1007/s00270-019-02325-3

Becker, M. S., Schmezer, P., Breuer, R., Haas, S. F., Essers, M. A., Krammer, P. H., et al. (2014). The traditional Chinese medical compound Rocaglamide protects nonmalignant primary cells from DNA damage-induced toxicity by inhibition of p53 expression. *Cell Death Dis* 5 (1), e1000. doi:10.1038/cddis.2013.528

Bruix, J., Han, K. H., Gores, G., Llovet, J. M., and Mazzaferro, V. (2015). Liver cancer: Approaching a personalized care. *J. Hepatol.* 62 (1 Suppl. l), S144–S156. doi:10.1016/j.jhep.2015.02.007

Chang, Y. L., Xu, G. L., Wang, X. P., Yan, X., Xu, X., Li, X., et al. (2020). Anti-tumor activity and linear-diarylheptanoids of herbal couple Curcumae Rhizoma-Sparganii Rhizoma and the single herbs. *J. Ethnopharmacol.* 250, 112465. doi:10.1016/j.jep.2019.112465

Chen, L., Xu, W., Yang, Q., Zhang, H., Wan, L., Xin, B., et al. (2020). Imperatorin alleviates cancer cachexia and prevents muscle wasting via directly inhibiting STAT3. *Pharmacol. Res.* 158, 104871. doi:10.1016/j.phrs.2020.104871

Cheng, M. F. (2015). Forty-Two Cases with Primary Liver Cancer Treated with Modified Liver-Benefiting and Distention-Reducing Decoction Combined with Interventional Therapy. *Henan Tradit Chin. Med.* 35 (11), 2657–2659.

Cheng, Y., Chen, T., and Chen, J. (2020). Erzhu Jiedu decoction ameliorates liver precancerous lesions in a rat model of liver cancer. *J. Cancer* 11 (24), 7302–7311. doi:10.7150/jca.49554

Chi, H. C., Hu, F. S., Han, D., and Zhang, Q. (2010). The Effectiveness of Liver-soothing and Spleen-strengthening Traditional Chinese Medicine Combined with Intra-arteriaI Infusion of Chemical Medicine for Advanced Primary Hepatocellular Cancer Patients. *Chin. J. Inf. TCM* 17 (06), 16–18.

Chon, Y. E., Park, H., Hyun, H. K., Ha, Y., Kim, M. N., Kim, B. K., et al. (2019). Development of a New Nomogram Including Neutrophil-to-Lymphocyte Ratio to Predict Survival in Patients with Hepatocellular Carcinoma Undergoing Transarterial Chemoembolization. *Cancers (Basel)* 11 (4), 509. doi:10.3390/cancers11040509

Deng, L., Peng, G. L., Jiang, Y. L., Jiang, M., and Yang, S. L. (2014). Clinical Observation of oral Jianpiyigan Prescription Combined with Hepatic Arterial Chemotherapy Embolism in Elderly Primary Liver Cancer. *Shandong Med. J.* 54 (16), 59–61. doi:10.3969/j.issn.1002-266X.2014.16.024

Ding, R. F. (2012). Clinical Observation of Fuzheng Decoction Combined with Transcatheter Arterial Chemoembolization in middle-advanced Hepatocellular Carcinoma. *J. Hebei Med. Univ.* 33 (6), 679–681. doi:10.3969/j.issn.1007-3205.2012.06.024

Du, H. P., Bai, L. J., Gong, Y. H., and Hu, Q. (2018). Clinical Observation of Biejiajian Pill with Transcatheter Arterial Chemoembolization in Hepatic Fibrosis. *Chin. J. Gerontol.* 38 (16), 3895–3897.

Feng, N., and Chen, W. (2015). Clinical Observation of Transcatheter Hepatic Arterial Chemoembolization Combined with Chinese Herbal Medicine in Treating 42 Cases with Primary Liver Cancer. *Chin. J. Ethomed Ethnopharm* 24 (05), 95–96.

Galle, P. R., Tovoli, F., Foerster, F., Wörns, M. A., Cucchetti, A., and Bolondi, L. (2017). The treatment of intermediate stage tumours beyond TACE: From surgery to systemic therapy. *J. Hepatol.* 67 (1), 173–183. doi:10.1016/j.jhep.2017.03.007

Galle, P. R., Forner, A., Llovet, J. M., Mazzaferro, V., Piscaglia, F., Raoul, J. L., et al. (2018). EASL Clinical Practice Guidelines: Management of hepatocellular carcinoma. *J. Hepatol.*, S0168827818302150. doi:10.1016/j.jhep.2018.03.019

Han, K. H., Kudo, M., Ye, S. L., Choi, J. Y., Poon, R. T., Seong, J., et al. (2011). Asian Consensus Workshop Report: Expert Consensus Guideline for the Management of Intermediate and Advanced Hepatocellular Carcinoma in Asia. *Oncology* 81 Suppl 1 (s1), 158–164. doi:10.1159/000333280

Higgins, J. P. T., Thomas, J., Chandler, J., Cumpston, M., Li, T., Page, M. J., et al. (2019). *Cochrane Handbook for Systematic Reviews of Interventions*. 2nd Edition. Chichester (UK): John Wiley & Sons.

Hill, J., Mills, C., Li, Q., and Smith, J. S. (2019). Prevalence of traditional, complementary, and alternative medicine use by cancer patients in low income and lower-middle income countries. *Glob. Public Health* 14 (3), 418–430. doi:10.1080/17441692.2018.1534254

Huang, J. Y., Fan, Q. X., and Sun, Y. (2009). Recent Clinical Observation of Shenyi Capsule with Cidan Capsule in Chemoembolizeing the Advanced Primary Liver Cancer. *Liaoning J. Tradit Chin. Med.* 36 (10), 1721–1723.

Imai, N., Ishigami, M., Ishizu, Y., Kuzuya, T., Honda, T., Hayashi, K., et al. (2014). Transarterial chemoembolization for hepatocellular carcinoma: A review of techniques. *World J. Hepatol.* 6 (12), 844–850. doi:10.4254/wjh.v6.i12.844

Intaraprasong, P., Siramolpiwat, S., and Vilaichone, R. K. (2016). Advances in Management of Hepatocellular Carcinoma. *Asian Pac. J. Clin. Cancer Prev.* 17 (8), 3697–3703. doi:10.1016/j.jceh.2016.03.006

Ji, J., Huang, H. X., Wang, X., Chen, B., and Zhang, T. (2012). Clinical Observation on Xiaoyao Powder Combined with Intervention of Hepatocellular Carcinoma of Liver-depression and Spleen-deficiency Syndrome. *Liaoning J. Tradit Chin. Med.* 14 (06), 80–82.

Jia, J., Li, X., Ren, X., Liu, X., Wang, Y., Dong, Y., et al. (2021). Sparganii Rhizoma: A review of traditional clinical application, processing, phytochemistry, pharmacology, and toxicity. *J. Ethnopharmacol.* 268, 113571. doi:10.1016/j.jep.2020.113571

Jiang, R. R., Wang, T. B., Man, T. T., Qin, Y. C., Hong, X. H., Rong, Z., et al. (2020). Short-term Curative and Plasma Angiogenic Responses to Fuhe Beihua Decoction with Transcatheter Arterial Chemoembolization in Primary Liver Cancer Patients with Liver Depression and Spleen Deficiency Syndrome. *Chin. J. Gerontol.* 23 (33), 4214–4221.

Li, J., Liu, Z., Chen, R., Hu, D., Li, W., Li, X., et al. (2014). The quality of reports of randomized clinical trials on traditional Chinese medicine treatments: a systematic review of articles indexed in the China National Knowledge Infrastructure database from 2005 to 2012. *BMC Complement. Altern. Med.* 14, 362. doi:10.1186/1472-6882-14-362

Li, L., and Xu, G. (2017). Clinical Observation of Applying TACE Combined with Traditional Chinese Medicine in thet Treatment of Primary Liver Cancer during Medium and Advanced Stage. *J. Sichuan Tradit Chin. Med.* 35 (05), 104–107.

Li, Y. H., Liang, H., and Zhang, C. H. (2011). Clinical Study of Transcatheter Hepatic Arterial Chemoembolization Combined with Chinese Herbal Medicine in Primary Liver Cancer. *J. Nanjing Med. Univ.* 31 (5), 742–745.

Liu, X., You, J. L., and Zhang, B. N. (2013). Thirty-Two Cases with Primary Liver Cancer Treated with WD-2 Combined with Intervention of Hepatocellular Carcinoma. *Shanxi J. Tradit Chin. Med.* 34 (05), 518–520.

Luan, X., Zhang, L. J., Li, X. Q., Rahman, K., Zhang, H., Chen, H. Z., et al. (2020). Compound-based Chinese medicine formula: From discovery to compatibility mechanism. *J. Ethnopharmacol.* 254, 112687. doi:10.1016/j.jep.2020.112687

Mason, M. C., Massarweh, N. N., Salami, A., Sultenfuss, M. A., and Anaya, D. A. (2015). Post-embolization syndrome as an early predictor of overall survival after transarterial chemoembolization for hepatocellular carcinoma. *HPB (Oxford)* 17 (12), 1137–1144. doi:10.1111/hpb.12487

Miksad, R. A., Ogasawara, S., Xia, F., Fellous, M., and Piscaglia, F. (2019). Liver function changes after transarterial chemoembolization in US hepatocellular carcinoma patients: the LiverT study. *BMC Cancer* 19 (1), 795. doi:10.1186/s12885-019-5989-2

Miller, K. D., Fidler-Benaoudia, M., Keegan, T. H., Hipp, H. S., Jemal, A., and Siegel, R. L. (2020). Cancer statistics for adolescents and young adults, 2020. *CA Cancer J. Clin.* 70 (1), 443–459. doi:10.3322/caac.2159010.3322/caac.21637

Moher, D., Liberati, A., Tetzlaff, J., and Altman, D. G. (2009). Preferred reporting items for systematic reviews and meta-analyses: the PRISMA statement. *BMJ* 339 (7), b2535. doi:10.1371/journal.pmed.1000097

Palmer, M. K. (1982). WHO Handbook for Reporting Cancer Treatment. *Br. J. Cancer* 45 (3), 14–27. doi:10.1038/bjc.1982.83

Quan, N. V., Dang Xuan, T., and Teschke, R. (2020). Potential Hepatotoxins Found in Herbal Medicinal Products: A Systematic Review. *Int. J. Mol. Sci.* 21 (14), 5011. doi:10.3390/ijms21145011

Raoul, J. L., Forner, A., Bolondi, L., Cheung, T. T., Kloeckner, R., and de Baere, T. (2019). Updated use of TACE for hepatocellular carcinoma treatment: How and when to use it based on clinical evidence. *Cancer Treat. Rev.* 72, 28–36. doi:10.1016/j.ctrv.2018.11.002

Raoul, J. L., Sangro, B., Forner, A., Mazzaferro, V., Piscaglia, F., Bolondi, L., et al. (2011). Evolving strategies for the management of intermediate-stage hepatocellular carcinoma: Available evidence and expert opinion on the use of transarterial chemoembolization. *Cancer Treat. Rev.* 37 (3), 212–220. doi:10.1016/j.ctrv.2010.07.006

Rong, Z., Mo, C. M., Huang, Y., Hu, Z. B., Bai, G. D., and He, S. Y. (2013). Dujieqing Oral Liquid Combined Hepatic Arterial Chemotherapy Embolism(TACE) in Treatment of Advanced Primary Liver Cancer. *Liaoning J. Tradit Chin. Med.* 15 (12), 18–20.

Shen, L. N., Lou, X. J., Liu, J., and Xu, J. (2020). Clinical Study on Gexia Zhuyu Tang for Advanced Liver Cancer after Precise TACE. *J. New Chin. Med.* 52 (07), 44–47.

Sieghart, W., Hucke, F., and Peck-Radosavljevic, M. (2015). Transarterial chemoembolization: Modalities, indication, and patient selection. *J. Hepatol.* 62 (5), 1187–1195. doi:10.1016/j.jhep.2015.02.010

So, T. H., Chan, S. K., Lee, V. H., Chen, B. Z., Kong, F. M., and Lao, L. X. (2019). Chinese Medicine in Cancer Treatment - How is it Practised in the East and the West. *Clin. Oncol. (R Coll. Radiol.* 31 (8), 578–588. doi:10.1016/j.clon.2019.05.016

Song, Y. N., Zhuang, J. H., Zhang, S. L., Wang, G. Y., Ni, J., He, S. F., et al. (2017). Clinical Research of Wenyang Jiedu Formula with TACE in the Treatment of Advanced Primary Hepatic Carcinoma. *J. Yunnan Univ. Tradit Chin. Med.* 40 (06), 22–25.

Sung, H., Ferlay, J., Siegel, R. L., Laversanne, M., Soerjomataram, I., Jemal, A., et al. (2021). Global cancer statistics 2020: GLOBOCAN estimates of incidence and mortality worldwide for 36 cancers in 185 countries. *CA A. Cancer J. Clin.* 71, 209–249. doi:10.3322/caac.21660

Tang, A., Hallouch, O., Chernyak, V., Kamaya, A., and Sirlin, C. B. (2018). Epidemiology of hepatocellular carcinoma: target population for surveillance and diagnosis. *Abdom. Radiol. (Ny)* 43 (1), 13–25. doi:10.1007/s00261-017-1209-1

Tang, Q. Y., Wei, A. L., Pan, Z., and Li, P. C. (2015). Clinical Observation of Aitongxiao Formula with TACE in the Treatment of Middle-advanced Primary liver cancer. *Lishizhen Med. Mater. Med. Res.* 26 (04), 906–908.

Therasse, P., Arbuck, S. G., Eisenhauer, E. A., Wanders, J., Kaplan, R. S., Rubinstein, L., et al. (2000). New guidelines to evaluate the response to treatment in solid tumors. European Organization for Research and Treatment of Cancer, National Cancer Institute of the United States, National Cancer Institute of Canada. *J. Natl. Cancer Inst.* 92 (3), 205–216. doi:10.1093/jnci/92.3.205

Trotti, A., Colevas, A. D., Setser, A., Rusch, V., Jaques, D., Budach, V., et al. (2003). CTCAE v3.0: development of a comprehensive grading system for the adverse effects of cancer treatment. *Semin. Radiat. Oncol.* 13 (3), 176–181. doi:10.1016/S1053-4296(03)00031-6

Wang, A. M., Tu, J. G., and Wang, J. Y. (2020). Clinical Observation of Modified Bazhen decoction on Adverse Reactions after TACE in Primary Liver Cancer. *Chin Mod. Doctor* 58 (12), 114–117.

Wang, J. (2015). The Effect of Yangzhengxiaoji Capsule on Tumor Marker and Quality of Life in Primary Liver Cancer Patients. *Chin. J. Gerontol.* 35 (20), 5827–5829.

Wang, M., Huang, C., Su, Y., Yang, C., Xia, Q., and Xu, D. J. (2017). Astragaloside II sensitizes human hepatocellular carcinoma cells to 5-fluorouracil via suppression of autophagy. *J. Pharm. Pharmacol.* 69 (6), 743–752. doi:10.1111/jphp.12706

Wang, Q. M., Wang, R. R., Zhang, D., Pan, M. Q., Pan, B., Deng, X. S., et al. (2016). Clinical Study on Treating Primary Hepatic Carcinoma with Syndrome of Stagnation of Liver Qi and Spleen Deficiency with Combination of Oral Ganxi Tablets and Arsenic Trioxide via Transcatheter Arterial Chemoembolization. *Chin. J. Tradit Chin. Med. Pharm.* 31 (03), 1121–1125.

Wang, X. D., Li, B., Cai, L. J., Huang, S. Q., and Wei, M. (2020). Short-term Clinical Observation of Fuzheng Quxie Yiai Recipe Combined with TACE in the Treatment of Patients with Advanced Primary Liver Cancer. *Asia-pacific Tradit Med.* 16 (09), 151–155.

Wang, X. M., Li, X. B., and Peng, Y. (2017). Impact of Qi-invigorating traditional Chinese medicines on intestinal flora: A basis for rational choice of prebiotics. *Chin. J. Nat. Med.* 15 (4), 241–254. doi:10.1016/S1875-5364(17)30041-9

Wang, Y., Zhang, Q., Chen, Y., Liang, C. L., Liu, H., Qiu, F., et al. (2020). Antitumor effects of immunity-enhancing traditional Chinese medicine. *Biomed. Pharmacother.* 121, 109570. doi:10.1016/j.biopha.2019.109570

Wei, P. L., Gu, H., Liu, J., and Wang, Z. (2018). Development of Fangjiomics for Systems Elucidation of Synergistic Mechanism Underlying Combination Therapy. *Comput. Struct. Biotechnol. J.* 16, 565–572. doi:10.1016/j.csbj.2018.10.015

Yang, J. D., Hainaut, P., Gores, G. J., Amadou, A., Plymoth, A., and Roberts, L. R. (2019). A global view of hepatocellular carcinoma: trends, risk, prevention and management. *Nat. Rev. Gastroenterol. Hepatol.* 16 (10), 589–604. doi:10.1038/s41575-019-0186-y

Ye, W. D., Xu, W. D., and Yu, Z. C. (2015). Clinical Observation on 68 Cases of Terminal-stage Liver Cancer Treated with TACE Combined Soothing Liver and Invigorating Spleen. *J. Zhejiang Chin. Med. Univ.* 39 (07), 541–544.

Yoon, S. Y., Lee, J. Y., Roh, D. H., and Oh, S. B. (2018). Pharmacopuncture With Scolopendra subspinipes Suppresses Mechanical Allodynia in Oxaliplatin-Induced Neuropathic Mice and Potentiates Clonidine-induced Anti-allodynia Without Hypotension or Motor Impairment. *J. Pain* 19 (10), 1157–1168. doi:10.1016/j.jpain.2018.04.015

Zhai, B., Zhang, N., Han, X., Li, Q., Zhang, M., Chen, X., et al. (2019). Molecular targets of β-elemene, a herbal extract used in traditional Chinese medicine, and its potential role in cancer therapy: A review. *Biomed. Pharmacother.* 114, 108812. doi:10.1016/j.biopha.2019.108812

Zhang, L. X., Lv, Y., Xu, A. M., and Wang, H. Z. (2019). The prognostic significance of serum gamma-glutamyltransferase levels and AST/ALT in primary hepatic carcinoma. *BMC Cancer* 19 (1), 841. doi:10.1186/s12885-019-6011-8

Zhang, N. (2020). The efficacy of Sanjinshusan Decoction Combined with TACE on Middle-Late Liver Cancer. *Chin. J. Liv Integr. Tradit West. Med.* 30 (02), 164–165.

Zhang, Q., Chi, H. C., Yu, J., Wang, X. M., and Zhao, W. S. (2007). Clinical Study of Guben Yiliu II Combined with Chemicals Arterial Perfusion for Advanced Hepatoma of 58 Cases. *J. Tradit Chin. Med.* 48 (03), 235–237.

Zhang, S., Sun, K., Zheng, R., Zeng, H., Wang, S., Chen, R., et al. (2021). Cancer incidence and mortality in China, 2015. *J. Natl. Cancer Cent.* 1, 2–11. doi:10.1016/j.jncc.2020.12.001

Zhang, Z. Y., Dong, B. Z., Li, F. F., and Rong, X. J. (2017). Clinical Research of Clearing Liver-fire for Removing Blood Stasis Prescription Combined with TACE in the Treatment of Patients with Advanced Primary Liver Cancer. *J. Sichuan Tradit Chin. Med.* 35 (07), 111–113.

Zhong, Y. Q., Fu, J. J., Liu, X. M., Diao, X., Mao, B., Fan, T., et al. (2010). The reporting quality, scientific rigor, and ethics of randomized placebo-controlled trials of traditional Chinese medicine compound formulations and the differences between Chinese and non-Chinese trials. *Curr. Ther. Res. Clin. Exp.* 71 (1), 30–49. doi:10.1016/j.curtheres.2010.02.001

Zhu, R. X., Seto, W. K., Lai, C. L., and Yuen, M. F. (2016). Epidemiology of Hepatocellular Carcinoma in the Asia-Pacific Region. *Gut Liver* 10 (3), 332–339. doi:10.5009/gnl15257

Conflict of Interest: The authors declare that the research was conducted in the absence of any commercial or financial relationships that could be construed as a potential conflict of interest.

Publisher's Note: All claims expressed in this article are solely those of the authors and do not necessarily represent those of their affiliated organizations or those of the publisher, the editors, and the reviewers. Any product that may be evaluated in this article or claim that may be made by its manufacturer is not guaranteed or endorsed by the publisher.

frontiers in Oncology

ORIGINAL RESEARCH
published: 09 November 2021
doi: 10.3389/fonc.2021.727130

Proteome Analysis of *Camellia nitidissima* Chi Revealed Its Role in Colon Cancer Through the Apoptosis and Ferroptosis Pathway

Yiwei Chen[1,2,3†], *Fan Zhang*[2,3†], *Zhengcai Du*[2,3,4], *Jinling Xie*[2,3], *Lei Xia*[2,3], *Xiaotao Hou*[2,3,4*], *Erwei Hao*[2,3,4*] and *Jiagang Deng*[2,3,4*]

[1] School of Pharmacy, Chengdu University of Traditional Chinese Medicine, Chengdu, China, [2] Guangxi Key Laboratory of Efficacy Study on Chinese Materia Medica, Guangxi University of Chinese Medicine, Nanning, China, [3] Collaborative Innovation Center for Research on Functional Ingredients of Agricultural Residues, Guangxi University of Chinese Medicine, Nanning, China, [4] Postdoctoral Workstation, Guangxi Institute of Medicinal Plants, Nanning, China

Colon cancer is the third most common cancer in the world with a high mortality rate. At present, surgery combined with radiotherapy and chemotherapy is the primary treatment, but patient prognosis remains poor. Traditional Chinese medicine (TCM) has become a complementary and alternative source of anti-cancer drugs. *Camellia nitidissima* Chi (CNC) is a TCM used to treat a variety of cancers. However, the role of CNC in cancer remains elusive, and its effect and mechanism on colon cancer have not been reported. Here, we show that CNC exerts an excellent inhibitory effect on colon cancer proliferation and apoptosis induction *in vitro* and *in vivo*. We performed label free-based quantitative proteomic analysis to evaluate the HCT116 cells treated with CNC. Our data revealed a total of 363 differentially expressed proteins, of which 157 were up-regulated and 206 down-regulated. Gene Ontology enrichment analysis showed that these proteins were involved in tumor occurrence and development through multiple biological processes such as cell proliferation, cell apoptosis, cell cycle, and cell death. Interestingly, we also found significant changes in ferroptosis pathways. The role of essential proteins glutathione peroxidase 4 (GPX4) and heme oxygenase-1 (HMOX1) were verified. CNC decreased the expression of GPX4 and increased the expression of HMOX1 at the mRNA and protein levels *in vivo* and *in vitro*. Collectively, these findings reveal that CNC regulates colon cancer progression *via* the ferroptosis pathway and could be an attractive treatment for colon cancer.

Keywords: ***Camellia nitidissima*** **Chi, colon cancer, ferroptosis, proteomics, 4D label-free**

OPEN ACCESS

Edited by:
Qingmin Sun,
Affiliated Hospital of Nanjing University of Chinese Medicine, China

Reviewed by:
Tingting Du,
Chinese Academy of Medical Sciences and Peking Union Medical College, China
Chao Sun,
Tianjin Medical University General Hospital, China

***Correspondence:**
Xiaotao Hou
xthou@126.com
Erwei Hao
ewhao@163.com
Jiagang Deng
dengjg53@126.com

[†]*These authors have contributed equally to this work*

Specialty section:
This article was submitted to Pharmacology of Anti-Cancer Drugs, a section of the journal Frontiers in Oncology

Received: *18 June 2021*
Accepted: *18 October 2021*
Published: *09 November 2021*

Citation:
Chen Y, Zhang F, Du Z, Xie J, Xia L, Hou X, Hao E and Deng J (2021) Proteome Analysis of Camellia nitidissima Chi Revealed Its Role in Colon Cancer Through the Apoptosis and Ferroptosis Pathway. Front. Oncol. 11:727130. doi: 10.3389/fonc.2021.727130

INTRODUCTION

According to 2021 American Cancer Society data, colon cancer ranks third in terms of morbidity and mortality, and it is the third most common cancer in the world after lung and breast cancer (1). While surgery, chemotherapy, radiotherapy, and vaccine therapy can be applied individually or in combination, they carry side effects that affect patient quality of life (2, 3). This underscores the urgent need to develop novel strategies for the treatment of colon cancer.

Clinical studies have shown that traditional Chinese medicine (TCM) has significant advantages as auxiliary anti-tumor treatment. It has become a supplementary and alternative source of anti-cancer drugs with high efficiency and few side effects (4, 5). *Camellia nitidissima* Chi (CNC) is a TCM that mainly composed of flavonoids, saponins, and polyphenols (6). It has been used as a traditional folk medicine to treat hypertension, hyperlipidemia, infection, and other diseases (7). Moreover, a growing body of modern pharmacological research demonstrated that CNC has a significant inhibitory effect on various cancers (8–11). Despite, evidence supporting beneficial effects of CNC, its anti-cancer mechanisms remains unknown due to its multi-target effects and multi-component characteristics.

In recent years, proteomics research based on mass spectrometry (MS) has been widely used to investigate protein alterations (12, 13), and it is increasingly used to study TCM (14, 15). In the current study, we performed high-resolution MS to detect changes in crucial proteins in HCT116 cells treated with CNC. Bioinformatics analysis was subsequently carried out to identify novel pathways and protein targets affected by CNC treatment, and functional analysis was performed to predict the effect of molecular and biological processes to better understand the potential mechanism of CNC against colon cancer.

MATERIALS AND METHODS

CNC Extract Preparation

In total, 400 g of dried CNC (harvested in Fangchenggang, Guangxi, China) was weighed, immersed in 10 L of 75% (v/v) ethanol for 30 min, and twice extracted in a reflux extraction for 1.5 h each time. The extracted solution was merged and evaporated by a rotary evaporator and then freeze-dried to obtain the extract powder. Dimethyl sulfoxide was dissolved into a 0.22-μM filter membrane with a concentration of 100 mg/mL for *in vitro* assays. Sterilized water was dissolved with a concentration of 1 g/mL (quantity of raw material) for *in vivo* assays and then frozen at -20°C.

Cell Lines and Animals

HCT116, SW480, and HCT15 cell lines (human colorectal adenocarcinoma) were obtained from the Type Culture Collection of the Chinese Academy of Sciences (Shanghai, China) and Procell Life Science &Technology Co., Ltd. (Wuhan, China). HCT116 was grown in McCoy's 5A (Procell, China) supplemented with 10% fetal bovine serum (FBS; Gibco/Thermo Fisher Scientific, Waltham, MA, USA). SW480 was grown in L-15 media (Gibco/Thermo Fisher Scientific) supplemented with 10% FBS. HCT15 was grown in RPMI 1640 (Keygen, Nanjing, China) supplemented with 10% FBS. All cells were maintained at 37°C in a humidified incubator containing 5% CO_2. Female BALB/c nude mice (5-6 weeks) purchased from Vital River (SCXK [Jing] 2016-0006, Beijing, China) were used for the *in vivo* experiments. Animals were housed at a controlled temperature of 20-22°C and relative humidity of 50-60% under12-h light-dark cycles.

Antibodies and Primer Sequences

The following antibodies were used: Caspase 3 (Cat# CST9661S), Caspase 9 (Cat# CST9507S), cyclin-dependent kinase (CDK4, Cat# 12790T), CDK6 (Cat# CST13331T), proliferating cell nuclear antigen (PCNA, Cat# CST13110T), glutathione peroxidase 4 (GPX4, Cat# CST52455S), heme oxygenase-1 (HMOX1, Cat# CST5853S), glyceraldehyde 3-phosphate dehydrogenase (GAPDH, Cat# CST5174S), all of which were from Cell Signaling Technology (CST, Danvers, MA, USA); Bax (Cat# ab77566) and Bcl-2 (Cat# ab59348) were from Abcam.

The primers used for the amplification of GPX4, HMOX1, P53, SLC7A11, FTH1, ACSL4 and GAPDH were synthesized by Generay Co., Ltd. (Shanghai, China). GPX4 sequence: forward primer (5'-3'), TTGCCGCCTACTGAAGC; reverse primer (5'-3'), ATGTGCCCGTCGATGTC. HMOX1 sequence: forward primer (5'-3'), CAGTCTTCGCCCCTGTCT; reverse primer (5'-3'), GCATGGCTGGTGTGTAGG. P53 sequence: forward primer (5'-3'), CAGCACATGACGGAGGTTGT; reverse primer (5'-3'), TCATCCAAATACTCCACACGC. SLC7A11 sequence: forward primer (5'-3'), TCTCCAAAGGAGGTTACCTGC; reverse primer (5'-3'), AGACTCCCCTCAGTAAAGTGAC. FTH1 sequence: forward primer (5'-3'), ATCTCATCAAGCCCTCTGTAGT; reverse primer (5'-3'), GGACGCAGGTCATGGAAGC. ACSL4 sequence: forward primer (5'-3'), ACTGGCCGACC TAAGGGAG; reverse primer (5'-3'), GCCAAAGGCAAG TAGCCAATA. GAPDH sequence: forward primer (5'-3'), GGACCTGACCTGCCGTCTAG; reverse primer (5'-3'), GTAGCCCAGGATGCCCTTGA.

Analysis of Chemical Constituents in CNC Extract

Chromatographic analysis of CNC was performed using the UltiMate 3000 RS liquid chromatography (LC) system (Thermo Fisher Scientific). The gradient system consisting of acetonitrile containing 0.1% formic acid (solvent A) and water containing 0.1% formic acid (solvent B) was as follows: 0-1 min, 98% B; 1-25 min, 98-5% B; 25-30 min, 5-98% B. The volume of sample was 5 μL for each injection. The column temperature and flow rate were 35°C and 0.3 mL/min, respectively. CNC chemical constituents were detected by a Q Exactive Orbitrap mass spectrometer (Thermo Fisher Scientific) with an electrospray ionization interface. The full scan range was from 150 to 2000 m/z.

Cell Proliferation Assays and Morphological Observation

Cell viability was assessed with MTS kits according to the manufacturer instructions (Promega, Madison, WI, USA).

Briefly, 3,000 cells/well were seeded in 96-well plates. After overnight incubation, the cells were treated with or without CNC extract (31.25, 46.875, 62.5, 93.75, 125, 187.5, 250 μg/mL) for 48 h prior to the MTS assays. The classic ferrostatin-1 rescue experiment was performed by MTS, the concentration of ferrostatin-1 was 1uM, and the concentration of CNC extract was 100ug/mL. Cells morphology was observed and photographed under an inverted microscope (Olympus, Tokyo, Japan).

Colony Formation Assays

To evaluate colony formation, 1,000 cells/well were seeded in 6-well plates. Then cells were treated with or without CNC extract (25, 50, 100 μg/mL). The plates were washed with phosphate-buffered saline (PBS) and stained with crystal violet on day 7. The cells were observed and photographed with the colony count analysis system of GelCount (Oxford Optronix, Abingdon, UK).

Apoptosis and Cell Cycle Assays

For apoptosis and cell cycle analyses, 1.5×10^5 cells/well were seeded in 6-well plates. After overnight incubation, the cells were treated with or without CNC extract (25, 50, 100, 150 μg/mL) for 48 h. Cells were collected and performed according to the protocol of the Annexin V FITC Apoptosis kit (and FxCycleTM PI/RNAse Solution (both from BD Biosciences, Franklin Lakes, NJ, USA). All cell samples were analyzed on the Attune Flow cytometer (Thermo Fisher Scientific) within 1 h.

Western Blotting

The concentrations of HCT116 cells protein samples were determined using a Pierce™BCA Protein Assay Kit (Thermo Fisher Scientific). The protein samples were then separated by 12% SDS-PAGE (Bio-Rad, Hercules, CA, USA) and transferred to polyvinylidene fluoride membranes (Millipore, Burlington, MA, USA). After blocking for 1 h, antibodies were incubated overnight at 4°C. Protein bands were visualized utilizing ECL detection reagents (Bio-Rad).

Proteomic Sample Preparation

HCT116 cell samples were disrupted in lysis buffer (1% Triton X-100, 1% protease inhibitor cocktail). Protein concentrations were determined by the BCA kit. 4D Label-free samples underwent reversed-phase peptide fractionation on a homemade rig followed by and LC-MS/MS analysis. Proteomic samples were analyzed by LC-MS/MS as described in **Supplement 1**.

Protein Identification and Quantitation

LC-MS/MS spectra were searched using the MaxQuant search engine (v.1.6.6.0) (16) embedded into the Homo sapiens 9606 SwissProt database (20366 entries). Trypsin/P was specified as the cleavage enzyme allowing up to two missing cleavages. All identified proteins were subjected to the annotation methods as described in **Supplement 2**.

Parallel Reaction Monitoring Analysis

Based on the method mentioned by Sun and colleagues (16), dithiothreitol and iodide acetamide were added to the protein solution. The mixture was hydrolyzed overnight at 37°C and the ratio of trypsin: protein was 1:50. Hydrolysis was continued for 4 h until the ratio of trypsin:protein was 1:100. The peptides were dissolved in 0.1% (v/v) aqueous formic acid, and the mobile phase was isolated using an EASY-nLC 1000 ultra high-performance LC (UHPLC) system (Thermo Fisher Scientific). The peptides were subjected to the nanospray ionization source followed by MS/MS in Q ExactiveTM Plus (Thermo Fisher Scientific) coupled online to the UHPLC. MS/MS data were processed using Skyline (v.3.6).

Transmission Electron Microscopy

HCT116 and HCT15 cells were seeded into 15-cm dishes. After 24 h of culture, cells were treated with or without CNC extract (100μg/mL) for 48 h. Cells were collected and fixed, then dehydrated and embedded. The embedded cells were cut into ultrathin sections at 60-80nm using an ultrathin slicer (Leica UC7, Wetzlar, Germany). Finally, mitochondria ultrastructure was observed under TEM (HT7700, Hitachi, Tokyo, Japan) and the images were collected.

Detection of Reactive Oxygen Species, Iron, and Glutathione

HCT116 cells were treated with or without CNC extract for 12 h. Then, cells were collected and incubated with 10 μM 2'-7'-dichlorofluorescein diacetate (DCFH-DA) at 37°C for 25 min. The ROS-induced fluorescence intensity of intracellular DCFH-DA was measured by Operetta CLS™ High Content (PerkinElmer, Waltham, MAUSA). The iron concentrations in HCT116 and HCT15 were measured by Tissue iron assay kit. The glutathione (GSH) concentrations in HCT116 were measured by Reduced GSH assay kit.

Reverse Transcription-Quantitative Polymerase Chain Reaction

According to the manufacturer's instructions, total RNA was extracted using an Eastep R Super Total RNA Extraction Kit (Promega). cDNA was synthesized using a GoScript TM Reverse Transcription System (Promega). RT-QPCR was performed in 96-well plates using the Step-Two Real-Time PCR system (Applied Roche LightCycler 96). For quantitative SYBR®Green real-time PCR, the following primers were used: GPX4, HMOX1, P53, SLC7A11, FTH1, ACSL4 and GAPDH (all synthesized by Generay Co., Ltd.). GAPDH was used as an internal standard, and the relative expression of each gene was normalized to GAPDH. The relative quantification of gene expression was analyzed using the $2^{-\Delta\Delta Ct}$ method. Each sample was analyzed in triplicate.

Immunofluorescence

Tumor specimens were fixed in 4% paraformaldehyde overnight and embedded in paraffin. Samples were incubated with primary antibodies against GPX4 (1:100, Proteintech), HMOX1 (1:100, Proteintech), CDK4 (1:300, CST), PCNA (1:600, CST), P53 (1:500, CST) or FTH1 in (1:300, CST) PBS overnight at 4°C. Samples were them incubated with secondary Cy3-labeled anti-rabbit antibody (Boster Biological Technology, Pleasanton, CA,

USA) for 1 h at ambient temperature. DAPI was added and incubated for 5min in the dark. Samples were visualized with an Olympus BX53 fluorescence microscope.

Subcutaneous Tumor Mouse Model

Nude mice were subcutaneously injected with 4×10^6 HCT116-Luc cells. Mice with a tumor diameter of $100mm^3$ were numbered and randomly divided into five groups (n = 6/group). CNC extract (1.2, 2.4, or 4.8 g/kg/d) given *via* gavage. Fluorouracil (25mg/kg/2d) was injected intraperitoneally as the positive control. Tumor growth data were recorded twice a week, and the tumor volume was calculated. The mice were sacrificed and photographed after 14 days. The animal study protocol was reviewed and approved by the Animal Ethics Committee of the Guangxi University of Chinese Medicine, and all procedures were followed the relevant regulations and guidelines.

Statistical Analysis

One-way analyses of variance followed by the LSD-t multiple comparison tests were performed to compare multiple groups. Each experiment was carried out in duplicate and repeated three times. Statistical analyses were performed using GraphPad 8.0.2 software (GraphPad Inc., San Diego, CA, USA) to perform a two-tailed t-test, and $p < 0.05$ was considered statistically significant. The results are presented as mean ± standard deviation (SD).

RESULTS

Identification of Anti-tumor Active Compounds in CNC Extracts

We analyzed the phytochemical ingredients of CNC extract using UHPLC-MS. According to the standard of the mzCloud database (https://www.mzcloud.org/Stats), a total of 116 compounds with mzCloud best match >80 were identified **(see Supplementary 3)**. In addition, by further alignment with published data from the literature, 10 compounds were reported to have been isolated from CNC, and were speculated to be the anti-tumor active components. The details of these 10 compounds are listed in **Table 1**, including flavonoids, polysaccharides, volatile components, and triterpenoids. The base peak chromatogram of CNC extract obtained by UHPLC-MS was constructed (see **Supplementary 4**).

CNC Extract Inhibits Cell Proliferation *In Vitro*

To evaluate the effect of CNC extract on colon cancer cell growth, we treated HCT116, SW480, and HCT15 cells with different concentrations. All of the tested cell lines were treated with various concentrations of CNC extract for 24, 48, and 72h and had increasingly lower cell viability with higher drug concentrations (**Figure 1A**). The half-maximal inhibitory concentrations (IC_{50}) of CNC extract in HCT116, SW480, and HCT15 cells were 124.2μg/mL (24h), 92.37μg/mL (48h), 108.6μg/mL (72h), 124.2μg/mL (24h), 103.5μg/mL (48h), 97.98μg/mL (72h); and 128.5μg/mL (24h), 97.17μg/mL (48h), 84.38μg/mL (72h) respectively. Cell morphology gradually became round, and nuclear condensation induced by CNC extract was observed in all three cell lines (**Figure 1B**). The colony formation abilities of HCT116, SW480, and HCT15 cells were dose-dependently inhibited after CNC extract incubation (**Figure 1C**). The effects of different CNC extract concentration were evaluated by flow cytometry. Higher concentrations resulted in increased percentages of apoptotic cells in SW480 and HCT15. However, the apoptosis rate of HCT116 did not show a good dose-dependent concentration, perhaps because HCT116 was less sensitive, and the concentration of CNC extract that induces the initiation of mass apoptosis of HCT116 may be between 100 and 150μg/mL. (**Figure 2A**) and a greater proportion of G2/M phase cells (**Figure 2B**) compared to control. CNC extract interrupted cell cycle progression by inducing G2/M arrest rather than by influencing G0/G1. Moreover, we examined classical apoptosis proteins by western blot and found an increased ratio of cleaved-caspase-9/caspase-9 (C-caspase9/caspase9)were up-regulated after treated with CNC extract treatment, while caspase-3 was down-regulated (**Figure 2C**). We also examined mitochondrial apoptosis proteins and found that although bcl-2 was down-regulated, the bax/bcl-2 ratio did not change significantly. These results may suggest that CNC extract induces apoptosis may through other signaling pathways. For cell cycle proteins, the results showed that CNC extract treatment decreased the levels of CDK4, 6, and PCNA in HCT116 cells.

TABLE 1 | Relevant analytical data for compounds isolated from CNC extract.

Retention time (min)	Experimental mass (m/z)	Molecular formula	Theoretical mass (m/z)	Adduct ion	Mass error (ppm)	Possible compounds	Score
0.492	180.06369	$C_6H_{12}O_6$	180.06339	$[M+H]^+$	1.6661	D- (+)-Glucose	86.2
7.654	289.0722	$C_{15}H_{14}O_6$	290.0793	$[M-H]^-$	-0.7968	Catechin	93.6
10.119	609.1463	$C_{27}H_{30}O_{16}$	610.1533	$[M-H]^-$	0.0719	Rutin	95
11.411	433.1122	$C_{21}H_{20}O_{10}$	432.1054	$[M+H]^+$	0.5708	Vitexin	85.6
12.328	303.0497	$C_{15}H_{10}O_7$	302.0424	$[M+H]^+$	0.7157	Quercetin	88.3
12.822	287.0548	$C_{15}H_{10}O_6$	286.0476	$[M+H]^+$	0.5325	Luteolin	82.9
18.539	151.0391	$C_8H_8O_3$	152.0463	$[M-H]^-$	6.7101	Methyl salicylate	77.3
19.451	439.36035	$C_{30}H_{48}O_3$	439.3563	$[M+H]^+$	-2.8705	Oleanolic acid	94.8
20.124	427.3926	$C_{30}H_{50}O$	426.3856	$[M+H]^+$	1.2408	Lupeol	86.8
21.471	283.2645	$C_{18}H_{36}O_2$	284.2718	$[M-H]^-$	-0.8516	Stearic acid	99.7

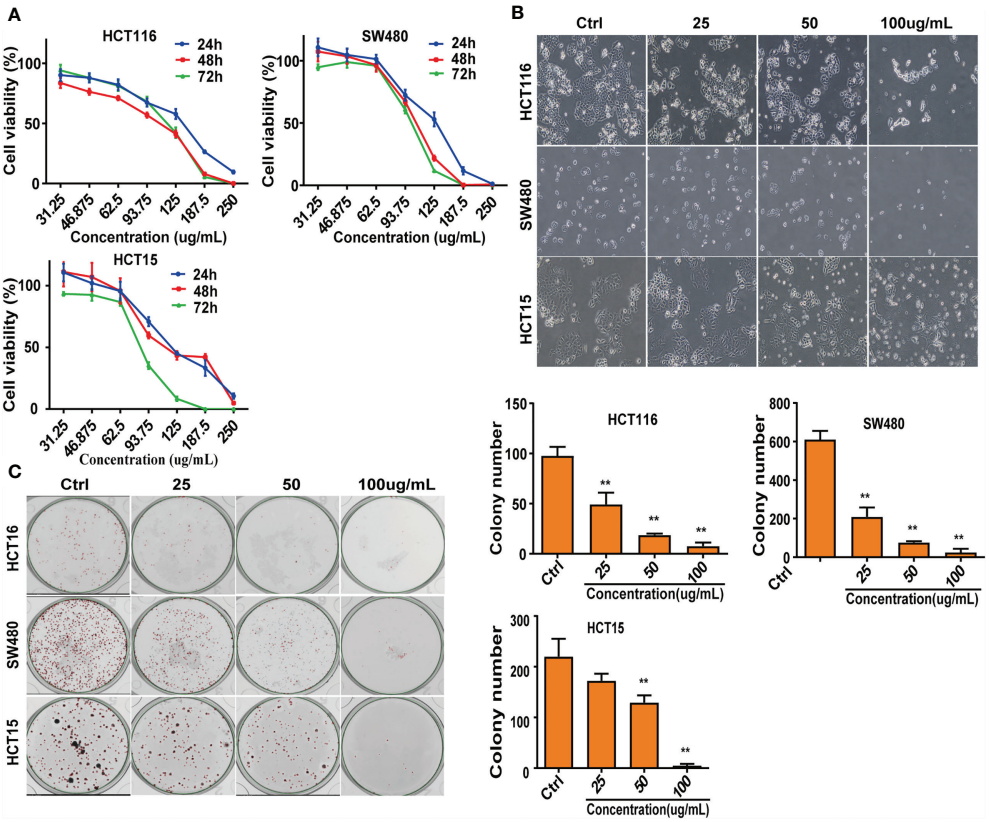

FIGURE 1 | Suppress of cell lines growth *in vitro*. **(A)** After intervention with CNC extract, cell viability was measured by MTS assay. **(B)** Cell morphology were observed after treatment with CNC extract. **(C)** Number of cell clones after treatment with CNC extract. There were three duplicate samples in each experiment. Data are expressed as mean ± SD. Compared with control group: **p < 0.01.

Quantitative Proteomics Analysis

Proteomic data were acquired by 4D-Label free technology and a timsTOF pro mass spectrometer (Bruker nanoElute system, Billerica, MA, USA). Peptides digested by trypsin were analyzed using high-resolution MS. The primary ions and secondary fragments of the peptides were also subjected to high-resolution MS. All obtained data were analyzed through a specific bioinformatics database (**Figure 3A**). Most peptide fragments were found to contain 7-20 amino acid residues, an observation that conforms with the general rules of trypsin enzymatic hydrolysis and higher-energy collisional dissociation fragmentation (**Figure 3B**). There was a negative correlation between molecular weight and the protein sequence coverage. Larger molecular weight proteins can produce more enzymatic fragments to achieve the same coverage. That is to say. It needs more peptides identified from a large protein to achieve the same coverage. The length of the peptide fragments identified met the quality control requirements (**Figure 3C**). In this experiment, we identified 6720 proteins, of which 6039 were quantified. Using 1.5-fold expression as the standard, we found that 363 proteins were differentially expressed in HCT116 cells treated with CNC extract. Among these, 157 and 206 proteins were up- and down-regulated, respectively. (**Figure 3D**).

Protein Function Classification and Enrichment Analysis

To thoroughly understand the role of the differentially expressed proteins in the anti-tumor effect of CNC extract, we annotated the function and characteristics of these proteins from the Gene Ontology (GO) and Kyoto Encyclopedia of Genes and Genomics (KEGG). GO analysis indicated that the most two significantly changed biological processes (BP) were cellular process and biological regulation. Other functional categories such as cellular component (CC) and molecular function (MF)are listed in **Figure 4A**. InterProScan (http://www.ebi.ac.uk/interpro/) was utilized to analyze the subcellular classification of the differentially expressed proteins. Out of the 363 proteins, 139 are in the nucleus (28.31%), 119 are located in the cytoplasm (24.24%), and 82 are extracellular (16.7%) (**Figure 4B**). In the GO enrichment analysis, multiple BPs such as regulation of cell proliferation, regulation of cell cycle, apoptotic process were involved in cancer development (**Figure 4C**). The KEGG pathway enrichment analysis identified the ferroptosis pathway as being cancer related (**Figure 4D**). Ferroptosis is a type of cell death characterized by elevated intracellular iron and ROS. The results suggest that CNC extract suppression of CC proliferation may be related to the ferroptosis pathway, and it might target

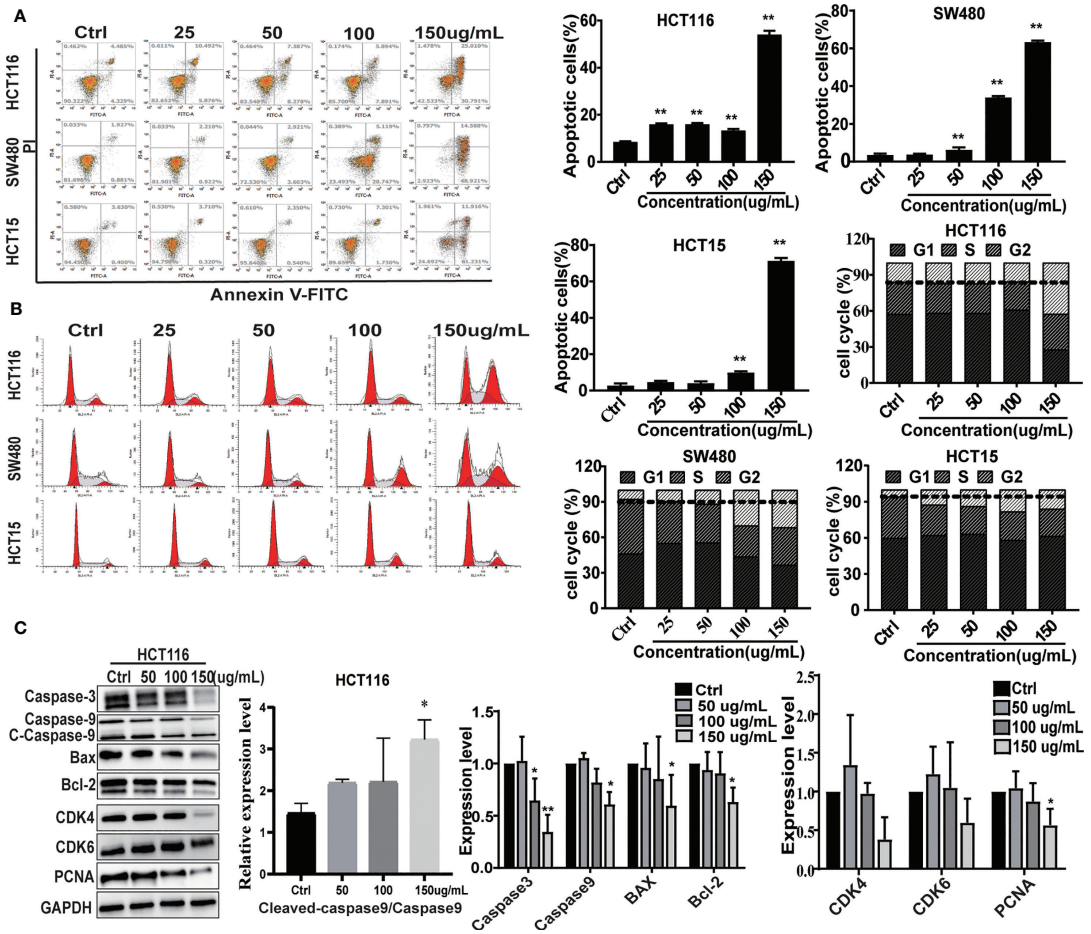

FIGURE 2 | The effect on cell apoptosis and cell cycle. **(A)** Apoptosis rate induced by CNC extract in cell lines. **(B)** The cell cycle distribution of cell lines incubated by CNC extract. **(C)** WB analysis of related proteins in HCT116 after intervention of CNC extract. There were three duplicate samples in each experiment. Data are expressed as mean ± SD. Compared with control group: *p < 0.5, **p < 0.01.

GPX4 and HMOX1. In addition, it is associated with cell apoptosis and cell cycle arrest.

CNC Extract Induces Cell Death by Promoting Ferroptosis

PRM analysis is principal method used to verify the proteomics data that selects specific peptides or target peptides and quantifies them (17). We analyzed 15 of the 363 differentially expressed proteins using PRM instead of traditional western blots (see **Supplementary 5**). First, according to the classic ferrostatin-1 rescue experiment, we found that the ferroptosis inhibitor ferrostatin-1 can effectively reverse the cell ferroptosis induced by CNC extract (**Figure 5A**). Among them, there were three proteins associated with the ferroptosis pathway. 4D Label-free analysis showed that the ferroptosis-associated proteins GPX4 and GPX1 decreased, whereas HMOX1 increased (**Figure 5B**). We observed the same results after the PRM analysis. Additionally, nuclear accumulation of ROS was increased in CNC extract-treated HCT116 cells (**Figure 5C**). We hypothesized that ferroptosis may be highly related to CNC extract-induced cell death, and TEM revealed that HCT116 and HCT15 cells treated with CNC extract exhibited characteristic features of ferroptosis and the most significantly changed mitochondria was indicated by red arrows. (**Figure 5D**), such as shrunken mitochondria with increased membrane density and the appearance of autophagy. While the iron content of HCT116 and HCT15 cells were significantly increased in the CNC extract group, there were no changes in HCT116 of GSH content (**Figures 5E, F**). The result of no significant change in GSH content was consistent with the research results of other scholars, and they found the second class inhibits GPX4 without GSH depletion, such as RSL3, which inhibits GPX4 directly (18). In ferroptosis, GPX4 protects against iron- and oxygen-dependent lipid peroxidation by converting lipid peroxides into nontoxic lipids. Inhibition of GPX4 will lead to peroxide accumulation and the occurrence of ferroptosis (19). HMOX1 can catalyze the degradation of heme to Fe^{2+}, biliverdin, and carbon monoxide. Excess Fe^{2+} promotes ferroptosis through the Fenton reaction (20). Other hallmarks of ferroptotic pathway, such as p53, SLC7A11, FTH1 and ACSL4 in HCT116 and HCT15 were determined.

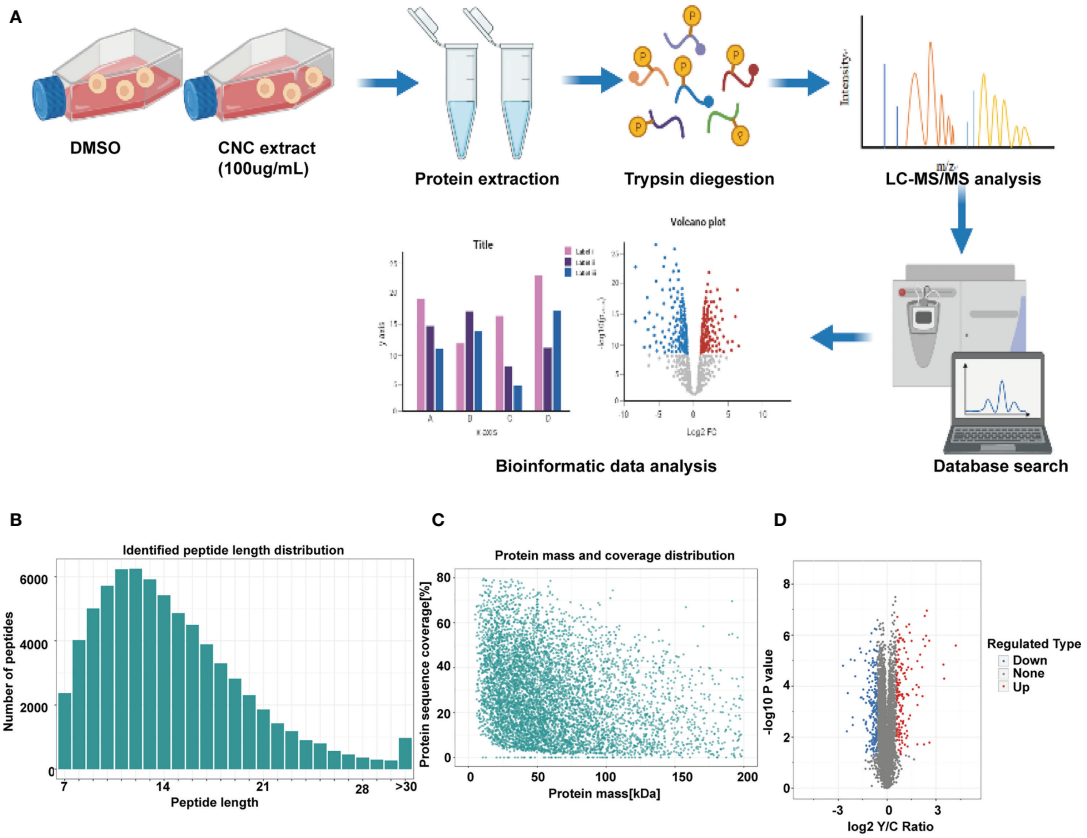

FIGURE 3 | Differentially expressed proteins were evaluated by proteomics. **(A)** Flow diagram of 4D Label-free proteomics. **(B)** Length distribution of the peptides identified by mass spectrometry. **(C)** Relationship between protein molecular weight and coverage. **(D)** Volcano plot of differentially expressed proteins. The blue dots are down-regulated proteins. The red dots are up-regulated proteins. There were three duplicate samples in each experiment.

Notably, it was found that CNC extract could reduce mRNA expression levels of GPX4, SLC7A11 and FTH1 in HCT116. And CNC extract could increase mRNA expression levels of HMOX1, P53 and ACSL4 in HCT116. Also, CNC extract could increase mRNA expression levels of HMOX1 and P53 in HCT15, but had no significant effect on the expression of other hallmarks of ferroptotic pathway (**Figure 5G**). Similar expression levels of HMOX1 protein were observed in western blot and R-PCR. As for GPX4, western blot and q-PCR showed the same results and down-regulated the expression of GPX4, but there was no significant difference in western blot (**Figure 5H**). These results provide further evidence that CNC extract may inhibit the proliferation of colon cancer cells through ferroptosis-related pathways.

CNC Extract Suppresses Tumor Growth and Regulates the Ferroptosis Pathway *In Vivo*

After 14 consecutive days of treatment with CNC extract, xenografts of CNC extract-treated groups had smaller tumors compared to the model group (**Figures 6A, B**). Bioluminescence imaging of HCT116 xenograft tumors in different groups showed consistent results for the measured tumor volume (**Figure 6C**). Pathological sections of tumor tissues were also observed with hematoxylin and eosin staining (**Figure 6D**). Immunofluorescence staining of ferroptosis- and cell proliferation-related markers (GPX4, FTH1, PCNA, and CDK4 positive ratio) decreased, while HMOX1 and p53 increased in the CNC extract-therapy group (**Figure 7A**). Consistent with the *in vitro* experiments, TUNEL assays showed that apoptosis rates were significantly increased in the CNC extract-therapy group compared to the model group (**Figure 7B**).

DISCUSSION

Colon cancer is a malignant tumor and the fourth leading cause of cancer-related deaths (21). Although progress has been made in diagnosis and treatment, the prognosis of the patients is still inferior (22). Recent years have seen the rapid rise and development of TCM. Compared with single-target chemical drugs with high toxicity, side effects, and poor efficacy, the clinical advantages of TCMs with multiple components, pathways, and targets are becoming more prominent (23–25). CNC is a TCM with a medicinal history of more than 2000 years. Modern pharmacological studies have suggested that CNC has a wide range of anti-tumor properties (26, 27), in liver cancer, lung cancer, esophageal cancer, and others. Here we studied the anti-

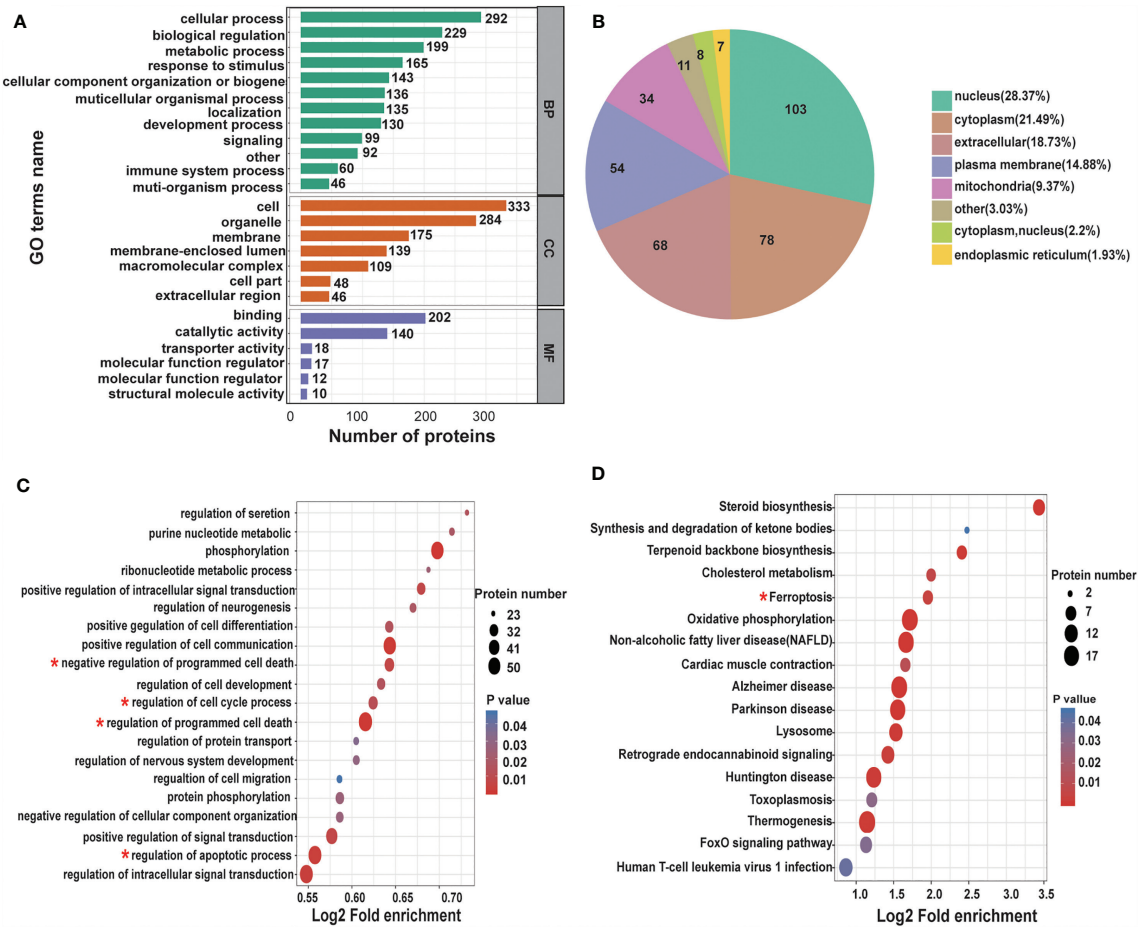

FIGURE 4 | Differentially expressed proteins under the presence of CNC extract in HCT116 cells analyzed by GO and KEGG. **(A)** BP, CC, and MF evaluated. **(B)** Subcellular localization and classification of differentially expressed proteins. **(C)** GO enrichment analysis of BP. **(D)** KEGG pathway enrichment analysis.

colon cancer efficacy of CNC *in vivo* and *in vitro* to explore potential mechanisms underlying these effects. Our results suggest that CNC is a promising candidate for the prevention and treatment of colon cancer.

Ferroptosis, a form of regulated cell death identified by Stockwell and colleagues in 2012, is mediated by iron-dependent accumulation of lipid ROS (28). In recent years, studies have found that the mechanism and treatment of tumors are closely related to ferroptosis (29, 30). Our study provides the first evidence that CNC can regulate ferroptosis signaling pathways, thus inhibiting the proliferation of colon cancer cells *in vitro* and *in vivo*. Ferroptosis is mainly related to intracellular iron metabolism, lipid peroxide (ROS) content, and GPX4 activity. Iron transporters are negatively regulated by ferritin. Studies have shown significantly increased ferritin in tumor patients with inhibited iron efflux (31). The anti-tumor mechanism of dihydroartemisinin in the human hepatoma cell line HepG2 is to induce ferroptosis by increasing ROS and reducing GSH expression in cancer cells through a Fenton-like reaction (32). Here, we verified the ferroptosis pathway of CNC against colon cancer. TEM revealed typical morphological characteristics of ferroptosis in CNC-treated HCT116 and HCT15 cells, such as shrunken mitochondria with increased membrane density. And we also found that the ferroptosis inhibitor ferrostatin-1 can effectively reverse the cell ferroptosis induced by CNC extract. Measuring the intracellular contents of ROS, Fe, and GSH revealed that CNC significantly induced the accumulation of ROS in HCT116 cells and induced the accumulation of Fe in HCT116 and HCT15 cells and finally mediated ferroptosis. Furthermore, the key ferroptosis pathway proteins were verified *in vitro*. qPCR results showed that significantly decreased mRNA expression of GPX4, SLC7A11 and FTH1 in HCT116 cells, while that of HMOX1, P53 and ACSL4 were significantly increased. Also, we observed the increase mRNA expression levels of HMOX1 and P53 in HCT15, but had no significant effect on the expression of other hallmarks of ferroptotic pathway. These results were corroborated by western blot analyses. In the immunofluorescence experiments of tumor tissues in nude mice, GPX4 and FTH1 expression were down-regulated and HMOX1 and p53 were up-regulated in the CNC extract group compared to the model group. These results suggested that the anti-colon cancer effect of CNC may be related to inhibition of GPX4, FTH1 and promotion of HMOX1, p53 expression, which

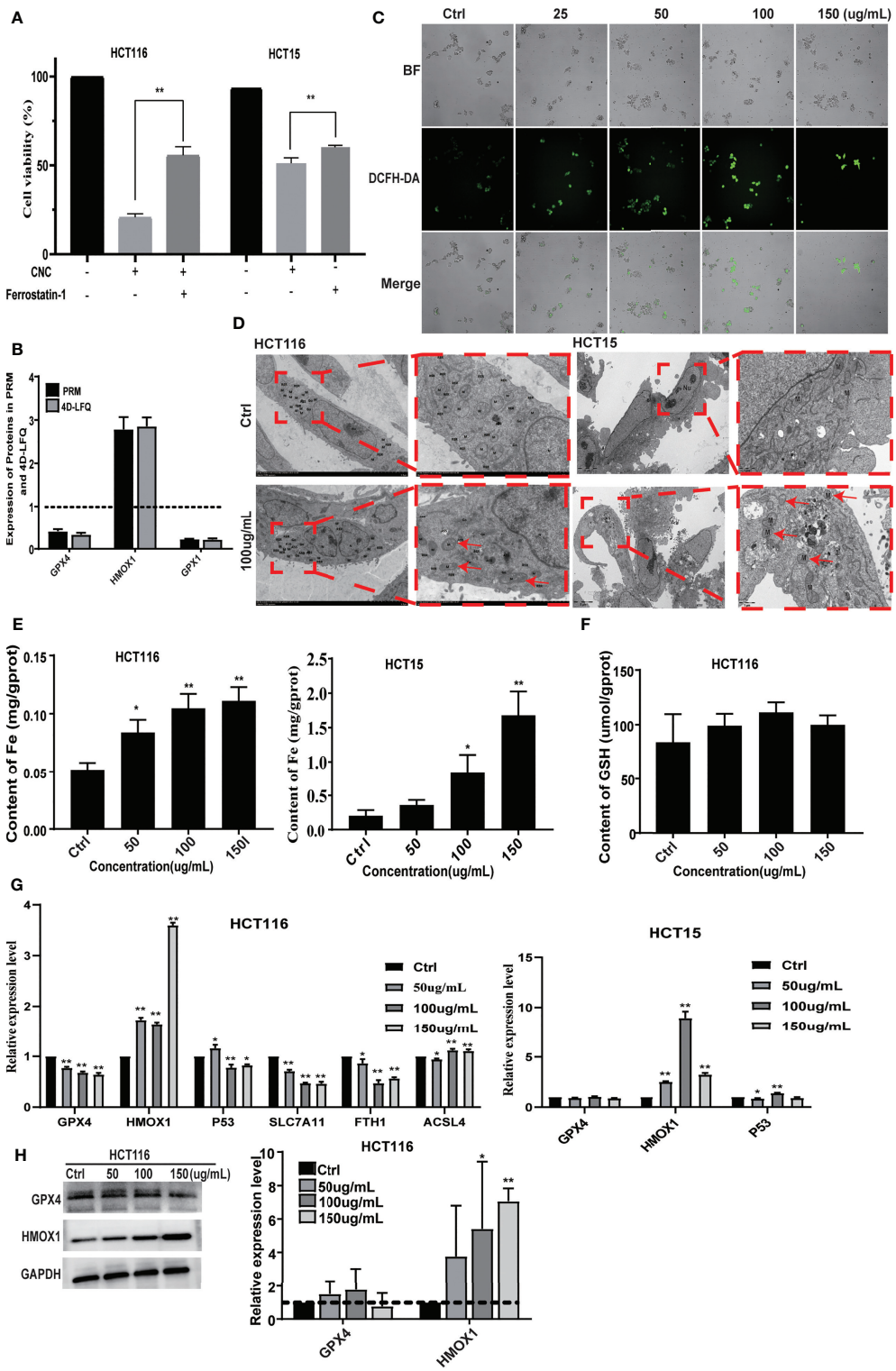

FIGURE 5 | CNC extract induce cell death by promoting ferroptosis. **(A)** The ferrostatin-1 rescue experiment. **(B)** Ferroptosis-associated proteins quantification by mass spectrometry-based targeted proteomics (PRM). **(C)** The detection of HCT116 cellular ROS accumulation. **(D)** The TEM analysis of HCT116 and HCT15 cells morphology. **(E, F)** The detection of cellular Fe and GSH content. **(F)** Expression of relevant proteins at mRNA level were detected by q-PCR. **(G)** Expression of GPX4 and HMOX1 in HCT116 cells was measured by western blot. There were three duplicate samples in each experiment. Data are expressed as mean ± SD. Compared with control group: *p < 0.5, **p < 0.01.

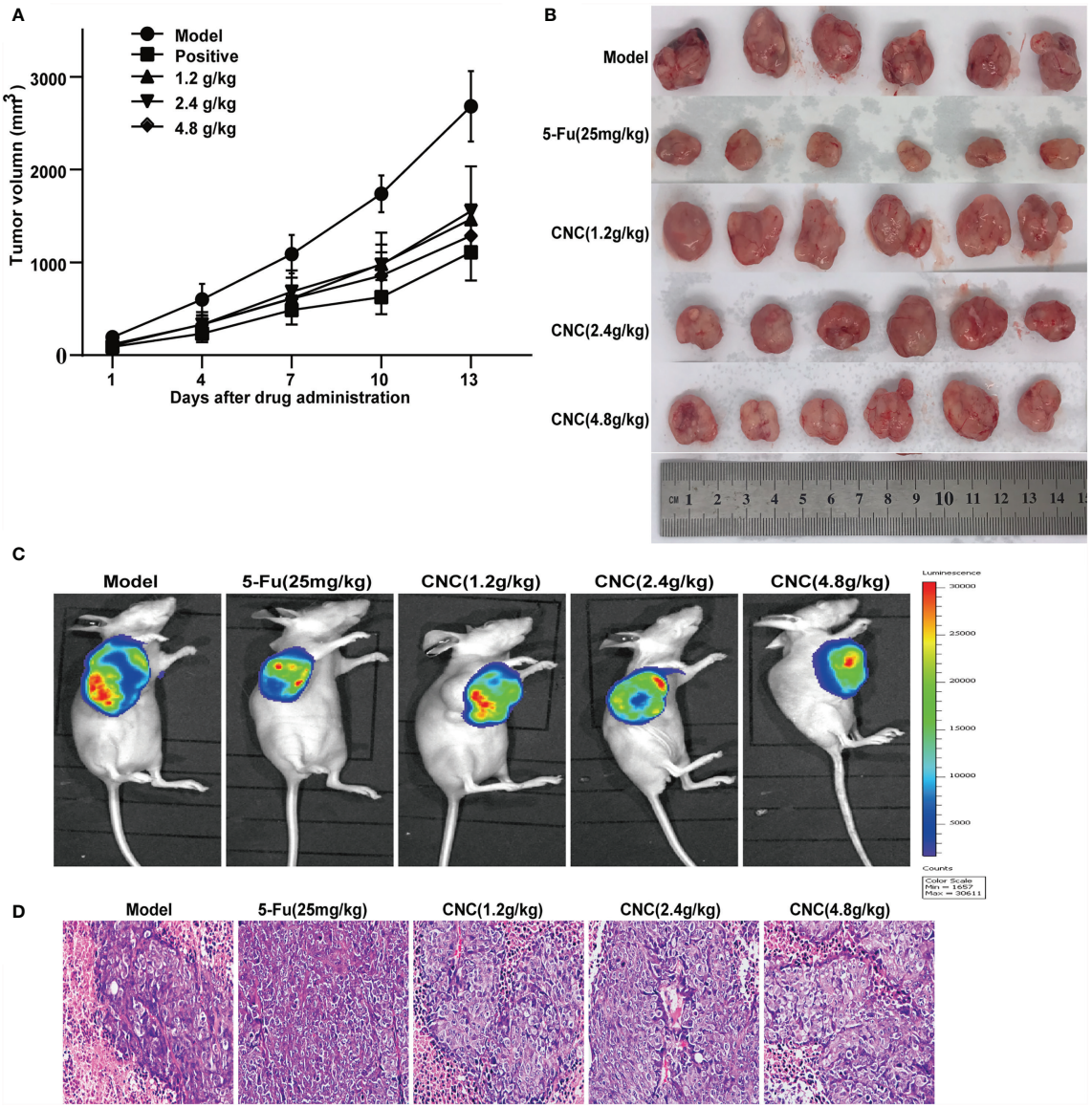

FIGURE 6 | CNC extract inhibited tumor growth in human HCT116 xenograft nude mouse model. **(A, B)** Tumor growth curves and volume in CNC extract-treatment and model groups. **(C)** Bioluminescence imaging of HCT116 xenograft tumors in different groups at the end of experiments. **(D)** HE staining of tumor tissues. There were six nude mice in each group.

is similar to the mechanism by which artesunate induces ferroptosis in tumor cells (33).

Proteomics is the study pertaining to protein products encoded and expressed by genes and is a powerful tool for understanding the interactions of protein molecules in the human body (34). The proteomics of cells or bodies under normal conditions, diseases, and during drug treatment helps clarify the molecular mechanisms underlying the actions of macromolecules and facilitates the identification of new drug targets, drug development, and the drafting of clinical treatment guidelines (35). In our study, we combined 4D Label-free quantitative proteomics with PRM to analyze protein changes in HCT116 cells to find potential pathways and targets of CNC. The results showed that CNC could regulate apoptosis, cell cycle, ferroptosis, and other pathways of colon cancer cells, and we further detected ferroptosis pathway proteins. In addition to effects on ferroptosis, CNC was also found to promote apoptosis and block cell cycling, indicating that CNC may exert anti-tumor effects through multiple pathways.

The main chemical components of CNC are flavonoids, polysaccharides, saponins, volatile components, and trace elements (36). In our research, 116 CNC compounds were detected by UHPLC-MS. According to published literature, 10 of these compounds have been isolated from CNC, although

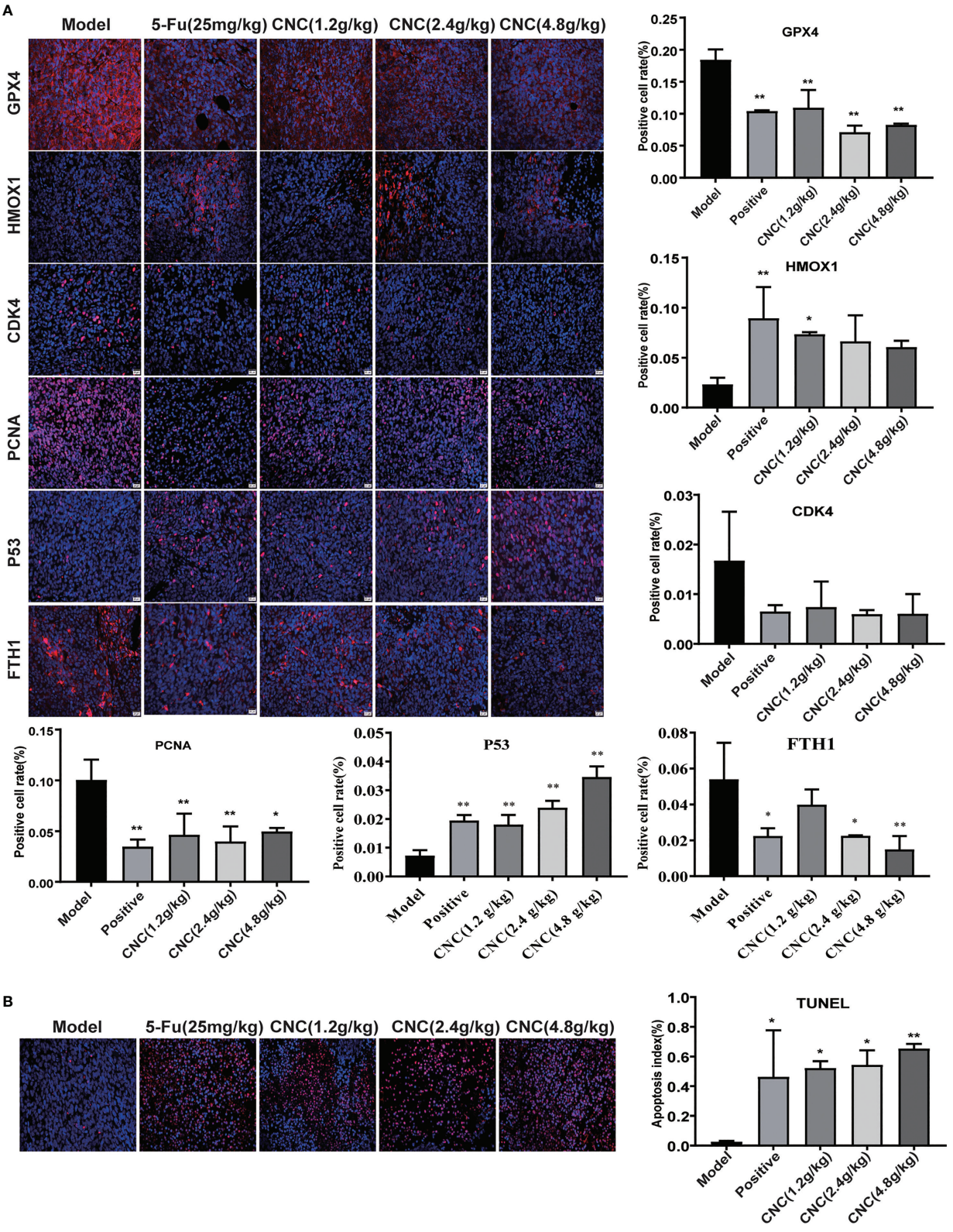

FIGURE 7 | IF detection and TUNEL analysis in tumor tissues. **(A)** IF expression of GPX4, HMOX1, CDK4, PCNA, p53 and FTH1proteins in tumor tissue. **(B)** TUNEL analysis in tumor tissues. There were six nude mice in each group. Data are expressed as mean ± SD. Compared with model group: *p < 0.5, **p < 0.01.

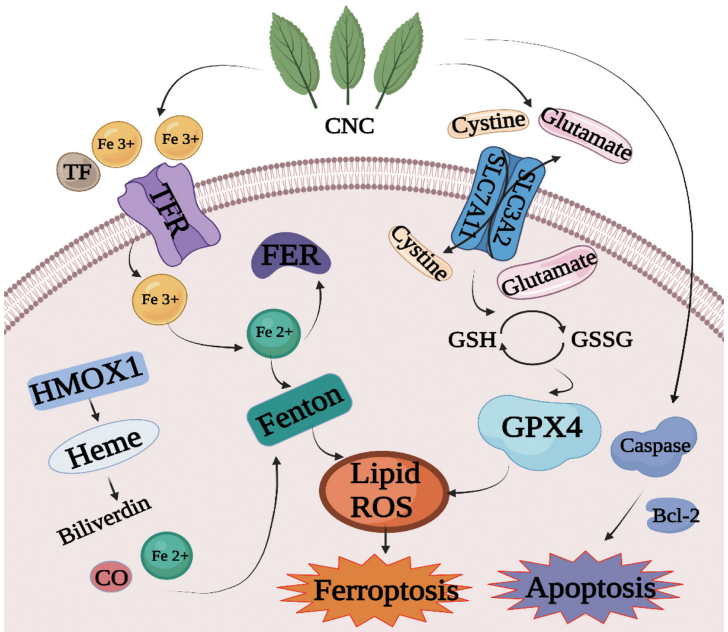

FIGURE 8 | Mechanism diagram of cell death induced by CNC extract through the apoptosis and ferroptosis pathway.

their contents were not among the highest. The mass spectrum of CNC contains several high intensity peaks that have not been resolved, indicating that there may be other anti-tumor components in CNC. Further studies are needed to clarify the detailed biochemical and physiological mechanisms of action associated with the anti-tumor effects of CNC.

In summary, we studied the chemical constituents, anti-tumor pharmacological effects, and mechanism of CNC. Flavonoids, polysaccharides, volatile components, and triterpenes were detected by UHPLC-MS. A combination of 4D Label-free quantitative proteomics and PRM technology was used to identify the potential targets and pathways underlying the anti-colon cancer effect of CNC. The results showed that CNC could regulate cell apoptosis, cell cycle, ferroptosis, and other pathways in colon cancer cells, indicating multi-pathway regulatory effects. We detected and verified components of the ferroptosis pathway and found that CNC regulates GPX4, HMOX1, SLC7A11, FTH1, p53 and ACSL4 protein expression to exert its anti-colon cancer effects. The potential mechanism by which CNC extract affects the apoptosis and ferroptosis pathway is shown in **Figure 8**. In conclusion, CNC is a promising candidate for the prevention and treatment of colon cancer.

DATA AVAILABILITY STATEMENT

The datasets presented in this study can be found in online repositories. The names of the repository/repositories and accession number(s) can be found below: https://www.jianguoyun.com/p/DTo3RE8Qh4fOCRio3P0D.

ETHICS STATEMENT

The animal study was reviewed and approved by Animal Ethics Committee of the Guangxi University of Chinese Medicine, and all procedures were followed the relevant regulations and guidelines.

AUTHOR CONTRIBUTIONS

JD, EH and XH designed the study. YC and FZ drafted the manuscript. YC and FZ conducted experiments, and the other authors took part in literature collection and data analysis. All authors contributed to the article and approved the submitted version.

FUNDING

This study was supported by grants from Guangxi Special Project for Innovation-Driven Development (AA18118049); Guangxi Science and Technology Plan Project (AD19110155); Guangxi Science and Technology Base and Talent Special Fund (GuiKe AD21075014).

SUPPLEMENTARY MATERIAL

The Supplementary Material for this article can be found online at: https://www.frontiersin.org/articles/10.3389/fonc.2021.727130/full#supplementary-material

REFERENCES

1. Siegel RL, Miller KD, Fuchs HE, Jemal A. Cancer Statistics, 2021. *CA Cancer J Clin* (2021) 71(1):7–33. doi: 10.3322/caac.21654
2. Focaccetti C, Bruno A, Magnani E, Bartolini D, Principi E, Dallaglio K, et al. Effects of 5-Fluorouracil on Morphology, Cell Cycle, Proliferation, Apoptosis, Autophagy and ROS Production in Endothelial Cells and Cardiomyocytes. *PloS One* (2015) 10(2):e0115686. doi: 10.1371/journal.pone.0115686
3. Advani S, Kopetz S. Ongoing and Future Directions in the Management of Metastatic Colorectal Cancer: Update on Clinical Trials. *J Surg Oncol* (2019) 119(5):642–52. doi: 10.1002/jso.25441
4. Yun CW, Kim HJ, Lee SH. Therapeutic Application of Diverse Marine-Derived Natural Products in Cancer Therapy. *Anticancer Res* (2019) 39 (10):5261–84. doi: 10.21873/anticanres.13721
5. Shi XQ, Zhu ZH, Yue SJ, Tang YP, Chen YY, Pu ZJ, et al. Studies on Blood Enrichment and Anti-Tumor Effects of Combined Danggui Buxue Decoction, Fe and rhEPO Based on Colon Cancer-Related Anemia Model and Gut Microbiota Modulation. *Chin J Nat Med* (2021) 19(6):422–31. doi: 10.1016/s1875-5364(21)60041-9
6. Wang W, Liu H, Wang Z, Qi J, Yuan S, Zhang W, et al. Phytochemicals From Camellia Nitidissima Chi Inhibited the Formation of Advanced Glycation End-Products by Scavenging Methylglyoxal. *Food Chem* (2016) 205:204–11. doi: 10.1016/j.foodchem.2016.03.019
7. Rahayu RP, Prasetyo RA, Purwanto DA, Kresnoadi U, Iskandar RPD, Rubianto M. The Immunomodulatory Effect of Green Tea (Camellia Sinensis) Leaves Extract on Immunocompromised Wistar Rats Infected by Candida Albicans. *Vet World* (2018) 11(6):765–70. doi: 10.14202/vetworld.2018.765-770
8. Dai L, Li JY, Shen XY, Tang YP, Feng Y, Li L, et al. Growth Inhibition and Apoptosis Induction by Camellia Chrysantha (Hu) Tuyama in Human Esophageal Squamous Carcinoma Cells. *Chin J Oncol Prev Treat* (2013) 5 (01):32–5. doi: 10.3969/j.issn.1674-5671.2013.01.08
9. Li L, Shen XY, Dai L, Li JY. LT Z. Effect of Camellia Nitidissima Chi Extract on Proliferation of HUMAN Gastric Cancer MGC-803 Cells. *Guangxi Med Univ* (2013) 30(03):344–6. doi: 10.16190/j.cnki.45-1211/r.2013.03.007
10. Zhu H, Zhao X, Sripanidkulchai B. Antioxidative and Cytotoxic Effect of the Extract From Camellia Nitidissima CW Chi. *Isan J Pharm Sci* (2011) 7:11–7. doi: 10.14456/ijps.2011.2
11. Kong GJ, Du HZ, Yuan ST. L S. Study Effect of Extrative Fraction of Camellia Chrysantha (Hu) Tuyama From N-Butyl Alcohol on Lung Carcinogenesis Induced by Urethane. *Asia-Pac Tradit Med* (2015) 11(21):4–7. doi: 10.11954/ytctyy.201521002
12. Zhang X, Feng H, Li D, Liu S, Amizuka N, Li M. Identification of Differentially Expressed Genes Induced by Aberrant Methylation in Oral Squamous Cell Carcinomas Using Integrated Bioinformatic Analysis. *Int J Mol Sci* (2018) 19 (6):1–15. doi: 10.3390/ijms19061698
13. Yu Y, Wang JL, Meng LL, Hu CT, Yan ZW, He ZP, et al. DDX54 Plays a Cancerous Role Through Activating P65 and AKT Signaling Pathway in Colorectal Cancer. *Front Oncol* (2021) 11:650360. doi: 10.3389/fonc.2021.650360
14. Leung EL, Clementi E, Wong WS. Advanced Technologies Charting a New Path for Traditional Chinese Medicine Drug Discovery. *Pharmacol Res* (2017) 117:65–6. doi: 10.1016/j.phrs.2016.12.010
15. Wu X, Han X, Li L, Fan S, Zhuang P, Yang Z, et al. iTRAQ-Based Quantitative Proteomics and Target-Fishing Strategies Reveal Molecular Signatures on Vasodilation of Compound Danshen Dripping Pills. *Chem Biol Interact* (2020) 316:108923. doi: 10.1016/j.cbi.2019.108923
16. Cox J, Mann M. MaxQuant Enables High Peptide Identification Rates, Individualized P.P.B.-Range Mass Accuracies and Proteome-Wide Protein Quantification. *Nat Biotechnol* (2008) 26(12):1367–72. doi: 10.1038/nbt.1511
17. Xu X, Liu T, Yang J, Chen L, Liu B, Wang L, et al. The First Whole-Cell Proteome- and Lysine-Acetylome-Based Comparison Between Trichophyton Rubrum Conidial and Mycelial Stages. *J Proteome Res* (2018) 17(4):1436–51. doi: 10.1021/acs.jproteome.7b00793
18. Zhang X, Sui S, Wang L, Li H, Zhang L, Xu S, et al. Inhibition of Tumor Propellant Glutathione Peroxidase 4 Induces Ferroptosis in Cancer Cells and Enhances Anticancer Effect of Cisplatin. *J Cell Physiol* (2020) 235(4):3425–37. doi: 10.1002/jcp.29232
19. Ishida T, Takahashi T, Kurokawa Y, Nishida T, Hirota S, Serada S, et al. Targeted Therapy for Drug-Tolerant Persister Cells After Imatinib Treatment for Gastrointestinal Stromal Tumours. *Br J Cancer* (2021). doi: 10.1038/s41416-021-01566-9
20. NaveenKumar SK, SharathBabu BN, Hemshekhar M, Kemparaju K, Girish KS, Mugesh G. The Role of Reactive Oxygen Species and Ferroptosis in Heme-Mediated Activation of Human Platelets. *ACS Chem Biol* (2018) 13(8):1996–2002. doi: 10.1021/acschembio.8b00458
21. Arnold M, Sierra MS, Laversanne M, Soerjomataram I, Jemal A, Bray F. Global Patterns and Trends in Colorectal Cancer Incidence and Mortality. *Gut* (2017) 66(4):683–91. doi: 10.1136/gutjnl-2015-310912
22. Van Cutsem E, Borràs JM, Castells A, Ciardiello F, Ducreux M, Haq A, et al. Improving Outcomes in Colorectal Cancer: Where do We Go From Here? *Eur J Cancer* (2013) 49(11):2476–85. doi: 10.1016/j.ejca.2013.03.026
23. Nourmohammadi S, Aung TN, Cui J, Pei JV, De Ieso ML, Harata-Lee Y, et al. Effect of Compound Kushen Injection, a Natural Compound Mixture, and Its Identified Chemical Components on Migration and Invasion of Colon, Brain, and Breast Cancer Cell Lines. *Front Oncol* (2019) 9:314. doi: 10.3389/fonc.2019.00314
24. Pan Z, Wang K, Chen Q, Zheng X, Song Z, Ding X. SFI Enhances Therapeutic Efficiency of Gefitinib: An Insight Into Reversal of Resistance to Targeted Therapy in Non-Small Cell Lung Cancer Cells. *J Cancer* (2020) 11(2):334–44. doi: 10.7150/jca.32989
25. Wei D, Wang L, Chen Y, Yin G, Jiang M, Liu R, et al. Yangyin Fuzheng Decoction Enhances Anti-Tumor Efficacy of Cisplatin on Lung Cancer. *J Cancer* (2018) 9(9):1568–74. doi: 10.7150/jca.24525
26. He X, Li H, Zhan M, Li H, Jia A, Lin S, et al. Camellia Nitidissima Chi Extract Potentiates the Sensitivity of Gastric Cancer Cells to Paclitaxel *via* the Induction of Autophagy and Apoptosis. *Onco Targets Ther* (2019) 12:10811–25. doi: 10.2147/ott.S220453
27. Dai L, Li JL, Liang XQ, Li L, Feng Y, Liu HZ, et al. Flowers of Camellia Nitidissima Cause Growth Inhibition, Cell-Cycle Dysregulation and Apoptosis in a Human Esophageal Squamous Cell Carcinoma Cell Line. *Mol Med Rep* (2016) 14(2):1117–22. doi: 10.3892/mmr.2016.5385
28. Dixon SJ, Lemberg KM, Lamprecht MR, Skouta R, Zaitsev EM, Gleason CE, et al. Ferroptosis: An Iron-Dependent Form of Nonapoptotic Cell Death. *Cell* (2012) 149(5):1060–72. doi: 10.1016/j.cell.2012.03.042
29. Yu H, Guo P, Xie X, Wang Y, Chen G. Ferroptosis, a New Form of Cell Death, and its Relationships With Tumourous Diseases. *J Cell Mol Med* (2017) 21 (4):648–57. doi: 10.1111/jcmm.13008
30. Zhang Q, Yi H, Yao H, Lu L, He G, Wu M, et al. Artemisinin Derivatives Inhibit Non-Small Cell Lung Cancer Cells Through Induction of ROS-Dependent Apoptosis/Ferroptosis. *J Cancer* (2021) 12(13):4075–85. doi: 10.7150/jca.57054
31. Miller LD, Coffman LG, Chou JW, Black MA, Bergh J, D'Agostino RJr., et al. An Iron Regulatory Gene Signature Predicts Outcome in Breast Cancer. *Cancer Res* (2011) 71(21):6728–37. doi: 10.1158/0008-5472.Can-11-1870
32. Yuan B, Liao F, Shi ZZ, Ren Y, Deng XL, Yang TT, et al. Dihydroartemisinin Inhibits the Proliferation, Colony Formation and Induces Ferroptosis of Lung Cancer Cells by Inhibiting PRIM2/SLC7A11 Axis. *Onco Targets Ther* (2020) 13:10829–40. doi: 10.2147/ott.S248492
33. Markowitsch SD, Schupp P, Lauckner J, Vakhrusheva O, Slade KS, Mager R, et al. Artesunate Inhibits Growth of Sunitinib-Resistant Renal Cell Carcinoma Cells Through Cell Cycle Arrest and Induction of Ferroptosis. *Cancers (Basel)* (2020) 12(11):1–24. doi: 10.3390/cancers12113150
34. Sun BB, Maranville JC, Peters JE, Stacey D, Staley JR, Blackshaw J, et al. Genomic Atlas of the Human Plasma Proteome. *Nature* (2018) 558(7708):73–9. doi: 10.1038/s41586-018-0175-2
35. Evans C, Noirel J, Ow SY, Salim M, Pereira-Medrano AG, Couto N, et al. An Insight Into iTRAQ: Where do We Stand Now? *Anal Bioanal Chem* (2012) 404(4):1011–27. doi: 10.1007/s00216-012-5918-6

36. He D, Li X, Sai X, Wang L, Li S, Xu Y. Camellia Nitidissima CW Chi: A Review of Botany, Chemistry, and Pharmacology. *Phytochem Rev* (2018) 17(2):327–49. doi: 10.1007/s11101-017-9537-x

Conflict of Interest: The authors declare that the research was conducted in the absence of any commercial or financial relationships that could be construed as a potential conflict of interest.

Publisher's Note: All claims expressed in this article are solely those of the authors and do not necessarily represent those of their affiliated organizations, or those of the publisher, the editors and the reviewers. Any product that may be evaluated in this article, or claim that may be made by its manufacturer, is not guaranteed or endorsed by the publisher.

frontiers in Oncology

ORIGINAL RESEARCH
published: 25 November 2021
doi: 10.3389/fonc.2021.753598

Periplocymarin Induced Colorectal Cancer Cells Apoptosis *Via* Impairing PI3K/AKT Pathway

Yi Cheng[1], Guiying Wang[2,3], Lianmei Zhao[4]*, Suli Dai[4], Jing Han[5], Xuhua Hu[2], Chaoxi Zhou[2], Feifei Wang[2], Hongqing Ma[2], Baokun Li[2] and Zesong Meng[2]*

[1] Department of Dermatology, The Fourth Hospital of Hebei Medical University, Shijiazhuang, China, [2] Department of General Surgery, The Fourth Hospital of Hebei Medical University, Shijiazhuang, China, [3] Department of Gastrointestinal Surgery, The Third Hospital of Hebei Medical University, Shijiazhuang, China, [4] Scientific Research Center, The Fourth Hospital of Hebei Medical University, Shijiazhuang, China, [5] Department of Medical Oncology, The Fourth Hospital of Hebei Medical University, Shijiazhuang, China

OPEN ACCESS

Edited by:
Chao Sun,
Tianjin Medical University General Hospital, China

Reviewed by:
Hamed Barabadi,
Shahid Beheshti University of Medical Sciences, Iran
Ajay Sharma,
University of Texas Health Science Center at Houston, United States

***Correspondence:**
Guiying Wang
wangguiying@hebmu.edu.cn
Lianmei Zhao
zhaolianmei@hbydsy.com

Specialty section:
This article was submitted to Pharmacology of Anti-Cancer Drugs, a section of the journal Frontiers in Oncology

Received: 05 August 2021
Accepted: 04 November 2021
Published: 25 November 2021

Citation:
Cheng Y, Wang G, Zhao L, Dai S, Han J, Hu X, Zhou C, Wang F, Ma H, Li B and Meng Z (2021) Periplocymarin Induced Colorectal Cancer Cells Apoptosis Via Impairing PI3K/AKT Pathway. Front. Oncol. 11:753598. doi: 10.3389/fonc.2021.753598

Colorectal cancer (CRC) is one of the most common cancers worldwide, and approximately one-third of CRC patients present with metastatic disease. Periplocymarin (PPM), a cardiac glycoside isolated from *Periploca sepium*, is a latent anticancer compound. The purpose of this study was to explore the effect of PPM on CRC cells. CRC cells were treated with PPM and cell viability was evaluated by CCK-8 assay. Flow cytometry and TUNEL staining were performed to assess cell cycle and apoptosis. Quantitative proteomics has been used to check the proteins differentially expressed by using tandem mass tag (TMT) labeling and liquid chromatography–tandem mass spectrometry. Bioinformatic analysis was undertaken to identify the biological processes that these differentially expressed proteins are involved in. Gene expression was analyzed by western blotting. The effect of PPM *in vivo* was primarily checked in a subcutaneous xenograft mouse model of CRC, and the gene expression of tumor was checked by histochemistry staining. PPM could inhibit the proliferation of CRC cells in a dose-dependent manner, induce cell apoptosis and promote G0/G1 cell cycle arrest. A total of 539 proteins were identified differentially expressed following PPM treatment, where among those there were 286 genes upregulated and 293 downregulated. PPM treatment caused a pro-apoptosis gene expression profile both *in vivo* and *in vitro*, and impaired PI3K/AKT signaling pathway might be involved. In addition, PPM treatment caused less detrimental effects on blood cell, hepatic and renal function in mice, and the anti-cancer effect was found exaggerated by PPM+5-FU combination treatment. PPM may perform anti-CRC effects by promoting cell apoptosis and this might be achieved by targeting PI3K/AKT pathway. PPM might be a safe and promising anti-cancer drug that needs to be further studied.

Keywords: colorectal cancer, periplocymarin, apoptosis, IRS1, PI3K/AKT pathway

INTRODUCTION

Global cancer statistics for 2020 showed that colorectal cancer (CRC) ranks third in terms of cancer incidence, but second in terms of cancer mortality, where more than 1.9 million new CRC cases and 935,000 deaths were estimated to occur worldwide (1). In developed countries, five-year survival of patients with CRC has been improved due to early screening, however, up to 25% patients still present with stage 4 disease, while 25 to 50% present with early-stage disease and subsequently go on to develop metastatic disease (2, 3). The prognosis for patients with metastatic CRC remains poor, with a median five-year survival of CRC in 2012–2015 just 56.9% in China (4). Chemotherapeutic agents such as FOLFOX, the main therapy strategy for CRC patients, are effective but combined with unwanted toxicity and side effects (5). Therefore alternative treatment options are urgently required.

To date, about 85% of all approved small-molecule anticancer drugs are from natural products directly or indirectly (6). Periplocymarin (PPM) is isolated from *cortex periplocae*, the dry root of *Periploca sepium* Bge, which is traditionally used as antirheumatic and diuretic agent in Chinese medicine (7). Previous studies have indicated that, PPM performed anti-tumor effects in various of cancer (8, 9). For example, it has been found that PPM promoted prostate adenocarcinoma (PC3) cell apoptosis and inhibit proliferation of U937, HCT-8, Bel-7402, BGC823, A549, and A2780 cell lines *in vitro* with IC50 values of 0.02–0.29 mM (10). Recently, PPM has been shown to exhibit the advantages of quick effect, short duration, and no accumulation (11). Furthermore, PPM is highly permeable with absence of P-glycoprotein efflux and cytochrome P450, indicating it is a potential natural compound for drug development (12). However, the effect of PPM on CRC has been seldom performed. In the present study, we have investigated the effect of PPM on CRC, to provide more candidate drugs for CRC patients and prolong their lives.

MATERIALS AND METHODS

Cell Culture

The CRC cell lines HCT 116, SW480, RKO, and HT-29 were purchased from Type Culture Collection of the Chinese Academy of Science (Shanghai, China) (catalogue numbers were TCHu 99, TCHu172, TCHu116, and TCHu103, respectively) and preserved by the Scientific Research Center of the Fourth Hospital of Hebei Medical University. All cells were cultured in DMEM (Gibco Invitrogen, Grand Island, NY, USA) supplemented with 10% heat-inactivated fetal bovine serum (FBS) (Gibco Invitrogen, Grand Island, NY, USA), penicillin (100 U/ml), and streptomycin (100 μg/ml) (Invitrogen, Carlsbad, California, USA) and incubated at 37°C in air containing 5% CO_2.

CCK-8 Assay

PPM (purity ≥98%) was obtained from Tauto Biotechnology Co., Ltd (catalogue number E-2462, Shanghai, China). PPM was dissolved in DMSO and diluted to 12.5, 25, 50, or 100 ng/ml using DMEM medium (final concentration of DMSO <0.01%). Cells (1×10^4 cells/well) were exposed to different concentrations of PPM (12.5, 25, 50, or 100 ng/ml) for 24 and 48 h separately. Cells with 0.01% DMSO but no PPM treatment were set as DMSO group. Cells without either PPM or DMSO treatment were set as control. Cell Counting Kit 8 (CCK-8) assay was performed to detect the proliferative ability of CRC cell lines according to the manufacturer's instructions. Briefly, 10 μl of CCK-8 solution ((Meilun Biotechnology, Dalian, China) was added to each well by incubation for 2 h at 37°C in the dark. The absorbance was measured at 450 nm using spectrophotometer. The proliferation rate was calculated by the formula: proliferation rate = (As − Ab)/(Ac − Ab), in which As represents the test group, Ac the negative control group, and Ab the blank control group.

According to the results, HCT 116 and RKO cells treated with PPM (12.5, 25, 50, or 100 ng/ml) for 24 h were used for apoptosis and cell cycle analysis.

Cell Apoptosis Detection

Cellular apoptosis was quantified by both flow cytometry and TUNEL staining kit. Briefly, approximately 5×10^5 cells were harvested and suspended in 500 μl of binding buffer containing Annexin V and propidium iodide (PI) (both 5 μl) (BD Biosciences, San Diego, CA, USA). Then cells were incubated and analyzed by Annexin V-FITC/PI Staining kit according to the manufacturer's instruction.

TUNEL staining was performed by using kit (Roche Diagnostic GmbH, Penzberg, Germany) following the manufacturer's protocol. Cells were fixed by 4% paraformaldehyde and washed twice with PBS, and then incubated in solution containing 10 μl of 0.1% Triton X-100 (Sigma-Aldrich, USA) and 10 ml of 0.1% sodium citrate for 2 min. After drying, the TUNEL staining reaction solution was added to the cells, which was followed by 60 min incubation at 37°C in the dark. The cells were observed under a fluorescence microscope. Cells with 0.01% DMSO but no PPM treatment were set as control group.

Cell Cycles Detection

Cell cycles were also determined by flow cytometry. Approximately 1×10^6 cells were harvested and suspended with 1 ml of DNA staining solution and 10 μl of permeabilization solution (MultiSciences Biotech, Hangzhou, China). Cells were incubated at room temperature in the dark for 30 min and then analyzed.

Liquid Chromatography–Mass Spectrometry/Mass Spectrometry Analysis

Proteins were extracted from HCT 116 cells treated by 50 ng/ml PPM for 24 h and untreated cells respectively by SDT [4% (*w*/*v*) SDS, 100 Mm Tris/HCL pH 7.6, 0.1 M DTT] lysis and quantified using a BCA Protein Assay Kit (Bio-Rad, Hercules, CA, USA). The proteins were digested using filter-aided sample preparation (FASP) and the peptide fraction was quantified. Peptides from each sample (100 μg) were labeled with TMTs (Thermo Fisher Scientific) according to the manufacturer's instructions.

The tryptic peptides were fractionated using a high-pH reverse-phase high-performance liquid chromatography (HPLC) system using a Thermo Betasil C18 column (10 cm, ID75 μm, 3 μm, C18-A2). Briefly, one unit of TMT reagent was thawed and reconstituted in acetonitrile. The peptide mixtures were then incubated for 2 h at room temperature and pooled, desalted, and dried by vacuum centrifugation. HPLC-MS/MS was performed using an Easy nLC system (Thermo Fisher Scientific) coupled to Q Exactive mass spectrometer (Thermo Scientific).

Bioinformatic Analysis

The gene ontology (GO) annotation of differentially expressed proteins (DEPs) was performed by Blast2GO software (http://blast2go.com). Functional annotation was based on the online Kyoto Encyclopedia of Genes and Genomes (KEGG) Automatic Annotation Server database (http://www.kegg.jp/). A fold-change <0.83 or >1.2 with a *P*-value (Student's *t*-test) <0.05 was selected as the cutoff criteria for the identification of DEPs. GO enrichment and KEGG pathway enrichment was performed based on the Fisher's exact test with a *P*-value <0.05 and a false discovery rate (FDR) value <0.01.

Western Blot Analysis

Total protein was extracted using RIPA lysis buffer containing protease inhibitors (APExBIO Technology, Houston, USA). Protein concentrations were determined using BCA Protein Assay Kit (Bio-Rad, Hercules, CA, USA). Then 10% SDS-PAGE gel electrophoresis was carried out using 50 μg of protein from each sample. After gel transfer, PVDF membranes were incubated with primary antibodies including rabbit anti-Bax (1:1,000, Proteintech, Wuhan, China), Bcl-2 (1:1,000, Proteintech, Wuhan, China), survivin (1:1,000, Proteintech, Wuhan, China), cleaved caspase-3 (1:1,000, Proteintech, Wuhan, China), cleaved caspase-9 (1:1,000, Proteintech, Wuhan, China), p21 (1:1,000, Proteintech, Wuhan, China), cyclin D1 (1:1,000, Proteintech, Wuhan, China), IRS1(1:1,000, Affinity, USA), p-PI3K (1:1,000, Affinity, USA), p-AKT (1:1,000, Affinity, USA), PI3K (1:1,000, Affinity, USA), and AKT (1:1,000, Affinity, USA) overnight at 4°C. After washing, membranes were further incubated with fluorochrome-labeled anti-rabbit IgG secondary antibody (1:10,000, Proteintech, Wuhan, China) for 1 h at room temperature. The membranes were imaged using the Odyssey Infrared Imaging System (LI-COR Biosciences, Lincoln, NE, USA), which was used to normalize relative expression level of each protein to GAPDH.

Animal Experiments

The animal studies were conducted in accordance with the international standards-3R principle of animal welfare, and approved by the Experimental Animal Ethics Committee of the Fourth Hospital of Hebei Medical University. Approximately 5–6 weeks old Male BALB/c nude mice were obtained from the Beijing Vital River Laboratory Animal Technology (Beijing, China) and were housed at the Fourth Hospital of Hebei Medical University Experiment Animal Centre. Approximately 1×10^6 HCT 116 cells suspended in 100 μl of PBS were subcutaneously injected into the right flank of each mouse. Tumor volume was measured every three days using a caliper and tumor volume was calculated by formula: tumor volume = (length × width^2)/2. When the tumors' volume reached 100 mm^3, the mice were randomly divided into four groups (n = 6 per group). Control group (CON): mice were intraperitoneally injected with 0.9% physiological saline every two days. PPM group (PPM): mice were intraperitoneally injected with 3 mg/kg PPM every two days. Fluorouracil group (5-FU): mice were intraperitoneally injected with 10 mg/kg fluorouracil every two days. PPM + fluorouracil group (PPM + 5-FU): mice were intraperitoneally injected with a combination of PPM (3 mg/kg) and fluorouracil (10 mg/kg) every two days. Approximately 21 days after treatment, mice were sacrificed by spinal dislocation and the tumors were harvested and weighed. Blood were collected from eyeball and used for further analysis. The tumors were fixed in formalin and used for histological study.

Histology and Immunohistochemistry

Six mice in each group were for pathologic examinations, included hematoxylin and eosin (HE) staining and immunohistochemistry (IHC) study. Tumor tissue were fixed, dehydrated and then embedded in paraffin. Slices were cut into 4 um and dewaxed and then dehydrated. HE staining was performed according to the protocol. Six xenografted tumors in each group were used for the quantification of the IHC studies. Immunohistochemistry (IHC) was carried out according to standard procedures. Primary antibodies of Bax (1:200, Proteintech, Wuhan, China), Bcl-2 (1:200, Proteintech, Wuhan, China), cleaved caspase-3 (1:200, Proteintech, Wuhan, China), IRS1 (1:200, Affinity, USA), p-PI3K (1:200, Affinity, USA), and p-AKT (1:200, Affinity, USA) were incubated overnight at 4°C. The staining intensity was scored as follows: 0 (negative), 1 (weak staining), 2 (moderate intense staining), or 3 (strong staining). The extent of the staining was scored based on the percentage of positive cells: 0 (no staining), 1 (1–10% staining), 2 (10–50% staining), and 3 (more than 50% staining). The final IHC score was obtained by multiplying the intensity and percentage scores as described previously (13).

Blood Analysis

Routine blood test was performed by using a Mindray BC-6800Plus hematology analyzer (Mindray Biomedical Electronics, Shenzhen, China). Serum parameters of liver and kidney function were measured by Beckman Coulter AU5800 chemistry analyzer (Beckman Coulter, USA).

Statistical Analysis

Data were analyzed using GraphPad Prism v5.0 and SPSS v21.0 and are presented as means ± standard error of the mean (SEM). One-way analysis of variance (ANOVA) was used for comparisons among multiple groups and repeated measure of ANOVA was used for analysis of tumor volume. For comparisons between two groups, the SNK-q test was used. $P < 0.05$ was considered statistically significant.

RESULTS

PPM Inhibits the Viability of CRC Cells

To explore the effects of PPM on CRC cells, the viability of CRC cells was assessed by CCK-8 assay. The results showed that, the viability of HCT 116, RKO, HT-29, and SW480 cells were inhibited by PPM in a dose- and time-dependent manner (P <0.001) (**Figure 1**), indicating PPM may inhibit CRC cells proliferation. The IC_{50} values of PPM against HCT 116, RKO, HT-29, and SW480 cells at 24 h were 35.74 ± 8.20 ng/ml, 45.60 ± 6.30 ng/ml, 72.49 ± 5.69 ng/ml, and 112.94 ± 3.12 ng/ml, respectively. HCT 116 and RKO cell lines were more prone to the inhibition by PPM, therefore used for further analysis.

PPM Induced Cell Apoptosis in CRC Cells

To clarify the effect of PPM on the apoptosis of CRC cells, HCT 116 and RKO cells were treated with different concentration of PPM for 24 h, and the number of apoptotic cells was detected by flow cytometry. Data indicated that, compared to control, PPM treatment caused significantly increased apoptotic ratio in both HCT 116 and RKO cells in a dose dependent manner (**Figure 2A**). Similar results were also exhibited in TUNEL staining, which indicated that PPM treatment caused increased TUNEL-positive CRC cell ratio (**Figure 2B**).

Previous studies have found that the increase in the Bax/Bcl-2 ratio can lead to cytochrome c release and the subsequent cleavage and activation of caspase-3 and caspase-9, which can result in the

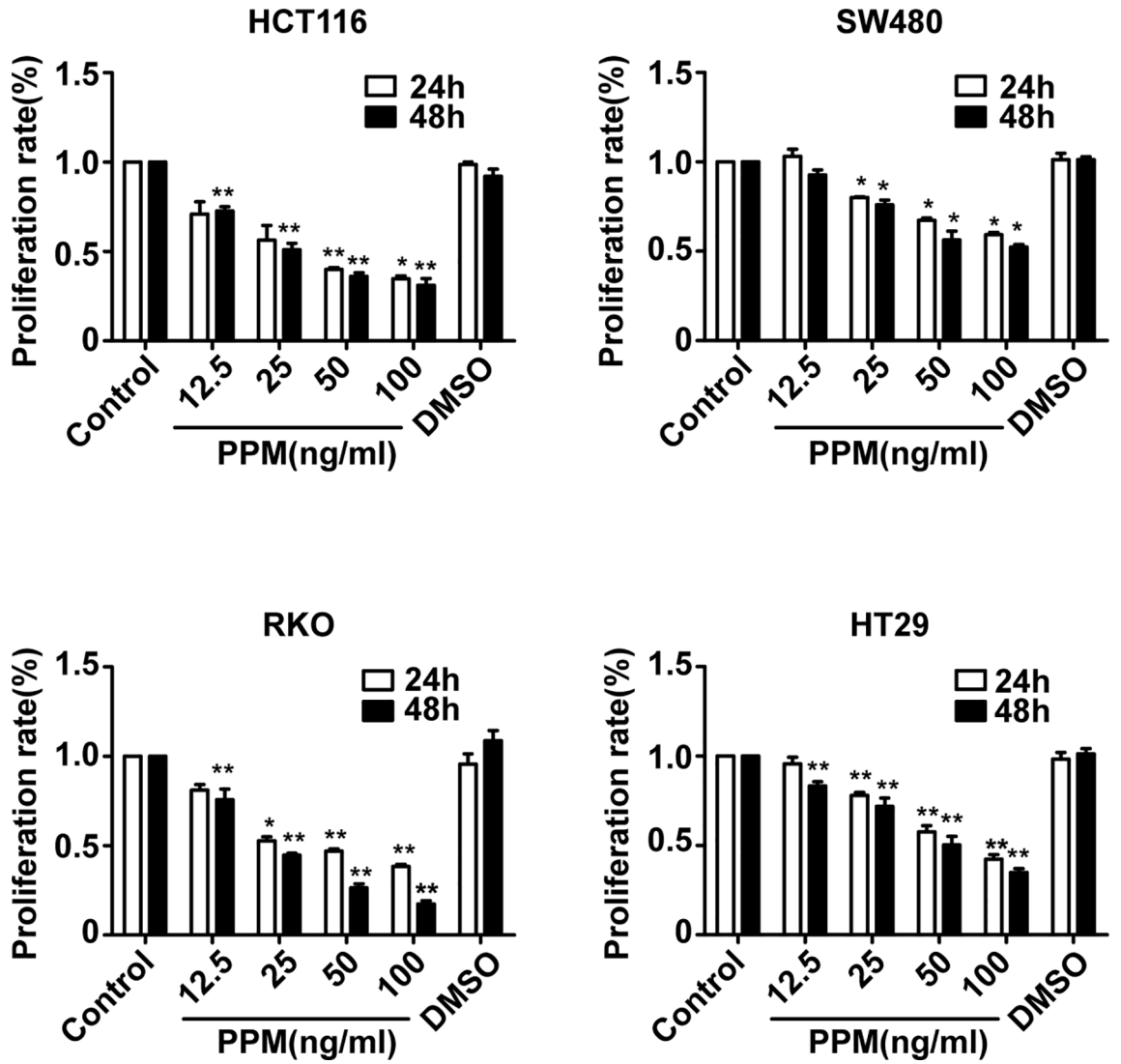

FIGURE 1 | The effect of periplocymarin (PPM) on the viability of colorectal cancer cells. Colorectal cancer cells (HCT 116, SW480, RKO, and HT-29) were treated with different concentrations of PPM (0, 12.5, 25, 50, or 100 ng/ml) and 0.01% DMSO for 24 and 48 h. Cell viability was determined by CCK-8 assays. Data are shown as means ± SEM. *P < 0.05, **P < 0.01, *vs*. untreated control group.

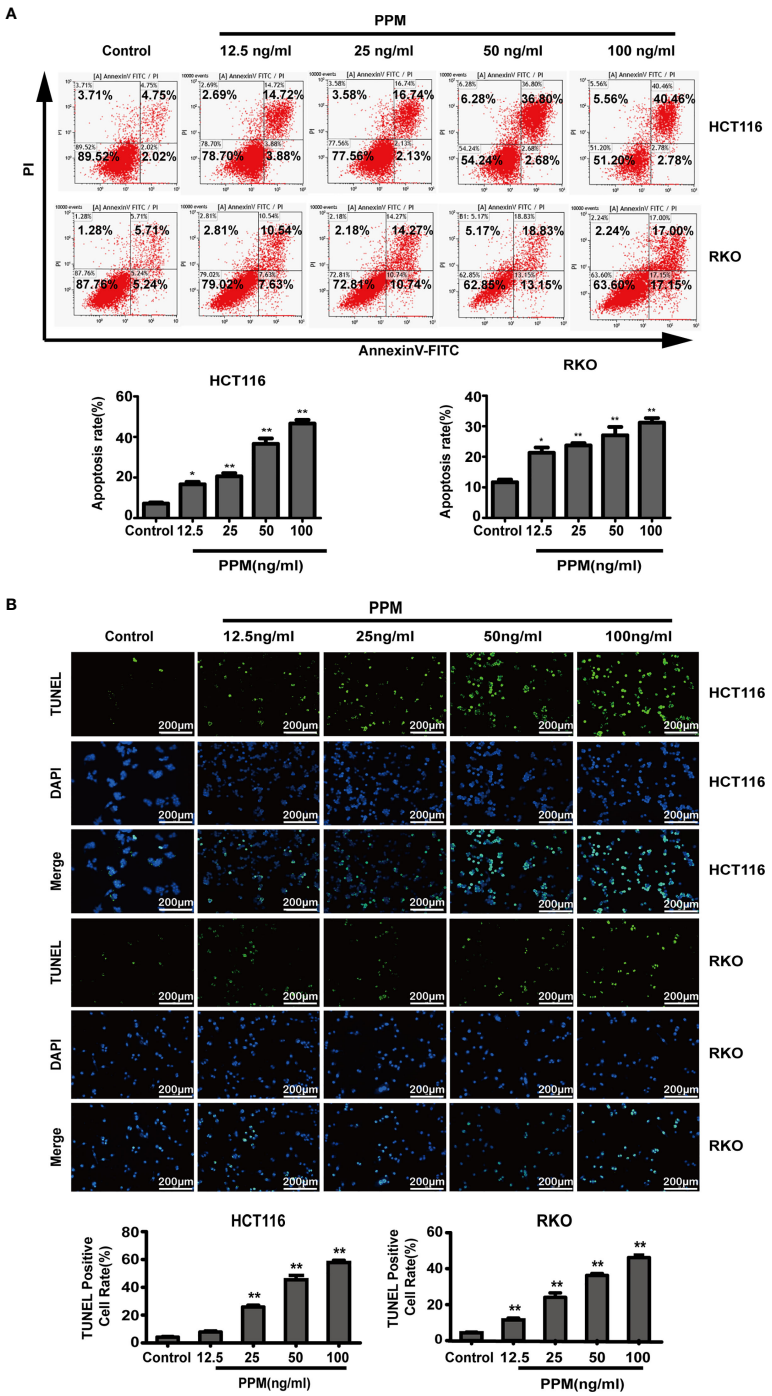

FIGURE 2 | Periplocymarin (PPM) induces apoptosis in colorectal cancer cells. **(A)** Flow cytometric analysis of HCT 116 and RKO cells treated with different concentrations of PPM (0, 12.5, 25, 50, or 100 ng/ml) for 24 h. The cells were examined by Annexin V-FITC staining. **(B)** TUNEL staining of HCT 116 and RKO cells treated with PPM (0, 12.5, 25, 50, or 100 ng/ml) for 24 h. Apoptotic cells (TUNEL-positive cells) exhibit green fluorescence. Scale bar, 200 μm. Data are shown as means ± SEM. *$P < 0.05$, **$P < 0.01$, *vs*. untreated control group.

degradation of intracellular substrates and apoptosis (14). This study detected these apoptosis related proteins. Data from western blot has shown that, PPM treatment caused pro-apoptotic gene expression profile, which exhibited increased pro-apoptotic gene expression such as Bax, cleaved caspase-3 and cleaved caspase-9, while decreased anti-apoptotic gene expression such as survivin and Bcl-2 (**Figures 3A, B**). Therefore, PPM may cause CRC cell apoptosis by targeting relative gene expression.

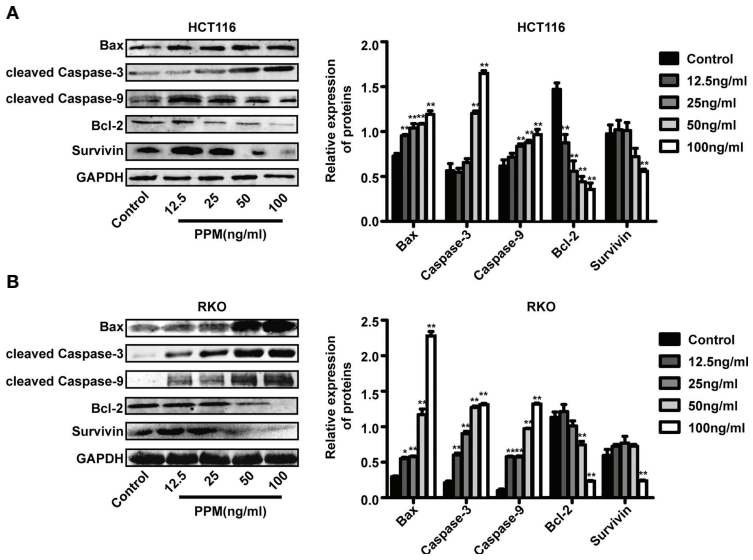

FIGURE 3 | Periplocymarin (PPM) altered gene expression involved in apoptosis. Western blot analysis of Bax, Bcl-2, cleaved caspase-3, cleaved caspase-9, and survivin protein levels in HCT 116 **(A)** and RKO cells **(B)** treated with different concentrations of PPM (0, 12.5, 25, 50, or 100 ng/ml) for 24 h. Values are shown as means ± SEM. $^{*}P < 0.05$, $^{**}P < 0.01$, *vs*. untreated control group.

PPM Induced Cell Cycle Arrest

We further examined whether PPM have regulated the cell cycle. Data from flow cytometry has indicated that, compared to control, PPM treatment may cause significantly increased ratio of cells in G0/G1 phase while decreased ratio of cells in S phase, indicating PPM may promote cycle arrest in CRC cells (**Figure 4A**) and the maximum effect of PPM observed in the present study was at concentration of 50 ng/ml.

Cyclin D1 and p21 are both involved in cell cycle regulation. Data from the present study has found that, compared to control, PPM treatment may increase p21 expression in a dose-dependent manner in both cell lines (**Figure 4B**). PPM treatment led to decreased cyclin D1 gene expression at concentration of 50 ng/ml onward in HCT 116 cells, while this inhibitory effect can be found in all PPM-treated RKO cells. The maximal effect of PPM on cyclin D1 expression was noted at 100 ng/ml in both cell lines.

DEPs Identification

Tag-based (TMT) quantitative proteomics technology was performed to detect proteins of CRC cells under PPM treatment. Of those DEPs, 286 were found upregulated and 293 were downregulated. Among them, 33 of the upregulated proteins and seven of the downregulated proteins showed >2 fold-changes with $P < 0.05$ (**Figure 5A** and **Table 1**). The most enriched GO terms were annotated as transmembrane receptor protein tyrosine kinase activity in the molecular function category (GO: 0004714, six proteins, P = 8.99E−05), low-density lipoprotein particle in the cellular compartment category (GO: 0034362, six proteins, P = 1.81E−06), and animal organ morphogenesis in regard to the biological process category (GO: 0009887, 46 proteins, P = 1.76E−07) (**Figure 5B**). KEGG pathway enrichment analysis was performed to check pathways associated with the DEPs. The results showed that 14 KEGG pathways were significantly enriched based on the number of proteins with $P < 0.05$. The top seven enriched pathways were Inflammatory bowel disease (five proteins, P = 0.001687), Complement and coagulation cascades (six proteins, P = 0.002066), Malaria (four proteins, P = 0.006051), Pancreatic cancer (proteins, P = 0.010368), Measles (10 proteins, P = 0.013437), Leishmaniasis (six proteins, P = 0.018835), and the PI3K/AKT signaling pathway (16 proteins, P = 0.028105). DEPs were more associated with the PI3K/AKT signaling pathway which might participate in the proapoptotic effects of PPM on CRC cells (**Figure 5C**).

PPM Impairs PI3K/AKT Signaling Pathway

PI3K/AKT signaling pathway activation has been found promotes tumor progression and cell survival by inhibition of apoptosis (15). PI3K and AKT are both the downstream target genes of IRS1 (16) and the phosphorylation forms are the active ones. In the present study, consistent with TMT-based results, PPM treatment caused significantly decreased IRS1 expression in HCT and RKO cells compared to control cells in almost a PPM concentration-dependent manner. Although gene expression of PI3K and AKT were not altered, both p-PI3K and p-AKT were significantly decreased by PPM treatment. Therefore, PPM treatment may impair PI3K/AKT signaling pathway, contributing to increased CRC cell apoptosis ratio (**Figures 6A, B**). The mass spectrometry proteomics data have been deposited to the ProteomeXchange Consortium (http://proteomecentral.proteomexchange.org) *via* the iProX partner repository (17) with the dataset identifier PXD029172.

The Effects of PPM on Blood Parameters

To examine the safety of PPM, blood parameters were checked in the nude mice. Data indicated that, compared to CON animals,

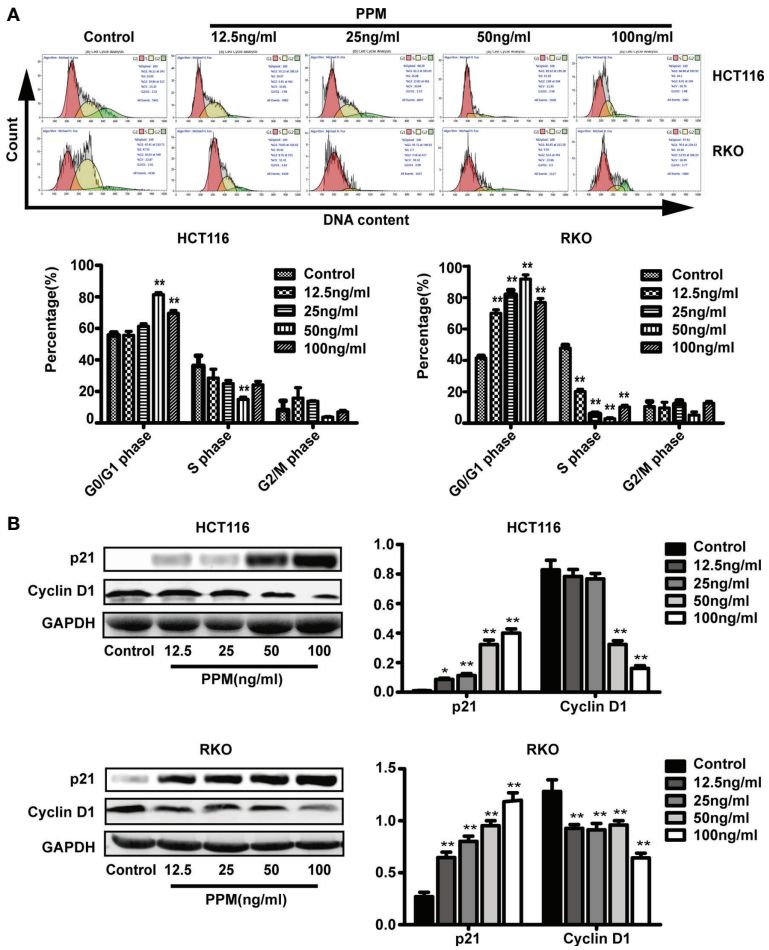

FIGURE 4 | Periplocymarin (PPM) induces cell cycle arrest in colorectal cancer cells. **(A)** PPM induced G0/G1 cell cycle arrest in HCT 116 and RKO cells as determined by flow cytometry. **(B)** The protein expression of cyclin D1 was decreased and that of P21was increased with PPM treatment. Values are shown as means ± SEM. *$P < 0.05$, **$P < 0.01$, *vs*. untreated control group.

PPM treatment caused no alterations in blood cells, hepatic and renal functional parameters. However, 5-FU treated animals exhibited lower WBC number and higher ALT and AST levels compared to CON animals (P all <0.05), indicating hypoleukemia and liver functional impairment. Only increased UN level was found in PPM + 5-FU group, indicating that 5-FU combined with PPM might cause renal functional impairment. Meanwhile, the WBC count and ALT, AST levels in PPM + 5-FU group showed no difference compared to those in CON group, suggesting PPM might alleviate the adverse effects of 5-FU on hepatic function and WBC (**Table 2**).

The Effects of PPM on Colorectal Tumor Formation *In Vivo*

To explore the effects of PPM on CRC cells *in vivo*, BALB/c nude mice with HCT 116 cells xenografted tumor were treated. Data from the present experiment has shown that, compared to control animals, PPM, 5-FU and PPM + 5-FU treatment all could impair tumor growth. There were no statistical differences in tumor volume between 5-FU and PPM-treated group (**Figures 7A, B**). At day 21, compared to control group, the weights of tumors were found reduced in PPM, 5-FU and PPM + 5-FU treated animals. There were no statistical differences in tumor weight between 5-FU and PPM-treated group (**Figure 7C**). The tumor weight in PPM + 5-FU-treated group was even lower when compared to PPM and 5-FU-treated groups separately (**Figure 7C**), indicating the anti-tumor effect might be exaggerated in PPM and 5-FU combination treatment.

Gene expression involved in cell apoptosis were also measured by immunohistochemistry, which indicated that PPM, 5-FU, and PPM + 5-FU treatment all led to increased gene expression of Bax and cleaved caspase-3 while decreased expression of IRS1, p-PI3K, and p-AKT (**Figure 7D**), indicating PPM may perform pro-apoptotic effects *in vivo*. Except p-PI3K, the most manifest effects in those gene expressions were found in PPM + 5-FU-treated animals, suggesting the pro-apoptotic effects might also be exaggerated by PPM and 5-FU combination therapy strategy.

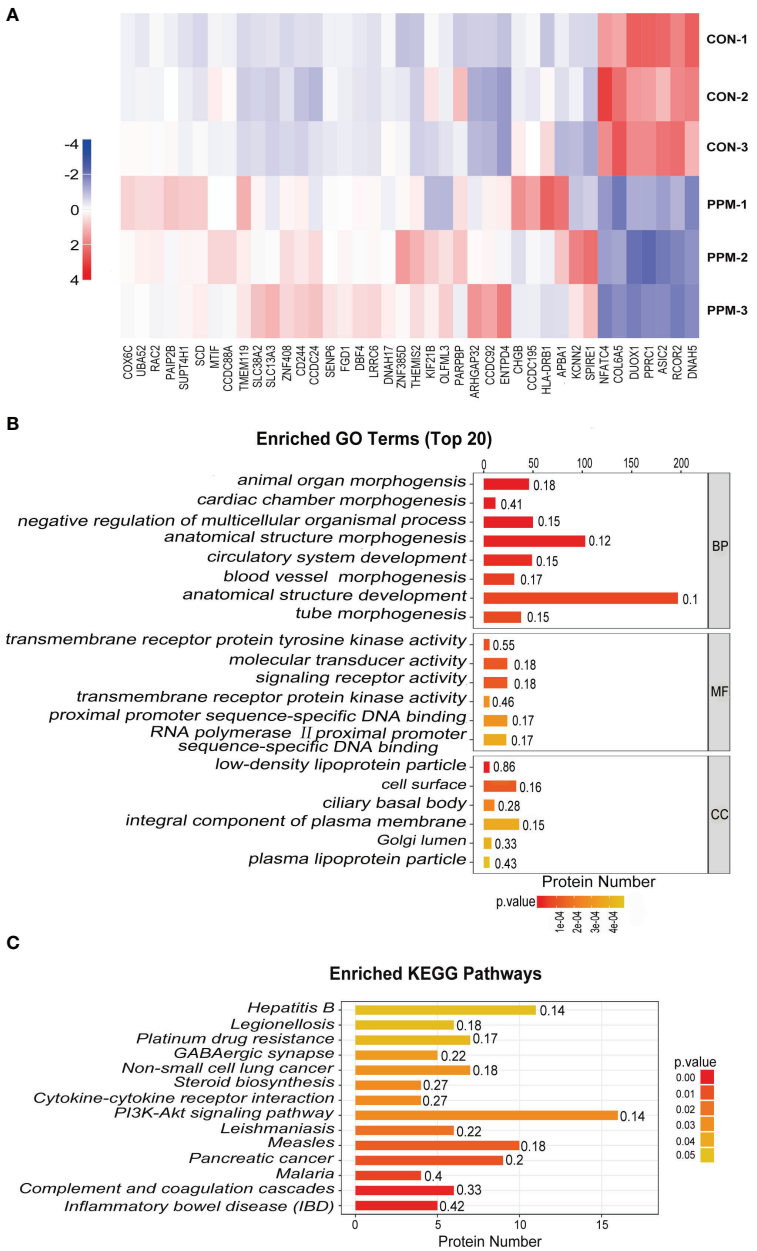

FIGURE 5 | Quantitative proteomic analysis of control and PPM-treated HCT 116 cells and bioinformatic analyses of the differentially expressed proteins (DEPs). **(A)** Hierarchical clustering of DEPs between the control and PPM-treated groups. The heatmap is a visualized demonstration of the protein distribution in different samples. Columns represent the proteins and rows represent the groups of cells. The red color represents high expression and blue color represents low expression. A total of 33 of the upregulated proteins and seven of the downregulated proteins showed >2 fold-changes with $P < 0.05$. **(B)** Top 20 enriched GO terms using Fisher's exact test for the biological process (BP), molecular function (MF), and cellular component (CC) categories. The vertical axis represents GO terms in each category; the horizontal axis demonstrates the protein number of each item. The numbers beside the bars are enrichment factors, which represent the significance and reliability of proteins enriched in each item. **(C)** Enriched KEGG pathways associated with the DEPs. The color of the bar represents the *P*-value calculated using Fisher's exact test.

DISCUSSION

Colorectal cancer (CRC) is one of the most common malignancies worldwide, and is the second leading cause of tumor death (18). For some stage IV colon and rectal cancers with metastases, radiotherapy and chemotherapy therapy are the main therapy strategies so far. However, the chemotherapy drugs are effective but combined with unwanted toxicity and side effects (5).

It has been found that, cardiac glycosides (CG) may have the ability to induce tumor cell death *in vitro* (19–21). Retrospective

TABLE 1 | DEPs between PPM-treated groups and control groups in HCT 116 cells.

Accession	Protein Name	Gene Name	Fold chang	p value
Up-regulated proteins				
Q8N4L8	Coiled-coil domain-containing protein 24	CCDC24	6.81	0.04
Q9GZR1	Sentrin-specific protease 6	SENP6	4.71	0.02
Q3V6T2	Girdin	CCDC88A	4.63	0.03
P98174	FYVE, RhoGEF and PH domain-containing protein 1	FGD1	4.44	0.04
Q9H6B1	Zinc finger protein 385D	ZNF385D	3.86	0.01
Q9Y227	Ectonucleoside triphosphate diphosphohydrolase 4	ENTPD4	3.35	0.02
Q8N511	Transmembrane protein 199	TMEM199	3.30	0.04
P05060	Secretogranin-1	CHGB	3.29	0.01
Q9H2S1	Small conductance calcium-activated potassium channel protein 2	KCNN2	3.20	0.00
Q5TEJ8	Protein THEMIS2	THEMIS2	3.19	0.02
Q30167	HLA class II histocompatibility antigen, DRB1-10 beta chain	HLA-DRB1	3.07	0.04
A0A1B0GUA6	Putative coiled-coil domain-containing protein 195	CCDC195	3.08	0.01
Q96QD8	Sodium-coupled neutral amino acid transporter 2	SLC38A2	3.00	0.00
Q02410	Amyloid-beta A4 precursor protein-binding family A member 1	APBA1	2.97	0.03
Q9NRN5	Olfactomedin-like protein 3	OLFML3	2.73	0.02
A8TX70	Collagen alpha-5(VI) chain	COL6A5	2.69	0.01
Q9NRD9	Dual oxidase 1	DUOX1	2.52	0.00
Q9NWS1	PCNA-interacting partner	PARPBP	2.51	0.02
Q86X45	Protein tilB homolog	LRRC6	2.50	0.04
A7KAX9	Rho GTPase-activating protein 32	ARHGAP32	2.33	0.01
Q53HC0	Coiled-coil domain-containing protein 92	CCDC92	2.29	0.02
Q9UBU7	Protein DBF4 homolog A	DBF4	2.26	0.03
Q8IZ40	REST corepressor 2	RCOR2	2.25	0.00
Q8WWT9	Solute carrier family 13 member 3	SLC13A3	2.24	0.03
Q08AE8	Protein spire homolog 1	SPIRE1	2.19	0.01
Q9H9D4	Zinc finger protein 408	ZNF408	2.15	0.00
Q9UFH2	Dynein heavy chain 17, axonemal	DNAH17	2.13	0.04
Q16515	Acid-sensing ion channel 2	ASIC2	2.12	0.00
Q8TE73	Dynein heavy chain 5, axonemal	DNAH5	2.12	0.00
O75037	Kinesin-like protein KIF21B	KIF21B	2.10	0.02
Q14934	Nuclear factor of activated T-cells, cytoplasmic 4	NFATC4	2.06	0.01
Q5VV67	Peroxisome proliferator-activated receptor gamma coactivator-related protein 1	PPRC1	2.02	0.00
Q9BZW8	Natural killer cell receptor 2B4	CD244	2.02	0.01
Down-regulated proteins				
O00767	Acyl-CoA desaturase	SCD	0.49	0.00
P04733	Metallothionein-1F	MT1F	0.47	0.01
P09669	Cytochrome c oxidase subunit 6C	COX6C	0.45	0.04
P62987	Ubiquitin-60S ribosomal protein L40	UBA52	0.45	0.01
P15153	Ras-related C3 botulinum toxin substrate 2	RAC2	0.45	0.04
Q9ULR5	Polyadenylate-binding protein-interacting protein 2B	PAIP2B	0.41	0.04
P63272	Transcription elongation factor SPT4	SUPT4H1	0.41	0.04

clinical analyses revealed that, CG digoxin administration during chemotherapy may improve overall survival in cohorts of breast, colorectal, head and neck, and hepatocellular carcinoma patients (22). Moreover, elevated plasma digitoxin levels have been found previously correlate with reduced incidence of leukemia, lymphoma, and kidney/urinary tract tumors in patients (23). PPM, a cardiac glycoside isolated from *Cortex Periplocae*, has been used for chronic congestive heart failure treatment due to its effect of strengthen myocardial contractility (24). Previous studies performed in some tumor cells, such as PC3, U937, MCF-7, and SMMC-7721, have found that, PPM has potent anti-cancer effect by inhibiting cells growth and promoting apoptosis (10, 12), suggesting PPM applications in anti-cancer treatment.

Most anti-cancer therapies trigger apoptosis to eliminate malignant cells (25, 26). Previous study indicated that PPM inhibited prostate cancer cell line PC3 growth by the activation of caspase-dependent apoptotic pathways (10). PPM also could sensitize U937 cells to TNF-related apoptosis, which was more quickly than the ouabain (10). In the present experiment, we have found that PPM promoted CRC cell apoptosis *in vitro*. Our study showed PPM treatment led to a significant reduction in the viability of several CRC cell lines and increased the rate of apoptosis in HCT 116 and RKO cells in a dose-dependent manner. In addition, we are first to discover that PPM could trigger an increase of expression profile for the pro-apoptotic proteins Bax, cleaved caspase-3, and cleaved caspase-9, and a decrease in those of the anti-apoptotic proteins Bcl-2 and survivin, contributing to increased apoptotic ratio in CRC cell (14, 27). However, mechanisms underlying PPM modulating apoptosis is still quite limited and detailed studies needs to be further performed.

Cell cycle disruption has been found in pathogenesis of tumors (28). In this study, we observed that PPM treatment could cause significantly increased ratio of cells in G0/G1 phase

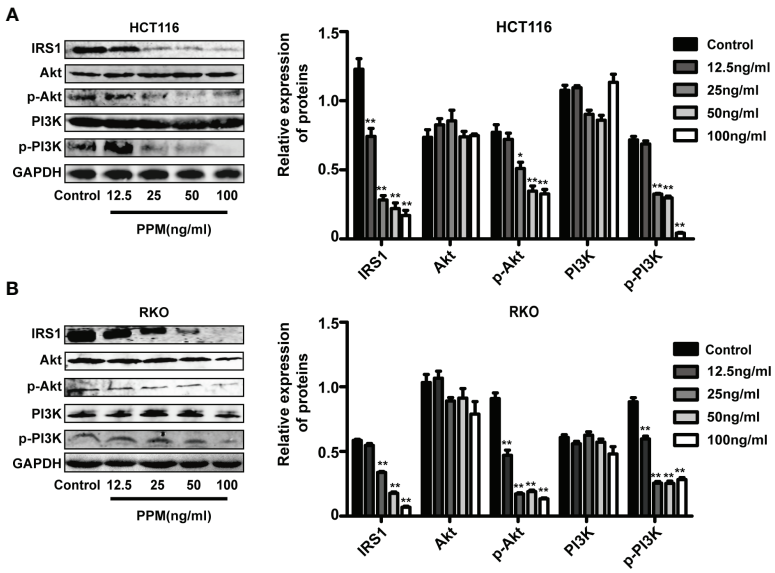

FIGURE 6 | Periplocymarin (PPM) modulates gene expression involved in PI3K/AKT signaling pathway. PPM treatment altered the expression levels of IRS1, PI3K, AKT, p-PI3K, and p-AKT in HCT 116 **(A)** and RKO cells **(B)**. Values are shown as means ± SEM. *$P < 0.05$, **$P < 0.01$, *vs*. untreated control group.

while decreased ratio of cells in S phase, indicating PPM promoted cycle arrest in CRC cells. But the maximum effect of PPM observed was at concentration of 50 ng/ml, suggesting that its effect on cell cycle does not enhance as the drug concentration increases when greater than 50 ng/ml. Protein p21 is a negative regulator of G1/S transition (29), and downregulation of p21 is involved in tumor promotion in various cancers (30, 31). Oncogene cyclin D1 has been found overexpressed in human cancers (32) and implicated in many activities, such as cell cycle promotion, chromosomal instability, mitochondrial function and cellular senescence (33). Previous studies have found that cyclin D1 binds and sequesters p21, thereby allowing the progression from G1 to S phase (34). In the present study, we found that PPM treatment increased p21 and decreased cyclin D1 gene expression, indicating that PPM reduced CRC cell proliferation mainly by causing cell cycle arrests, and this effect might be achieved by increasing p21 and reducing cyclin D1 expression. Similar results have also been found in some other traditional Chinese medicine, such as curcumol and pigallocatechin-3-gallate (35, 36). But the maximal effect of PPM on p21 and cyclin D1 expression was noted at 100 ng/ml, indicating that there might be other proteins involved in the cell cycle regulation of PPM treatment, which needs further research.

Quantitative proteomic techniques have been widely applied due to their ability to reveal the dynamics of protein expression and protein-protein interactions from a global perspective, which greatly help to understand the gene function in cellular processes (37). In this study, the proteomic approach has been introduced to identify PPM treatment-associated DEPs. A total of 6,645 proteins were identified, of these, 539 were found to be differentially expressed. Gene Ontology (GO) analysis suggests these proteins have important functions in various metabolic processes, (e.g., transmembrane receptor protein tyrosine kinase activity, signaling receptor activity, and molecular transducer activity). PI3K/AKT signaling pathway was selected for further mechanism research owing to its high enrichment factor and more DEPs associated according to the KEGG analysis. At the same time, the results also showed that IRS1, as the upstream of PI3K, was down-regulated after PPM treatment.

PI3K/AKT signaling pathway plays an important role in tumor cell growth, proliferation and survival by regulating apoptosis-related genes (15). Elevated level of phosphorylated PI3K and

TABLE 2 | The effects of periplocymarin (PPM) and 5-FU on blood cell counts and liver and kidney function.

	WBC ($\times10^9$/L)	RBC ($\times10^{12}$/L)	PLT ($\times10^9$/L)	ALT (U/L)	AST (U/L)	CREA (μmol/L)	UN (mmol/L)
CON	0.64 ± 0.06	3.33 ± 0.04	309.67 ± 11.57	10.63 ±1.20	57.40 ± 10.06	2.27 ± 0.46	2.47 ± 0.09
5-FU	0.32 ± 0.04*	3.37 ± 0.11	276.00 ± 26.01	47.53 ±13.43*	113.67 ± 20.07*	4.67 ± 0.44	6.77 ± 1.26
PPM	0.68 ± 0.06	3.42 ± 0.01	327.33 ± 16.76	8.00 ± 1.66	37.03 ± 0.58	2.33 ± 0.18	2.20 ± 0.17
PPM + 5-FU	0.54 ± 0.08	3.51 ± 0.09	336.00 ± 7.21	25.13 ± 4.0	77.03 ± 4.71	3.93 ± 1.66	5.23 ± 0.27*

WBC, white blood cell; RBC, red blood cell; PLT, platelet; ALT, alanine aminotransferase; AST, aspartate aminotransferase; CREA, creatinine; UN, urea nitrogen.
Data were present as mean±SEM. N=3 per/group.
**P < 0.05 vs. CON group.*

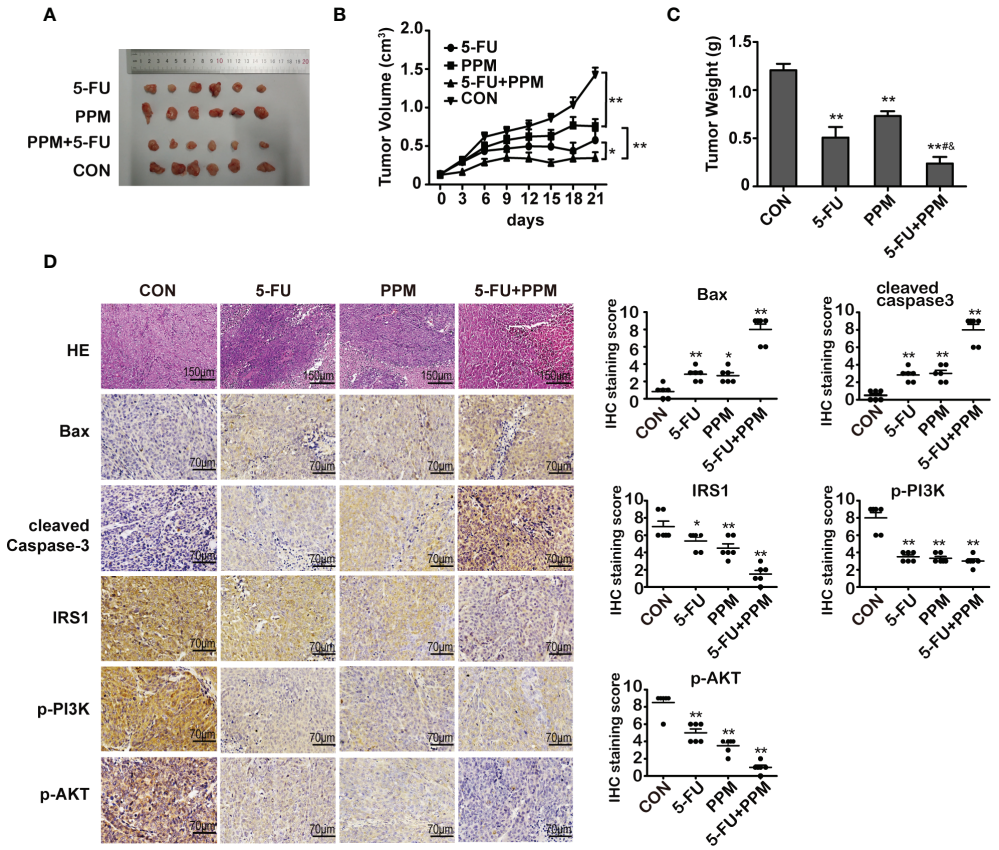

FIGURE 7 | The effect of periplocymarin (PPM) on colorectal cancer cells in nude mice. **(A)** Images of tumors derived from mice in each group. **(B)** Tumor volumes were calculated in each group every 3 days from days 1 to 21. **(C)** Tumor weights were measured on day 21. **(D)** Hematoxylin/eosin-stained sections of tumor tissues derived from mice in each treatment group were presented. Magnification: 200×. Scale bar, 150 μm. The expression of Bax, cleaved caspase-3, IRS1, p-PI3K, and p-AKT in tumor tissues of mice from each treatment group was examined by immunohistochemistry. Magnification: 400×. Scale bar, 70 μm. $^{*}P < 0.05$, $^{**}P < 0.01$, *vs*. untreated control group. $^{\#}P < 0.05$, *vs*. 5-FU treatment group. $^{\&}P < 0.05$, *vs*. PPM treatment group. n =6 per group.

AKT were found in human CRC samples, which was correlated with a poor disease outcome (38). Activated PI3K/AKT signaling pathway has been suggested favorable for cells survival through inhibiting apoptosis and impair cell cycle arrest by targeting downstream genes, including Bcl-2 family, caspase family, survivin, p21, and cyclin D (39–43). Inhibition of PI3K/AKT signaling pathway has been found effective in inhibition of tumor cells of different tissues (44–46). IRS1, upstream of PI3K and major substrate of insulin, insulin-like growth factors and cytokine signaling, plays an important role in mediating apoptosis, cell differentiation, and cell transformation (47). IRS1 is constitutively activated in a variety of solid tumors, namely, CRC, breast cancers, leiomyomas, Wilms tumors, rhabdomyosarcomas, liposarcomas, leiomyosarcomas, and adrenal cortical carcinomas (48). In the present study, we found that PPM reduced IRS1, p-PI3K, p-AKT gene expression and caused impaired PI3K/AKT signaling pathway in CRC cells, which might lead to increased apoptotic ratio and promoted cell cycle arrest.

Also, in the present experiment, we have checked the effect and safety of PPM in animal models. We have found that, PPM performed comparable anti-tumor effect with 5-FU, but with less negative effects in white cells and liver function. Studies about PPM on blood, renal and hepatic function is little. It has been found that the toxicity of *Cortex Periplocae* is mainly cardiac glycoside poisoning (49). However, previous study has found that, *Cortex Periplocae* extract may reverse the white blood cell decline caused by cyclophosphamide (50). Wan et al. (51) found that periplocoside A, another nature product compound isolated from *Cortex Periplocae*, may prevent liver damage caused by concanavaline A. Intriguingly, the PPM + 5-FU combination therapy strategy seemed more effective in tumor suppression than single drug treatment, and only slightly renal function impairment was observed, indicating PPM might be added to other traditional anti-tumor therapy, more favorable effects would be achieved with less side effects. However, long-term *in vivo* effect of PPM still needs to be investigated. In addition, the cardiovascular safety of PPM is still needed to be warranted.

In conclusion, data from this experiment indicated that PPM performed anti-tumor effects both *in vivo* and *in vitro*. Inhibited PI3K/AKT signaling pathway might be involved in this process. A diagram for the mechanism of PPM-induced apoptosis and cell

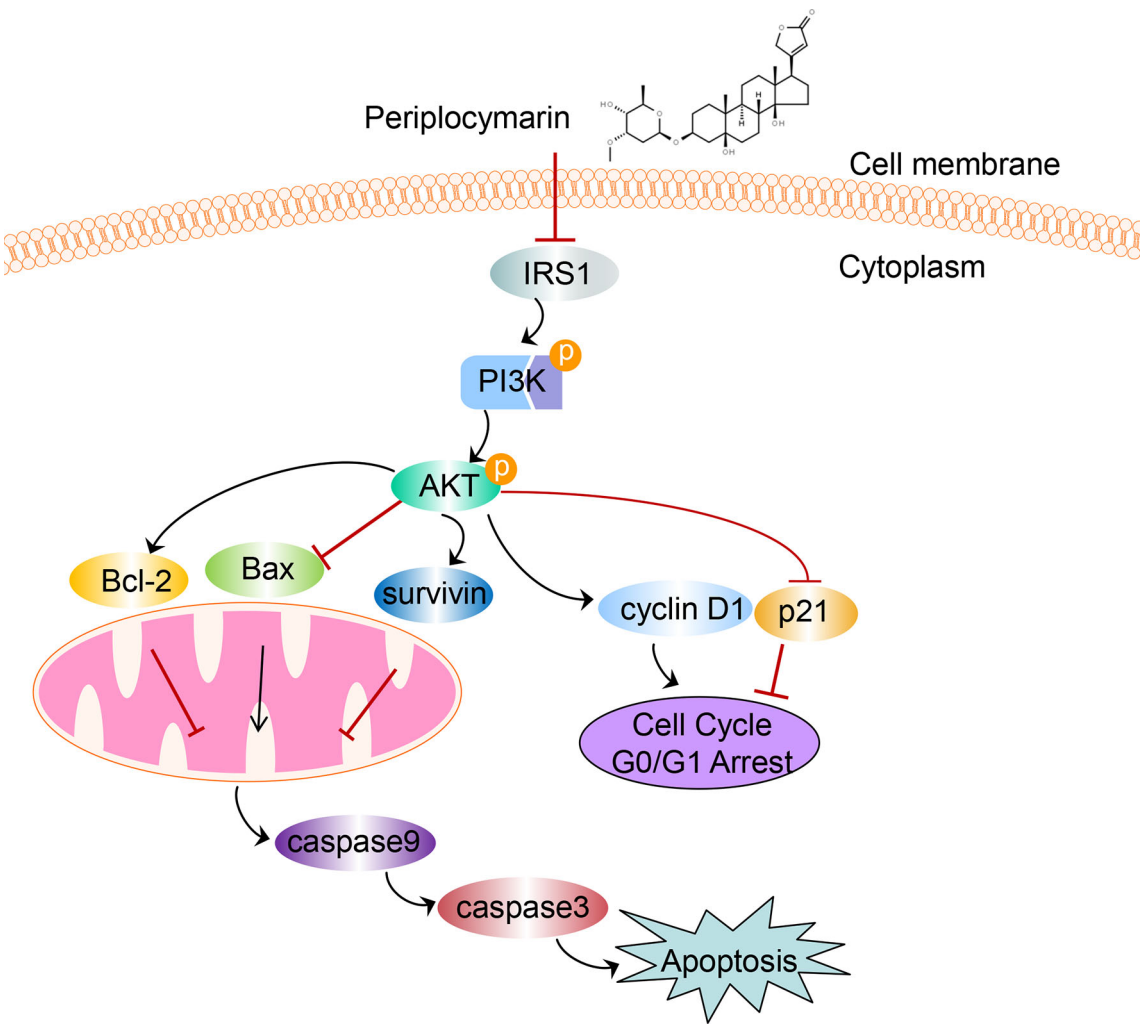

FIGURE 8 | The schematic diagram depicts the mechanism of PPM-induced apoptosis and cell cycle arrest *via* impairing PI3K/AKT signaling pathway in CRC cells. We supposed that PPM may inhibit the expression of IRS1, p-PI3K, and p-AKT and modulate the expression of Bcl-2 family, survivin, p21, and cyclin D1, which further promotes apoptosis and cell cycle arrest in G0/G1 phase of CRC cells.

cycle arrest *via* impairing PI3K/AKT signaling pathway in CRC cells is shown in **Figure 8**. PPM is a promising chemotherapeutic drug for CRC treatment but extended safety evaluation should be performed.

DATA AVAILABILITY STATEMENT

The original contributions presented in the study are included in the article/supplementary material. Further inquiries can be directed to the corresponding authors.

ETHICS STATEMENT

The animal study was reviewed and approved by the Experimental animal ethics committee of the Fourth Hospital of Hebei Medical University.

AUTHOR CONTRIBUTIONS

GW and LZ conceived the study. YC, SD, and CZ performed the experiment. JH and XH analyzed experimental results. HM, BL, and ZM provided advice on the study design and data interpretation. YC and FW wrote the manuscript. All authors contributed to the article and approved the submitted version.

FUNDING

This work was supported by the Natural Science Foundation of China (Grant No. 81772550), Natural Science Foundation precision medicine joint project of Hebei Province, China

(Grant No. H2020206485), Department of science and technology key project of Hebei Province, China (Grant No. 206Z7705G) and Precision Medicine Joint Fund Cultivation Project of Hebei Province, China (Grant No. H2021206253).

ACKNOWLEDGMENTS

Thanks for the contributions of teachers from the Scientific Research Center of the Fourth Hospital of Hebei Medical University.

REFERENCES

1. Sung H, Ferlay J, Siegel RL, Laversanne M, Soerjomataram I, Jemal A. Global Cancer Statistics 2020: GLOBOCAN Estimates of Incidence and Mortality Worldwide for 36 Cancers in 185 Countries. *CA Cancer J Clin* (2021) 71:209–49. doi: 10.3322/caac.21660
2. Garborg K, Holme Ø, Løberg M, Kalager M, Adami HO. M. Bretthauer. Current Status of Screening for Colorectal Cancer. *Ann Oncol* (2013) 24:1963–72. doi: 10.1093/annonc/mdt157
3. Schreuders EH, Ruco A, Rabeneck L, Schoen RE, Sung JJ, Young GP, et al. Colorectal Cancer Screening: A Global Overview of Existing Programmes. *Gut* (2015) 64:1637–49. doi: 10.1136/gutjnl-2014-309086
4. Zeng H, Chen W, Zheng R, Zhang S, Ji JS, Zou X, et al. Changing Cancer Survival in China During 2003-15: A Pooled Analysis of 17 Population-Based Cancer Registries. *Lancet Glob Health* (2018) 6:e555–67. doi: 10.1016/s2214-109x(18)30127-x
5. Chibaudel B, Tournigand C, Bonnetain F, Richa H, Benetkiewicz M, André T, et al. Therapeutic Strategy in Unresectable Metastatic Colorectal Cancer: An Updated Review. *Ther Adv Med Oncol* (2015) 7:153–69. doi: 10.1177/1758834015572343
6. Newman DJ, Cragg GM. Natural Products as Sources of New Drugs From 1981 to 2014. *J Nat Prod* (2016) 79:629–61. doi: 10.1021/acs.jnatprod.5b01055
7. C. P. Commission. *Chinese Pharmacopoeia. 2015 edition* Vol. First volume. Beijing: China Medical Science and Technology Press (2015) p. 257–8.
8. Zhang HY, Xu WQ, Zheng YY, Omari-Siaw E, Zhu Y, Cao X, et al. Octreotide-Periplocymarin Conjugate Prodrug for Improving Targetability and Anti-Tumor Efficiency. Synthesis, *In Vitro* and *In Vivo* Evaluation. *Oncotarget* (2016) 7:86326–38. doi: 10.18632/oncotarget.13389
9. Zhang H, Xu W, Omari-Siaw E, Liu Y, Chen B, Chen D, et al. Redox-Responsive PEGylated Self-Assembled Prodrug-Nanoparticles Formed by Single Disulfide Bond Bridge Periplocymarin-Vitamin E Conjugate for Liver Cancer Chemotherapy. *Drug Delivery* (2017) 24:1170–8. doi: 10.1080/10717544.2017.1365393
10. Bloise E, Braca A, De Tommasi N, Belisario MA. Pro-Apoptotic and Cytostatic Activity of Naturally Occurring Cardenolides. *Cancer Chemother Pharmacol* (2009) 64:793–802. doi: 10.1007/s00280-009-0929-5
11. Li M-y, Yang X, Yan C-y, Xiao Z-j, Jiang W-q, Wang X-y, et al. Research Progress on Chemical Composition and Pharmacological Effects of Periplocae Cortex and Predictive Analysis on Q-Marker. *Chin J Chin Matieral Med* (2020) 45:2772–83. doi: 10.19540/j.cnki.cjcmm.20200327.202
12. Martey ON, He X, Xing H, Deng F, Feng S, Li C, et al. Periplocymarin is a Potential Natural Compound for Drug Development: Highly Permeable With Absence of P-Glycoprotein Efflux and Cytochrome P450 Inhibitions. *Biopharm Drug Dispos* (2014) 35:195–206. doi: 10.1002/bdd.1884
13. Gu J, Huang W, Zhang J, Wang X, Tao T, Yang L, et al. TMPRSS4 Promotes Cell Proliferation and Inhibits Apoptosis in Pancreatic Ductal Adenocarcinoma by Activating ERK1/2 Signaling Pathway. *Front Oncol* (2021) 11:628353. doi: 10.3389/fonc.2021.628353
14. Czabotar PE, Lessene G, Strasser A, Adams JM. Control of Apoptosis by the BCL-2 Protein Family: Implications for Physiology and Therapy. *Nat Rev Mol Cell Biol* (2014) 15:49–63. doi: 10.1038/nrm3722
15. Jiang N, Dai Q, Su X, Fu J, Feng X, Peng J. Role of PI3K/AKT Pathway in Cancer: The Framework of Malignant Behavior. *Mol Biol Rep* (2020) 47:4587–629. doi: 10.1007/s11033-020-05435-1
16. Haeusler RA, McGraw TE, Accili D. Biochemical and Cellular Properties of Insulin Receptor Signalling. *Nat Rev Mol Cell Biol* (2018) 19:31–44. doi: 10.1038/nrm.2017.89
17. Ma J, Chen T, Wu S, Yang C, Bai M, Shu K, et al. Iprox: An Integrated Proteome Resource. *Nucleic Acids Res* (2019) 47:D1211–d1217. doi: 10.1093/nar/gky869
18. Bray F, Ferlay J, Soerjomataram I, Siegel RL, Torre LA, Jemal A. Global Cancer Statistics 2018: GLOBOCAN Estimates of Incidence and Mortality Worldwide for 36 Cancers in 185 Countries. *CA Cancer J Clin* (2018) 68:394–424. doi: 10.3322/caac.21492
19. Howard CM, Estrada M, Terrero D, Tiwari AK, Raman D. Identification of Cardiac Glycosides as Novel Inhibitors of Eif4a1-Mediated Translation in Triple-Negative Breast Cancer Cells. *Cancers (Basel)* (2020) 12:2169. doi: 10.3390/cancers12082169
20. Newman RA, Yang P, Pawlus AD, Block KI. Cardiac Glycosides as Novel Cancer Therapeutic Agents. *Mol Interv* (2008) 8:36–49. doi: 10.1124/mi.8.1.8
21. Ramirez-Ortega M, Maldonado-Lagunas V, Melendez-Zajgla J, Carrillo-Hernandez JF, Pastelín-Hernandez G, Picazo-Picazo O, et al. Proliferation and Apoptosis of HeLa Cells Induced by. *Vitro Stimulation Digitalis Eur J Pharmacol* (2006) 534:71–6. doi: 10.1016/j.ejphar.2006.01.035
22. Menger L, Vacchelli E, Adjemian S, Martins I, Ma Y, Shen S, et al. Cardiac Glycosides Exert Anticancer Effects by Inducing Immunogenic Cell Death. *Sci Transl Med* (2012) 4:143ra99. doi: 10.1126/scitranslmed.3003807
23. Haux J, Klepp O, Spigset O, Tretli S. Digitoxin Medication and Cancer; Case Control and Internal Dose-Response Studies. *BMC Cancer* (2001) 1:11. doi: 10.1186/1471-2407-1-11
24. Yun W, Qian L, Cheng Y, Tao W, Yuan R, Xu H. Periplocymarin Plays an Efficacious Cardiotonic Role *via* Promoting Calcium Influx. *Front Pharmacol* (2020) 11:1292. doi: 10.3389/fphar.2020.01292
25. Zhang L, Ren X, Alt E, Bai X, Huang S, Xu Z, et al. Chemoprevention of Colorectal Cancer by Targeting APC-Deficient Cells for Apoptosis. *Nature* (2010) 464:1058–61. doi: 10.1038/nature08871
26. Liu S, Lin H, Wang D, Li Q, Luo H, Li G, et al. PCDH17 Increases the Sensitivity of Colorectal Cancer to 5-Fluorouracil Treatment by Inducing Apoptosis and Autophagic Cell Death. *Signal Transduct Target Ther* (2019) 4:53. doi: 10.1038/s41392-019-0087-0
27. Tamm I, Schriever F, Dörken B. Apoptosis: Implications of Basic Research for Clinical Oncology. *Lancet Oncol* (2001) 2:33–42. doi: 10.1016/s1470-2045(00)00193-5
28. Hou PF, Jiang T, Chen F, Shi PC, Li HQ, Bai J. KIF4A Facilitates Cell Proliferation *via* Induction of P21-Mediated Cell Cycle Progression and Promotes Metastasis in Colorectal Cancer. *Cell Death Dis* (2018) 9:477. doi: 10.1038/s41419-018-0550-9
29. Niculescu AB, Chen 3X, Smeets M, Hengst L, Prives C, Reed SI. Effects of P21 (Cip1/Waf1) at Both the G1/S and the G2/M Cell Cycle Transitions: pRb is a Critical Determinant in Blocking DNA Replication and in Preventing Endoreduplication. *Mol Cell Biol* (1998) 18:629–43. doi: 10.1128/mcb.18.1.629
30. Nie FQ, Sun M, Yang JS, Xie M, Xu TP, Xia R, et al. Long Noncoding RNA ANRIL Promotes non-Small Cell Lung Cancer Cell Proliferation and Inhibits Apoptosis by Silencing KLF2 and P21 Expression. *Mol Cancer Ther* (2015) 14:268–77. doi: 10.1158/1535-7163.Mct-14-0492
31. Abbas T, Dutta A. P21 in Cancer: Intricate Networks and Multiple Activities. *Nat Rev Cancer* (2009) 9:400–14. doi: 10.1038/nrc2657
32. Tchakarska G, Sola B. The Double Dealing of Cyclin D1. *Cell Cycle* (2020) 19:163–78. doi: 10.1080/15384101.2019.1706903
33. Casimiro MC, Pestell RG. Cyclin D1 Induces Chromosomal Instability. *Oncotarget* (2012) 3:224–5. doi: 10.18632/oncotarget.476
34. LaBaer J, Garrett MD, Stevenson LF, Slingerland JM, Sandhu C, Chou HS, et al. New Functional Activities for the P21 Family of CDK Inhibitors. *Genes Dev* (1997) 11:847–62. doi: 10.1101/gad.11.7.847
35. Wang J, Li XM, Bai Z, Chi BX, Wei Y. X. Chen. Curcumol Induces Cell Cycle Arrest in Colon Cancer Cells *via* Reactive Oxygen Species and Akt/Gsk3β/Cyclin D1 Pathway. *J Ethnopharmacol* (2018) 210:1–9. doi: 10.1016/j.jep.2017.06.037
36. Zhang X, Min KW, Wimalasena J, Baek SJ. Cyclin D1 Degradation and P21 Induction Contribute to Growth Inhibition of Colorectal Cancer Cells Induced by Epigallocatechin-3-Gallate. *J Cancer Res Clin Oncol* (2012) 138:2051–60. doi: 10.1007/s00432-012-1276-1
37. Li Z, Li N, Shen L, Fu J. Quantitative Proteomic Analysis Identifies MAPK15 as a Potential Regulator of Radioresistance in Nasopharyngeal Carcinoma Cells. *Front Oncol* (2018) 8:548. doi: 10.3389/fonc.2018.00548

38. Itoh N, Semba S, Ito M, Takeda H, Kawata S, Yamakawa M. Phosphorylation of Akt/PKB is Required for Suppression of Cancer Cell Apoptosis and Tumor Progression in Human Colorectal Carcinoma. *Cancer* (2002) 94:3127–34. doi: 10.1002/cncr.10591
39. Chang F, Lee JT, Navolanic PM, Steelman LS, Shelton JG, Blalock WL, et al. Involvement of PI3K/Akt Pathway in Cell Cycle Progression, Apoptosis, and Neoplastic Transformation: A Target for Cancer Chemotherapy. *Leukemia* (2003) 17:590–603. doi: 10.1038/sj.leu.2402824
40. Tewari D, Patni P, Bishayee A, Sah AN, Bishayee A. Natural Products Targeting the PI3K-Akt-mTOR Signaling Pathway in Cancer: A Novel Therapeutic Strategy. *Semin Cancer Biol* (2019), S1044–579X(19)30405-5. doi: 10.1016/j.semcancer.2019.12.008
41. Bahrami A, Khazaei M, Hasanzadeh M, ShahidSales S, Joudi Mashhad M, Farazestanian M, et al. Therapeutic Potential of Targeting PI3K/AKT Pathway in Treatment of Colorectal Cancer: Rational and Progress. *J Cell Biochem* (2018) 119:2460–9. doi: 10.1002/jcb.25950
42. Stiles BL. PI-3-K and AKT: Onto the Mitochondria. *Adv Drug Delivery Rev* (2009) 61:1276–82. doi: 10.1016/j.addr.2009.07.017
43. Wheatley SP, Altieri DC. Survivin at a Glance. *J Cell Sci* (2019) 132:223826–34. doi: 10.1242/jcs.223826
44. Huang Z, Liu CA, Cai PZ, Xu FP, Zhu WJ, Wang WW, et al. Omega-3pufa Attenuates MNU-Induced Colorectal Cancer in Rats by Blocking PI3K/AKT/Bcl-2 Signaling. *Onco Targets Ther* (2020) 13:1953–65. doi: 10.2147/ott.S241298
45. Sui Y, Zheng X. D. Zhao. Rab31 Promoted Hepatocellular Carcinoma (HCC) Progression *via* Inhibition of Cell Apoptosis Induced by PI3K/AKT/Bcl-2/BAX Pathway. *Tumour Biol* (2015) 36:8661–70. doi: 10.1007/s13277-015-3626-5
46. Surmeli Z, Gursoy P, Erdogan AP, Bozkurt E, Atmaca H, Uzunoglu S, et al. Combination of Zoledronic Acid and Serine/Threonine Phosphatase Inhibitors Induces Synergistic Cytotoxicity and Apoptosis in Human Breast Cancer Cells *via* Inhibition of PI3K/Akt Pathway. *Tumour Biol* (2016) 37:3665–73. doi: 10.1007/s13277-015-3265-x
47. White MF. IRS Proteins and the Common Path to Diabetes. *Am J Physiol Endocrinol Metab* (2002) 283:E413–22. doi: 10.1152/ajpendo.00514.2001
48. Chang Q, Li Y, White MF, Fletcher JA, Xiao S. Constitutive Activation of Insulin Receptor Substrate 1 is a Frequent Event in Human Tumors: Therapeutic Implications. *Cancer Res* (2002) 62:6035–8.
49. Li Y, Li J, Zhou K, He J, Cao J, An M, et al. A Review on Phytochemistry and Pharmacology of Cortex Periplocae. *Molecules* (2016) 21:1702. doi: 10.3390/molecules21121702
50. XU Shuo JP, Xu W, Wu X, Jiang W, Kuang Y, Ma J. Advances on Chinese Herbal Medicine Periplocae Cortex. *Northwest Pharm J* (2017) 32:118–21. doi: 10.3969/j. issn. 1004-2407.2107.01.032
51. Wan J, Zhu YN, Feng JQ, Chen HJ, Zhang RJ, Ni J, et al. Periplocoside A, a Pregnane Glycoside From Periploca Sepium Bge, Prevents Concanavalin A-Induced Mice Hepatitis Through Inhibiting NKT-Derived Inflammatory Cytokine Productions. *Int Immunopharmacol* (2008) 8:1248–56. doi: 10.1016/j.intimp.2008.05.001

Conflict of Interest: The authors declare that the research was conducted in the absence of any commercial or financial relationships that could be construed as a potential conflict of interest.

Publisher's Note: All claims expressed in this article are solely those of the authors and do not necessarily represent those of their affiliated organizations, or those of the publisher, the editors and the reviewers. Any product that may be evaluated in this article, or claim that may be made by its manufacturer, is not guaranteed or endorsed by the publisher.

frontiers in Oncology

ORIGINAL RESEARCH
published: 02 December 2021
doi: 10.3389/fonc.2021.767116

PKM2 Is the Target of a Multi-Herb-Combined Decoction During the Inhibition of Gastric Cancer Progression

Qingmin Sun[1†], Mengyun Yuan[1,2†], Hongxing Wang[1,2†], Xingxing Zhang[1], Ruijuan Zhang[1,2], Haidan Wang[1], Xu Chen[1,2], Min Zhu[1], Shenlin Liu[1] and Jian Wu[1]*

[1] Jiangsu Province Hospital of Chinese Medicine, Affiliated Hospital of Nanjing University of Chinese Medicine, Nanjing, China, [2] No. 1 Clinical Medical College, Nanjing University of Chinese Medicine, Nanjing, China

Gastric cancer is the third leading cause of cancer death worldwide. Traditional Chinese medicine (TCM) is increasingly extensively applied as a complementary therapy for gastric cancer (GC) in China, which shows unique advantages in preventing gastric cancer metastasis. Previous study indicates modified Jian-pi-yang-zheng (mJPYZ) decoction inhibit the progression of gastric cancer by regulating tumor-associated macrophages (TAM). However, it is unclear whether mJPYZ can affect metabolic reprogramming of gastric cancer cells. Here, we showed that mJPYZ effectively attenuated GC cells proliferation, migration and invasion. Meantime, mJPYZ reduced the aerobic glycolysis level of GC cells *in vivo* and *in vitro* by regulating the expression and nuclear translocation of PKM2. Overexpression of PKM2 that could reverse the inhibitory effect of mJPYZ, migration and epithelial to mesenchymal transition (EMT). Our results showed PKM2/HIF-1α signaling was the key metabolic regulator of mJPYZ in GC cells. In summary, our present study suggested that abnormal PKM2 is required for maintaining the malignant phenotype of GC cells. The TCM decoction mJPYZ inhibited GC cells growth and EMT by reducing of glycolysis in PKM2 dependent manner. This evidence expanded our understanding of the anti-tumor mechanism of mJPYZ and further indicated mJPYZ a potential anti-tumor agent for GC patients.

Chemical Compounds Studied in this Article: Rutin (PubChem CID: 5280805); Lobetyolin (PubChem CID: 53486204); Calycosin-7-glucoside (PubChem CID: 71571502); Formononetin (PubChem CID: 5280378); Calycosin (PubChem CID: 5280448); Ononin (PubChem CID: 442813); P-Coumaric Acid (PubChem CID: 637542).

Keywords: traditional Chinese medicine, PKM2, gastric cancer, aerobic glycolysis, cancer metabolism

OPEN ACCESS

Edited by:
Vincent Kam Wai Wong, Macau University of Science and Technology, Macao SAR, China

Reviewed by:
Weidong Li, China Academy of Chinese Medical Sciences, China
Run-Ze Li, Macau University of Science and Technology, Macao SAR, China

***Correspondence:**
Jian Wu
jianwu@njucm.edu.cn

†These authors have contributed equally to this work and share first authorship

Specialty section:
This article was submitted to Pharmacology of Anti-Cancer Drugs, a section of the journal Frontiers in Oncology

Received: *30 August 2021*
Accepted: *16 November 2021*
Published: *02 December 2021*

Citation:
Sun Q, Yuan M, Wang H, Zhang X, Zhang R, Wang H, Chen X, Zhu M, Liu S and Wu J (2021) PKM2 Is the Target of a Multi-Herb-Combined Decoction During the Inhibition of Gastric Cancer Progression. Front. Oncol. 11:767116. doi: 10.3389/fonc.2021.767116

INTRODUCTION

According to the latest global cancer statistics, gastric cancer is still the fifth most commonly diagnosed cancer and the fourth leading cause of cancer mortality worldwide in 2020 (1). There is an urgent need to develop strategy to prevent the recurrence and metastasis of gastric cancer patients. Traditional Chinese medicine (TCM) has been well accepted and is increasingly extensively applied as a complementary and alternative therapy for gastric cancer (GC) in China, which show unique advantages in preventing and treating gastric cancer metastasis (2). Our previous study showed that Jianpi Yangzheng Xiaozheng (JPYZXZ) decoction could significantly improve life quality and prolong the survival of patients with advanced stage gastric cancer (3). Our recent study further indicated that the components of JPYZXZ also inhibited the progress of gastric cancer *in vivo* and *in vitro* (4). Moreover, mechanism research showed modified Jianpi Yangzheng decoction (mJPYZ) alleviates gastric cancer progression *via* macrophages immune checkpoint PI3Kγ (5). However, it is unclear whether mJPYZ can affect metabolic reprogramming of gastric cancer cells.

Cell metabolic reprogramming exist in various cancer cells and are implicated as salient hallmarks of cancer (6). "Aerobic glycolysis" or "Warburg effect", as a classic metabolic reprogramming pathway of tumor cells, refers to the fact that cancer cells give priority to glycolysis instead of oxidative phosphorylation (OXPHOS) to produce energy under normoxic conditions (7). Numerous studies have shown that aerobic glycolysis is closely related to occurrence, metastasis, and poor prognosis of gastric cancer (8, 9). Meanwhile, in the tumor microenvironment, lactate, a by-product of glycolysis, can also facilitate tumor immunosuppression (10). Mechanistically, a variety of oncogenes and their targeted metabolic enzymes, including phosphofructokinase (PFK), hexokinase (HK), lactate dehydrogenase (LDHA), and pyruvate kinase1/2 (PKM1/2), can promote glycolysis, resulting in cancion genesis, progression, and metastasis. Therefore, target glycolysis has become a novel therapeutic strategy for the treatment of gastric cancer.

PFK, HK, PK are three important rate-limiting enzymes in aerobic glycolysis. Among them, PK is considered to be the central kinase that reprograms cell metabolism, which catalyzes the conversion of phosphoenolpyruvate to pyruvate (11).

There are four isoforms of the PK protein family, PKM1, PKM2, PKL, and PKR. PKM2 has been revealed to be dramatically increased in gastric cancer cells. When PKM2 is deleted in GC cells, the PI3K/AKT/mTOR pathway and autophagy are inhibited, resulting in a decrease in the proliferation and invasion phenotype of GC cells (8, 12). Specially, studies have demonstrated that PKM2 promote transcription of HIF-1α to enhance glycolysis by translocate to the nucleus (13).

Recent studies indicate that TCM have a regulatory effect on glucose metabolism, and metabolism-related factors and enzymes may be their targets (14). mJPYZ decoction contains Astragalus mongholicus (Huangqi); Codonopsis pilosula (Dangshen); Sparganium stoloniferum (Sanleng); Curcuma phaeocaulis (Erzhu), which is an optimized version compared to JPYZXZ and could inhibit gastric cancer growth and metastasis (4). In the current study, we hypothesized that mJPYZ could inhibit PKM2 and remodel aerobic glycolysis in GC cells. We elucidated the potential mechanism of mJPYZ decoction in reducing the aerobic glycolysis level and alleviating the progression of gastric cancer.

MATERIALS AND METHODS

Cell Culture

The MGC-803, SGC-7901 and BGC-823 human gastric cancer cell lines were obtained from the Cell Bank of Type Culture Collection of the Chinese Academy of Sciences (Shanghai, China), and were cultured in RPMI 1640 supplemented with 10% Newborn calf serum in a humidified incubator at 37°C with 5% CO_2.

Preparation of mJPYZ

All herbs were supplied by SANYUE Chinese Traditional Medicine Co. (Nantong, China) and were identified by a Chinese pharmacist. The herbs were soaked and boiled with double-distilled water for 30 min, then the extracted solutions were quantified to 1 g/mL. The extract was stored at −20°C after sterilization and filtering by a 0.22 μm filter.

MTT Assay

GC cells (5×10^3 cells/well) were seeded into 96-well plates separately for 24 h to allow adherence to the walls. To determine the decoction dose, the IC50 of the MGC-803, SGC-7901 and BGC-823 was calculated and the dose range of 2, 4, 8 mg/mL was selected. Then mJPYZ decoction was added at different concentrations (0, 1, 2, 4, 8, 16 mg/mL) for 24, 48, 72 h. MTT (120 μL, 5 mg/mL) (Sigma, USA) was added after the medium was removed, and the cells were incubated for 4 h in the incubator. The supernatant was removed, and 150 μL of dimethyl sulfoxide (DMSO) was added for 10 min. Absorbance at 490 nm was detected on an ELX800 Automatic microplate reader (Bio-Tek, USA) to calculate the absorption value.

Colony Formation

GC cells were seeded at 2000 cells/well in 6-well plates. After a 24h cells adherence, mJPYZ decoction was added to treat the cells for another 10 days. At the end of treatment, the cells were fixed with 95% ethanol and stained with 0.1% Crystal Violet. Photos of each group were taken under a microscope, and the number of colonies formed was then counted.

Wound-Healing Assay

GC cells (5×10^5 cells/well) were seeded into 6-well plates, and a straight line was drawn on the bottom of the plates with a pipette tip when 80% of the cells were adherent to the walls. The plates were washed lightly with PBS 3 times. mJPYZ decoction with different concentrations were set into the wells, and pictures were taken again after incubation for 48 h, and the area between wound boundaries was recorded.

Transwell Invasion Assay

Matrigel (100 μL, diluted 1:29 with PBS) (Corning, USA) was vertically added to the inside bottom of the 8-μm Transwell chambers (Merck & Millipore, Germany), and the chambers were dried 1 h before use. After a 24 h serum withdrawal, cells (2×10^5 cells/mL) were added to the chamber, and mJPYZ decoction with different concentrations were set into the 24-well plates. After 48 h, the migrated cells were fixed with 95% ethanol and stained with crystal violet. Photos of each group were taken under a microscope, and sections were counted randomly.

Flow Cytometry Analysis of Apoptosis and Cell Cycle

Cells were seeded in 6-well plates for 24 h, and treated with 0, 2, 4, and 8 mg/mL mJPYZ for 48 h. Cells were then harvested and stained with annexin V-FITC and PI, and detected by flow cytometry. For cell cycle, cells were then harvested and fixed with 75% ethanol, and was determined using propidium iodide (PI) staining and FACSAria III flow cytometer (BD Biosciences, USA) analysis according to the manufacturer's protocol.

Western Blotting Analysis

Total protein was extracted from cells using RIPA lysis buffer. The nuclear and cytoplasmic protein was extracted using a commercial kit (Yeasen Biotechnology, Shanghai, China). The protein concentration was determined with a BCA kit. Different groups of protein were separated using sodium dodecyl sulfate polyacrylamide gel electrophoresis (SDS-PAGE) and transferred to polyvinylidene difluoride (PVDF) membranes (Millipore, Billerica, MA, USA). After blocking with 5% nonfat milk for 1 h at room temperature, the membranes were incubated with 1:1000 primary antibodies E-cadherin (Cell Signaling Technology, #3195), N-cadherin (Proteintech, 22018-1-AP), Vimentin (Cell Signaling Technology, #5741), MMP-9 (Cell Signaling Technology, #13667), MMP-2 (Cell Signaling Technology, #40994), β-Actin (Cell Signaling Technology, #8457), HK2 (Proteintech, 22029-1-AP), PFKFB3 (Proteintech, 13763-1-AP), PDK1 (Cell Signaling Technology, #3062), PDK4 (Abcam, ab89295), PKM2 (Proteintech, 15922-1-AP), HIF-1α (Bioss, bs-0737R/Abcam, ab51608), Lamin B1 (Proteintech, 12987-1-AP) at 4°C overnight. Then the membranes were incubated with secondary antibodies at room temperature for 1 h. The membranes were finally scanned with a Bio-rad ChemiDoc XRS+ (Berkeley, CA, USA).

Co-Immunoprecipitation (Co-IP) Assay

To analyze interactions of HIF-1α protein with related proteins, cells seeded in 10-cm-diameter culture dishes were lysed, followed by centrifugation at 15,000 ×g for 15 min. Supernatants were precipitated with Rabbit IgG or HIF-1α specific Polyclonal antibody (Abcam, Cambridge, UK) and incubated with gentle rocking overnight at 4°C. Protein A/G beads washed with cell lysate were added to supernatant fractions and incubated with gentle rocking for 12 h at 4°C. The beads were then washed four times with cold cell lysate and boiled with 1 × SDS loading buffer for 10 min, followed by SDS-PAGE. The same ways to analyze interactions of HIF-1α protein with related proteins.

Biochemical Assays

The lactate concentration of the cell supernatant or the plasma were determined using a Lactate Testing Kit (Jian cheng Bioengineering Institute, Nanjing, China), according to the manufacture's protocol. And the glucose concentration of the cell supernatant or the plasma were determined using a Glucose Assay Kit (Rongsheng Biotechnology, Shanghai, China), according to the manufacture's protocol.

Immunofluorescence Staining

Cells were seeded in glass coverslips for 24 h, and treated with 8mg/mL mJPYZ for 48 h. The treated cell slices were fixed with 4% paraformaldehyde, washed with PBS, and incubated with primary antibodies against PKM2 at 4°C overnight. The next day, after incubation with fluorescence secondary antibody and 4′,6-diamidine-2-phenylindole, the slices were mounted and observed with an FV1000 laser scanning confocal microscope (Leica, Wetzlar, Germany). All double immunofluorescence images were captured under the same conditions. The co-localization analysis was performed using Image J software (NIH Image, Bethesda, MD, USA).

Plasmid Construction, Lentivirus Packaging, and Cell Transfection

The PKM2 overexpression lentivirus was synthesized by Shanghai Engineering Research Center of Cancer Drug Targets (Shanghai, China). Briefly, to create a recombinant plasmid overexpressing PKM2-OE, a full-length cDNA encoding the PKM2 sequence was amplified and cloned into the GV358 vector, which contained the component order Ubi-MCS-3FLAG-SV40-EGFR-IRES-puromycin. Then the recombinant plasmid was under identification and sequencing analysis. Finally, after plasmid extraction, got the highly-purified plasmid.

To establish a stable lentivirus transfection GC cell line, MGC-803, SGC-7901 and BGC-823 cells were seeded in 6-well plates, and when 60–70% confluent, they were transfected with PKM2-OE lentivirus in the presence of 5 μg/mL polybrene for 24 h. The positive cells were selected by puromycin and transfection efficiency was determined by inverted fluorescence microscope and western blotting.

Establishment of Xenograft Tumor Model

Mice (615-strain) were purchased from the Tianjin Institute of Blood (6 weeks old, weighing 18–22 g). All mice were maintained under standard conditions of 50% relative humidity, 21 ± 2°C, and a 12 h light cycle. Each mouse was inoculated with 0.2 mL of cell suspension (5×10^7/mL, MFC murine gastric cancer cells)in the right armpit after disinfection. The diameter of the induration reached 3–7 mm after 10 days, which shows the establishment of a successful model. Fifteen mice were divided randomly into 3 groups: control group (normal saline, NS 0.2 mL/10 g *via* gavage), 5-Fluorouracil (5-Fu) group (5-Fu 25 mg/kg *via* intraperitoneal injection) and mJPYZ group

(mJPYZ 15g/kg, 0.2mL/10 g *via* gavage). All the mice were medicated for 14 days (5-Fu intraperitoneal injection every other day) continuously. The weight of mice was recorded every 4 days and sacrificed on day 21. Tumors were excised from the animals and weighed immediately.

Mice (BALB/c-nu) were also purchased from the Tianjin Institute of Blood (6 weeks old, weighing 18–22 g). After adaptive culturing, nude mice were randomly divided into negative control (NC) group, PKM2 overexpression (PKM2-OE group) group and PKM2 overexpression with mJPYZ mediated (PKM2-OE+mJPYZ) group. SGC-7901 cells with stable expression of PKM2 were taken, cellular concentration was adjusted to 1×10^7 cells and they were inoculated beneath right axilla skin of each nude mouse with the inoculation density being 0.2ml. The growth status of subcutaneous xenograft in nude mice was closely observed.

The Experimental Animal Ethics Committee of Nanjing Medical University approved all animal experiments.

Extracellular Acidification Rate (ECAR) and Glycolysis Proton Efflux Rate (glycoPER)

Assays were performed using a Seahorse XFe24 analyzer (Seahorse Bioscience, Agilent Technologies) according to the Manufacturer's instructions. The ECAR was measured using a Seahorse XF Glycolytic Rate Assay Kit (Seahorse Bioscience, Agilent, 103344-100). The glycolytic capacities of cells were analyzed with the Seahorse XF Glycolysis Rate/Stress Test Report Generator package. The %PER from glycolysis was calculated by subtracting the acidification from CO_2 produced by the mitochondria, also called glycoPER.

Statistical Analysis

Each experiment was repeated at least three times. All quantitative data are expressed as the mean ± standard deviation (SD) and analyzed using GraphPad Prism 7.0 software (GraphPad Software, San Diego, CA, USA). The comparisons between two groups were analyzed by Student's t-tests (unpaired, two-tailed) or the one-way analysis of variance (ANOVA) (followed by Tukey's *post-hoc* tests). Statistical significance was defined as $P < 0.05$.

RESULTS

mJPYZ Inhibited Gastric Cancer Cells Proliferation, Migration and Invasion

MTT assay was used to determine the toxicity of mJPYZ on GC cell lines (MGC-803, SGC-7901, BGC-823), As shown in **Figure 1A**, mJPYZ inhibited the GC cells proliferation in a dose- and time-dependent manner. Meantime, the results of Scratch-healing showed that the wound healing speed of GC cells was significantly reduced when mJPYZ treatment, indicating that the cell migration ability was decreased, and it was positively correlated with the concentration of mJPYZ (**Figure 1B**). Transwell assay also confirmed that mJPYZ could inhibit the migration and invasion of gastric cancer (**Figures 1C, D**). Moreover, Western blot analyses of E-cadherin, N-cadherin, Vimentin, MMP-2 and MMP-9, which were all metastasis related proteins, suggested mJPYZ significantly inhibited EMT and invasion of GC cells (**Figures 1E, F**). Taken together, these results showed that mJPYZ significantly inhibited GC cells proliferation, migration and invasion.

mJPYZ Decreased Tumor Load and Metastasis in a Xenograft Tumor Model

Next, we established a xenograft tumor model using SGC-7901 GC cells to verify the effect of mJPYZ *in vivo*. As shown in **Figures 2A, B**, the treatment groups exhibited decreased tumor volume compared to the NC group after 15g/kg mJPYZ per day administration. The weights of the mice treated with 5-Fu was significantly reduced, while mJPYZ groups had no statistical difference (**Figure 2C**). Similar to the results of *in vitro*, we also found mJPYZ increased the protein expression levels of E-cadherin and decreased the levels of N-cadherin, Vimentin, which indicated that mJPYZ inhibited gastric cancer growth and EMT in the xenograft tumor (**Figures 2D–G**). These data suggested that mJPYZ controlled GC cells growth and metastasis by modulating EMT *in vivo*.

mJPYZ Reduced the Aerobic Glycolysis Level in GC Cells

To determine the underlying mechanism of mJPYZ on GC cells, we used network pharmacology and Gene Oncology (GO) analysis to investigate mJPYZ corresponding pathways participate in progress of gastric cancer. The results suggested that underlying modulate mechanism of mJPYZ on GC cells including cellular energy metabolism, HIF-1αsignaling etc. (**Figure 3A**). Previous studies have shown that robust aerobic glycolysis is associated with tumor invasion and metastasis. Therefore, we explored whether the anti-tumor activity of mJPYZ is related to aerobic glycolysis. As shown in **Figures 3B, C**, mJPYZ treatment for 48 h significantly inhibited glucose uptake and supernatant lactate levels in a dose-dependent manner. Moreover, mJPYZ administration decreased extracellular acidification rates (ECARs), glucose consumption and lactate production in GC cells compared with control group. Consistently, both basal glycolysis and compensatory glycolysis were abrogated by mJPYZ (**Figures 3D, E**). Additionally, microPET-CT images also confirmed the reduced ^{18}F-fluorodeoxyglucose (^{18}FDG) accumulation on tumor-bearing nude mice of mJPYZ treatment (**Figures 3F, G**). Therefore, target glucose metabolism may be a potential mechanism of mJPYZ in treatment of gastric cancer.

mJPYZ Inhibited the Expression and Nuclear Translocation of PKM2 in GC Cells

Given the rate-limiting enzymes role of HK2, PFKFB3 and PKM2 in aerobic glycolysis, we investigated the effect of mJPYZ on three key enzymes. Moreover, we observed the expression of pyruvate dehydrogenase kinases (PDKs), which dominate the synthesis of biological macromolecules in the

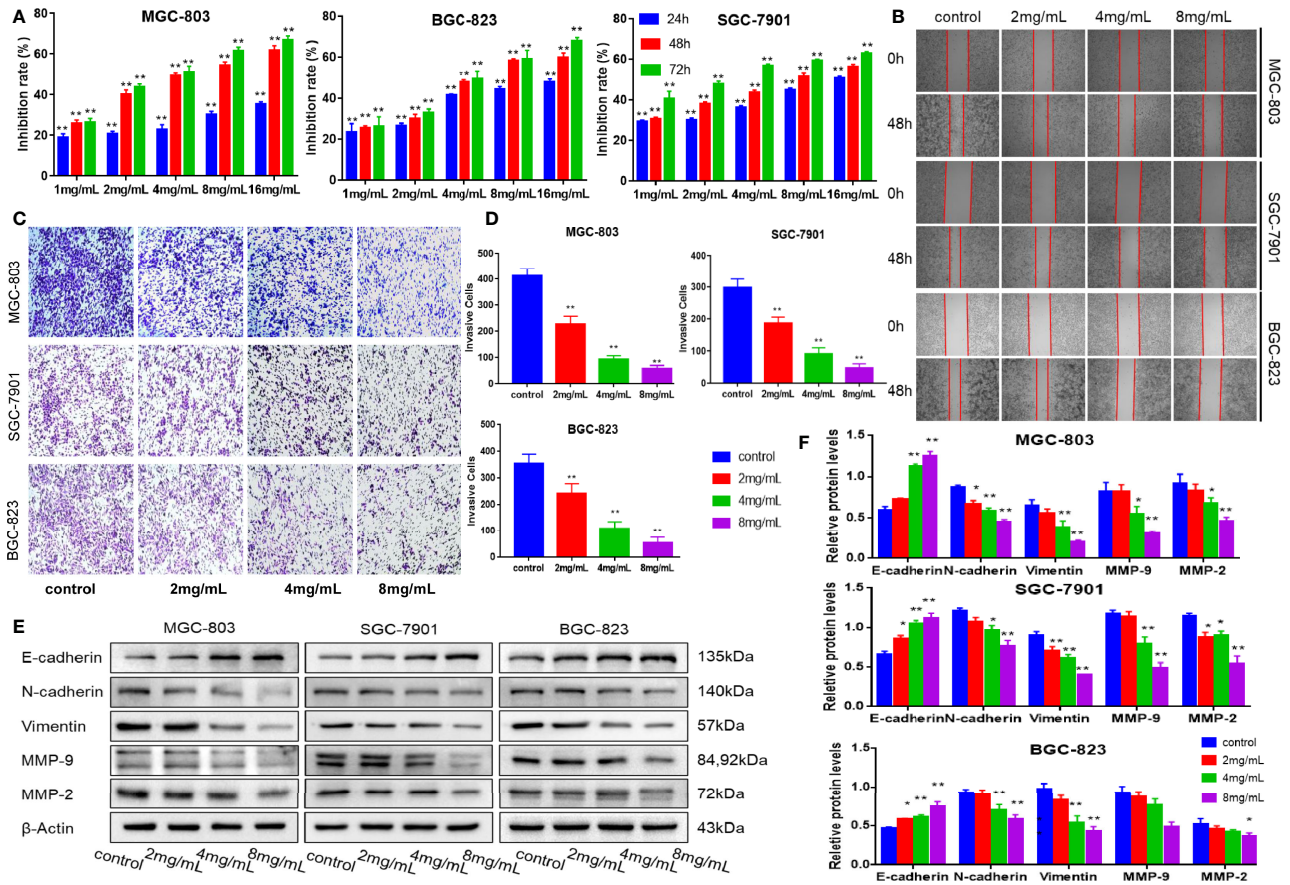

FIGURE 1 | mJPYZ inhibited the proliferation, migration and invasion of gastric cancer cells *in vitro*. **(A)** Viability of cancer cells interfered by mJPYZ was determined using the MTT assay. mJPYZ inhibited the GC cells proliferation in a dose- and time-dependent manner. **(B)** Migration of gastric cancer cells were detected by wound healing assay. The cell migration ability was decreased after mJPYZ treatment, and was positively correlated with the concentration of mJPYZ. **(C, D)** Invasion of gastric cancer cells were detected by Transwell invasion assay. The cell invasion ability was decreased after mJPYZ treatment, and was positively correlated with the concentration of mJPYZ. **(E, F)** Western blotting analysis of fundamental proteins related to EMT. mJPYZ treatment increased E-cadherin expression, while it decreased the expression of N-cadherin, Vimentin, MMP-9 and MMP-2 in a dose-dependent manner. Data are represented as mean ± SD, n=3 independent experiments. *P < 0.05, **P < 0.01 versus control group by one-way analysis of variance (ANOVA) followed by Tukey's *post-hoc* tests.

glycolysis of tumor cells. Western blot results showed that mJPYZ inhibited the expression of PKM2, which catalyses the last step of glycolysis, but had no obvious effect on the levels of HK2, PFKFB3, PDK1 and PDK4 (**Figures 4A, B**). Similarly, immunofluorescence results also revealed that mJPYZ treatment could reduce the intensity of PKM2 (**Figure 4C**).

In general, PKM2 functions as a metabolic kinase by forming the homotetramer in the cytoplasm. In our study, we discovered that mJPYZ suppressed PKM2 translocating into the nucleus, but increased in the cytoplasm *in vitro*, which might be important for the inhibitory effect of mJPYZ (**Figures 4D, E**). *In vivo*, western blot and immunofluorescence results also supported that mJPYZ decreased the expression of PKM2 (**Figures 4F–H**). Thus, it was confirmed that mJPYZ inhibited aerobic glycolysis in GC cells, which is related to the downregulated nuclear translocation of PKM2 both *in vivo* and *in vitro.*

Effect of mJPYZ in Gastric Cancer Aerobic Glycolysis Was Largely Dependent on PKM2

To verify whether mJPYZ reduced glucose uptake and lactate levels were depended on PKM2, we further examined the glucose uptake and lactate levels when PKM2 was over-expression (PKM2-OE) in GC cell lines (MGC-803,SGC-7901,BGC-823). The data showed PKM2-OE group displayed higher glucose consumption and lactate levels than the NC group, while mJPYZ treatment could inhibited GC lactate levels and glucose uptake effectively (**Figures 5A, B**). Consistent with these results, the ECAR and %PER from glycolysis were decreased with mJPYZ treatment, but this phenomenon was reversed by over expression of PKM2 (**Figures 5C, D**). Together, our results suggested that mJPYZ regulated metabolic reprogramming was obviously dependent on PKM2.

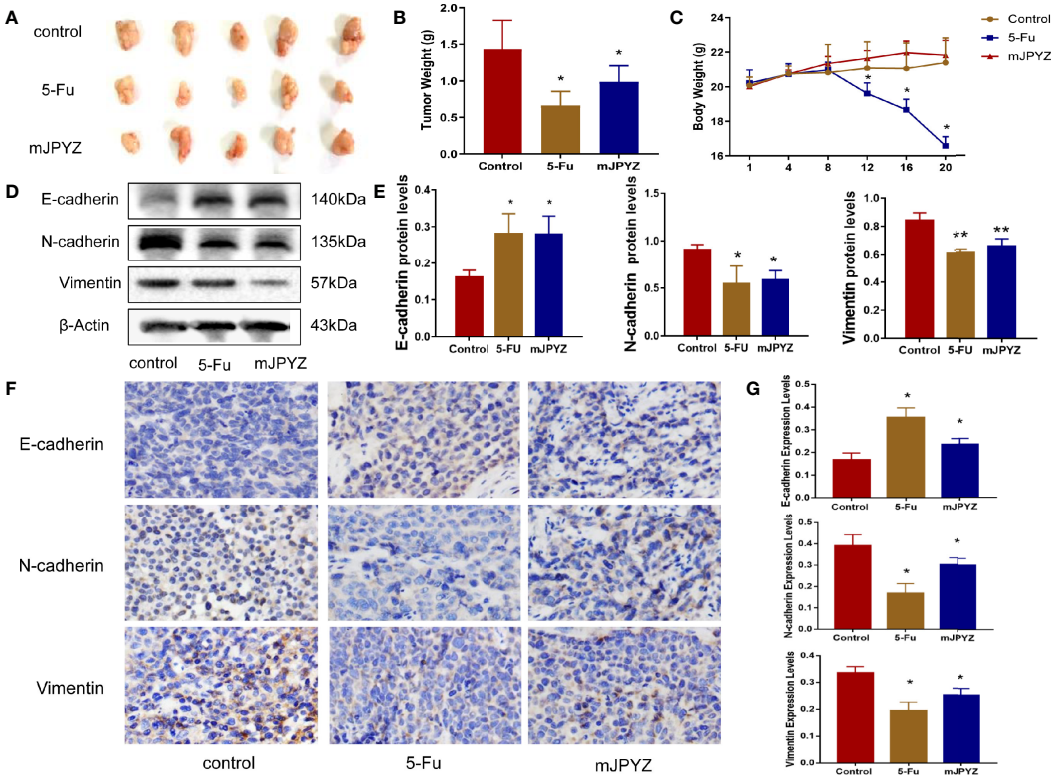

FIGURE 2 | mJPYZ decreased tumor growth and metastasis *in vivo*. **(A)** The gross manifestation and volumes of tumors. **(B)** The tumor weight. **(C)** The weight of the mice which recorded every 4 days. Effect of mJPYZ on the growth of SGC-7901 xenograft tumors (n = 5). **(D, E)** Western blotting analysis xenograft tumor tissues of essential proteins related to EMT. **(F, G)** Immunohistochemistry showed the rates of E-cadherin, N-cadherin and Vimentin expression. Compared to control, mJPYZ treatment increased the levels of E-cadherin, while decreased the levels of N-cadherin and Vimentin. Data are represented as mean ± SD, n=5 mice or n=3 independent experiments. *P < 0.05, **P < 0.01 versus control group by one-way analysis of variance (ANOVA) followed by Tukey's *post-hoc* tests.

mJPYZ Disrupted the PKM2/HIF-1α Signaling Pathway in GC Cells

It has been indicated that PKM2 may directly interact with HIF-1α in nuclear and promote transcriptional activation of HIF-1α target genes (15). Therefore, we firstly checked the influence of mJPYZ to HIF-1α in GC cell lines. As expect, our results showed the expression of HIF-1α was significantly suppressed by mJPYZ, and PKM2 could induce the expression of HIF-1α (**Figures 6A, B**). Similarly, we also found mJPYZ inhibited the HIF-1α expression *in vivo* (**Figures 6C, D**). Furthermore, co-immunoprecipitation was then conducted to determine the relationship between PKM2 and HIF-1α in GC cell lines, the results clearly confirmed the strong interaction of HIF-1α and PKM2 (**Figures 6E, F**). Moreover, mJPYZ treatment increased HIF-1α ubiquitination levels in a dose-dependently manner (**Figure 6G**). Above results suggested PKM2/HIF-1α was the key metabolic regulator of mJPYZ in GC cells.

Overexpression of PKM2 Could Reverse the Inhibitory Effect of mJPYZ on GC Cells Proliferation, Migration and EMT

Further, we determined the role of PKM2 in migration and EMT of GC cell lines. As shown in **Figure 7A**, the protein levels of N-cadherin and vimentin were enhanced, while the levels of E-cadherin were decreased in the PKM2-OE group, and mJPYZ treatment could reverse it (**Figures 7A, B**). Similarly, we also showed PKM2 overexpression partially reversed the migration inhibitory effect of mJPYZ in GC cells (**Figures 7C, D**). In addition, *in vivo* study revealed that mJPYZ treatment could disrupt PKM2 induced tumor growth. Western blot analysis tissue of GC also indicated that mJPYZ interfered PKM2 overexpression caused EMT related gene expression (**Figures 7E–I**). These results further indicated that PKM2 was actually the target of mJPYZ, and mJPYZ induced GC cell growth inhibition and migration were partially regulated by PKM2-mediated glycolysis.

Chemical Components in mJPYZ and Binding Site Analysis of the mJPYZ-PKM2

To investigate whether chemical constituents are involved in the regulation of activation of PKM2 by direct interaction, we performed LC-ESI-MS/MS. The mass spectrometer parameters were: spray voltage, 3 000 eV (-), 4 000 eV (+); capillary temperature, 350℃; shealth gas pressure, 30 psi; auxiliary gas, 10 psi; The ions were detected (selective reaction monitoring) under positive and negative mode with the optimized parameters

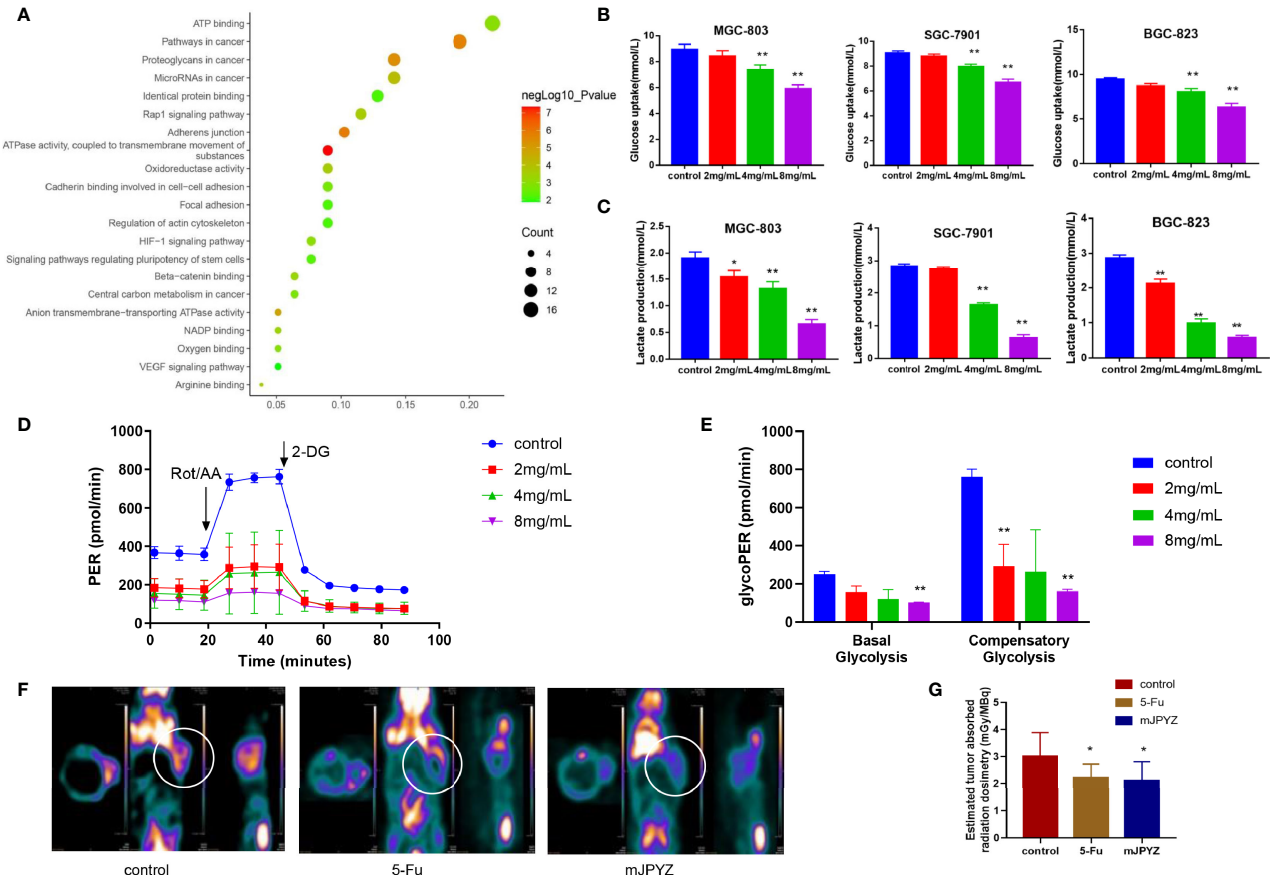

FIGURE 3 | The effects of mJPYZ on EMT of gastric cancer cells depended on aerobic glycolysis. **(A)** Network pharmacology and Gene Oncology (GO) analysis investigated mJPYZ corresponding pathways participate in progress of gastric cancer and found related to aerobic glycolysis. **(B, C)** The effect of mJPYZ on the glucose uptake and lactate production levels in gastric cancer cells. **(D, E)** Extracellular acidification rates (ECAR) and Proton Efflux Rate (PER) were measured in SGC-7901 cells by Seahorse XFe assays. Quantification of the PER from glycolysis of mJPYZ with control group. mJPYZ administration decreased ECARs, PER, glucose consumption and lactate production in GC cells compared with control group. **(F, G)** MicroPET-CT on tumor-bearing nude mice. After mJPYZ treatment, 18F-fluorodeoxyglucose (^{18}FDG) accumulation was reduced in tumor. Data are represented as mean ± SD, n=3 independent experiments. *P < 0.05, **P < 0.01 versus control group by one-way analysis of variance (ANOVA) followed by Tukey's *post-hoc* tests.

(**Table S1**). Typical XIC chromatograms of 7 major constituents in mJPYZ and mixture standards are shown in **Figures 8A, B** The contents of rutin, lobetyolin, calycosin-7-glucoside, formononetin, calycosin, ononin and p-coumaric acid in the decoction were finally determined as 0.89 μg/g, 2.01 μg/g, 105.22 μg/g, 25.88 μg/g, 71.26 μg/g, 80.48 μg/g and 19.56 μg/g, respectively. Then we conducted a molecular docking of the binding modes of PKM2 with the 7 compounds. The results showed rutin, calycosin, formononetin and calycosin-7-glucoside had strong affinity with PKM2 (**Figures 8B, C**). These data suggested that chemical compounds from mJPYZ had unerlying binding sites with PKM2 that may influence the activity or stability of PKM2.

DISCUSSION

Cancer cells undergo complex metabolic regulations and alterations, and targeting metabolic reprogramming refers to a novel therapeutic approaches for cancer treatment (16). Recent studies show chemically synthesized small molecule inhibitors of critical metabolic enzymes are regarded as potentially promising antitumor agents. However, their coexisting non-specific cytotoxicity impairs the proliferation of normal cells, such as immune cells and stem cells, and may lead to severe side effects or drug resistance (17). Therefore, finding or developing more effective and safer drugs or decoctions from herbs is of constructive significance to the development of anticancer drugs. Here, we reported a multi-herb-combined decoction with no obvious cytoxicity, and found mJPYZ significantly reduced the aerobic glycolysis level in GC *in vivo* and *in vitro*, and identified PKM2 is the main target.

As well known, TCM has been widely used a complementary approach for cancer treatment in China over hundreds of years (18). GC is the most prevalent cancer in East Asia (1). Extensive evidence indicated that TCM possesses definite advantages in GC, especially for advanced patients (19, 20). According to the

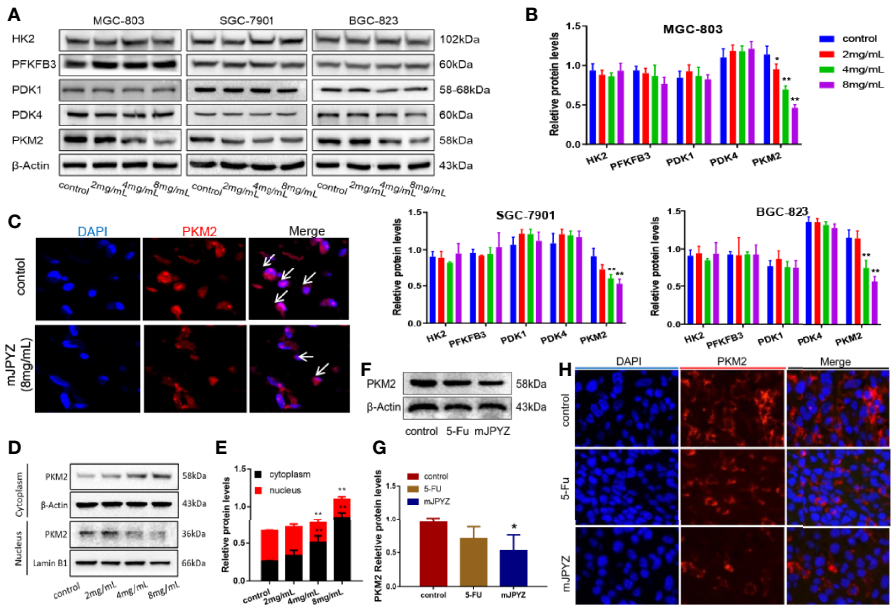

FIGURE 4 | mJPYZ effected the expression and location of PKM2 in gastric cancer. **(A, B)** Western blotting analysis of three rate-limiting enzymes and ATP related enzymes. mJPYZ treatment decreased the expression of PKM2 in a dose-dependent manner, while the others expression unchanged. **(C)** Immunofluorescence showed PKM2 expression was reduced after mJPYZ treatment *in vitro*. **(D, E)** mJPYZ suppressed PKM2 translocating into the nucleus, meanwhile increased in the cytoplasm. **(F, G)** Western blotting analysis of PKM2 expression *in vivo*. mJPYZ treatment decreased the expression of PKM2. **(H)** Immunofluorescence showed PKM2 expression was reduced after mJPYZ *in vivo*. Data are represented as mean ± SD, n=3 independent experiments. *P < 0.05, **P < 0.01 versus control group by the one-way analysis of variance (ANOVA) followed by Tukey's *post-hoc* tests.

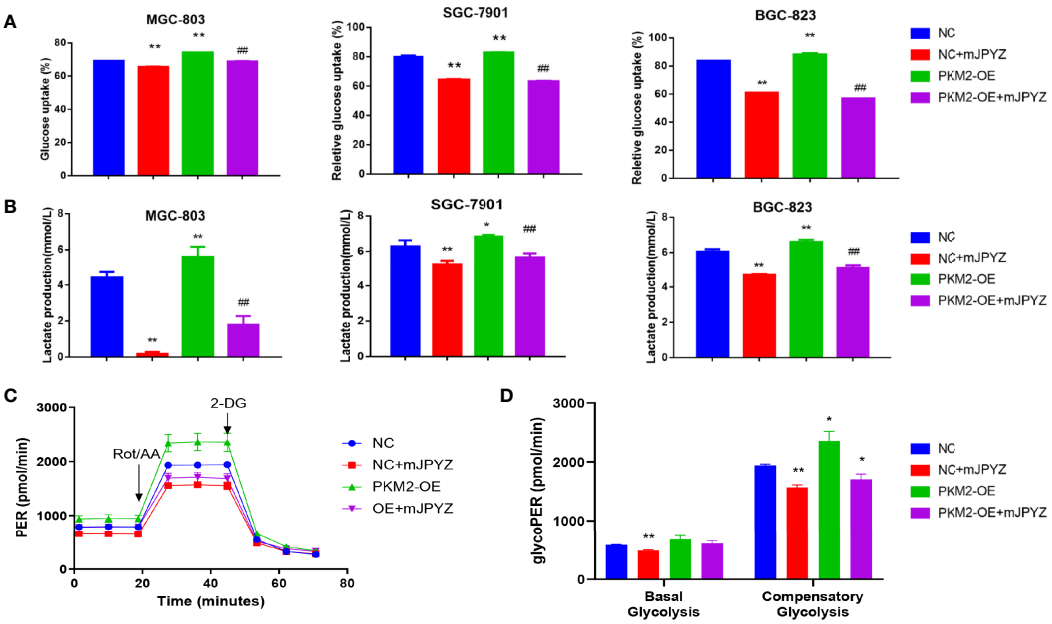

FIGURE 5 | mJPYZ modulated PKM2 and influenced gastric cancer aerobic glycolysis. **(A, B)** The effects of mJPYZ on the glucose uptake and lactate production levels in Negative Control (NC) and PKM2 overexpression gastric cancer cells. **(C, D)** Extracellular acidification rates (ECAR) and Proton Efflux Rate (PER) were measured in gastric cancer cells by Seahorse XFe assays. mJPYZ administration decreased ECARs, PER, glucose consumption and lactate production in NC or PKM2-OE compared with untreated control. Data are represented as mean ± SD, n=3 independent experiments. *P < 0.05, **P < 0.01 versus NC group, ##P < 0.01 versus PKM2-OE group by one-way analysis of variance (ANOVA) followed by Tukey's *post-hoc* tests.

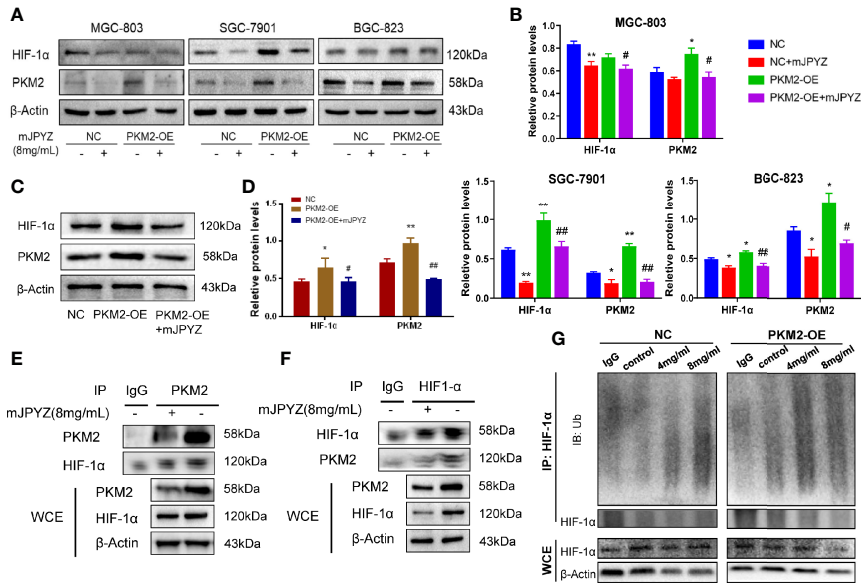

FIGURE 6 | mJPYZ impaired PKM2/HIF-1α signaling pathway. **(A–C)** The effects of PKM2 overexpression on interacted HIF-1α by western blotting. PKM2-OE induced increased PKM2 and HIF-1α, while mJPYZ treatment decreased the expression of PKM2 and HIF-1α whether in NC or PKM2-OE, compared with untreated control. **(D)** Western blotting showed mJPYZ treatment decreased the expression of PKM2 and HIF-1α *in vivo*. **(E, F)** Co-IP analysis of the interaction between PKM2 and HIF1-α in gastric cancer cells. **(G)** mJPYZ treatment increased HIF-1α ubiquitination degradation in a dose-dependently manner. Data are represented as mean ± SD, n=3 independent experiments. *P < 0.05, **P < 0.01 versus NC group, #P < 0.05, ##P < 0.01 versus PKM2-OE group by one-way analysis of variance (ANOVA) followed by Tukey's *post-hoc* tests.

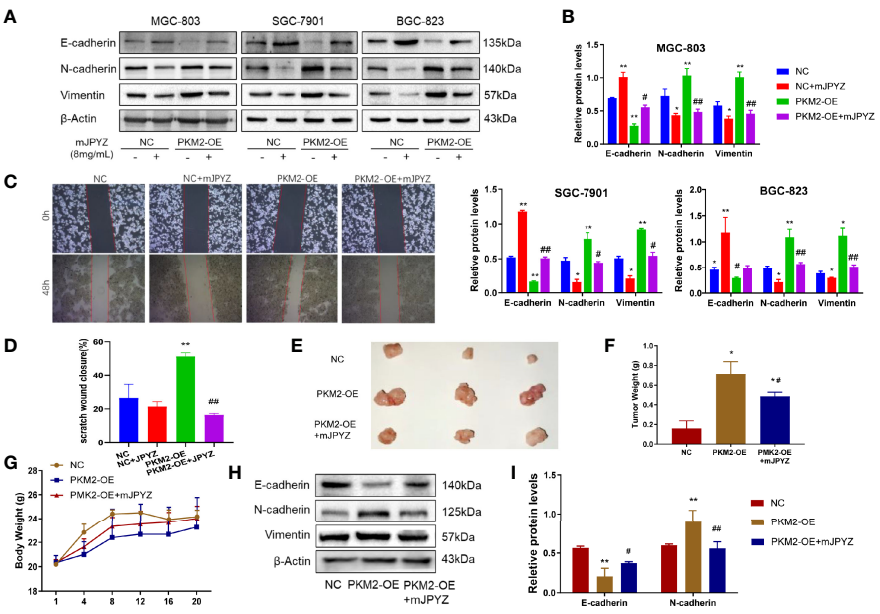

FIGURE 7 | Overexpression of PKM2 reversed the effect of mJPYZ on gastric cancer. **(A, B)** PKM2 affected the effect of mJPYZ on gastric cancer EMT related proteins. **(C, D)** Wound healing assay showed overexpression of PKM2 reversed the mJPYZ influence on migration. **(E–G)** mJPYZ still significantly inhibited the xenograft tumors growth although overexpression of PKM2, while the mice body weight still. **(H, I)** Western blotting analysis of overexpression of PKM2 affected the EMT essential proteins *in vivo*. Data are represented as mean ± SD, n=3 mice or n=3 independent experiments. #P < 0.05, ##P < 0.01 versus PKM2-OE group. *P < 0.05, **P < 0.01 versus control group by one-way analysis of variance (ANOVA) followed by Tukey's *post-hoc* tests.

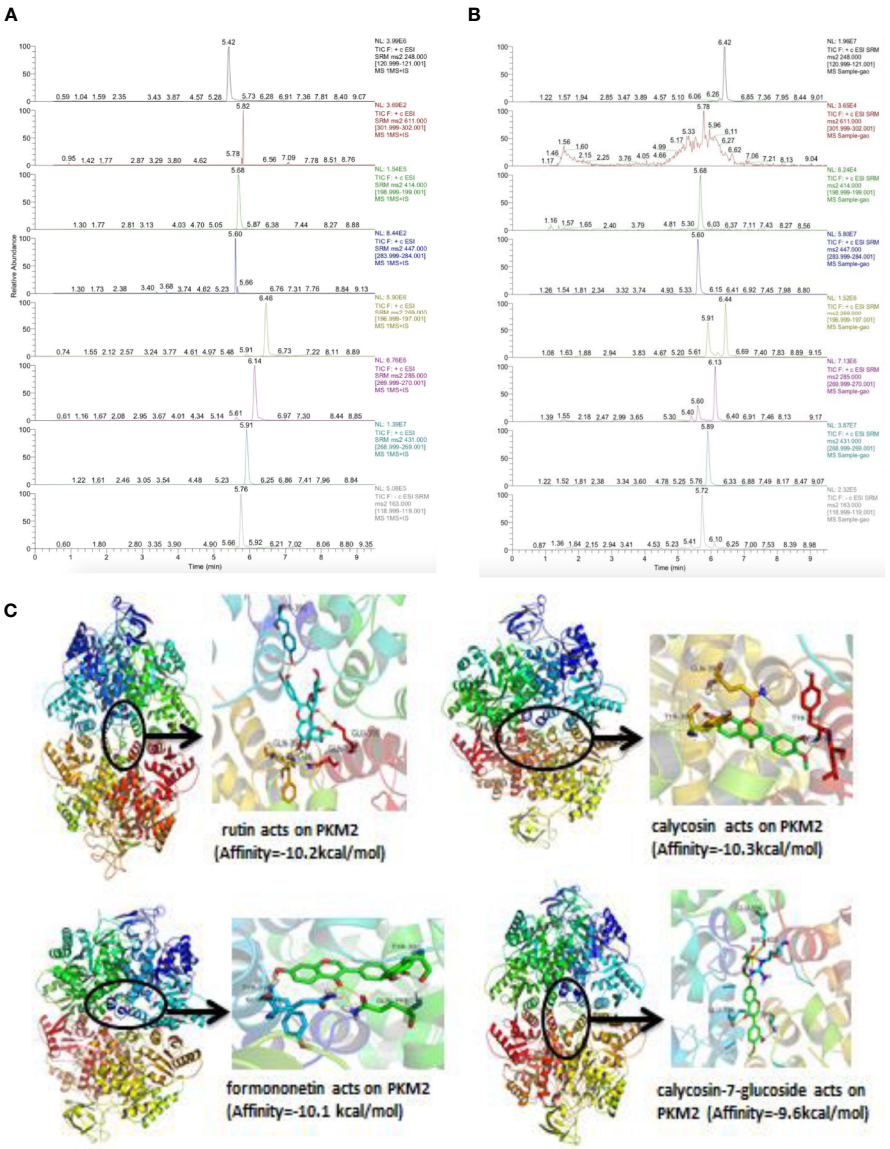

FIGURE 8 | Chemical components in mJPYZ showed strong affinity with PKM2. **(A, B)** The major chemical constituents in mJPYZ and mixture standards were analyzed by LC-ESI-MS/MS analysis. **(C)** Molecular docking of the binding modes of PKM2 with the major compounds in mJPYZ. The results showed rutin, calycosin, formononetin and calycosin-7-glucoside had strong affinity with PKM2.

clinical practice, we use the "Qi-invigorating, spleen-strengthening and stasis-removing" method in treating gastric cancer, and obtain a good efficacy in patients (4). mJPYZ as a representative decoction shows obvious advantage for gastric cancer by modulating TAM differentiation (5). In tumor microenvironment, lactate produced by cancer cells has a critical function in TAM polarization (21). Therefore, combined network pharmacology, we speculated that mJPYZ may affect tumor cells glucose metabolic reprogramming by regulating glycolysis. Consequently, we found mJPYZ significantly inhibited gastric cancer cells proliferation and invasion, and reduced the aerobic glycolysis level by dependent on PKM2 in GC cells.

Numerous studies suggest a key role for PKM2 in aerobic glycolysis of cancer. PKM2 is the rate-limiting enzyme that catalyzes the conversion of phosphoenolpyruvate to pyruvate, which is the final step in the glycolytic pathway (22). It has been indicated that PKM2 might be promising molecular target for the treatment of gastric cancer (8). PKM2 exists primarily as an inactive monomer or dimer, when it translocate to the nucleus, which will interact with HIF-1α and regulate expression of numerous proglycolytic enzymes (23). Our study showed mJPYZ inhibited the expression of PKM2, and suppressed PKM2 translocating into the nucleus in GC cells. Moreover, our study also revealed that the overexpression of PKM2 displayed higher glucose consumption and lactate levels.

Hence, the inhibition of abnormal PKM2 was critical for the suppression effect of mJPYZ on GC.

As previously mentioned, PKM2 may translocates into the nucleus and forms a complex with HIF-1α to cause an glucose metabolism reprogramming from OXPHOS to glycolysis, as well as facilitates angiogenesis and EMT in cancer by stimulating the target genes (24–26). HIF-1α regulates a variety of tumor processes for adaptation, including metabolism, angiogenesis, invasion and cell proliferation. Studies showed that HIF-1α could modulate various EMT transcription factors, histone modifiers, enzymes (MMPs), chemokine receptors (27). Therefore, we checked the effect of mJPYZ to HIF-1α in GC cells, and observed that decreased expression level of HIF-1α when mJPYZ treatment. The positive correlation between PKM2 and HIF-1α was also confirmed by PKM2-OE. In agreement with previous reports, we verified that HIF-1α could interact with PKM2 using Co-IP in GC cells. PKM2 lead to a positive feedback loop that amplifies HIF-1 activity and may enhance metabolic reprogramming. Prolyl-hydroxylated HIF-1α binds to the von Hippel-Lindau (VHL) tumor suppressor protein, which recruits the E3- ubiquitin-ligase complex and causes proteasome degradation of HIF-1α (26). Thus, HIF-1α ubiquitination degradation is the key to blocking downstream signal activation. Here we identified that mJPYZ treatment increased HIF-1α ubiquitination levels in a dose-dependently manner.

CONCLUSION

In summary, our present study suggested that high expression of PKM2 is required for maintaining the malignant phenotype of GC cells. The TCM decoction mJPYZ inhibited GC cells growth and EMT by reducing of glycolysis in PKM2/HIF-1α signaling-dependent manner. This evidence expanded our understanding of the anti-tumor mechanism of mJPYZ and further indicated mJPYZ a potential anti-tumor agent for GC patients.

DATA AVAILABILITY STATEMENT

The original contributions presented in the study are included in the article/**Supplementary Material**. Further inquiries can be directed to the corresponding author.

ETHICS STATEMENT

The animal study was reviewed and approved by The Experimental Animal Ethics Committee of Nanjing Medical University.

AUTHOR CONTRIBUTIONS

QS and JW conceptualized the research hypothesis and designed the study. MY, HXW, XZ, RZ, HDW, XC, and MZ performed the laboratory experiments. MY and HXW performed the statistical analysis and data interpretation. QS, JW, and MY interpreted the results and wrote the manuscript. All authors performed critical revision of the final manuscript. SL supervised the study. All authors contributed to the article and approved the submitted version.

FUNDING

This study was supported by National Natural Science Foundation of China (No. 81973609, 81973782, 82174197, 81704031), Science and Technology Planning Project of Jiangsu Province, China (No. BK20211392), Jiangsu Provincial Medical Youth Talent (QNRC2016641), "333" Project of Jiangsu Province (LGY2018065), Jiangsu Provincial Hospital of Traditional Chinese Medicine Academic Talent Program (Y2018RC33); A Project Funded by the Priority Academic Program Development of Jiangsu Higher Education Institutions (PAPD), The Open Projects of the Discipline of Chinese Medicine of Nanjing University of Chinese Medicine Supported by the Subject of Academic priority discipline of Jiangsu Higher Education Institutions (ZYX03KF019, ZYX03KF021, ZYX03KF029). Postgraduate Research &Practice Innovation Program of Jiangsu Province (SJCX21_0692).

SUPPLEMENTARY MATERIAL

The Supplementary Material for this article can be found online at: https://www.frontiersin.org/articles/10.3389/fonc.2021.767116/full#supplementary-material

REFERENCES

1. Sung H, Ferlay J, Siegel RL, Laversanne M, Soerjomataram I, Jemal A, et al. Global Cancer Statistics 2020: GLOBOCAN Estimates of Incidence and Mortality Worldwide for 36 Cancers in 185 Countries. *CA: Cancer J Clin* (2021) 71(3):209–49. doi: 10.3322/caac.21660
2. Wang K, Chen Q, Shao Y, Yin S, Liu C, Liu Y, et al. Anticancer Activities of TCM and Their Active Components Against Tumor Metastasis. *BioMed Pharmacother* (2021) 133:111044. doi: 10.1016/j.biopha.2020.111044
3. Zou X, Chen YC, Shou-You HU, Wang RP, Wang XX, Liu SL, et al. Effect of Jianpi Yangzheng Xiaozheng Fang on Survival and Life Quality of Cases With Late Stage Gastric Cancer. *J Nanjing Univ Traditional Chin Med* (2015) 31 (3):201–5. doi: 10.14148/j.issn.1672-0482.2015.0201
4. Wu J, Zhang XX, Zou X, Wang M, Wang HX, Wang YH, et al. The Effect of Jianpi Yangzheng Xiaozheng Decoction and Its Components on Gastric Cancer. *J Ethnopharmacol* (2019) 235:56–64. doi: 10.1016/j.jep.2019.02.003
5. Yuan M, Zou X, Liu S, Xu X, Wang H, Zhu M, et al. Modified Jian-Pi-Yang-Zheng Decoction Inhibits Gastric Cancer Progression *via* the Macrophage Immune Checkpoint PI3Kgamma. *BioMed Pharmacother* (2020) 129:110440. doi: 10.1016/j.biopha.2020.110440
6. DeBerardinis RJ, Chandel NS. Fundamentals of Cancer Metabolism. *Sci Adv* (2016) 2(5):e1600200. doi: 10.1126/sciadv.1600200
7. Cairns RA, Harris IS, Mak TW. Regulation of Cancer Cell Metabolism. *Nat Rev Cancer* (2011) 11(2):85–95. doi: 10.1038/nrc2981
8. Kitayama K, Yashiro M, Morisaki T, Miki Y, Okuno T, Kinoshita H, et al. Pyruvate Kinase Isozyme M2 and Glutaminase Might be Promising

Molecular Targets for the Treatment of Gastric Cancer. *Cancer Sci* (2017) 108 (12):2462–9. doi: 10.1111/cas.13421
9. Liu Y, Zhang Z, Wang J, Chen C, Tang X, Zhu J, et al. Metabolic Reprogramming Results in Abnormal Glycolysis in Gastric Cancer: A Review. *Oncol Targets Ther* (2019) 12:1195–204. doi: 10.2147/OTT.S189687
10. Zhang T, Suo C, Zheng C, Zhang H. Hypoxia and Metabolism in Metastasis. *Adv Exp Med Biol* (2019) 1136:87–95. doi: 10.1007/978-3-030-12734-3_6
11. Yang W, Lu Z. Regulation and Function of Pyruvate Kinase M2 in Cancer. *Cancer Lett* (2013) 339(2):153–8. doi: 10.1016/j.canlet.2013.06.008
12. Wang C, Jiang J, Ji J, Cai Q, Chen X, Yu Y, et al. PKM2 Promotes Cell Migration and Inhibits Autophagy by Mediating PI3K/AKT Activation and Contributes to the Malignant Development of Gastric Cancer. *Sci Rep* (2017) 7 (1):2886. doi: 10.1038/s41598-017-03031-1
13. Hamanaka RB, Chandel NS. Cell Biology. Warburg Effect and Redox Balance. *Science* (2011) 334(6060):1219–20. doi: 10.1126/science.1215637
14. Wang S, Fu JL, Hao HF, Jiao YN, Li PP, Han SY. Metabolic Reprogramming by Traditional Chinese Medicine and Its Role in Effective Cancer Therapy. *Pharmacol Res* (2021) 170:105728. doi: 10.1016/j.phrs.2021.105728
15. van, den, Bosch MWM, Craig T, Jian-kang J. Pyruvate Kinase M2 Regulates Hif-1 Alpha Activity and IL-1 Beta Induction and Is a Critical Determinant of the Warburg Effect in LPS-Activated Macrophages (Vol 21, Pg 65, 2015). *Cell Metab* (2015) 21(2):347–7. doi: 10.1016/j.cmet.2015.01.017
16. Altman BJ, Stine ZE, Dang CV. From Krebs to Clinic: Glutamine Metabolism to Cancer Therapy. *Nat Rev Cancer* (2016) 16(12):773. doi: 10.1038/nrc.2016.131
17. Erez A, DeBerardinis RJ. Metabolic Dysregulation in Monogenic Disorders and Cancer - Finding Method in Madness. *Nat Rev Cancer* (2015) 15(7):440–8. doi: 10.1038/nrc3949
18. Wang Z, Qi F, Cui Y, Zhao L, Sun X, Tang W, et al. An Update on Chinese Herbal Medicines as Adjuvant Treatment of Anticancer Therapeutics. *Biosci Trends* (2018) 12(3):220–39. doi: 10.5582/bst.2018.01144
19. Huang WJ, Ruan S, Wen F, Lu XN, Gu SP, Chen XX, et al. Multidrug Resistance of Gastric Cancer: The Mechanisms and Chinese Medicine Reversal Agents. *Cancer Manag Res* (2020) 12:12385–94. doi: 10.2147/CMAR.S274599
20. Lee YK, Bae K, Yoo HS, Cho SH. Benefit of Adjuvant Traditional Herbal Medicine With Chemotherapy for Resectable Gastric Cancer. *Integr Cancer Ther* (2018) 17(3):619–27. doi: 10.1177/1534735417753542
21. Elia I, Haigis MC. Metabolites and the Tumour Microenvironment: From Cellular Mechanisms to Systemic Metabolism. *Nat Metab* (2021) 3(1):21–32. doi: 10.1038/s42255-020-00317-z
22. Gao X, Wang H, Yang JJ, Liu X, Liu ZR. Pyruvate Kinase M2 Regulates Gene Transcription by Acting as a Protein Kinase. *Mol Cell* (2012) 45(5):598–609. doi: 10.1016/j.molcel.2012.01.001
23. Dong T, Yan Y, Chai H, Chen S, Xiong X, Sun D, et al. Pyruvate Kinase M2 Affects Liver Cancer Cell Behavior Through Up-Regulation of HIF-1alpha and Bcl-xL in Culture. *BioMed Pharmacother* (2015) 69:277–84. doi: 10.1016/j.biopha.2014.12.010
24. Wang HJ, Hsieh YJ, Cheng WC, Lin CP, Lin YS, Yang SF, et al. JMJD5 Regulates PKM2 Nuclear Translocation and Reprograms HIF-1alpha-Mediated Glucose Metabolism. *Proc Natl Acad Sci USA* (2014) 111(1):279–84. doi: 10.1073/pnas.1311249111
25. Feng J, Wu L, Ji J, Chen K, Yu Q, Zhang J, et al. PKM2 is the Target of Proanthocyanidin B2 During the Inhibition of Hepatocellular Carcinoma. *J Exp Clin Cancer Res* (2019) 38(1):204. doi: 10.1186/s13046-019-1194-z
26. Luo W, Hu H, Chang R, Zhong J, Knabel M, O'Meally R, et al. Pyruvate Kinase M2 is a PHD3-Stimulated Coactivator for Hypoxia-Inducible Factor 1. *Cell* (2011) 145(5):732–44. doi: 10.1016/j.cell.2011.03.054
27. Tam SY, Wu VWC, Law HKW. Hypoxia-Induced Epithelial-Mesenchymal Transition in Cancers: HIF-1alpha and Beyond. *Front Oncol* (2020) 10:486. doi: 10.3389/fonc.2020.00486

Conflict of Interest: The authors declare that the research was conducted in the absence of any commercial or financial relationships that could be construed as a potential conflict of interest.

Publisher's Note: All claims expressed in this article are solely those of the authors and do not necessarily represent those of their affiliated organizations, or those of the publisher, the editors and the reviewers. Any product that may be evaluated in this article, or claim that may be made by its manufacturer, is not guaranteed or endorsed by the publisher.

frontiers in Pharmacology

ORIGINAL RESEARCH
published: 03 December 2021
doi: 10.3389/fphar.2021.670167

Antiproliferative, Antiangiogenic, and Antimetastatic Therapy Response by Mangiferin in a Syngeneic Immunocompetent Colorectal Cancer Mouse Model Involves Changes in Mitochondrial Energy Metabolism

Julio César Rodriguez-Gonzalez[1†], Ivones Hernández-Balmaseda[2†], Ken Declerck[3], Claudina Pérez-Novo[3], Emilie Logie[3], Claudia Theys[3], Patrycja Jakubek[3,4], Olga Luisa Quiñones-Maza[1], Geovanni Dantas-Cassali[5], Diego Carlos dos Reis[5], Guy Van Camp[6], Miriam Teresa Lopes Paz[5], Idania Rodeiro-Guerra[2], René Delgado-Hernández[7,8] and Wim Vanden Berghe[3]**

[1]Centro de Investigación y Desarrollo de Medicamentos (CIDEM), La Habana, Cuba, [2]Laboratorio de Farmacología, Instituto de Ciencias del Mar (ICIMAR), CITMA, La Habana, Cuba, [3]Laboratory of Protein Science, Proteomics and Epigenetic Signaling (PPES) and Integrated Personalized and Precision Oncology Network (IPPON), Department of Biomedical Sciences, University of Antwerp, Campus Drie Eiken, Antwerp, Belgium, [4]Department of Food Chemistry, Technology and Biotechnology, Faculty of Chemistry, Gdansk University of Technology, Gdansk, Poland, [5]Departamento de Farmacología, Instituto de Ciencias Biológicas (ICB), Universidad Federal de Minas Gerais (UFMG), Horizonte, Brazil, [6]Center of Medical Genetics, University of Antwerp and Antwerp University Hospital, Antwerp, Belgium, [7]Centro de Estudios para las Investigaciones y Evaluaciones Biológicas (CEIEB), Instituto de Farmacia y Alimentos (IFAL), Universidad de La Habana, La Habana, Cuba, [8]Facultad de Ciencias Naturales y Agropecuarias, Universidat de Santander (UDES), Bucaramanga, Colombia

In spite of the current advances and achievements in cancer treatments, colorectal cancer (CRC) persists as one of the most prevalent and deadly tumor types in both men and women worldwide. Drug resistance, adverse side effects and high rate of angiogenesis, metastasis and tumor relapse remain one of the greatest challenges in long-term management of CRC and urges need for new leads of anticancer drugs. We demonstrate that CRC treatment with the phytopharmaceutical mangiferin (MGF), a glucosylxanthone present in Mango tree stem bark and leaves (*Mangifera Indica L.*), induces dose-dependent tumor regression and decreases lung metastasis in a syngeneic immunocompetent allograft mouse model of murine CT26 colon carcinoma, which increases overall survival of mice. Antimetastatic and antiangiogenic MGF effects could be further validated in a wound healing *in vitro* model in human HT29 cells and in a matrigel plug implant mouse model. Interestingly, transcriptome pathway enrichment analysis demonstrates that MGF inhibits tumor growth, metastasis and angiogenesis by multi-targeting of mitochondrial oxidoreductase and fatty acid β-oxidation metabolism, PPAR, SIRT, NFκB, Stat3, HIF, Wnt and GP6 signaling pathways. MGF effects on fatty acid β-oxidation metabolism and carnitine palmitoyltransferase 1 (CPT1) protein expression could be further confirmed *in vitro* in human HT29 colon cells. In conclusion, antitumor, antiangiogenic and antimetastatic effects of MGF treatment hold promise to reduce

OPEN ACCESS

Edited by:
Cristiana Perrotta, University of Milan, Italy

Reviewed by:
Seung Ho Shin, Gyeongsang National University, South Korea
Olga Krysko, Ghent University, Belgium

***Correspondence:**
René Delgado-Hernández
rdelgado@ifal.uh.cu
rdh231259@gmail.com
Wim Vanden Berghe
wim.vandenberghe@uantwerpen.be

[†]These authors have contributed equally to this work and share first authorship

Specialty section:
This article was submitted to Pharmacology of Anti-Cancer Drugs, a section of the journal Frontiers in Pharmacology

Received: *23 February 2021*
Accepted: *03 November 2021*
Published: *03 December 2021*

Citation:
Rodriguez-Gonzalez JC, Hernández-Balmaseda I, Declerck K, Pérez-Novo C, Logie E, Theys C, Jakubek P, Quiñones-Maza OL, Dantas-Cassali G, Carlos dos Reis D, Van Camp G, Lopes Paz MT, Rodeiro-Guerra I, Delgado-Hernández R and Vanden Berghe W (2021) Antiproliferative, Antiangiogenic, and Antimetastatic Therapy Response by Mangiferin in a Syngeneic Immunocompetent Colorectal Cancer Mouse Model Involves Changes in Mitochondrial Energy Metabolism. Front. Pharmacol. 12:670167. doi: 10.3389/fphar.2021.670167

adverse toxicity and to mitigate therapeutic outcome of colorectal cancer treatment by targeting mitochondrial energy metabolism in the tumor microenvironment.

Keywords: Mangiferin (PubChem CID: 5081647), antitumor, antiangiogenesis, antimetastasic, colon carcinoma, mitochondrial metabolism

INTRODUCTION

The latest GLOBOCAN 2018 database showed that colorectal cancer (CRC) is placed third in incidence and second in mortality worldwide, respectively; being responsible for 10% of all newly diagnosed cancer cases, and 9% of all cancer deaths worldwide (Bray et al., 2018). In Cuba, CRC ranked fifth in incidence and third in mortality in 2013, being more frequently in female and in adult people over 60 years of age in both indicators (Ministerio de Salud Pública.Dirección de Registros Médicos y Estadísticas de Salud and de Cuba, 2017). Despite advances in the prevention and diagnosis of CRC, between 60 and 70% of patients are detected at middle- or late-stage CRC, which results in difficult clinical management and less favourable prognosis (Petrelli et al., 2017). This contributes to 40–50% mortality rate within the first 5 years since the diagnosis, accounting for almost 10% of the cancer mortalities each year (Torre et al., 2016). Most of the CRC patients die from metastases (mCRC), predominantly in the liver, lungs, lymph nodes, and the peritoneum (Vatandoust et al., 2015). The main therapeutic options to mCRC are the surgical removal of liver metastases and/or chemotherapy. The former has increased patient survival in the first 5 years, but only 20–25% of these patients are eligible for surgery (Dhir and Sasson, 2016). The effectiveness of current chemotherapies is limited (Pritchard et al., 2012) due to suppression of host immune antitumor responses (Teng et al., 2015; Bhatia and Kumar, 2016), therapy-induced tumor resistance, tumor relapse (Shaked, 2016) local/systemic toxicities and increased risk of secondary tumorigenesis (Pritchard et al., 2012; Abdullah and Chow, 2013). In this scenario more than 80% of patients with mCRC die during the long-term follow-up (Ting et al., 2013). The progression of CRC is also closely related to angiogenesis associated with a poor prognosis and relapse of the disease (Mihalache and Rogoveanu, 2014) and has become an alternative valid therapeutic target in the treatment of colon cancer (Wang et al., 2015; Wang and Zhu, 2016). Since 2004, conventional chemotherapy is combined with targeted monoclonal antibody therapies specifically directed against vascular endothelial growth factor (VEGF) and epidermal growth factor (EGF) and their receptors to block angiogenic and proliferative tumor actions (Mihalache and Rogoveanu, 2014), (Mayer, 2009). Unfortunatedly, resistance and adverse effects have also been reported for these targeted treatments (Wang et al., 2015; Wang and Zhu, 2016). This has renewed interest in phytochemicals from medicinal plants for CRC treatment. Herbs with a rich ethnomedicinal history represent a rich resource of bioactive compounds with polypharmaceutical effects with multiple targets in cell growth, cell differentiation, and apoptosis regulation (Chen et al., 2008; Newman and Cragg, 2020; Atanasov et al., 2021). The public WHO global report on traditional and complementary medicine indicates that in developing countries, 80% of population relies on plant-derived medicines for the health care (World Health Organization, 2019). The number of phytochemical products submitted to the FDA is particularly high in the oncological area.

Mangiferin (MGF) is a polyphenolic phytochemical of the C-glycosylated xanthone type (1,3,6,7-tetrahydroxyxanthone-C2-β-d glucoside) present in all parts of *Mangifera indica* L. (*Anacardiaceae*), and in some medicinal plants. We and others have previously demonstrated promising antiproliferative, anti-angiogenic, anti-invasive and antimetastatic antitumor effects by poorly characterized mechanisms in different cancer cell types ((Leiro et al., 2004; Sarkar et al., 2004; García-Rivera et al., 2011; Khurana et al., 2016; Núñez Selles et al., 2016; Imran et al., 2017; Zou et al., 2017; Tan et al., 2018; He et al., 2019; Delgado-Hernández et al., 2020)).

Taking into account the interesting pharmacological properties of MGF described above, we applied a systems biology transcriptomics approach to resolve the molecular mechanism of action for the *in vivo* antitumor effects of MGF in a syngeneic immunocompetent allograft mouse model of murine CT26 colon carcinoma.

MATERIALS AND METHODS

Reagents

Mangiferin (MGF) was purified and characterized from the aqueous extract of the stem bark and leaves of *Mangifera indica* L to 95,5% purity at the Departments of Pharmacognosy, Institute of Food and Pharmacy, Havana University and Department of Analytical Chemistry of Center of Drugs Research and Development, CIDEM (Núñez Sellés et al., 2002; García-Rivera et al., 2011; Gil et al., 2014). Cisplatin (cis-diamminedichloroplatinum(II), CDDP) was purchased from Shandong Boyuan Pharmaceutical Co., Ltd, China. The culture medium RPMI-1640, dimethylsulfoxide (DMSO), fetal bovine serum, penicillin-streptomycin (100x), L-Glutamine, trypsin, ethylenediaminetetraacetic acid (EDTA), sodium dodecyl sulphate (SDS), reduced Matrigel (196 USP unit/ mg) and set of Drabkin reagents were purchased from Sigma-Aldrich Inc. (Saint Louis, MO, United States). 3-(4,5-Dimethyl-2-thiazolyl)-2,5-diphenyl-2H-tetrazolium bromide (MTT), 2-propanol, ethanol, hydrochloric acid (HCl), formaldehyde and acetic acid were obtained from Merck KGaA (Germany). Solutions of test compounds were routinely prepared in DMSO or MilliQ water and sterilized using syringe-driven 0.22 μm filters. The final concentration of DMSO in culture medium did never exceed 0.5%.

Tumor Cell Lines and Culture Conditions

CT26. WT is an *N*-nitroso-*N*-methylurethane-(NNMU) induced undifferentiated murine adenocarcinoma of the colon, syngeneic with the BALB/c mouse, which was provided by the Molecular Immunology Center, Havana. CT26. WT cells were grown in cell culture as monolayers in T-75 cm^2 culture flasks (BD Falcon) in RPMI-1640 with 2 mM of L-Glutamine supplemented with 10% fetal bovine serum, 100 UI/mL of penicillin, and 100 μg/ ml of streptomycin. Only cells of the first two serial passages after cryostorage were used in the syngeneic allograft models (Evans et al., 2016). At the day of implantation, the cells were harvested from subconfluent cultures (70–85%) by trypsinization (0.05% trypsin and 0.02% EDTA), and washed twice in phosphate-buffered saline solution before they were resuspended in non-supplemented RPMI culture medium. Human colon adenocarcinoma cell line HT29 (ATCC HTB-38) was cultured in McCoy's 5 A medium (Gibco, ThermoFisher, United States) supplemented with 1.5 mM L-glutamine, 2.2 g/L sodium bicarbonate, 100 ml/ L of fetal bovine serum and 100 U/ mL penicillin and 100 g/ L streptomycin. All cell lines were cultured in a humidified atmosphere (37°C, 5% CO_2).

Cell Viability Assays

MTT assays were performed to assess cell viability and/or growth inhibition of CT26 and HT29 colon cancer cell lines after exposure to MGF essentially, as previously described (Hernandez-Balmaseda et al., 2021). Briefly, cells were seeded in 96-well tissue culture plates at the concentration of 5,000 cells per well. The next day cells were treated with MGF in a concentration range of 10–400 μM for 24, 48, and 72 h. Control cells were exposed to 0.5% DMSO solvent control. Following treatment, the medium supernatant was aspirated from the wells and replaced with fresh medium. Next, 50 μL of MTT solution was added to all the wells and cells were incubated for another 4 h at 37°C. Subsequently, medium was aspirated and formazan crystals were dissolved in 50 μL of DMSO. The measurement of absorption was performed at 595 nm using (Envision 2103 multilabel reader, Perkin Elmer, United States) plate reader. The experiments were repeated with four technical replicates per treatment.

Cell Migration Wound Scratch Assay

HT29 cells were seeded at a concentration of 35,000 cells per well and left to grow at 37°C under 5% CO_2 until they reached 95–100% confluence. Then, cells were treated with 10 μg/ ml of MMC for 4 h to block cell proliferation and distinguish it from cell migration. When the incubation time was finished, a scratch was made in each well with the Incucyte Woundmaker tool. Next, cells were gently washed with PBS to remove any cell debris formed after making a scratch. Afterwards PBS was removed and exchanged with serum-free McCoy's 5 A medium to prevent cell division. The cells were treated either with MGF alone (at 1, 50 and 400 μM concentrations) or in combination with a proangiogenic cell migration growth factor VEGF (at 10 ng/ ml) for 24 h and incubated at 37°C under 5% CO_2 in the Incucyte Live-Cell Analysis system (Sartorius, Germany). Control cells were treated with an appropriate solvent, which in the case of MGF was 0.5% DMSO and in the case of VEGF–MilliQ water. Imaging was performed every 2 h for a total duration of 24 h with a × 10 objective. The area of wound closure was calculated and analysed using the Incucyte Scratch Wound Cell Migration software module of the ZOOM imaging system. The experiments were performed in three biological replicates with three technical replicates for each treatment.

Fatty Acid β-oxidation and Ketone Body Assays

Intracellular lipid accumulation induced by free fatty acid exposure leads to enhanced fatty acid oxidation (FAO) and ketogenesis (beta-hydroxybutyrate production). Protein expression levels of CPT1 (carnitine palmitoyltransferase 1), a key regulatory enzyme of mitochondrial fatty acid β-oxidation were determined by Western analysis. Ketone body (beta-hydroxybutyrate) levels were assessed using a colorimetric assay kit (Cayman Chem). Briefly HT29 cells were seeded at a density of $18*10^6$ cells in a T175 flask. The next day cells were treated with 0.2 mM FFA and 40 μM or 400 μM MGF for 24 h. Stock solutions of 0.66 M oleic acid and (1.32 M) palmitic acid (Sigma-Aldrich, Germany) were prepared in isopropanol. Equal amounts of oleic and palmitic acid were mixed to prepare a FFA stock of 1 mM FFA. Free fatty acid-free bovine serum albumin (BSA) was dissolved in serum-free McCoy's 5 A or RPMI medium without antibiotics at the final concentration of 1% and then sterilized using syringe-driven 0.22 μm filters. Afterwards, medium was supplemented with the mixture of FFA at a final concentration of 0.2 mM and sonicated for 6–8 h until FFA were completely dissolved using a Branson 3,200 sonication bath. FFA medium was protected from light and stored at 4°C. Following treatment, cell pellets were collected with a cell scraper and used immediately to extract ketone bodies according to the manufacturers protocol. The measurement of absorption was performed at 450 nm using (Envision 2103 multilabel reader, Perkin Elmer, United States) plate reader at room temperature. The experiments were performed in one biological replicate, with three technical replicates per each treatment. Similarly, RNA was extracted using RNeasy Mini Kit (Qiagen, Germany) from the collected cell pellets. RNA quantity was determined using Qubit™ RNA Broad Range Assay Kit with the aid of the Invitrogen Qubit™ 4 Fluorometer (Thermo Fisher Scientific, United States). The extracted RNA was stored at -80°C until further QPCR analysis. For protein analysis, cell pellet was washed once with cold PBS, centrifuged (1,500 rpm, 3 min, 4°C) then cells were lysed using 1x RIPA buffer (Cell Signalling, United States) with a cocktail of protease inhibitors (Sigma-Aldrich, Germany) and left on ice for 15 min. Afterwards, cell lysates were centrifuged (13,000 rpm, 15 min, 4°C) and the supernatants were transferred to the new test tubes. Protein concentration was measured using Pierce™ BCA Protein Assay Kit (Thermo Fisher Scientific, United States) and the measurement of absorption was performed at 560 nm using (Envision 2103 multilabel reader, Perkin Elmer, United States) plate reader.

Prior to SDS-PAGE electrophoresis, protein lysates were mixed with Laemmli buffer (Biorad, United States) and 50 mM 1,4-dithiothreitol (DTT) and then heated at 70°C for 10 min. Then, the samples and protein ladder (BenchMark™ Protein Ladder, Thermo Fisher Scientific, United States) were loaded on SDS-PAGE polyacrylamide gels (stacking 6%, resolving 12%) at protein concentration equal to 10 μg/well. The electrophoresis was run in Mini-PROTEAN Tetra Cell System (Biorad, United States) using the high molecular weight buffer (100 mM MOPS, 100 mM Tris, 0.2% SDS, 2 mM EDTA, 5 mM sodium bisulfite) at 70 V until the samples reached the separating gel and then the voltage was increased up to 120 V. Afterwards, the proteins were transferred on pre-wet nitrocellulose membranes (Cytiva, United States) in Power Blotter 1-step transfer buffer (Invitrogen, United States) using Power Blotter XL System (Invitrogen, United States) (7 min at 1.3 A). Nitrocellulose membranes were blocked in blocking buffer (5% milk solution in TBST) for 1 h at room temperature and incubated overnight at 4°C with primary antibodies diluted in blocking buffer as follows: 1:4000 for anti-CPT1A (Proteintech, UK). Next day, membranes were washed three times with TBST and then incubated with HRP-conjugated anti-rabbit secondary antibody diluted in blocking buffer (1:2000). Anti-GAPDH (Cell signaling, United States) antibodies (diluted 1:2000) in blocking buffer were used as loading controls for CPT1A. Protein detection was performed on the Amershan imager 680 (Cytiva, United States) using Pierce™ ECL Western Blotting Substrate (Thermo Fisher Scientific, United States) and quantified using Image-J software.

In vivo Experiments

Housing and all procedures involving animals were performed according to protocols approved by the Drug Research and Development Center Ethics Committee for Animal Research and in compliance with the Cuban National Guidelines for the Care and Use of Laboratory Animals (CECMED Resolution No. 37 2012 for Good Laboratory Practice for Quality Control). Male BALB/c mice were purchased at National Laboratory Animal Production Center, Havana, Cuba. BALB/c mice were used at 6–8 weeks of age with weight between 18 and 22 g, in all experiments. They were supplied with water and food at *libitum* and were kept in quarantine for 15 days for adaptation to temperature (22°C ± 2°C), humidity (77 ± 3%) and alternating cycles of 12 h light/dark environment. For allograft studies, the animals were inoculated (as specified in more detail for each specific model below) with $1x10^5$ CT26. WT cells/mouse in 100 μL of non-supplemented RPMI-1640 culture medium. The following day, they were weighted, labeled and placed in separate boxes.

Ectopic Subcutaneous Syngeneic CT26. WT Tumor Model

The animals were inoculated subcutaneously with CT26. WT cells on the right dorsal side. Once tumors grew up to 30 mm^3, mice were randomly divided at day 14 into five groups (10 animals/group) and treated for 14 days (28 days protocol). The products, doses, and treatment schedules were as follows: *Group I*, carboxymethylcellulose (CMC) 0.05% as the negative control; *Group II*, MGF 10 mg/ kg b. w.; *Group III*, MGF 50 mg/ kg b. w.; *Group IV*, MGF 100 mg/ kg b. w.; and *Group V*, CDDP 5 mg/kg b. w. as positive control. MGF doses were prepared in 0.05% CMC and CDDP in sterile saline solution (0,9% NaCl). MGF and CMC were administered daily intragastrically and CDDP every 6 days by intraperitoneal injections in three treatment cycles. The tumor growth was monitored and tumor size was measured by length and width with caliper every 2 days by the same operator, and the tumor volume was calculated (V, mm^3 = length x $width^2$ x 0.5). At the end of the experiment, all mice were sacrificed and dissected. The tumors were recovered for photographic imaging and weighed. Three independent experiments were performed.

Lung Metastasis Model

The animals were challenged by an intravenous puncture in the tail veins and distributed in five groups (10/group). The products, doses, and treatment regimens were as follows: *Group I*, 0.05% CMC; *Group II*, MGF 10 mg/kg b. w.; *Group III*, MGF 50 mg/ kg b. w.; *Group IV*: MGF 100 mg/ kg b. w.; and *Group V*, CDDP 5 mg/kg b. w. The preparation, route, and frequency of administration were the same as those described in the ectopic/subcutaneous model. The animals were treated for 17 days and sacrificed at day 18. The trachea-lung were extracted, photographed and perfused with 20 Gx1½ tracheal needles with 1 ml 15% Chinese ink in PBS pH 7.2–7.4. The trachea was excised and the lungs were soaked for discoloration and fixation for 5 min in Fekete's solution (Bao et al., 2011). The lungs were photographed and the superficial metastatic nodules were counted using a stereoscope (Olympus, Japan) and fixed with 4% formaldehyde. Lungs presented with more than 250 nodules, were assigned a cut-off value of 250 (due to the difficulty of counting a larger number because of high nodule density). A survival analysis was performed until the treatments were completed. Three independent experiments were performed.

Angiogenesis Model by Matrigel Implant

The animals were divided into four groups (5/group). The control groups were implanted with 200 μL of a cold mixture of Matrigel, heparin (32 IU) and PBS (*negative or basal control: implant A*) and another mixture equal to the previous one plus CT26. WT cells (5×10^5) as *positive control: implant B*. For the treatment groups, two concentration of MGF: *2*00 μg/ ml (*implant C*) and 100 μg/ ml(implant D) were included into the implant volume B. The implants were subcutaneously applied in the in the inguinal region. The experimentation time was extended by 12 days. The animals were sacrificed, the plugs were excised, photographed and cleaved with residues of surrounding tissue to facilitate histological orientation. They were weighed and measured with caliper by their length, width, and height, and the volume was calculated using the formula of an ellipsoid: V (mm^3) = length x width x height x π/6). The plugs were liquified in 300 μL PBS by incubation at 4°C, overnight (Beatty and Paterson, 2001), and the hemoglobin (Hb) released was quantified by the Drabkin method (Drabkin

and Austin, 1935). For histological analysis, the plugs were fixed in 10% formalin in PBS, embedded in paraffin and cut (5–7 μm). Histological staining was initially performed with hematoxylin-eosin and whereas specific staining for blood vessel counts was done with Masson's trichrome. A microscopic count of the blood vessels was performed throughout the periphery of the tumor.

Immunohistochemical Studies

Subcutaneous tissue tumors were fixed in formalin (10% w/v in phosphate-buffered saline–PBS pH 7.4) during 24 h and sections (4 μm) were processed for immunohistochemistry analysis. A biotin-peroxidase system was used with identification of the secondary antibody by polymer (ADVANCE HRP). Antigen retrieval was performed in water bath at 98°C, with a citrate buffer solution (pH 6.0) (Target Retrieval Solution) for 20 min. In order to block the endogenous peroxidase activity, slides were incubated with a solution of H_2O_2 3% in methyl alcohol. Reagents were applied manually with 1 h incubation for the primary antibody and 30 min for the reagents, except for chromogen diaminobenzidine, incubated for 5 min. Minichromosome maintenance complex component 7 (MCM 7 or CDC47), a marker of cell proliferation, was measured using a specific monoclonal antibody CDC47 (clone 47DC141, Neomarkers, 1/300) (Zorde Khvalevsky et al., 2013). Positive and negative controls were included in each bath. The index for CDC47 staining was obtained by counting the percentage of positive cells in 500 tumor cells.

RNA Extraction and Isolation

Subcutaneous and pulmonary tumor tissue samples from each animal (n = 5/group) were individually treated with RNA*later*® (Qiagen, Benelux, Belgium) by 24 h at 4°C, and immediately stored at −80°C until the RNA isolation procedure. Up to 30 mg tissue were completely disrupted and homogenized in 700 μL QIAzol® Lysis Reagent (Qiagen, Benelux, Belgium) by the Tissue Lyser II (Qiagen®, Benelux, Belgium) with 5 mm stainless steel beads diameter to extract total RNA. Total RNA was isolated using RNeasy® Microarray Tissue kit (Qiagen, Benelux, Belgium), according to manufacturer's protocol. Total RNA was purified on RNeasy Mini spin columns according to the manufacturer's protocol. During the purification process contaminating genomic DNA was removed by means of DNase digestion. Purity and concentration total RNA samples were evaluated by ultraviolet spectroscopy (NanoDrop, Thermo Scientific, Wilmington, United States). The integrity of the RNA samples was evaluated by the Experion Automated Electrophoresis System (BioRad, CA, United States) according to the manufacturer instructions. Good quality of the RNA material samples with A260/280 ratio between 1,9–2,1 were used for further analysis.

RNA Bead Array and Data Processing

Five hundred ng of total RNA from 18 samples (3 replicates by group) subcutaneous and pulmonary tissue tumors were amplified using the Illumina TotalPrep RNA Amplification kit (Life Technologies, Carlsbad, CA, United States). RNA was reverse transcribed using T7 oligo(dT) primers after which biotinylated cRNA was synthesized through *in vitro* transcription reaction. Seven hundred 50 ng of amplified cRNA was hybridized to a corresponding array on a Mouse WG-6 2v bead chip (Illumina, San Diego, CA, United States). The beadchip array was incubated for 18 h at 58°C in a hybridization oven whilst continuous rocking. After several consecutive washing steps, bead intensities were read on Illumina iScan. Raw data intensities were read in R using the "bead array" package (v2.8.1) (Dunning et al., 2007). Intensities were quantile normalized and differential gene expression between samples was estimated using "limma" (v3.14.1) (Ritchie et al., 2015). Genes were considered to be differentially expressed when they had a p-value < 0.05 and a fold change of at least 1.25 in comparison to controls. Transcriptomic analysis was done by uploading Illumina bead array gene expression data into Ingenuity Pathway Analysis (IPA) software (Ingenuity® Systems, www.ingenuity.com, Redwood City, CA, United States and QIAGEN Inc., https://digitalinsights.qiagen.com/products-overview/discovery-insights-portfolio/analysis-and-visualization/qiagen-ipa/?), and performing a core analysis according to the instructions provided. Each identifier was mapped to its corresponding gene object in the Ingenuity knowledge base. Fisher's exact test was used to calculate a p-value determining the probability that each biological function and/or disease assigned to that data set is due to chance alone. Metascape systems biology freeware (https://metascape.org/) was used for correlating the transcriptomic profiles of the different *in vivo* data (Zhou et al., 2019). The Circos plot visualization allows to show how genes from different input gene lists overlap. Heatmaps show Metascape enrichment analysis of all statistically enriched ontology terms (GO/KEGG terms, canonical pathways, hall mark gene sets). Accumulative hypergeometric p-values and enrichment factors are calculated and used for filtering. Remaining significant terms are then hierarchically clustered into a tree dendrogram based on Kappa-statistical similarities among their gene memberships. The term with the best p-value are selected within each cluster as a representative term to be displayed in a hierarchical tree dendrogram. The heatmap cells are colored by their p-values (see color legend). Along the same line, Metascape enrichment analysis of all statistically enriched transcription factor (TF)-target interaction networks is dermined by the TRRUST database (Han et al., 2018). Protein-protein interactions (PPI) among all input gene lists are extracted from PPI data source to form a PPI network. GO enrichment analysis is applied to the network to assign biological "meanings" of sub-protein networks. GO enrichment analysis is applied to each MCODE network to assign "meanings" to the network component, where top three best p-value terms were retained. MCODE components were identified from the merged network. Each MCODE network is assigned a unique color.

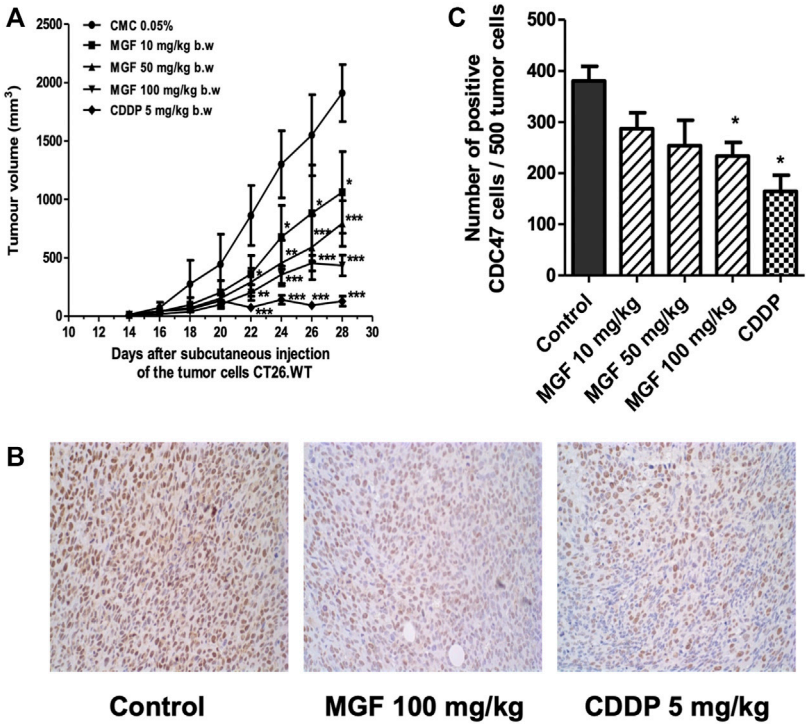

FIGURE 1 | MGF treatment induces tumor regression in CT26. WT colorectal cancer model. BALB/c mouse colorectal cancer cells CT26. WT (1×10^5 cells) were injected subcutaneously into 6–8 weeks-old BALB/c mice. After 14 days of tumor allograft growth, the mice were daily treated for 14 days by (oral) cannulation with MGF at low (10 mg/ kg), intermediate (50 mg/ kg) and high (100 mg/ kg) doses or carboxymethyl cellulose (CMC) 0,05% as vehicle control. Standard chemotherapeutic CDDP treatment (5 mg/ kg) was intraperitoneal injected each 6 days. **(A)** Tumor volume changes induced by different treatments. **(B)** Immunohistochemical staining of tumor sections to CDC47 monoclonal antibody. **(C)** Barplot representation of quantified immunohistochemical CDC47 positive staining cells in the different experimental setups (mean ± standard error of the mean (SEM) of three independent experiments). Statistical significant differences have been determined by two-way ANOVA * $p < 0.05$; ** $p < 0.01$; *** $p < 0.001$.

Reverse Transcription-PCR and Real-Time Quantitative PCR Validation

Total RNA (700 ng) isolated by RNeasy Mini Kit (Qiagen), was reverse transcribed to cDNA by the GoScript™ Reverse Transcriptase kit (Promega, United States) according to the manufacturer's protocol. RT-qPCR was performed using GoTaq® qPCR master mix (Promega, United States) on Rotor-Gene Q (Qiagen, Germany). Gene expression was calculated with the ΔΔCt method after normalization against the glyceraldehyde-3-phosphate dehydrogenase (*GAPDH*), actinB (*ACTB*) or beta-2-microtubulin (*B2M*) housekeeping genes, as further specified. Following gene specific primersets were used for array validation experiments of C-C Motif Chemokine Ligand 3 (*CCL3*), Collagen Type VI Alpha three chain (*COL6A3*), C-X-C Motif Chemokine Ligand 9 (*CXCL9*) and Metalloproteinase 13 (*MMP13*); and the following gene specific primer sets: *CCL3* forward primer: 5′-CAGCCAGGTGTCATTTTCCTG-3′ and reverse primer: 5′-AGGTCTCTTTGGAGTCAGCG-3′. *COL6A3* forward primer: 5′-GGAACCACGGAAGAGAGCAA-3′ and reverse primer: 5′-CAGGGAACTGACCCAAGACA-3′.*CXCL9* forward primer: 5′-TGTGGAGTTCGAGGAACCCT-3′ and reverse primer: 5′-AGTCCGGATCTAGGCAGGTT-3′. *MMP13* forward primer: 5′- GGAGCCCTGATGTTTCCCAT-3′ and reverse primer: 5′- GTCTTCATCGCCTGGACCATA-3′. The experiment was carried out in duplicate in three independent biological replicates. The thermal cycling conditions included initial denaturation at 95°C for 2 min and subsequent 40 cycles of two-step protocol: denaturation at 95°C for 15 s and annealing/extension at 60°C for 60 s.

Statistical Analysis

One-way or two-way ANOVA with Dunnett post hoc test (comparison every mean to control mean) were performed to evaluate statistical significance, as indicated in Figure legends. Survival analysis was done with the log-rank (Mantel-Cox) statistical test. All statistical analyses were performed using GraphPad Prism® (GraphPad Software, La Jolla California, United States) statistical package. P value < 0.05 was considered significant.

RESULTS

Mangiferin Induces CT26.WT Colorectal Tumor Regression *in vivo*

The CT26 syngeneic colorectal cancer tumor model was used to investigate the effect of MGF on tumor growth *in vivo*. CT26.

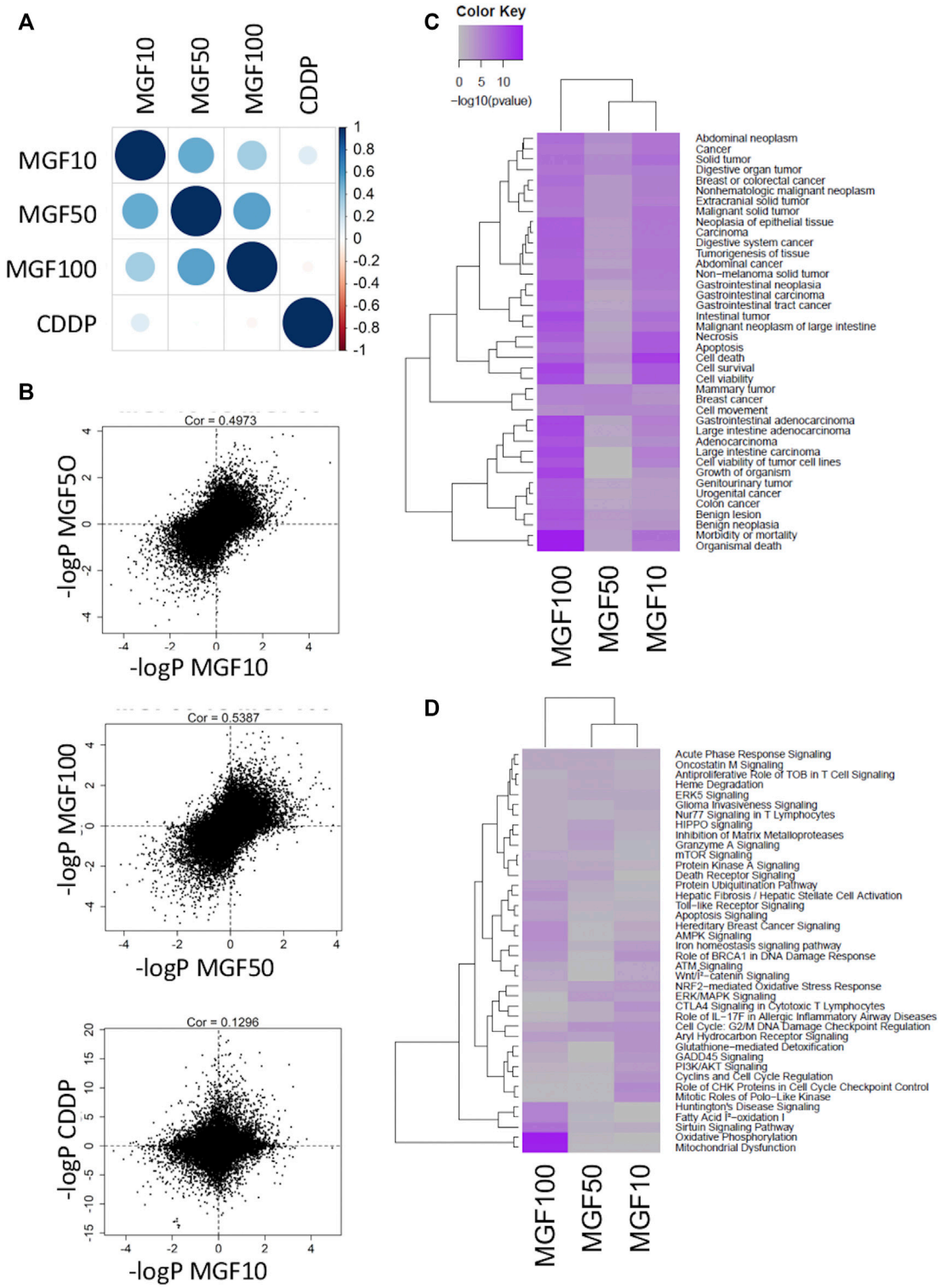

FIGURE 2 | MGF treatment of CT26. WT colorectal cancer model reshapes gene expression patterns controlling cell death, cell growth, cell motility and mitochondrial disease functions. **(A)** Cross-comparison of common transcriptional changes of the different treatments by correlating the -log10 p-values for every treatment combination. **(B)** Scatter plot pearson correlations of transcriptional gene responses for different MGF doses and for MGF versus CDDP treatments **(C)** IPA pathway enrichment analysis of disease functions. **(D)** IPA pathway enrichment analysis of biological pathways.

WT cells were grown for 14 days after subcutaneous injection. Changes in tumor volume by MGF treatment were measured during 2 weeks of treatment protocol. As shown in **Figure 1A**, allgrafts treated with MGF show dose dependent tumor regression, comparable to the volume reduction observed upon treatment with the reference chemotherapeutic drug CDDP. Significant treatment antitumor effects start to be observed from day 22, following 8 days of treatment (**Figure 1A**), reaching a maximal reduction in tumor size of 75% at 100 mg/kg. Overall, CDDP treatment revealed the strongest antitumor effect (approximately 90% tumor size reduction). Along the same line, MGF and CDDP dependent reduction of tumor volume corresponds with decreased immunohistochemical staining intensity of the cell proliferation marker CDC47 reflecting arrest of tumor growth (**Figures 1B,C**).

Mangiferin Inhibition of Tumor Cell Motility (Invasion), Angiogenesis, Vasculogenesis Involves Transcriptional Changes in Fatty Acid Metabolism, PPAR, NFκB, Wnt and GP6 Signaling Pathways

To get more insight in the molecular mechanism of the antitumor of MGF, a gene expression microarray experiment was performed. Gene expression profiles of subcutaneous tumor tissue obtained from mice treated for 2 weeks with 5 mg/ kg CDDP, 10 mg/ kg MGF, 50 mg/ kg MGF and 100 mg /kg were compared to untreated control mice with tumors. In general, MGF showed mild transcriptional changes as compared to CDDP treatment. Using a fold change difference of at least 1.25 and a p-value below 0.05, 454 genes were found to be differentially expressed in the 10 mg/ kg MGF condition, 263 genes in the 50 mg/ kg MGF condition, 812 genes in the 100 mg/ kg MGF condition and 3,340 genes after 5 mg/ kg CDDP treatment (**Supplementary Table S1**). Highly significant positive correlations could be observed upon comparing the log2 microarray gene expression values and the ΔCt qPCR expression values of *CCL3, COL6A3, CXCL9* and *MMP13* target genes, supporting the validity our microarray results (**Supplementary Figure S1**).

Next, bioinformatic analysis of transcriptome changes of the different treatments was performed by correlating the -log10 p-values for every treatment combination (**Figure 2A**). Whereas strong positive correlations were observed for transcriptional responses for the different MGF doses ($r = \geq 0.5$), only weak overlap could be observed for MGF and CDDP treatments ($r = 0.13$), suggesting a different mechanism of action (**Figure 2B**). Next, we focused on pathway enrichment analysis of disease and biological pathways of the MGF treatment specific transcriptional changes using Ingenuity Pathway Analysis (IPA®, QIAGEN Redwood City) (**Figures 2C,D**; **Supplementary Table S1**). Differentially expressed genes for all MGF doses are enriched for regulation of cancer and colon cancer related disease functions, including cell death and survival and cell motility, gastrointestinal neoplasia, gastrointestinal carcinoma, malignant neoplasm of large intestine, and digestive system cancer (**Figure 2C**).

Along the same line, significant transcriptional changes could be observed at the gene expression level in cytokine signaling (acute phase response, oncostatinM), mitochondrial metabolic stress (oxidative phosphorylation, fatty acid oxidation, Nrf2, Glutathione detoxification, SIRT, and AMPK/mTOR signaling), cell cycle (cyclins, checkpoints, mitotic PLK kinases), metalloproteases (MMPs), cell death (death receptors), iron homeostasis (heme degradation) DNA damage (ATM, BRCA1, GADD45 signaling), cell death (ubiquitination), differentiation (Wnt/catenin) and xenobiotic-metabolizing hormone receptor signaling (Aryl hydrocarbon and aldosterone receptor signaling) (**Figure 2D**; **Supplementary Figure S3**; **Supplementary Table S1**).

Next, we used the IPA regulation z-score algorithm to identify biological functions and pathways that are most significantly activated (Z-score >1) or repressed (Z-score < -1) by MGF based on direction of gene expression changes (increase/decrease). Interestingly, MGF dose dependently suppresses expression of multiple genes involved in tumor cell motility (invasion), angiogenesis, vasculogenesis and development of vasculature functions (**Figure 3A**). Furthermore, when analyzing possible protein interaction networks of MGF responsive gene targets by the STRING algorithm (https://string-db.org/), we identified various interconnected protein network clusters involved in cell motility, angiogenesis and cell death/autophagy/ proliferation, or dysfunctional mitochondrial oxidoreductase metabolism, in line with the results of our IPA analysis (**Figures 2D**, **3A** and **Supplementary Figure S2**).

Mangiferin Suppresses Cell Motility *in vitro*

To further characterize MGF anticancer effects on cell viability and cell motility *in vitro*, we next performed MTT and wound scratch assays in mouse CT26 and human HT29 colon cancer *in vitro* cell models. First, CT26 and HT29 were treated with MGF for 24, 48, and 72 h with a MGF concentration range from 10 to 400 μM, followed by a colorimetric MTT assay, as previously described (Hernandez-Balmaseda et al., 2021). As can be observed from **Figure 3B**, MGF does not significantly decrease cell viability in the dose range tested and shows no adverse toxicity. Next, MGF effects on prometastic and proangiogenic cell motility were analyzed for 24 h in a wound scratch assay in VEGF treated HT29 cells by realtime Incucyte Live Cell imaging in IncuCyte® ImageLock 96-well microplates, after scratching cells with the Incucyte Woundmaker tool (Kobelt et al., 2021). Time dependent changes in wound closure of the different treatments were quantified by the Incucyte Scratch Wound Cell Migration software module of the ZOOM imaging system. In line with our gene expression pathway analysis in mouse CT26 cells, MGF treatment was also found to significantly suppress VEGF induced prometastatic and proangiogenic cell motility in human HT29 cells (**Figures 3C,D**).

Mangiferin Exerts Antiangiogenic Effects *in vivo* in a Matrigel Plug Angiogenesis Mouse Model

Next, we further verified whether inhibition of vasculogenesis by MGF could also be experimentally confirmed in a CT26. WT cells

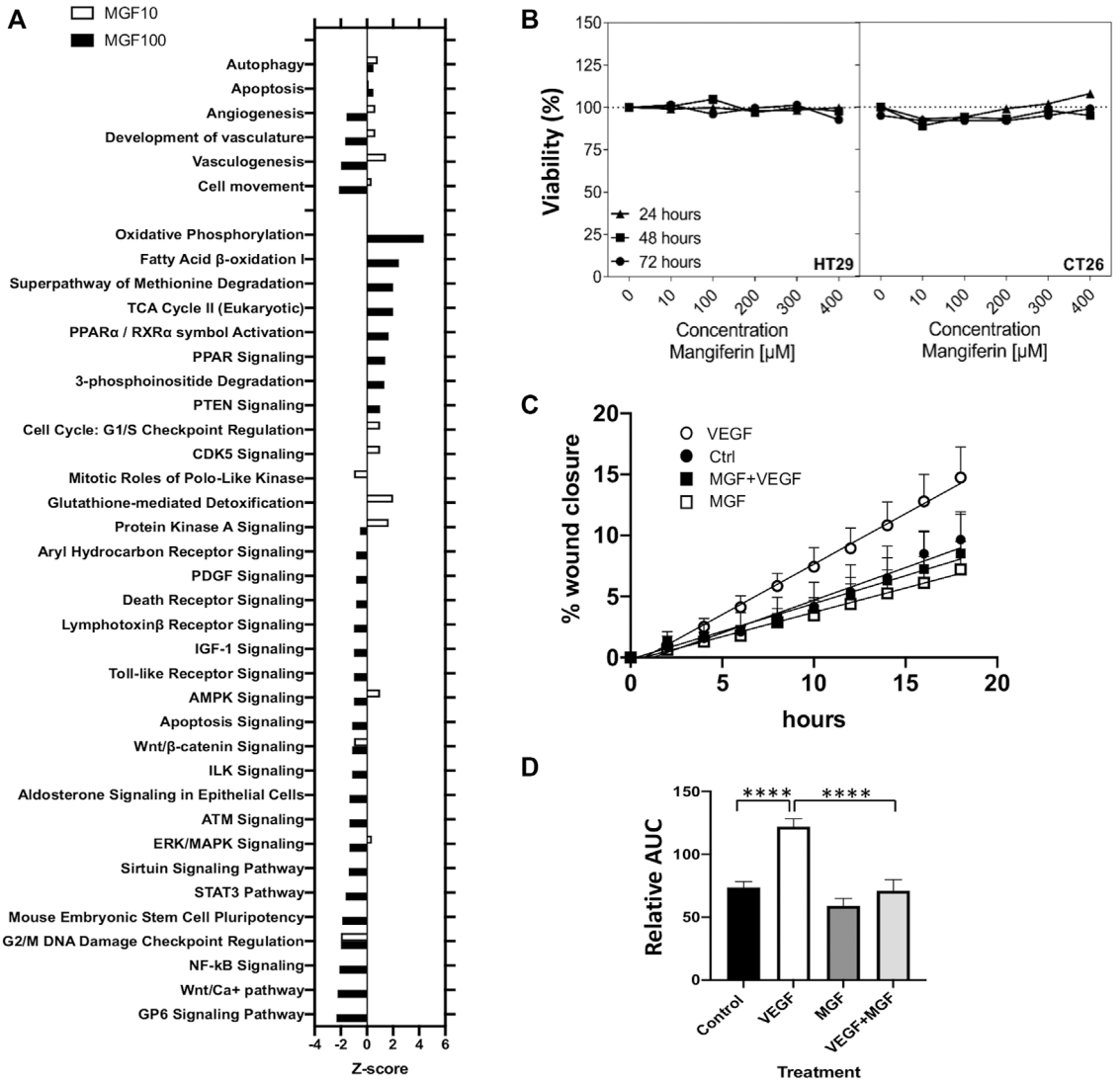

FIGURE 3 | MGF treatment inhibits prometastatic tumor cell motility in a wound scratch assay *in vitro* without adverse toxicity.**(A)** Z-score barplot of most significantly enriched disease functions and canonical pathways **(B)** Assessment of cell viability by MTT assay of HT29 cells and CT26. WT colorectal cells after 24, 48 and 72 h treatment with MGF. **(C)** Realtime image quantification (0–18 h) of *in vitro* migration and wound closure of HT29 cells in the presence of 10 ng/ ml VEGF, 400 μM MGF a combination thereof or solvent matched controls. **(D)** Bar plot quantitation of the wound closure after cell scratching following different treatments by measuring each area under the curve in **Figure 3C** (0–18 h). Data are given as mean ± SD (n = 3). Statistics were calculated with 1-way ANOVA ***p < 0.0001.

engrafted matrigel plug assay, allowing to measure effects on neovascularization of tumor cells *in vivo* (Kastana et al., 2019). Angiogenesis is an attractive cancer therapeutic target, not only because it supplies oxygen and nutrients for the survival of tumor cells, but also provides the route for metastatic spread of these cancer cells.

Tumor formation in the subcutaneous matrigel plug tissue, with abundant blood supply, was observed in the CT26. WT engrafted control animals. In contrast, the plug in control animals colors yellow lacking blood irrigation in the matrigel subcutaneous implant (**Figure 4A**). Clearly, MGF treatment promotes a reduction of peritumoral and intratumoral blood vessel supply and tumor size in a dose-dependent manner (**Figure 4A** from left to right). Moreover, quantitative analysis of Hb content shows that MGF dose dependently inhibits angiogenesis, i.e. 58% and 81% decrease of Hb levels at respectively 100 and 200 μg/ml MGF treatment (p < 0.05) (**Figure 4B**). As expected, CT26. WT tumor cells show an adequate proangiogenic response in matrigel (81% increase in Hb content) as compared to the control setup (**Figure 4B**). Besides, the antiangiogenic effect of MGF also results in dose dependent reduction in tumor volume (84% reduction at 200 μg/ml MGF, **Figure 4C**) or tumor weight (73% reduction at 200 μg/ml MGF, **Figure 4D**). Besides, a histological study was performed using the hematoxylin-eosin and Masson's trichrome staining. This allows clear differentiation of the collagen fibers (colored in

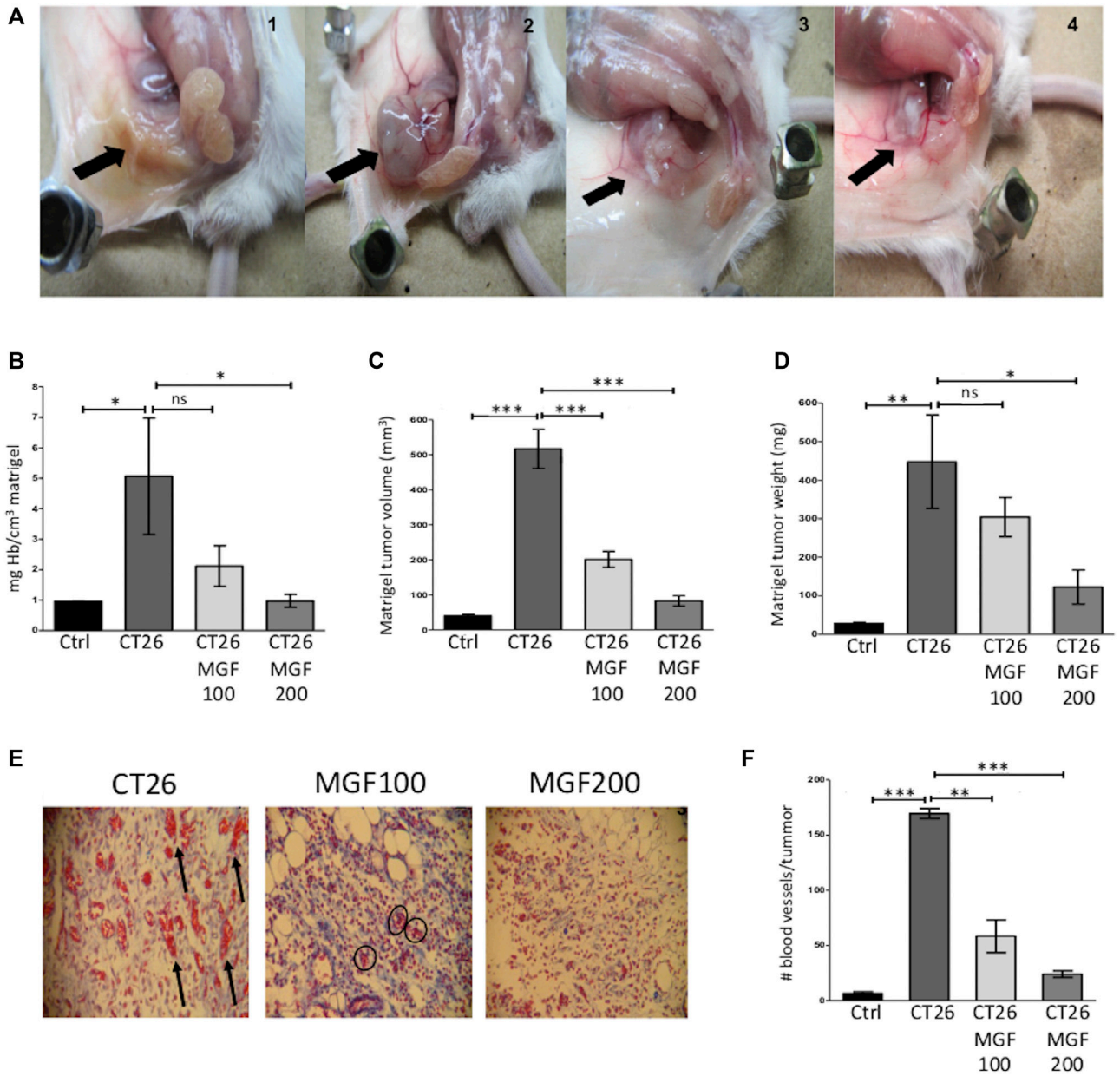

FIGURE 4 | MGF treatment has antiangiogenic effects *in vivo* CT26. WT matrigel plug angiogenesis model. BALB/c mice were subcutaneously implanted bith a *basal control* plug (Matrigel + heparin + PBS), CT26 tumor plug (basal control plug + CT26. WT cells (5 x 10^5). Treatment groups were implanted with a MGF200 plug (MGF 200 µg/ ml + Matrigel, heparin, CT26. WT, PBS) or MGF100 plug (MGF 100 µg/ ml + Matrigel, heparin, CT26. WT, PBS). Twelve days post-implantation, the subcutaneous matrigel plugs were weighed, measured, and the corresponding volumes were calculated. Hb release of liquified plugs was quantified by the Drabkin method. The histological analysis were staining by haematoxylin-eosin and subsequently with Masson's trichrome dye. A microscopic count of the blood vessels was performed throughout the periphery of the tumours. **(A)** Macroscopic subcutaneous plug images from left to right basal control, CT26 tumor control, MGF 100 µg/ ml treatment, MGF 200 µg/ ml treatment **(B)** quantification of Hb content plug relative to tumor control plug (arbitrarily set at 100%) **(C)** volume of Matrigel plug (mm^3) **(D)** weight of Matrigel plug (mg) **(E)** staining with Masson's Trichrome of tumour samples. Left picture, tumour positive control plug shows numerous macro- and microvessels in the tumour periphery area, the arrow points are indicative of larger calibre blood vessels; middle picture, tumor plug with MGF100 µg/ mL shows few remaning small vessels in the matrigel (circle marks); right picture, in tumor plug with MGF 200 µg/ ml no blood vessels can be observed in the matrigel, magnification ×100. **(F)** Quantification of the number of blood vessels in the entire tumour periphery area. Data are represented as mean ± SD; not significant (ns), significant, * $p < 0.05$; *** $p < 0.001$.

blue) from the blood vessels (colored in red). As can be observed in the histological staining (**Figure 4E**) or blood vessel count (**Figure 4F**), MGF dose dependently inhibits the formation of blood vessels in the tumor periphery of the CT26. WT engrafted Matrigel ($p < 0.001$). Altogether, these results support our gene expression pathway enrichment analysis which identified various

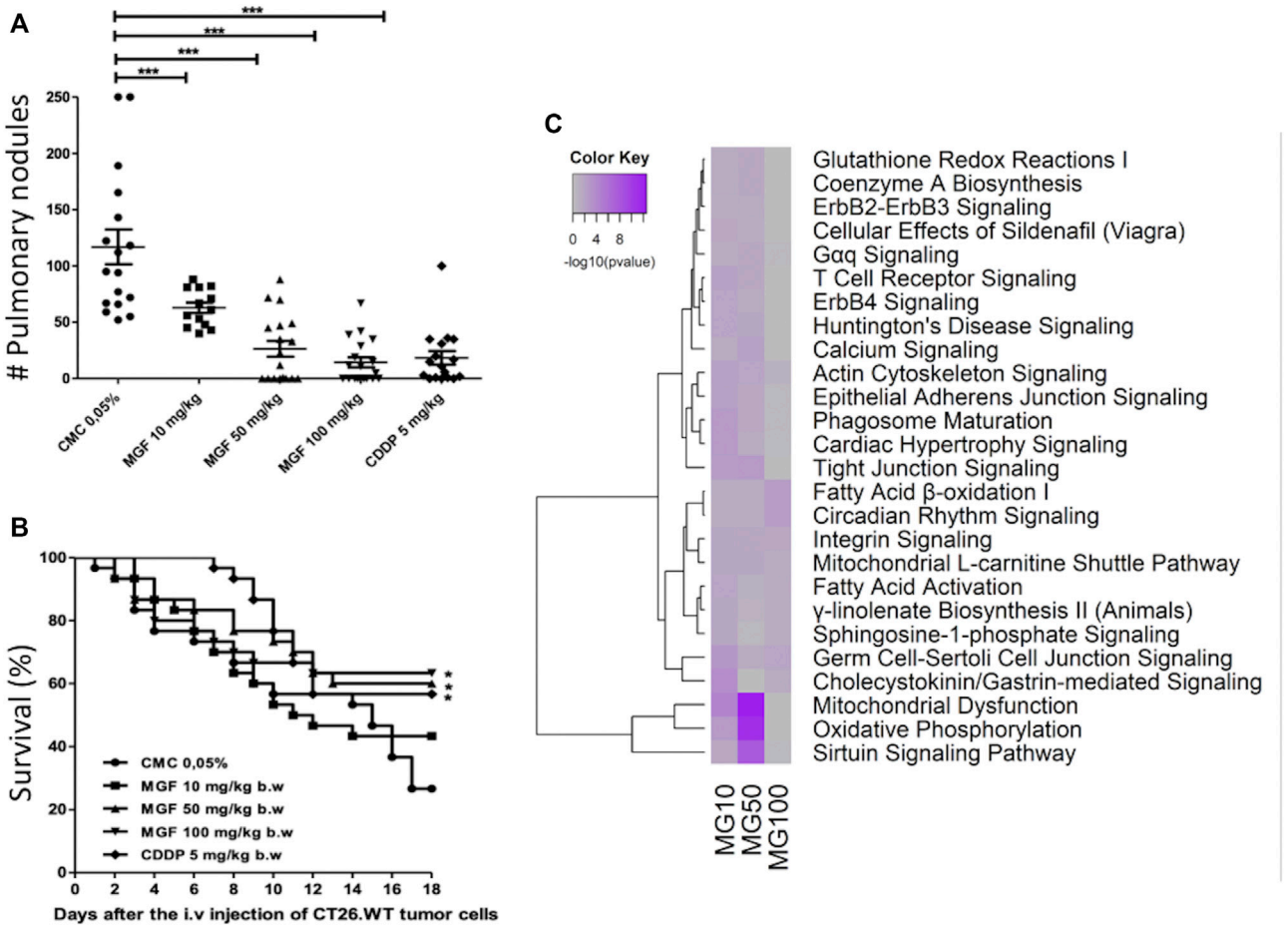

FIGURE 5 | MGF inhibits CT26. WT-induced experimental lung metastasis. BALB/c mice (15/group) were orally treated with 0.05% CMC, MGF 10 mg/ kg b. w., 50 mg/ kg b. w., and 100 mg/ kg b. w. for 17 days, or intraperitoneally with 5 mg/ kg b. w of CDDP (three cycles every days), after injection of CT26. WT cells ($1x10^5$ cells/100 μL non-supplemented RPMI culture medium). **(A)** number of pulmonary surface nodules counted by experimental group. **(B)** survival curves during 18 days (sacrifice) of the experiment to each experimental group. Values are shown as mean ± standard error of the mean (SEM) of three independent experiments. MGF significantly inhibited (*** $p < 0.001$) tumor lung metastasis as shown in panel A and significantly increased survival of mice as shown in panel B, as compared to vehicle control treatment response. **(C)** heatmap representations of most significantly enriched pathways associated with gene expression changes in response to MGF treatment.

MGF responsive target genes involved in suppression of angiogenesis-vasculogenesis.

Mangiferin Inhibits Lung Metastasis of CT26 Cells in an Experimental Metastasis Mouse Model

To further evaluate suppression of cancer cell motility-migration in response to MGF, as predicted in our transcriptome analysis, we next investigated whether MGF could reduce number of lung metastasis nodules upon intravenous puncture of colorectal cells in the mouse tail veins. The number of CT26 metastasis nodules in lungs were quantified following 17 days treatment in the different experimental setups as shown in **Figure 5**. A significant reduction ($p < 0.001$) in the number of pulmonary surface metastatic nodules could be observed by increasing doses of MGF, respectively 46, 77, and 88% decrease upon treatment with 10, 50 or 100 mg/ kg b. w. MGF as compared to the vehicle control group (**Figure 5A**). Similarly, metastatic nodules could be reduced 83% upon treatment with 5 mg/kg b. w. CDDP (83%) (**Figure 5A**). Treatments with 50 and 100 mg/ kg b. w. MGF, or 5 mg/ kg b. w. CDDP also resulted in a significant improvement of longterm survival rate as compared to the vehicle control group (MGF 50 mg/ kg: $p = 0.027$; MGF 100 mg/ kg: $p = 0.020$; CDDP: $p = 0.022$) (**Figure 5B**). Remarkably, gene expression analysis of pulmonary metastatic colon tumor tissue biopsies from mice treated with MGF revealed similar gene expression patterns and pathway enrichment as in the primary CT26 tumor model (**Figure 5C**; **Supplementary Table S2**). Accordingly, MGF treatment targets mitochondrial energy metabolism (fatty acid oxidation, sirtuin, TCA) NFκB, PPAR, Wnt and GP6 signaling to suppress cancer cell migration-metastasis processes (**Figure 5C**). Since tumor tissue biopsies are a heterogenous mixture of CT26 tumor metastasis and healthy lung cells, tumor gene expression

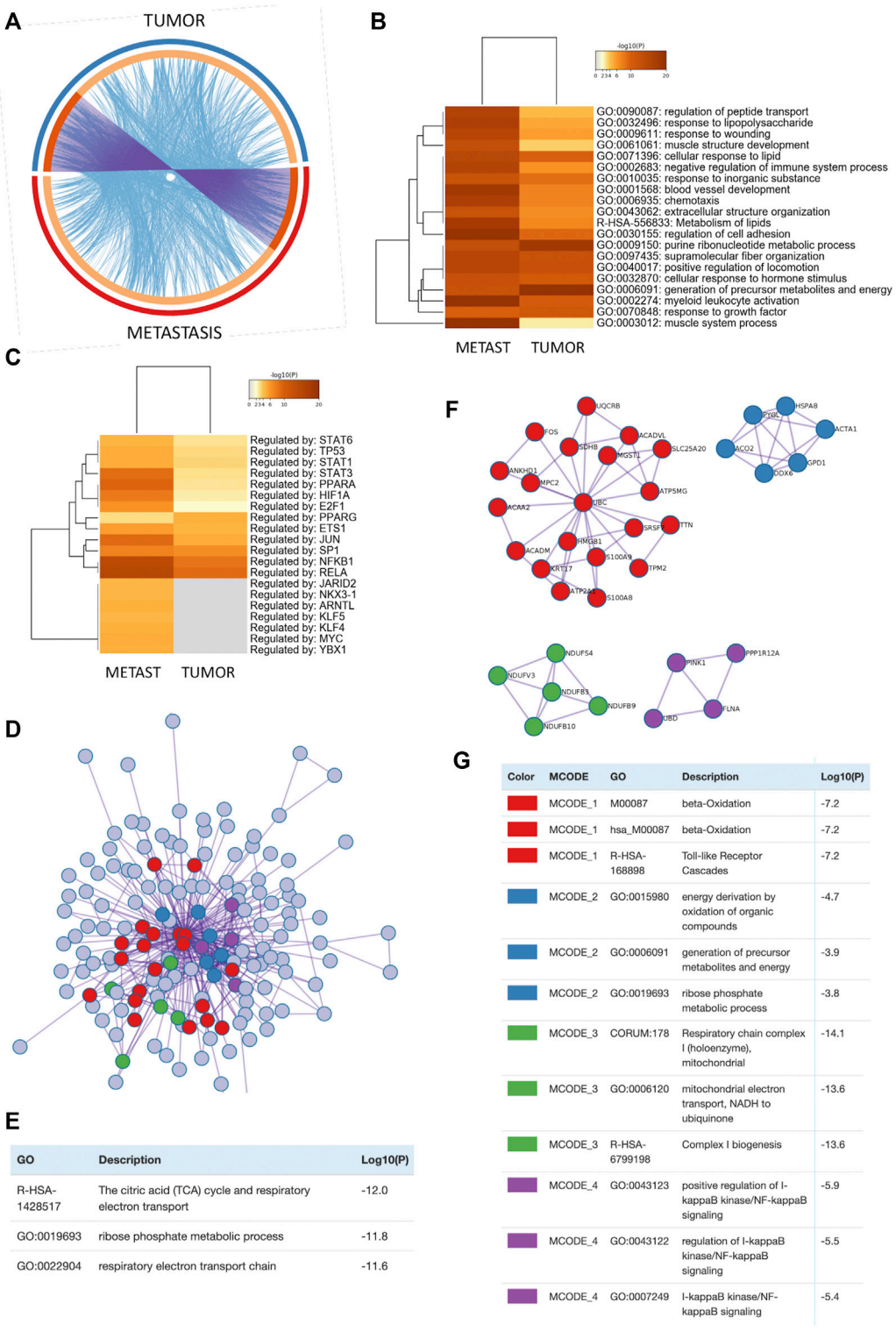

GO	Description	Log10(P)
R-HSA-1428517	The citric acid (TCA) cycle and respiratory electron transport	-12.0
GO:0019693	ribose phosphate metabolic process	-11.8
GO:0022904	respiratory electron transport chain	-11.6

Color	MCODE	GO	Description	Log10(P)
	MCODE_1	M00087	beta-Oxidation	-7.2
	MCODE_1	hsa_M00087	beta-Oxidation	-7.2
	MCODE_1	R-HSA-168898	Toll-like Receptor Cascades	-7.2
	MCODE_2	GO:0015980	energy derivation by oxidation of organic compounds	-4.7
	MCODE_2	GO:0006091	generation of precursor metabolites and energy	-3.9
	MCODE_2	GO:0019693	ribose phosphate metabolic process	-3.8
	MCODE_3	CORUM:178	Respiratory chain complex I (holoenzyme), mitochondrial	-14.1
	MCODE_3	GO:0006120	mitochondrial electron transport, NADH to ubiquinone	-13.6
	MCODE_3	R-HSA-6799198	Complex I biogenesis	-13.6
	MCODE_4	GO:0043123	positive regulation of I-kappaB kinase/NF-kappaB signaling	-5.9
	MCODE_4	GO:0043122	regulation of I-kappaB kinase/NF-kappaB signaling	-5.5
	MCODE_4	GO:0007249	I-kappaB kinase/NF-kappaB signaling	-5.4

FIGURE 6 | Analysis of MGF regulated protein interaction network in colorectal cancer reveals key roles for mitochondrial energy metabolism and inflammatory signaling to mediate its anticancer effects **(A)** The Circos plot shows how genes from the different input gene lists of tumor (TUMOR) *vs*. metastasis (METAST) mouse models overlap. On the outside, arc represents the identity of each gene list. On the inside, orange color represents the gene names that appear in both lists and light orange color represent unique gene names that are part of common enriched pathways (same ontology term). Purple lines link the same gene shared by multiple gene lists. Blue lines link the genes where they fall into the same ontology term (the term has to be statistically significantly enriched). The greater the number of purple links and the longer the dark orange arcs implies greater overlap among the input gene lists. Blue links indicate the amount of functional overlap among the input gene

(*Continued*)

FIGURE 6 | lists. **(B)** Metascape enrichment analysis of all statistically enriched ontology terms (GO/KEGG terms, canonical pathways, hall mark gene sets). **(C)** Metascape enrichment analysis of all statistically enriched TF-target interaction networks. **(D)** All protein-protein interactions (PPI) among all input gene lists were extracted from PPI data source and formed a PPI network. **(E)** GO enrichment analysis was applied to assign biological "meanings" of the PPI network. **(F)** MCODE sub-protein network components were identified from the merged PPI network. Each MCODE network is assigned a unique color. **(G)** GO enrichment analysis was applied to assign biological "meanings" of MCODE sub-protein networks, where top three best p-value terms were retained.

changes by MGF treatment at 100 mg/kg are less pronounced than at 50 mg/kg since the fraction of CT26 tumor cells is strongly decreased at the highest MGF concentration, which significantly reduces the MGF effect size in the mixed cell population.

Mangiferin Regulated Protein Interaction Networks Target Mitochondrial Energy Metabolism and Inflammatory Signaling to Elicit Antitumor and Antimetastatic Therapy Response *in vivo*

To further characterize molecular mechanism of action of MGF, we further crosscompared MGF responsive genes in the primary CT26 tumor model and the metastatic cancer models by Metascape systems biology freeware (https://metascape.org/) (Zhou et al., 2019) (**Supplementary Figure S4**; **Supplementary Table S3**). As can be observed in the circos plot (**Figure 6A**), we observe significant overlap between gene expression changes as well as biological pathways, as both experiments probably target similar biological processes. This is also clear in the overlapping heatmap representation (**Figure 6B**), showing highly significant pathway enrichment related to blood vessel development, lipid metabolism, chemotaxis, locomotion, wound healing, generation of energy metabolites, hormone stimulus, growth factor response and leukocyte activation among others (**Supplementary Table S3**). Further TRRUST analysis of all statistically enriched TF-target interaction networks (Koundouros and Poulogiannis, 2020) identified major regulatory roles for STAT3, PPARA/G, HIF1A and NFκB1/RelA transcription factor families, which are key players in lipid metabolism, hypoxia and inflammatory tumor signaling (**Figure 6C**). Furthermore, Metascape protein-protein-interaction (PPI) analysis of all MGF responsive target genes reveals a global protein network involved in reprogramming of mitochondrial energy metabolism in CT26 tumor cells (**Figures 6D,E**). More specifically, 4 major protein interaction subnetworks could be identified (**Figure 6F**) involved in fatty acid β-oxidation and toll like receptor signaling (MCODE1), generation of energy metabolites (oxidation organic compounds, ribose phosphate metabolism) (MCODE2), mitochondrial respiratory chain complex 1 (MCODE3) and NFκB signaling (MCODE4) (**Figure 6G**).

Mangiferin Targets Fatty Acid β-oxidation Metabolism in Human HT29 Colon Cancer Cells

To verify whether MGF directly targets fatty acid β-oxidation energy metabolism in colon cancer cells, we measured ketone body concentrations (β-hydroxybutyrate) upon exposure of human HT29 colon cancer cells to free fatty acids (to mimick free fatty acids present in the tumor microenvironment *in vivo*) in presence or absence of MGF. **Figure 7A** shows that 24 h treatment of HT29 cells with 0.2 mM free fatty acids (FFA) increases intracellular concentrations of β-hydroxybutyrate as compared to untreated HT29 cells. Of special note, cotreatment with 400 μM MGF reverses this effect to levels observed in untreated cells. Along the same line we measured changes in protein expression of carnitine palmitoyltransferase (CPT1), a key metabolic enzyme involved in fatty acid β-oxidation. Similarly, FFA treatment increases CPT1 expression levels whereas, MGF reverses the effect to control levels (**Figure 7B**).

DISCUSSION

Today, various pharmacological anticancer properties of MGF have already been described *in vitro*, including antiproliferative, pro-apoptotic, anti-invasive, antimetastatic and antiangiogenic bioactivities (García-Rivera et al., 2011; Khurana et al., 2016; Núñez Selles et al., 2016; Imran et al., 2017; Delgado-Hernández et al., 2020). Here, we further demonstrate *in vivo* antitumor efficacy of MGF in different syngeneic immune competent colon cancer (CT26) mouse allograft models and propose a novel "metabolic" anti-cancer mechanism of action.

To further characterize the corresponding molecular mechanisms involved in tumor regression we have applied systems biology pathway enrichment analysis (IPA) of gene expression patterns of tumor samples of the various treatments. This revealed that cell motility, invasion and metastasis are the most significantly suppressed biological pathways upon MGF treatment. This could be confirmed human and mouse colon cancer cells in a wound scratch assay *in vitro* and a lung metastasis model *in vivo*. At the gene expression level, MGF suppresses various prometastatic genes, including MMP13, COL4A1, COL4A2, INHBA, KMT2A, ZEB1/2. Tumour invasion and metastasis involves degradation of different components of the extracellular matrix and basement membranes (Type IV collagen), catalysed by proteolytic enzymes such as matrix metalloproteinases (MMPs). Degradation of type IV collagen correlates with metastatic potential, whereas MMP-13 gene expression has been identified as a reliable predictor of liver metastasis in patients with CRC (Yamada et al., 2010).

Serum levels of Collagen IV (Col4A1, Col4A2) abundant in are elevated in patients with colorectal liver metastases and facilitate invasion (Wang et al., 2020; Liu et al., 2020). The heterodimeric TGF-β family ligand Inhibin (INHA) is a novel paracrine factor involved in cancer angiogenesis and metastasis (Singh et al., 2018a). The histone methyltransferase KMT2A promotes colorectal cancer metastasis via activation of

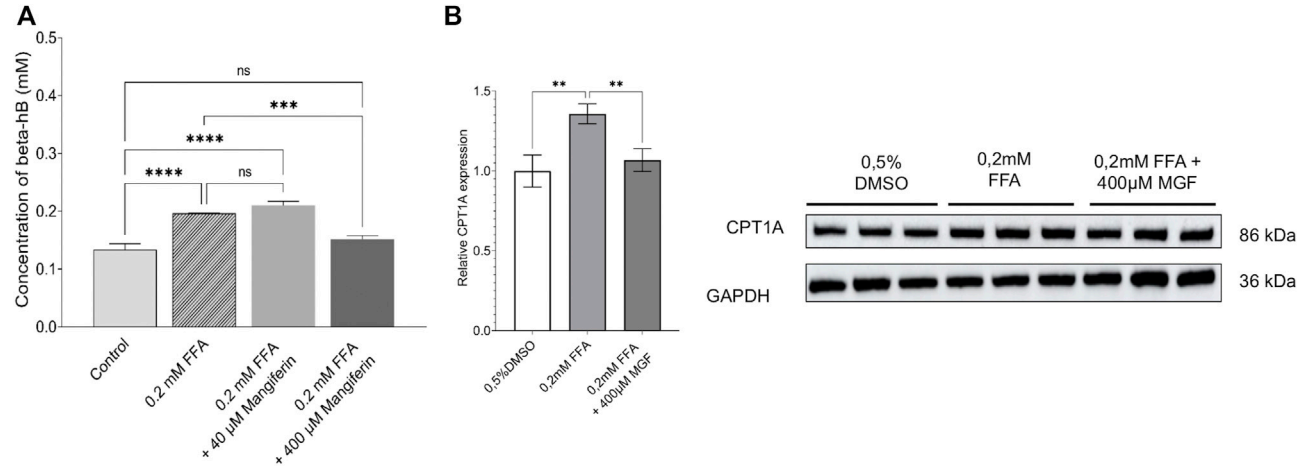

FIGURE 7 | MGF decreases free fatty acid induced fatty acid β-oxidation metabolism in human HT29 colon cancer cells. **(A)** Intracellular concentrations of β-hydroxybutyrate in HT29 cells in response to 24 h treatment with 0.2 mM free fatty acids (FFA) increase significantly compared to untreated HT29 cells. Cotreatment with 400 µM MGF reverses this effect. Data are given as mean ± SD ($n = 3$ wells). Statistics were calculated with 1-way ANOVA and Tukey post-test; ***$p < 0.001$; ****$p < 0.0001$; ns indicates not significant. **(B)** Representative quantification **(left)** of western blot analysis of relative CPT1A protein expression **(right)** in HT29 cells after treatment with 0.2 mM FFA or 0.2 mM FFA with 400 µM MGF. The relative levels of CPT1A were quantified by normalizing to GAPDH which was used as a loading control. Data are given as mean ± SD of three biological replicates. Statistics were calculated with 1-way ANOVA and Dunnett's adjustments; **$p < 0.01$ compared to FFA treated cells.

cathepsin Z (Fang et al., 2019). Finally PDPK1 and ZEB1/2 members drive tumor metastasis spread via regulating epithelial–mesenchymal transition (EMT) during hypoxia (Dupuy et al., 2015; Du et al., 2016; Stemmler et al., 2019; Saxena et al., 2020). Since angiogenesis is one route for metastatic spread of cancer cells, it can be noticed that various transcriptional changes blocking angiogenesis, indirectly also reduce metastatic cell migration and both pathways are interconnected (**Supplementary Figure S2**). Accordingly, MGF decreased expression of various proangiogenic genes such as HMOX1, MMP13, IGF1R, INSR, TGFB3, PDGFR A/B and SEMA5A among others. HMOX1 promotes vascularisation in a hypoxic environment by stimulating paracrine proangiogenic functions of bone marrow derived cells (BMDCs) (Grochot-Przeczek et al., 2014). Besides, HMOX1 also promotes proangiogenic effects in endothelial cells by reciprocal regulation of VEGF and SDF1 (Ayer et al., 2016). TGFB3 induces angiogenesis by promoting transdifferentiation of mesenchymal stem cells into endothelial cells (Batlle et al., 2019). PDGFRA and PDGFRB play different roles in neosvascularisation and promoting vessel stability (Zhang et al., 2009). Matrix metalloprotein (MMP13) by degrading extracellular matrix (ECM) stimulates the release of VEGF from ECM and thereby promoting angiogenesis and metastasis in skin squamous cell carcinoma and colitis induced colon cancer (Lederle et al., 2010; Ai et al., 2015). SEMA5A promotes angiogenesis by increasing endothelial cell proliferation, migration (Sadanandam et al., 2010). Furthermore, oncogenic angiogenic and metastatic functions have been described for INS and IGF1R (Heidegger et al., 2014). Finally, in line with the bioinformatic analysis, the predicted inhibition of angiogenesis, and suppression of vasculogenesis could also be confirmed in an *in vivo* matrigel plug implant mouse model.

By crosscomparing MGF responsive genes in the primary CT26 tumor model and the metastatic cancer models by Metascape systems biology freeware (https://metascape.org/), we searched for a common molecular mechanism of action (**Figure 6**). Interestingly, significant enrichment of various common pathways could be observed related to blood vessel development, lipid metabolism, chemotaxis, locomotion, wound healing, generation of energy metabolites, hormone stimulus, growth factor response and leukocyte activation among others Furthermore, we identified major regulatory roles for STAT3, PPARA/G, SIRT, HIF1A and NFκB1/RelA transcription factor families, which are key players in lipid metabolism, hypoxia and inflammatory tumor signaling. Ultimately, protein-protein-interaction (PPI) analysis of all MGF responsive target genes established a global protein network with 4 major protein interaction subnetworks involved in fatty acid β-oxidation and toll like receptor signaling (MCODE1), generation of energy metabolites (oxidation organic compounds, ribose phosphate metabolism) (MCODE2), mitochondrial respiratory chain complex 1 (MCODE3) and NFκB signaling (MCODE4). MGF regulation of fatty acid β-oxidation metabolism could further be experimentally validated in human HT29 colon cancer cells by colorimetric detection of decrease in β-hydroxybutyrate concentrations and protein expression of the key metabolic enzyme CPT1. Ketone bodies are interwoven with crucial mammalian metabolic pathways such as β-oxidation (FAO), the tricarboxylic acid cycle (TCA), gluconeogenesis, glycolysis and the pentose phosphate pathway (PPP) (Puchalska and Crawford, 2017), which were identified in Metascape protein-protein interaction analysis as key protein (sub)networks affected by MGF treatment (**Figure 6**). A common feature of cancer cells is their ability to rewire their metabolism to sustain the production of ATP and macromolecules needed for cell growth, division and

survival. These alterations are pivotal to the development and maintenance of the malignant phenotype of cancer cells in unfavorable tumor microenvironment or metastatic sites. In particular, the importance of altered fatty acid metabolism in cancer has received renewed interest as, aside their principal role as structural components of the membrane matrix, they are important secondary messengers, and can also serve as fuel sources for energy production (Koundouros and Poulogiannis, 2020; Nagarajan et al., 2021). The ways in which cancer cells utilize lipids are often influenced by the complex interactions within the tumor microenvironment and adjacent stroma (Ma et al., 2018; Corn et al., 2020). Cancer cells survive in challenging hypoxic or nutrient depleted tumor micro-environments. For example tumor-stroma localized adipocytes can be activated by cancer cells to lipolyze their triglyceride stores, delivering secreted fatty acids to cancer cells for uptake through numerous fatty acid transporters. Cancer-associated fibroblasts are also implicated in lipid secretion for cancer cell catabolism and lipid signaling leading to activation of mitogenic and migratory pathways (Koundouros and Poulogiannis, 2020; Nagarajan et al., 2021). As these cancer-stromal interactions are exacerbated during tumor progression, fatty acids secreted into the microenvironment can impact infiltrating immune cell function and phenotype. Regulation of TLR/NFκB/PPAR pathways by (un)saturated fatty acids plays a key role in tumor-immune responses (Hwang et al., 2016). Lipid metabolic abnormalities such as increased fatty acid oxidation and *de novo* lipid synthesis can provide survival advantages for the tumor to resist chemotherapeutic and radiation treatments and alleviate cellular stresses involved in the metastatic cascade. Fatty acid oxidation is also reprogrammed in cancer-associated immune and other host cells, which may contribute to immune suppression and tumorpromoting microenvironment. New evidence indicates that cancer stem cells show high metabolic plasticity and can dynamically transform their metabolic state to favor glycolysis or oxidative metabolism depending on the tumor microenvironment (Belisario et al., 2020; Zhu et al., 2020). This illustrates that fatty acids regulate each part of the cancer lifecycle and suggests that therapeutic intervention targeting lipid and fatty acid metabolism signaling pathways by MGF holds promise for colorectal cancer treatment (Kadochi et al., 2017; Nakamura et al., 2018; Li et al., 2021). Fatty acid catabolism and anabolism pathway crosstalk are pivotal in cell fate decision during redox regulated ferroptosis cancer therapy and maybe strongly context dependent (Hassannia et al., 2018; Kumar et al., 2021; Yuan et al., 2021). In clinical trials, MGF treatment was already found to improve metabolic health (diabetes, hyperlipidemia, insulin resistance) by optimization of mitochondrial bioenergetic pathways (fuel switching between fatty acid and carbohydrates) *via* sirtuin (SIRT) and PPAR (in)dependent metabolic mechanisms (Guo et al., 2011; Niu et al., 2012; Apontes et al., 2014; Na et al., 2015; Singh et al., 2018b; Li et al., 2018; Liu et al., 2018; Zhang et al., 2019). Sirtuin NAD + -dependent histone deacetylase enzymes are central players in the maintenance of cellular energy and metabolic homeostasis, whereas impaired SIRT functions result in several pathological conditions and contribute to the altered metabolic phenotype (metastasis, drug resistance) of malignantly transformed (colorectal) cancer cells, referred to as the Warburg effect (Chalkiadaki and Guarente, 2015; Gaál and Csernoch, 2020). Natural product SIRT modulators (such as MGF) are receiving growing interest to optimize mitochondrial bioenergetic pathways in cancer treatment (Iside et al., 2020; Karaman Mayack et al., 2020). Similarly, PPAR transcription factors are fatty acid sensors that enhance mitochondrial fatty acid β-oxidation (Poulsen et al., 2012; Puchalska and Crawford, 2017). Besides their lipid metabolic effects, PPARs also suppress angiogenesis, metastasis by targeting HIF, NFκB and STAT3 TF functions which regulate cancer hypoxia, inflammatory pathways, chemotaxis, cell adhesion (tight junctions), epithelial-mesenchymal transition (wnt signaling) in the tumor-microenvironment ((Michalik et al., 2004; Wang et al., 2004; Panigrahy et al., 2005; Moraes et al., 2010; Zhou et al., 2012; Woolf et al., 2015; Gou et al., 2017; Ju et al., 2017; Vu and Datta, 2017; Vallée and Lecarpentier, 2018; Mammadova-Bach et al., 2020), in line with our systems biology network analysis. Today, various natural and pharmacological PPAR ligands have already been described with anti-metastatic and anti-angiogenic therapeutic properties (Panigrahy et al., 2005; Gou et al., 2017), which increase the efficacy of chemotherapeutics with minimal toxicity (Girnun et al., 2007; Girnun et al., 2008). Similarly, our results further suggest that MGF has potential value to be used as adjuvant phytotherapeutic treatment against CRC to reduce adverse toxicity and to mitigate outcome of colon cancer treatment. To further develop its application in clinical practice, more molecular combination studies with different MGF formulations (du Plessis-Stoman et al., 2011; Morozkina et al., 2021; Baán et al., 2019) as well as uniformly controlled clinical trials are needed.

DATA AVAILABILITY STATEMENT

All transcriptome data have now been deposited in a public depository (https://zenodo.org/) and can be accessed *via* https://doi.org/10.5281/zenodo.5185362.

ETHICS STATEMENT

The animal study was reviewed and approved by Drug Research and Development Center Ethics Committee for Animal Research and in compliance with the Cuban National Guidelines for the Care and Use of Laboratory Animals (CECMED Resolution No. 37 2012 for Good Laboratory Practice for Quality Control). No human studies were conducted.

AUTHOR CONTRIBUTIONS

Conceptualization, JR-G, IH-B, WVB, RD-H, and IR-G; methodology, JR-G, IH-B, OQ-M, CP-N, EL, CT, PJ, GVC, DC, and ML; software, KD; validation, JCR-G, IH-B; formal analysis, KD, JR-G, IH-B, and WVB; investigation, JR-G, IH-B, OQ-M, CP-N, EL, GVC, ML, WVB, RD-H, IR-G; resources, WVB, RD-H, IR-G; data curation KD, WVB; writing, review and editing, JR-G, IH-B, WVB, RD-H, and IR-G; supervision, WVB,

RD-H, IR-G; project administration, WVB, RD-H, IR-G; funding acquisition, WVB, RD-H, IR-G; All authors have read and agreed to the published version of the manuscript.

FUNDING

This work was supported by the P211LH005-019 project (CITMA), Cuba; Visiting Research Program, PVE400768/2014–3 project (CNPq), Brazil, and the projects ZEIN2011PR383 and ZEIN2016PR418 (Flemish VLIR collaboration program), Belgium. This work was partially supported by the project PN223LH010-035 from Ministerio de Ciencia, Tecnologia y Medio Ambiente (Cuba), Programa de Ciencias Basicas y Naturales.

SUPPLEMENTARY MATERIAL

The Supplementary Material for this article can be found online at: https://www.frontiersin.org/articles/10.3389/fphar.2021.670167/full#supplementary-material

REFERENCES

Abdullah, L. N., and Chow, E. K. (2013). Mechanisms of Chemoresistance in Cancer Stem Cells. *Clin. Transl Med.* 2 (1), 3. doi:10.1186/2001-1326-2-3

Ai, F., Zhang, X., Li, X., Qin, Z., Ye, Q., Tian, L., et al. (2015). Up-regulation of Matrix Metalloproteinases in a Mouse Model of Chemically Induced Colitis-Associated Cancer: the Role of microRNAs. *Oncotarget* 6 (7), 5412–5425. doi:10.18632/oncotarget.3027

Apontes, P., Liu, Z., Su, K., Benard, O., Youn, D. Y., Li, X., et al. (2014). Mangiferin Stimulates Carbohydrate Oxidation and Protects against Metabolic Disorders Induced by High-Fat Diets. *Diabetes* 63 (11), 3626–3636. doi:10.2337/db14-0006

Atanasov, A. G., Zotchev, S. B., Dirsch, V. M., and Supuran, C. T.International Natural Product Sciences Taskforce (2021). Natural Products in Drug Discovery: Advances and Opportunities. *Nat. Rev. Drug Discov.* 20, 200–216. doi:10.1038/s41573-020-00114-z

Ayer, A., Zarjou, A., Agarwal, A., and Stocker, R. (2016). Heme Oxygenases in Cardiovascular Health and Disease. *Physiol. Rev.* 96 (4), 1449–1508. doi:10.1152/physrev.00003.2016

Baán, A., Adriaensens, P., Lammens, J., Delgado Hernandez, R., Vanden Berghe, W., Pieters, L., et al. (2019). Dry Amorphisation of Mangiferin, a Poorly Water-Soluble Compound, Using Mesoporous Silica. *Eur. J. Pharm. Biopharm.* 141, 172–179. doi:10.1016/j.ejpb.2019.05.026

Bao, L., Haque, A., Jackson, K., Hazari, S., Moroz, K., Jetly, R., et al. (2011). Increased Expression of P-Glycoprotein Is Associated with Doxorubicin Chemoresistance in the Metastatic 4T1 Breast Cancer Model. *Am. J. Pathol.* 178 (2), 838–852. doi:10.1016/j.ajpath.2010.10.029

Batlle, R., Andrés, E., Gonzalez, L., Llonch, E., Igea, A., Gutierrez-Prat, N., et al. (2019). Regulation of Tumor Angiogenesis and Mesenchymal-Endothelial Transition by P38α through TGF-β and JNK Signaling. *Nat. Commun.* 10 (1), 3071. doi:10.1038/s41467-019-10946-y

Beatty, G., and Paterson, Y. (2001). IFN-gamma-dependent Inhibition of Tumor Angiogenesis by Tumor-Infiltrating CD4+ T Cells Requires Tumor Responsiveness to IFN-Gamma. *J. Immunol.* 166 (4), 2276–2282. doi:10.4049/jimmunol.166.4.2276

Belisario, D. C., Kopecka, J., Pasino, M., Akman, M., De Smaele, E., Donadelli, M., et al. (2020). Hypoxia Dictates Metabolic Rewiring of Tumors: Implications for Chemoresistance. *Cells* 9 (12), 2598. doi:10.3390/cells9122598

Bhatia, A., and Kumar, Y. (2016). Cancer Stem Cells and Tumor Immunoediting: Putting Two and Two Together. *Expert Rev. Clin. Immunol.* 12 (6), 605–607. doi:10.1586/1744666X.2016.1159133

Bray, F., Ferlay, J., Soerjomataram, I., Siegel, R. L., Torre, L. A., and Jemal, A. (2018). Global Cancer Statistics 2018: GLOBOCAN Estimates of Incidence and Mortality Worldwide for 36 Cancers in 185 Countries. *CA Cancer J. Clin.* 68 (6), 394–424. doi:10.3322/caac.21492

Chalkiadaki, A., and Guarente, L. (2015). The Multifaceted Functions of Sirtuins in Cancer. *Nat. Rev. Cancer* 15 (10), 608–624. doi:10.1038/nrc3985

Chen, S. T., Dou, J., Temple, R., Agarwal, R., Wu, K. M., and Walker, S. (2008). New Therapies from Old Medicines. *Nat. Biotechnol.* 26 (10), 1077–1083. doi:10.1038/nbt1008-1077

Corn, K. C., Windham, M. A., and Rafat, M. (2020). Lipids in the Tumor Microenvironment: From Cancer Progression to Treatment. *Prog. Lipid Res.* 80, 101055. doi:10.1016/j.plipres.2020.101055

Delgado-Hernández, R., Hernández-Balmaseda, I., Rodeiro-Guerra, I., Cesar Rodriguez Gonzalez, J., De Wever, O., Logie, E., et al. (2020). Anti-angiogenic Effects of Mangiferin and Mechanism of Action in Metastatic Melanoma. *Melanoma Res.* 30 (1), 39–51. doi:10.1097/CMR.0000000000000647

Dhir, M., and Sasson, A. R. (2016). Surgical Management of Liver Metastases from Colorectal Cancer. *J. Oncol. Pract.* 12 (1), 33–39. doi:10.1200/JOP.2015.009407

Drabkin, D., and Austin, J. (1935). Spectrophotometric Studies. II. Preparations from Washed Blood Cells: Nitric Oxide Hemoglobin and Sulfhemoglobin. *J. Biol. Chem.* 112 (51), 1935–1936. doi:10.1016/s0021-9258(18)74968-5

Du, J., Yang, M., Chen, S., Li, D., Chang, Z., and Dong, Z. (2016). PDK1 Promotes Tumor Growth and Metastasis in a Spontaneous Breast Cancer Model. *Oncogene* 35 (25), 3314–3323. doi:10.1038/onc.2015.393

du Plessis-Stoman, D., du Preez, J., and van de Venter, M. (2011). Combination Treatment with Oxaliplatin and Mangiferin Causes Increased Apoptosis and Downregulation of NFκB in Cancer Cell Lines. *Afr. J. Tradit Complement. Altern. Med.* 8 (2), 177–184. doi:10.4314/ajtcam.v8i2.63206

Dunning, M. J., Smith, M. L., Ritchie, M. E., and Tavaré, S. (2007). Beadarray: R Classes and Methods for Illumina Bead-Based Data. *Bioinformatics* 23 (16), 2183–2184. doi:10.1093/bioinformatics/btm311

Dupuy, F., Tabariès, S., Andrzejewski, S., Dong, Z., Blagih, J., Annis, M. G., et al. (2015). PDK1-Dependent Metabolic Reprogramming Dictates Metastatic Potential in Breast Cancer. *Cell Metab* 22 (4), 577–589. doi:10.1016/j.cmet.2015.08.007

Evans, J. P., Sutton, P. A., Winiarski, B. K., Fenwick, S. W., Malik, H. Z., Vimalachandran, D., et al. (2016). From Mice to Men: Murine Models of Colorectal Cancer for Use in Translational Research. *Crit. Rev. Oncol. Hematol.* 98, 94–105. doi:10.1016/j.critrevonc.2015.10.009

Fang, Y., Zhang, D., Hu, T., Zhao, H., Zhao, X., Lou, Z., et al. (2019). KMT2A Histone Methyltransferase Contributes to Colorectal Cancer Development by Promoting Cathepsin Z Transcriptional Activation. *Cancer Med.* 8 (7), 3544–3552. doi:10.1002/cam4.2226

Gaál, Z., and Csernoch, L. (2020). Impact of Sirtuin Enzymes on the Altered Metabolic Phenotype of Malignantly Transformed Cells. *Front. Oncol.* 10, 45. doi:10.3389/fonc.2020.00045

García-Rivera, D., Delgado, R., Bougarne, N., Haegeman, G., and Berghe, W. V. (2011). Gallic Acid Indanone and Mangiferin Xanthone Are strong Determinants of Immunosuppressive Anti-tumour Effects of Mangifera Indica L. Bark in MDA-Mb231 Breast Cancer Cells. *Cancer Lett.* 305 (1), 21–31. doi:10.1016/j.canlet.2011.02.011

Gil, E., Hernández, R. G., Nuevas, L., and Hoogmartens, J. (2014). Determination of Mangiferin in Mangifera Indica L. Stem Bark Extract (Vimang®) and Pharmaceuticals by Liquid Chromatography. *Emirates J. Food Agric.* 26, 592–601. doi:10.9755/ejfa.v26i7.18186

Girnun, G. D., Chen, L., Silvaggi, J., Drapkin, R., Chirieac, L. R., Padera, R. F., et al. (2008). Regression of Drug-Resistant Lung Cancer by the Combination of Rosiglitazone and Carboplatin. *Clin. Cancer Res.* 14 (20), 6478–6486. doi:10.1158/1078-0432.CCR-08-1128

Girnun, G. D., Naseri, E., Vafai, S. B., Qu, L., Szwaya, J. D., Bronson, R., et al. (2007). Synergy between PPARgamma Ligands and Platinum-Based Drugs in Cancer. *Cancer Cell* 11 (5), 395–406. doi:10.1016/j.ccr.2007.02.025

Gou, Q., Gong, X., Jin, J., Shi, J., and Hou, Y. (2017). Peroxisome Proliferator-Activated Receptors (PPARs) Are Potential Drug Targets for Cancer Therapy. *Oncotarget* 8 (36), 60704–60709. doi:10.18632/oncotarget.19610

Grochot-Przeczek, A., Kotlinowski, J., Kozakowska, M., Starowicz, K., Jagodzinska, J., Stachurska, A., et al. (2014). Heme Oxygenase-1 Is Required for Angiogenic Function of Bone Marrow-Derived Progenitor Cells: Role in Therapeutic Revascularization. *Antioxid. Redox Signal.* 20 (11), 1677–1692. doi:10.1089/ars.2013.5426

Guo, F., Huang, C., Liao, X., Wang, Y., He, Y., Feng, R., et al. (2011). Beneficial Effects of Mangiferin on Hyperlipidemia in High-Fat-Fed Hamsters. *Mol. Nutr. Food Res.* 55 (12), 1809–1818. doi:10.1002/mnfr.201100392

Han, H., Cho, J. W., Lee, S., Yun, A., Kim, H., Bae, D., et al. (2018). TRRUST V2: an Expanded Reference Database of Human and Mouse Transcriptional Regulatory Interactions. *Nucleic Acids Res.* 46 (D1), D380–D386. doi:10.1093/nar/gkx1013

Hassannia, B., Wiernicki, B., Ingold, I., Qu, F., Van Herck, S., Tyurina, Y. Y., et al. (2018). Nano-targeted Induction of Dual Ferroptotic Mechanisms Eradicates High-Risk Neuroblastoma. *J. Clin. Invest.* 128 (8), 3341–3355. doi:10.1172/JCI99032

He, W., You, Y., Du, S., Lei, T., Wang, H., Li, X., et al. (2019). Anti-neoplastic Effect of Mangiferin on Human Ovarian Adenocarcinoma OVCAR8 Cells via the Regulation of YAP. *Oncol. Lett.* 17 (1), 1008–1018. doi:10.3892/ol.2018.9708

Heidegger, I., Kern, J., Ofer, P., Klocker, H., and Massoner, P. (2014). Oncogenic Functions of IGF1R and INSR in Prostate Cancer Include Enhanced Tumor Growth, Cell Migration and Angiogenesis. *Oncotarget* 5 (9), 2723–2735. doi:10.18632/oncotarget.1884

Hernandez-Balmaseda, I., Guerra, I. R., Declerck, K., Herrera Isidrón, J. A., Pérez-Novo, C., Van Camp, G., et al. (2021). Marine Seagrass Extract of Thalassia Testudinum Suppresses Colorectal Tumor Growth, Motility and Angiogenesis by Autophagic Stress and Immunogenic Cell Death Pathways. *Mar. Drugs* 19 (2), 52. doi:10.3390/md19020052

Hwang, D. H., Kim, J. A., and Lee, J. Y. (2016). Mechanisms for the Activation of Toll-like Receptor 2/4 by Saturated Fatty Acids and Inhibition by Docosahexaenoic Acid. *Eur. J. Pharmacol.* 785, 24–35. doi:10.1016/j.ejphar.2016.04.024

Imran, M., Arshad, M. S., Butt, M. S., Kwon, J. H., Arshad, M. U., and Sultan, M. T. (2017). Mangiferin: a Natural Miracle Bioactive Compound against Lifestyle Related Disorders. *Lipids Health Dis.* 16 (1), 84. doi:10.1186/s12944-017-0449-y

Iside, C., Scafuro, M., Nebbioso, A., and Altucci, L. (2020). SIRT1 Activation by Natural Phytochemicals: An Overview. *Front. Pharmacol.* 11, 1225. doi:10.3389/fphar.2020.01225

Ju, K. D., Lim, J. W., and Kim, H. (2017). Peroxisome Proliferator-Activated Receptor-Gamma Inhibits the Activation of STAT3 in Cerulein-Stimulated Pancreatic Acinar Cells. *J. Cancer Prev.* 22 (3), 189–194. doi:10.15430/JCP.2017.22.3.189

Kadochi, Y., Mori, S., Fujiwara-Tani, R., Luo, Y., Nishiguchi, Y., Kishi, S., et al. (2017). Remodeling of Energy Metabolism by a Ketone Body and Medium-Chain Fatty Acid Suppressed the Proliferation of CT26 Mouse colon Cancer Cells. *Oncol. Lett.* 14 (1), 673–680. doi:10.3892/ol.2017.6195

Karaman Mayack, B., Sippl, W., and Ntie-Kang, F. (2020). Natural Products as Modulators of Sirtuins. *Molecules* 25 (14), 3287. doi:10.3390/molecules25143287

Kastana, P., Zahra, F. T., Ntenekou, D., Katraki-Pavlou, S., Beis, D., Lionakis, M. S., et al. (2019). Matrigel Plug Assay for *In Vivo* Evaluation of Angiogenesis. *Methods Mol. Biol.* 1952, 219–232. doi:10.1007/978-1-4939-9133-4_18

Khurana, R. K., Kaur, R., Lohan, S., Singh, K. K., and Singh, B. (2016). Mangiferin: a Promising Anticancer Bioactive. *Pharm. Pat Anal.* 5 (3), 169–181. doi:10.4155/ppa-2016-0003

Kobelt, D., Walther, W., and Stein, U. S. (2021). Real-Time Cell Migration Monitoring to Analyze Drug Synergism in the Scratch Assay Using the IncuCyte System. *Methods Mol. Biol.* 2294, 133–142. doi:10.1007/978-1-0716-1350-4_9

Koundouros, N., and Poulogiannis, G. (2020). Reprogramming of Fatty Acid Metabolism in Cancer. *Br. J. Cancer* 122 (1), 4–22. doi:10.1038/s41416-019-0650-z

Kumar, N., Perez-Novo, C., Shaw, P., Logie, E., Privat-Maldonado, A., Dewilde, S., et al. (2021). Physical Plasma-Derived Oxidants Sensitize Pancreatic Cancer Cells to Ferroptotic Cell Death. *Free Radic. Biol. Med.* 166, 187–200. doi:10.1016/j.freeradbiomed.2021.02.026

Lederle, W., Hartenstein, B., Meides, A., Kunzelmann, H., Werb, Z., Angel, P., et al. (2010). MMP13 as a Stromal Mediator in Controlling Persistent Angiogenesis in Skin Carcinoma. *Carcinogenesis* 31 (7), 1175–1184. doi:10.1093/carcin/bgp248

Leiro, J., Arranz, J. A., Yáñez, M., Ubeira, F. M., Sanmartín, M. L., and Orallo, F. (2004). Expression Profiles of Genes Involved in the Mouse Nuclear Factor-Kappa B Signal Transduction Pathway Are Modulated by Mangiferin. *Int. Immunopharmacol* 4 (6), 763–778. doi:10.1016/j.intimp.2004.03.002

Li, J., Liu, M., Yu, H., Wang, W., Han, L., Chen, Q., et al. (2018). Mangiferin Improves Hepatic Lipid Metabolism Mainly through its Metabolite-Norathyriol by Modulating SIRT-1/AMPK/SREBP-1c Signaling. *Front. Pharmacol.* 9, 201. doi:10.3389/fphar.2018.00201

Li, J., Zhang, H., and Dai, Z. (2021). Cancer Treatment with the Ketogenic Diet: A Systematic Review and Meta-Analysis of Animal Studies. *Front. Nutr.* 8, 594408. doi:10.3389/fnut.2021.594408

Liu, Y., Zhang, J., Chen, Y., Sohel, H., Ke, X., Chen, J., et al. (2020). The Correlation and Role Analysis of COL4A1 and COL4A2 in Hepatocarcinogenesis. *Aging (Albany NY)* 12 (1), 204–223. doi:10.18632/aging.102610

Liu, Z., Apontes, P., Fomenko, E. V., Chi, N., Schuster, V. L., Kurland, I. J., et al. (2018). Mangiferin Accelerates Glycolysis and Enhances Mitochondrial Bioenergetics. *Int. J. Mol. Sci.* 19 (1), 201. doi:10.3390/ijms19010201

Ma, Y., Temkin, S. M., Hawkridge, A. M., Guo, C., Wang, W., Wang, X. Y., et al. (2018). Fatty Acid Oxidation: An Emerging Facet of Metabolic Transformation in Cancer. *Cancer Lett.* 435, 92–100. doi:10.1016/j.canlet.2018.08.006

Mammadova-Bach, E., Gil-Pulido, J., Sarukhanyan, E., Burkard, P., Shityakov, S., Schonhart, C., et al. (2020). Platelet Glycoprotein VI Promotes Metastasis through Interaction with Cancer Cell-Derived Galectin-3. *Blood* 135 (14), 1146–1160. doi:10.1182/blood.2019002649

Mayer, R. J. (2009). Targeted Therapy for Advanced Colorectal Cancer-Mmore Is Not Always Better. *N. Engl. J. Med.* 360 (6), 623–625. doi:10.1056/NEJMe0809343

Michalik, L., Desvergne, B., and Wahli, W. (2004). Peroxisome-proliferator-activated Receptors and Cancers: Complex Stories. *Nat. Rev. Cancer* 4 (1), 61–70. doi:10.1038/nrc1254

Mihalache, A., and Rogoveanu, I. (2014). Angiogenesis Factors Involved in the Pathogenesis of Colorectal Cancer. *Curr. Health Sci. J.* 40 (1), 5–11. doi:10.12865/CHSJ.40.01.01

Ministerio de Salud Pública. Dirección de Registros Médicos y Estadísticas de Salud, L. H., and de Cuba, República. (2017). *Anuario Estadístico de Salud 2016*.

Moraes, L. A., Spyridon, M., Kaiser, W. J., Jones, C. I., Sage, T., Atherton, R. E., et al. (2010). Non-genomic Effects of PPARgamma Ligands: Inhibition of GPVI-Stimulated Platelet Activation. *J. Thromb. Haemost.* 8 (3), 577–587. doi:10.1111/j.1538-7836.2009.03732.x

Morozkina, S. N., Nhung Vu, T. H., Generalova, Y. E., Snetkov, P. P., and Uspenskaya, M. V. (2021). Mangiferin as New Potential Anti-cancer Agent and Mangiferin-Integrated Polymer Systems-A Novel Research Direction. *Biomolecules* 11 (1), 79. doi:10.3390/biom11010079

Na, L., Zhang, Q., Jiang, S., Du, S., Zhang, W., Li, Y., et al. (2015). Mangiferin Supplementation Improves Serum Lipid Profiles in Overweight Patients with Hyperlipidemia: a Double-Blind Randomized Controlled Trial. *Sci. Rep.* 5, 10344. doi:10.1038/srep10344

Nagarajan, S. R., Butler, L. M., and Hoy, A. J. (2021). The Diversity and Breadth of Cancer Cell Fatty Acid Metabolism. *Cancer Metab.* 9 (1), 2. doi:10.1186/s40170-020-00237-2

Nakamura, K., Tonouchi, H., Sasayama, A., and Ashida, K. (2018). A Ketogenic Formula Prevents Tumor Progression and Cancer Cachexia by Attenuating Systemic Inflammation in Colon 26 Tumor-Bearing Mice. *Nutrients* 10 (2), 206. doi:10.3390/nu10020206

Newman, D. J., and Cragg, G. M. (2020). Natural Products as Sources of New Drugs over the Nearly Four Decades from 01/1981 to 09/2019. *J. Nat. Prod.* 83 (3), 770–803. doi:10.1021/acs.jnatprod.9b01285

Niu, Y., Li, S., Na, L., Feng, R., Liu, L., Li, Y., et al. (2012). Mangiferin Decreases Plasma Free Fatty Acids through Promoting its Catabolism in Liver by Activation of AMPK. *PLoS One* 7 (1), e30782. doi:10.1371/journal.pone.0030782

Núñez Selles, A. J., Daglia, M., and Rastrelli, L. (2016). The Potential Role of Mangiferin in Cancer Treatment through its Immunomodulatory, Anti-angiogenic, Apoptopic, and Gene Regulatory Effects. *Biofactors* 42 (5), 475–491. doi:10.1002/biof.1299

Núñez Sellés, A. J., Vélez Castro, H. T., Agüero-Agüero, J., González-González, J., Naddeo, F., De Simone, F., et al. (2002). Isolation and Quantitative Analysis of Phenolic Antioxidants, Free Sugars, and Polyols from Mango (Mangifera Indica L.) Stem Bark Aqueous Decoction Used in Cuba as a Nutritional Supplement. *J. Agric. Food Chem.* 50 (4), 762–766. doi:10.1021/jf011064b

Panigrahy, D., Huang, S., Kieran, M. W., and Kaipainen, A. (2005). PPARgamma as a Therapeutic Target for Tumor Angiogenesis and Metastasis. *Cancer Biol. Ther.* 4 (7), 687–693. doi:10.4161/cbt.4.7.2014

Petrelli, F., Tomasello, G., Borgonovo, K., Ghidini, M., Turati, L., Dallera, P., et al. (2017). Prognostic Survival Associated with Left-Sided vs Right-Sided Colon Cancer: A Systematic Review and Meta-Analysis. *JAMA Oncol.* 3 (2), 211–219. doi:10.1001/jamaoncol.2016.4227

Poulsen, Ll., Siersbæk, M., and Mandrup, S. (2012). PPARs: Fatty Acid Sensors Controlling Metabolism. *Semin. Cell Dev Biol* 23 (6), 631–639. doi:10.1016/j.semcdb.2012.01.003

Pritchard, J. R., Lauffenburger, D. A., and Hemann, M. T. (2012). Understanding Resistance to Combination Chemotherapy. *Drug Resist. Updat* 15 (5-6), 249–257. doi:10.1016/j.drup.2012.10.003

Puchalska, P., and Crawford, P. A. (2017). Multi-dimensional Roles of Ketone Bodies in Fuel Metabolism, Signaling, and Therapeutics. *Cell Metab* 25 (2), 262–284. doi:10.1016/j.cmet.2016.12.022

Ritchie, M. E., Phipson, B., Wu, D., Hu, Y., Law, C. W., Shi, W., et al. (2015). Limma powers Differential Expression Analyses for RNA-Sequencing and Microarray Studies. *Nucleic Acids Res.* 43 (7), e47. doi:10.1093/nar/gkv007

Sadanandam, A., Rosenbaugh, E. G., Singh, S., Varney, M., and Singh, R. K. (2010). Semaphorin 5A Promotes Angiogenesis by Increasing Endothelial Cell Proliferation, Migration, and Decreasing Apoptosis. *Microvasc. Res.* 79 (1), 1–9. doi:10.1016/j.mvr.2009.10.005

Sarkar, A., Sreenivasan, Y., Ramesh, G. T., and Manna, S. K. (2004). Beta-D-Glucoside Suppresses Tumor Necrosis Factor-Induced Activation of Nuclear Transcription Factor kappaB but Potentiates Apoptosis. *J. Biol. Chem.* 279 (32), 33768–33781. doi:10.1074/jbc.M403424200

Saxena, K., Jolly, M. K., and Balamurugan, K. (2020). Hypoxia, Partial EMT and Collective Migration: Emerging Culprits in Metastasis. *Transl Oncol.* 13 (11), 100845. doi:10.1016/j.tranon.2020.100845

Shaked, Y. (2016). Balancing Efficacy of and Host Immune Responses to Cancer Therapy: the Yin and Yang Effects. *Nat. Rev. Clin. Oncol.* 13 (10), 611–626. doi:10.1038/nrclinonc.2016.57

Singh, A. K., Raj, V., Keshari, A. K., Rai, A., Kumar, P., Rawat, A., et al. (2018). Isolated Mangiferin and Naringenin Exert Antidiabetic Effect via PPARγ/GLUT4 Dual Agonistic Action with strong Metabolic Regulation. *Chem. Biol. Interact* 280, 33–44. doi:10.1016/j.cbi.2017.12.007

Singh, P., Jenkins, L. M., Horst, B., Alers, V., Pradhan, S., Kaur, P., et al. (2018). Inhibin Is a Novel Paracrine Factor for Tumor Angiogenesis and Metastasis. *Cancer Res.* 78 (11), 2978–2989. doi:10.1158/0008-5472.CAN-17-2316

Stemmler, M. P., Eccles, R. L., Brabletz, S., and Brabletz, T. (2019). Non-redundant Functions of EMT Transcription Factors. *Nat. Cell Biol* 21 (1), 102–112. doi:10.1038/s41556-018-0196-y

Tan, H. Y., Wang, N., Li, S., Hong, M., Guo, W., Man, K., et al. (2018). Repression of WT1-Mediated LEF1 Transcription by Mangiferin Governs β-Catenin-Independent Wnt Signalling Inactivation in Hepatocellular Carcinoma. *Cell Physiol Biochem* 47 (5), 1819–1834. doi:10.1159/000491063

Teng, M. W., Galon, J., Fridman, W. H., and Smyth, M. J. (2015). From Mice to Humans: Developments in Cancer Immunoediting. *J. Clin. Invest.* 125 (9), 3338–3346. doi:10.1172/JCI80004

Ting, W. C., Chen, L. M., Pao, J. B., Yang, Y. P., You, B. J., Chang, T. Y., et al. (2013). Common Genetic Variants in Wnt Signaling Pathway Genes as Potential Prognostic Biomarkers for Colorectal Cancer. *PLoS One* 8 (2), e56196. doi:10.1371/journal.pone.0056196

Torre, L. A., Siegel, R. L., Ward, E. M., and Jemal, A. (2016). Global Cancer Incidence and Mortality Rates and Trends--An Update. *Cancer Epidemiol. Biomarkers Prev.* 25 (1), 16–27. doi:10.1158/1055-9965.EPI-15-0578

Vallée, A., and Lecarpentier, Y. (2018). Crosstalk between Peroxisome Proliferator-Activated Receptor Gamma and the Canonical WNT/β-Catenin Pathway in Chronic Inflammation and Oxidative Stress during Carcinogenesis. *Front. Immunol.* 9, 745. doi:10.3389/fimmu.2018.00745

Vatandoust, S., Price, T. J., and Karapetis, C. S. (2015). Colorectal Cancer: Metastases to a Single Organ. *World J. Gastroenterol.* 21 (41), 11767–11776. doi:10.3748/wjg.v21.i41.11767

Vu, T., and Datta, P. K. (2017). Regulation of EMT in Colorectal Cancer: A Culprit in Metastasis. *Cancers (Basel)* 9 (12), 171. doi:10.3390/cancers9120171

Wang, J., and Zhu, C. (2016). Anticoagulation in Combination with Antiangiogenesis and Chemotherapy for Cancer Patients: Evidence and Hypothesis. *Onco Targets Ther.* 9, 4737–4746. doi:10.2147/OTT.S103184

Wang, L. H., Yang, X. Y., Zhang, X., Huang, J., Hou, J., Li, J., et al. (2004). Transcriptional Inactivation of STAT3 by PPARgamma Suppresses IL-6-responsive Multiple Myeloma Cells. *Immunity* 20 (2), 205–218. doi:10.1016/s1074-7613(04)00030-5

Wang, T., Jin, H., Hu, J., Li, X., Ruan, H., Xu, H., et al. (2020). COL4A1 Promotes the Growth and Metastasis of Hepatocellular Carcinoma Cells by Activating FAK-Src Signaling. *J. Exp. Clin. Cancer Res.* 39 (1), 148. doi:10.1186/s13046-020-01650-7

Wang, Z., Dabrosin, C., Yin, X., Fuster, M. M., Arreola, A., Rathmell, W. K., et al. (2015). Broad Targeting of Angiogenesis for Cancer Prevention and Therapy. *Semin. Cancer Biol.* 35 Suppl (Suppl. l), S224–S243. doi:10.1016/j.semcancer.2015.01.001

Woolf, E. C., Curley, K. L., Liu, Q., Turner, G. H., Charlton, J. A., Preul, M. C., et al. (2015). The Ketogenic Diet Alters the Hypoxic Response and Affects Expression of Proteins Associated with Angiogenesis, Invasive Potential and Vascular Permeability in a Mouse Glioma Model. *PLoS One* 10 (6), e0130357. doi:10.1371/journal.pone.0130357

World Health Organization (2019). *WHO Global Report on Traditional and Complementary Medicine 2019*. Geneva: World Health Organization.

Yamada, T., Oshima, T., Yoshihara, K., Tamura, S., Kanazawa, A., Inagaki, D., et al. (2010). Overexpression of MMP-13 Gene in Colorectal Cancer with Liver Metastasis. *Anticancer Res.* 30 (7), 2693–2699.

Yuan, Z. H., Liu, T., Wang, H., Xue, L. X., and Wang, J. J. (2021). Fatty Acids Metabolism: The Bridge between Ferroptosis and Ionizing Radiation. *Front Cell Dev Biol* 9, 675617. doi:10.3389/fcell.2021.675617

Zhang, J., Cao, R., Zhang, Y., Jia, T., Cao, Y., and Wahlberg, E. (2009). Differential Roles of PDGFR-Alpha and PDGFR-Beta in Angiogenesis and Vessel Stability. *FASEB J.* 23 (1), 153–163. doi:10.1096/fj.08-113860

Zhang, Q., Kong, X., Yuan, H., Guan, H., Li, Y., and Niu, Y. (2019). Mangiferin Improved Palmitate-Induced-Insulin Resistance by Promoting Free Fatty Acid Metabolism in HepG2 and C2C12 Cells via PPARα: Mangiferin Improved Insulin Resistance. *J. Diabetes Res.* 2019, 2052675. doi:10.1155/2019/2052675

Zhou, J., Zhang, S., Xue, J., Avery, J., Wu, J., Lind, S. E., et al. (2012). Activation of Peroxisome Proliferator-Activated Receptor α (PPARα) Suppresses Hypoxia-Inducible Factor-1α (HIF-1α) Signaling in Cancer Cells. *J. Biol. Chem.* 287 (42), 35161–35169. doi:10.1074/jbc.m112.367367

Zhou, Y., Zhou, B., Pache, L., Chang, M., Khodabakhshi, A. H., Tanaseichuk, O., et al. (2019). Metascape Provides a Biologist-Oriented Resource for the Analysis of Systems-Level Datasets. *Nat. Commun.* 10 (1), 1523–1533. doi:10.1038/s41467-019-09234-6

Zhu, X., Chen, H. H.ik, Gao, C. Y., Zhang, X. X., Jiang, J. X., Zhang, Y., et al. (2020). Energy Metabolism in Cancer Stem Cells. *World J. Stem Cell* 12 (6), 448–461. doi:10.4252/wjsc.v12.i6.448

Zorde Khvalevsky, E., Gabai, R., Rachmut, I. H., Horwitz, E., Brunschwig, Z., Orbach, A., et al. (2013). Mutant KRAS Is a Druggable Target for Pancreatic Cancer. *Proc. Natl. Acad. Sci. U S A.* 110 (51), 20723–20728. doi:10.1073/pnas.1314307110

Zou, B., Wang, H., Liu, Y., Qi, P., Lei, T., Sun, M., et al. (2017). Mangiferin Induces Apoptosis in Human Ovarian Adenocarcinoma OVCAR3 Cells via the Regulation of Notch3. *Oncol. Rep.* 38 (3), 1431–1441. doi:10.3892/or.2017.5814

Conflict of Interest: The authors declare that the research was conducted in the absence of any commercial or financial relationships that could be construed as a potential conflict of interest.

Publisher's Note: All claims expressed in this article are solely those of the authors and do not necessarily represent those of their affiliated organizations, or those of the publisher, the editors and the reviewers. Any product that may be evaluated in this article, or claim that may be made by its manufacturer, is not guaranteed or endorsed by the publisher.

frontiers in Pharmacology

ORIGINAL RESEARCH
published: 23 March 2022
doi: 10.3389/fphar.2022.847905

Silibinin Therapy Improves Cholangiocarcinoma Outcomes by Regulating ERK/Mitochondrial Pathway

Yang Bai[1,2†], *Jiaqi Chen*[3†], *Weijian Hu*[2], *Lei Wang*[4], *Yulian Wu*[1*] *and Shi'an Yu*[2*]

[1]*Department of Surgery, The Second Affiliated Hospital, Zhejiang University School of Medicine, Hangzhou, China,* [2]*Department of Hepatobiliary and Pancreatic Surgery, Affiliated Jinhua Hospital, Zhejiang University School of Medicine, Jinhua, China,* [3]*Stomatology Hospital, School of Stomatology, Zhejiang University School of Medicine, Clinical Research Center for Oral Diseases of Zhejiang Province, Key Laboratory of Oral Biomedical Research of Zhejiang Province, Cancer Center of Zhejiang University, Hangzhou, China,* [4]*Department of Urology Surgery, Affiliated Jinhua Hospital, Zhejiang University School of Medicine, Jinhua, China*

OPEN ACCESS

Edited by:
Qingmin Sun,
Affiliated Hospital of Nanjing University of Chinese Medicine, China

Reviewed by:
Xiaodong Liu,
The Chinese University of Hong Kong, China
Wansong Chen,
Central South University, China

***Correspondence:**
Shi'an Yu
ysa513513@gmail.com
Yulian Wu
yulianwu@zju.edu.cn

[†]*These authors have contributed equally to this work*

Specialty section:
This article was submitted to Pharmacology of Anti-Cancer Drugs, a section of the journal Frontiers in Pharmacology

Received: *03 January 2022*
Accepted: *07 March 2022*
Published: *23 March 2022*

Citation:
Bai Y, Chen J, Hu W, Wang L, Wu Y and Yu S (2022) Silibinin Therapy Improves Cholangiocarcinoma Outcomes by Regulating ERK/Mitochondrial Pathway. Front. Pharmacol. 13:847905. doi: 10.3389/fphar.2022.847905

Background: Silibinin is widely utilized drug in various cancer treatments, though its application in cholangiocarcinoma has not yet been explored. For the first time, we evaluated the anticancer potential and underlying molecular mechanism of silibinin in treatment of cholangiocarcinoma treatment.

Methods: HuCCT-1 and CCLP-1 cells were chosen to be an *in vitro* study model and were exposed to various concentrations of silibinin for indicated times. Cell viability was evaluated by the cell counting kit-8 (CCK-8) assay and half maximal inhibitory (IC50) concentrations were calculated. Cell proliferation capacity was determined through the use of colony formation and 5-Ethynyl-2′- deoxyuridine (EdU) assays. Cell apoptosis and cycle arrest were assessed by Live/Dead staining assay and flow cytometry (FCM). The protein levels of extracellular regulated protein kinases (ERK)/mitochondrial apoptotic pathway were evaluated through western blotting (WB). Mitochondrial membrane potential changes were determined *via* 5,5′,6,6′-Tetrachloro-1,1′,3,3′-tetraethyl-imidacarbocyanine iodide (JC-1). A cholangiocarcinoma cell line xenograft model was used to assess the anti-tumor activity of silibinin *in vivo*.

Results: Inhibition of the ERK protein by silibinin led to a significant decrease in mitochondrial membrane potential, which, in turn, caused Cytochrome C to be released from the mitochondria. The activation of downstream apoptotic pathways led to apoptosis of cholangiocarcinoma cells. In general, silibinin inhibited the growth of cholangiocarcinoma cell line xenograft tumors.

Abbreviations: CCK-8, cell counting kit-8; CDKs, cyclin dependent kinases; EdU, 5-Ethynyl-2′- deoxyuridine; ERK, extracellular regulated protein kinases; FCM, flow cytometry; FITC, Fluorescein isothiocyanate isomer; HE, hematoxylin and eosin; IC50, half maximal inhibitory; IHC, immunohistochemistry; JC-1, 5,5',6,6'-Tetrachloro-1,1',3,3'-tetraethyl-imidacarbocyanine iodide; LC3B, microtubule-associated proteins light chain 3B; MAPK, mitogen activated protein kinase; PI, propidium iodine; PMSF, Phenylmethanesulfonyl fluoride; PVDF, polyvinylidene fluoride; TUNEL, TdT mediated dUTP Nick End Labeling; WB, western blotting.

Conclusions: Silibinin is able to inhibit cholangiocarcinoma through the ERK/mitochondrial apoptotic pathway, which makes silibinin a potential anti-tumor drug candidate for cholangiocarcinoma treatment.

Keywords: silibinin, cholangiocarcinoma, ERK, mitochondrial membrane potential, anti tumor drug

INTRODUCTION

Cholangiocarcinoma is a highly malignant tumor that originates from the bile duct epithelial cells and occurs from the capillary bile duct to the common bile duct. It is the second most common hepatobiliary pancreatic tumor in the world, accounting for 3% of all gastrointestinal malignancies (Banales et al., 2020). Cholangiocarcinoma exhibits different biological behavior than hepatocellular carcinoma, as cholangiocarcinoma is more likely to infiltrate into the bile duct wall, and invade the surrounding liver tissue, blood vessels, nerves and lymphoid tissue. Therefore, the surgical resection rate is low and the overall prognosis of patients remains poor (Rizvi et al., 2018). Thus far, most patients are in the advanced stage of the disease at time of diagnosis, and systemic treatment remains the main treatment (Kelley et al., 2020). However, due to differences in molecular pathology and gene mutations between biliary systemic tumors at different anatomical sites, the effects of systematic treatments are quite different (Chaisaingmongkol et al., 2017; Montal et al., 2020). Therefore, there is an urgent need to develop novel drugs for the treatment of cholangiocarcinoma.

Silibinin is an antioxidant that has been extracted from a plant called milk thistle (Bosch-Barrera et al., 2017). It can stabilize the hepatocyte membrane and maintain its integrity. It is also able to promote the recovery of hepatocyte ultrastructure, as it is the most effective flavonoid found in the world (Salomone et al., 2017). Additionally, studies have demonstrated that silibinin can also inhibit growth and differentiation of liver cancer (Mao et al., 2018), prostate cancer (Vue et al., 2016), breast cancer (Si et al., 2020) and cervical cancer (García-Maceira and Mateo, 2009). It is very well-known that the malignant degree of cholangiocarcinoma is high, and conventional treatment is limited. Therefore, in this study, we evaluated the use of silibinin for the treatment of cholangiocarcinoma in order to find a novel treatment for this disease.

ERK is a member of the mitogen activated protein kinase (MAPK) family (Guo et al., 2020). After it becomes activated, it has an important role in cell growth, development, division, death, as well as malignant transformation. ERK-mediated signal transduction pathway receives various mitogen stimulation, as well as stress of cells from inside and outside. It activates ERK substrate, and regulates cell proliferation, apoptosis and invasion (Lavoie et al., 2020). Activated ERK plays an anti-apoptotic role by phosphorylating the anti-apoptotic molecule Bcl-2, activating transcription factors and interfering with TRAIL, which finally promotes tumor cell growth. Overactivation of ERK has been found in oral cancer (Gao et al., 2020), melanoma (Savoia et al., 2019), breast cancer (Peng et al., 2017) and others. However, there are few studies on ERK protein in cholangiocarcinoma. In this paper, we were aiming to observe the therapeutic effect of silibinin on cholangiocarcinoma *in vivo* and *in vitro*, as well as to explore its potential mechanism.

MATERIAL AND METHODS

Materials

Silibinin (cat. no. S109809) was purchased from Aladdin. Primary antibodies against Caspase-9 (cat. no. ab202068), Caspase-3 (cat. no. ab184787), PARP (cat. no. ab191217), p53 (cat. no. ab26) and GAPDH (cat. no. ab181602) were bought from Abcam. CDK2 (cat. no. 10122-1-AP), cdc25a (cat. no. 55031-1-AP), ERK (cat. no. 16443-1-AP), CDK4 (cat. no. 11026-1-AP), Bcl-2 (cat. no. 12789-1-AP), Bcl-xl (cat. no. 10783-1-AP), and Cytochrome C (cat. no. 10993-1-AP) were purchased from Proteintech. Cyclin E2 (cat. no. #4132) was bought from Cell Signaling Technology. p-ERK (cat. no. AF1015) and VDAC (cat. no. DF6140) were bought from Affinity. The antibodies were utilized at the recommended concentrations following the manufacturer's instructions.

Cell Culture

HuCCT-1 and CCLP-1, two human cholangiocarcinoma cell lines, were acquired from the American Tissue Culture Collection (Manassas, VA, USA). The cell lines were cultured in RPMI 1640 medium (cat. no. 01-100-1A, Biological Industries) that was supplemented with 10% FBS (cat. no. 04-001-1B, Biological Industries), 100 U/ml penicillin and 100 μg/ml streptomycin (Invitrogen, CA, USA). All cells were incubated at 37°C in a humidified atmosphere with 5% CO_2.

Cell Counting Kit-8 Assay

For concentration-dependent cell viability experiments, cells were seeded onto 96-well plates ($4*10^3$ cells/well), 18 h prior to treatment with varying concentrations of silibinin for an additional 48 h. Overall, 10 μl CCK-8 (cat. no. C0037, Beyotime) was added into each well for 2 h, and the absorption value was then measured. For time-dependent cell viability experiments, HuCCT-1 and CCLP-1 cells were plated onto 96-well plates 18 h prior to treatment with an IC50 and 2*IC50 concentrations of silibinin for 0, 6, 12, 24, 48, and 72 h. The absorption value was measured at different time points. Curves were fitted and analyzed using the GraphPad Prism 8.4.0 software (GraphPad Software, Inc.).

Colony Formation Assay

Cholangiocarcinoma cells were seeded onto a 6-well plate (Jet Bio-Filtration Co., Ltd.) at 5,000 cells per well 18 h prior to treatment with silibinin or SCH772984. Then, after treatment

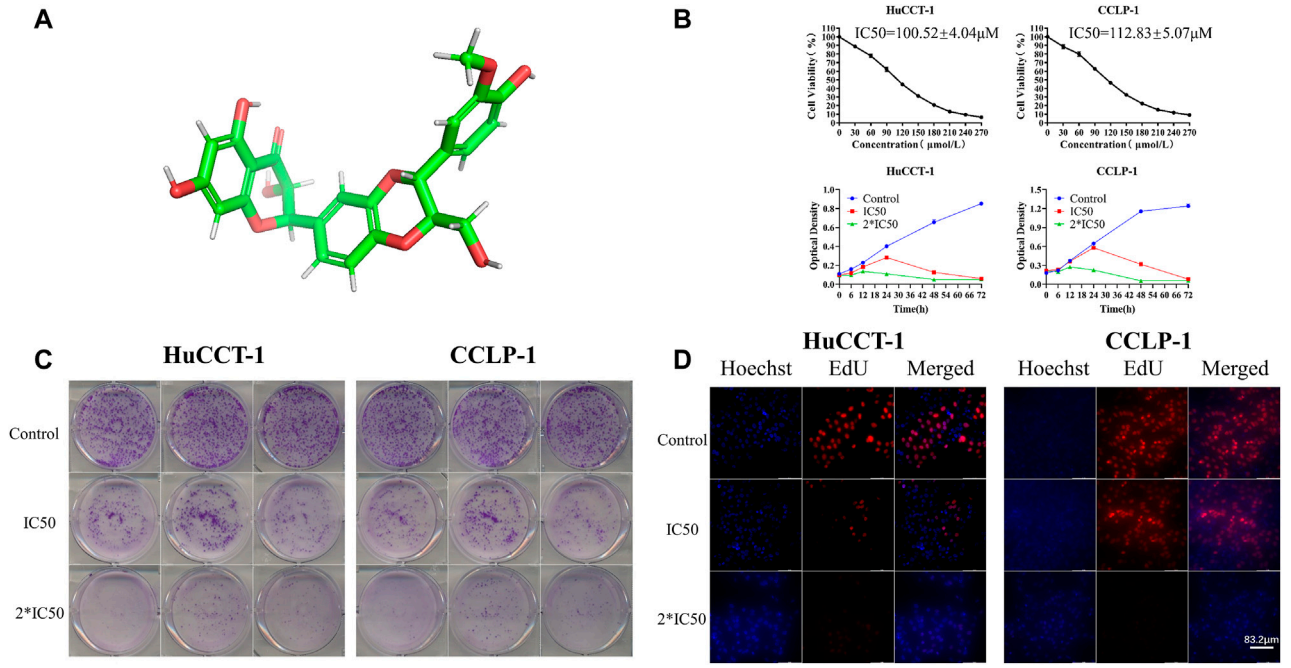

FIGURE 1 | Silibinin inhibits cell viability in cholangiocarcinoma cells. **(A)**. Diagram of the three-dimensional structure of silibinin. **(B)**. Silibinin inhibited cell viability of HuCCT-1 and CCLP-1 cell lines in a concentration-dependent and time-dependent manner. Cells were treated with varying concentrations of silibinin for indicated time points (6, 12, 24, 48 and 72 h) and cell viability was examined by the CCK-8 assay. **(C)**. Colony formation assay results of HuCCT-1 and CCLP-1 cell lines treated with different concentrations of silibinin. **(D)**. EdU proliferation assay results of HuCCT-1 and CCLP-1 cell lines treated with different concentrations of silibinin.

cells were incubated for another 14 days and then stained with crystal violet. More than 50 cells were defined as a clone.

EdU Proliferation Assay

The BeyoClick™ EdU Cell Proliferation Kit with Alexa Fluor 594 (cat. no. C0078S; Beyotime) was used to evaluate the effect of silibinin and SCH772984 on the cholangiocarcinoma cell lines, according to the manufacturer's instructions. After treatment for 48 h, cholangiocarcinoma cells were EdU-labeled and cultured for another 2 hours. Next, Hoechst33342 staining was carried out. Fluorescence microscopy (Olympus Corporation, Japan) was utilized to take a picture.

Apoptosis and Cell Cycle Analysis

Cell apoptosis was assessed using Annexin V-FITC Apoptosis Detection Kit (cat. no. C1062M, Beyotime), according to the manufacturer's protocol. In brief, cells were seeded onto six-well plates at a density of $4*10^5$ cells per well. After being exposed to silibinin or SCH772984 for 48 h, cells were then cultured with fluorescein isothiocyanate isomer (FITC) and propidium iodine (PI) at 37°C for 30 min. Then, cell cycle distribution was evaluated utilizing the Cell Cycle and Apoptosis Analysis Kit (cat. no. C1052, Beyotime). After exposure to IC50 and 2*IC50 concentrations of silibinin for 48 h, the cells were collected and fixed with 75% pre-cooled ethanol. Then, cells were stained with PI for 30 min prior to detection. Finally, apoptosis and cell cycle distribution were detected by FCM, and then analyzed utilizing Flowjo 10.4 (FlowJo LLC) and Modifit LT 5 (Verity Software House, Inc.).

Live/Dead Staining Assay

Live/dead staining assay was conducted utilizing a Calcein/PI Live/Dead Viability/Cytotoxicity Assay Kit (cat. no. C2015M, Beyotime). In brief, after exposure to IC50 and 2*IC50 concentrations of silibinin for 48 h, cells were collected and stained using Calcein and PI for 20 min at room temperature. The pictures were taken by a fluorescence microscope (Olympus IX71).

Cell Mitochondria Isolation

Mitochondria isolation assay was carried out according to the manufacturer's protocol. Briefly, after exposure to IC50 and 2*IC50 concentrations of silibinin for 48 h, cells were collected and then incubated with mitochondria isolation reagents that contain 1% Phenylmethanesulfonyl fluoride (PMSF) in an ice bath for 15 min. Subsequently, cell suspensions were then homogenized for appropriate times, and the proportion of cells that were positive for trypan blue staining was examined microscopically (**Supplementary Figure S1A**). When the positive ratio exceeded 50%, then the homogenate was stopped and mitochondria were isolated using differential centrifugation.

Western Blotting

Western blotting analysis was carried out, as previously described (Chen et al., 2021). Briefly, cells were collected and dissolved

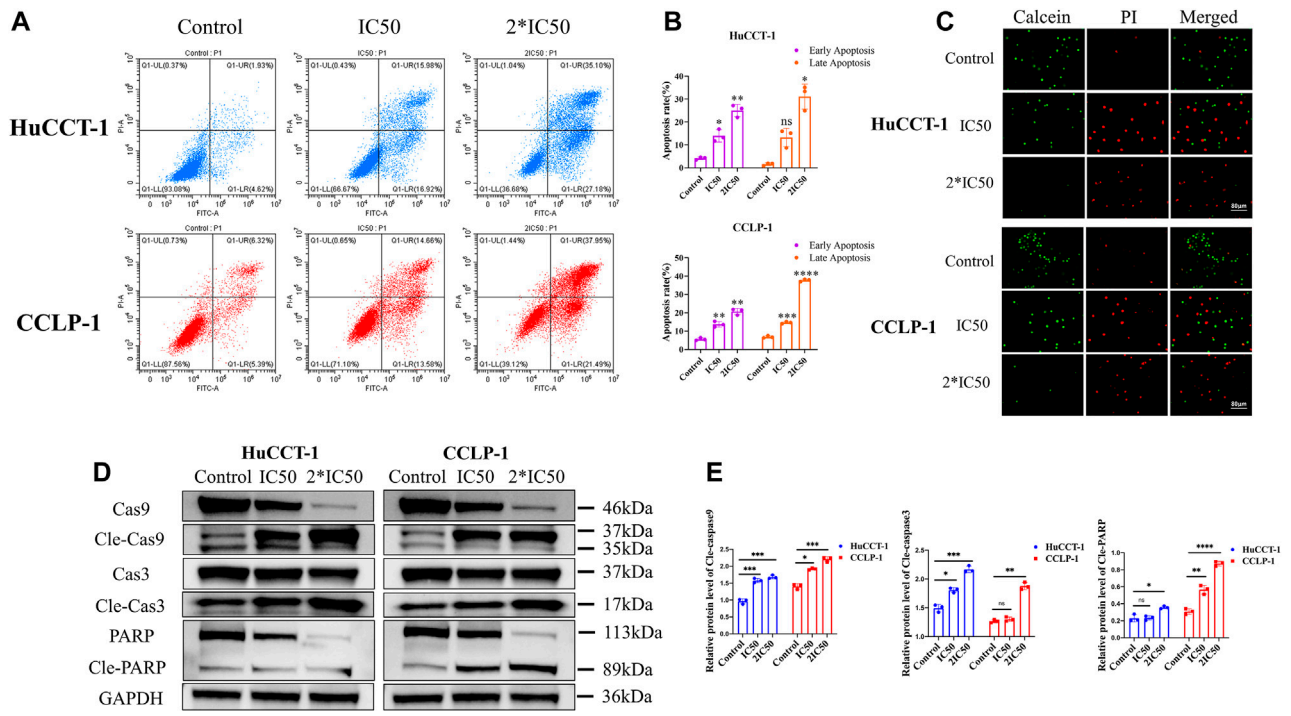

FIGURE 2 | Silibinin induced apoptosis in HuCCT-1 and CCLP-1 cells. **(A,B)**. Detection of apoptosis by FCM and quantitative analysis of the apoptosis rate. HuCCT-1 and CCLP-1 cells were treated with IC50 and 2*IC50 concentrations of silibinin for 48 h **(C)**. The live/dead staining assay results of the HuCCT-1 and CCLP-1 cell lines treated with silibinin for 48 h. Red dots represent dead cells and green dots represent surviving cells. **(D)**. Western blotting results of HuCCT-1 and CCLP-1 cell lines treated with IC50 and 2*IC50 concentrations of silibinin for 48 h. The apoptosis-related proteins were identified. **(E)**. The quantification results of cle-caspase-9, cle-caspase-3 and cle-PARP. Data are shown as mean ± SD. $*p < 0.05$, $**p < 0.01$, $***p < 0.001$, $****p < 0.0001$, significantly difference compared to the control group.

within the Lysis Buffer (cat. no. P0013B, Beyotime) containing 1 mM PMSF (cat. no. ST506, Beyotime). The protein concentration was detected through the use of an enhanced BCA Protein Assay Kit (cat. no. P0010, Beyotime). Next, equivalent amounts of protein were separated on SurePAGE Bis-Tris gels (GenScript) for electrophoresis, and then transferred to polyvinylidene fluoride (PVDF) membranes. Then, the membranes were blocked *via* a blocking buffer (cat. no. P0252, Beyotime) for 1 h, and then cultured with primary antibodies overnight. After incubation with secondary antibodies at appropriate concentration for an hour at room temperature, the protein bands on the membrane were eventually identified using a Hypersensitivity Chemiluminescence Kit (cat. no. G2020, Servicebio). The band intensity was quantified using the ImageJ software (National Institutes of Health).

Mitochondrial Membrane Potential Analysis

Briefly, after exposure to IC50 and 2*IC50 concentrations of silibinin for 48 h, cells were collected and then incubated with the JC-1 staining working solution at 37°C for 30 min. The treated cells underwent subsequent FCM or fluorescence photographs by confocal microscopy.

In Vivo Experiments

Animal experiments were carried out, as described previously (Chen et al., 2021). Until tumors reached approximately 30 mm^3, the mice were randomly assigned into three different groups. First, the mice were assigned to a control group (n = 4; 0.9% physiological saline). Second, the mice were assigned to a low-dose silibinin group (n = 4; 100 mg/kg). Third, they were assigned to a high-dose silibinin group (n = 4, 200 mg/kg). Finally, compounds were administered in a peritumoral manner once a day. Tumor volume was calculated using the following formula: volume = length*width^2/2 and mice were sacrificed 3 weeks after injection.

Immunohistochemistry Staining Analysis

For immunohistochemistry (IHC) staining assay, sections that were 5 um thick were stained with hematoxylin and eosin (HE) for analysis of proliferation and apoptosis. For total ERK (t-ERK) and phosphorylated ERK (p-ERK) detection of protein expression, tissue sections were incubated with anti-ERK and p-ERK primary antibodies overnight, and then incubated with HRP-conjugated secondary antibody. The proliferative capacity of tumors was analyzed using Ki-67 staining, and apoptotic cells were determined through the use of a TdT mediated dUTP Nick End Labeling (TUNEL) Apoptosis Assay Kit (cat. no. C1091, Beyotime), as per the manufacturer's introductions.

Statistical Analysis

Data and figures were processed through the use of GraphPad Prism 8.4.0 (GraphPad Software, Inc.). The values were expressed

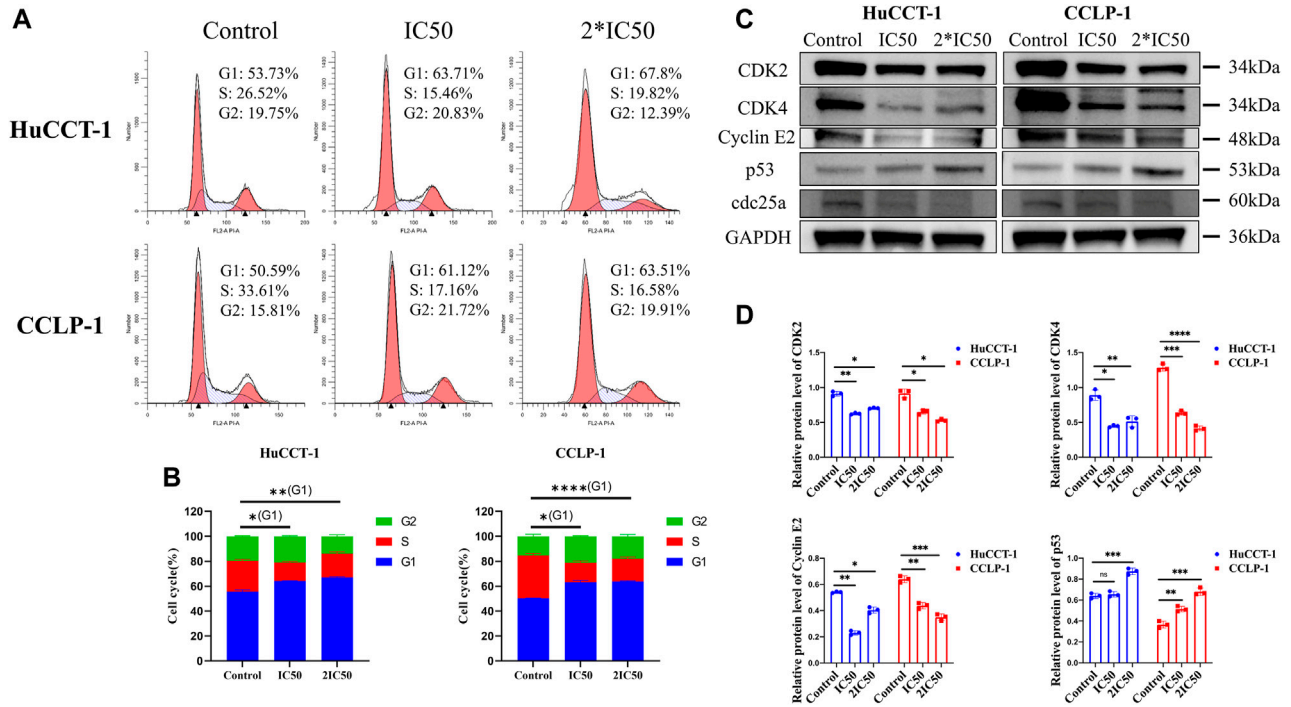

FIGURE 3 | Silibinin induced G1 arrest in cholangiocarcinoma. **(A,B)**. Cholangiocarcinoma cell cycle distribution was determined using FCM analysis after treatment with IC50 and 2*IC50 concentrations of silibinin. The histograms show the percentage of HuCCT-1 and CCLP-1 cells in each phase. **(C,D)**. Western blotting results of G1 checkpoint proteins. Cells were treated with IC50 and 2*IC50 concentrations of silibinin for 48 h. The quantification results of CDK2, CDK4, Cyclin E2 and p53 are demonstrated by histograms. Data are shown as mean ± SD, $*p < 0.05$, $**p < 0.01$, $***p < 0.001$, $****p < 0.0001$, significantly difference compared with control group.

as mean ± standard deviation, and then assessed using Student's t-test or the one-way analysis of variance procedure. Dunnett's multiple comparisons test was chosen as the post test for data satisfying the homogeneity of variance. Furthermore, Dunnett's T3 multiple comparisons test was chosen as a post-hoc test for data that did not meet the homogeneity of variance. With the exception of animal experiments (four mice allocated per group to ensure a sufficient group size for statistical analysis), which was carried out once, all other experiments were performed in triplicate with at least three independent experiments. $p < 0.05$ was considered to be a statistically significant difference.

RESULTS

The Viability of Cholangiocarcinoma Cells was Significantly Inhibited by Silibinin

In order to illustrate the therapeutic efficacy of silibinin (**Figure 1A**)on cholangiocarcinoma, two cholangiocarcinoma cell lines, HuCCT-1 and CCLP-1, were chosen to be *in vitro* cell models. The cell viability of HuCCT-1 and CCLP-1 was significantly inhibited by silibinin after administering the drug for 48 h and the IC50 was 100.52 ± 4.04 μmol/L and 112.83 ± 5.07 μmol/L, respectively (**Figure 1B**). In addition, cholangiocarcinoma cells were inhibited by silibinin in a time-dependent manner. The ability to proliferate is one aspect of cell viability. Therefore, the proliferation of cholangiocarcinoma after silibinin treatment was determined. The colony formation ability and the proliferation ability of cholangiocarcinoma cells treated with silibinin were significantly inhibited (**Figures 1C,D**). These results illustrate that silibinin can act as a tumor suppressor by inhibiting the proliferation of cholangiocarcinoma.

Apoptosis was Induced by Silibinin in Cholangiocarcinoma Cells

In addition to their proliferative capacity, apoptosis can significantly affect cell viability as well. Therefore, the effect of silibinin on cholangiocarcinoma cell apoptosis was examined. After treatment with IC50 and 2*IC50 concentrations of silibinin for 48 h, the apoptosis rate of HuCCT-1 and CCLP-1 cells was significantly increased compared to the control group, as shown by FCM with FITC/PI double staining (**Figures 2A,B**). Consistent with results from FCM, Live/Dead cell staining assay indicated a significant transition from calcein signal to PI signal (**Figure 2C**), demonstrating that silibinin induced apoptosis of cholangiocarcinoma cells in a dose-dependent manner. In order to further determine whether cholangiocarcinoma cells underwent apoptosis, rather than necrosis or other types of cell death, western blotting was utilized to determine the expression of the downstream apoptosis-related proteins, Caspase-3 and PARP. The

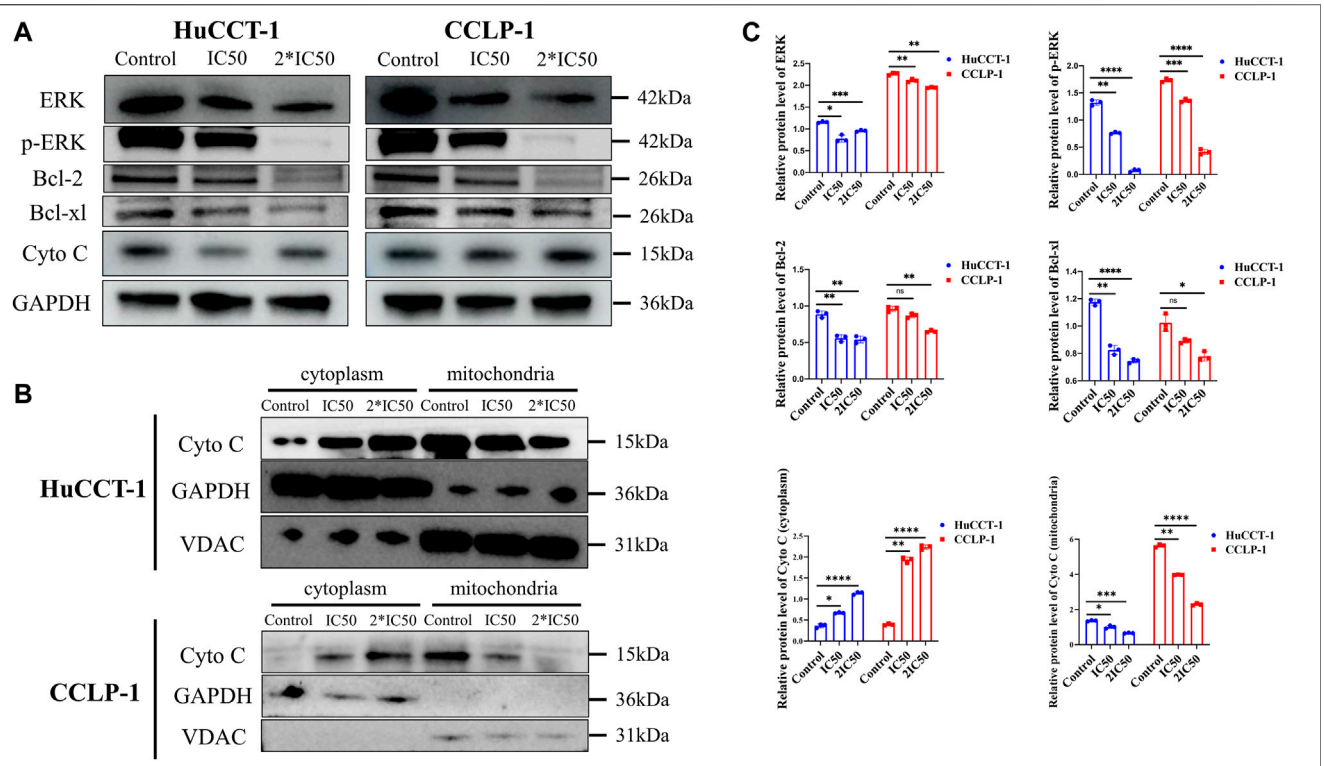

FIGURE 4 | Silibinin induced apoptosis of cholangiocarcinoma cells through the ERK/Cytochrome c pathway. **(A)**. Expression of upstream proteins of the mitochondrial apoptosis pathway, as detected by western blotting. Cells were treated with IC50 and 2*IC50 concentrations of silibinin for 48 h **(B)**. Cytochrome C expression in different parts after mitochondrial isolation. **(C)**. The quantification results of western blotting. Data are shown as mean ± SD, $*p < 0.05$, $**p < 0.01$, $***p < 0.001$, $****p < 0.0001$, significantly different compared to the control group.

expression of cleaved Caspase-3 and cleaved PARP1 significantly increased after silibinin treatment, which means that silibinin induced cholangiocarcinoma cell death by activating apoptosis pathways (**Figures 2D,E**). Furthermore, we discovered that expression of cleaved Caspase-9 significantly increased after silibinin administration, which implies that apoptosis of cholangiocarcinoma cells may be mitochondria-related.

G1 Arrest was Induced by Silibinin in Cholangiocarcinoma Cells

In order to explore more underlying mechanisms resulting in loss of cell viability after silibinin treatment, FCM was utilized to evaluate the cell cycle distribution of both cell lines. The percentage of cells in the G1 phase increased significantly in the HuCCT-1 and CCLP-1 cell line after being treated with IC50 concentration of silibinin for 48 h, from 53.73 to 63.71% ($p < 0.05$) and from 50.59 to 61.12% ($p < 0.05$), respectively (**Figures 3A,B**). This ratio was further enhanced when 2*IC50 concentration of silibinin was administered. Next, the expression of the G1 checkpoint protein was determined by WB. The CDK2, CDK4 and Cyclin E2 levels decreased markedly with a significant increase in p53, indicating that treatment with silibinin might result in G1 arrest in cholangiocarcinoma cells (**Figures 3C,D**).

Silibinin-Mediated Apoptosis of Cholangiocarcinoma Cells was Associated with Mitochondrial Apoptosis

From prior results, it can be determined that the apoptosis of cholangiocarcinoma cells is associated with mitochondria whose reduced membrane potential can cause cell apoptosis. Changes of the mitochondrial membrane potential is related to ERK protein expression. Therefore, the expression of ERK and p-ERK were initially examined. The expression of both proteins was significantly reduced after silibinin administration (**Figures 4A,C**). At the same time, the ratio of p-ERK to ERK also significantly decreased, which means that silibinin treatment was associated with ERK degradation and possibly ERK dephosphorylation (**Supplementary Figure S1B**). Additionally, Phosphorylated ERK can indirectly activate Bcl-2 and Bcl-xl protein on the downstream mitochondrial membrane, in order to change the mitochondrial membrane potential. As hypothesized, a decrease of p-ERK expression led to a significant decrease in the expression of Bcl-2 and Bcl-xl. The decrease of Bcl-2 and Bcl-xl protein led to a reduction in the mitochondrial membrane potential, as indicated by JC-1 assay, making JC-1 unable to aggregate within the matrix of mitochondria, leading to a transition from aggregates to monomers (**Figures 5A,B**). Consistent with FCM results, confocal microscopy results demonstrated a significant

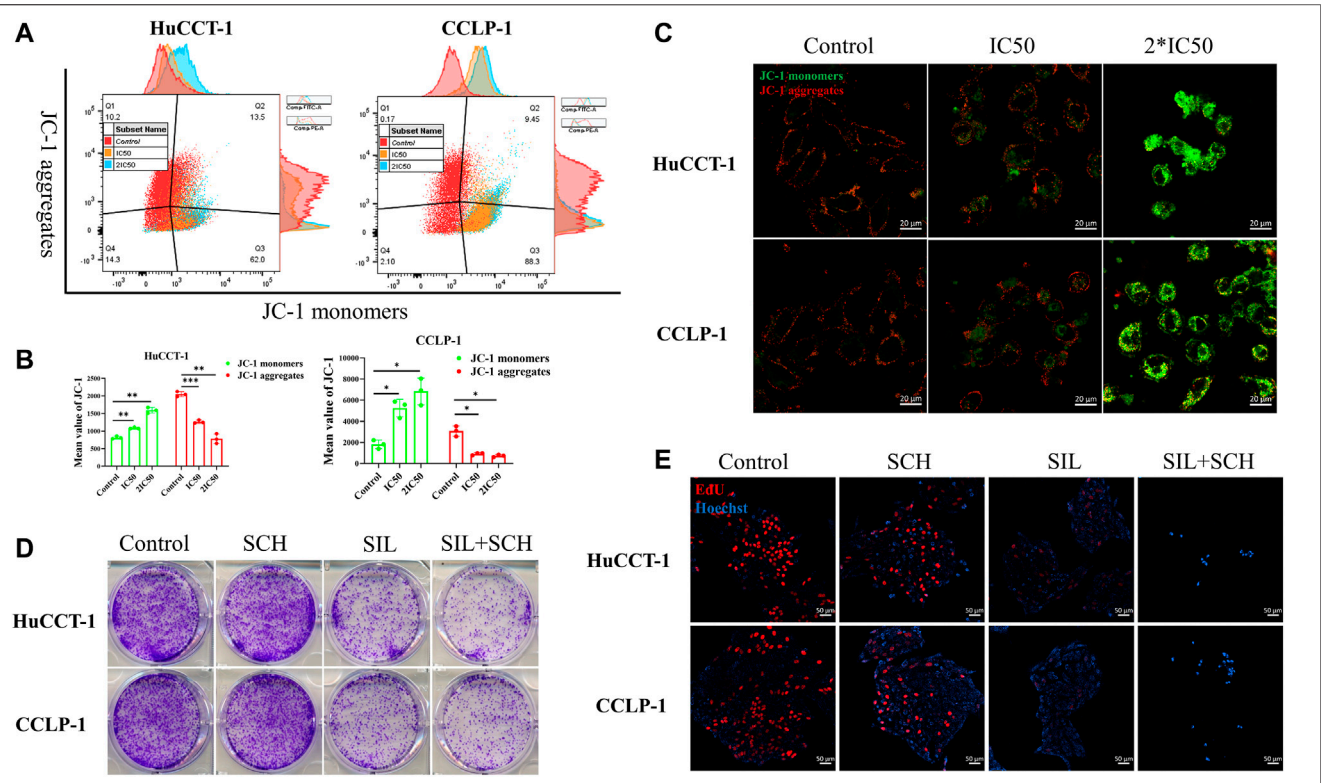

FIGURE 5 | Silibinin acts on the ERK protein, causing a decrease in mitochondrial membrane potential. **(A,B)**. FCM results of the mitochondrial membrane potential changes in cholangiocarcinoma cells. Cells were treated with IC50 and 2*IC50 concentrations of silibinin for 48 h. Data is shown as mean ± SD, $^{*}p < 0.05$, $^{**}p < 0.01$, $^{***}p < 0.001$, significantly different compared to the control group. **(C)**. Mitochondrial membrane potential changes were observed by confocal microscopy after silibinin treatment. Red fluorescence indicates aggregates and green fluorescence indicates monomers. **(D)**. Colony formation assay results of HuCCT-1 and CCLP-1 cell lines treated with silibinin and SCH772984. **(E)**. EdU proliferation assay results of HuCCT-1 and CCLP-1 cell lines treated with silibinin and SCH772984.

transition from red signal to green signal after silibinin treatment (**Figure 5C**). A reduction in mitochondrial membrane potential was a hallmark event within the early stages of apoptosis, which can further trigger release of Cytochrome C from mitochondria to cytoplasm. Cytochrome C was significantly decreased within the mitochondria, but increased in the cytoplasm after silibinin administration, which further activated downstream Caspase-9, causing cholangiocarcinoma cell apoptosis (**Figures 4B,C**).

ERK Regulated Silibinin-Mediated Apoptosis in Cholangiocarcinoma Cells

From these results, we speculated that ERK proteins have an important function in silibinin-mediated apoptosis of cholangiocarcinoma cells. Therefore, SCH772984, which is an inhibitor of ERK proteins, was utilized to explore the effect of selective inhibition of ERK on cholangiocarcinoma cells. The colony formation and proliferation ability of cholangiocarcinoma cells were significantly inhibited *via* silibinin, and the inhibitory effect was more significant after the addition of SCH772984 (**Figures 5D,E**). The cholangiocarcinoma cell apoptosis caused by silibinin was significantly aggravated following SCH772984 treatment (**Figures 6A,B**). In addition, the combination of silibinin and SCH772984 led to a significant increase in the expression of apoptosis-related proteins (**Figures 6C,D**).

Silibinin Suppressed Growth of Tumors *In Vivo*

In order to investigate the effect of silibinin in cholangiocarcinoma growth *in vivo*, mice bearing cholangiocarcinoma subcutaneous xenografts were utilized. After silibinin was administered for 3 weeks, tumor size and weight were significantly reduced (**Figures 7A,B**). From the 14th day after silibinin treatment, the tumor growth rate was significantly reduced compared to the control group. Additionally, the greater the dose administered, the more significant the difference (**Figure 7C**). IHC analysis indicated a significant reduction of Ki-67 staining, as well as a dramatic increase of TUNEL staining in tumor tissues of mice treated with silibinin, suggesting that tumor proliferation was inhibited and apoptosis played an important role (**Figure 7D**, **Supplementary Figure S1C**). Finally, ERK and p-ERK protein expression in tumor tissues was detected. Similar to the results *in vitro*, silibinin was able to significantly reduce expression of two proteins (**Figures 7D–F**, **Supplementary Figure S1C**). These

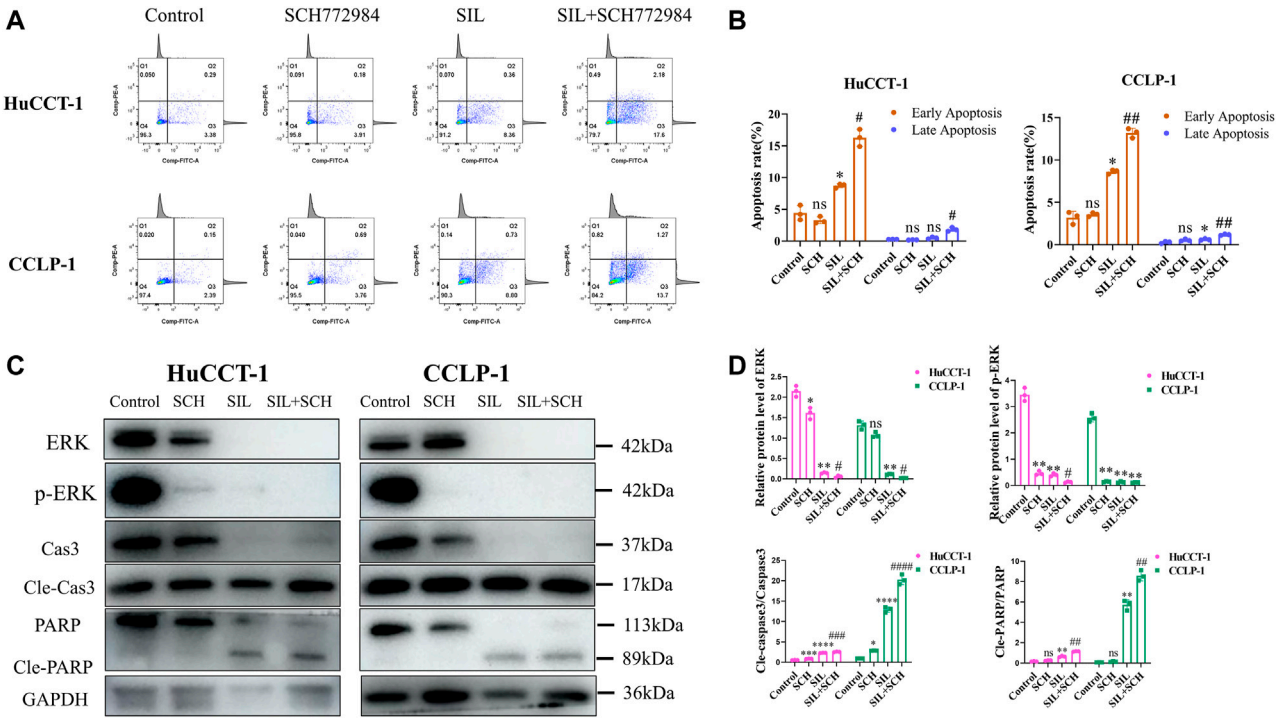

FIGURE 6 | The combined application of SCH772984 significantly aggravated apoptosis of cholangiocarcinoma cells. **(A,B)**. Apoptosis detection by FCM and quantitative analysis of the apoptosis rate. **(C,D)**. The expression of apoptosis-related proteins was identified in HuCCT-1 and CCLP-1 cell lines, and quantification results were shown by histograms. Data is shown as mean ± SD, $^{*}p < 0.05$, $^{**}p < 0.01$, $^{***}p < 0.001$, $^{****}p < 0.0001$, significantly difference compared to the control group. $\#p < 0.05$, $\#\#p < 0.01$, $\#\#\#p < 0.001$, significantly difference compared to the SIL group.

results demonstrate that silibinin suppressed cholangiocarcinoma growth *in vivo* in a similar manner.

DISCUSSION

Silymarin, a traditional Chinese medicine, is the dried and mature fruit of *Silybum marianum Gaertn*, with several functions including bring down a fever, detoxifying, soothing the liver and gallbladder (Federico et al., 2017). Silibinin, which is extracted from the shell of silybin seed, is one of the components with the highest content, as well as the strongest anti-inflammatory activity (Chen J et al., 2020). Due to its effect as an antioxidant (Chen YH et al., 2020), anti-lipid peroxidation, anti-fibrosis (Liu R et al., 2020) and immune regulation (Luo et al., 2019), silibinin is known to be a "natural liver protecting medicine". It is widely used in the treatment of hepatitis, liver cirrhosis and metabolic liver injury (Abenavoli et al., 2010). In recent years, studies have demonstrated that silibinin has activities other than liver protection, including a strong anti-tumor activity, which has attracted more attention from researchers (Bosch-Barrera et al., 2017). Cholangiocarcinoma is a type of tumor with high molecular and genetic heterogeneity, as its location can occur anywhere from ductus arteriosus to the common bile duct (Rizvi et al., 2018). Due to the different molecular pathology and genetic mutations between tumors of the biliary system across different anatomic locations, it is more difficult to treat cholangiocarcinoma compared to other neoplasms (Rizvi and Gores, 2013). From the perspective of cell biology, the process of carcinogenesis involves cell proliferation, differentiation, apoptosis, angiogenesis and as well as others. From the perspective of molecular biology, it involves a series of proteins, kinases, transcription factors and cellular pathways. Silibinin can have an important function across different stages of carcinogenesis, including inhibiting proliferation of cancer cells, regulating cell cycle and inducing apoptosis in order to play a considerable role in anti-tumor activity (Bosch-Barrera and Menendez, 2015). Many studies have demonstrated that silibinin has promising anticancer effects across both androgen dependent and independent prostate, skin, bladder, lung, colon, breast and liver cancers (Polachi et al., 2016; Vue et al., 2016; Barros et al., 2020; Liu Y et al., 2020). However, thus far, there have been no reports on the application of silibinin on cholangiocarcinoma treatment. With this in mind, this study utilized silibinin in the treatment of cholangiocarcinoma for the first time and explored the underlying mechanisms in order to search for a new therapeutic approach for cholangiocarcinoma.

The cell cycle is a fundamental process of cellular life activities, fueled by the sequential activation of corresponding cyclin-dependent kinases (CDKs) by cyclins (Dalton, 2015). Cyclin periodic accumulation and disassembly positively regulates cell cycle progression, whereas CDK inhibitors negatively regulate cell cycle progression by inhibiting activity of CDKs at appropriate time points during the cell cycle. Cyclins, CDKs, and CDK

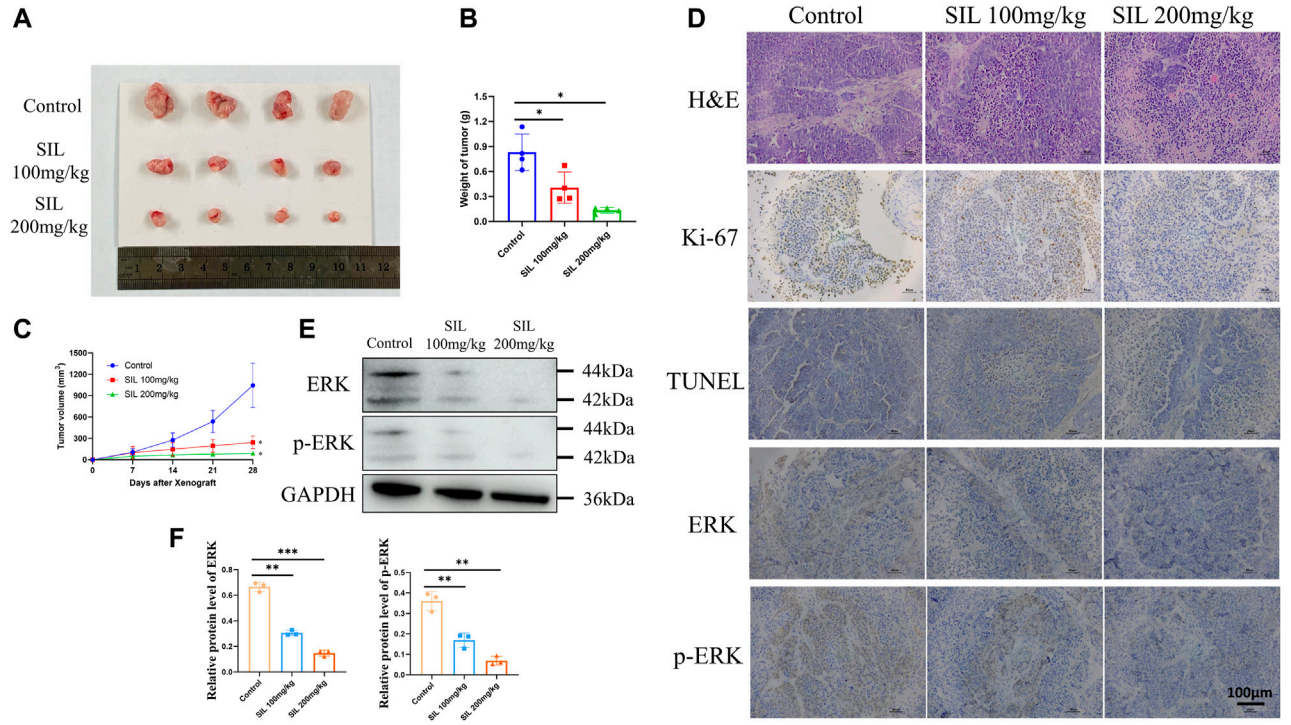

FIGURE 7 | Silibinin suppressed tumor growth in the cholangiocarcinoma xenograft model. **(A)**. Anti-tumor activity of silibinin in tumor-bearing mice. Representative xenografts are shown. **(B)**. Tumor weights of each group measured at the end of treatment. Data are shown as mean ± SD, $*p < 0.05$, significantly different compared to the control group. **(C)**. Tumor volumes of each group are measured in the indicated days of treatment. $*p < 0.05$ meant a significant difference compared to the control group at the end of the treatment. **(D)**. H&E, Ki-67 and immunohistochemistry assays of cholangiocarcinoma tissue. **(E,F)**. The expression of ERK and p-ERK proteins was detected *in vivo,* and quantification results are shown by histograms. Data is shown as mean ± SD, $**p < 0.01$, $***p < 0.001$, significantly different compared to the control group.

inhibitors coordinate with each other in order to regulate cell cycle progression (Kar, 2016). Silibinin caused G1 arrest by decreasing the expression of Cyclin D1, Cyclin E2 and CDK4 and inducing increased expression of p21 and p15 in the human pancreatic adenocarcinoma cell line SW1990 (Zhang et al., 2018). In the colon cancer cell line HT-29, a significant dose-dependent G1 arrest was observed after treatment with silibinin at doses of 50–100 μg/ml. On the other hand, a G2 arrest occurred after a prolonged (48 h) exposure to high doses of silibinin (Agarwal et al., 2003). Similar to these findings, our results revealed a significant G1 arrest in cholangiocarcinoma cell line when treated with silibinin at IC50 and 2*IC50 concentrations for 48 h. This was different from prior reports that indicated that silibinin led to a G2 arrest in tumors, including cervical (You et al., 2020) and gastric cancer (Zhang et al., 2013). This illustrates that there are different mechanisms of action of silibinin across different tumors and that silibinin mainly acts as a tumor suppressor by causing G1 arrest in cholangiocarcinoma.

Autophagy occurs continuously at a basal rate under normal cellular conditions in order to maintain a balance of intracellular recycling and metabolic regulations (Mizushima and Komatsu, 2011). The normal level of autophagy in cells is low, which is needed to maintain normal physiological metabolism. However, when itis activated by external adverse factors, it may cause cell autophagic death (Kim and Lee, 2014). Cells need to undergo many changes related to metabolic machinery before they become cancerous, and autophagy becomes downregulated during carcinogenesis. Cancer cells are able to express a panel of anti-autophagy genes, such as *Bcl-2*, *Akt*, and *PI3KC1*, suggesting that autophagy can inhibit the transformation of normal cells into cancer cells. Most autophagy regulators are oncogenes and tumor suppressors, which is also a reason why autophagy in cancer has not been fully defined. In glioma cell lines U87 and U251, silibinin promoted the up-regulated expression of BNIP3, as well as translocation of the protein into the mitochondria by activating autophagy. This, in turn, led to the translocation of AIF from the mitochondria into the nucleus, and ultimately caused cell death (Wang et al., 2020). In breast cancer, silibinin was able to induce autophagy in MCF-7 cells by decreasing Akt/mTOR expression, thus enhancing its inhibitory effect on estrogen receptors and finally causing breast cancer cell death (Zheng et al., 2015). We observed the same phenomenon in cholangiocarcinoma after treatment with silibinin. There was significant dose-dependent autophagy induced by silibinin in cholangiocarcinoma (Data not shown). We suggested that there was a relationship between autophagy and apoptosis induced by silibinin, but we did not validate this conjecture, which is also a limitation in our experiments.

ERK is a member of the MAPK family, and an important related molecule downstream of EGFR (Corcoran et al., 2012). After phosphorylation on threonine and tyrosine residues of ERK, p-ERK (the active form of ERK) enters the nucleus where it phosphorylates several substrates for other kinases and transcription factors. It eventually causes cell cycle progression, as well as changes in cell proliferation, differentiation, metabolism, apoptosis and other behaviors. Unlike the high mutation rates of *RAS* (Prior et al., 2020), *BRAF* (Davies et al., 2002), and others genes in cancer cells, acquired mutations in *ERK* have thus far been virtually absent in cancer cells. The reason may be that ERK in cells is able to regulate many substrates (i.e., kinases and transcription factors), and once the drug resistance mutation occurs in *ERK*, the effective regulation of these substrates becomes lost, affecting normal cell activities and being unable to guarantee cell survival. Moreover, an increasing number of preclinical findings show that ERK inhibitors have better outcomes than RAF and MEK inhibitors (Hatzivassiliou et al., 2012; Qin et al., 2012). Recently, several ERK inhibitors have entered clinical studies, including GDC-0994, Ulixertinib (BVD-523), KO-947, LY3214996, and others (Blake et al., 2016; Sullivan et al., 2018). In the present study, we applied silibinin, a natural extract of silymarin, to effectively inhibit the expression of ERK, causing a reduction in the expression of anti-apoptotic proteins, such as Bcl-2 and Bcl-xl. The ratio of p-ERK to t-ERK density is a common indicator for the interpretation of ERK inhibition. From the ratio of p-ERK to total ERK, we found that there was no significant difference in the ratio between different groups. This phenomenon suggests that the decrease of p-ERK after silibinin treatment may be due to the decrease of t-ERK, rather than silibinin inhibiting the phosphorylation of ERK. The decreased protein expression led to a decrease in the mitochondrial membrane potential, which, in turn, triggered Cytochrome C efflux from the mitochondria and finally activated downstream Caspase-9, Caspase-3 and other apoptotic proteins, causing cell apoptosis.

Silibinin is poorly water-soluble, and nano-formulations of silibinin constructs have been reported to effectively improve the bioavailability of silibinin (Liu et al., 2017). Constructing nanoparticles with silibinin as the core in order to treat cholangiocarcinoma is also the next direction of our endeavors.

CONCLUSION

For the first time, our study confirmed that silibinin can have an effective therapeutic effect on cholangiocarcinoma, such as treatment of other tumors, and its mechanism may be associated with intervening ERK and mitochondrial membrane potential. At the cellular level, silibinin treatment can significantly cause degradation and dephosphorylation of ERK protein, which further reduces cell membrane potential and causes outflow of Cytochrome C. The accumulation of Cytochrome C in the cytoplasm initiates the downstream apoptotic cascade, and causes cell death. This research inspired us to treat cholangiocarcinoma by intervening ERK in the future.

DATA AVAILABILITY STATEMENT

The original contributions presented in the study are included in the article/**Supplementary Materials**, further inquiries can be directed to the corresponding authors.

ETHICS STATEMENT

The animal study was reviewed and approved by Experimental animal welfare ethics committee of Zhejiang Experimental Animal Center.

AUTHOR CONTRIBUTIONS

SY and YW conceived and designed the study. YB and JC conducted the study. WH and LW contributed to the acquisition of data. YB and JC analyzed and interpreted the data. SY and YW reviewed and edited the article. All authors read and approved the final manuscript.

FUNDING

This research was supported by Zhejiang basic public welfare research program under Grant No. LGF20H160028.

SUPPLEMENTARY MATERIAL

The Supplementary Material for this article can be found online at: https://www.frontiersin.org/articles/10.3389/fphar.2022.847905/full#supplementary-material

Supplementary Figure S1 | (A). Trypan blue staining results of the HuCCT-1 and CCLP-1 cell lines after mitochondrial isolation. **(B)**. The ratio of p-ERK to ERK related to **Figure 4A**. Data are shown as mean ± SD, * $p < 0.05$, ** $p < 0.01$, **** $p < 0.0001$, significantly difference compared to the control group. **(C)**. The quantification results of IHC in **Figure 7D**. Data are shown as mean ± SD, ** $p < 0.01$, *** $p < 0.001$, **** $p < 0.0001$, significantly different compared to the control group.

REFERENCES

Abenavoli, L., Capasso, R., Milic, N., and Capasso, F. (2010). Milk Thistle in Liver Diseases: Past, Present, Future. *Phytother Res.* 24 (10), 1423–1432. doi:10.1002/ptr.3207

Agarwal, C., Singh, R. P., Dhanalakshmi, S., Tyagi, A. K., Tecklenburg, M., Sclafani, R. A., et al. (2003). Silibinin Upregulates the Expression of Cyclin-dependent Kinase Inhibitors and Causes Cell Cycle Arrest and Apoptosis in Human colon Carcinoma HT-29 Cells. *Oncogene* 22 (51), 8271–8282. doi:10.1038/sj.onc.1207158

Banales, J. M., Marin, J. J. G., Lamarca, A., Rodrigues, P. M., Khan, S. A., Roberts, L. R., et al. (2020). Cholangiocarcinoma 2020: the Next Horizon in Mechanisms and Management. *Nat. Rev. Gastroenterol. Hepatol.* 17 (9), 557–588. doi:10.1038/s41575-020-0310-z

Barros, T. M. B., Lima, A. P. B., Almeida, T. C., and da Silva, G. N. (2020). Inhibition of Urinary Bladder Cancer Cell Proliferation by

Silibinin. *Environ. Mol. Mutagen* 61 (4), 445–455. doi:10.1002/em.22363

Blake, J. F., Burkard, M., Chan, J., Chen, H., Chou, K. J., Diaz, D., et al. (2016). Discovery of (S)-1-(1-(4-Chloro-3-fluorophenyl)-2-hydroxyethyl)-4-(2-((1-methyl-1H-pyrazol-5-yl)amino)pyrimidin-4-yl)pyridin-2(1H)-one (GDC-0994), an Extracellular Signal-Regulated Kinase 1/2 (ERK1/2) Inhibitor in Early Clinical Development. *J. Med. Chem.* 59 (12), 5650–5660. doi:10.1021/acs.jmedchem.6b00389

Bosch-Barrera, J., and Menendez, J. A. (2015). Silibinin and STAT3: A Natural Way of Targeting Transcription Factors for Cancer Therapy. *Cancer Treat. Rev.* 41 (6), 540–546. doi:10.1016/j.ctrv.2015.04.008

Bosch-Barrera, J., Queralt, B., and Menendez, J. A. (2017). Targeting STAT3 with Silibinin to Improve Cancer Therapeutics. *Cancer Treat. Rev.* 58, 61–69. doi:10.1016/j.ctrv.2017.06.003

Chaisaingmongkol, J., Budhu, A., Dang, H., Rabibhadana, S., Pupacdi, B., Kwon, S. M., et al. (2017). Common Molecular Subtypes Among Asian Hepatocellular Carcinoma and Cholangiocarcinoma. *Cancer Cell* 32 (1), 57. doi:10.1016/j.ccell.2017.05.009

Chen J, J., Li, D. L., Xie, L. N., Ma, Y. R., Wu, P. P., Li, C., et al. (2020). Synergistic Anti-inflammatory Effects of Silibinin and Thymol Combination on LPS-Induced RAW264.7 Cells by Inhibition of NF-κB and MAPK Activation. *Phytomedicine* 78, 153309. doi:10.1016/j.phymed.2020.153309

Chen YH, Y. H., Lin, H., Wang, Q., Hou, J. W., Mao, Z. J., and Li, Y. G. (2020). Protective Role of Silibinin against Myocardial Ischemia/reperfusion Injury-Induced Cardiac Dysfunction. *Int. J. Biol. Sci.* 16 (11), 1972–1988. doi:10.7150/ijbs.39259

Chen, J., Pan, Q., Bai, Y., Chen, X., and Zhou, Y. (2021). Hydroxychloroquine Induces Apoptosis in Cholangiocarcinoma via Reactive Oxygen Species Accumulation Induced by Autophagy Inhibition. *Front. Mol. Biosci.* 8, 720370. doi:10.3389/fmolb.2021.720370

Corcoran, R. B., Ebi, H., Turke, A. B., Coffee, E. M., Nishino, M., Cogdill, A. P., et al. (2012). EGFR-mediated Re-activation of MAPK Signaling Contributes to Insensitivity of BRAF Mutant Colorectal Cancers to RAF Inhibition with Vemurafenib. *Cancer Discov.* 2 (3), 227–235. doi:10.1158/2159-8290.CD-11-0341

Dalton, S. (2015). Linking the Cell Cycle to Cell Fate Decisions. *Trends Cel Biol.* 25 (10), 592–600. doi:10.1016/j.tcb.2015.07.007

Davies, H., Bignell, G. R., Cox, C., Stephens, P., Edkins, S., Clegg, S., et al. (2002). Mutations of the BRAF Gene in Human Cancer. *Nature* 417 (6892), 949–954. doi:10.1038/nature00766

Federico, A., Dallio, M., and Loguercio, C. (2017). Silymarin/Silybin and Chronic Liver Disease: A Marriage of Many Years. *Molecules* 22 (2), 191. doi:10.3390/molecules22020191

Gao, Y., Xu, H., and Pu, T. (2020). MicroRNA-1179 Suppresses the Proliferation and Enhances Vincristine Sensitivity of Oral Cancer Cells via Induction of Apoptosis and Modulation of MEK/ERK and PI3K/AKT Signalling Pathways. *AMB Express* 10 (1), 149. doi:10.1186/s13568-020-01082-8

García-Maceira, P., and Mateo, J. (2009). Silibinin Inhibits Hypoxia-Inducible Factor-1alpha and mTOR/p70S6K/4E-BP1 Signalling Pathway in Human Cervical and Hepatoma Cancer Cells: Implications for Anticancer Therapy. *Oncogene* 28 (3), 313–324. doi:10.1038/onc.2008.398

Guo, Y. J., Pan, W. W., Liu, S. B., Shen, Z. F., Xu, Y., and Hu, L. L. (2020). ERK/MAPK Signalling Pathway and Tumorigenesis. *Exp. Ther. Med.* 19 (3), 1997–2007. doi:10.3892/etm.2020.8454

Hatzivassiliou, G., Liu, B., O'Brien, C., Spoerke, J. M., Hoeflich, K. P., Haverty, P. M., et al. (2012). ERK Inhibition Overcomes Acquired Resistance to MEK Inhibitors. *Mol. Cancer Ther.* 11 (5), 1143–1154. doi:10.1158/1535-7163.MCT-11-1010

Kar, S. (2016). Unraveling Cell-Cycle Dynamics in Cancer. *Cell Syst.* 2 (1), 8–10. doi:10.1016/j.cels.2016.01.007

Kelley, R. K., Bridgewater, J., Gores, G. J., and Zhu, A. X. (2020). Systemic Therapies for Intrahepatic Cholangiocarcinoma. *J. Hepatol.* 72 (2), 353–363. doi:10.1016/j.jhep.2019.10.009

Kim, K. H., and Lee, M. S. (2014). Autophagy--a Key Player in Cellular and Body Metabolism. *Nat. Rev. Endocrinol.* 10 (6), 322–337. doi:10.1038/nrendo.2014.35

Lavoie, H., Gagnon, J., and Therrien, M. (2020). ERK Signalling: a Master Regulator of Cell Behaviour, Life and Fate. *Nat. Rev. Mol. Cel Biol.* 21 (10), 607–632. doi:10.1038/s41580-020-0255-7

Liu, C. H., Lin, C. C., Hsu, W. C., Chung, C. Y., Lin, C. C., Jassey, A., et al. (2017). Highly Bioavailable Silibinin Nanoparticles Inhibit HCV Infection. *Gut* 66 (10), 1853–1861. doi:10.1136/gutjnl-2016-312019

Liu R, R., Wang, Q., Ding, Z., Zhang, X., Li, Y., Zang, Y., et al. (2020). Silibinin Augments the Antifibrotic Effect of Valsartan through Inactivation of TGF-β1 Signaling in Kidney. *Drug Des. Devel. Ther.* 14, 603–611. doi:10.2147/DDDT.S224308

Liu Y, Y., Xie, X., Hou, X., Shen, J., Shi, J., Chen, H., et al. (2020). Functional Oral Nanoparticles for Delivering Silibinin and Cryptotanshinone against Breast Cancer Lung Metastasis. *J. Nanobiotechnol.* 18 (1), 83. doi:10.1186/s12951-020-00638-x

Luo, H., Vong, C. T., Chen, H., Gao, Y., Lyu, P., Qiu, L., et al. (2019). Naturally Occurring Anti-cancer Compounds: Shining from Chinese Herbal Medicine. *Chin. Med.* 14, 48. doi:10.1186/s13020-019-0270-9

Mao, J., Yang, H., Cui, T., Pan, P., Kabir, N., Chen, D., et al. (2018). Combined Treatment with Sorafenib and Silibinin Synergistically Targets Both HCC Cells and Cancer Stem Cells by Enhanced Inhibition of the Phosphorylation of STAT3/ERK/AKT. *Eur. J. Pharmacol.* 832, 39–49. doi:10.1016/j.ejphar.2018.05.027

Mizushima, N., and Komatsu, M. (2011). Autophagy: Renovation of Cells and Tissues. *Cell* 147 (4), 728–741. doi:10.1016/j.cell.2011.10.026

Montal, R., Sia, D., Montironi, C., Leow, W. Q., Esteban-Fabró, R., Pinyol, R., et al. (2020). Molecular Classification and Therapeutic Targets in Extrahepatic Cholangiocarcinoma. *J. Hepatol.* 73 (2), 315–327. doi:10.1016/j.jhep.2020.03.008

Peng, W. X., Huang, J. G., Yang, L., Gong, A. H., and Mo, Y. Y. (2017). Linc-RoR Promotes MAPK/ERK Signaling and Confers Estrogen-independent Growth of Breast Cancer. *Mol. Cancer* 16 (1), 161. doi:10.1186/s12943-017-0727-3

Polachi, N., Bai, G., Li, T., Chu, Y., Wang, X., Li, S., et al. (2016). Modulatory Effects of Silibinin in Various Cell Signaling Pathways against Liver Disorders and Cancer - A Comprehensive Review. *Eur. J. Med. Chem.* 123, 577–595. doi:10.1016/j.ejmech.2016.07.070

Prior, I. A., Hood, F. E., and Hartley, J. L. (2020). The Frequency of Ras Mutations in Cancer. *Cancer Res.* 80 (14), 2969–2974. doi:10.1158/0008-5472.CAN-19-3682

Qin, J., Xin, H., and Nickoloff, B. J. (2012). Specifically Targeting ERK1 or ERK2 Kills Melanoma Cells. *J. Transl. Med.* 10, 15. doi:10.1186/1479-5876-10-15

Rizvi, S., and Gores, G. J. (2013). Pathogenesis, Diagnosis, and Management of Cholangiocarcinoma. *Gastroenterology* 145 (6), 1215–1229. doi:10.1053/j.gastro.2013.10.013

Rizvi, S., Khan, S. A., Hallemeier, C. L., Kelley, R. K., and Gores, G. J. (2018). Cholangiocarcinoma - Evolving Concepts and Therapeutic Strategies. *Nat. Rev. Clin. Oncol.* 15 (2), 95–111. doi:10.1038/nrclinonc.2017.157

Salomone, F., Barbagallo, I., Godos, J., Lembo, V., Currenti, W., Cinà, D., et al. (2017). Silibinin Restores NAD^+ Levels and Induces the SIRT1/AMPK Pathway in Non-Alcoholic Fatty Liver. *Nutrients* 9 (10), 1086. doi:10.3390/nu9101086

Savoia, P., Fava, P., Casoni, F., and Cremona, O. (2019). Targeting the ERK Signaling Pathway in Melanoma. *Int. J. Mol. Sci.* 20 (6), 1483. doi:10.3390/ijms20061483

Si, L., Fu, J., Liu, W., Hayashi, T., Nie, Y., Mizuno, K., et al. (2020). Silibinin Inhibits Migration and Invasion of Breast Cancer MDA-MB-231 Cells through Induction of Mitochondrial Fusion. *Mol. Cel Biochem.* 463, 189–201. doi:10.1007/s11010-019-03640-6

Sullivan, R. J., Infante, J. R., Janku, F., Wong, D. J. L., Sosman, J. A., Keedy, V., et al. (2018). First-in-Class ERK1/2 Inhibitor Ulixertinib (BVD-523) in Patients with MAPK Mutant Advanced Solid Tumors: Results of a Phase I Dose-Escalation and Expansion Study. *Cancer Discov.* 8 (2), 184–195. doi:10.1158/2159-8290.CD-17-1119

Vue, B., Zhang, S., Zhang, X., Parisis, K., Zhang, Q., Zheng, S., et al. (2016). Silibinin Derivatives as Anti-prostate Cancer Agents: Synthesis and Cell-Based Evaluations. *Eur. J. Med. Chem.* 109, 36–46. doi:10.1016/j.ejmech.2015.12.041

Wang, C., He, C., Lu, S., Wang, X., Wang, L., Liang, S., et al. (2020). Autophagy Activated by Silibinin Contributes to Glioma Cell Death via Induction of Oxidative Stress-Mediated BNIP3-dependent Nuclear Translocation of AIF. *Cell Death Dis.* 11 (8), 630. doi:10.1038/s41419-020-02866-3

You, Y., He, Q., Lu, H., Zhou, X., Chen, L., Liu, H., et al. (2020). Silibinin Induces G2/M Cell Cycle Arrest by Activating Drp1-dependent Mitochondrial Fission in Cervical Cancer. *Front. Pharmacol.* 11, 271. doi:10.3389/fphar.2020.00271

Zhang, Y., Li, Q., Ge, Y., Chen, Y., Chen, J., Dong, Y., et al. (2013). Silibinin Triggers Apoptosis and Cell-Cycle Arrest of SGC7901 Cells. *Phytother Res.* 27 (3), 397–403. doi:10.1002/ptr.4733

Zhang, X., Liu, J., Zhang, P., Dai, L., Wu, Z., Wang, L., et al. (2018). Silibinin Induces G1 Arrest, Apoptosis and JNK/SAPK Upregulation in SW1990 Human Pancreatic Cancer Cells. *Oncol. Lett.* 15 (6), 9868–9876. doi:10.3892/ol.2018.8541

Zheng, N., Zhang, P., Huang, H., Liu, W., Hayashi, T., Zang, L., et al. (2015). ERα Down-Regulation Plays a Key Role in Silibinin-Induced Autophagy and Apoptosis in Human Breast Cancer MCF-7 Cells. *J. Pharmacol. Sci.* 128 (3), 97–107. doi:10.1016/j.jphs.2015.05.001

Conflict of Interest: The authors declare that the research was conducted in the absence of any commercial or financial relationships that could be construed as a potential conflict of interest.

Publisher's Note: All claims expressed in this article are solely those of the authors and do not necessarily represent those of their affiliated organizations, or those of the publisher, the editors and the reviewers. Any product that may be evaluated in this article, or claim that may be made by its manufacturer, is not guaranteed or endorsed by the publisher.

frontiers | Frontiers in Pharmacology

REVIEW
published: 02 June 2022
doi: 10.3389/fphar.2022.820474

Molecular Mechanism of Anti-Colorectal Cancer Effect of *Hedyotis diffusa* Willd and Its Extracts

Zihong Wu[1], *Bei Yin*[2]* *and Fengming You*[3]*

[1]Hospital of Chengdu University of Traditional Chinese Medicine, Chengdu, China, [2]School of Second Clinical Medicine, Guangzhou University of Chinese Medicine, Guangzhou, China, [3]TCM Regulating Metabolic Diseases Key Laboratory of Sichuan Province, Hospital of Chengdu University of Traditional Chinese Medicine, Chengdu, China

With the sharp change in our diet and lifestyle, the incidence of colorectal cancer (CRC) is increasing among young people and has become the second most common malignant tumor worldwide. Although the current treatment of CRC is getting updated rapidly, recurrence and metastasis are still inevitable. Therefore, new anticancer drugs are needed to break existing limitations. In recent years, *Hedyotis diffusa* Willd (HDW) extracts have been proved to demonstrate excellent anti-colorectal cancer effects and have been widely used in clinical practices. In this review, we aim to explore the advantages, potential signaling pathways, and representative active ingredients of HDW in the treatment of CRC from the perspective of molecular mechanism, in order to provide new ideas for the future treatment of CRC.

Keywords: colorectal cancer, *Hedyotis diffusa* Willd, advantages, signaling pathways, active ingredients, molecular mechanism

OPEN ACCESS

Edited by:
Youhua Xu,
Macau University of Science and Technology, Macao SAR, China

Reviewed by:
Cui-Ting Peng,
Sichuan University, China
Sung-Gook Cho,
Korea National University of Transportation, South Korea

***Correspondence:**
Bei Yin
17817315916@163.com
Fengming You
yfmdoc@163.com

Specialty section:
This article was submitted to Pharmacology of Anti-Cancer Drugs, a section of the journal Frontiers in Pharmacology

Received: *23 November 2021*
Accepted: *06 April 2022*
Published: *02 June 2022*

Citation:
Wu Z, Yin B and You F (2022) Molecular Mechanism of Anti-Colorectal Cancer Effect of Hedyotis diffusa Willd and Its Extracts. Front. Pharmacol. 13:820474. doi: 10.3389/fphar.2022.820474

INTRODUCTION

Colorectal cancer (CRC) is one of the leading causes of cancer-related death in Western and developing countries, and it is the second most common cancer after lung cancer (Hemminki et al., 2021). Epidemiology results show that the global cases of CRC reached over 1.9 million in 2020 (Alyabsi et al., 2021). Global data indicate that although the incidence of CRC has declined significantly over the past few decades among people over the age of 50, an annual increase of about 1.8% has been observed in younger patients, and it is projected that the average incidence of CRC may increase by about 107.1% in patients aged 20–34 years by 2030 (Thanikachalam et al., 2019; Vidri et al., 2020). About 33% of CRC patients have distant metastasis at the time of diagnosis, although many advances in systematic approaches have occurred such as chemotherapy, targeted therapy, and immunotherapy, while about 86% of patients with advanced colorectal cancer still die within 5 years of diagnosis (Wrobel et al., 2019). These gloomy data present a challenging goal for clinicians and researchers, that is, to explore new anticancer drugs to overcome the limitations of existing therapies.

Hedyotis diffusa Willd (HDW) is a kind of Rubiaceae of Chinese herbal medicine, which is a famous Chinese herbal medicine with thousands of years of clinical practice history. HDW is an important ingredient of various anticancer formulations; it has been reported to inhibit tumor cell proliferation and metastasis and alleviate side effects after chemotherapy as well (Song et al., 2019). Early pharmacological studies have confirmed that HDW has medicinal properties like antitumor, anti-inflammatory, immunomodulatory, antioxidant, and other biological activities (Shen et al., 2016). As an antitumor herbal medicine, HDW and its extracts have been widely used in the

treatment of CRC, breast cancer, prostate cancer, and so on (Wazir et al., 2021; Huang et al., 2021). In this review, we explore the advantages, potential signal pathways, and representative active ingredients of HDW in the treatment of CRC. To write this review, we tried to use the latest published articles in highly reputated journals.

ADVANTAGES OF HDW

HDW is a widely used clinical herbal medicine. Meng et al. (2013) found 199 anticancer herbs by searching PubMed and SciFinder databases; they then ranked each herb by frequency of occurrence and found that HDW was in the top five; subsequently, MTS cell viability assay was used to confirm that HDW, and its extracts showed good anticancer cell proliferation activity. HDW is also a representative of many heat-clearing and detoxifying anticancer herbs, whose anticancer activity is second only to yew and equivalent to matrine, especially in the treatment of CRC highlighted more advantages (Song et al., 2019).

Although there are a variety of treatments for colorectal cancer, chemotherapy is still one of the main therapies for most patients. However, the resistance of cancer cells to chemotherapy drugs limits its long-term application, which is also the primary reason for clinical chemotherapy failure. Lai et al. (2017) demonstrated that HDW can inhibit the activity, migration, and invasion of drug-resistant colorectal cancer cells of HCT-8/5-FU, and reverse multiple drug resistance (MDR) of colorectal cancer cells. Compared with oxaliplatin alone, combined use of HDW can reduce toxicity, increase efficacy, reduce the incidence of bone marrow suppression after chemotherapy, enhance immune response, improve the quality of life of cancer patients, and prolong their survival (Chen et al., 2016; Ho, 2018). In addition, HDW also has multiple pharmacological effects such as antioxidant, anti-inflammatory, anti-fibroblast, and immune regulation, and it also has a certain blocking effect on the transformation of colitis cancer (DanQing et al., 2021).

The role of HDW in CRC is quite important. Next, we will make a systematic, comprehensive, and detailed review framework for the molecular mechanism of HDW and its extracts in the treatment of CRC.

POTENTIAL SIGNALING PATHWAYS

To investigate the potential mechanism of HDW in inhibiting CRC cell growth, we will review the potential signaling pathways of HDW acting on CRC over the years, including the *in vivo* and *in vitro* experiments (**Table 1**).

Yan et al. (2017) suggested that the chloroform extract of HDW(CEHDW) may play an anticancer role by suppressing phosphorylation of PI3K/AKT and RAS/ERK signaling pathways: CEHDW could inhibit proliferation and promote apoptosis of the SW620 CRC cell lines, and in addition, it plays this role by decreasing the expression levels of B-cell lymphoma 2(Bcl-2), cyclin D1, cyclin-dependent kinase 4(CDK4), surviving and proliferating cell nuclear antigen (PCNA), and increasing the expression levels of Bcl-2-associated X (Bax) protein. CEHDW also inhibits the activation of protein kinase B (AKT) and extracellular signal-regulated kinase (ERK).

Multiple drug resistance (MDR) is one of the main causes of chemotherapy failure. Li et al. (2015); Li et al. (2018) proposed for the first time that the ethanol extract of HDW (EEHDW) may overcome drug resistance of HCT-8/5-FU cells by downregulating the expression of ABC subfamily G member 2 (ABCG2) and P-glycoprotein (P-gp), or via inhibiting the phosphorylation of the PI3K/AKT signaling pathway. It mainly suppresses the expression of PI3K and p-Akt key target genes; downregulates the expression of Bcl-2, cyclin D1, and CDK4; and upregulates the expression of Bax, p21, and phosphatase-tensin homolog (PTEN) to reduce the viability of cancer cells, inhibit cell colony formation, induce cell apoptosis and then reverse MDR.

Li et al. (2019) constructed a human lymphatic endothelial cell (HLEC) model stimulated by vascular endothelial growth factor C (VEGF-C) and found that EEHDW regulates PI3K/AKT, ERK, and signal transducer and activator of transcription 3(STAT3) signaling pathways to inhibit VEGF-C-mediated lymphatic formation of HCT-116 and HCT-8 cell lines, thus blocking the migration of cancer cells and lymphangiogenesis. These signaling pathways are interrelated and can occur in parallel; important downregulated molecules in this process include cyclin D1, CDK4, MMP2, MMP9, and VEGFR-3.

In 2012, a CRC mice xenograft (CMX) model was used by some researchers to demonstrate the anticancer activity of EEHDW *in vivo* (Cai et al., 2012); they found EEHDW reduced tumor weight and volume in model mice. This may be attributed to EEHDW hobbling the phosphorylation of STAT3 signaling pathway. Feng et al. (2017) further confirmed that EEHDW has strong anti-colorectal cancer activity both *in vivo* and *in vitro*, and also built a CMX model and some human CRC cell lines (HCT-8, HT-29, HCT-116, and SW620 cells). The results show that EEHDW could regulate various inflammatory (IL-1β, IL-6, IL-4, IL-10, TNF-α) and angiogenic factors (COX-2, iNOS, eNOS, HIF-1α) and downregulate the expression of various oncogenes (Bcl-2, Bax, Pim-1, p53), thus affecting the proliferation and apoptosis of cancer cells and tumor angiogenesis. The changes in these key molecules suggest that EEHDW may play an important role in decreasing the activation of multiple signaling pathways, such as ERK1/2, AKT, STAT3, JNK, and p38.

Lin et al. (2015) studied the activity of EEHDW in a carcinogenic inflammatory environment and demonstrated that EEHDW treatment significantly reduced IL-6-induced STAT3 pathway phosphorylation and induced activation of pro-apoptotic factors Bax, caspase-9, and caspase-3, and downregulated Bcl-2, cyclin D1, and CDK4, thereby enhancing the local inflammatory environment and promoting tumor progression. In addition, Lin et al. (2011); Lin et al. (2015) also confirmed that EEHDW could prevent G1 to S progression of HT-29 cells and inhibit the expression levels of VEGF-A, to counteract tumor angiogenesis. In the early years, Lin et al. (2013) verified that EEHDW can reduce intra-tumor

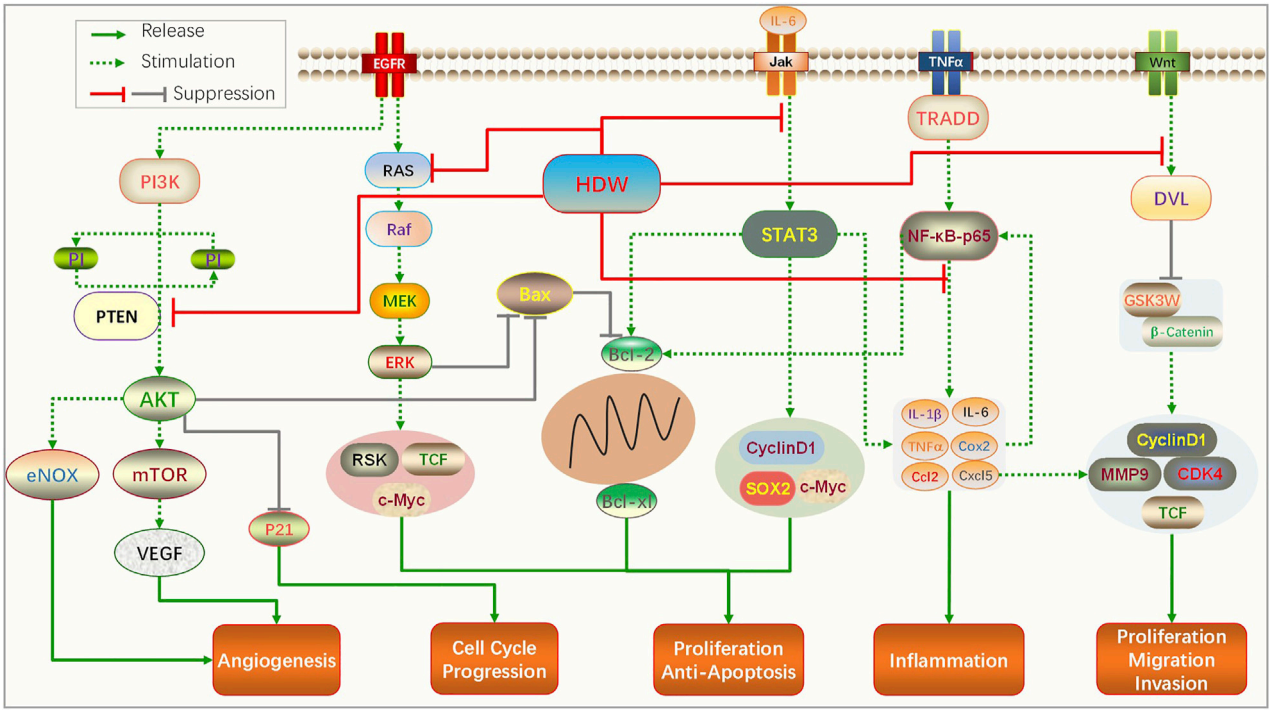

FIGURE 1 | Main signaling pathways and molecules of HDW act on CRC.

microvascular density (MVD) in a CMX model by inhibiting the expression of VEGF-A and VEGFR2, the target gene of the Sonic hedgehog (SHH) signaling pathway. Lin et al. (2010) also observed that EEHDW treatment could break the DNA, decrease the mitochondrial membrane potential, and increase the ratio of Bax/Bcl-2 of HT-29 cells, suggesting that EEHDW inhibited the growth of HT-29 cells via the mitochondrion-dependent pathway.

Lin et al. (2012) also believed that EEHDW could block the cell cycle G1 to S progression by decreasing the expression of cyclin D1, PCNA, and CDK4 but increasing the p21, which was positively correlated with the treatment time and concentration of EEHDW. Sun et al. (2016) showed that HDW may inhibit CRC stem cells; EEHDW can significantly reduce the expression of Lgr5, PCNA, ABCB1, survivin, *β*-catenin, and c-Myc in HT-29 SP cells and reduce the proportion of SP in HT-29 cells. These are associated with the inhibition of the Wnt/*β*-catenin signaling pathway and the expression of ABC transporters. Both Lai et al. (2017) and Chen et al. (2018) found that EEHDW inhibited metastasis of HCT-8/5-FU cells by regulating the transforming growth factor-*β* (TGF-*β*) signaling pathway, which showed inhibition of cell adhesion, migration, and invasion.

In summary, PI3K/AKT, RAS/ERK, STAT3, and cell cycle arrest are the most common signaling pathways for HDW extracts to intervene in CRC. Other signaling pathways include TGF-*β*, Wnt/-*β*-catenin, SHH, ABC, and mitochondrion-dependent pathways, which are closely related to the anticancer activity of HDW. It exerts anti-colorectal cancer activity mainly by promoting cells apoptosis; inhibiting cell proliferation, migration, and invasion; and suppressing tumor and lymphangiogenesis. It can also reverse the drug resistance of CRC cells. A network pharmacology research shows that the main targets of HDW therapy for CRC are AKT, PIK, TP53, BRAF, CDK2, and RAF, Gene Ontology (GO) analysis suggested that HDW may exert anticancer activity through regulating tumor-related pathways, cell motility and cell community, which is consistent with the main molecular mechanisms reviewed in this article (Liu X et al., 2018). The following is a schematic diagram of the main signaling pathways that HDW acts on CRC (**Figure 1**).

REPRESENTATIVE ANTITUMOR CONSTITUENTS

Modern technologies have helped us identify 58 kinds of antitumor active components in HDW (Han et al., 2020). We will review several representative chemical constituents.

Anthraquinones

Anthraquinones are one of the main anticancer components of HDW, and their anticancer activity is similar to that of paclitaxel. Meng et al. (2013) evaluated the effects of 10 active components of HDW on seven cancer cell lines and peripheral blood mononuclear cells (PBMCs). They found that anthraquinones inhibit cancer cell vitality in a dose-dependent manner within a certain concentration range, especially 2-hydroxymethyl-1-

TABLE 1 | Potential signaling pathways of HDW extracts against CRC.

Formulation	Models	End point or mechanisms of action	Signaling pathways			Experiment	References
			Molecular mechanisms	Decrease↓	Increase ↑		
CEHDW (0.0125-0.1 mg/ml)	SW620 cells	Inhibit proliferation and promote apoptosis of cells	Inhibit the phosphorylation of PI3K/AKT and RAS/ERK	Bcl-2 Cyclin D1 CDK4 Survivin PCNA	Bax	*In vitro*	Yan et al. (2017)
EEHDW (0.5-2 mg/ml)	HCT-8/5-FU cells	Inhibit viability, colony formation and promote apoptosis of cells	Inhibit the activation of the PI3K/AKT signaling pathway	Bcl-2 Cyclin D1 CDK4 PI3K, AKT	Bax p21 PTEN	*In vitro*	Li et al. (2018)
EEHDW (0.25-2 mg/ml)	HCT116 and HCT-8 cells	Suppress lymphangiogenesis and attenuate the migration of cells and their tube formation abilities	Inhibit VEGF-C-mediated lymphangiogenesis in CRC by the suppression of multiple (PI3K/AKT, ERK, and STAT3) signaling pathways	Cyclin D1 CDK4 MMP2 MMP9 VEGFR-3		*In vitro*	Li et al. (2019)
EEHDW (0.5-2 mg/ml)	HCT-8, HT-29 HCT-116 and SW620 cells	Inhibit proliferation and promote apoptosis of CRC cells	Decrease the levels of phosphorylated AKT, ERK1/2, JNK, p38, p70S6K, and STAT3	Bcl-2 Pim-1	Bax cytochrome c	*In vitro*	Feng et al. (2017)
(0.1 g/ml)	CMX model			COX-2 iNOS, eNOS HIF-1α, IL-1β,IL-6 TNF-α	Caspase-3 Caspase-9 PARP IL-4 and IL-10 p-p53	*In vivo*	
EEHDW (0.6 g/ml)	CMX model	Inhibit the proliferation and promote apoptosis of CRC cells	Inhibit the phosphorylation of STAT3	Bcl-2 Cyclin D1 CDK4	Bax p21	*In vivo*	Cai et al. (2012)
EEHDW (1-5 mg/ml)	HT-29 cells	Inhibit the growth and promote apoptosis of cells	Inactivate the IL-6/STAT3 signaling pathway Block the cell cycle G1 to S progression	Bcl-2 Cyclin D1 CDK4	Bax and caspase-9 Caspase-3	*In vitro*	Lin et al. (2015)
EEHDW (1-5 mg/ml)	HT-29 cells	Suppress the expression of VEGF-A in both HT-29 and HUVEC cells	Block the cell cycle G1 to S progression	VEGF-A		*In vitro*	Lin et al. (2011)
EEHDW (1-5 mg/ml)	HT-29 cells	Inhibit the proliferation of cells	Block the cell cycle G1 to S progression	Cyclin D1 CDK4 PCNA	p21	*In vitro*	Lin et al. (2012)
EEHDW (0.5-2 mg/ml)	HCT-8/5-FU cells	Reduce viability and reverse MDR of cells	Inhibit ABCG2-mediated drug resistance by downregulating the expression of ABCG2 and P-gp	ABCG2 P-gp		*In vitro*	Li et al. (2015)
EEHDW (1-5 mg/ml)	HT-29 SP cells	Inhibit viability and sphere formation, and induce cell morphological changes	Inhibit the expression of ABC transporters and the Wnt/β-catenin signaling pathway	ABCB1 Lgr5 β-Catenin c-Myc Survivin PCNA		*In vitro*	Sun et al. (2016)
EEHDW (0.5-2 mg/ml)	HCT-8/5-FU cells	Inhibit viability, adhesive, migratory, and invasion potential of cells	Suppress the TGF-β signaling pathway	TGF-β SMAD4 n-cadherino	E-cadherin	*In vitro*	Lai et al. (2017)
EEHDW (0.5-2 mg/ml)	HCT-8 cells	Reduce migration and invasion of cells	Inhibit the TGF-β/Smad signaling pathway-induced EMT	TGF-β p-Smad2/3 Smad4	E-cadherin	*In vitro*	Chen et al. (2018)
EEHDW (0.6 g/ml)	CMX model	Inhibit tumor growth and reduce intratumoral MVD	Suppress the SHH signaling pathway	SHH and Gli-1 Ptch-1 and Smo VEGF-A VEGFR2		*In vivo*	Lin et al. (2013)
EEHDW (1-5 mg/ml)	HT-29 cells	Inhibit the viability, change the morphology, and promote apoptosis of cells	Mitochondrion-dependent pathway	Bcl-2	Bax cytochrome c	*In vitro*	Lin et al. (2010)

hydroxyanthraquinone (IC50 = 45.33 μM) could significantly inhibit the proliferation of the colorectal cancer cell line Caco-2, followed by 2-methyl-3-methoxyanthraquinone, 2-hydroxymethylanthraquinone, and 2-hydroxy-3-methylanthraquinone (IC50 = 93–155 μM). Meanwhile, anthraquinones have almost no effect on PBMCs. Li et al.

TABLE 2 | Representative antitumor constituents isolated from the HDW.

Constituent	Cell lines/models	IC50=(μM)		Reference
		Compounds	Paclitaxel (P); 5-FU (F); TMZ; doxorubicin (D)	
Anthraquinones	Caco-2	45.33-93.25	P:31.81-35.31	Meng et al. (2013)
	HeLa, HepG2, RPMI8226, DU145, PC-3, LNCaP	28.82-92.82	P:14.15-58.37	
Iridoids	HCT15	9.50-96.10	F:3.90-4.70	Wang et al. (2018); Wang et al. (2017)
	HL-60, A459, HepG2, PC-3, CNE-2, BCG-823	11.40-97.90	F:7.50-22.80	
Flavonoid: quercetin	HT29, HCT15, HCT116	5.57-45.94	D:759.40-763.5	Ayoup et al. (2021); Devaraj and Devaraj (2017)
Triterpene: ursolic acid	Caco-2	67.60-73.78	P:31.81-35.31	Meng et al. (2013)
	HeLa, HepG2, RPMI8226, DU145, PC-3, LNCaP	22.33-65.02	P:14.15-58.37	
Coumarins: scopoletin, esculetin	HCT-116	18.64-29.91	P:30.56-37.31	Yuan et al. (2021); Yu et al. (2021)
Esculetin	MCF-7, SKM-1, A549, Ishikawa, HEC-1B	0.37-142.5	P:13.16-56.49	
Alkaloids	HCT-116, HCT-8, HT-29	0.89-11.25	F:4.20-25.61	Dey et al. (2019); Jiang et al. (2017)
	HepG2, HeLa, K562, McF-7, A549	2.10-8.00		
Cyclotides	SH-SY5Y, U-87 MG	2.15-7.92	TMZ:312.50-489.90	Gerlach et al. (2022)
Sterols: stigmasterol	Caco-2, HT29	>200	P:14.15-35.31	Meng et al. (2013); Gao et al. (2019)
	HeLa, HepG2, RPMI8226, DU145, PC-3, LNCaP			

(2016) confirmed that the active component of the 1, 3-dihydroxy-2-methylanthraquinone fraction from HDW with a much high inhibitory rate up to 48.9 ± 3.3% against HepG2 carcinoma cells at 125 μMol/L, mainly mediating by death receptor and mitochondrial apoptosis pathways. 2-Hydroxymethylanthraquinone found in HDW has been demonstrated to significantly reduce LPS-induced acute lung injury and suppress the level of inflammatory factors by regulating the TLR4/NF-κB pathway, thereby inhibiting inflammatory cancer transformation (Tan et al., 2018).

Iridoids

Iridoids are also one of the main components of HDW in their anticancer activities and are widely found in plants (Wang et al., 2020). Wang et al. (2017) isolated nine iridoids (1–3, 5–10) from HDW and measured the cytotoxic effects of all the compounds on various human tumor cell lines *in vitro*. Iridoid glycosides of Shecaoiridoidside C (compound 3) were found to be highly cytotoxic to HCT15 (human colon cancer cells) and other tumor cells (IC50 = 9.6–62.2 μM), and compounds 1, 7, 9(IC50 = 37.6–86.6 μM, 34.2–71.3 μM, 78.3–97.9 μM) also showed certain cytotoxicity to HCT15, A459, and HepG2 cells. In 2018, Wang et al. (2018) further confirmed that compounds 1 and 2 (IC50 = 9.5–28.2 μM, 15.8–26.2 μM) obvious cytotoxicity to HCT15 and all tumor cells. In addition, compound 8 (IC50 = 16.5–40.4 μM) also showed a significant inhibitory effect on HCT15, CNE-2, HL-60, A459, and HepG2 cancer cells.

Flavonoids

Flavonoids are a class of polyphenols with a wide range of biological activities, their anticancer and antioxidant effects have been the focus of research for many years. Epidemiological studies have confirmed that dietary intake of flavonoids can reduce the risk of cancer (Maleki et al., 2019; Selvakumar et al., 2020). Badar et al. (2021) found that flavonoids can target the PI3K/Akt/mTOR signaling pathway in the treatment of cancer. It could also modulate and regulate reactive oxygen species (ROS) of colorectal cancer HCT15, HCT116, and SW480 cell lines to activate caspases, thus o stimulating cell apoptosis (Kopustinskiene et al., 2020). Li Y. L et al. (2020) also suggested that the flavonoids from HDW may inhibit the upstream of the H2O2-induced pathway by lowering ROS and increasing the levels of Trx1 and TrxR1, thereby blocking the ASK1/P38 MAPK signaling pathway and reversing cellular malignant transformation. It is believed that flavonoids have the therapeutic potential of epigenetic regulation of cancer pathogenesis (Khan et al., 2021). Quercetin is a representative compound of flavonoids; it has many preventive effects in colorectal cancer, such as promoting apoptosis and antioxidant and inhibiting angiogenesis, and it is very sensitive to HCT116 cells (IC50 = 5.57–45.94 μM) (Ayoup et al., 2021).

Triterpenes

Triterpenes are essential for human health; they could suppress nuclear factor kappa B (NF-κB), STAT3, nuclear factor erythroid-2-related factor 2 (Nrf2), and other key signaling pathways to activate the antioxidant and anti-inflammatory ability, cell cycle regulation, and epigenetic to prevent tumor development (Li S et al., 2020). Four triterpenes have been isolated from HDW, namely, ursolic acid, oleanolic acid, isoarborinol, and arborinone (Chen et al., 2016). Studies have shown that ursolic acid has strong anti-inflammatory activity, via interfering with various biological processes such as free radical scavenging, pro-apoptotic and antiapoptotic protein expression, and G1/G2 cell cycle arrest, leading to apoptosis of cancer cells and inhibition of cell proliferation and angiogenesis (Yin et al., 2018; Alam et al.,

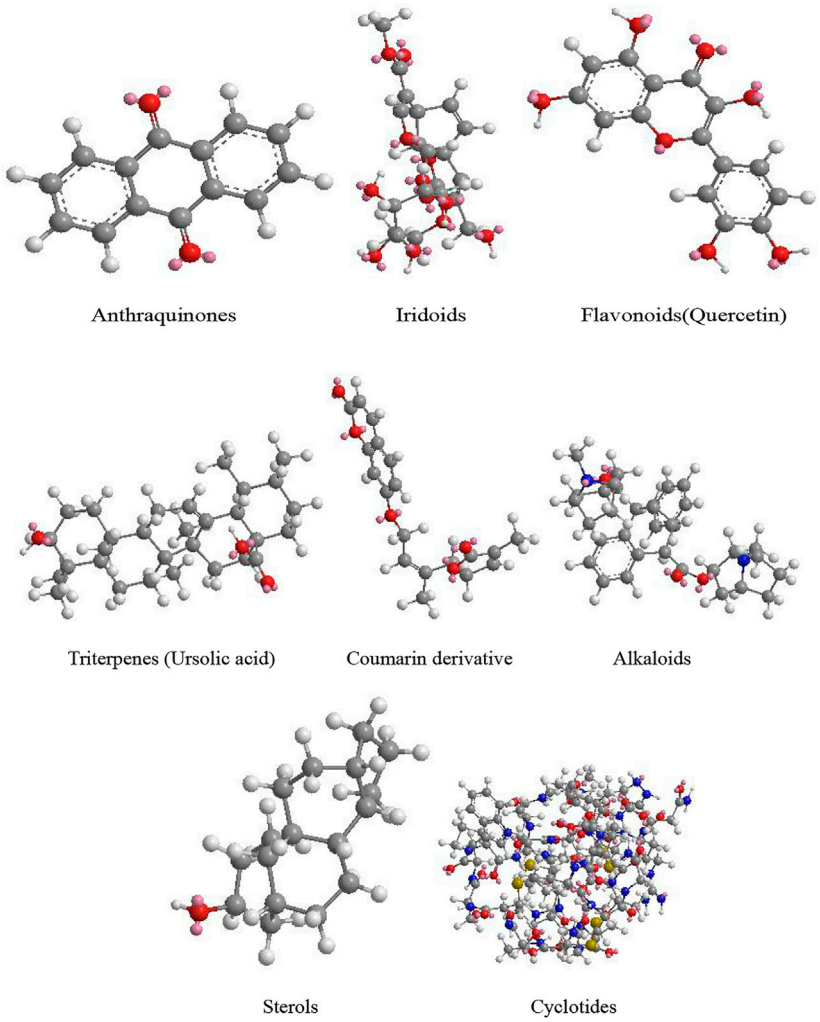

FIGURE 2 | Three-dimensional structures of representative antitumor constituents.

2021). Meng et al. (2013) found that ursolic acid (IC50 = 71 μM) had the strongest inhibitory effect on Caco-2 cells among compounds isolated from HDW, and it also had a strong inhibitory effect on Hep G2, DU145, PC-3, LNCaP, and HeLa cancer cells (IC50 = 22.33–65.02 μM), which was close to the activity of paclitaxel. However, oleanolic acid has a less toxic effect on cancer cells than ursolic acid (IC50 = 65.18–198.10 μM).

Coumarins

The total coumarins of HDW, including scopoletin and esculetin, showed significant antiproliferative activity. Jiang et al. (2017) identified that HDW contains two kinds of coumarins, with a total content of 87.4% coumarins, which can activate caspases and inhibit PI3K/Akt pathway proteins, thus inducing SkM-1 cell apoptosis in a dose-dependent manner (IC50 = 104.48 μg/ml, 100.66 μg/ml). Yu et al. (2021) synthesized a new class of scopoletin derivatives and found that compound 18e exhibited antiproliferative activity against different cancer cells, especially MCF-7 cells (IC50 = 0.37 μM). A study proved that scopoletin could inhibit the proliferation of HCT-116 and A549 cells by reducing the level of RAS-Raf-MEK-ERK and PI3K/AKT pathways (IC50 = 32 μg/ml, 16 μg/ml) (Yuan et al., 2021). In addition, esculetin can target hnRNPa1 and downregulate the expression of Bcl-xl and Xiap, resulting in cell apoptosis and restricted proliferation of Ishikawa (IC50 = 95 μM) and HEC-1B (IC50 = 142.5 μM) (Jiang et al., 2021).

Alkaloids

Alkaloids can inhibit the proliferation of colorectal cancer cells by interfering with the cell cycle, which shows certain anticancer potential (Khan et al., 2022). Modern pharmacological studies show that steroidal alkaloids have anticancer, anti-inflammatory, bactericidal, analgesic, and other biological activities and showed strong cytotoxicity to HCT-116 (IC50 = 3.8 μM) and HepG2, HeLa, K562, McF-7, and A549 cells (IC50 = 2.1–8.0 μM); the application of this compound is promising (Dey et al., 2019; Jiang et al., 2016).

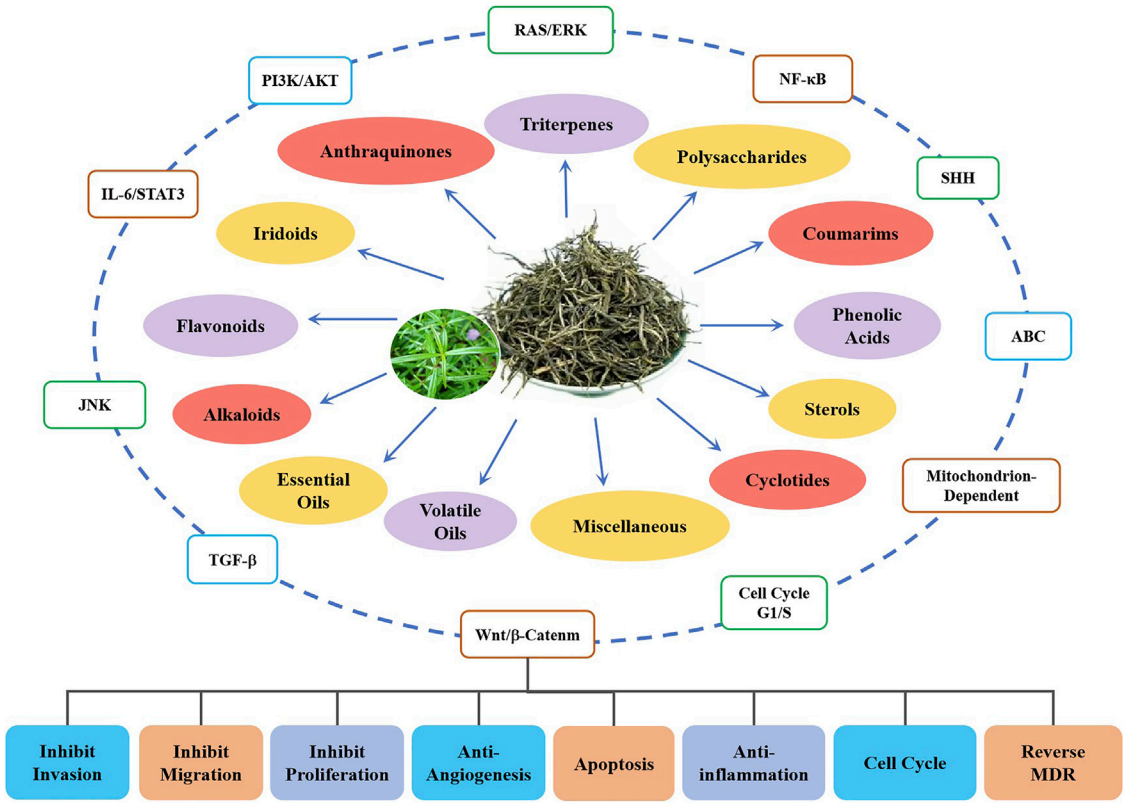

FIGURE 3 | Schematic diagram of anti-colorectal cancer components from HDW and their related mechanisms.

Sterols

Sterols are also common chemical constituents of HDW. Interestingly, the reduction of squalene epoxidase caused by sterol accumulation can activate the *β*-catenin oncogenic pathway and inhibit the p53 tumor suppressor pathway, leading to the progression of CRC (Jun et al., 2021). Gao et al. (2019) also observed that sterol regulatory element-binding protein-1 is overexpressed in HT29 cells, promoting the vascular endothelial generation, activating the NF-κB-P65 pathway, and thus causing uncontrolled proliferation of cancer cells. Meng et al. (2013) confirmed that stigmasterol showed very low anticancer activity (IC50 > 200 μM). This indicates that among many active ingredients, sterols may play a neutralizing or even opposite role.

Cyclotides

The unique ring structure of cyclotides shows great promise in the treatment of cancer as it is stable and difficult to be enzymatically hydrolyzed (Mehta et al., 2020). Gerlach et al. (2022) found that multiple cyclotides (CyO2, CyO13) were cytotoxic to SH-SY5Y and U-87 MG cells (IC50 = 2.15–7.92 μM), and combined application could enhance the efficacy of temozolomide (TMZ).

The representative antitumor constituents isolated from the HDW are organized and listed in **Table 2**, and their 3D structure is shown in **Figure 2**.

CONCLUSION AND DISCUSSION

Hedyotis diffusa Willd is a representative of heat-clearing and detoxifying herbs with strong anticancer activity and is widely used in clinical adjuvant therapy for postoperative patients with colorectal cancer. In many anticancer TCM formulations, its frequency is as high as 5.1% (Chao et al., 2014). In this study, we covered almost all relevant studies on the anti-colorectal cancer effects of HDW and its extracts *in vitro* and *in vivo* and summarized its advantages, potential signaling pathways, and representative active ingredients in the treatment of CRC as well. We found that the ethanol extract of HDW (EEHDW) had the best anticancer activity, and its anticancer ability was dose- and time-dependent, with a general study concentration of 0.5–2 mg/ml. HDW is less toxic to normal cells than chemotherapy, and it can also reverse MDR in colorectal cancer cells.

HDW exerts anti-colorectal cancer activity through multiple pathways and targets. PI3K/AKT, RAS/ERK, STAT3, NF-κB, Wnt/*β*-catenin, and cell cycle arrest are the most common signaling pathways for its intervention in colorectal cancer. The activation of the PI3K/AKT pathway is a very classic molecular event in the development process of colorectal cancer. Studies have found it plays an important role in regulating cell autophagy, inhibiting epithelial–mesenchymal transition (EMT), and promoting the G1/S-phase cell cycle

(Duan et al., 2018; Wei et al., 2019). The RAS/ERK pathway also plays a vital role in the invasion and proliferation of CRC, and cyclin D1 secreted after its activation can cause the uncontrolled proliferation of colorectal cells (Zhu et al., 2019). Although these pathways are involved in the regulation of different oncogenic mechanisms, they contain common upstream and downstream effector factors and are linked at multiple levels. For example, the interaction of Wnt/β-catenin and PI3K/AKT/mTORC1 signaling pathways is one of the mechanisms of drug resistance in CRC patients (Prossomariti et al., 2020), and oncogene doublecortin-like kinase-1 (DCLK1) can activate NF-κBp65 and induce EMT through the PI3K/Akt/Iκα pathway (Liu W et al., 2018).

Up to 170 compounds have been isolated from HDW, these anthraquinones, iridoids, flavonoids, triterpenes, coumarins, alkaloids, and cyclotides are the main components of anticancer activity. Interestingly, the compound sterols could activate the Wnt/β-catenin pathway, which may play a neutralizing or even opposite role in many compounds. The IC50 of these constituents in colorectal cancer cell lines were close to chemical drugs such as paclitaxel and 5-FU and had no inhibitory effect on normal cell lines (IC50 > 200 μM). They upregulate pro-apoptotic proteins and downregulate antiapoptotic proteins by acting on these key signaling pathways, promote cell apoptosis, inhibit cell proliferation, and inhibit the formation of tumor blood vessels and lymphatics (**Figure 3**).

Modern research technology has provided much evidence for the anti-colorectal cancer effect and molecular mechanism of HDW, which has provided a scientific basis for its wide clinical application, and it is good news for colorectal cancer patients. However, most of the research objects are model mice or cancer cells, which are different from human physiological and pathological environments. On the other hand, traditional Chinese medicine prescription is a combination of several herbs, with the structure of monarch, minister, assistant, and guide. These studies only involve one HDW or one of its components, which obviously cannot fully reflect the anticancer thought of TCM. Moreover, many studies have shown that the combination of multiple components or extracts has more advantages in the intervention of tumor-related signaling pathways than a single herbal. Therefore, the clinical practice of HDW and its extract in the treatment of CRC needs to be further verified, and more suitable options should be explored in future studies.

AUTHOR CONTRIBUTIONS

WZH is responsible for collecting and organizing the data and writing the review. YB is responsible for perfecting graphics and tables, as well as reviewing the full text. In the process of revising the manuscript. YFM is responsible for the critical framework resetting, methodology designing and overall writing quality control. All authors listed have made a substantial, direct, and intellectual contribution to the work and approved it for publication.

FUNDING

This research is supported by the National Nature Science Foundation of China(No.8274315), with the project title of "Tongxieyaofang, Effect in Delaying Colon Cancer Progression through Inhitibion of Stress-induced TSC22D3 Over-expression and Recovering of Th1/Tc1 Immune Responses from the Perspective of 'Simultaneous Regulation of Form, Qi, and Spirit'".

REFERENCES

Alam, M., Ali, S., Ahmed, S., Elasbali, A. M., Adnan, M., Islam, A., et al. (2021). Therapeutic Potential of Ursolic Acid in Cancer and Diabetic Neuropathy Diseases. *Int. J. Mol. Sci.* 22 (22), 12162. doi:10.3390/ijms222212162

Alyabsi, M., Algarni, M., and Alshammari, K. (2021). Trends in Colorectal Cancer Incidence Rates in Saudi Arabia (2001-2016) Using Saudi National Registry: Early- versus Late-Onset Disease. *Front. Oncol.* 11, 730689. doi:10.3389/fonc.2021.730689

Ayoup, M. S., Abu-Serie, M. M., Awad, L. F., Teleb, M., Ragab, H. M., and Amer, A. (2021). Halting Colorectal Cancer Metastasis via Novel Dual Nanomolar MMP-9/MAO-A Quinoxaline-Based Inhibitors; Design, Synthesis, and Evaluation. *Eur. J. Med. Chem.* 222, 113558. doi:10.1016/j.ejmech.2021.113558

Badar Ul Islam, B., Khan, M. S., Husain, F. M., Rehman, M. T., Zughaibi, T. A., Abuzenadah, A. M., et al. (2021). mTOR Targeted Cancer Chemoprevention by Flavonoids. *Curr. Med. Chem.* 28 (39), 8068–8082. doi:10.2174/0929867327666201109122025

Cai, Q., Lin, J., Wei, L., Zhang, L., Wang, L., Zhan, Y., et al. (2012). Hedyotis Diffusa Willd Inhibits Colorectal Cancer Growth *In Vivo* via Inhibition of STAT3 Signaling Pathway. *Int. J. Mol. Sci.* 13 (5), 6117–6128. doi:10.3390/ijms13056117

Chao, T. H., Fu, P. K., Chang, C. H., Chang, S. N., Chiahung Mao, F., and Lin, C. H. (2014). Prescription Patterns of Chinese Herbal Products for post-surgery colon Cancer Patients in Taiwan. *J. Ethnopharmacol* 155 (1), 702–708. doi:10.1016/j.jep.2014.06.012

Chen, R., He, J., Tong, X., Tang, L., and Liu, M. (2016). The Hedyotis Diffusa Willd. (Rubiaceae): A Review on Phytochemistry, Pharmacology, Quality Control and Pharmacokinetics. *Molecules* 21 (6), 710. doi:10.3390/molecules21060710

Chen, W., Jin, Y., Yang, H., Wei, L., and Lin, J. (2018). Hedyotis Diffusa Willd Reduces Migration and Invasion through Inhibition of TGF-β-Induced EMT in Colorectal Cancer Cells. *Eur. J. Integr. Med.* 23, 57–63. doi:10.1016/j.eujim.2018.09.008

DanQing, L., YuJie, G., ChengPeng, Z., HongZhi, D., Yi, H., BiSheng, H., et al. (2021). N-butanol Extract of Hedyotis Diffusa Protects Transgenic Caenorhabditis elegans from Aβ-Induced Toxicity. *Phytother Res.* 35 (2), 1048–1061. doi:10.1002/ptr.6871

Devaraj, H., and Devaraj, S. N. (2017). Differential Cytotoxic Activity of Quercetin on Colonic Cancer Cells Depends on ROS Generation through COX-2 Expression. *Food Chem. Toxicol.* 106 (Pt A), 92–106. doi:10.1016/j.fct.2017.05.006

Dey, P., Kundu, A., Chakraborty, H. J., Kar, B., Choi, W. S., Lee, B. M., et al. (2019). Therapeutic Value of Steroidal Alkaloids in Cancer: Current Trends and Future Perspectives. *Int. J. Cancer* 145 (7), 1731–1744. doi:10.1002/ijc.31965

Duan, S., Huang, W., Liu, X., Liu, X., Chen, N., Xu, Q., et al. (2018). IMPDH2 Promotes Colorectal Cancer Progression through Activation of the PI3K/AKT/mTOR and PI3K/AKT/FOXO1 Signaling Pathways. *J. Exp. Clin. Cancer Res.* 37 (1), 304. doi:10.1186/s13046-018-0980-3

Feng, J., Jin, Y., Peng, J., Wei, L., Cai, Q., Yan, Z., et al. (2017). Hedyotis Diffusa Willd Extract Suppresses Colorectal Cancer Growth through Multiple Cellular Pathways. *Oncol. Lett.* 14 (6), 8197–8205. doi:10.3892/ol.2017.7244

Gao, Y., Nan, X., Shi, X., Mu, X., Liu, B., Zhu, H., et al. (2019). SREBP1 Promotes the Invasion of Colorectal Cancer Accompanied Upregulation of MMP7 Expression and NF-Kb Pathway Activation. *BMC Cancer* 19 (1), 685. doi:10.1186/s12885-019-5904-x

Gerlach, S. L., Dunlop, R. A., Metcalf, J. S., Banack, S. A., and Cox, P. A. (2022). Cyclotides Chemosensitize Glioblastoma Cells to Temozolomide. *J. Nat. Prod.* 85 (1), 34–46. doi:10.1021/acs.jnatprod.1c00595

Han, X., Zhang, X., Wang, Q., Wang, L., and Yu, S. (2020). Antitumor Potential of Hedyotis Diffusa Willd: A Systematic Review of Bioactive Constituents and Underlying Molecular Mechanisms. *Biomed. Pharmacother.* 130, 110735. doi:10.1016/j.biopha.2020.110735

Hemminki, K., Försti, A., and Hemminki, A. (2021). Survival in colon and Rectal Cancers in Finland and Sweden through 50 Years. *BMJ Open Gastroenterol.* 8 (1), e000644. doi:10.1136/bmjgast-2021-000644

Ho, K. (2018). Hedyotis Diffusa and Panax Ginseng Combination: Better Anticancer Properties. *Appl. Food Sci.* 2, 15.

Huang, L., Xu, H., Wu, T., and Li, G. (2021). Hedyotis Diffusa Willd. Suppresses Hepatocellular Carcinoma via Downregulating AKT/mTOR Pathways. *Evid. Based Complement. Alternat Med.* 2021, 5210152. doi:10.1155/2021/5210152

Jiang, J., Wang, B., Li, J., Ye, B., Lin, S., Qian, W., et al. (2017). Total Coumarins of Hedyotis Diffusa Induces Apoptosis of Myelodysplastic Syndrome SKM-1 Cells by Activation of Caspases and Inhibition of PI3K/Akt Pathway Proteins. *J. Ethnopharmacol* 196, 253–260. doi:10.1016/j.jep.2016.12.012

Jiang, Q. W., Chen, M. W., Cheng, K. J., Yu, P. Z., Wei, X., and Shi, Z. (2016). Therapeutic Potential of Steroidal Alkaloids in Cancer and Other Diseases. *Med. Res. Rev.* 36 (1), 119–143. doi:10.1002/med.21346

Jiang, R., Su, G., Chen, X., Chen, S., Li, Q., Xie, B., et al. (2021). Esculetin Inhibits Endometrial Cancer Proliferation and Promotes Apoptosis via hnRNPA1 to Downregulate BCLXL and XIAP. *Cancer Lett.* 521, 308–321. doi:10.1016/j.canlet.2021.08.039

Jun, S. Y., Brown, A. J., Chua, N. K., Yoon, J. Y., Lee, J. J., Yang, J. O., et al. (2021). Reduction of Squalene Epoxidase by Cholesterol Accumulation Accelerates Colorectal Cancer Progression and Metastasis. *Gastroenterology* 160 (4), 1194–1207. doi:10.1053/j.gastro.2020.09.009

Khan, H., Alam, W., Alsharif, K. F., Aschner, M., Pervez, S., and Saso, L. (2022). Alkaloids and Colon Cancer: Molecular Mechanisms and Therapeutic Implications for Cell Cycle Arrest. *Molecules* 27 (3), 920. doi:10.3390/molecules27030920

Khan, H., Belwal, T., Efferth, T., Farooqi, A. A., Sanches-Silva, A., Vacca, R. A., et al. (2021). Targeting Epigenetics in Cancer: Therapeutic Potential of Flavonoids. *Crit. Rev. Food Sci. Nutr.* 61 (10), 1616–1639. doi:10.1080/10408398.2020.1763910

Kopustinskiene, D. M., Jakstas, V., Savickas, A., and Bernatoniene, J. (2020). Flavonoids as Anticancer Agents. *Nutrients.* 12 (2), 457. doi:10.3390/nu12020457

Lai, Z., Yan, Z., Chen, W., Peng, J., Feng, J., Li, Q., et al. (2017). Hedyotis Diffusa Willd Suppresses Metastasis in 5-fluorouracil-resistant Colorectal Cancer Cells by Regulating the TGF-β Signaling Pathway. *Mol. Med. Rep.* 16 (5), 7752–7758. doi:10.3892/mmr.2017.7500

Li, H., Lai, Z., Yang, H., Peng, J., Chen, Y., and Lin, J. (2019). Hedyotis Diffusa Willd. Inhibits VEGF-C-mediated Lymphangiogenesis in Colorectal Cancer via Multiple Signaling Pathways. *Oncol. Rep.* 42 (3), 1225–1236. doi:10.3892/or.2019.7223

Li, Q., Lai, Z., Yan, Z., Peng, J., Jin, Y., Wei, L., et al. (2018). Hedyotis diffusa Willd Inhibits Proliferation and Induces Apoptosis of 5-FU Resistant Colorectal Cancer Cells by Regulating the PI3K/AKT Signaling Pathway. *Mol. Med. Rep.* 17 (1), 358–365. doi:10.3892/mmr.2017.7903

Li, Q., Wang, X., Shen, A., Zhang, Y., Chen, Y., Sferra, T. J., et al. (2015). Hedyotis Diffusa Willd Overcomes 5-fluorouracil Resistance in Human Colorectal Cancer HCT-8/5-FU Cells by Downregulating the Expression of P-Glycoprotein and ATP-Binding Casette Subfamily G Member 2. *Exp. Ther. Med.* 10 (5), 1845–1850. doi:10.3892/etm.2015.2762

Li, S., Kuo, H. D., Yin, R., Wu, R., Liu, X., Wang, L., et al. (2020). Epigenetics/epigenomics of Triterpenoids in Cancer Prevention and in Health. *Biochem. Pharmacol.* 175, 113890. doi:10.1016/j.bcp.2020.113890

Li, Y. L., Chen, X., Niu, S. Q., Zhou, H. Y., and Li, Q. S. (2020). Protective Antioxidant Effects of Amentoflavone and Total Flavonoids from Hedyotis Diffusa on H2 O2 -Induced HL-O2 Cells through ASK1/p38 MAPK Pathway. *Chem. Biodivers* 17 (7), e2000251. doi:10.1002/cbdv.202000251

Li, Y. L., Zhang, J., Min, D., Hongyan, Z., Lin, N., and Li, Q. S. (2016). Anticancer Effects of 1,3-Dihydroxy-2-Methylanthraquinone and the Ethyl Acetate Fraction of Hedyotis Diffusa Willd against HepG2 Carcinoma Cells Mediated via Apoptosis. *PLoS One* 11 (4), e0151502. doi:10.1371/journal.pone.0151502

Lin, J., Chen, Y., Wei, L., Chen, X., Xu, W., Hong, Z., et al. (2010). Hedyotis Diffusa Willd Extract Induces Apoptosis via Activation of the Mitochondrion-dependent Pathway in Human colon Carcinoma Cells. *Int. J. Oncol.* 37 (5), 1331–1338. doi:10.3892/ijo_00000785

Lin, J., Li, Q., Chen, H., Lin, H., Lai, Z., and Peng, J. (2015). Hedyotis Diffusa Willd. Extract Suppresses Proliferation and Induces Apoptosis via IL-6-inducible STAT3 Pathway Inactivation in Human Colorectal Cancer Cells. *Oncol. Lett.* 9 (4), 1962–1970. doi:10.3892/ol.2015.2956

Lin, J., Wei, L., Shen, A., Cai, Q., Xu, W., Li, H., et al. (2013). Hedyotis Diffusa Willd Extract Suppresses Sonic Hedgehog Signaling Leading to the Inhibition of Colorectal Cancer Angiogenesis. *Int. J. Oncol.* 42 (2), 651–656. doi:10.3892/ijo.2012.1753

Lin, J., Wei, L., Xu, W., Hong, Z., Liu, X., and Peng, J. (2011). Effect of Hedyotis Diffusa Willd Extract on Tumor Angiogenesis. *Mol. Med. Rep.* 4 (6), 1283–1288. doi:10.3892/mmr.2011.577

Lin, M., Lin, J., Wei, L., Xu, W., Hong, Z., Cai, Q., et al. (2012). Hedyotis Diffusa Willd Extract Inhibits HT-29 Cell Proliferation via Cell Cycle Arrest. *Exp. Ther. Med.* 4 (2), 307–310. doi:10.3892/etm.2012.599

Liu, W., Wang, S., Sun, Q., Yang, Z., Liu, M., and Tang, H. (2018). DCLK1 Promotes Epithelial-Mesenchymal Transition via the PI3K/Akt/NF-Kb Pathway in Colorectal Cancer. *Int. J. Cancer* 142 (10), 2068–2079. doi:10.1002/ijc.31232

Liu, X., Wu, J., Zhang, D., Wang, K., Duan, X., and Zhang, X. (2018). A Network Pharmacology Approach to Uncover the Multiple Mechanisms of Hedyotis Diffusa Willd. On Colorectal Cancer. *Evid. Based Complement. Alternat Med.* 2018, 6517034. doi:10.1155/2018/6517034

Maleki, S. J., Crespo, J. F., and Cabanillas, B. (2019). Anti-inflammatory Effects of Flavonoids. *Food Chem.* 299, 125124. doi:10.1016/j.foodchem.2019.125124

Mehta, L., Dhankhar, R., Gulati, P., Kapoor, R. K., Mohanty, A., and Kumar, S. (2020). Natural and Grafted Cyclotides in Cancer Therapy: An Insight. *J. Pept. Sci.* 26 (4-5), e3246. doi:10.1002/psc.3246

Meng, Q. X., Roubin, R. H., and Hanrahan, J. R. (2013). Ethnopharmacological and Bioactivity Guided Investigation of Five TCM Anticancer Herbs. *J. Ethnopharmacol* 148 (1), 229–238. doi:10.1016/j.jep.2013.04.014

Prossomariti, A., Piazzi, G., Alquati, C., and Ricciardiello, L. (2020). Are Wnt/β-Catenin and PI3K/AKT/mTORC1 Distinct Pathways in Colorectal Cancer? *Cell Mol Gastroenterol Hepatol* 10 (3), 491–506. doi:10.1016/j.jcmgh.2020.04.007

Selvakumar, P., Badgeley, A., Murphy, P., Anwar, H., Sharma, U., Lawrence, K., et al. (2020). Flavonoids and Other Polyphenols Act as Epigenetic Modifiers in Breast Cancer. *Nutrients* 12 (3), 761. doi:10.3390/nu12030761

Shen, H., Bai, Y., and Huo, Z. (2016). The Protective Effect of Hedyotis Diffusa on Collagen Induced Arthritis Rats. *Int. J. Clin. Exp. Med.* 9, 12880–12887.

Song, Y., Wang, H., Pan, Y., and Liu, T. (2019). Investigating the Multi-Target Pharmacological Mechanism of Hedyotis Diffusa Willd Acting on Prostate Cancer: A Network Pharmacology Approach. *Biomolecules* 9 (10), E591. doi:10.3390/biom9100591

Sun, G., Wei, L., Feng, J., Lin, J., and Peng, J. (2016). Inhibitory Effects of Hedyotis Diffusa Willd. On Colorectal Cancer Stem Cells. *Oncol. Lett.* 11 (6), 3875–3881. doi:10.3892/ol.2016.4431

Tan, J., Li, L., Shi, W., Sun, D., Xu, C., Miao, Y., et al. (2018). Protective Effect of 2-Hydroxymethyl Anthraquinone from Hedyotis Diffusa Willd in Lipopolysaccharide-Induced Acute Lung Injury Mediated by TLR4-NF-Kb Pathway. *Inflammation* 41 (6), 2136–2148. doi:10.1007/s10753-018-0857-9

Thanikachalam, K., and Khan, G. (2019). Colorectal Cancer and Nutrition. *Nutrients* 11 (1), 164. doi:10.3390/nu11010164

Vidri, R. J., and Fitzgerald, T. L. (2020). GSK-3: An Important Kinase in colon and Pancreatic Cancers. *Biochim. Biophys. Acta Mol. Cel Res* 1867 (4), 118626. doi:10.1016/j.bbamcr.2019.118626

Wang, C., Gong, X., Bo, A., Zhang, L., Zhang, M., Zang, E., et al. (2020). Iridoids: Research Advances in Their Phytochemistry, Biological Activities, and Pharmacokinetics. *Molecules* 25 (2), 287. doi:10.3390/molecules25020287

Wang, C., Xin, P., Wang, Y., Zhou, X., Wei, D., Deng, C., et al. (2018). Iridoids and Sfingolipids from Hedyotis Diffusa. *Fitoterapia* 124, 152–159. doi:10.1016/j.fitote.2017.11.004

Wang, C., Zhou, X., Wang, Y., Wei, D., Deng, C., Xu, X., et al. (2017). The Antitumor Constituents from Hedyotis Diffusa Willd. *Molecules* 22 (12), 2101. doi:10.3390/molecules22122101

Wazir, J., Ullah, R., Khongorzul, P., Hossain, M. A., Khan, M. W., Aktar, N., et al. (2021). The Effectiveness of Hedyotis Diffusa Willd Extract in a Mouse Model of Experimental Autoimmune Prostatitis. *Andrologia* 53 (1), e13913. doi:10.1111/and.13913

Wei, R., Xiao, Y., Song, Y., Yuan, H., Luo, J., and Xu, W. (2019). FAT4 Regulates the EMT and Autophagy in Colorectal Cancer Cells in Part via the PI3K-AKT Signaling axis. *J. Exp. Clin. Cancer Res.* 38 (1), 112. doi:10.1186/s13046-019-1043-0

Wrobel, P., and Ahmed, S. (2019). Current Status of Immunotherapy in Metastatic Colorectal Cancer. *Int. J. Colorectal Dis.* 34 (1), 13–25. doi:10.1007/s00384-018-3202-8

Yan, Z., Feng, J., Peng, J., Lai, Z., Zhang, L., Jin, Y., et al. (2017). Chloroform Extract of Hedyotis Diffusa Willd Inhibits Viability of Human Colorectal Cancer Cells via Suppression of AKT and ERK Signaling Pathways. *Oncol. Lett.* 14 (6), 7923–7930. doi:10.3892/ol.2017.7245

Yin, R., Li, T., Tian, J. X., Xi, P., and Liu, R. H. (2018). Ursolic Acid, a Potential Anticancer Compound for Breast Cancer Therapy. *Crit. Rev. Food Sci. Nutr.* 58 (4), 568–574. doi:10.1080/10408398.2016.1203755

Yu, N., Li, N., Wang, K., Deng, Q., Lei, Z., Sun, J., et al. (2021). Design, Synthesis and Biological Activity Evaluation of Novel Scopoletin-NO Donor Derivatives against MCF-7 Human Breast Cancer *In Vitro* and *In Vivo*. *Eur. J. Med. Chem.* 224, 113701. doi:10.1016/j.ejmech.2021.113701

Yuan, C., Wang, M. H., Wang, F., Chen, P. Y., Ke, X. G., Yu, B., et al. (2021). Network Pharmacology and Molecular Docking Reveal the Mechanism of Scopoletin against Non-small Cell Lung Cancer. *Life Sci.* 270, 119105. doi:10.1016/j.lfs.2021.119105

Zhu, D., Zhou, J., Zhao, J., Jiang, G., Zhang, X., Zhang, Y., et al. (2019). ZC3H13 Suppresses Colorectal Cancer Proliferation and Invasion via Inactivating Ras-ERK Signaling. *J. Cel Physiol* 234 (6), 8899–8907. doi:10.1002/jcp.27551

Conflict of Interest: The authors declare that the research was conducted in the absence of any commercial or financial relationships that could be construed as a potential conflict of interest.

Publisher's Note: All claims expressed in this article are solely those of the authors and do not necessarily represent those of their affiliated organizations, or those of the publisher, the editors, and the reviewers. Any product that may be evaluated in this article, or claim that may be made by its manufacturer, is not guaranteed or endorsed by the publisher.

Advantages of publishing in Frontiers

OPEN ACCESS
Articles are free to read for greatest visibility and readership

FAST PUBLICATION
Around 90 days from submission to decision

HIGH QUALITY PEER-REVIEW
Rigorous, collaborative, and constructive peer-review

TRANSPARENT PEER-REVIEW
Editors and reviewers acknowledged by name on published articles

Frontiers
Avenue du Tribunal-Fédéral 34
1005 Lausanne | Switzerland

Visit us: www.frontiersin.org
Contact us: frontiersin.org/about/contact

REPRODUCIBILITY OF RESEARCH
Support open data and methods to enhance research reproducibility

DIGITAL PUBLISHING
Articles designed for optimal readership across devices

FOLLOW US
@frontiersin

IMPACT METRICS
Advanced article metrics track visibility across digital media

EXTENSIVE PROMOTION
Marketing and promotion of impactful research

LOOP RESEARCH NETWORK
Our network increases your article's readership